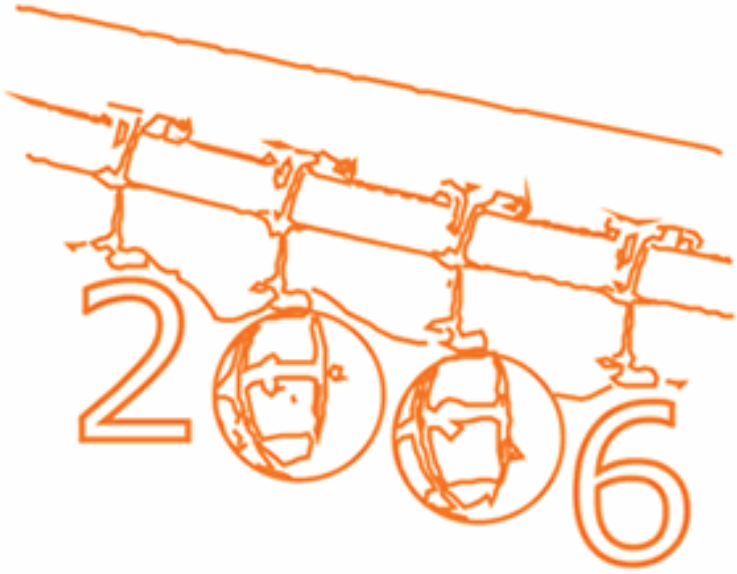
TNT



Trends in NanoTechnology

Grenoble (France) – September 04-08, 2006



PHANTOMS FOUNDATION

Universidad de Oviedo

UAM UNIVERSIDAD AUTONOMA DE MADRID

Georgia Tech

NIMS Nanomaterials Laboratory

DLPG

cea leti

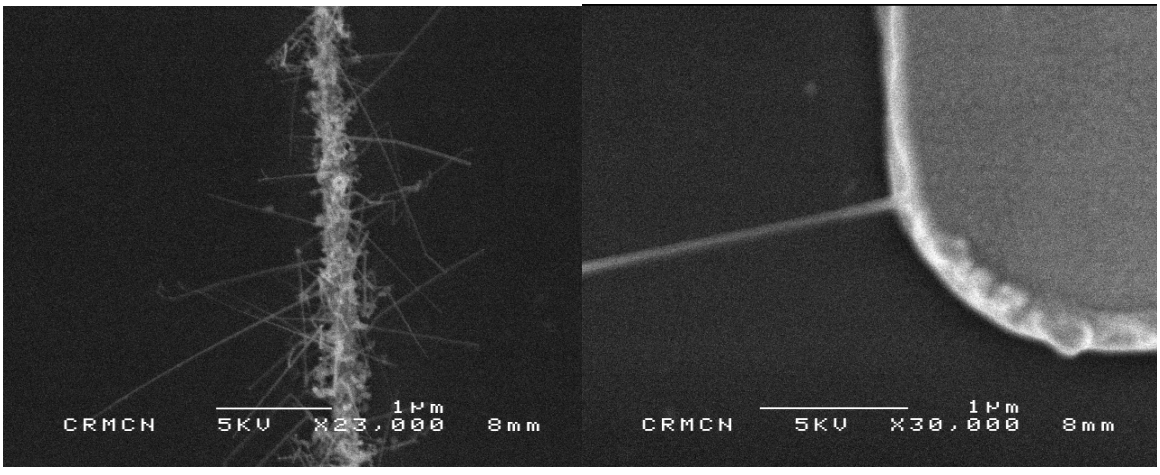
DRFMC

CONNECTED SILICON NANOWIRE FABRICATION FROM CVD OF SILANE

H. ABED, H. JAMGOTCHIAN, H. DALLAPORTA, V. SAFAROV, D. TONNEAU
CRMCN, Faculté des Sciences de Luminy, case 901, 13288 Marseille cedex 09, France
Contact : abed@crmcn.univ-mrs.fr

Semiconducting nanowires (NWs) present several interesting physical properties among which electrical properties are probably the most important from the point of view of applications (electronic devices, sensors…). The formation of silicon whiskers has already been studied from the dissociation of tetrachlorosilane ($SiCl_4$) molecules on silicon surface coated with gold clusters [1]. The growth of whiskers occurs via the so-called Vapor-Liquid-Solid (VLS) technique [2,3]. The mechanism involves a step of eutectic Au-Si alloy formation at sample temperature higher than 363°C, ie above the cracking temperature of $SiCl_4$ molecule (180°C). The permanent gaseous molecule decomposition induces the sur-saturation of the alloy and consequently the precipitation of silicon from the liquid alloy. Finally, one can observe on the sample silicon crystalline NWs, whose diameter is identical to the diameter of the gold clusters. The gold cluster 'catalysing' the gas decomposition remains always at the extremity of the NW during growth. The process feasibility has clearly been demonstrated and the actual challenge remains in the connection of a single Si NWs to integrate it in a device.

We have studied the growth of Si NWs from the decomposition of silane molecules (SiH_4) on gold nanoparticles [4]. To solve the problem of NWs connection, we have tried to initiate the growth reaction from a micronscale tungsten track, connected to aluminium pads, and preliminary coated with gold particles. The tungsten track is then heated by Joule effect in the CVD reactor in an atmosphere of silane. The growth reaction starts above a threshold of electrical power injected in the wire and SiNWs grow at the centre of the tungsten wire, where the temperature is the highest. Ex-situ HRTEM analyses have shown that the SiNWs are coated with a 2 nm thick oxide sheath and the gold particle, whose diameter is identical to the diameter of silicon nanowire [5], remains at the NW extremity. Preliminary results on electrical measurements will be presented.



References

[1] R. S. Wagner, J. Appl. Phys., 38(4), 1554-1560 (1966).
[2] R. S. Wagner, and W. C. Ellis, Appl. Phys. Lett., 4, 89 (1964).
[3] H. I. Givargizov, J. Cryst. Growth 32, 20 (1975).
[4] H. Abed, A. Charrier, H. Dallaporta, V. Safarov, H. Jamgotchian, D. Tonneau, JVSTB24(3), 1248-1253 (2006).

[5] Y. Cui, J. L. Lauhon, M. S. Gudiksen, J. Wang, and C. M. Lieber, Appl. Phys. Lett. 78, 2214 (2001)

POLARON STATES IN SELF-ASSEMBLED QUANTUM DOT MOLECULES WITH DIFFERENT SHAPES

Miguel Angel Adames, A. S. Camacho B.
Departamento de Física, Universidad de Los Andes, Bogota, Colombia
madames@uniandes.edu.co

In realistic semiconductor quantum dots (QDs) the optical phonon emission is a powerful source of relaxation. It has been shown that the polaron formation in these systems is a crucial process in relation with the energy loss processes. Furthermore, it offers a theoretical explanation to the experimental results in QDs [1]. Recently have been grown quantum dots molecules (QDM) in which can be observed interesting behaviour relating with the coupling mechanism of QDs [2].

We focus on the polaron formation and its lifetime in these artificial molecules set up of two coupled QDs with different shapes. In particular, we investigate the optical transitions in self-assembled InAs/GaAs QDM with varying the quantum coupling parameter for spheres, cylinders and truncated cones

We calculate the coupling between the electron and the LO-phonon states by using the Fröhlich Hamiltonian, from which we determine the polaron states which are shown in figure 1. We also calculate of the dipolar electric transitions (figure 2)

We study the dependence on the polaron formation with the coupling between the dots. Since polaron formation strongly modifies the optical spectra due to the appearance of several anticrossings in the excited states, we present a study of the parameter ranges in which the polaronic presence is relevant for the behaviour of the molecule.

In addition we calculate the polaron decay time through irreversible emission of acoustic phonons that is shown in figure 3 for several coupling magnitudes and different shapes of QDs.

References:

[1] V. Preisler, T. Grande, R. Ferreira, L. A. de Vaulchier, Y. Guldner, F.J. Teran, M. Potemski, and A. Lemaitre Phys. Rev. **B 73**, 075320 (2006)

[2] E.A. Stinaff, M. Scheibner, A.S. Bracker, I.V. Ponomarev, V.L. Korenev, M.E. Ware, M.F. Doty, T.L. Reinecke, and D. Gammon, Science **311**, 636 (2006).

Figures:

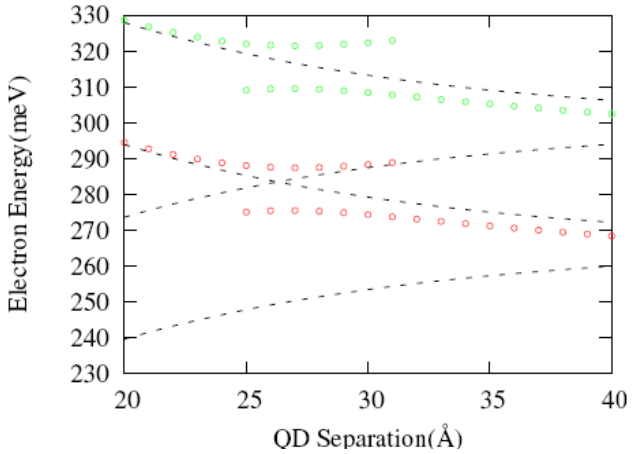


Figure 1. Electron (dashed line) and polaron (dots) states as a function of quantum dot separation for QDM with a harmonic confining potential.

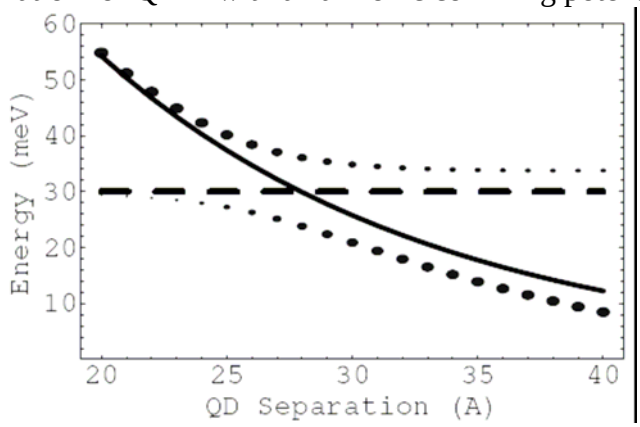


Figure 2. Optical transitions energies as a function of quantum dot separation

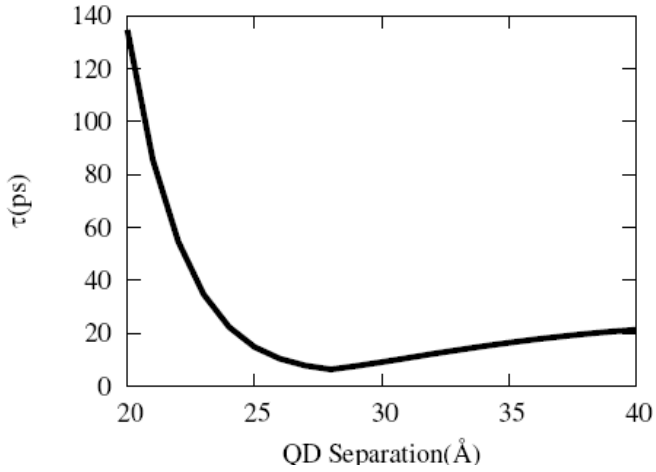


Figure 3. Polaron decay time through irreversible emission of two longitudinal acoustic (LA) phonons as a function of quantum dot separation.

Poster

SIMULATION OF CARBON NANOTUBE FIELD EFFECT TRANSISTORS WITH PALLADIUM CONTACTS

[1]C. Adessi, [2]F. Triozon, [3]S. Roche, and [1]X. Blase

(1)LPMCN, Université Claude Bernard Lyon 1 et CNRS, Domaine Scientifique de la Doua – Batiment Léon Brillouin, 43 Boulevard du 11 novembre 1918, 69622 Villeurbanne, France
(2) LETI and (3) DRFMC/SPSMS, Commissariat à l'Energie Atomique, 25 rue des Martyrs, 38054 Grenoble cedex 9, France
christophe.adessi@lpmcn.univ-lyon1.fr

The use of carbon nanotubes in field effect transistors (CNTFET) represents a promising way to develop new electronic devices. However, its development has raised a lot of questions regarding the contact with the electrodes and the electrostatic response of the nanotube. Actually, the fine structure of the interface between the metal and the nanotube and the chemical environment play an important role in the transport properties [1-3]. For instance, it has been proven that the use of Palladium contacts tends to reduce the Schottky barrier [1]. Moreover, the electrostatic influence of the gate over the nanotube is taking place over several ten or hundred nanometers. For these reasons, it is mandatory to use multiscale simulation in order to take into account the complexity of the interface at the atomic scale, and the geometry and electrostatics of the complete device.

The system considered to model the interface between the metal and the nanotube in the CNTFET is an infinite palladium nanowire connected to the nanotube (see figure). To model this interface, we start with a ground-state calculation of the system of interest using the SIESTA *ab-initio* package. The locality of the basis and the local density approximation lead to the partitioning of the system into "nearest-neighbor" sections so that the Hamiltonian H and overlap S matrices are tri-diagonal by blocks. This property allows to calculate with an O(N) scaling the Green's function of the system. We have thus been able to study the transmission across a semi-infinite metallic nanowire and a semiconducting carbon nanotube when different conformations for the contact are considered (flat connection or embedded nanotube into the metallic nanowire).

As the transport along the nanotube close to the Fermi level is mainly governed by the π-π^* bands, the *ab initio* calculation with a large orbital basis (used to model the contact between the metal and the nanotube) is unnecessary when we deal with the nanotube itself. Especially, the part of the tube submitted to the gate potential does not require such a large basis and a single orbital description is enough.

We have thus developed a technique to couple the *ab initio* calculations needed to describe the contact and the tight binding calculation for the part of the tube submitted to the gate potential. This has been performed by first computing with the *ab-initio* results the self-energy of a finite length nanotube connected to the palladium lead and then to use these self-energies to perform the self-consistent calculation of the influence of the gate on the nanotube using a simple π-π^* tight-binding basis. With this technique, the transmission properties of the contact are fully described without the inconvenience of the large basis used to model the contact.

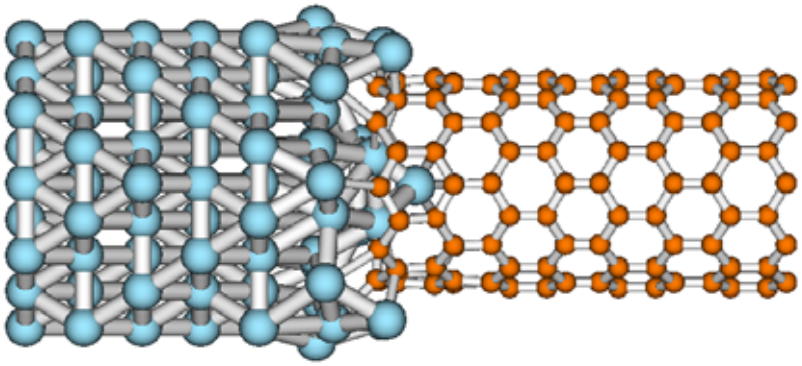
Using this reduction of the tight-binding basis, quantum simulations of CNTFETs with coaxial gate have been performed. The Green's function formalism is used to compute the Landauer-Büttiker conductance and the charge on each orbital of the channel, similarly to the method used by Guo and co-workers [4]. The self-consistency is obtained iteratively by solving the Poisson equation, correcting the potential on the nanotube within the Hartree scheme, and recalculating the charge along the nanotube with the Green's function method. Once self-consistency is achieved, the Landauer-Büttiker conductance is computed. The

present study is performed at T = 300 K. It is limited to coherent transport in the low bias regime (V_{DS} smaller than kT). The current-gate voltage characteristics $I(V_G)$ are calculated. We study the influence of gate the parameters (distance to the contacts and to the channel). The results with "*ab initio*" Pd-CNT self-energies are compared to those obtained with a very simple model of metal contacts, in order to discriminate the contribution of the contacts in the $I(V_G)$ characteristics.

References:

[1] A. Javey, J. Guo, Q. Wang, M. Lundstrom, and H. Dai, Nature, **424** (2003) 654; W. Kim, A. Javey, R. Tu, H. Dai, Applied Physics Letters, **87** (2005) 173101.
[2] Z. Chen, J. Appenzeller, J. Knoch, Y. Lin, and Ph. Avouris, NanoLetters, **5** (2005) 1497.
[3] S. Auvray, J. Borghetti, M. F. Goffman, A. Filoramo, V. Derycke, J. P. Bourgoin, and O. Jost, Applied Physics Letters, **84** (2004) 5106.
[4] J. Guo, S. Datta, and M. Lundstrom, IEEE Transactions on Electron Devices, **51** (2004) 172.

Figure:



Junction between a Pd nanowire and a (10,0) carbon nanotube

COILED MULTIWALLED CARBON NANOTUBES AS ELECTROMECHANICAL RESONATORS

M. Ahlskog[1], A. Volodin[2] and C. Van Haesendonck[2]
1) University of Jyväskylä, Nanoscience Center, P.O.B 35 (YFL), FIN-40014, Finland.
2) Laboratorium voor Vaste-Stoffysica en Magnetisme, Katholieke Universiteit Leuven, B-3001 Leuven, Belgium.
E-mail: ahlskog@phys.jyu.fi

Freestanding carbon nanotubes are being intensively studied as electromechanical resonators. Usually they are constructed from straight, freely suspended nanotubes and the mode of vibration being either lateral or torsional motion of the tube. We have constructed a nanotube resonator according to a very different design, based on coiled multiwalled carbon nanotubes. The nanotube material that we use is synthesized by a CVD technique [1]. The degree of disorder may be substantial, resulting generally in rather curved shape of the tubes. Regularly coiled nanotubes emerge under certain conditions from the CVD reactor. After deposition on a substrate, these nanotube coils have nearly freestanding windings (Figure 1). When exciting the nanotube windings either electrically, via an AFM tip, or acoustically, the fundamental resonances (ranging from 100 to 400 MHz) can be detected. The resonators are sensitive to mass changes as small as a few tens of attograms [2].

References:

[1] K. Hernadi, A. Fonseca, J. B.Nagy, D. Bernaerts, A. Fudala, A.A. Lucas, Zeolites, **17** (1996) 416.
[2] A. Volodin, D. Buntinx, M. Ahlskog, A. Fonseca, J. B.Nagy, C. Van Haesendonck, Nanoletters, **4** (2004) 1775.



Figure 1. A SEM image of a coiled multiwalled nanotube deposited on a substrate.

Poster

ION BEAMS IRRADIATION EFFECT ON NANOHARDESS OF SILICON

Shahjada Ahmed Pahlovy[*1], Sadao Momota[1], Yao Yingxue[2], M.Kashihara[1], K.Nishimura[1]

[1]*Intelligent Mechanical System Engineering Department, Kochi University of Technology, Kochi-782-8502, Japan.*

[2]*Mechanical Electronics Engineering Department, Harbin Institute of Technology, Harbin-150001, China.*

096402c@gs.kochi-tech.ac.jp

Abstract

Nanohardness is defined as a materials resistance to permanent or plastic deformation at the nano-micro scale. Nanohardness is a significant mechanical properties of materials used to characterize the wear resistance of materials mailny. Most mechanical parts like bearings, gears, and shafts are produced by finishing processes such as hard turning, grinding and/or honing. The durability and reliability of these precision products are directly influenced by mechanical behavior specially nanohardness. This paper describes how ion beam irradiation influence the nanohardness property of materials i.e. effects on nanohardness of silicon.

If mechanical parts are in micro nano scale such as micro interconnector, micro valve, micro actuator, micro switch in those case nanohardness is an important factor for better performance. In the present paper discusses ion beams irradiation effects on hardness in micronano scale is discussed.

The experiment was completed by a 10- GHz NANOGAN ECR ion source installed at Kochi University of Technology (KUT), Japan. Ar^{+4} ions with energy 60 keV, 100 keV, 200 keV and 400 keV were irradiated on Si through a Cu stencil mask at room temperature. The dimension of the used mask thickness was 10 µm with square hole size 43µm x 43 µm. For the three different energies, the dose on sample was 500 qµC/cm^2 constant where q denotes the charge states of the irradiated Ar ions. After ion beam irradiation the nano indentation was done by Nano Indenter-II at Harbin Institute of Technology (HIT) ,China.

Nanohardness for 60 keV, 100 keV, 200 keV and 400 keV were measured to be 10.807 GPa, 10.187GPa, 10.029 GPa and 9.84 GPa respectively. Finally the effect of ion beams irradiation on nanohardness of silica is compared graphically for different accelerating energy. It shows hardness property depends on accelerating energy

Figure 1 shows the relation between accelerating energy and nanohardness on irradiated surface. The relation shows nanohardness decreases with the increases of accelerating energy. It also noted that it decreases very sharply between 60keV and 100 keV accelerating energy. After 100 keV the hardness decreases smoothly.

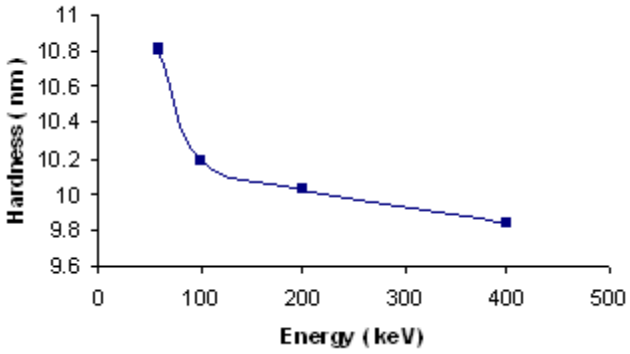


Figure 1 Energy vs. Hardness of irradiated Si.

.

Nanotechnology is an outgrowth and extension of microfabrication. Newly developments in mechatronics and robotics expand their application fields. Superior functions with advanced control are required in mechatronics system and robotic system. In those systems nanohardess of materials are important factor for better performance in micro nano scale. The current paper gives the idea how nanohardness property changes with different acceleration energy during micro nano scale fabrication by ECR ion beam irradiation. It seems this technique will helpful to improve mechanical properties during micro nano fabrication.

References:

[1] Sadao Momota, Y. Nojiri, Y. Hamagawa,K. Hamaguchi, J. Taniguchi, H. Ohno ,Application of highly charged Ar ion beams to ion beam lithography , Nuclear Instruments and Methods in Physics Research B 242 (2006) 247-249.

[2] Sami Franssila, Introduction to micro fabrication, 2005 Edition.

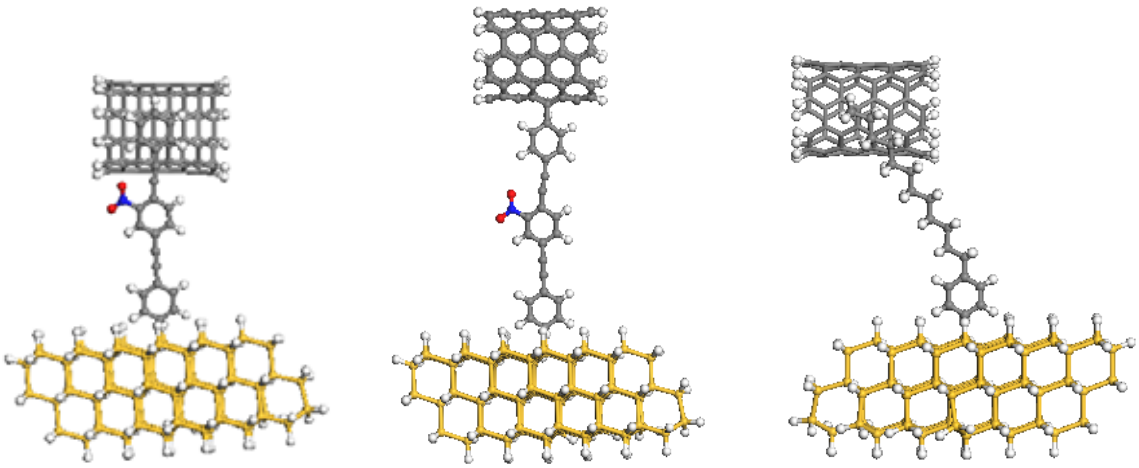
[3] Bernhard Wolf, Handbook of Ion Sources, 1995 Edition.

SWITCHING BEHAVIOR IN SILICON-MOLECULE-SWCNTS DEVICES: A DENSITY FUNCTIONAL THEORY STUDY

Brahim Akdim, Ruth Pachter
Air Force Research Laboratory, Materials and Manufacturing Directorate
Wright-Patterson Air Force Base, OH 45433
Brahim.Akdim@wpafb.af.mil

Most recently, a new testbed for exploring the electrical properties of single molecules has been developed [1], in order to eliminate the possibility of metal nanofilament formation and to ensure that molecular effects are measured, whereby Si and single-wall carbon nanotubes (SWCNTs) are used as electrodes for the molecular monolayer, demonstrated, for example, for molecules such as those based on oligo(phenylene-ethynylene) in a Si-OPE/NO_2-SWCNT device configuration. Interestingly, the use of such structures with π-conjugated organic molecules resulted in a hysteresis loop with current-voltage measurements that are useful for a memory device [1]. Devices without π-conjugated molecules ((Si-H) surface only), or with alkyl-bearing molecules produced no hysteresis, indicating that the observed memory effects is molecular relevant.

In this work, we present a density functional theory study of the OPE derivative either physisorbed or chemisorbed (**a, b** in Fig. 1) at a SWCNT, and covalently bonded at the Si slab, as well as of an alkyl derivative (**c**, cf. Fig. 1), with respect to conformational changes, taking place under an applied field. Structural parameters, electronic structure, and charge transfer as a function of an applied field will be discussed in detail.



a **b** **c**

Figure 1: Models representing a physisorption (a) and a chemisorption (b) in the Si—OPE/NO_2—CNT complex, and a physisorption of alkyl derivative (c).

References:

1 He, J., Flatt, A. K., Stephenson, J. J., Condell, D. Doyle, J. M. Tour, Nature Materials 5, 63 (2006).

Synthesizing Silicon Nanocrystals in Silicon Dioxide Matrix by Magnetron Sputtering Technique for Optical and Electrical Applications

A. S. Alagoz, A. Imer, A. Seyhan, R. Turan
Department of Physics, Middle East Technical University, 06531, Ankara, TURKEY
alagoz@metu.edu.tr

Charge storage and light emitting properties of Silicon (Si) nanocrystals embedded in silicon dioxide (SiO_2) matrix is of interest due to possible applications in nonvolatile memories and Si based optoelectronics. Floating nanocrystal based memory systems provide improved reliability with long retention time and higher density with low power consumption. It has been shown that Si nanocrystals can replace the classical floating gate electrode to improve Flash memory performance [1]. Photonic application of Si nanocrystals is based on the light emission generated by the Si nanocrystal as a result of the quantum size effect. This is expected to lead to the fabrication of Si based optoelectronic components such as Light Emitting Diodes (LED) [2].

Si nanocrystals can be synthesized by different techniques such as Ion Implantation [2], Chemical Vapor Deposition [3], Magnetron Sputtering [4], etc. Magnetron Sputtering is a superior in the synthesis of Si nanocrystals due to low process temperature, precise deposition control and good quality oxide production. Both floating Si nanocrystal non-volatile flash memory and Si nanocrystal based LED applications require good control over the material and device parameters such as the nanocrystal size uniformity, positioning nanocrystals in SiO_2 and the quality of SiO_2 matrix. With magnetron Sputtering technique, nanocrystal and matrix composition can easily be engineered, single and multilayer structures can be designed [5] and good quality thin SiO_2 layers can be achieved [6,7].

In this study, the effect of annealing temperature and time on the formation of Si nanocrystals in Si-rich SiO_2 layer prepared by Magnetron Sputtering have been studied systematically, shown in Fig. 1. The effect of post annealing under hydrogen and oxygen atmosphere are investigated with Photoluminescence Spectroscopy (PL), Fourier Transform Infrared Spectroscopy (FTIR), Capacitance-Voltage Characterization and Transmission Electron Microscopy (TEM). It is shown that the PL efficiency can be improved substantially with hydrogen annealing as a result of passivation of non-radiative transition centers. Post annealing under O_2 ambient has led to blue shift in the PL peak position, shown in Fig. 2, indicating size controlled light emission from Si nanocrystals.

References:

[1] S. Tiwari, F. Rana, H. Hanafi, A. Hartstein, et.al., Applied Physics Letter, **68** (1996) 1377.
[2] Serincan U., Aygun G., Turan R., Journal of Luminescence, **113** (2005) 299-234
[3] R.A. Rao, R.F. Steimle, M. Sadd, C.T. Swift, et.al., Soli-State Electronics, **48** (2004) 1463
[4] J. u. Schmidt, B. Schmidt, Materials Science & Engineering B **101** (2003) 28
[5] W. K. Choi, W.K. Chim, C. L. Heng, L.W. Ho, et.al., Applied Physics Letter **80** (2002) 2014
[6] T. Serikawa, S. Shirai, Vacuum **51** (1998) 781
[7] S. Suyuma, A. Okamoto, T. Serikawa, Journal of Applied Physics **62** (1987) 2360

Figures:

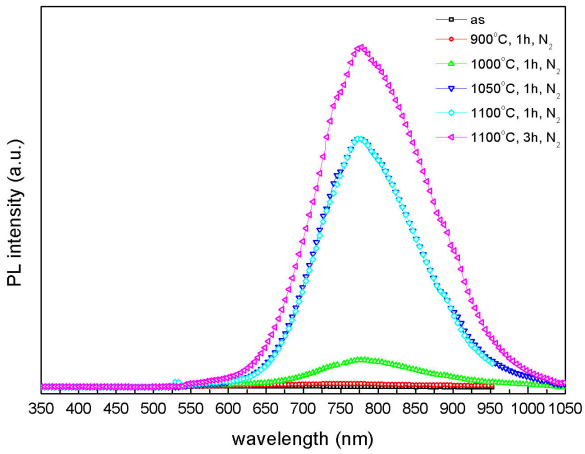


Fig.1. Photoluminescence spectra of Si reach SiO_2 layer for different annealing temperatures and annealing time

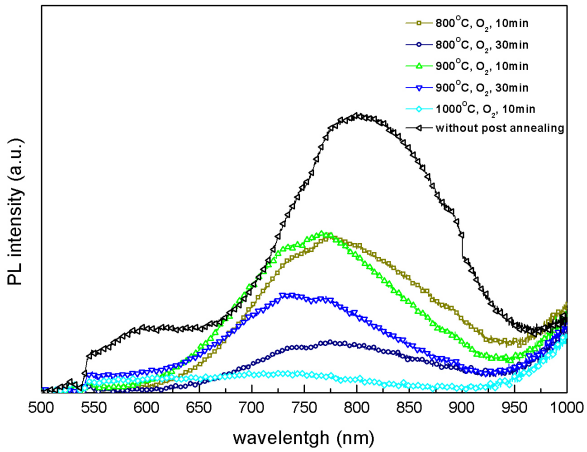


Fig. 2. Effect of post annealing under O_2 on Photoluminescence

EMPIRICAL ANALYTICAL DISTRIBUTION FUNCTION ON SIZE OF DISPERSE SYSTEMS OF MAGNETITE NANOPARTICLES

Rasim A.Ali-zade
Institute of Physics Azerbaijan National Academy of Sciences
H.Javid str.33, Baku Az-1143, Azerbaijan
alizade@lan.ab.az

Distribution functions of magnetite nanoparticles on size are one of main characteristic of disperse systems. This allowed to analysis mechanism of growth of nanoparticles, its behavior in external electrical, magnetic fields. This is necessary for determination of other physical characteristic of disperse systems by statistical averaging. Distribution function of magnetite nanoparticles on size has been determined by different methods.

Analytical size distribution function of six samples of magnetite nanoparticles has been determined on the base analysis of agreement of known analytical functions: normal, logarithmic-normal, combination of normal and logarithmic-normal functions, modified logarithmic-normal, β, γ, χ^2, III order Pirson functions with frequency distribution [1]. Parameters of used distribution functions (average size $(\bar{x})$, standard deviation (σ) ant etc.) have been determined by statistical analysis of electron microscopy data of magnetite nanoparticle size. Parameters of distribution $(\bar{x}, \sigma)$ are: (9.48, 2.363), (7.76, 2.305), (7.33, 1.71), (5.44, 1.164), (10.194, 1.574), (4.83, 1.47), for samples I-VI, correspondingly.

The agreement of distribution functions with frequency distribution has been investigated by nearest two functions and χ^2 criterion methods [2]. It has been determined that initial part of distribution of magnetite nanoparticles on size may be described by normal, final part - logarithmic-normal function. Diameter of magnetite nanoparticles, corresponding to transition of normal distribution to logarithmic-normal has been determined by equation:

$$F_N(x) - F_L(X) = 0$$

where $F_N(x)$, $F_L(X)$ normal and logarithmic-normal distribution functions correspondingly. Transition diameter is: 9.3, 7.5, 7.2 and 5.4 for samples I-IV, correspondingly.

Analytical distribution function of disperse systems magnetite nanoparticles consisting normal and logarithmic-normal functions has been constructed. However, using such analytical function in analytical calculations is not conveniently.

We constructed analytical function of distribution on the base of moments of distribution. It's known, distribution function $(F(x))$ may be determined on the base of characteristics function $(\Psi(x))$ [3].

$$F(x) = \int_0^1 \Psi(\omega) e^{-i\omega x} dx \qquad (1)$$

As $\Psi(x)$ may be presented by Taylor set:

$$\Psi(x) = \Psi(0) + \Psi'(0)\cdot\omega + \frac{1}{2!}\cdot\Psi''(0)\cdot\omega^2 + \frac{1}{3!}\cdot\Psi^3(0)\cdot\omega^3 + ... = \frac{1}{2\pi}\sum_{n=0}^{10}\omega^n x^n \frac{i^n}{n!}..$$

where $\Psi^{(n)}(0) = \overline{x^n}\frac{i^n}{2\pi}$, $\overline{x^n}$ is distribution moment in *n* order.

After substitution $\Psi(x)$ in (1) obtained:

$$F(x)=\frac{1}{2\pi}+\frac{1}{2\pi}\sum_{n=1}^{10}\frac{1}{n!}\overline{x^n}\,\frac{1}{(ix)^n}\int_0^1 t^n e^{-t}dt=\frac{1}{2\pi}+F_1(x)+F_2(x)+F_3(x)+.....F_{10}(x)$$

Last expression has been simplified:

$$F(x)=\frac{1}{2\pi}+\frac{1}{2\pi}\left(a_1x+a_2x^2+a_3x^3+.....a_{10}x^{10}\right)$$

where

$$a_n=\left(-(i)^{n+1}\right)\frac{1}{(n-1)!}\sum_{m=1}^{5}(-1)^m\,\frac{\overline{x^{2m}}}{2m!}\,\frac{1}{(2m+n)} \qquad \text{for } n=1,3,5,7,9$$

$$a_n=\left((i)^{n+1}\right)\frac{1}{(n-1)!}\sum_{m=1}^{5}(-1)^{m+1}\,\frac{\overline{x^{2m-1}}}{(2m-1)!}\,\frac{1}{(2m+n-1)} \qquad \text{for } n=2,4,6,8,10$$

Exact moments of distribution have been determined as described in [4].

Constructed analytical function has been compared with frequency distribution and agreeable results have been obtained. Moreover, constructed analytical function has been used in calculation of magnetization of disperse systems of magnetite nanoparticles by:

$$M(H)=M_s\cdot\varphi_m\int_0^1 F(m)\cdot L\left(\frac{mH}{kT}\right)\cdot dm$$

where $F(m)$ is distribution function on magnetic moment, which has been obtained on the base of distribution function on size, $L\left(\frac{mH}{kT}\right)=cth\left(\frac{mh}{kT}\right)-\frac{1}{\overline{\frac{mh}{kT}}}$ is Langevan function. Magnetizations curves obtained by calculation and experimentally are agree.

Thus obtained analytical distribution function described distribution of magnetite nanoparticles on size well enough and it is convenient in use in mathematical calculations.

References:

[1] Handbook of mathematical functions with formulas, graphs, and mathematical tables. Edited by M.Abramovich, I.A.Stegun, NAtionakl Bureau of Standards applied mathematics series 55, (1964)832.

[2] V.I.Krilov, B.B.Bobkov, P.I.Monastirniy, Vichislitelniye metodi t.1, M., Nauka, (1976)304.

[3] V.G.Levich, Kurs teoreticheskoi fiziki. t.1, Nauka M., (1969)912.

[4] R.A.Ali-zade, Transactions of Azerbaijan Academy of Sciences 24(2004)15.

Poster

PROBING THE TRANSVERSAL MAGNETO-OPTICAL KERR EFFECT AT THE NANOMETRIC SCALE

L.M. ÁLVAREZ-PRADO[1], J.-J. GREFFET[2], Y. SOUCHE[3], R. CARMINATI[2].

[1]Departamento de Física, Universidad de Oviedo, Av. Calvo Sotelo, 33007 Oviedo, Spain,
[2]Laboratoire EM2C CNRS, Ecole Centrale Paris, 92295 Châtenay-Malabry cedex, France.
[3]Laboratoire Louis Néel, CNRS/UJF, BP 166, Grenoble cedex 9, France.

lmap@uniovi.es

Nano-objects are becoming quite common in magnetism: dots, wires, constrictions, domains, walls…Magnetic Force Microscopy (MFM) and Spin Polarized Scanning Tunneling Microscopy (SP-STM) are currently used near-field techniques for studying such tiny objects. On the other hand, the magneto-optical Kerr effect (MOKE) is a widely used probe of magnetism in solid-sate physics. In the far-field version, the transverse configuration of the magneto-optical Kerr effect (TMOKE) is sensitive to one of the in-plane components of magnetization. Recently, a transverse MOKE-like configuration was adopted for a near-field setup [1,2].

We present a theoretical study of the transverse Kerr effect observed when an optical nanosource is scanned close to a magnetic material (within a nanometric distance). In order to achieve this task several calculations has been performed. The interaction between the nanoprobe and the magnetic structure can result in a complex electric field distribution. As a first approximation of the electric field felt by the sample we have used the expressions stemming from the Bethe and Bouwkamp theory [3]. From this field we have calculated the currents excited in the magnetic sample. The field radiated by these currents and observed in the far-field was obtained by using the electromagnetic theorem of reciprocity [3].

Some results showing the magnetic contrast for simple magnetic structures will be presented. In particular, we have studied a dot (0-D) in a single domain magnetic state and an isolated wire (1-D) containing a Bloch-type wall. The magnetic material used is $Co_{70.4}Fe_{4.6}Si_{15}B_{10}$ 60-nm thick. We will show the magnetic contrast which appears in two frequently used scanning modes: the “constant-distance” mode and the “constant-height” mode.

References:

[1] - J. Schoenmaker, A.D. Santos, Y. Souche, and L. C. Sampaio, Appl. Phys Lett, 88 (2005) 062506.

[2] - L. M. Álvarez-Prado, J. Schoenmaker, A.D. Santos, T. Fournier and Y. Souche, Phys. Stat. Sol. (a), 203 (2006) 1425.

[3] J. N. Walford, J.-A. Porto, R. Carminati, J.-J. Greffet, J. Opt. Soc. Am. A, **19** (2002) 572.

Poster

PHOTOTRANSFORMATION OF C_{60} THIN FILMS BY UV PULSED LASER IRRADIATION: COMPARATIVE PHOTOACOUSTIC, AFM, AND RAMAN STUDIES

E. Alvarez-Zauco*, E. V. Basiuk (Golovataya-Dzhymbeeva), R. Castañeda-Guzmán, R. Y. Sato-Berrú, J.M. Saniger-Blesa, M. Villagrán-Muniz

CCADET, Universidad Nacional Autónoma de México, Ciudad Universitaria, Coyoacán, 04510 México D.F., México. Phone (52-55) 5622-8602, Fax (52-55) 5622-8651

*e-mail: ezauco@ciencias.unam.mx

Abstract.

Fullerene C_{60} films deposited by sublimation were irradiated with Kr-F laser in a wide fluence interval from 15 to 40 mJ/cm^2. In situ photoacoustic analysis was applied to study the phase transformation during the irradiation. The results obtained were discussed in conjunction with atomic force microscopy (AFM) and Raman spectroscopy data. It was found that for a irradiation fluence interval from 22 to 30 mJ/cm^2, 80% of C_{60} undergoes photopolymerization (presumably through 2+2 cycloaddition). For a laser energy higher than 30 mJ/cm^2, a new amorphous carbon phase forms, having a large content of diamond-like, tetra-amorphous carbon (ta-C).

IMAGING DEFECTS IN CARBON NANOTUBES WITH AN STM

H. Amara[1,2], V. Meunier[3], J.-Ch. Charlier[2] and Ph. Lambin[1]
[1]*LPS, FUNDP, Rue de Bruxelles 61, 5000 Namur, Belgium*
[2]*PCPM, Université Catholique de Louvain, 1348 Louvain-la-Neuve, Belgium*
[3]*ORNL, Oak Ridge, TN 37831, USA*
hakim.amara@fundp.ac.bel

Scanning tunnelling microscopy (STM) and scanning tunnelling spectroscopy (STS) are powerful techniques for investigating the electronic topographic properties of nanomaterials. Whereas the already large amount of experimental STM data obtained so far on perfect nanotubes is perfectly understood, the identification of topological and non-topological modifications of the hexagonal lattice of a carbon nanotube remains an experimental challenge. Thanks to a simple, though accurate theoretical approach, it is possible to simulate the topographic and spectroscopic signatures of many types of defects in graphene and single-walled nanotubes, and to contribute therby to their identification from STM and STS observations. Several illustrations will be provided during the talk.

Development of a Silicon-based Single Electron Transistor

S.J. Angus[a,b], A.S. Dzurak[a,b], R. Brenner[a], M. Prunnila[c] and R.G. Clark[a]

[a] *Centre for Quantum Computer Technology, University of New South Wales, Sydney, NSW, Australia.*
[b] *School of Electrical Engineering and Telecommunications, University of New South Wales, Sydney, NSW, Australia.*
[b] *VTT Information Technology, P.O. Box 1208, FIN-02044 VTT, Espoo, Finland*

Email: susan.angus@student.unsw.edu.au

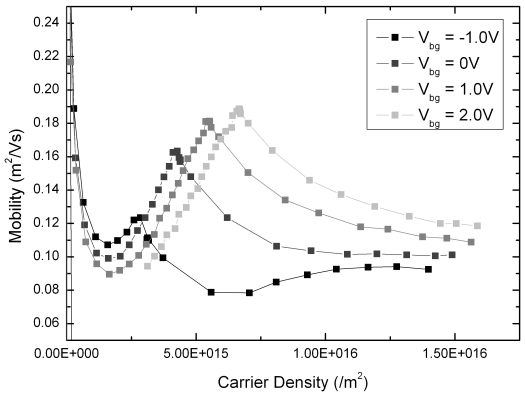
Single electron transistors (SETs) are of great interest for future nanoelectronic circuits [1] due to their small size, low power consumption, and ability to perform fast and sensitive charge measurements [2]. Silicon SETs in particular are advantageous since they have been shown to operate with remarkable stability [3], and they may be fabricated using techniques which are compatible with conventional integrated circuit technology.

The silicon SET studied in this work is designed for controllable and reproducible low temperature operation. It comprises a dual gate structure on a silicon-on-insulator substrate. A silicon quantum wire is formed in a high-resistivity superficial silicon layer using reactive ion etching. Carriers are induced in the silicon wire by utilizing the low-resistivity silicon substrate as a back gate, which is separated from the superficial silicon by an ∼80 nm thick buried oxide. The tunnel barriers are created electrostatically, using lithographically defined metallic electrodes (∼40 nm width). These electrodes surround the quantum wire, producing strong electrostatic confinement. This architecture provides independent control of tunnel barrier height and island occupancy, thus permitting excellent control of Coulomb blockade oscillations, as has been shown recently in a similar device [4]. The tunnel barrier gates also allow silicon quantum dots to defined electrostatically within the silicon wire. A schematic of the device is shown in Figure 2(a).

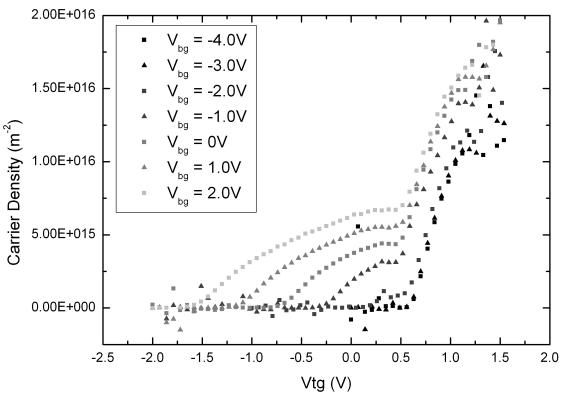
The use of the SOI substrate as a back-gate has been demonstrated in double-gated MOSFETs and in silicon wires. The double-gated MOSFETs were fabricated with a superficial silicon thickness of approximately 100 nm. Hall measurements performed on these devices confirmed the formation of two inversion layers, which were independently controllable by the top and back gates of the device. The results of these Hall measurements are shown in Figure 1. Preliminary measurements carried out on 50 nm thick, 1 μm wide silicon wires confirm the control of carriers in the superficial silicon by the back-gate, as seen in Figure 3. Silicon SETs, including gates for electrostatic tunnel barrier control, are currently in fabrication. An SEM image of one of these devices is provided in Figure 2(b). Latest results will be presented at the conference.

[1] K.K. Likharev, *Proceedings of the IEEE* **87**, 606 (1999).
[2] M.H. Devoret and R.J. Schoelkopf, *Nature* **406**, 1039 (2000).
[3] N.M. Zimmerman, W.H. Huber, A. Fujiwara and Y. Takahashi, *Appl. Phys. Lett.* **79**, 3188 (2001).
[4] A. Fujiwara, H. Inokawa, K. Yamazaki, H. Namatsu, Y. Takahashi, N.M. Zimmerman and S.B. Martin *Appl. Phys. Lett.* **88**, 053121 (2006).

Figure 1: Results from Hall measurements taken on a double-gated SOI MOSFET at 4 K

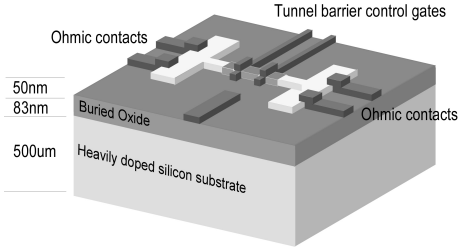


(a) Mobility as a function of carrier density

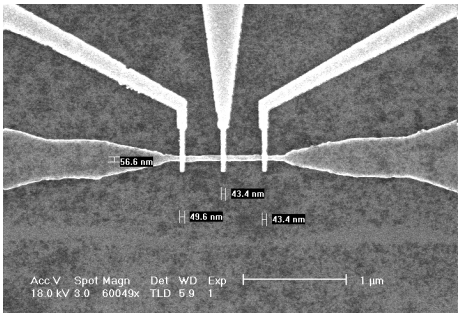


(b) Carrier density as a function of applied top-gate voltage

Figure 2: Silicon SET



(a) Schematic diagram of the Si SET studied in this work.



(b) SEM image of an Si SET in fabrication.

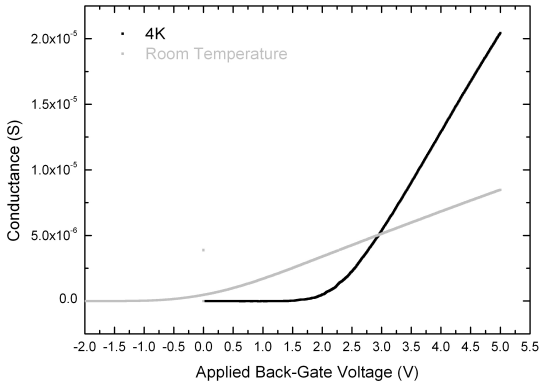


Figure 3: Conductance of a 50 nm thick, 1 μm wide silicon wire as a function of applied back-gate voltage.

DOUBLE-GATE ORGANIC FIELD EFFECT TRANSISTORS

A. Anthore, A. Mangin, and P. Lafarge
Laboratoire Matériaux et Phénomènes Quantiques, Université Paris 7, case courrier 7021, 2 place Jussieu, 75251 Paris Cedex 5, France
anne.anthore@paris7.jussieu.fr

We have realized organic field effect transistor using pentacene or dihexylsexithiophene as the organic semiconductor. The geometry of the transistor consists of a source, a drain and two gates: the typical back gate and a local gate used to fine tune the width of the current path between source and drain. I will present results showing that the fine tuning of the current path is not controlled at scales smaller than 10 µm. Two phenomena can explain this result : either the injection dominates the electronic transport through the channel, either a parasitic parallel channel, which is not sensitive to the local gate width, dominates.

Poster

INVESTIGATION OF CELL ATTACHMENT ON THE SCAFFOLDS MANUFACTURED BY ELECTROSPUN PCL-HYALURONAN BLENDS

Yang Y[1], Ylikauppila H[2], Nikkola L[2], Ashammakhi N[1,2]

[1]Institute of Science and Technology in Medicine, Keele University, UK
[2]Institute of Biomaterials, Tampere University of Technology, Tampere, Finland
nureddin.ashmmakhi@tut.fi

INTRODUCTION. Recently, nanofibre-based scaffolds were developed to mimic natural extracellular matrix (ECM). Various synthetic and natural polymers have been used (1-3). Polycaprolactone (PCL) is one of the commonly studied synthetic polymers (4). However, PCL is associated with high hydrophobicity. Among other factors such as topography or the biological receptors on the scaffold surface, hydrophilicity is an important factor for cell attachment. It is known that hyaluronan is an important natural material found in ECM. But it suffers from low mechanical properties. Thus, to combine mechanical strong structure provided by PCL and the hydrophilicity provided by hyaluronan, a blend of PCL and hyaluronan was hypothesized to be a better option for cell attachment and function.

MATERIALS AND METHODS Either acetic acid or a mixture of acetic acid with 26% chloroform was used to dissolve PCL. To half of specimens 5% of hyaluronan was added to PCL solution. Both pure PCL and PCL-hyaluronan blend solutions were then electrospun using a voltage source (20 kV) to produce non-woven structures that were collected on glass coverslides. UV light was used for sterilisation of the scaffolds. Osteofiboblast cell line (MG63) was seeded on the scaffolds and incubated. Constructs were examined at 12h, 48h and 1 week. Actin staining was made after one week of culture and examined by fluorescent microscopy.

RESULTS AND DISCUSSION Scaffolds made from PCL-hyaluronan blends have formed more homogenous nanofibers as compared to neat PCL. Fibre diameter of neat and blend PCL fibres ranged from 150 to 250 nm. Cell attachment on the blend fibres was much faster and earlier and appeared healthier shape compared to that on neat PCL nanofibres. After 12 and 48 hour cell seeding, round shape cells were still seen on neat PCL nanofiber scaffold but not on blend fibres (Fig. 1). No relation between the type of used solvent and cell morphology could be demonstrated. Actin staining demonstrated the presence of dense filaments and elongated cell bodies on PCL blend scaffolds mesh indicating better cell attachment and focal adhesion (Fig. 2). It seems that hyaluronan which is naturally occurring polysaccharide present in connective tissues with high hydrophilicity can be beneficial for enhancing cell growth and cell attachment on PCL scaffolds. Although, in gel form, pure hyaluronan was found not to favour cell attachment [5]. However, when PCL was blended with small portion of hyaluronan, cell attachment was improved as compared to hydrophobic neat PCL. UV sterilization of the scaffolds in the current study may have affected hyaluronan structure, and contributed to improved cell attachment. However, such explanations need to be studied further, which is the subject of undergoing studies. From the current results, one can conclude that hyaluronan blended with PCL in 5% can improve osteofibroblast cell attachment and spread on electrospun nanofibre based scaffolds. This can further applied in tissue engineering.

References:

[1] Ashammakhi *et al*. (2006) J Nanosci Nanotechnol (In press)
[2] Ndreu *et al*. (2006) Biomaterials (Submitted)
[3] Piras *et al*. (2006) J Nanosci Nanotechnol (In press)

[4] Nikkola *et al*. (2006) J Nanosci Nanotechnol (In press)
[5] Shu *et al*. Biomaterials, 24, (2003) 3825.

Figures:

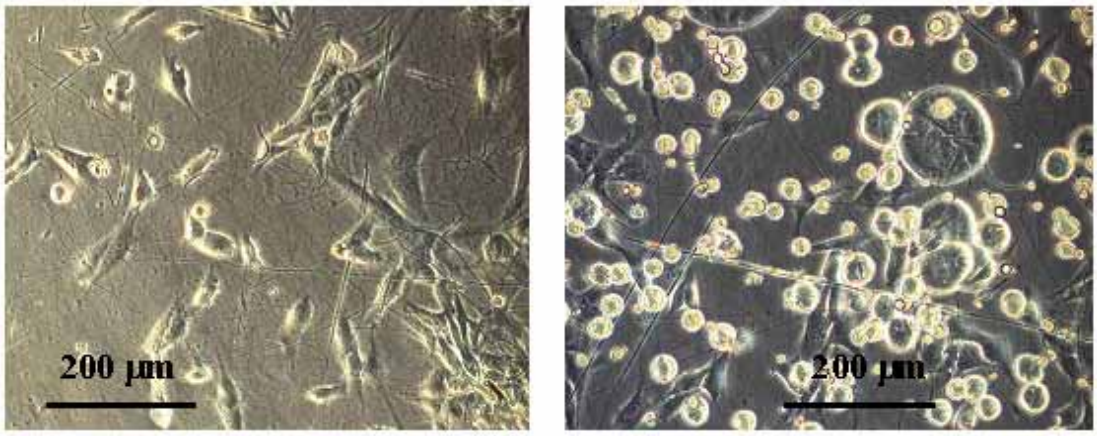


Figure 1 Light microscopic images of MG63 cells grown on nanofiber based scaffolds after 12 hour of culture on either neat PCL (Left) or PCL hyaluronan blend (Right).

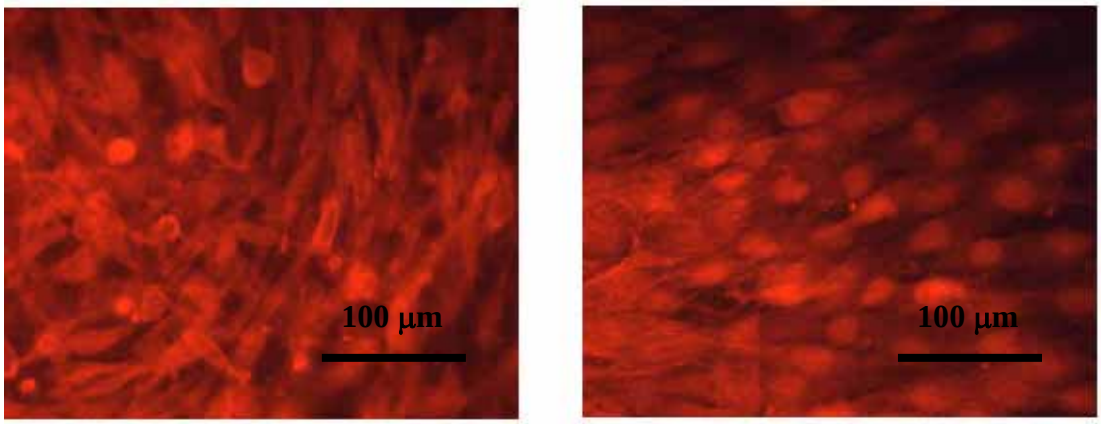


Figure 2 Actin stain images images of MG63 cells grown on nanofiber based scaffolds after 1 week hour of culture on either neat PCL (Left) or PCL hyaluronan blend (Right).

Investigating Chemical Disorder Strength in Carbon Nanotubes : Magnetic Tuning of Quantum Transport Regimes

Rémi Avriller[1],*S.Latil*[2],*F.Triozon*[3],*X.Blase*[4],*and S.Roche*[1]
[1]*CEA/DRFMC/SPSMS/GT, 17 avenue des martyrs, 38054 Grenoble, France*
[2]*LPS, University of Namur, 61 rue de Bruxelles, 50000 Namur, Belgium*
[3]*CEA/DRT/LETI, 17 rue des martyrs, 38054 Grenoble Cedex 9, France*
[4]*LPMCN, CNRS, Université Claude Bernard Lyon I and CNRS UMR 5586, 43 Bd du 11 Novembre 1918, 69622 Villeurbanne, France*
E-mail : remi.avriller@cea.fr

We have studied the various transport regime that develop in nitrogen doped metallic carbon nanotubes under magnetic fields [3]. By combining *abinitio* and *semi-empirical* models [1], a scaling analysis of the Landauer conductance has been performed and characteristic transport length scales extracted from phenomenological laws.

A quantitative analysis of the relationship between energy-dependant elastic mean free path and localization length has been done, and an external magnetic field applied perpendiculary to the nanotube axis is shown to induce a shift in energies of quasibound states, a phenomenon that results in giant magnetoconductance fluctuations under Fermi level shift.

References

[1] Ch. Adessi, Stephan Roche, and X. Blase. Reduced backscaterring in potassium doped nanotubes : ab-initio and semiempirical simulations. *Physical Review B*, 73(125414), March 2006.

[2] Hyoung Choi and Jisoon Ihm. Defects, quasibound states, and quantum conductance in metallic carbon nanotubes. *Physical Review Letters*, 84(13), March 2000.

[3] Sylvain Latil, Stephan Roche, Didier Mayou, and Jean-Christophe Charlier. Mesoscopic transport in chemically doped carbon nanotubes. *Physical Review Letters*, 92(25), June 2004.

OPTICAL AND ELECTRICAL INVESTIGATIONS OF THE InAs QUANTUM DOTS IN THE AlO MATRIX.

O.R. Bajutova, A.G. Milechin,O.V. Naumova, A.I. Toropov, A. Gutakovsky
Institute of Semiconductor Physics,630090 Novosibirsk ,Russia
bajutova@thermo.isp.nsc.ru

The technique of selective wet oxidation of Al(Ga)As has been widely used in the fabrication of various optical devices such as photon crystals[1], light emitting diodes, vertical-cavity quantum dot lasers. Oxidized Al(Ga)As layers are used as a current aperture for achieving both optical and electrical confinements and for making of a AlO/ GaAs distributed Bragg reflector mirrors with high reflection too. The application of this process to vertical cavity quantum dot lasers has led to significant performance improvements[2,3].
In this paper we report on using the technique of selective wet oxidation in the formation of InAs quantum dots in an AlO matrix and the investigation of optical and electrical properties. The InAs QD/AlO system can be considered as a promising candidate for possible application of as an active media for vertical cavity QD lasers because higher barriers of an aluminum oxide matrix produce shifts of the InAs QD bandgap energy.
The structure with InAs self – assembled quantum dots in an AlAs matrix was grown by molecular beam epitaxy on GaAs (001) oriented substrate. The lateral oxidation of the AlAs layers was then performed in horizontal quarz tube at 360^0C with N_2 as the carrier gas passing through a H_2O bubbler maintained at 95^0C.
Transmission electron microscopy results reveal, that the obtained AlO matrix has the amorphous structure. The optical investigations was performed by micro-Raman spectroscopy and micro-PL spectroscopy. Micro- Raman spectra measured from non-oxidised area reveals the phonon features at 274, 361 and 405 cm^{-1} attributed to LO GaAs-like phonon from InAs QDs and TO and LO phonons from AlAs layer, respectively. Intensity of the lines decreases when the laser spot approaches the oxidized area. No additional lines due the amorphous and crystalline As clusters observed earlier for InAs/AlAs QD structures [4] appear in the Raman spectra of annealed samples that reflect the improved selective oxidation procedure.
Micro-PL spectrum of InAs QDs samples taken from non-oxidized area reveals a PL peak by 1.69 eV attributed to the transition from the first electron excited states to the ground hole state in InAs QDs. The peak energy position shifts gradually towards lower energy (1.59 eV) by approaching the oxidized area while its intensity decreases. This fact can be explained by narrowing of the QD size distribution towards larger QDs upon oxidation.
The current-voltage characteristics of structures was measured at different temperatures. One can see current jump in the I-V curve at room temperature and two peaks in the I-V curve at nitric temperature. This behavior of the I-V dependencies suggests the resonant tunneling through the states in Al_2O_3 dielectric. The comparison of the structures, prepared with different modes, it makes it possible to determine which of these states correspondent to the InAs QDs embedded in AlO dielectric matrix.

References:

[1] A.M. Yacomotti,F. Raineri, G. Vecchi at all , Appl.Phys. B **81**, 333-336(2005)
[2] J.J. Wierer, P.W. Evans, N Holonyak, and D.A.Kellogg, Appl. Phys. Lett. **72**, 2742(1998).
[3] Z. Zou, D.L. Huffaker, S.Csutak, and D.G. Deppe, Appl. Phys. Lett. **75,** 22(1999)
[4] D.A. Tenne, O.R. Bajutova, A.K Bakarov, A.K. Kalagin,A.G. Milechin, A.I. Toropov,D.R.T. Zahn, Tech. Phys. Lett. **28**, 554(2002)

Poster

STRUCTURAL CHARACTERIZATION OF NANOGRANULAR $BATIO_3$-$COFE_2O_4$ THIN FILMS DEPOSITED BY LASER ABLATION ON SI/PT SUBSTRATES

J. Barbosa, B.G. Almeida, J.A. Mendes, A. Rolo, J.P. Araújo
Dep. Física, Universidade do Minho, Campus de Gualtar, 4710-057 Braga, Portugal
Dep. de Física and IFIMUP, Univ. Porto, Rua Campo Alegre, 687, 4169-007 Porto, Portugal
bernardo@fisica.uminho.pTt

Magnetoelectric nanocomposite thin films constructed by mixing magnetostrictive and piezoelectric materials have attracted recently much scientific and technological interest [1]. The stress mediated coupling between the magnetic and the electric component phases engenders a material presenting properties which are not available in the individual materials. As a result, the properties and performance of these nanostructures depend critically on the phase morphology and internal stress distribution, which, in turn, are determined by the elastic phase/phase and phase/substrate interactions.

In order to address this problem, nanogranular thin films composed by $BaTiO_3$ (piezoelectric) and $CoFe_2O_4$ (magnetostrictive) were prepared by pulsed laser ablation, on platinum covered Si(001) substrates. The depositions were done with a KrF excimer laser (wavelength λ = 248 nm), at a fluence of 1.5 mJ/cm^2. The oxygen pressure during deposition was 1 mbar, and the substrate temperature was 600ºC. The ablation targets were prepared by sintering $CoFe_2O_4$ and $BaTiO_3$ powders with different concentrations. Structural studies were performed by X-ray diffraction (XRD) and were carried out with a Philips PW-1710 diffractometer using Cu Kα radiation. Raman studies were performed using a Jobin-Yvon T64000 spectrometer.

Figure 1 shows the X-ray diffraction spectra measured on the nanocomposites with cobalt ferrite concentrations in the range 20% - 70%. They are polycrystalline and composed by a mixture of tetragonal-$BaTiO_3$ and $CoFe_2O_4$ with the cubic inverse spinnel structure. The grain sizes measured from the X-ray diffraction peak widths for both phases ((112) for $BaTiO_3$ and (311) for $CoFe_2O_4$), were determined by using the Scherrer equation. They are in the range 30nm to 100nm. The lattice parameter of the $CoFe_2O_4$ phase was obtained from the (311) peak position, and varied from 8.26Å for x=20% to 8.35Å for x=70%, with an almost linear trend. Comparing with the bulk cubic inverse spinnel $CoFe_2O_4$ lattice parameter (a=8.3874Å), it is observed that in the films the cobalt ferrite is under compressive stress, that relaxes as its concentration progressively increases. On the other hand the $BaTiO_3$ lattice parameters (*a,c*) were obtained using the (111) and (110) peaks. The lattice parameter *a* is approximatly constant as function of concentration (*a*~4.04Å) and expanded relative to the bulk phase. However, the lattice parameter *c* decreases from 4.006Å for x=20% to 3.93Å for x=70%, so that the $BaTiO_3$ *c* axes is increasingly compressed as the quantity of the barium titanate phase is reduced in samples. This behavior is the opposite of the observed one in $CoFe_2O_4$.

Figure 2 shows the Raman spectra of the thin film samples deposited with cobalt ferrite concentrations in the range 20%-70%. In order to understand the contributions of the different phases to the Raman spectra of the nanocomposite films the individual $BaTiO_3$ and $CoFe_2O_4$ bulk powders that were used to prepare the ablation targets were also measured. Two main peaks are observed in the spectrum of the $CoFe_2O_4$ powder. They appear at 470 cm^{-1} and 690 cm^{-1} and their positions are represented by doted lines in figure 2. In the $BaTiO_3$ powder the main observed peaks appear at 520 cm^{-1} and 716 cm^{-1}, and their positions are represented by solid lines in figure 2. The $BaTiO_3$ peak at 307 cm^{-1} coincides with a smaller one from $CoFe_2O_4$.

$CoFe_2O_4$ has a cubic inverse spinnel structure with $O_h^7(Fd\bar{3}m)$ space group. The metallic cations can occupy two types of positions: either surrounded by six oxygen ions forming an octahedron or by four oxygen ions forming a tetrahedron[2]. The modes appearing

at 470 cm^{-1} and 690 cm^{-1} were assigned to octahedral site (O-site) and tetrahedral site (T-site) modes, respectively [2]. On the other hand, the tetragonal form of $BaTiO_3$ belongs to the $C_{4v}^{1}(P4mmm)$ space group, and in the $BaTiO_3$ powder the peaks appearing in the Raman spectrum at 520 cm^{-1} and 716 cm^{-1} correspond, respectively, to transverse optical (TO) and longitudinal optical (LO) vibrations of the A_1 and E phonon modes [3].

Based on the peaks observed in the powders, the nanocomposite films spectra were deconvoluted by using Lorentzian line-shape functions to least-squares fit the Raman peaks as shown in figure 2. In the nanocomposite thin films, the main observed peaks appear near 470 cm^{-1} and 690 cm^{-1} and they correspond to the cubic inverse spinnel $CoFe_2O_4$ O-site and T-site modes referred above. The peaks from $BaTiO_3$ are not so visible, but two slight bumps appear near 520 cm^{-1} and 716 cm^{-1}, corresponding to the $BaTiO_3$ modes referred above. Their positions remain approximately the same in this concentration range. On the other hand, as the $CoFe_2O_4$ concentration increases, the O-site mode decreases from 491 cm^{-1}, for x=20%, to 473 cm^{-1}, for x=70%, being systematically above the bulk 470 cm^{-1} value (figure 3). A similar trend was observed for the T-site mode. This blueshift of the $CoFe_2O_4$ modes results from the lattice strain, as already observed also by X-ray diffraction and shown in figure 1.

References:

[1] - Zheng H., Wang J., Lofland S.E., Ma Z., Mohaddes-Ardabili L., Zhao T., Salamanca-Riba L., Shinde S.R., Ogale S.B., Bai F., Viehland D., Jia Y., Schlom D.G., Wuttig M., Roytburd A., Ramesh R. Science, **303** (2004) 661

[2] - T. Yu, Z.X. Shen, Y. Shi and J. Ding, J. Phys.: Condens. Matter, **14** (2002) L613

[3] - U.V. Venkateswaran, V.M. Naik and R. Naik, Phys. Rev. B, **58** (1999) 14256

Figures:

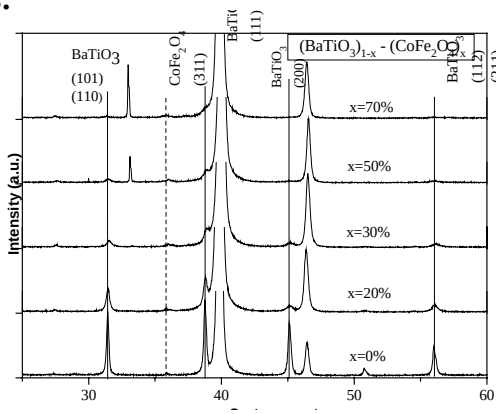


Figure 1: X-ray diffraction spectra of the samples deposited with cobalt ferrite concentrations in the range 20%-70%.

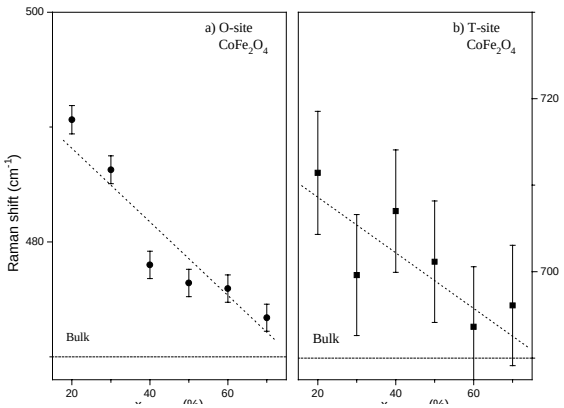


Figure 3: Raman shift as a function of the $CoFe_2O_4$ concentration, for the a) O-site and b) T-site modes. The lines are a guide to the eye.

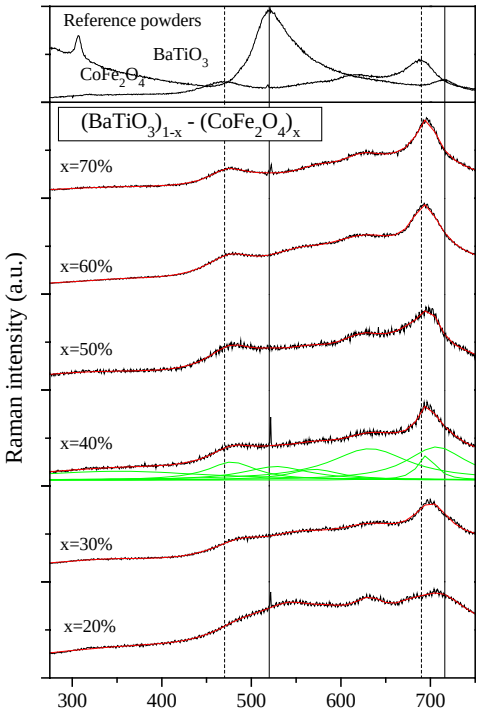


Figure 2: Raman spectra of the samples deposited with $CoFe_2O_4$ concentrations in the range 20%-70%, along with the corresponding fitting curves. Also shown are the $BaTiO_3$ and $CoFe_2O_4$ reference powders, and the Lorentzians obtained from the fit to the spectrum of the sample with x=40%.

THREE-DIMENSIONAL ELECTRON BEAM INDUCED DEPOSITION TO OVERCOME EDGE EFFECTS IN WIRING OF NANO STRUCTURES

S. Bauerdick, D. Hoering, A. Kricke[1], H. Hillmer[1], C. Stampfer[2], T. Helbling[2], C. Hierold[2] and H.W.P. Koops[3]

Raith, Hauert 18, 44227 Dortmund, Germany
[1]INA and CINSaT, University of Kassel, Heinrich-Plett-Strasse 40, 34132 Kassel, Germany
[2]Micro and Nanosystems, ETH Zurich, 8092 Zurich, Switzerland
[3]Ernst Ludwig Strasse 16, 64372 Ober-Ramstadt, Germany
bauerdick@raith.de

Electron Beam Induced Deposition (EBID) has been successfully applied to wiring of nano structures like carbon nanotubes [1, 2]. Moreover the development of easy to handle precursors yielding good conductivity of the deposit is very promising for further improvements of this technique [3]. Basically, a focused electron beam in combination with a gas injection system supplying a vapour precursor is used for direct patterning of conducting leads.

In general, creating a connection from a nano object to the outside world in the millimetre dimensions represents a challenge, whereas one would like to achieve this wiring easily, *in-situ* and with good electrical quality. Therefore all parts of the connection including wire bonding or electrical probes, metal electrodes fabricated by optical or e-beam lithography and the final wiring of the nano structure as well as the interfaces of these parts have to be examined carefully. Particularly the integrated combination of a nano manipulator, EBID and pre-patterned electrodes provides excellent flexibility. Moreover for suspended or 3-dimensional structures like in Nano Electro-Mechanical Systems (NEMS) (Fig. 3) direct patterning EBID can be used for wiring even during one of the final process steps [2].

Bonding or probing contacts show a good ohmic contact and the conductivity of metal lines is sufficient at a thickness of 100 nm to 200 nm. Fine line deposition however generates structures of 20 nm to 50 nm in thickness, and the connection to the metal pad is known to be a critical part of the rather high resistance of various EBID leads [2, 4]. In addition most gas injection systems deliver the precursor from one or several nozzles to the sample, resulting in a directed beam of precursor molecules and thus shadow effects. Figure 1 illustrates the adsorbed precursor layers on a 3-dimensional connector environment in cross-sectional view. In the semi or complete shadow region close to the step, the deposition rate is reduced and a different material quality is generated. To overcome these limited conditions an additionally fabricated connecting bridge pier and arc structure is designed here and serves as a height compensation regarding the edge scattering effects and precursor flux. The arc can thus be fabricated using the unshadowed adsorption rate of the precursor. A micrograph of such a special connecting structure made by deposited Pt/C lines for a 2-point (or 4-point) measurement is shown in Figure 2. The resistance of the additional parts with respect to their position to the nozzle is measured in 2-point and 4-point measurements. Results for various exposure and deposition parameters will be presented and a comparison with connections made by conventional EBID structures will be drawn.

References:

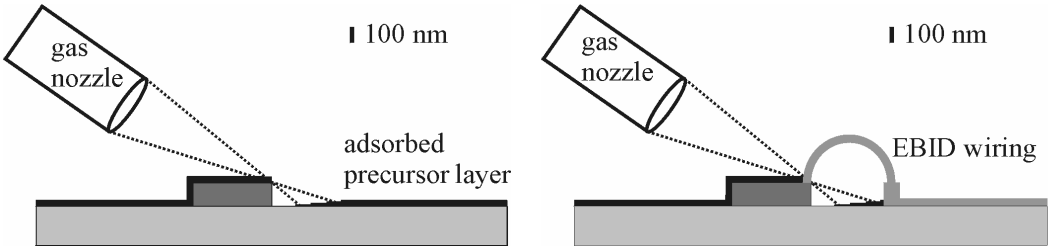
[1] T. Brintlinger et al., JVST B 23, 3174 (2005)

[2] S. Bauerdick et al., extended abstract at EIPBN 2006, Baltimore

[3] J. D. Barry et al., extended abstract at EIPBN 2006, Baltimore

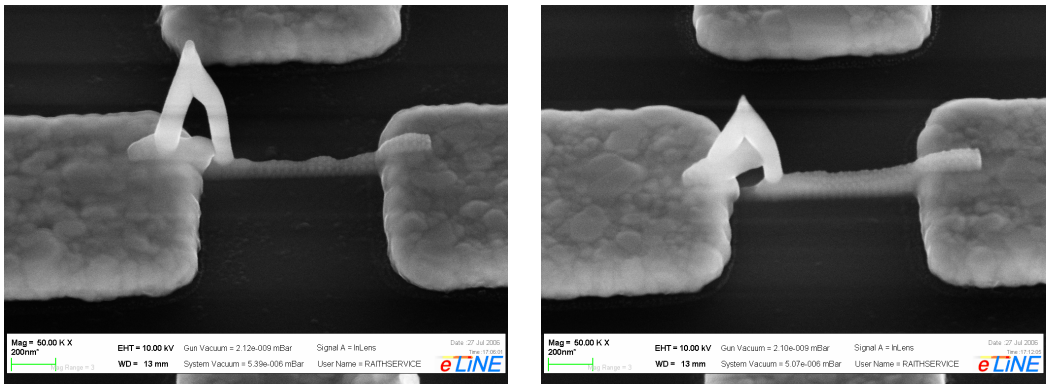
[4] M. D. Croitoru et al., JVST B 23, 2789 (2005).

Figures:



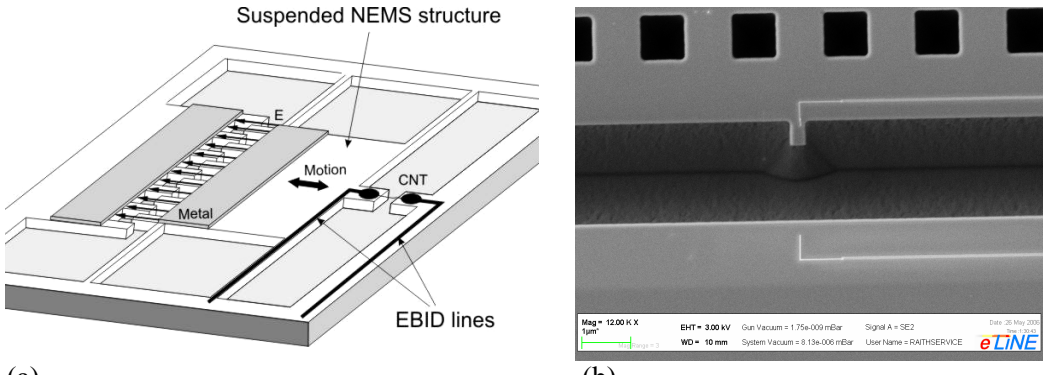
(a) (b)

Fig. 1: Schematic setup of gas injection system and sample with micro electrodes for wiring of nano structures showing (a) the distribution of the adsorbed precursor layers and (b) the 3-dimensional EBID structure to overcome step and shadow effects.



(a) (b)

Fig. 2: Scanning electron micrographs of 3-dimensional platinum EBID nano structures providing an improved contact to the pre-patterned electrodes.



(a) (b)

Fig 3: Nano electro-mechanical system (NEMS) with EBID leads used for wiring of nano structures: (a) schematic and (b) scanning electron micrograph.

ADAPTIVE ALGORITHMS FOR REAL-TIME STM IMAGING

S. Bedwani[1], *F. Guibault*[2] *and A. Rochefort*[1]
Département de génie physique[1] *et informatique*[2], *École Polytechnique de Montréal,*
et Réseau québécois sur les matériaux de pointes[1] *(RQMP)*
Montréal, Canada
Stephane.Bedwani@polymtl.ca

Our present understanding of electronic transport theories enables us to compute STM images of large and complex molecular systems such as carbon nanotubes or self-assemblies. The production of numerical STM images is generally limited to relatively small systems and needs substantial computational resources. Nevertheless, through the fast evolution of computer power, in conjunction with new parallel algorithmic strategies, the synthesis of real-time STM images now appears feasible. A rapid evaluation of STM images will allow both experimentalists and theoreticians to work on a common platform that will simplify the analysis of experimental data and favor exploration of new materials.

In order to produce real-time STM images, a two stage strategy is envisionned: the parallelization of tunneling current calculations (as STM image pixels), and the discretization of space where these currents are computed. For the current calculations, we have already successfully implemented a parallel approach using the extended Hückel formalism based on periodic systems. The present work focuses on the second stage, which is based on an iterative process involving adaptive algorithms. The process is a step by step image analysis in which zones of interest, such as contrasts related to adsorbed molecules or structural defects, are identified. This significantly decreases the computational time to produce STM images by reducing the number of calculations to perform in a specific areas.

The main steps of our adaptive algorithm are described in Figure 1(a). First, the surface of a molecular system such as the one illustrated in Figure 1(b) is discretized using an initial mesh. This step is performed either by taking a uniform coarse square grid or by using the position of adsorbed atoms. Several tunneling currents are then computed simultaneously for all mesh points on a parallel computer. For maximum flexibility, the tunneling currents can be probed anywhere on the surface, and the generated images are analyzed on an unstructured mesh obtained from a Delaunay triangulation. To locate the zones of interest, solutions are analyzed by detecting the edges, based on image contrast. Typical edge detection algorithms apply a convolution filter on a grid image to approximate the Laplacian. Although this process cannot be performed on unstructured meshes, it is still possible to approximate the Laplacian with a quadratic fit[1]. This fitting method approximates the second derivative for each pixel by applying a least square regression of a quadratic surface over a small area around a specific pixel. The Laplacian of the fitted surface yields a simple value that is assigned to the surface point studied. Once the edge detection is complete, weights are assigned to the triangles to determine which points of the surface need to be adapted to improve the image resolution. This adaptive cycling is then repeated until the desired resolution is obtained.

A sequence of adapted meshes is shown in Figure 1(c) where the final adapted solution contains only 945 pixels but has an equivalent resolution to a square grid of 3600 pixels. In this particular

case, the adapted image is generated almost four times faster then the typical grid image. In addition to the molecular adaptive mesher, we will present advances in the virtual STM project.

Reference:

[1] C. Manole, M.-G. Vallet, J. Dompierre, and F. Guibault, “Benchmarking Second Order Derivatives Recovery of a Piecewise Linear Scalar Field”, In *Proceedings of the 17th IMACS World Congress Scientific Computation, Applied Mathematics and Simulation*, (2005).

Figure:

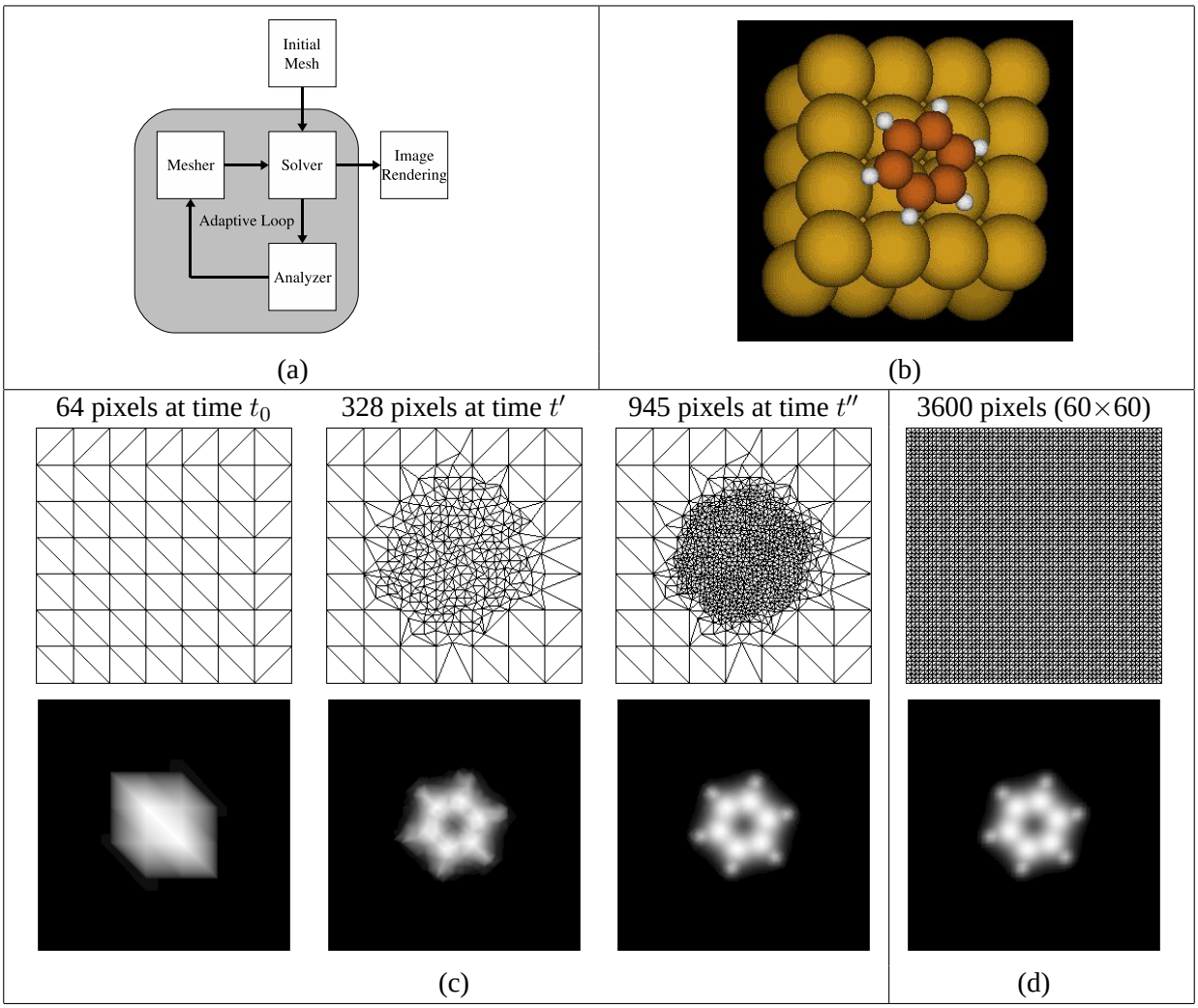


FIG. 1 – (a) Data flow of our adaptive molecular mesher; computations are performed on an initial mesh, then the surface is analyzed, and a new mesh is generated containing the next pixels to be solved. The surface analysis and solving process is repeated until the target resolution is obtained. (b) Benzene molecule adsorbed on Cu(100) surface is a simple example of an input system that can be used to generate numerical STM images. (c) Sequence of meshes and their ideal solution based on benzene’s van der Waals surface for different stages of the adaptive algorithm; first image is an initial coarse grid, second is an intermediate unstructured mesh, and third is the final adapted solution. (d) Reference grid of 3600 pixels and a solution for comparison with the final adapted solution.

FLAME SYNTHESIS AND DIAGNOSTICS OF TITANIA, VANADIA AND SILICA NANOPOWDERS

C. Bellomunno, S. Maffi, F. Cignoli, G. Angella, G. Zizak
Istituto per l'Energetica e le Interfasi (IENI) - C.N.R., via Cozzi, 53-20125, Milano – ITALY
Carla.Bellomunno@ieni.cnr.it

Nanostructured inorganic materials are routinely produced in manufacture industry by the gas-to particle conversion process using flame reactors. This route allows to obtain inexpensive, pure products with tailored characteristics for the different destination fields [1-2]. Catalysis, coatings, electronics, gas sensing, fuel cells and ceramics are just few meaningful examples of the potential application areas. For instance, carbon black, silica and titania are "historical" flame-made materials. In the last decades an increasing number of more and more sophisticated materials were obtained by flame synthesis.

In this work an investigation on the synthesis of oxides nanoparticles having very interesting applications is presented. TiO_2 from titanium tetraisopropoxide (TTIP), V_2O_5 from Vanadium oxytriethoxide and SiO_2 from Tetraethyl-orthosilicate were produced. The apparatus (see fig.1) consisted of a hybrid burner reactor [3-4] that allowed the injection of precursor vapours generating a diffusion flame in the middle of a premixed lean CH_4/air flame. Lean stoichiometry was adopted to guarantee the oxidizing environment. Powders samples were collected at different heights along the flame in two ways: sucking probe and rapid insertion technique (50 ms residence time). The samples were analyzed by X-Ray diffraction (XRD), Transmission Electron Microscopy (TEM) and Fourier Transform Infrared Spectroscopy (FTIR). Some comparisons between the sampling techniques are reported. Moreover, insights on reaction dynamics were pursued through flame emission spectroscopy in the spectral window from 231 nm to 847 nm. Spectra were recorded at the same height of the sampling locations, with the help of an alignment laser.

Overall results showed titania reaction to follow the expected dynamics, exhibiting a particle size increase and a change towards rutile in crystalline phase percentage along the flame. Vanadium oxides nanoparticles exhibited composite features: crystalline or amorphous, acicular or spherical. Analysis on silica revealed an amorphous structure and a high tendency of the nanoparticles to gather into aggregates. Light emission data of the three different flames showed as a common feature the typical spectral signatures of the post-burnt zone of premixed hydrocarbon-air flames and a signal at long wavelengths attributable to soot radiation. Beside this, data comparison from all flames made evident signatures peculiar to each of them, especially in the UV-blue spectral region from TiO_2 flame. A band in this region is particularly strong and becomes dominant in the higher part of the flame. Provided the similar nature of the precursors ligand, it seems to be reasonable to attribute this spectral behavior to species containing Titanium. Moreover, spectrum from isopropyl alcohol (being TTIP titanium isopropylate) injected in the premixed flame were recorded, and did not show any signature in the blue region, thus supporting the hypothesis. About titania peculiar flame characteristics, more efforts will be spent in the direction of a deeper interpretation. The investigation was carried out using the hybrid burner reactor, which proved to be well suited for reaction dynamics studies. The porous plug premixed flame produced a burnt gases region with smooth variations, and the precursor injection method allowed a stretched reaction flame and a separation of the two feeding systems. Moreover, reaction conditions could be changed by acting on several variables, such as flame composition, precursor concentration, region of injection in the burnt gases, according to the specific aim pursued.

References:

[1] M.S. Wooldridge, Prog. Energy Combust. Sci., **24** (1998) 63.
[2] K. Wegner, S.E. Pratsinis, Powder Technology, **150** (2005) 117.
[3] M.S. Wooldridge, S.A Danczyk., J. Wu, NanoStructured Materials, **11** (1999) 955.
[4] C. Bellomunno, F. Cignoli, S. De Iuliis, S. Maffi, G. Zizak, Proceedings of 29th Meeting of the Italian Section of the Combustion Institute, Pisa, Italy, June, (2006).

Figures:

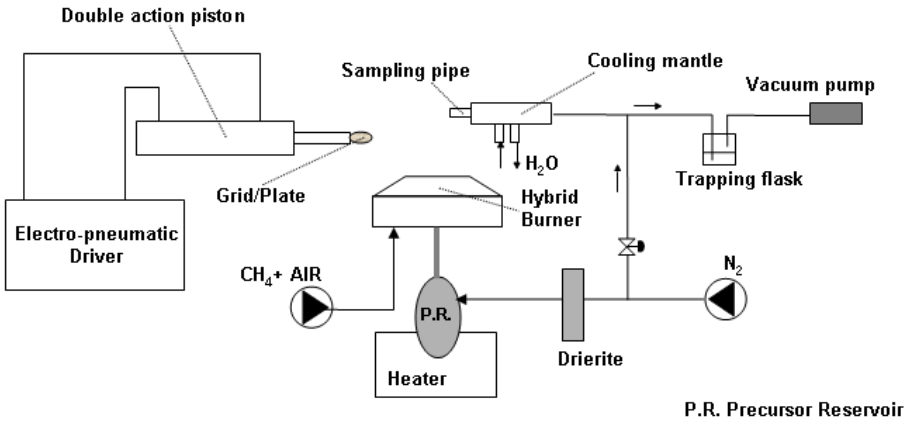
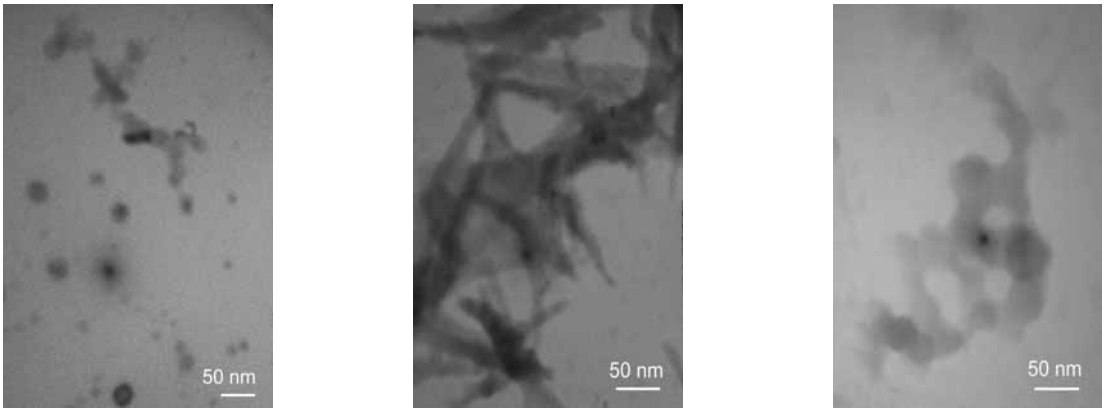


Fig.1 Experimental apparatus for nanopowders production and sampling**.**



TiO_2 **V_2O_5** **SiO_2**

Fig.2 TEM micrographs of nanoparticles synthesized in the hybrid flame reactor.

Mechanical modulation of tunnel junction as an ultra sensitive NEMS

Bogdan Bercu, Laurent Montès, Guillaume Bacles, Jacques Zimmermann, Panagiota Morfouli
Institute of Microelectronics, Electromagnetism and Photonics, UMR 5130 (INPG/UJF/CNRS),
3 parvis Louis Néel, 38016 Grenoble, France
E-mail : bercu@enserg.fr Tel.: +33 (0)4 56 52 94 77

Abstract

In this contribution we present a series of results, obtained by Finite Element Analysis (FEA), concerning a novel type of NEMS: tunnel junctions mounted on thin membranes. The current is modulated via a mechanical stress applied on the barrier material (SiO_2) instead of a modulation of the electrical field. The tunnel junction can be obtained by vertically oxidizing a thin bar of silicon or aluminum, the choice for silicon being made due to the IC compatibility of the technology employed.

A mechanical stress applied to the junction induces changes in the height and length of the barrier, related to the modifications induced by the structure deformation into the semiconductor band structure and to the oxide thickness. A particular way of applying the stress is to mount the structure on a thin silicon membrane, micromachined in a SOI (Silicon On Insulator) wafer [1]. In this case it is not the piezoresistivity that one seeks to implement but the dilation thickness of oxide tunnel because of the exponential dependence of the tunnel current on the oxide thickness. Another important advantage is that one can achieve an applied stress on the structure in the order of GPa without special equipment. Moreover, the tunneling current can be dynamically modulated using the resonance frequencies of the membrane. Maintained in resonance by an external forced oscillation (e.g. by a piezoelectric stack), frequencies in the order of hundreds of MHz can be achieved with a fine tune related to the geometrical dimensions of the membrane. The available technology allows us to micromachine in silicon different types of membrane, from large ones of 3x3mm², 30µm thick, down to thin membranes of 150x150µm², 1µm thick, micromachined on SOI wafers, therefore offering a wide range of membrane deformation (for a specific domain of applied pressure) and of resonance frequencies. For an in-plane stress sufficiently small for that the variation of the band gap in the semiconductor remains small [2], one can investigate the tunnel current modulation related to the oxide thickness variation.

The studied structure geometry (Figure 1a) is sufficiently large in order to avoid, in a first approach, other effects related to the geometry. The thickness considered for the oxide is 3nm (which is achievable by local AFM oxidation) and is sufficiently small for direct tunneling through the barrier. The structure is mounted on a thin membrane (Figure 1b), 1µm thick, which is micro machined in a SOI wafer. The membrane deformation and the corresponding stress distribution (Figure 2a) are simulated as a function of the applied pressure, allowing to determine optimal positioning and dimensions for a maximal response as a function of the membrane type and size [3]. The SiO_2 thickness variation resulting from the membrane deformation (Figure 2b) is used for tunneling current calculations. The relative variation of the tunneling current calculated as a function of the applied pressure is in the order of 5% for 100kPa of applied pressure (Figure 3a), and increases up to 30% for 1MPa of applied pressure. A comparison to existing experimental results have been performed in order to validate the models utilized. The tunneling current modulation through a 2.1nm thick oxide barrier was simulated as a function of the applied field. Figure 3b shows a good agreement with the experimental values.

The results concerning the tunnel current and the equivalent sensitivity to the applied pressure for the simulated structure are very promising and open a novel approach for new NEMS devices with a broad field of application. A first prototype is currently under development.

References

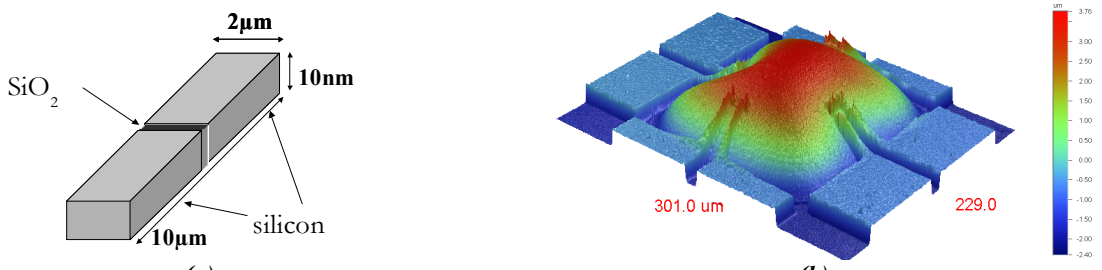
[1] "SOI-Silicon as structural layer for NEMS applications", M. Villarroya, E. Figueras, F. Pérez-Murano, F. Campabadal, J. Esteve, N. Barniol, Proc. SPIE, Vol. 5116 (2003)

[2] "Band structure, deformation potentials, and carrier mobility in strained Si, Ge, and SiGe alloys", M.V. Fischetti, S.E. Laux, Journal of Applied Physics, **80**(4) (1996), pp. 2234-52

[3] B. Bercu, L. Montès, P. Morfouli, Smart Pressure Sensor on SOI optimized by Finite Element Analysis, 2006 NSTI Nanotechnology Conference and Trade Show, May 7-11, 2006, Boston, Massachusetts, U.S.A.

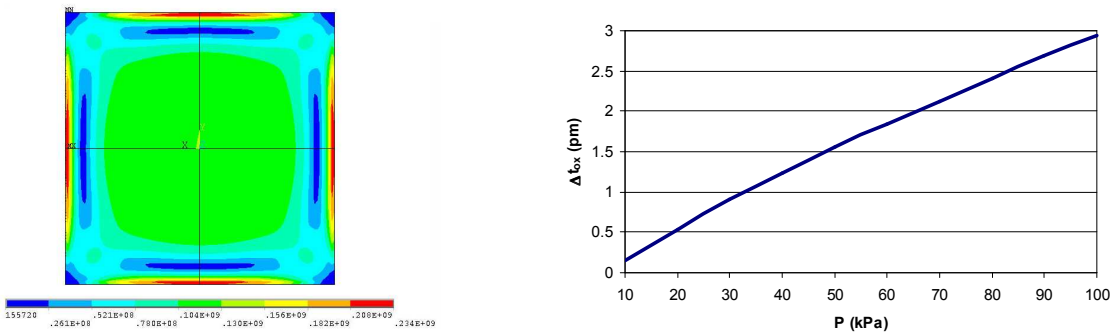
[4] W. K. Chim, P. S. Lim, "Improved model for the stress-induced leakage current in thin silicon dioxide based on conduction-band electron and valence band electron tunneling", J. App. Phys., 91(1), pp. 1577-1588 (2002)

Figures



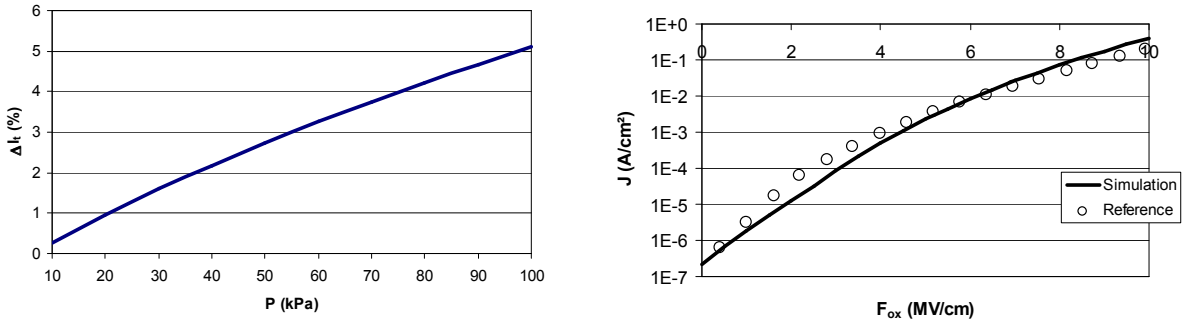
(a) *(b)*

Figure 1(a) *Schematic view of the structure ($Si/SiO_2/Si$) used for simulation;*
(b) *Measurement of a thin silicon membrane deformation (optical profilometer).*



(a) *(b)*

Figure 2 (a) *Stress distribution, calculated for a 1µm thick stressed membrane (P=50kPa);*
(b) *Thickness variation of the oxide as a function of the applied pressure.*



(a) *(b)*

Figure 3 (a) *Tunnel current relative variation as a function of the applied pressure;*
(b) *Simulation results for application on existing experimental data (t_{ox}=2.1nm) [4].*

PHOTOINDUCED PERIODIC NANOSTRUCTURES IN GLASS BY FEMTOSECOND PULSES

M. Bernier, R. Vallée, A. Saliminia, S.Gagnon, Y. Sheng and S.L. Chin
Centre d'optique, photonique et lasers (COPL), Laval University, Quebec, Canada

E-mail: martin.bernier.1@ulaval.ca

The use of ultrashort pulse sources in conjunction with a diffractive element was recently shown as a very promising way to photoinduce permanent periodic nanostructures in glass. Accordingly, high quality and high index modulation structures were written in silica both with UV [1] and IR [2-3] femtosecond (fs) sources. The fs-induced structure can be made very stable at elevated temperatures –where standard UV-written index change would erase. Still, important issues related to the underlying physical process responsible for the fs-induced FBG formation remain unanswered. One of these issues is the role that nonlinear processes such as multi-photon absorption and filamentation are playing in the context of the focusing of a Gaussian beam by a cylindrical lens through a diffractive element. In this presentation, we report the formation of high aspect-ratio nanostructures in silica by the use of the interference of femtosecond pulses in optical fibers. The photoinduced periodic nanostructures are typically less than 250nm width, 800nm height and 50um length formed in a periodic grating over many millimeters long as shown in figure 1.

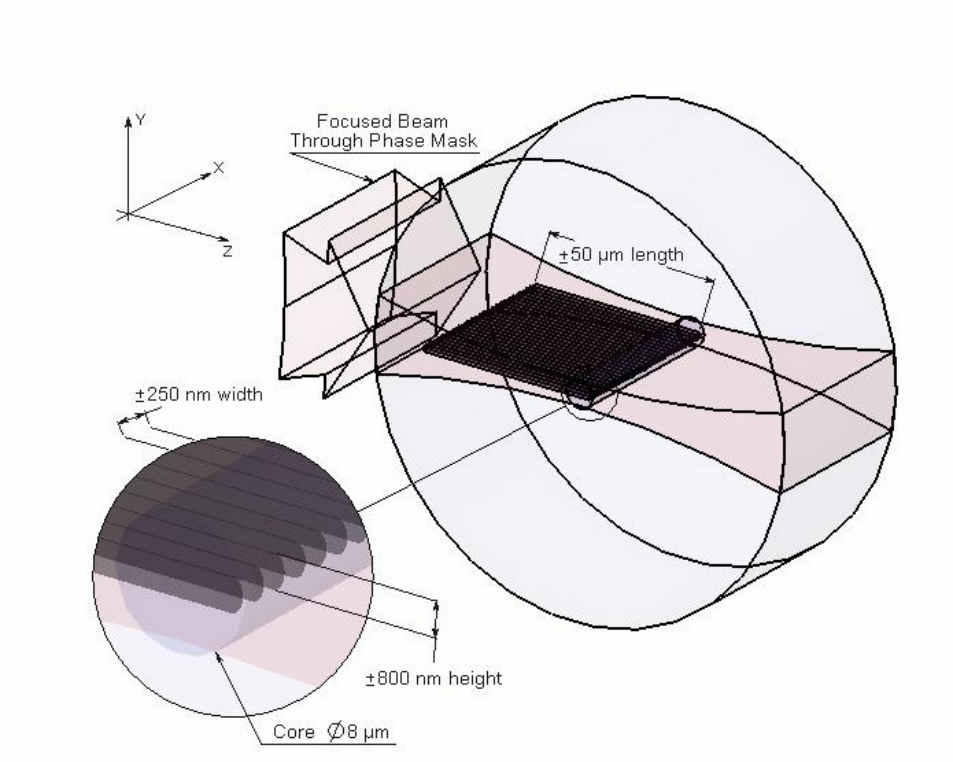


Figure 1: Scheme of the writing conditions and resulting photoinduced nanostructures

We further demonstrate via a high resolution measurement across the transverse plane of the fiber, that the refractive index change is bearing the signature of the filamentation of the femtosecond pulses crossing the fiber as shown in figure 2. We also demonstrate that filamentation process limit the height of the structure to wavelength by high-order solitonic compression and can be tunable from wavelength to many tenth of microns by scanning the beam over the fiber. This phenomenon permit to decrease the nanostructure height to ~300nm and also the structure width to ~75nm by the use of UV femtosecond laser at 266nm. Figure 2 is showing the refractive index profile of the SMF-28 fiber before(left) and after(right) inscription in H_2-free fiber during 60s at 1.4mJ/pulse. One can clearly observe the trace (filament) left by the passage of the fs-pulse across the core and also give a measurement of the nanostructure height to ~800nm FWHM.

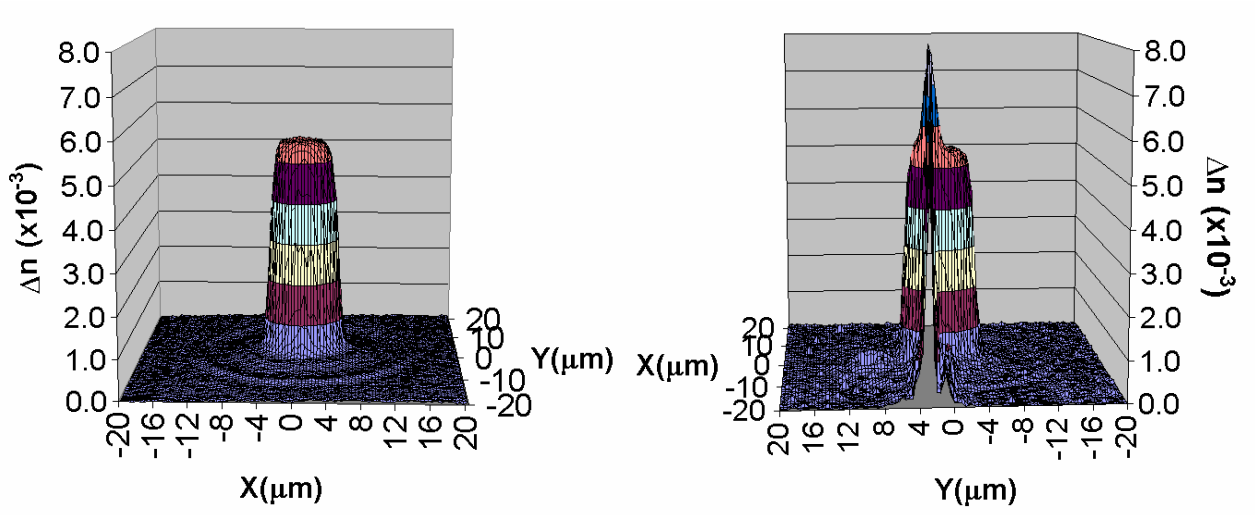


Figure 2: Refractive index profile before(left) and after(right) inscription.

References:

[1] A. Dragomir, D.N. Nikogosyan, K.A. Zagorulko, P.G. Kryukov, E.M. Dianov, "Inscription of fiber Bragg gratings by ultraviolet femtosecond radiation," Opt. Lett. **28**, 2171-2173 (2003).

[2] C.W. Smelser, S.J. Mihailov, D. Grobnic, P. Lu, R.B. Walker, H. Ding, X. Dai, "Multiple-beam interference patterns in optical fiber generated with ultrafast pulses and a phase mask" Opt. Lett. **29**, 1458-1461 (2004).

[3] S.J. Mihailov, C.W. Smelser, D. Grobnic, R.B. Walker, P. Lu, H. Ding, J. Unruh, "Bragg gratings written in All-SiO_2 and Ge-doped core fibers with 800 nm femtosecond radiation and a phase mask", J. Lightwave Technol. **22**, 94-100 (2004).

POLY(3-HEXYLTHIOPHENE) FIBRES FOR PHOTOVOLTAIC APPLICATIONS

Solenn Berson[a], *Rémi De Bettignies*[b], *Stéphane Guillerez*[b]

[a] *CEA –DRFMC/SPrAM/LEMOH, Structures et Propriétés d'Architectures Moléculaires – UMR5819, 17 rue des martyrs 38054 Grenoble cedex 09*
[b] *CEA – DRT/LITEN/DTS/LCS, INES – RDI, Laboratoire des Composants Solaires, 50 avenue du Lac Léman BP 332, 73377 Le Bourget du Lac, France*

stephane.guillerez@cea.fr

We present here a new polymeric composition with photovoltaic properties, its elaboration process and its performance in photovoltaic cells.
Recently, Yang and al. [1] have shown that the molecular order of the active layer of a solar cell, formed by an interpenetrated network of Poly(3-hexylthiophene) (P3HT) as donor material and [6,6]-phenyl C61 butyric acid methyl ester (PCBM) as acceptor is dependant to the process conditions (pristine/annealed film). The annealing of the active layer permits to control the morphology and the organization of the polymeric chains and the formation of fibrillar structures of P3HT leading to high performances.
More recently, Reyes-Reyes and al. [2] obtained 5.2% of Power Conversion Efficiency (PCE) by annealing the photovoltaic cell composed of P3HT/PCBM active layer.
However, the annealing process may be not compatible with the use of flexible substrates and alternative processing procedures leading to the required nanomorphology without thermal treatment may constitute a real step for the development of efficient and flexible solar cells.

In the work presented here, the fibrillar structures of P3HT have been obtained in solution and deposited on glass substrate or silicon (Figure 1). It was possible to separate the fibres from the well-dissolved polymeric chains and then to control the ratio of each material in new solutions.

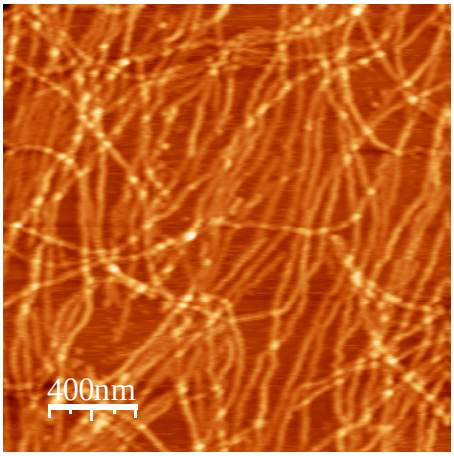


Figure 1: Atomic Force Microscopy image (tapping mode) of P3HT fibres deposited on silicon.

The effect on charge transport of the fibrillar P3HT percentage in a film was studied and showed a dependance. Photovoltaic performances obtained without annealing, with a fibrillar

P3HT/PCBM blend and with a controlled percentage of P3HT fibres in the active layer are also presented. Best cells reach a PCE of 3.59% without annealing under AM 1.5, 100 mW.cm^{-2} conditions (Figure 2) [3].

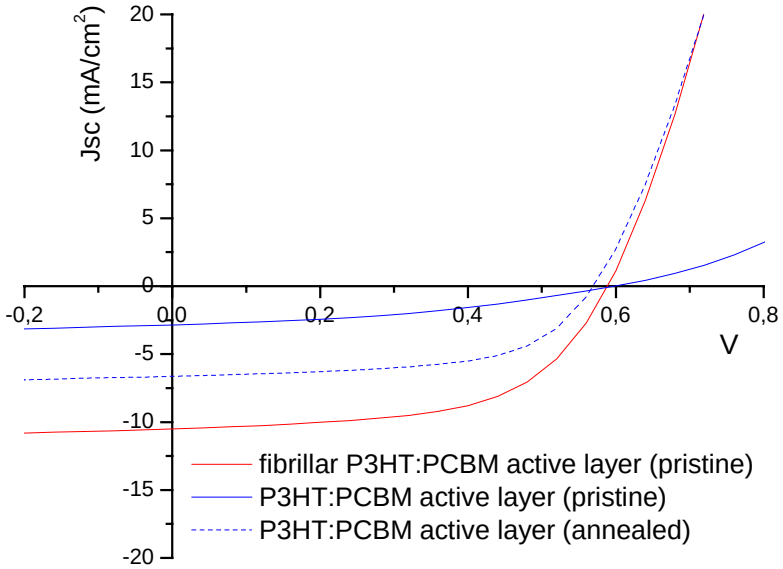


Figure 2: Current-voltage (J-V) curves of different composition of the active layer in the photovoltaic cell measured under AM 1.5 conditions.

References:

[1] X. Yang and al., Nanoletters, **5** (2005) 579
[2] M. Reyes-Reyes and al., Organic letters, **7** (2005) 5749
[3] S. Guillerez, S. Berson, R. De Bettignies, M. Firon, deposited patent

AB INITIO STUDY OF HIGH PERMITTIVITY HF OXIDES FOR CMOS NANOELECTRONIC

Pierre-Yves Prodhomme, Philippe Blaise, Jacky Even[*]*, Chris Hobbs*[**]
CEA/DRT/LETI/D2NT/LSCDP, 17 rue des Martyrs, 38054 Grenoble, France
[*]*INSA Rennes, France*
[**]*Freescale Crolles II, France*
pierre-yves.prodhomme@cea.fr

In the downscaling context, the MOS transistor dimensions shrink regularly. In order to follow the ITRS road map, the gate oxide has to be replaced (to avoid leakage current) by a new material with a high permittivity called « high-k » material (in order to thicken oxide keeping the property of the capacity). During the last few years the new material which has shown the most interesting properties is the hafnium dioxide (HfO_2). However the use of this new MOS stack involves new challenges, namely concerning the comprehension of its electronics properties. The scale of the devices being of the order of a nanometer, it becomes interesting and necessary to study this new stack with an atomistic approach using ab initio methods. The ab initio methods we are using rely on the density functional theory (DFT[1,2]). Mainly, the abinit program www.abinit.org has been employed.

Firstly our study purpose has been to reproduce the material structure existing in a MOS stack. Several publications [4,5] have shown the cubic, the tetrahedral and the monoclinic structure for HfO_2 bulk material. But, experimentally, the phase caught in a thin MOS stack is polycrystalline including the monoclinic and orthorhombic phases. So, we tried and succeed to obtain those 2 phases separately, by DFT/LDA energy minimization techniques.

Besides, we have already obtained the band structure of monoclinic HfO2, with DFT density functional theory and then we corrected it with the GW approximation [3] in order to get a band gap in good agreement with experiment. The value of the GW corrected band gap we obtained is 7.1 eV. This is in good agreement with a band gap of 6.7 eV, recently obtained by a mixed computational (DFT) and experimental approach [7]. (Let's recall that the GW approximation take into account electrons interactions within a perturbative many body approach which is not possible simply using DFT).

Following that, we will soon obtain the band structure of metal gate and then we will be able to simulate the whole structure of a nanometric MOS stack, in order to study the band alignment between a chosen metal and a highK material and the associated effective work function, which is critical for the future nanoelectronic devices.

References:

[1] P.Hohenberg & W. Kohn, Phys. Rev. **136** (1964), B864
[2] W. Kohn & L.J. Sham, Phys. Rev., **140** (1965), A1133.
[3] L. Hedin & S. Lundquist, Solid State Physics, **23** (1969) p.1.
[4] X. Zhao & D. Vanderbilt, Phys. Rev. B, **65** (2002) 233106.
[5] A. A. Demkov, Phys. Stat. Sol., **226** (2001) 57.
[6] A. Kokalj, Comp. Mat. Sci., **28** (2003) 155.
[7] S. Sayan & al., J. Appl. Phys., **96** (2004) 7485.

Figures:

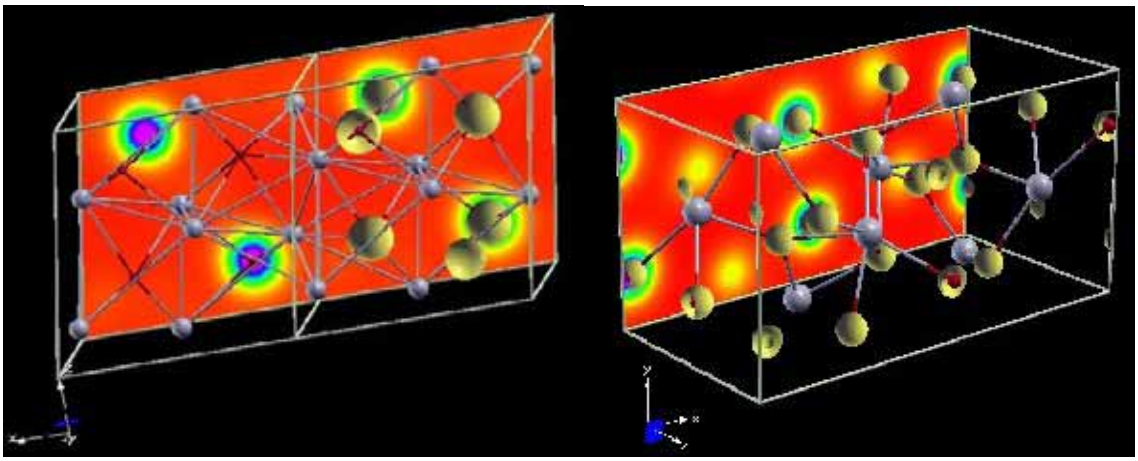


Fig. 1: HfO_2 monoclinic and orthorhombic phases, showing electronic contours (XCrysden [6]).

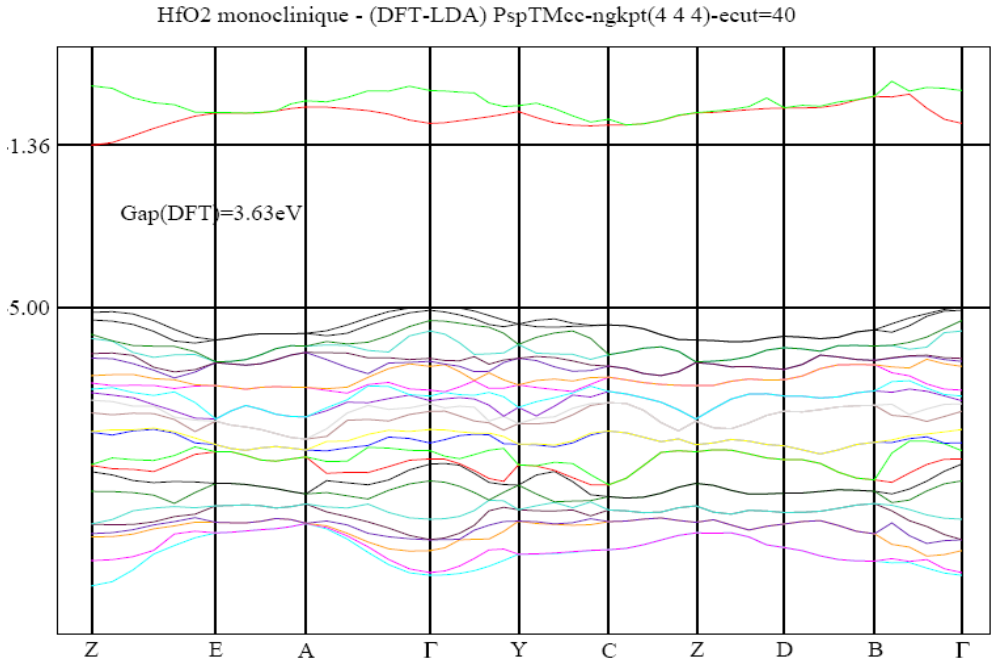


Fig. 2: HfO_2 monoclinic DFT band structure with a 3.63 eV indirect band gap ; the GW corrected band gap value for the same phase value is 7.1 eV.

WAFER SCALE CNT TIP GRAFTING GROWTH PROCESS BY HOT FILAMENT ASSISTED CVD

A. S. Rollier[1], A. M. Bonnot[2], C. Bernard[3], A. Iaia[2], D. Mariolle[4], L. Buchaillot[1], J. P. Aimé[3]

[1]IEMN/CNRS, 59652 Villeneuve d'Ascq Cedex, France
[2]LEPES/CNRS, 38042 Grenoble Cedex 9, France
[3]CPMOH/CNRS, 33405 Talence, France
[4]CEA-DRT-LETI, 38042 Grenoble Cedex 9, France

E-mail : bonnot@grenoble.cnrs.fr

Because of their high aspect ratio and small diameter, CNTs are very attractive tips for Scanning Probe Microscopy (SPM). Interest in CNT tip is also reinforced by the CNT high stiffness and high strength and by the inertness of carbon, which prevent from chemical probe surface modification. CNT tips could become standard probes, if one succeeds in the finalisation of a batch process.

In this aim, we have set up a self assembled procedure which leads to the growth of SWNTs or DWNTs at the apex of commercial Si probes [1]. These tips will be denoted as CNT tips.

Our self assembled technique involves two stages. A thin layer of Co is evaporated on the whole substrate and then, CNTs are deposited by HFCVD.

Investigation of our CNT tip mechanical properties [2] has demonstrated the interest of the fabrication technique. The CNTs appeared to be firmly stuck on the Si tip and so long as their length does not exceed 1 µm, the main parameter governing their mechanical response is the contact between the free CNT end and the surface.

By the way, our self assembled CNT tips have unique potentiality for SPM applications. However, the process needs still to be improved, in particular concerning the grafting probability is of only 20 % and the control of the CNT length.

In that spirit, fields of Si tips with different shapes have been fabricated. Optimisation of the process has allowed us to increase the grafting probability up to 40-60 % and to limit the length of the CNT tip in the 100-500 nm range (fig. 1).

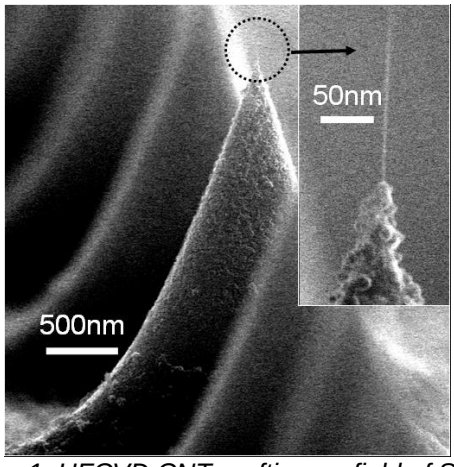


Figure 1: HFCVD CNT grafting on field of Si tips

[1] L. Marty at al. *Thin Sol. Films* 501 (2006) 299
[2] D. Dietzel at al. *Nanotech.* **16** (2005) S73

Optoelectronic switch and memory devices based on polymer functionalized carbon nanotube transistors

Julien Borghetti[1], Vincent Derycke[1], Stephane Lenfant[2], Pascale Chenevier[1], Arianna Filoramo[1], Marcelo Goffman[1], Dominique Vuillaume[2] and Jean-Philippe Bourgoin[1]

[1]**Lab. Elec. Mol., CEA-Saclay Service de Physique de l'Etat Condens, 91191 Gif-sur-Yvette, France**
[2]**IEMN, Avenue Poincare, 59652 Villeneuve d'Ascq, France**

Associating carbon nanotubes with conjugated polymers or molecules has been recently recognized as an efficient way to improve performances of organic electronic devices and to achieve new functionality, in particular for optoelectronic applications. This approach maintains the main advantages of organic electronics for low cost, flexible and/or transparent applications. A particularly interesting example of such a nanotube/polymer combination consists of a carbon nanotube field effect transistor coated with a polymer thin film (1; 2). Indeed, such a device can ideally combine the very high carrier mobility of carbon nanotubes (100000 $cm^2/V.s$) with the excellent optical properties of polymers (or molecules in general). Carbon nanotube transistors can, by themselves, emit or detect photons at wavelengths defined by the nanotube chirality. But, to extend their capabilities in optoelectronics, it is important to be able to tune these wavelengths independently of the nanotube structure. Functionalizing the nanotube with a polymer is an efficient way to achieve such a goal. In the present study (2), we demonstrate that drastic photo-induced modifications of the electrical characteristics of self-assembled (3) nanotube transistors functionalized by photo-conductive polymers can be achieved.

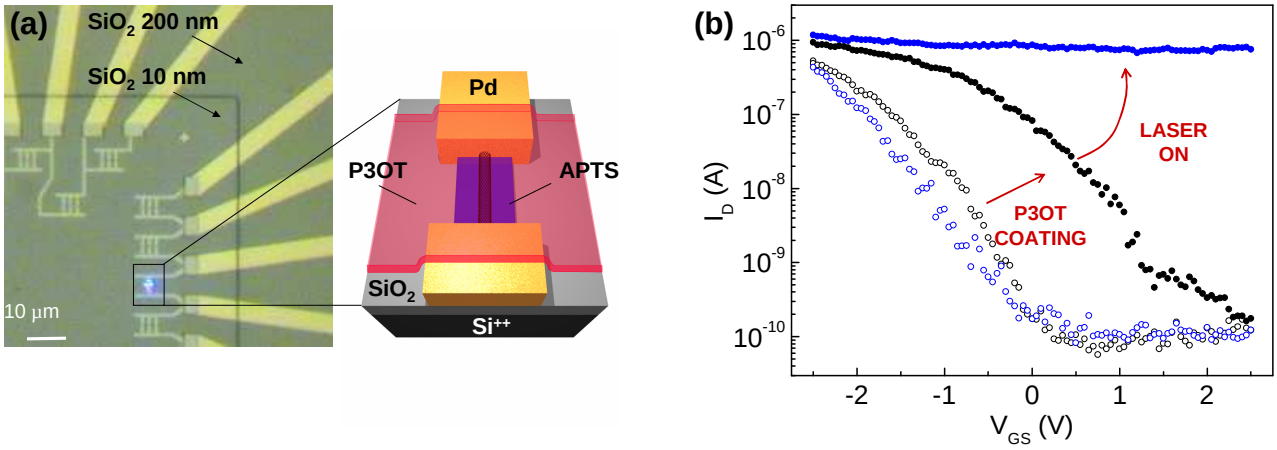


Figure 1 Self assembled CNTFETs and their response to the polymer photoexcitation. (a) Optical microscope picture of the sample showing a series of self-assembled CNTFETs and the blue laser spot focused on an individual transistor. Right: scheme of the CNTFET showing a single nanotube connected by Pd electrodes separated by $\sim$ 100 nm and coated by the P3OT film. (b) Transfer characteristics $I_D(V_{GS})$ at V_{DS}= -400 mV of an 'as-made' CNTFET in the dark (open black circles) and upon illumination (steady state, λ = 457 nm, P= 60 μW, spot size $\sim$2 μm) (open blue circles) and of the same transistor coated with P3OT ($\sim$ 5 nm thick film) in the dark (filled black circles) and upon illumination (filled blue circles).

The figure 1 shows that the polymer film acts as a wavelength dependent 'optical gate', which is significantly more efficient than a conventional electrostatic gate. The process impacts both the on- and the off-states of the transistor with a maximum change of conductance reaching four orders of magnitude between the dark and illuminated states. Depending on the applied biases and polymer characteristics the device can be optimized

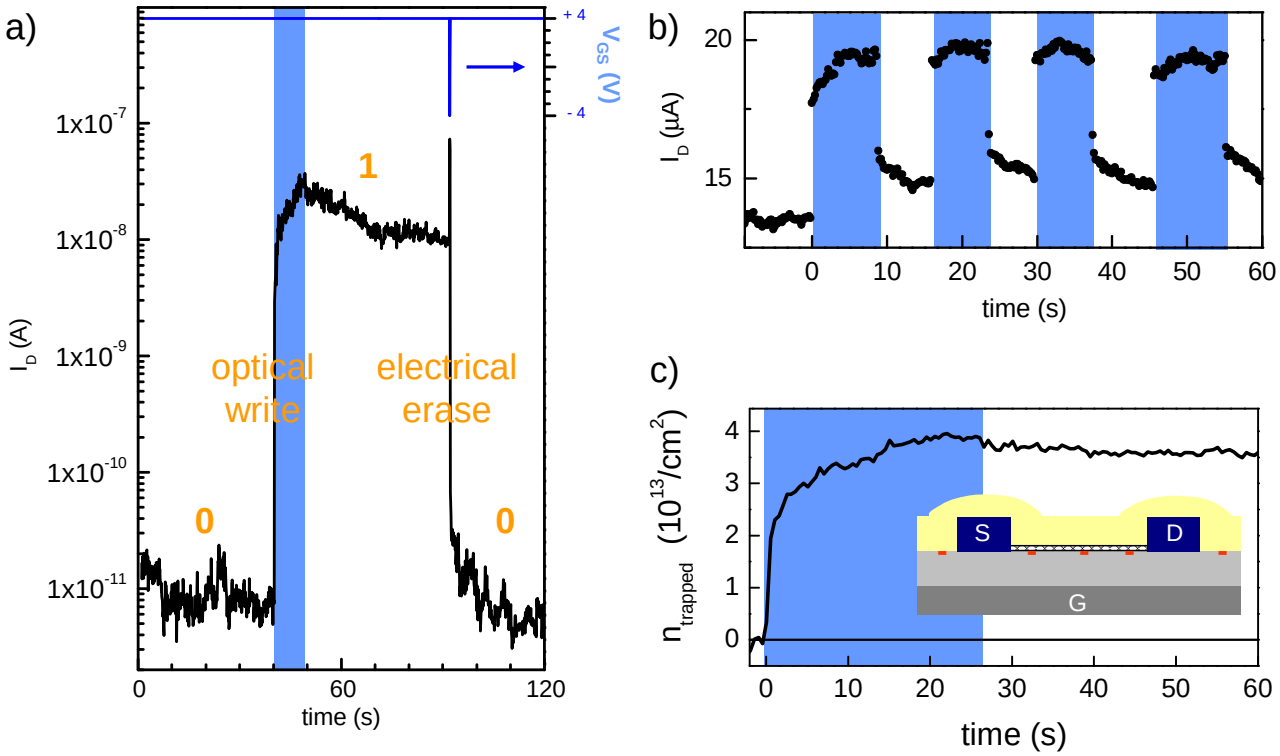


Figure 2 Optical memory and switch based on the OG-CNTFET (a) $I_D(t)$ response at V_{GS}= +4 V of an OG-CNTFET to a light pulse at $\lambda = 457$ nm (laser on in the blue shaded area). The current magnitude difference before and after illumination allows memory applications. The memory erase action is also shown. After the light pulse has been applied, a short (100 ms) negative V_{GS} pulse at -4 V is used to bring the device back to its initial state. (b) $I_D(t)$ response at V_{GS}= -3 V of a device composed of multiple nanotubes to a light pulse at $\lambda = 457$ nm. The negative gate bias allows rapid optically driven modulation of the current. (c) Evaluation of the trapped electrons density $n_{trapped}$ obtained by comparing the $I_D(t)$ response at V_{GS}= +4 V with the transfer characteristic $I_D(V_{GS})$ in the dark. An I_D increase of 3 orders of magnitude for $V_{GS} = +4$ V is equivalent to a negative gate shift of -5 V, created by 4.10^{14} charges/cm^2 ($Q = C_{ox}V_{GS}$) at the Si++/SiO_2 interface. Because the APTS layer is $\sim$ 1 nm thick (SiO_2 is 10nm thick), the same effective equivalent potential on the nanotube is created by $\sim 4.10^{13}$ charges/cm^2. The inset shows those interfacial traps (red dashes).

as a memory element (Fig 2a) or as an optical switch (Fig 2b). On the basis of a set of experiments performed with either CNTFETs or P3OT thin film transistors (TFT), we propose a mechanism based on the trapping of photo-generated electrons at the nanotube-gate dielectric interface. The results are consistent with the generally observed p-type conduction in organic TFTs (4). Thanks to its very high charge sensitivity, the nanotube transistor proves a good tool to study the spatial distribution and relaxation rate of trapped carriers in organic thin films transistors (Fig 2c). In particular, the non exponential type of decay of the persistent photo-conductivity in TFTs can be studied with improved sensitivity using a nanotube transistor as charge sensor.

References

[1] Star, A., Lu, Y., Bradley, K., and Gruner, G. *Nano Lett.* **4**, 1587–1591 (2004).
[2] Borghetti, J. *et al. Submitted to Adv. Mater.* (2006).
[3] Choi, K., Bourgoin, J., Auvray, S., Esteve, D., Duesberg, G., Roth, S., and Burghard, M. *Surf. Sci.* **462**, 195 (2000).
[4] Chua, L. L., Zaumseil, J., Chang, J. F., Ou, E. C. W., Ho, P. K. H., Sirringhaus, H., and Friend, R. H. *Nature* **434**, 194–199 (2005).

SECOND HARMONIC GENERATION AND IMAGING OF FUNCTIONALIZED CRYSTALLINE NANOAGGREGATES

Jonathan Brewer[1], *M. Schiek*[2], *A. Luetzen*[2], *K.Al-Shamery*[2] and *H.-G. Rubahn*[1]
1: Department of Physics and Chemistry and Mads Clausen Institute
University of Southern Denmark
DK- 5230 Odense M, Denmark
2: University of Oldenburg, Physical Chemistry I
D-26129 Oldenburg, Germany
Brewer@fysik.sdu.dk

Para-hexaphenylene (p6P) and methyloxylated quaterphenylene (MOP4) molecules form well-aligned, needle-like and blue light emitting aggregates (nanofibers) on mica substrates with interesting optical properties (1;2;3). Experiments have shown that these nanofibers have a high potential for applications in submicron-scaled photonics and electronics due to their extraordinary optical, morphological and also electrical properties.

One important application of organic nanoaggregates would be an implementation as frequency doubling elements in future integrated optical circuits. The possibility to functionalize para-phenylenes with electron push and pull groups and to obtain nanofibers from asymmetrically functionalized para-phenylenes should open a new route to nanoscaled frequency doublers.

In this work functionalized phenylene nanoneedles made from amino-methyloxylated quaterphenylenes (MOP4NH2) are grown on mica and are transferred onto SiO substrates for optical examination. When excited with femtosecond laser pulses the fibers are found to have a large non linear optical response and they exhibit pronounced second harmonic generation (SHG). In contrast, nanoneedles generated from non-functionalized phenylenes show SHG orders of magnitude weaker (Fig.1). The intensity of the SHG is investigated for single fibers as a function of excitation wavelength and excitation intensity. It is also shown using a laser scanning microscope that it is possible to image the fibers using second harmonic generation (Fig.2). This proofs that SHG imaging is an interesting, label-free new method which can be used as a complement to traditional fluorescence laser scanning microscopy.

Acknowledgments:

We are indebted to L.Bagatolli for support with the confocal microscope. We thank the Danish research agencies FTP and SNF for financial support. JB thanks the graduate school of molecular biophysics for a stipend.

References:

[1] F.Balzer and H.-G. Rubahn, Growth control and optics of organic nanoaggregates. Adv.Funct.Mat., **15**:17 -- 24, 2005.
[2]M.Schiek, A. Luetzen, R. Koch, K. Al-Shamery, F. Balzer, R. Frese and H.-G. Rubahn, Nanofibers from functionalized para-phenylene molecules. App.Phys.Lett. **86** : 153107, 2005.
[3] J. Brewer, C. Maibohm, L. Jozefowski, L. Bagatolli and H.-G. Rubahn A 3D view on free-floating, space-fixed and surface-bound para-phenylene nanofibres. Nanotechnology, **16**:2396 -- 2401, 2005.

Figures:

Fig.1: Measured Second harmonic (red curves) and two-photon luminescence (blue curve) intensity from MOP4NH2, MOP4Cl and p6P nanofibers, transferred to SiO surfaces. Excitation at 790 nm with 100 fs and 4.5 mW.

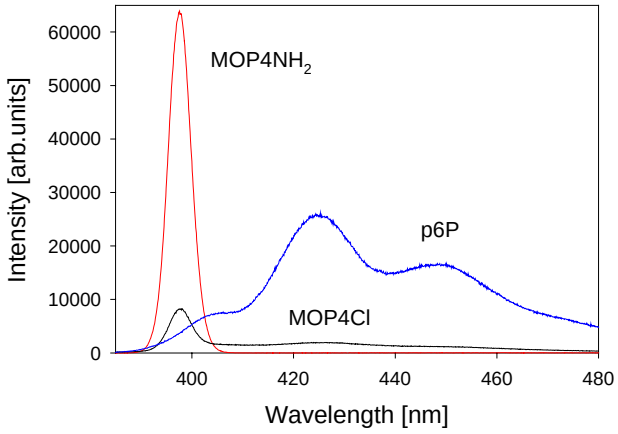
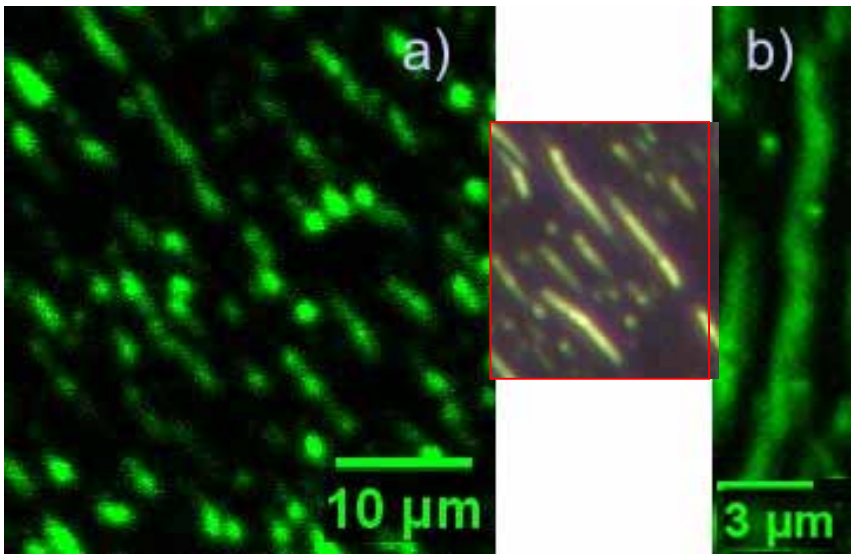


Fig.2: Two-dimensional imaging of MOP4NH2 nanofibers, using a femtosecond confocal microscope. The inset shows a dark field image of the same fibers.



Poster

TUNING FORK BASED NANO-TOOLBOX FOR MOLECULAR AND ORGANIC ELECTRONIC

M. Brun[1], I. Duszynski[1], S. Decossas[2], F. Triozon[1], Y. Luo[3], P. Rannou[3], and B. Grévin[3]

[1]CEA/DRT/LETI, 17 Rue des Martyrs 38054 Grenoble cedex 09, France, [2]*LTM/CNRS, CEA/LETI/DTS, 17 rue des Martyrs, 38054 Grenoble Cedex 09, France,* [3] *LEMOH, UMR5819-SPrAM (CEA-CNRS-Univ.Grenoble I), DRFMC CEA-Grenoble, 17 rue des Martyrs 38054 Grenoble Cedex09, France*

mickael.brun@cea.fr

The development of a new electronics based on nanoscale building blocks in the bottom up approach needs new techniques for visualising, probing and connecting the building blocks at the nanometre scale. This is especially true for organic and molecular materials which are, most of time, incompatible with standard lithography and deposition techniques. In this purpose, scanning probe microscopies already allow characterizing at the atomic scale the topological arrangement of these building blocks, and thus, open the way for probing and controlling the assembling process of the future architectures. In addition, the spectroscopic capabilities associated with both STM or AFM allow probing the electronic or mechanical properties at the atomic scale. Single molecules properties can be investigated without any wiring technology, to reveal the intrinsic behaviour of these molecular building blocs.

However, an important problem which remains to be resolved is the electrical connectivity between individual electro-active molecules and the macro-world. Without solving it, no further progress in the molecular electronics can be achieved and the great integration potentiality of the molecular materials can be lost. This step is then considered as a crucial milestone towards operational molecular devices. In return, solving it will allow fundamental studies. This is especially important for understanding the connexion behaviour at this length scale where the contact interface plays a dominant role in the whole device characteristic. In this purpose, one can expect to develop a nanometric toolbox for the manipulation and connection of functional molecules.

In this presentation, the developments of such a toolbox based on quartz tuning forks will be presented. We will first demonstrate that frequency-modulated atomic force microscopy with these rigid cantilever can be used to image the microphase separation of soft materials, i.e., a polystyrene/poly(methylmethacrylate) block copolymer [1]. Two-dimensional force spectroscopy images revealing a clear contrast originating from local variations in the mechanical properties of the two microsegregated phases will be presented. The force versus tip-sample distance dependence extracted from the frequency shift data will be discussed in the frame of the contact forces theories.

These results illustrate the possibility to use quartz tuning forks for imaging and probe soft material. Then we will discuss how it can be used for “driving” dynamic nanostencils with integrated AFM tip for both the imaging and wiring single organic nano-objects. Some preliminary results on the dynamic nanostencils realisation by conventional microelectronic routes will be shown. They are based on the standard Si_3N_4 suspended membrane with an integrated AFM tip and nanostencil holes realized by focused ion beam deposition and

milling. The possibility to drive this functionalised chip in close proximity of the nano-objects with tuning forks will be discussed.

References:

[1] M. Brun, S. Decossas, F. Triozon, P. Rannou, and B. Grévin , Applied Physics Letters, **87** (2005) 133101.

Figures:

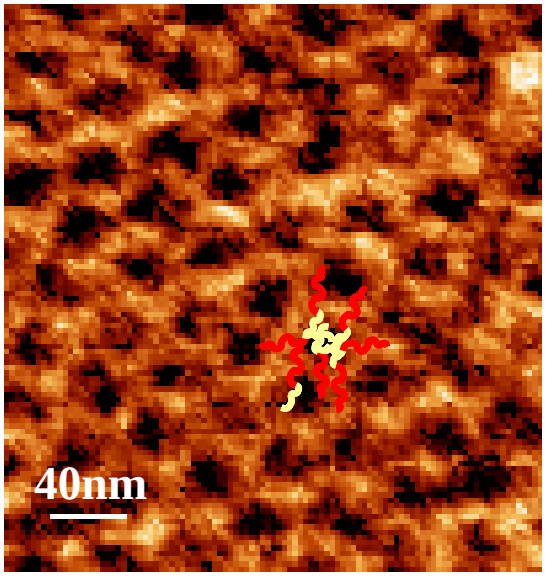


Fig 1. TF-AFM dissipation image (HV, 300K) of a PS:PMMA copolymer. The red and yellow sketch illustrates copolymer chain segregation.

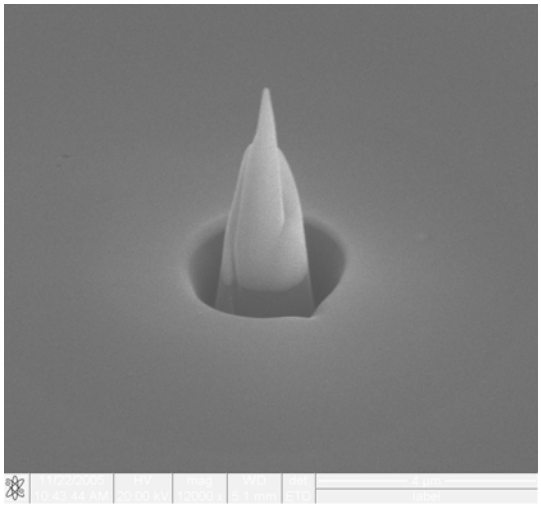


Fig 2. AFM tip grown on Si_3N_4/Si substrate and subsequently shaped by focused ion beam.

Poster

MAGNETIC PROPERTIES OF SCREEN-PRINTED $(Y_{0.5}Sm_{0.5})Co_5$ MAGNET ARRAYS

D. Bueno-Baques, L. Maldonado,J. L. Hidalgo-Gonzalez, V. Corral-Flores and J. A. Matutes-Aquino
Centro de Investigacion en Materiales Avanzados, S.C. Miguel de Cervantes 120, Complejo Industrial Chihuahua, Chihuahua, Chih. 31109, Mexico
dbueno@mailaps.org

Screen printing is a modern materials deposition technique, widely applied in high-volume industrial applications and more recently for a patterned magnet deposition in MEMs devices [1]. Despite of the well adaptivity of this technique to MEMs microfabrication process, the magnetic properties of the resulting bonded printed magnets are, in general, inferior compared to the bulk sintered magnets. In this work, a study of the magnetic properties of magnet arrays based on $(Y_{0.5}Sm_{0.5})Co_5$ nanoparticles prepared on Si substrates by screen-printing method is presented.

$(Y_{0.5}Sm_{0.5})Co_5$ nanoparticles were obtained by mechanical milling starting from arc melted ingots and heat treated in Ar atmosphere. High magnetic properties, with a saturation magnetization M_s = 92.3 emu/g, remanent magnetization M_r = 63.3 emu/g and coercive field iH_c = 26 kOe were observed.

A well controlled paste like ink prepared with the nanoparticles and a mixture of organic solvent and polymer was used to print three different pattern arrays of square μdots of 200 μm, predefined in a polyester screen mesh with an opening of w = 150 μm and a thread diameter of d = 60 μm. After drying, well defined patterns with good adherence to the substrate were obtained. Patterns were cut in samples of 3 by 3 mm.

The microstructure of the samples was studied by optic and scanning electron microscopy (SEM). An isotropic homogeneous distribution of the nanoparticles inside the μdots was bserved. The final shape of the μdots in the array was found to be highly dependent on the squeeze pressure and speed over the mesh. Magnetic properties were studied by pulsed field magnetometry and VSM at room temperature. Samples showed lower saturation magnetization and a slightly increase in the coercive field. The influence of the polymeric matrix, size and distribution of nanoparticles in the arrays on the magnetic properties is discussed in detail.

A micromagnetic simulation of the magnetic behavior of the arrays were carried out with the MagPar software suite [2]. Pattern arrays with different separations between the bonded nanoparticles, as well as particle size and distributions were considered. Results of the simulations are presented and discussed.

References

[1] Orphee Cugat, Jerome Delamare, and Gilbert Reyne, IEEE Trans. Magn. **39** 5 (2003) 3607
[2] W. Scholz, J. Fidler, T. Schrefl, D. Suess, R. Dittrich, H. Forster and V. Tsiantos, Comp. Mat. Sci. **28** (2003) 366

Poster

THE ROLE OF THE MESOPOROUS SILICA STRUCTURE ON THE NANODESIGN OF TITANIA/SILICA PHOTOCATALYSTS

A.M. Busuioc[1,2*], M. Mertens[3], P. Cool[1], N. Bilba[2] and E.F. Vansant[1]

[1] *Laboratory of Adsorption and Catalysis, University of Antwerp, Universiteitsplein 1, B-2610, Wilrijk, Belgium*
[2] *Laboratory of Materials Chemistry,"Al.I. Cuza" University of Iasi, B-dul Carol 11, 700506, Iasi, Romania*
[3] *VITO – Flamish Institute for Technological Research, Boeretang 200, B-2400, Mol, Belgium*
*alina.busuioc@ua.ac.be

The world now faces tremendous challenge in various environmental problems. As a result, extensive research is done on advanced methods for elimination of hazardous chemical compounds from air and water. Photocatalytic oxidation of organic compounds in water and air has received much attention as a potential technology for pollution abatement. Titania has proved to be the most active photocatalytic semiconductor because it allows complete degradation of pollutants under ultraviolet irradiation [1-3]. To improve TiO_2 photoactivity, particles should be small enough to offer a high number of active centres by unit mass. Unfortunately, a small particle size leads to high filtration costs to remove the catalyst, hindering its industrial application. For this reason, a major focus of current photocatalysis research is the achievement of titania-based materials with suitable properties to present simultaneously high photoactivity and effective separation properties. Titania nanoparticles supported on silica might be materials capable of accomplishing both requests since they do not only take the advantage of high surface areas but of improved recovery properties as compared to pure titania, which may facilitate the separation.

In this work, we report the synthesis and photocatalytic behaviour of TiO_2/SiO_2 materials prepared by acid catalysed sol-gel method. As silica support, we have used hexagonally packed MCM-41 and SBA-15 mesostructures. Titania sol was obtained by controlled hydrolysis of titanium isopropoxide in nitric acid. The main objective of this work was to study the effect of the support's structure on the growth and properties of titania nanoparticles. The obtained materials were characterized by X-ray diffraction (XRD), N_2-sorption measurements, chemical analysis, Raman, UV-Vis diffuse reflectance spectroscopy. Based on the combined data from the structural characterization and chemical analysis, a mechanism for the growth of TiO_2 nanocrystals within the channels of MCM-41 and SBA-15 is proposed. In figure 1, the growth and localisation of the titania nanoparticles governed by mesoporous structure of the silica supports is presented schematically.

Throughout this study it is shown that the mesoporous structure of the support influences significantly the growth of titania nanoparticles. Moreover, deposition of different amounts TiO_2 leads to important modifications of the silica support structural characteristics and properties. This has a great impact on the overall adsorption capacity and photocatalytic activity of the TiO_2/SiO_2 catalyst towards the removal of organic dyes in aqueous solutions. The photodecomposition of rhodamine 6G (R6G) in aqueous medium was selected as probe reaction to test the photoactivity of the prepared materials and to verify the potential use of these materials for wastewater treatment. In table 1 are summarized the properties and photocatalytic performances of titania/silica prepared catalysts in R6G photo-oxidation process. For a better understanding of the tremendous role that the silica mesostructure plays on the nansostructuring and photocatalytic behaviour of titania, in table 1are presented the catalytic performances of the pure TiO_2 prepared by ACSG-method. Prior to irradiation, the suspension was magnetically stirred for 30 minutes in order to establish the adsorption – desorption equilibrium between the catalyst surface and the dye. During this time, the dye could not be decomposed, because anatase needs UV-light for its catalytic activity. Because of the absence of UV-light, the decrease of the R6G concentration is due to the

adsorption of the dye on the surface of the catalyst (*adsorbed dye*). At time 0, the solution was irradiated with UV-light and during 1h the photocatalytic decomposition of R6G was followed (*degradated dye*). As it can be seen from table 1, all supported catalysts show lower catalytic activities than P25 in this reaction. However, important differences are obtained, depending on the titania loading, titania nanoparticles size and on the location of these nanoparticles within the mesopores of the support. The catalysts prepared using MCM-41 as support show higher adsorption capacity towards bulky molecules of R6G, due to the fact that the mesopores are not blocked by titania nanoparticles. In contrast, the channels of SBA-15 are choked by titania nanoparticles, limiting the access of R6G molecules inside the pores. Moreover, these catalyst show lower photocatalytic activity, in comparison with the TiO_2/MCM-41 materials. Since the titania nanoparticles are too big to enter inside the pores of MCM-41, they locate on the outer surface of the silica support. Thus a better accessibility of R6G molecules to the active sites is provided, resulting in a significantly increased photocatalytic activity.

References:

[1] E. Barraud, F. Bosc, D. Edwards, N. Keller and V. Keller, J. Catal., **235** (2005) 318

[2] A.G. Rincon and C. Pulgarin, Appl. Cat. B: Env., **63** (2006) 161.

[3] S. Preis, J.L. Falconer, R. Del Prado Asensio, N. Capdet Santiago, A. Kachina and J. Kallas, Appl. Cat. B: Env.**, 64** (2006) 79.

Figures:

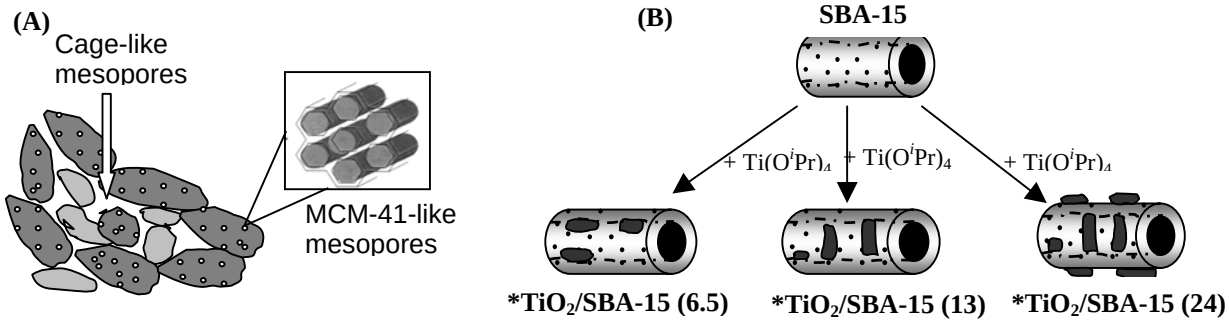


Figure 1. Nanostructuting of titania particles using **(A)** MCM-41 and **(B)** SBA-15 mesoporous silica as supports; * the numbers between brakets represent the initial titania concentration (in mmols Ti^{4+}) used for deposition.

Tables 1: Properties and photocatalytic performances of TiO_2/SiO_2 prepared catalysts

Catalyst	Final loading (mmols Ti^{4+})	TiO_2 particles size (nm)	Adsorbed dye (%)	Degradated dye (%)	Removed dye (%)
TiO_2/MCM-41 (1.95)	1.69	2.46	98	41	999
TiO_2/MCM-41 (6.5)	0.39	3.87	89	73	97
TiO_2/MCM-41 (13)	0.32	4.61	61	52	81
TiO_2/MCM-41 (19.5)	0.43	4.85	64	32	75
TiO_2/MCM-41 (24)	0.44	4.61	70	56	87
TiO_2/SBA-15 (1.95)		0.74	88	14	90
TiO_2/SBA-15 (6.5)		3.86	43	28	59
TiO_2/SBA-15 (13)		4.48	30	15	41
TiO_2/SBA-15 (19.5)		4.83	40	34	60
TiO_2/SBA-15 (24)		5.03	32	21	46
TiO_2 (24)	-	15.26	13	14	25
P25	-	-	16	88	90

SILICON NANOWIRES GROWTH IN A NANOPOROUS ALUMINA TEMPLATE

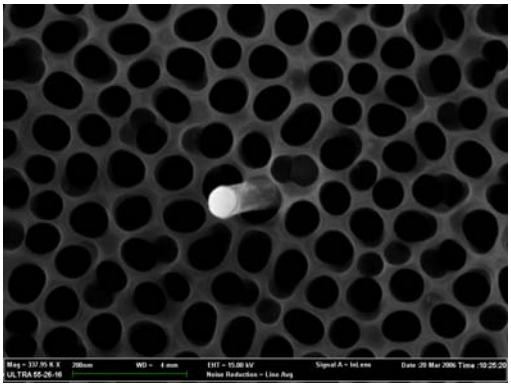
D. Buttard, T. David, and P. Gentile
CEA-Grenoble/DRFMC/SP2M/SINAPS
17 rue des Martyrs
38054 Grenoble Cedex – France
denis.buttard@cea.fr

The growth of semi-conductors nanowires is now of a great interest for nanoelectronic technology, which leads to new electrical or optical properties. The case of silicon nanowires is especially interesting since the silicon is a key material for the nanoelectronic technology. The realization of devices like sensors nanowires leads to technological stresses in terms of mechanical behaviour and positioning of the nanowires. For example the encapsulation and the planarization are difficult to realize after the growth of nanowires on a bulk substrate. We propose another way which consists to grow nanowires directly in a nanoporous cylindrical template made of porous alumina.
Porous alumina layers are composed of uniform porous structure with cylindrical pores parallel to the current lines [1]. They are obtained by direct electrochemical process under a constant voltage value in an aqueous acid solution. They are usually used in several fields of applications in physics, chemistry and biology as a host matrix. This nanoholes array can be used for nanoelectronics applications by filling the cylindrical pores with semi-conductive, electric or magnetic materials, and thus giving a nanowires array.
We show in this communication the growth of silicon nanowires in a nanoporous structure. We present the realization of the anodic oxidation of aluminium and we adjust parameters like the cell size, the pores diameter, the layer thickness and the lateral distribution. The silicon nanowires growth with chemical vapour deposition conditions is then performed in the particular vapour-liquid-solid (VLS) mode [2]. Previous results show the growth of nanowires on bulk substrate [3]. The growth condition of a nanowire in a nanopore is different from those on a bulk surface and will be discussed.

References:

[1] H. Masuda and K. Fukuda, Science, **268** (1995) 1466.
[2] R.S. Wagner and W. C. Ellis, Appl. Phys.Lett., **4** (1964) 89.
[3] J.W. Dailey, J. Taraci, T. Clement, D. J. Smith, J. Drucker and S.T. Picraux, J. Appl. Phys., **96** (2004) 7556.

Figures:



Spontaneous growth of uniformly distributed In nanodots and InI_3 nanowires on InP induced by a focused ion beam

Victor Callegari, Philipp M. Nellen
EMPA, Überlandstr. 129, CH-8600 Dübendorf, Switzerland
victor.callegari@empa.ch

Focused ion beam (FIB) milling can be used both as a top-down (patterning) as well as a bottom-up structuring tool. Bottom-up applications include self-assembly at random or specific locations during or after ion irradiation. Nano-crystallite growth on FIB irradiated areas has been shown for GaAs and InAs[1].

We show spontaneous growth of hemispherical nanodots due to differential sputtering by the 30 keV Ga^+ ions and of wires due to chemical reactions with iodine on the surface of FIB-irradiated areas on a (100)InP substrate.

Hemispherical islands consisting mainly of In grow on InP during sputtering. Diameter and height of a typical island are 42 nm and 7 nm, respectively, determined by scanning electron and atomic force microscopy (Figures 1 and 2). Density of the nanodots was measured to be $2x\ 10^{10}$ cm^{-2}. The size of the nanodots is relatively stable over a wide range of ion fluences ($5x\ 10^{12}$ -$1x\ 10^{15}$ cm^{-2}). Size can be increased by heating the substrate above 156°C, the melting point of pure In. Ga content even reduces the melting point. The differential sputtering rate, due to differences in the surface binding energies of binary semiconductor materials was identified as the main cause for the growth of the nanodots. The surface is depleted from the light element and the heavier element coalesces to form dots. Formation of dots is thought to be enhanced by ion-enhanced surface diffusion, considering a temperature-dependent diffusion coefficient. As a comparison, it has been reported that the minimum Ga droplet size on GaAs is 120 nm[2]. The minimum size in this case is limited by the low melting point of Ga (29.8°C) and the precipitation of Ga on the surface originating from the Ga^+ ion beam. Similar growth is expected for all materials with a significant differential sputtering rate (e.g. GaX, InX, where X=P, As, N, Sb).

Reactive gases can be inserted into the FIB-chamber to enhance sputtering rate (focused ion beam gas enhanced etching, FIB-GAE) or to deposit metals, insulators or carbon (focused ion beam chemical vapor deposition, FIB-CVD). These gases may form involatile reaction products on areas previously irradiated by the FIB. For InP, iodine was used to enhance the sputtering rate. The reaction between InP and I_2 does not require simultaneous ion irradiation. The main reaction products are GaI_3, PI_3 and InI_3. InI_3 stays on the surface due to its low vapor pressure. By patterning the area along parallel lines with FIB and heating the substrate, InI_3 wires with diameter below 100 nm could be grown. Ion trenching creates sharp V-shaped grooves at the bottom of which wire growth is confined to 2 dimensions. Surface rippling with controllable wavelength under ion bombardment has been reported for different materials[3] and could be also be used as a template for nanowire fabrication.

Localization and density of the islands and wires can be controlled with beam current, scanning strategy, irradiation time and substrate temperature.

References:

[1] A. Lugstein et. al, Journal of vacuum science and technology B, **22(6)** (2004) 2995.
[2] A. Lugstein et. al, Journal of vacuum science and technology B, **22(3)** (2004) 888.
[3] L. Jie et. al, Applied physics letters, **88** (2006) 093112.

Figures:

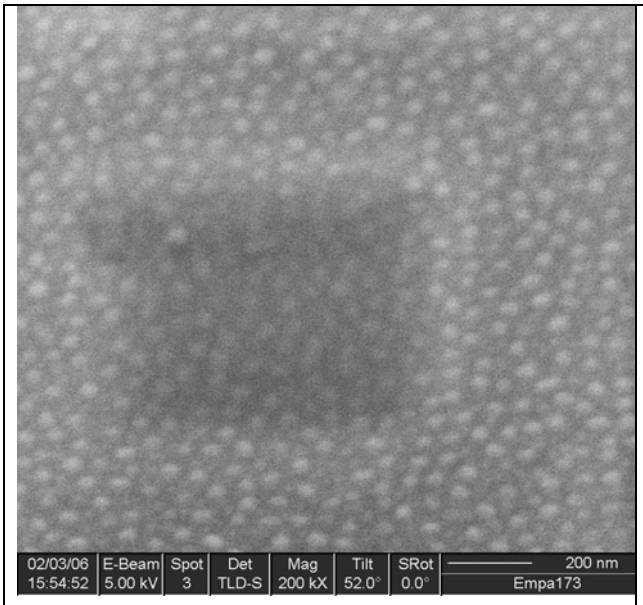


Figure 1: Indium-Gallium quantum dots grown under ion beam irradiation

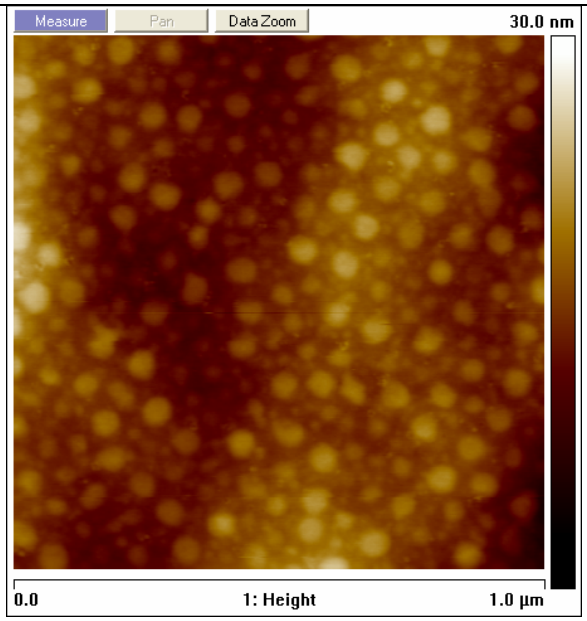


Figure 2: AFM image of the as-sputtered InP surface

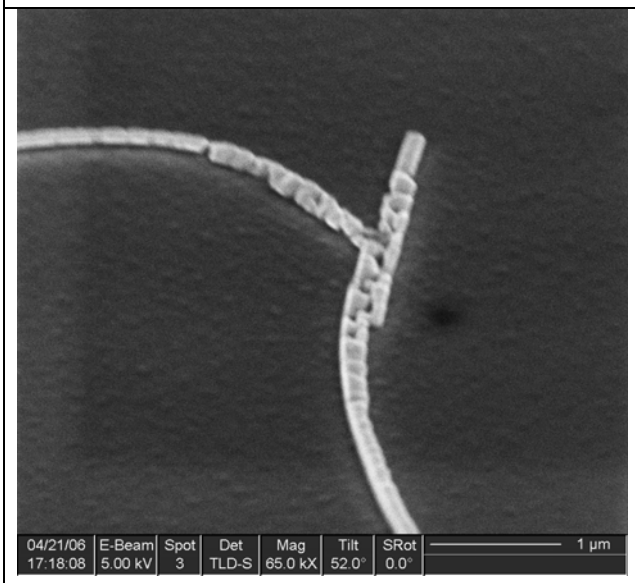


Figure 3: InI_3 nanowire which grows spontaneously under FIB-GAE of InP with I_2.

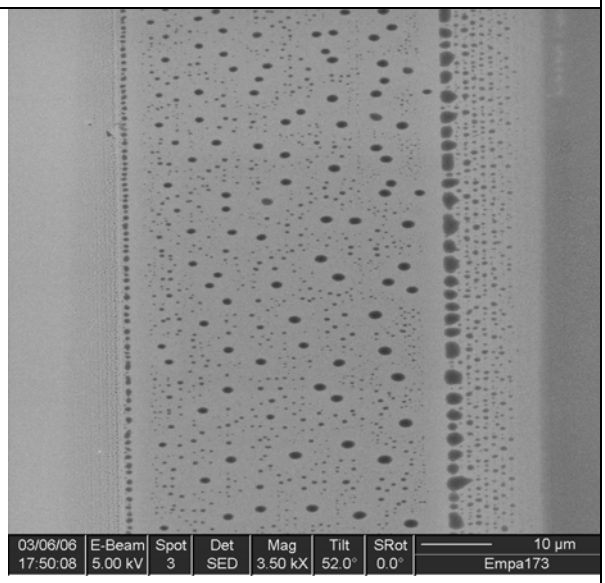


Figure 4: InI_3 rearranges along previously milled lines after heating 10 minutes at 160°C on air.

ELECTROCHEMICAL FABRICATION AND CHARACTERIZATION OF GOLD NANOWIRES.

M.R. Calvo, V. Climent, C. Untiedt.

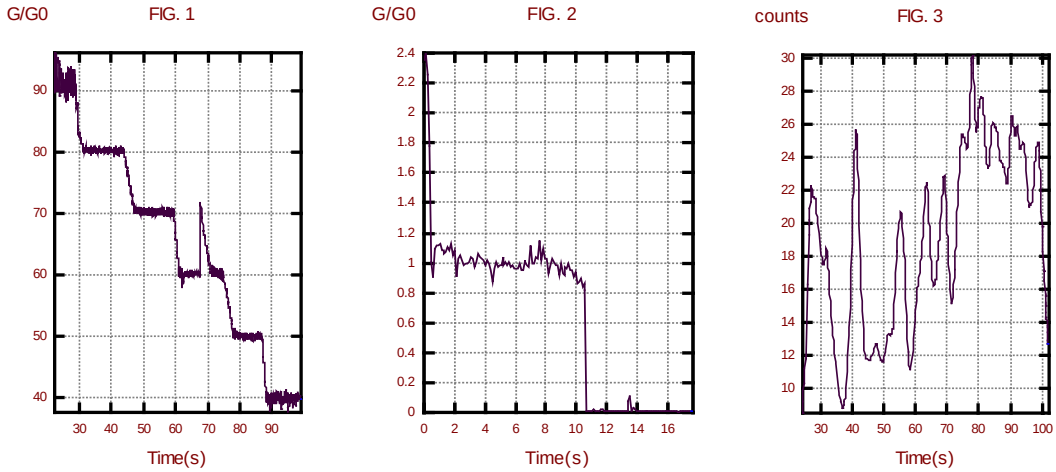
LT-Nanolab. Depto. Física Aplicada. Facultad de Ciencias. Universidad de Alicante.

Electrochemical methods have recently become an interesting tool for fabricating and characterizing nanostructures at room temperature such as nanocontacts or nanowires [1,2]. The controllable fabrication of nanogaps and nanocontacts is crucial in the development of nanoscale electronics devices [3]. Simplicity, low cost and reversibility are some of the advantages of this technique that allows to work at nanoscale without requiring sophisticated instrumentation.

In our experimental setup, we measure the conductance across a nanocontact fabricated either by disolving a macroscopic gold wire or depositing it in between two separated gold electrodes. The conductance is directly related with the radious of the contact. We have achieved a high level of control on the electrochemical fabrication of very small contacts (just a few atoms) in gold [fig. 1]. Also, it is possible to reach stable one-atom contacts, whose conductance is just the quantum unit of conductance G_0 [fig. 2].

We have observed “plateaus” in conductance during the electrochemical growth and etching of gold nanowires. Histograms reveal a certain periodicity of these plateaus [fig. 3], indicating the presence of some stable diameters. The analysis of the data exhibits a behaviour that is similar to the refered in previous works about shell structure in gold, using other tecniques like STM [4] or Mechanically Controlled Break Junction [5].

Our aim is to get the maximum control over the electrochemical fabrication process at nanoscale. Making of electrochemistry a reproducible technique to prepare nanocontacts will open several possibilities that are not feasible with other instruments. Some examples could be to deposite multilayers with atomic precision, to produce molecular junctions or to change the nanocontacts properties by adding reactives to the solution. It involves, also, the possibility of reproducing experiments that today are made by more expensive, complicated or irreversible methods.



.

.

[1] A.F. Morpurgo, C.M. Marcus, D.B. Robinson. Appl. Phys. Lett. **74**, 14 (1999)

[2] J. Li, Y. Yamada, K. Murakoshi, Y. Nakato. Chem. Comun. 2001, 2170-2171

[3] J. Xiang, B. Liu, B. Liu, B. Ren, Z-Q. Tian, Elecrochem. Commun. 577-580 (2000)

[4] E. Medina, J.L., M. Díaz, N. León, C. Guerrero, A. Hasmy, P.A. Serena, J.L. Costa-Krämer. Phys. Rev. Lett. **91**, 026802 (2003).

[5] A.I. Mares, A.F. Otte, L.G. Soukiassian, R.H.M. Smith, J.M. van Ruitenbeck. Phys. Rev. B, **70**, 073401 (2004).

DISLOCATION GENERATION AND MOTION IN AU(001) AT THE NANOMETRIC SCALE

E. Carrasco, O. Rodríguez de la Fuente and J. M. Rojo
Departamento de Física de Materiales. Universidad Complutense.
Av. Complutense s/n, 28040 Madrid
e-mail address: esthercarrasco@fis.ucm.es

Nanoindentation, in conjunction with surface sensitive techniques, such as atomic force microscopies (AFM), are beginning to be used to study the elastic-plastic transition on the nanoscale and examine the dislocation and related defects involved in those first stages of plasticity [1,2]. However, the atomic processes taking place at the initial stages of plasticity in solid surfaces are still full of uncertainties. In particular, more information would be required in relation to the mechanisms involving the nucleation of dislocations, and the possible role played by the surface at the incipient stages of plasticity. Elucidating the role of surfaces is particularly relevant in view of the growing interest in the physical properties of nanostructures.

In previous articles we have used scanning tunnelling microscopy (STM) to image the Au(001) surface after nanoindentation with the microscope tip [3,4]. Local analysis around the nanoindentation point has shown that two special types of dislocation configurations are generated around the latter: 'mesas' and 'screw-loops', both of which intersect the surface and give rise to permanent features that can be disclosed by STM and AFM [5]. In this work, we present new scanning tunnelling microscopy (STM) results about the characterization and motion of these types of dislocation configurations around a nanoindentation. In particular, we report about the spatial distribution of 'mesas' around nanoindentations and their movement as a result of additional nanoindentations in their proximities. We also show and analyse the generation of two types of terraces, resulting from the cross-slip of 'screw-loops' of opposed Burgers vector. We further include theoretical calculations (atomistic simulations and standard dislocation theory calculations) which help to explain the dislocation mechanisms which are responsible for the plastic processes observed in the neighbourhood of the surface. We show that these new data fit very well into a joint description of the mechanical response of surfaces to a nanoindentation and the processes taking place at the atomistic level which results in surface defects.

References

[1] J. Li, K.J. Van Vliet, T. Zhu, S. Yip and S. Suresh, Nature, **418**, (2002) 307.
[2] S.G. Corcoran, R.J. Colton, E.T. Lilleoden and W.W. Gerberich, Phys. Rev. B, **55,** (1997) R16057.
[3] O. Rodríguez de la Fuente, J.A. Zimmerman, M.A. González, J. de la Figuera, J.C. Hamilton, W.W. Pai and J.M. Rojo, Phys. Rev. Lett., **88**, (2002) 036101.
[4] E. Carrasco, O. Rodríguez de la Fuente, M.A. González and J.M. Rojo, Phys.Rev. B (Rapid Communications), **68**, (2003) 180102(R).
[5] A. Asenjo, M. Jafaar, E. Carrasco and J. M. Rojo, Phys. Rev. B, **73**, (2006) 075431.

VISIBLE AND IR PHOTOLUMINESCENCE STUDY OF ERBIUM-DOPED SILICON NANOCRYSTALS PRODUCED BY RF SPUTTERING

M.F. Cerqueira[1], M. Losurdo[2], T. Monteiro[3], M. J. Soares[3], M. Peres[3], P. Alpuim[1]

[1]Departamento de Física, Universidade do Minho, Braga, Portugal.
[2]Plasma Chemistry Research Center, CNR, Bari, Italy
[3]Departamento de Física, Universidade de Aveiro, Aveiro, Portugal.

Since the discovery of the 'size effect' on the silicon band gap and the observation of room temperature photoluminescence (PL) in the visible range from porous silicon**,** the research on nanostructured silicon-based materials aimed at the fabrication of efficient optoelectronic integrated systems has been intensified.

Erbium-doping of nanostructured silicon allows such systems to emit in the infra-red region (1.54 μm that corresponds to the minimum in absorption within the transparent window of silica fibers) leading the way to the design of devices for optical communications.

In this paper, erbium-doped low dimensional Si-based heterogeneous matrices were grown by reactive magnetron sputtering on glass substrates using different oxygen/hydrogen ratios and showing different microstructures. Amorphous, micro- and nanocrystalline samples were obtained and their optical properties are shown to be dependent on the film crystalline fraction and matrix chemical composition. For the structural characterisation, X-ray in the grazing incidence geometry and Raman spectroscopy were used. The chemical studies were done using the RBS/ERD technique. Spectroscopic ellipsometry (SE) has been combined with the previous techniques to resolve the film microstructure and composition. In particular, the distribution along the film thickness of the volume fractions of nanocrystalline/amorphous silicon and SiO_x phases has been obtained from SE analysis.

In this contribution visible photoluminescence from thin silicon films as a function of oxygen/ hydrogen ratio present in the matrix and the sample microstructure is discussed.

Acknowledgment

This work was partially supported by a FCT Project POCTI/CTM/39395/2001 and INTAS Project #03-51-6486.

The Influence of Surface Preparation and Probe Configuration on the Reliability of Work Function Measurement using Kelvin Probe Microscopy

Amal Chabli[1], Denis Mariolle[1], François Bertin[1], Nicolas Gaillard[2], Rémy Gassilloud[1], François Martin[1]
[1]CEA-DRT-LETI-CEA-/G, 17 rue des Martyrs, 38054, Grenoble Cedex 9, France
[2]STMicroelectronics, Central R&D Labs, 850 rue Jean Monnet, BP16, 38926 Crolles, France
francois.bertin@cea.fr

The electrode Work Function (WF) is a key parameter which defines the electrical characteristics of major devices such as the MOSFET threshold voltage (Vth) and the optimization of Metal/Insulator/Metal capacitors. For the 45 nm gate-width and below, the standard polysilicon electrodes of MOSFETs are expected to be replaced by metals in order to suppress high resistance and double depletion phenomena. To solve those issues, new metals deposition processes such as Atomic Layer Deposition (ALD) technique as well as metal WF engineering are under investigation [1,2]. Thus, the understanding of the impact of deposition processes on both metal WF value and its variations within the layer becomes an important issue in the development of advanced devices [3].
Based on charge-transfer cancellation between a metal coated AFM tip and the sample connected as a capacitor, Kelvin Force Microscopy (KFM) is a spatially resolved technique (50 nm) well suited to characterize local WF variations on metal layers with a sensitivity of about 5 meV. We have reported elsewhere, WF mappings at the decananometer scale using KFM on various metal layers to study the impact of the deposition process on the electrical properties of the devices [4]. This approach, which is a variation of the well known Kelvin Probe technique [5], can be operated at both normal pressure or in UHV. However KFM is sensitive to environmental artefacts when operated in air [6].
In this paper, we report on the influence of the environmental conditions to the image contrast using KFM to image the WF of polycrystalline metals. We demonstrate that the WF is related to the grain orientation as observed on Cu layers (figure 1) [4]. However, the measurement contrast decreases as the relative humidity (RH) increases, as confirmed by successive KFM measurements performed on the same area at different RH values. This behaviour is associated with the contribution of the surface to the bulk WF [7]. Therefore, to obtain a reliable WF value, it is important to maintain the RH value as low as possible while scanning.

Secondly we investigate the effect of the surface oxidation on the WF measurement. It has been demonstrated using X-ray Photoelectron Spectroscopy that $WSi_{2.58}$ layers fabricated using ALD show the presence of only a Si oxide after annealing. The WF change with the surface oxidation of the sample is analysed. KFM measurements are performed on 15-nm-thick $WSi_{2.58}$ layers both before and after annealing. In addition, measurements are performed both with and without HF cleaning. The WF of the tip is determined using a reference sample (Pt layer). Figure 2 shows the WF obtained from $WSi_{2.58}$ samples both with and without the presence of a surface oxide. The reliability of the measurements is confirmed by the low dispersion in the values of an AlCu test sample. For the $WSi_{2.58}$ layers, the WF value is higher for annealed layers than for the as deposited ones. After HF cleaning to remove the surface oxide, the WF values are lower, as expected from an oxide-free material. These results show that the extracted WF value depends on the chemical composition of the sample surface, therefore careful specimen preparation is required to avoid surface artefacts.
It is well known that the tip aspect-ratio limits dramatically the spatial resolution of the KFM. To solve this issue, we have deposited on a commercially available tip a high-aspect-ratio tungsten needle, using an electron beam induced deposition process. First results obtained from the measurement of copper lines show a contrast enhancement of about 70% using these new tips.

References:

[1] G. S. Lujan *et al.*, Proceedings of the 32nd ESSDERC, (2002) **583.**
[2] H. N. Alshareef *et al.*, Appl., Phys. Lett., **87**, (2005) 052109.
[3] A. Yagashita *et al.*, IEEE Trans. Electron Devices, **48**, (2001) 1604.
[4] N. Gaillard *et al.*, as discussed at the 2006 MAM conference, O7.01, Grenoble, France.
[5] L. Kelvin, Philosophical Magazine **46** (1898).
[6] H. Sugimura *et al.*, Appl. Phys. Lett. **80**, (2002) 1459.
[7] H. Luth, « Surfaces and Interfaces of Solid Materials », Springer Verlag, 4th, rev. and extended ed., (2001) .

Figures:

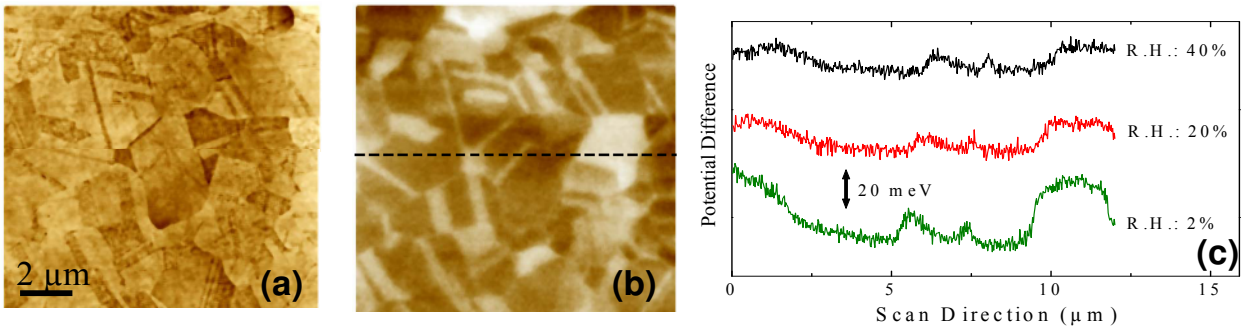


Figure 1 – (a) Surface topography of the copper layer (Zscale= 10 nm), (b) measured potential on the same area and (c) potential profile along the dashed line for three RH values.

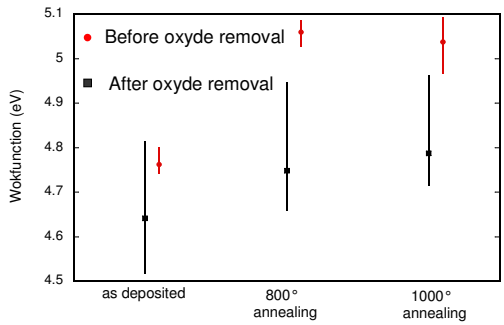


Figure 2 – Evolution of Work function measure by KFM (reference set on a platinum layer at 5.3eV) for three different samples of $WSi_{2.58}$ material (thickness = 15 nm) deposited onto silicon dioxide (thickness = 200 nm). For each sample, analysis has been done both before and after oxide (top surface) removal (dip FH 1%, 15 s). Error bars are reported for a set of 10 measurements with two tips (same tips used before and after oxide removal)

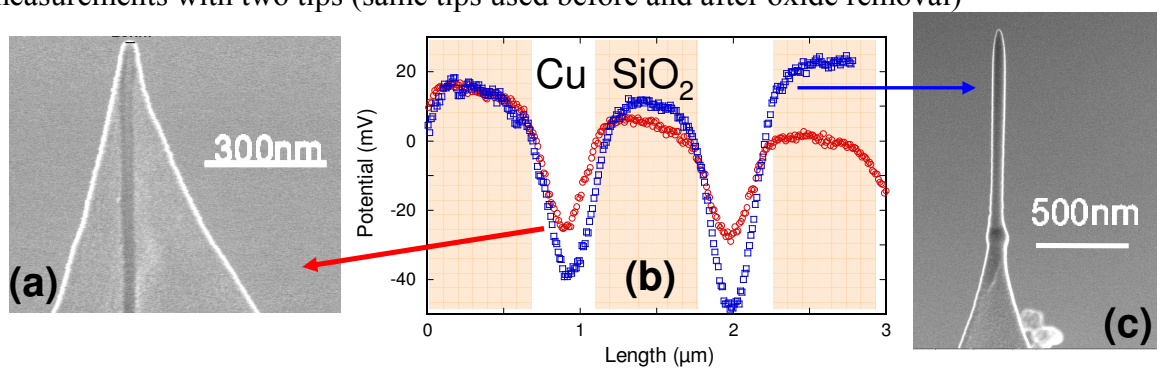


Figure 3 - (a) Conventional PtIr tip, (b) Potential measurements with tip shown on and 3-a (red circles) ad figure 3-c (blue squares), (c) W EBID needle deposited on a conventional tip.

CONTROL OF THE TEMPERATURE DEPENDENCE OF THE PHOTOLUMINESCENCE FROM InAs/GsAs SELF ASSEMBLED QUANTUM DOTS

Adil Chahboun [1,3], N. V. Baidus [1,2], E. Alves [4], M. J. M. Gomes [1], B. N. Zvonkov [2] and M. I. Vasilevskiy [1]

[1] *Universidade do Minho, Departamento de Física,4170-057 Braga,Portugal*
[2] *NIFTI, N.I. Lobachevsky State University, 603600 Nihznii Novgorod, Russia*
[3] *LPS, Dhar Mehraz Science Faculty, BP 1796 FES, Morocco*
[4] *Instituto Técnico Nuclear ITN, EN10, 2686-953 Sacavèm, Portugal*
chahboun@fisica.uminho.pt

Self assembled InAs/GaAs quantum dots (QD's) have demonstrated their ability to emit in the telecommunication wavelength range (1.3-1.55 µm). They showed a big potential to be used as active elements of low threshold lasers and light emitting diodes. However, as it is usually reported, their emission is strongly temperature dependent. In fact, the photoluminescence (PL) from these structures was shown to decrease dramatically at room temperature or even below. This is commonly explained by a thermally activated escape of carriers from the QD's to the surrounding matrix, followed by the non-radiative recombination [1].
In this work, we present a new approach to overcome the PL quenching phenomenon, by using tetrachloromethane (CCl_4) during the growth [2]. The PL emission is shown to remain constant or to increase slowly with the increase of the temperature. A decrease in defect concentration in the GaAs matrix is suggested to explain this effect. We also show that it is possible to control the PL intensity from InAs QD's by changing the defect concentration in the matrix. In fact, irradiation of defect free samples in order to generate defects in the matrix leads to the quenching phenomenon. A simple theoretical model allowing for calculation of the concentrations of free carriers in the system and their evolution with temperature is provided to support our arguments.

References:

[1] E. C. Le Ru, J. Fack, and R. Murray, Phys. Rev. B **67**, 245318 (2003)
[2] N.V. Baidus, A. Chahboun, M. J. M. Gomes, M. I. Vasilevskiy, P. B. Demina, E. A. Uskova, and B. N. Zvonkov, Appl. Phys. Lett. **87**, 53109 (2005).

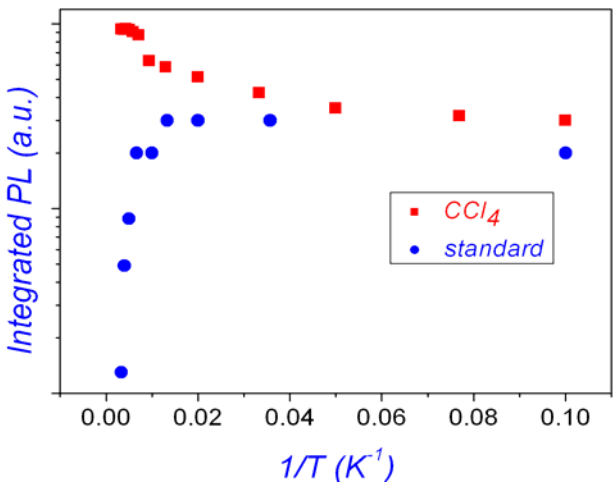


Fig 1: Temperature dependence of PL from InAs QD's indicating two different behaviours at room temperature.

ELECTROCHEMICAL GRAFTING OF POLYMERS ON ALIGNED MULTI-WALLED CARBON NANOTUBES

J. Chancolon[1], T. Matrab[2], M. Chehimi[2], G. Deniau[3], J. N. Rouzaud[4] C. Reynaud[1], and M. Mayne-L'Hermite[1]

[1] Laboratoire Françis Perrin, CEA Saclay, DSM/DRECAM/SPAM, France

[2] ITODYS, Université Paris VII and CNRS (UMR 7086), France

[3] Laboratoire de Chimie des Surfaces et Interfaces, CEA Saclay, DSM/DRECAM/SPCSI, France

[4] Laboratoire de Géologie, Ecole Normale Supérieur de Paris, France

jerome.chancolon@cea.fr

Due to their interesting properties, carbon nanotubes (CNTs) have attracted particular attention for different application fields such as composite materials, microelectronics [1] and biology. Processing CNTs is a key point which often requires appropriate chemical modification of their surface in order to enhance their dispersability or to improve their compatibility with polymers. Regarding the numerous methods reported in the literature, chemical functionalisation is based on covalent grafting, or on molecular stacking or on wrapping of the CNTs surface with surfactants or polymers. Covalent functionalisation is usually performed chemically. More recently, methods of electrografting were reported [2, 3].

In this context, the aim of this study is to demonstrate the potentialities of electrochemical grafting of polymers on carpets of aligned CNTs. Two different methods designed to tether polymeric chains at the surface of aligned carbon nanotubes will be reported. First, grafting of BUMA (Butyl Methacrylate) by an electropolymerization method [2] will be detailed. Then, we will demonstrate that Surface-Initiated Atom Transfer Radical Polymerization (SI-ATRP) is an attractive two-step way to *graft onto* CNTs surface polymers with controlled molecular weight and thickness [4]. We have recently found that the surface"diazonium salt/ATRP" process [5a] is an effective route for carbon nanotubes functionalization with PS (PolyStyrene) and PMMA (PolyMetylMethAcrylate) [5b].

The CNTs synthesis has been performed by aerosol-assisted catalytic chemical vapour deposition (CCVD) process. Briefly, this process involves the use of solutions containing both liquid hydrocarbon and metal precursors. This method consists in producing and subsequently pyrolysing mixed liquid aerosols generated from the solutions. The starting solution is composed of ferrocene (5 wt%) dissolved in toluene and the aerosol, carried by an argon flow, is pyrolysed at 850 °C during 7 min. The resulting sample is composed of multi-walled carbon nanotubes perpendicularly aligned and attached to the substrate surface and looks like a carpet. In this case, we choose a conducting substrate (Si-n). The nanotube length reaches 130 µm, the average inter-tube spacing is around 100 nm and the external diameter of carbon nanotubes is varying between 10 and 100 nm [6, 7].

Regarding the electropolymerization process, the set-up consists in a three-electrode electrochemical cell under inert atmosphere. The working electrode was the CNTs carpet grown on Si-n, the auxiliary electrode was a graphitic carbon foil and the reference electrode was based on the Ag/Ag^+ couple. Finally, voltametric cycles (20 mV/s) were conducted in an electrolyte containing the monomer (BUMA). SEM images show that CNTs are mainly covered (fig 1). HRTEM observations on individual nanotubes confirm theses observations showing an amorphous layer deposited on all CNTs.

For the "diazonium salt/ATRP" protocol, phenyl ethyl bromide groups were electrochemically grafted onto CNTs using the diazonium salt $BF_4^-,^+N_2\text{-}C_6H_4\text{-}CH_2CH_2\text{-}Br$. The as-prepared $BrCH_2CH_2\text{-}C_6H_4$-modified CNTs (CNT-Br) served as a platform for the growth of PS and PMMA chains by ATRP. The overall synthesis process is illustrated in

figure 2. TEM images (Fig.3) show that for raw CNTs, the external surface of the nanotubes is well organized and corresponds to stacked graphene layers (Figure 3a). On the contrary, CNT-PMMA or CNT-PS hybrids exhibit amorphous layers corresponding to the grafted polymer chains the thickness of which is ~ 1 and 2 nm (Figs. 3b and 3c).

References:

[1] C. A Dike, J. M. Tour, J. Am. Chem. Soc., **51** (2004) 11151.
[2] T. Defever, G. Deniau, S. Palacin, L. Goux-Capes, S. Barrau, M. Mayne-L'Hermite, J. P. Bourgoin, J. Electroanal. Chem., **589** (2006) 46.
[3] G. Deniau, L. Azoulay, P. Jegou, G. Le Chevallier, S. Palacin, Surf. Sci., **600** (2006) 675.
[4] S. Edmondson, V. L. Osborne, W. T. Shuck, Chem. Soc. Rev., **33** (2004) 14.
[5] (a)T. Matrab, M. M. Chehimi , C. Perruchot, A. Adenier, A. Guillez, M. Save, B. Charleux, E. Cabet-Deliry, J. Pinson, Langmuir, **21** (2005) 4686; (b) T. Matrab, J. Chancolon, M. Mayne-l'hermite, G. Deniau, J. P. Boudou, M. Chehimi, M. Delamar, Submitted to Colloids Surf. A.
[6] M. Pinault, V. Pichot, H. Khodja, P. Launois, C. Reynaud, M. Mayne-l'hermite, Nanoletters, **5** (2005) 2394.
[7] M. Pinault, M. Mayne, C. Reynaud, O. Beyssac, J. N. Rouzaud, C. Clinart, Diam. Relat. Mater, **13** (2004) 1266.

Figures:

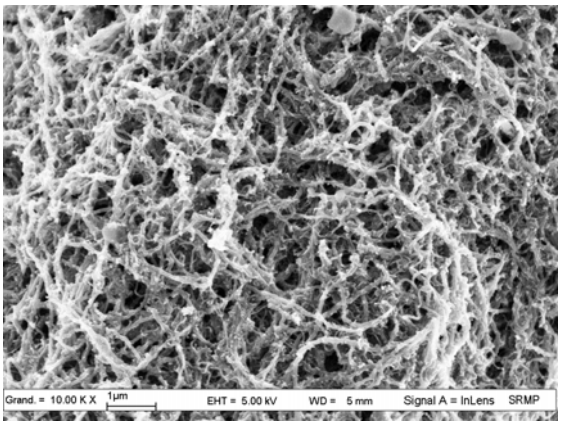


Figure 1. SEM image of CNTs grafted with BUMA

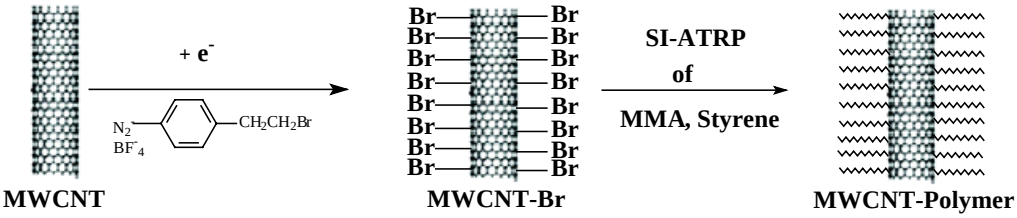


Figure 2 . Brominated initiators are attached to CNTs via electrochemical reduction of the diazonium salt precursor. PS and PMMA chains are grafted by SI-ATRP from the CNT-Br platform.

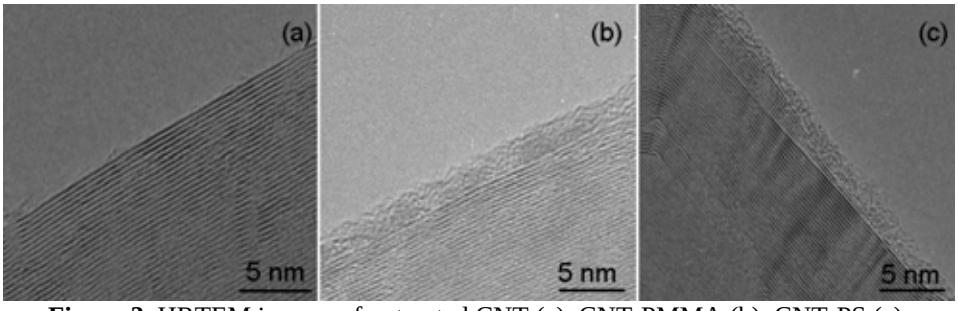


Figure 3. HRTEM images of untreated CNT (a), CNT-PMMA (b), CNT-PS (c).

Poster

SWIFT HEAVY ION INDUCED SURFACE RESTRUCTURING OF THE THIN FILM

R. S. Chauhan[1], D. C. Agarwal[1], S. Kumar[1,4], S. A. Khan[2], D. Kabiraj[2], I. Sulania[2], D. K. Avasthi[2] and W. Bolse[3]

[1]Department of Physics, R. B. S. College, Agra-282 002, India
[2]Inter-University Accelerator Centre, New Delhi-110 067, India
[3]Institut fuer Strahlenphysik, Universitaet Stuttgart, Allmandring 3, 70569 Stuttgart, Germany
[4]CITM, Aravali Hills, Sector-43, Faridabad-121 001, India

Contact e-mail: rvschauhan@yahoo.com

Abstract

Recently, it has been shown that self-organization of thin film surfaces during high-energy heavy ion irradiation results in structure formation at a sub-micrometer scale, creating peculiar surface morphologies of quite regular patterns [1-3]. In the present work, we report on the self-organization of the surface of NiO thin films on different substrates (SiO_2, Si and Al) using 100 MeV Ag ions at LN_2 temperature and at an incidence angle of 75^o with the beam axis. The surface morphology of the irradiated surface is studied by Atomic force microscopy (AFM). AFM images of ion-beam irradiated samples show the restructuring of the initially flat and coherent NiO film into an almost periodic NiO lamellae structure induced by the swift heavy ion bombardment. The quite regular lamellae are oriented perpendicular to the beam direction and show an average distance of the order of 1 ❍ m. Their final height is also of the order of 1 ❍ m, while their widths are of hundreds of nm. Section analysis of the AFM images reveal that the width of the lamellae, at the same irradiation fluence, is less in case of NiO films deposited on SiO_2 substrate in comparison to Al substrate. It is also observed that the cracking and development of lamellae structure are seen at higher fluence in the case of Al substrate.

References:

[1] W. Bolse, et al., *Appl. Phys. A 76 (2003) 1*

[2] W. Bolse, et al., *Surf. Coat. Technol. 200 (2005) 1430*

[3] W. Bolse, *Nucl. Instr. Meth. B* 244 (2006) 8

AC MAGNETIC PROPERTIES OF NANOGRANULAR FeCoAlN FILMS.

Oleksandr Chayka, Luděk Kraus, František Fendrych, Sergiy Veljko
Institute of Physics ASCR, Na Slovance 2, CZ-18221 Prague 8, Czech Republic
chayka@fzu.czl

Nowadays, electronic devices such as microinductors, transformers and magnetic recording heads are demanded to operate in the GHz frequency range that has stimulated intensive research of new magnetic materials with high frequency permeability. Soft magnetic nanogranular films consisting of magnetic grains embedded in an insulating matrix are appropriate candidates for these applications due to the follows reasons: (a) the intrinsic maze structure of nanogranular films leads to high resistivity which reduces eddy current losses (b) the ferromagnetic resonance (FMR), which is the second main loss mechanism, can be shifted to higher frequencies in materials with high saturation magnetization M_s and anisotropy field H_a. FeCo-based oxide or nitride films, which satify these requirements have recently attracted much attention [1,2].

In the present paper we report on AC magnetic properties of ferromagnetic nanogranular FeCo-based nitride films. The samples were prepared by UHV plasma jet technique [3]. External magnetic field was applied during the deposition. The FeCoAlN films consist of FeCo grains with the size of about 10 nm (evaluated from X-ray diffraction measurements) embedded in an insulating AlN matrix. Magnetic properties of the as-deposited samples were investigated using an AC hysteresis loop tracer. The evaluation of the relative effective permeability frequency dependence was based on a short-circuited strip line method. [4]. The network analyzer (AGILENT E8364B) was used for this kind of measurements.

Figs. 1a and b show the hysteresis loops of a film measured along the easy and hard axis of magnetization, respectively. The coercive field along the easy axis, measured at the frequency of 200 Hz, is about 4 kA/m. The broadening and the roughness of the loop measured along the hard axis indicate the easy axis distribution in the film plane, as was proved by the magneto-optical Kerr effect measurements [5]. Fig. 2 shows the frequency dependence of real μ_{eff}' and imaginary μ_{eff}'' parts of the relative effective permeability. The characteristic frequency at which the natural ferromagnetic resonance occurs is about 1.7 GHz.

References:

[1] K. Seemann, H. Leister, V. Bekker, J. Magn. Magn. Mater., **283** (2004) 310.
[2] N.D. Ha, T.S. Yoon, H.B. Kim, J.J. Lim, C.G. Kim and C.O. Kim, J. Magn. Magn. Mater., **290** (2005) 1571.
[3] F. Fendrych, L. Kraus, O. Chayka, P. Lobotka, I. Vávra, J. Touš, V. Studnička, and Z. Frait, Monatshefte J. Chemie, **133** (2002) 773.
[4] V. Bekker, K. Seemann, H. Leister, J. Magn. Magn. Mater., **270** (2004) 327.
[5] O. Životský, F. Fendrych, L. Kraus, K. Postava, O. Chayka, L. Halagačka, and J. Pištora, J. Magn. Magn. Mater., to be published.

Figures:

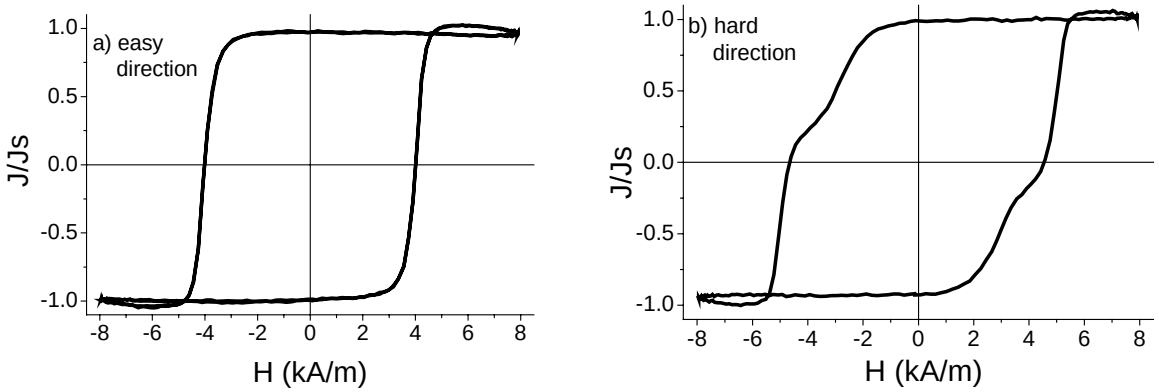


Figure 1: Hysteresis loops of $Fe_{50}Co_{50}$-AlN film measured along a) easy and b) hard axis directions.

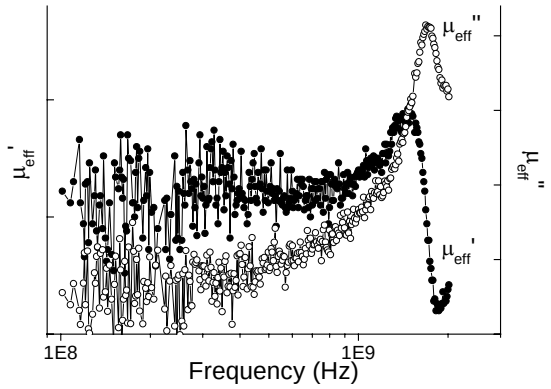


Figure 2: The frequency dependence of relative permeability.

CARBONE NANOTUBE MAT SENSORS FOR TOXIC GAS DETECTION

Nicolas Izard[1], Pascale Chenevier[1], Fabien Dubois[2], Eric Doris[2], Charles Mioskowski[2] and Jean-Philippe Bourgoin[1]

[1] Molecular Electronics Laboratory, DSM/DRECAM/SPEC, CEA/Saclay, Gif-sur-Yvette, France

[2] Lab. for Tagged Molecules in Chemistry and Biology, DSV/DBJC, CEA/Saclay, Gif-sur-Yvette, France

pascale.chenevier@cea.fr

Carbon nanotubes are especially well suited to chemical sensor design. Indeed, they show remarkable electrical characteristics, high conductivity for metallic, sharp on/off transition for semiconducting nanotubes. Beside their conductivity is extremely sensitive to changes in the environment of the nanotube. They can also be chemically functionalized by covalent grafting onto the nanotube walls.

Snow et al [1] have built gas sensors based on carbon nanotube networks as the reactive sensor, using filters to achieve chemical selectivity. In the current project, we implemented chemical selectivity directly onto the nanotubes by grafting reactive probes onto the nanotube walls (Scheme 1). The functionalized nanotubes were then deposited onto a chip using dielectrophoresis, forming connected micron sized carbon nanotube network transistors, the conductivity of which was measured as a function of reaction with toxic agents. Gas reaction with probes changed their electrical charge, inducing a local chemical gating effect onto nanotube conductivity.

Two kinds of probe were grafted through diazobenzene addition onto nanotubes. Diazopyridine was used as a model probe for alkylant detection. A selective cyclizing probe, designed for highly toxic organophosphonate detection [2], has been modified to add an amino moiety, later converted into a diazo group. Grafting rate was characterized by Raman spectroscopy and XPS. A low grafting rate was achieved to preserve nanotube conductivity.

Grafted and pristine carbon nanotubes were then deposited onto chips using dielectrophoresis. Diluted suspensions of nanotubes in NMP submitted to a relatively low frequency (100kHz-1MHz) electrical field between gold electrodes resulted in dense, thin networks of carbon nanotubes of 2-3kΩ resistance (figure 2).

Preliminary tests of alkylating agent reactivity onto pyridine derivatized nanotube sensors have shown a 2 fold increase in resistance compared to a 8% resistance increase for pristine nanotube networks. Further XPS analysis has shown that the gas-probe reaction was not complete, probably because of low probe availability in nanotube bundles. Work is in progress to increase the probe availability to gas and achieve gate bias enhanced sensitivity in electrical detection.

References:

[1] Novak, J. P., E. S. Snow, et al., Applied Physics Letters, **83** (2003) 4026.
Snow, E. S., F. K. Perkins, et al., Science, **307** (2005) 1942.
[2] Zhang, S. W. and T. M. Swager., Journal of the American Chemical Society, **125** (2003) 3420.

Figures:

Scheme 1: gas sensor detection principle

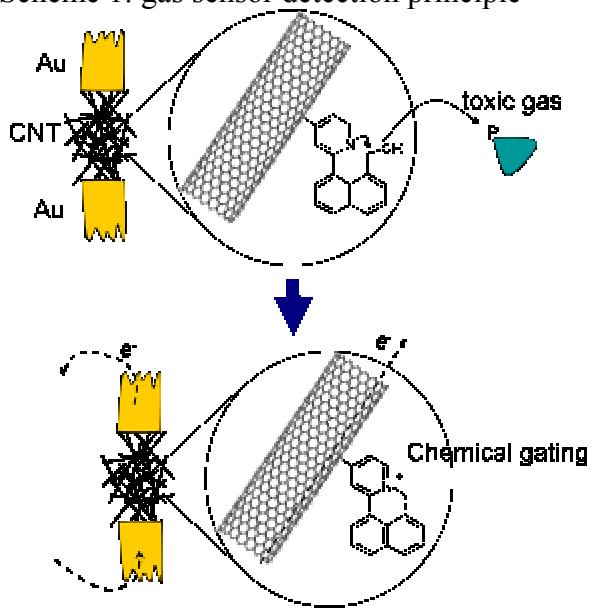
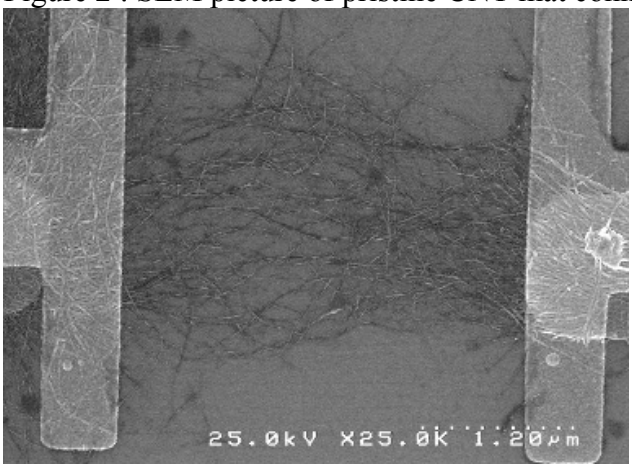


Figure 2 : SEM picture of pristine CNT mat connected onto chip.



FUNCTIONAL NANOCOMPOSITES BASED ON SINGLE-WALLED CARBON NANOTUBES – SYNTHESIS AND INVESTIGATION

M.V. Chernysheva[1], A.A. Eliseev[1], A.V. Lukashin[1], Yu.D. Tretyakov[1], S.V. Savilov[2], N.A. Kiselev[3], O.M. Zhigalina[3], A.S. Kumskov[3], A.V. Krestinin[4], J.L. Hutchison[5]
[1]Department of Materials Science, Moscow State University, Moscow 119992, Russia
[2]Department of Chemistry, Moscow State University, Moscow 119992, Russia
[3]Institute of Crystallography, Moscow 119333, Russia
[4]Institute of Problems of Chemical Physics, Chernogolovka 142432, Moscow Region, Russia
[5]Department of Materials, University of Oxford, Oxford OX1 3PH, UK
marina@inorg.chem.msu.ru

Single-walled carbon nanotubes (SWNTs) first produced in 1991 by arc-discharge vaporation method nowadays draw close attention of scientific community worldwide due to their unique electronic and structural properties accompanied by extraordinary mechanical behavior depending on the diameter and conformation of tubes. Well-defined atomic structure, ultra small diameter (from 0.4 nm) and the highest length to diameter ratio makes SWNTs extremely attractive as the perfect templates for the formation of 1D nanocrystals inside the channels. Chemical design of SWNTs via filling of tubes with favourable conductive, optical or magnetic materials impulses the development of novel class of nanotube architectures and nanoscale materials. For instance intercalation of the electron donors (with Fermi level located in the conductance band) to the metallic tubes will lead to increase of electron density on carbon walls resulting in better conductance through the composite wire while intercalation of electron acceptors (with Fermi level below one of SWNT) may cause the system to demonstrate semiconductor behavior. This concept allows to tune electronic structure of SWNTs by intercalation of metallic, semiconductor or dielectric materials enabling their great potential applications as active elements of electronic devices and circuits.

The present study is focused on the controllable growth of 1D conductive nanocrystals in channels of carbon nanotubes with inner diameter 1-1.4 nm and investigation of their effect on electronic properties of nanocomposites. SWNTs were obtained by catalytical arc-discharge method with following purification and pre-opening by treatment at 500ºC in dry air for 0,5 hour. The nanocomposites were prepared using capillary technique via impregnation of oxidized SWNTs in static vacuum of 0.01 mbar by molten salts CuI, CuCl or AgI at temperatures 100ºC above the melting point of the correspondent salt.

SWNTs and filled carbon nanotubes were characterized by high resolution TEM, Raman and impedance spectroscopy, EDX and surface analyses. According to capillary adsorption studies the specific BJH surface area of pre-opened SWNTs decreases after the impregnation procedure (for example, with CuI) from 1073 m^2/g down to 43 m^2/g nearly with unchanged pore size distribution pointing out the incorporation of guest material into inner channels of nanotubes. EDX microanalysis and HRTEM imaging of all obtained nanocomposites proved the successful filling of SWNTs channels with fine nanocrystals of chosen materials (up to ~73 wt.%). Raman spectroscopy data of CuI, CuCl and AgI@SWNTs demonstrated the changing of electronic properties of composites resulting in the shift of RBM- и G-peaks as compare to row nanotubes. The Raman spectra of CuI@SWNTs, for instance, showed considerable broadening of G-modes and shifts to lower frequencies, both with the disappearing of G–-line of metallic tubes which can be ascribed to the shift of electronic band structure of filled SWNTs and transition of the metallic tubes to the semiconductive state.

Besides, the additional resistance measurements of single SWNTs bundle with diameter <100 nm and length of ~20 μm were performed indicating the resistance value of ~1 MΩ, which

corresponds to the metallic conductivity. The investigation of I-V curves and electrical impedance of individual SWNTs shelled with amorphous carbon showed the metallic behavior with the resistivity of inner channel equal $0{,}7 \cdot 10^{-5}$ Om·cm.

This work was supported by RFBR (06-03-33052 and 06-03-33136) and Russian Federal Program (IN-12.3/005).

TRANSPARENT CARBON NANOTUBE FIELD EMISSION DEVICES FOR DISPLAY AND LAMP

*Yousuk Cho, Sunhee Lee, Myungchan An, Dojin Kim**

School of Nano Science and Technology, Chungnam National University, Daejeon, Korea
dojin@cnu.ac.kr

Abstract

A simple new method to fabricate transparent carbon nanotube field emission devices was developed. The highly graphitized single wall carbon nanotubes (SWNTs) were attached in-situ in an arc-discharge chamber on Sn/ITO glass substrate. The post heat-treatment carried out below the deformation temperature of soda-lime glass guaranteed good mechanical adhesion and electrical contact between the carbon nanotubes emitters and the electrode by using the particulated Sn as a bonding agency. When the Sn particles were oxidized at <400℃, the SWNT-Sn composite changes to SWNT-SnOx composite and becomes transparent. The emission current density of thus fabricated SWNT-Sn composite emitters was about 1 mA/cm2 at 3V/μm of electric field. The emission current density of the SWNT-SnOx composite was also about 1 mA/cm^2 at the same electric field. As the oxidation temperature is higher, it showed a more stable emission property with increased life time of the emitter.

Keywords: carbon nanotube, field emission device, carbon nanotube composites, SnOx

HYBRID MATERIALS CONTAING NANOSIZED CLAY AND NATURAL FIBRE

Tanushree Choudhury and Nirendra M. Misra
Indian School of Mines, Department of Applied Chemistry, Dhanbad, INDIA
tanu_c79@yahoo.co.in

Clay particles that have the sizes a few nanometre thick, if properly dispersed in the polymer matrix impart unique combinations of physical and chemical properties that make these composites suitable for making coatings and films for a variety of industrial applications. Physical properties of nanocomposites can depend on the size of the incorporated colloids [1]. Clay minerals have also been used in making nanocomposites. A delaminated clay-polymer composite exhibit improvements in strength, modulus, thermal resistance etc [2]. Delamination (or, exfoliation) of clay depends on the dispersion of clay, and property of the composites depend on the interaction of delaminated clay with the polymer or, fibre. Natural fibre reinforced composites are employed as substitutes for synthetic fibre reinforced composites [3].
In the study hybrid material was prepared using montmorillonite clay and agave fibre. A natural dispersant was used for preparing exfoliated clay. Characterization of the materials were done using DSC, FTIR and SEM (Fig 1) Results show a show better dispersion of clay (by using a natural dispersant) and greater compatibility with natural fibres with finely dispersed clay particle. Such materials have great potential as a eco-friendly composite.

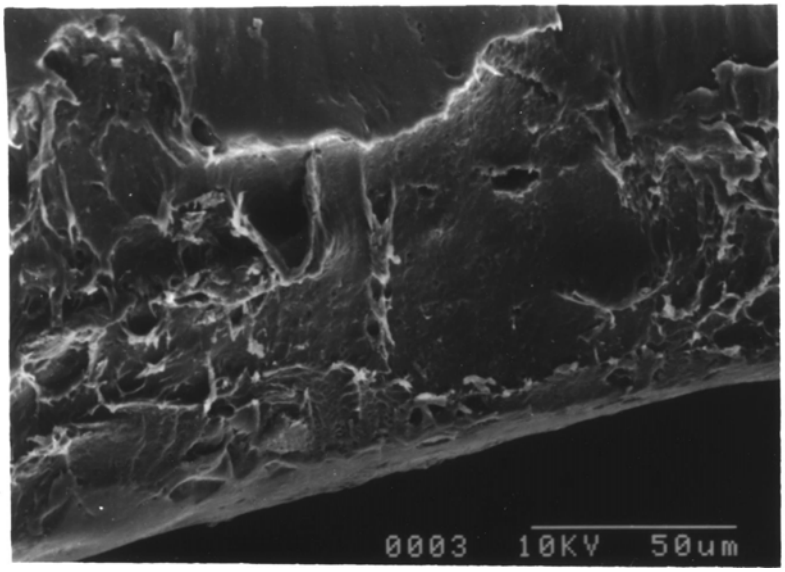


FIG.1 SEM of Hybrid material containing dispersed clay and natural fibre

References

[1] W. Caseri, The Chemistry of Nanostructured Materials (Peidong Yang, ed.), World Scientific, Singapore, (2003).
[2] D. Schmidt, D. Shah, E. P. Giannelis, Current Opinion in Solid State and Materials Science 6 (2002) 205.
[3] M. M. Thwe and K. Liao, J. Materials Science, 38 (2003) 363.
[4] Y. Deng, J. B. Dixon and G. N. White, Clays and Clay Minerals, 51 (2003) 150.
[5] R. D. Davis, J. W. Gilman, T. E.Sutto, J. H. Callahan, P. C. Trulove and H. C. De Long, Clays and Clay Minerals, 52 (2004) 171.

Poster

THE EFFECTS OF SILVER OXIDE ADDITIONS ON THE ELECTRICAL PROPERTIES AND MICROSTRUCTURE OF LOW-CURING-TEMPERATURE SILVER PASTE WITH MOD ADDED

Chun-An Lu [a#], *Pang Lin* [a]

[a]*Department of Materials Science and Engineering, National Chiao Tung University, 1001 Ta Hsueh Road, Hsinchu, Taiwan 300, Repubic of China.*

luchunan@itri.org.tw

Hong-Ching Lin [b], *Ying-Chang Hung* [b], *Tzeng Ya-Chung* [b]

[b]*Materials Research Laboratories, Industrial Technology Research Institute, Bldg. 77, 195 Section 4, Chung Hsing Road, Chutung, Hsinchu, Taiwan 310, Repubic of China.*

Sea-Fue Wang [c,]

[c]*Department of Materials and Mineral Resources Engineering, National Taipei University of Technology, 1, Sec. 3, Chung-Hsiao E. Rd., Taipei, Taiwan 106, Repubic of China.*

Abstract

In this paper, the effects of the silver(I) oxide (Ag_2O) and silver(II) oxide (AgO) additions on the thermal decomposition behaviors of the MOD silver 2-ethylhexanoate addition silver paste were investigated. In this study, low-curing-temperature silver pastes from Ag flake, α-terpineol, silver 2-ethylhexanoate and various amounts of silver(I) oxide and silver(II) oxide were prepared and characterized. The silver oxides usually are applied in optical and magneto-optical data storage. And for high rate battery applications, the silver oxides catalysts are used in cathodes application. Furthermore, the silver oxides have specially heat reduction property[1] at 150 .

Thermal decomposition effects of silver 2-ethylhexanoate for silver oxide catalytic reaction are evidenced by TGA and the decomposition activation energy E_a calculated analysis. The microstructures and resistivities of screen-printed films on alumina substrate after thermally treated were characterized and discussed. The electrical properties of the films were measured using four-point probe method at the curing temperature of 200°C. The results indicate that electrical resistivities of < 20Ω · cm were obtained.

References:

[1] B. V. L'VOV., Thermochimica acta, 333(1999), 13-19.

[2] K. F. Teng and R. W. Vest., IEEE, Trans. Components, Hybrid, and Manufacturing., V CHMT-12(4)(1987), 545-549.

[3] P. H. Kydd: PCT pattern, WO 98/37133 (1998).

[4] C.A. Lu, P. Lin, H.C. Lin and S.F. Wang: to be published in Jpn. J. Appl. Phys.

Figure:

[1] Derivative thermogravimetric analysis of silver 2-ethylhexanoate mixing with (a)no addition, (b)10wt% Ag_2O, (c)10wt% AgO, (d)20wt% Ag_2O, and (e)20wt% AgO.

[2] Resistivities of silver films with additions of no addition, 10wt% Ag_2O, 10wt% AgO, 20wt% Ag_2O, and 20wt% AgO and cured at 200 with different dwell time.

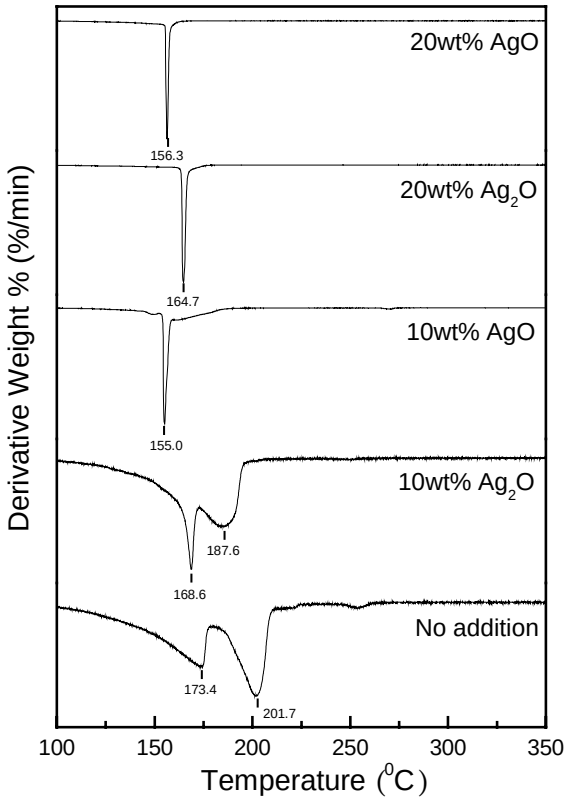


Figure 1

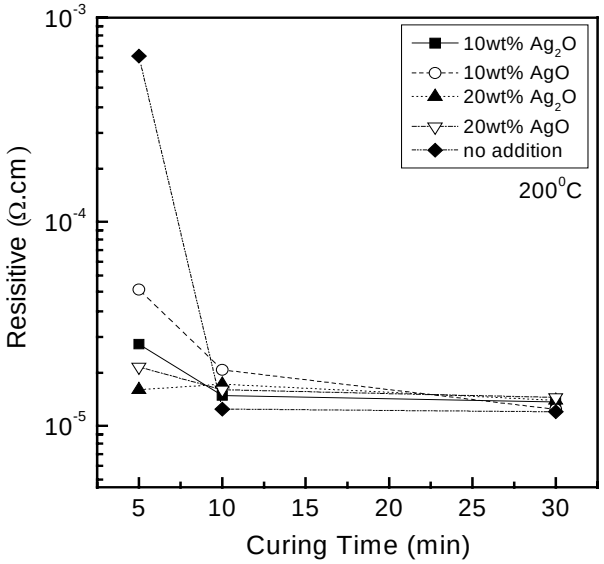

10wt% Ag2O
10wt% AgO
20wt% Ag2O
20wt% AgO
no addition
200°C
Resisitive (Ω.cm)
10-3
10-4
10-5
5
10
15
20
25
30
Curing Time (min)

Figure 2

Poster

ELECTRICAL TRANSPORT MEASUREMENTS ON SELF-ASSEMBLED ORGANIC MOLECULAR WIRES

N. Clément[1], J.-C. G. Flores[2], O.J. Dautel[2], F. Serein-Spirau[2], J.P. Lère-Porte[2], J. J. E. Moreau[2] D. Tondelier[1], D.Guérin[1], S. Lenfant[1], D. Vuillaume[1]

[1] Institut d'Electronique, de Micro-électronique et de Nanotechnologie,(IEMN) – CNRS, BP0069, Avenue Poincare, F-59652 cedex, Villeneuve d'Ascq, France.

[2] Hétérochimie Moléculaire et Macromoléculaire, UMR CNRS 5076,ENSCM, 8 rue de l'Ecole Normale,34296 Montpellier Cedex 05, France.

Nicolas.Clement@iemn.univ-lille1.fr

The electrical properties of nanorods and nanorings designed by supramolecular assemblies of highly π-conjugated oligomers are studied. On the chemist point of view, the best way to build nanostructure is to use molecular building blocks which form supramolecular structures through the use of non covalent interactions [1]. By using this bottom-up technique, it is possible to obtain numerous nanostructures such as nanorods, nanotubes or nanorings [2]. We report here the study of oligo(phenylenethienylene) bisurea which assemble itself in nanorings under specific conditions of dilution.

We synthesized a five benzene and thiophene sequence functionalized with two urea moieties (Fig.1). Thanks to hydrogen bonding [3,4], bisurea compounds self assemble into nanowires or nanorings (depending of the concentration fig 2). UV-visible absorption reveals that 1 forms H-aggregates where the π-oligomers are stacked one over each other. Evidence of H-bond association is observed from infrared spectroscopy, the NH strech region and the amide regions show characteristic peaks of a strong association of the urea moities. In these nano structures the distance between π-conjugated oligomers such as bithiophene is reduced. This leads to a better delocalisation of electron wave functions [4]. Charges injections and delocalisation with Electric Force Microscope (E.F.M) [5] have shown that electrical transport is governed preferentially by positive charges in these nanostructures (Fig.3). Holes are locally injected from the apex of the tip (at +2V for 2 mins) and the EFM image is recorded (at -2V, lift 50nm). In these conditions the darkness of the nanoring (after injections), which corresponds to a negative shift of the cantilever frequency, reveals that holes are injected and delocalized in the entire nanoring. The EFM signal amplitude corresponds to 500-1400 injected holes. Same experiments to inject electrons (at negative tip bias) were unsuccesfull. The delocalisation of positive charges inside these structures confirms that molecules assembled in these objects are well organized.

References:

[1] Lehn J.M Supramolecular Chemistry: Concept and Perspective, VCH Weinheim (1995).
[2] J.-C.G. Flores, O.J.Dautel, F.Serein-Spirau, J.P.Lère-Porte, J.J.E.Moreau, D.Tondelier, D.Guerin, S.Lenfant, D.Vuillaume submitted to JACS.
[3] Van Esch J., De Feyter S., Kellog R.., De Schryver F., Feringa B.L., Chem.Eur.J. **3** (1997) 1238.
[4] Rochefort A., Martel R., and Avouris P. Nanoletters, **2** (2002), 877
[5] Heim, T.; Lmimouni, K.; Vuillaume, D. Nanoletters, **4** (2004), 2145

Figures:

1

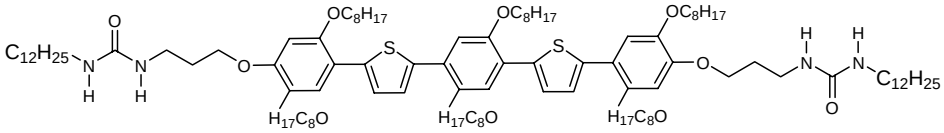


Fig.1 Molecular structure of oligo(phenylenethienylene) bisurea

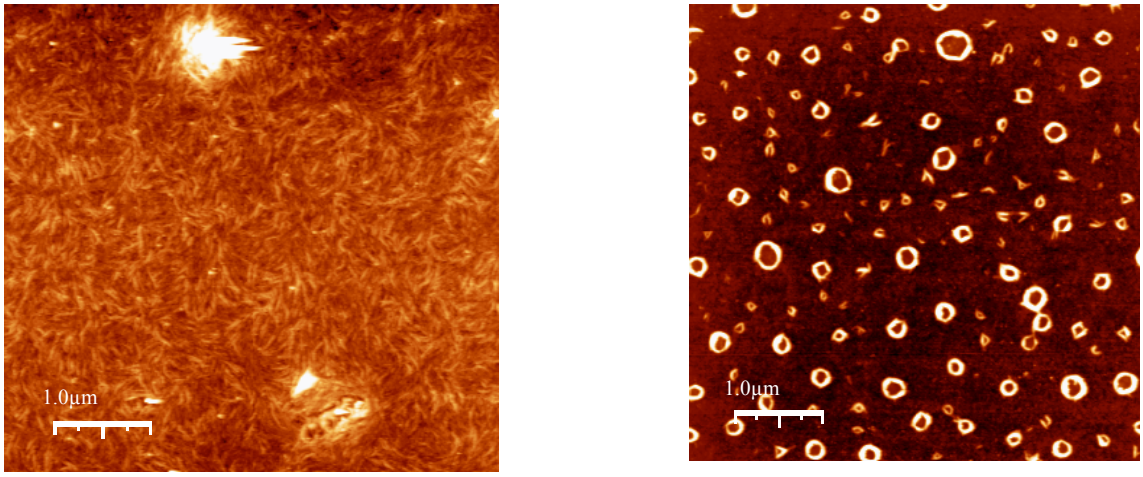


Fig.2 AFM topographic image (tapping mode) of solution-deposited film of the gel of **1** diluted in dichloromethane at 0.5 $g.L^{-1}$; we formed nanowires (SiO_2 substrate) (left) and of solution-deposited film of the gel of **1** diluted in dichloromethane at 0.05 $g.L^{-1}$; we formed nanorings (SiO_2 substrate) (right)

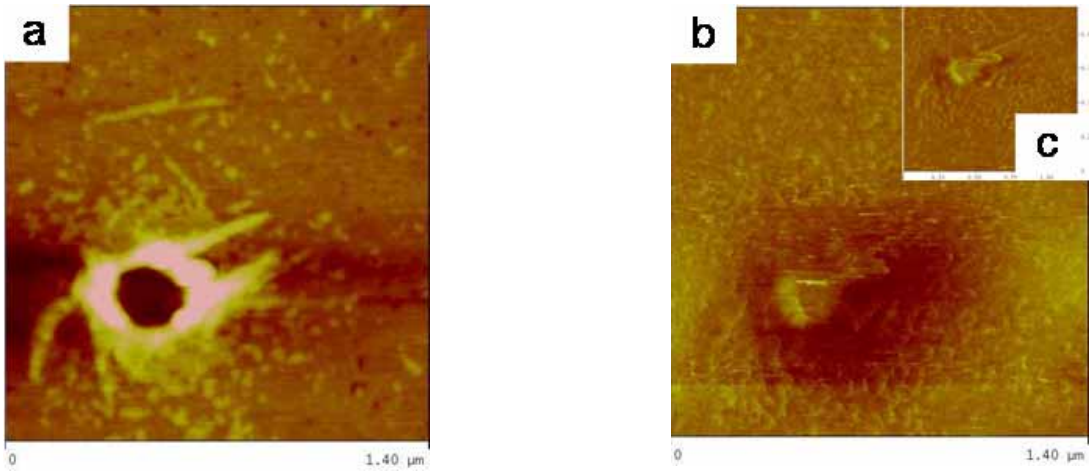


Fig.3 Topographic image of a nanoring after injecting holes (2V for 2 minutes) (a). EFM image corresponding to the topographic image recorded at -2V and lift 50 nm (b). Inset (c) is EFM image before injection.

Tunable supercurrent through single walled carbon nanotubes

J.-P. Cleuziou[1], W. Wernsdorfer[2], V. Bouchiat[3], Th. Ondarçuhu[1], M. Monthioux[1]

1 Centre d'Elaboration des Matériaux et d'Etudes Structurales, CEMES-CNRS,
29 rue Jeanne Marvig, 31055 Toulouse Cedex 4, France
2 Laboratoire L. Néel,
LLN-CNRS, associé à l'UJF, BP 166, 38042 Grenoble Cedex 9, France
3Centre de Recherches sur les Très Basses Température, CRTBT-CNRS,
associé à l'UJF, BP 166, 38042 Grenoble Cedex 9, France
Cleuziou@cemes.fr

Recent progress in improving the contact of single-walled carbon nanotubes (SWNTs) to superconducting nanoelectrodes showed that such molecules can accommodate a superconducting current[1] and behave as gate-controlled Josephson junctions[2]. Such nanotube junctions allow to implement a new type of weak link that can be coupled quantum dots reminiscent to the well studied superconducting single-electron transistor[3] but with the added presence of strong quantum confinement.

In this paper, we present results on the fabrication and low temperature characterization of gated superconducting junctions made of single walled carbon nanotube. We started from a degenerately n-doped silicon substrate with thermally grown SiO_2 layer on top, which was used as a backgate. The silica surface was then functionalized using standard silanization technique. The substrate is then dipped in an aqueous solution of sonicated SWNTs. SWNTs were prepared by the laser vaporation method, then dispersed using surfactant, and nanotube alignment was achieved using a combing technique. The nanotube location was imaged by atomic force microscopy (AFM) and aligned e-beam lithography was carried out to pattern the superconducting contacts made of a bilayer of Aluminum and Paladium (Fig.1). Only devices with a contact resistance below 30 kΩ and no significant gate effect at room temperature were used for our studies.

Our device is based on a SWNT-based Josephson junction, and can be modelled by a quantum dot in between two superconducting leads. The position of the quantum levels can be tuned with a gate voltage V_G. When a quantum level is aligned with respect to the Fermi

energy of the superconducting leads (*on*-state), a supercurrent of a few nanoampers can flow by resonant tunnelling through the SWNT. A detailed study of the *on*-states shows that they occur at the Kondo ridges, in agreement to previous studies. When the quantum levels are far from the Fermi energy (*off*-state), the supercurrent is strongly reduced (typically by a factor of 10 to 10^3) but not completely suppressed. This effect, not seen before[2], might be to due to a Josephson effect via a non-zero electron density between the levels of the CNT. Perspectives toward a phase control of the nanotube superconducting junction will be presented.

References:

[1] Kasumov, A.Y. et al. Supercurrents through single-walled carbon nanotubes, *Science*, **397**, 598-601, (1999).

[2] Herrero-Jarillo, P., van Dam, J.A. & Kouwenhoven, L. P. Quantum supercurrent transistors in carbon nanotubes, *Nature* **439**, 953-956 (2006).

[3] Joyez, P., Lafarge, P., Filipe, A., Esteve, D. & Devoret, M. H. Observation of Parity-Induced Suppression of Josephson Tunneling in the Superconducting Single-Electron Transistor. Phys. Rev. Lett. **72**, 2458-2461 (1994).

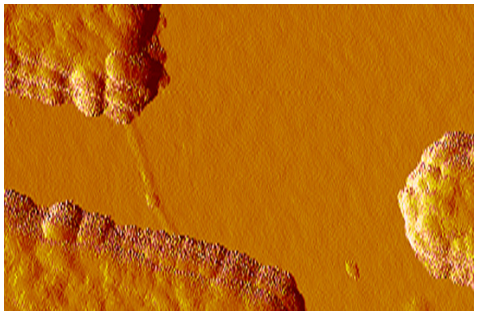


FIG 1. AFM micrograph of a nanotube based Josephson junction connected between Aluminum/Paladium contacts. Lateral gate is on the right side of the image (scale bar = 100 nm)

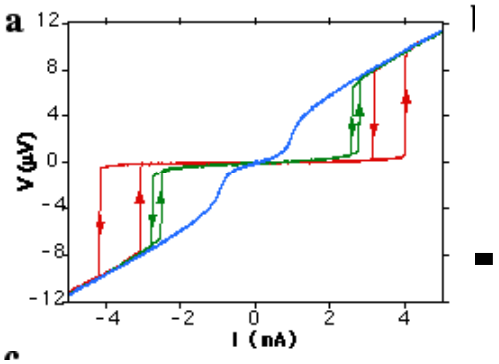


FIG. 2 : Voltage versus current characteristics of a SWNT junction devices measured at 50mK at three different setpoints, showing modulation of the superconducting current

Realization and characterization of vertical self-both-ends-bonded SW nanotubes grown at 550°C in a via-like metal/insulator/metal structure by in situ PECVD

JC Coiffic, M.Delaunay, P.Pantigny and M.Fayolle
CEA Grenoble, 17 av. des martyrs 38054 Cedex 9, GRENOBLE, FRANCE
jean-christophe.coiffic@cea.fr

Single Walled Carbon Nanotubes (SWCNTs) have focused a considerable research effort due to their outstanding properties and potential large application area. They are promising candidates to be integrated in future nanoelectronic devices [1], high sensitivity sensors [2] or used for heat removal in chips [3]. Many studies on SWCNTs devices fabrication are based on a SWCNT ex situ growth at high temperature (>700°C) and a second assembling step is needed. Some studies also report vertical interconnects with in-situ growth [4] but they require a post growth top contact realization. To be compatible with CMOS technology and to achieve manufacturable devices, CNT growth and integration processes have to comply both with low thermal budgets and large scale integration on silicon wafers.

In the following work, SWCNTs are grown and both-ends self connected in situ by a Plasma Enhanced Chemical Vapor Deposition (PECVD) at a low temperature of 550°C. We have developed a vertical via-like metal/insulator/metal structure on 200mm silicon wafers that allows bottom to top metal-to-metal nanotube self interconnections during growth. Morphological and electrical investigations of these interconnects are presented.

The structures used are described on Figure 1**.** A first metal layer is deposited on a highly doped Si wafer as a bottom electrode. A 200nm insulator layer of TEOS-SiO_2 is then deposited by PECVD and covered by a metal layer as a top electrode. Vertical 300-500nm diameter via-hole etching is then performed and stopped on the bottom metal surface. After sub-layer SiO_2 recessing, a Fe based catalyst is sputtered through a shadow mask. The CNT growth is then performed using an Electron Cyclotron Resonance (ECR) PECVD method. After a reduction step, a low pressure CH_4 gas mixture is introduced at 550°C. The final nanotube-connected structure is shown on Figure 2**.**

The process has been optimized to selectively grow single wall CNT. TEM image on Figure 3 shows the high quality structure of as grown 1.4nm diameter SWCNTs. Some SWCNTs bundles are also observed. In order to investigate their electrical behaviour we have performed I(V) and I(time) measurements by applying a sweep bias voltage between the two metal electrodes. Electrical characteristics of the tested devices do not give evidence of any hysteresis or instability which show the structure stability. The breakdown behaviour of such device has been tested by increasing bias voltage up to 40V. Preliminary measurements, as shown on Figure 4, have exhibited very high current density around 10^9 A/cm^2 followed by a sequential current drop until reaching zero with increasing voltage. Each drop can be attributed to a breakdown of one of the SWCNTs that interconnects the metal layers. These results are consistent with those of Dai team [5] who has performed similar measurements on horizontal SWCNTs between two planar electrodes.

Additional electrical measurements are on-going. They will be carried out at different temperatures to investigate the semi-conducting versus metallic behaviour of self interconnected SWCNTs.

Acknowledgments: This work was supported by the Micro and Nanotechnology Program from French Ministry of Research under the grant RTB: Post CMOS moléculaire 200 mm and by the CEA CHIMTRONIQUE program.

References:

[1] R. Seidel, Nano letters, **Vol. 4**, No. 5 (2004) 831-834
[2] K. Besteman, Nano letters, **Vol. 3**, (2003) 727–730
[3] T. Iwai, IEDM 2005
[4] G.S.Duesberg, Nano letters, **Vol. 3** No.2 (2003), 257-259
[5] Y.Li, Nano letters, **Vol. 4** (2004) 317-321

Figures:

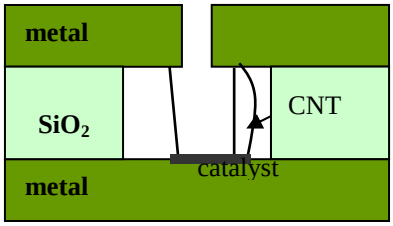


Figure 1: metal/SiO_2/metal structure in which base-growth SWCNTs self interconnect the bottom and top metal electrodes during growth

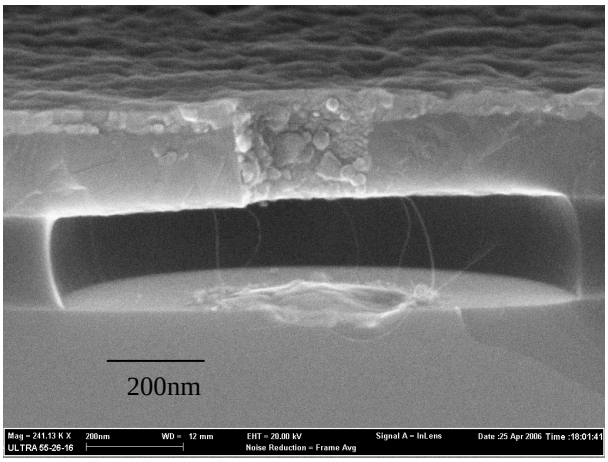


Figure 2: SEM image SWCNTs vertically self interconnected between two metal layers. The SWCNT array is grown at 550°C by an ECR-PECVD method from a CH_4 mixture

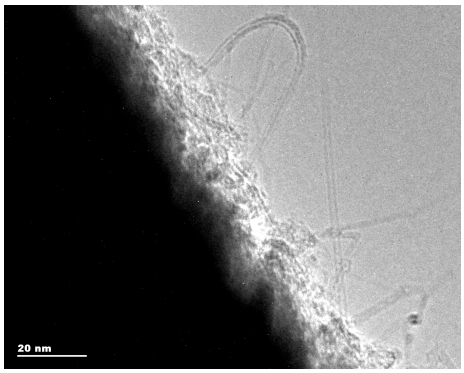


Figure 3: TEM image of SWCNTs grown in the same run as the previous structure. Straight 1.4nm diameter SWCNTs and some bundles (curved) are observed

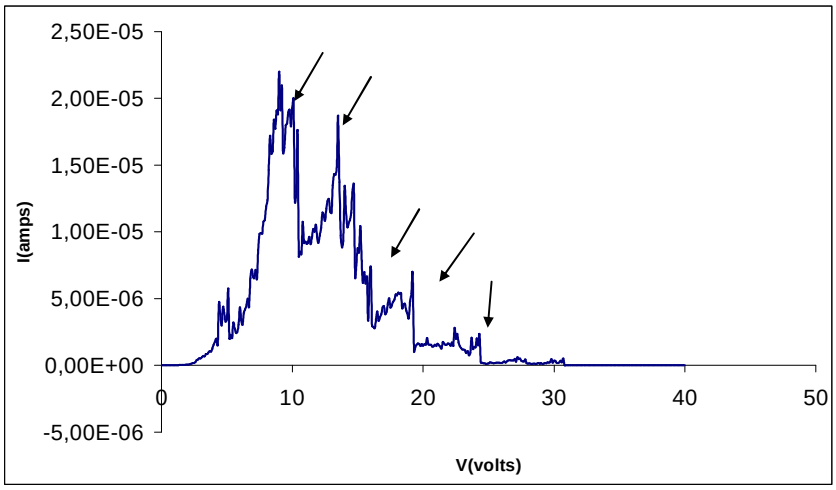


Figure 4: Electrical I(V) measured on the device described in figure 2 with increasing bias voltage between the two metal electrodes. Each arrow points up a current drop which could be related to a single SWCNT breakdown. After all SWCNT has been disconnected the current reaches zero. Considering that only a few SWCNT participate to the current conduction, the maximum current density is estimated to be around10^9A/cm^2

Poster

Nanostenciling and Pulsed Laser Deposition: a Versatile Combination for Parallel Patterning and Prototyping of Functional Materials

C.V. Cojocaru, C. Harnagea, A. Pignolet and F. Rosei
INRS – Énergie, Matériaux et Télécommunications, Université du Québec,
1650 Boul. Lionel-Boulet, Varennes, QC, J3X 1S2, Canada
cojocaru@emt.inrs.ca

Research in semiconductor physics is continuously motivated by the aim of improving device performance, which typically translates into increasing the density of the integrated individual components by decreasing their size. For most applications, nanostructure fabrication is the foremost challenge. In this context top-down and bottom-up fabrication approaches are both being explored to tailor structures at the nanometer scale and to pattern them in a desired fashion [1].

The trend towards device miniaturization has been sustained so far by the constant development of advanced optical lithography for parallel large scale production. For serial, small scale patterning, electron-beam lithography has been proposed as the technique of choice as it is capable of providing the best feature resolution. However, for this technique, production costs become formidable for surface patterning in the nanometer range.

Unconventional patterning approaches have emerged as low–cost, high–resolution alternatives to optical projection lithography. An important approach in this field falls into an area known as "soft lithography" (e.g. μ-contact printing, replica molding). Significant advances in defining nano-patterns have been made by nanoimprint lithography (NIL) as well as by its related variant, step and flash imprint lithography (S-FIL) both showing great potential for the semiconductor industry. All these techniques are based on the mechanical transfer of a pattern from an elastomeric stamp or a hard mold to the substrate by direct contact.

The common drawback of these alternative solutions, as well as of all lithographic approaches, is that they require resist or polymer processing and consequently many chemical, thermal and etch associated steps. Thus, the ability to fabricate arrays of structures with controlled size and shape, with limited interaction with the substrate of choice and using a minimal number of processing steps, is an ongoing challenge in nanotechnology.

Controlled deposition through a miniature shadow–mask or nanostenciling has been recently revisited and considered as a suitable method to grow directly patterned nanostructures, in a single step, either in dynamic or static modes [2], [3]. While offering unlimited freedom in choosing the physical vapor deposition method, pattern formation using nanostencils turned out to be a straightforward, low–cost and reliable method. Moreover, it drastically reduces the number of processing operations with respect to resist–based lithography.

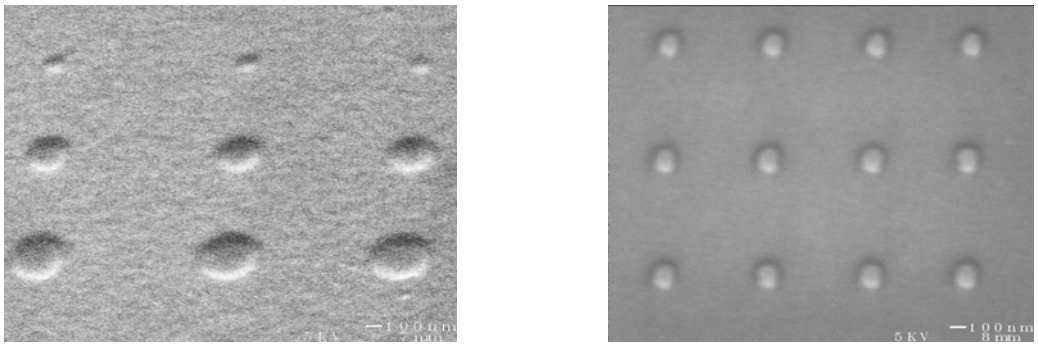
This approach that we are currently expanding on and investigating in detail is in principle directly applicable to the deposition of any material on any substrate [4], [5]. We will describe our recent work on the fabrication and patterning of three major classes of materials, namely metals (e.g. Pt, Cr), semiconductor hetero–structures (Ge/Si) and complex functional oxides (ABO_3 perovskite-type ferroelectrics) by nanostenciling and pulsed laser deposition (PLD). PLD emerged as a convenient deposition method because of its high versatility in growing stoichiometric thin films on a wide range of substrates. Moreover it offers the possibility of fine-tuning and controlling deposition parameters and therefore, the properties of the films and structures.

The combination of stenciling and PLD allows for the accurate organizing of structures into desired architectures. Selective deposition is obtained by interposing a sieve with apertures down to 100 nm between source and substrate. And, the material deposited through the stencil mask conserves the desired functionality even at the level of the individual nanostructures (e.g. piezo and ferroelectricity at the nanoscale proven by piezoresponse force microscopy (PFM)).

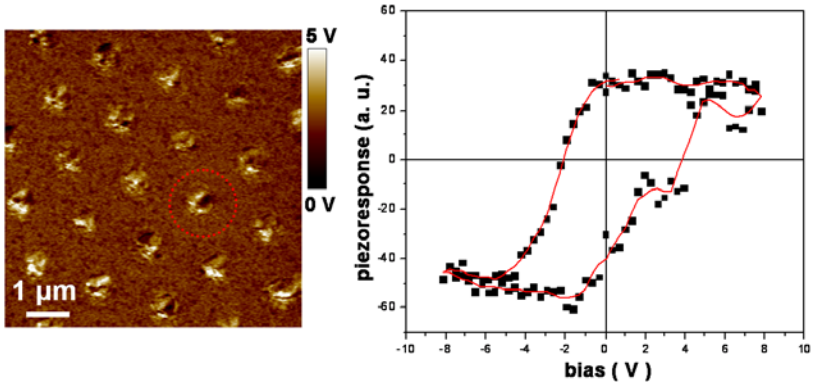
We will also discuss the application of a nanoscale multi-level-stenciling approach which may enable rapid prototyping of functional heterostructures composed of stacks of different materials (e.g. metal-oxide-metal and multiferroic structures grown by sequential depositions). The morphology and composition of theses nanostructures were characterized by SEM, AFM, XRD and XPS techniques and their local ferroelectric properties were detected using PFM.

The application of this process is meant for research (e.g. studying the size effects on the functional properties of the structures) but also represents a promising universal "tool" for parallel deposition of high-resolution and purity nanostructures of functional materials under high and ultra-high vacuum. Nanostenciling can be performed under these controlled conditions and is suitable for parallel prototyping of fragile or functionalized surfaces. Further developments of this approach are expected to lead to novel architectures and devices, also providing solutions for critical patterning issues not yet solved.

[1] C.V. Cojocaru, F. Ratto, C. Harnagea, A. Pignolet and F. Rosei, Microelectron. Eng. 80, (2005), 448
[2] J. Brugger, J.W. Berenschot, S. Kuiper, W. Nijdam, B. Otter and M. Elwenspoek, Microelectron. Eng. 53, (2000), 403
[3] R. Luthi, R.R. Schlittler, J. Brugger, P. Vettiger, M.E. Welland, and J.K. Gimzewski, Appl. Phys. Lett.75, (1999), 1314
[4] C.V. Cojocaru, C. Harnagea, F.Rosei and A. Pignolet, M. van den Boogaart, J. Brugger, Appl. Phys. Lett86, (2005), 183107
[5] C.V. Cojocaru, C. Harnagea, A. Pignolet and F. Rosei, IEEE, Transactions on Nanotechnology, (2006), in press



SEM micrographs of ordered Ge structures (100-350 nm in width) on Si(100) (left) and $BaTiO_3$ structures (125 nm in width) on Nb doped $SrTiO_3$ (100) oriented substrates (right) deposited at room temperature



Piezoresponse domain image (left) of patterned ferroelectric $BaTiO_3$ on 0.1% Nb doped $SrTiO_3$ and piezoresponse hysteresis loop obtained from an individual structure

IMPROVEMENT OF SURFACE HARDNESS IN NITROGEN IMPLANTED V-5%Ti ALLOYS: INFLUENCE OF THE PREFERENTIAL SPUTTERING IN THE ELEMENTAL COMPOSITION DETERMINATION.

I.Colera[*], E. Roman[**] , J.A. García[***], D. Cáceres[*] and J.L. de Segovia[**]

[*]*Universidad Carlos III de Madrid, Dpto de Física, Avda de la Universidad 30, Leganés 28911 Madrid.*
[**]*Instituto de Ciencia de Materiales de Madrid, CSIC, Cantoblanco, 28049 Madrid*
[***]*AIN-Centro de Ingeniería Avanzada de Superficies, Cordobilla, 31191- Pamplona, Spain*
icolera@fis.uc3m.es

Among the binary vanadium alloys, the V-5wt% Ti composition is interesting because of its low ductile-brittle transition temperature, very low void swelling and high creep resistance[1]. The origin of these useful properties is attributed to the microstructure of defects induced by the Ti atoms.

Ion implantation represents one surface treatment allowing the wear resistance of materials to be enhanced and their tribological properties to be improved. For metals, ion implantation is effective under high doses, exceeding 10^{16} cm^{-2} and ion energies exceeding 20 keV [2].

The main aim of this work has been to study the influence of the preferential sputtering in the elemental composition of nitrogen implanted V-5at%Ti at high energy and to characterize the improvements achieved in the tribological performance of this alloy.

Vanadium alloy ball shaped with a Ti concentration of 5 at% was produced from 99.9% V and 99.5% Ti by repeated arc melting in a high-purity He atmosphere and was annealed at 1573 K for 6 hours. Samples were prepared by cutting discs and the surfaces were polished with 1 μm diamond past. V-5%Ti sample was implanted with atomic N^+ ion at 100 KeV (5×10^{17} cm^{-2}), and with two successive molecular N_2^+ implantation at 100 KeV (9×10^{16} cm^{-2}) and at 50 KeV (4.4×10^{16} cm^{-2}). Using a simulation computer program flat profiles for the nitrogen concentration with values of 40% were obtained.

To obtain experimental depth profile for the relative concentration of elements on these vanadium alloys, surface were etching layer by layer with incident argon ions at 3 keV of energy and was studied by X-ray photoelectron Spectroscopy (XPS) and Auger electron Spectroscopy (AES) techniques. However, changes of surface-layer composition were obtained when surface was bombarded with 1.4 keV Ar^+ incident energy. The selective sputtering of carbon and oxygen atoms is energy depending and could change a factor of a 50%. However, the AES intensity corresponding to nitrogen, vanadium and titanium does not decrease in the same amount and preferential sputtering is not so evident at these two energies. By the contrary, Ar^+ ion sputtering at 6 keV previously reported [3] estimated a value of 1.4 of the nitrogen selective sputtering coefficient relative to titanium. Consequently different element concentration is obtained when studying samples at different Ar^+ ion sputtering energy. XPS spectra from the core electron level and valence bands are discussed.

In the present work, high energy nitrogen implantation (> 50 keV) samples [4] was studied (i) at maximum indentation loads of 2, 5, 25, 100 and 750 mN, (ii) the friction coefficient at contact pressure of 0.4. 0.5 0.6 and 0.65 GPa and (iii) the wear coefficient (m^2/N) at load of 0.25 ,0.5, 0.75 and 1N. Hardness increase is associated with the N implantation, suggesting nitride precipitation. XPS structure of the C_{1s}, N_{1s}, V_{2p} and Ti_{2p} obtained at different depths from the surface were deconvoluted using Gaussians after background subtraction. Nitride formation is studied and compared with previously reported values for V-N [5] and Ti-N [6].

The improvements achieved in the tribological performance of V-5 at%Ti alloy ion implanted with nitrogen at high energy are compared with those previously reported at low energy (1.2 keV) and at a temperature between 700-800 K [7],[8]. Hardness enhancement of these thermally activated nitrogen implanted alloys were due to the increasing of both, the thickness of the diffusion layer and the relative nitrogen content in the solid solution.

References:

[1] T. Leguey, A. Muñoz, and R. Rami. Journal of Nuclear Materials 275 (1999) 138-145.
[2] J.-K. Hirvonen, Ann. Rev. Mater Sci 19 (1989) 401-417.
[3] M.V. Kuznetsov, Ju.F. Zhuravlev, V.A. Zhilyaev and V.A. Gubanov. Journal of Electron Spectroscopy and Related Phenomena, 58 (1992) 1-9.
[4] García JA, ,Sánchez R, Martínez R, Medrano A , Rico M, Rodríguez R ,Varela M, Colera I, Cáceres D,Vergara I, Ballesteros C, Roman E, de Segovia JL. Surface & Coatings Technology 158-159 (2002) 669-673.
[5] Wiame H, Bois L., Lharidon P., Laurent Y., Grange P. Solid State Ionics 101-103 (1997) 755-759.
[6] Zhao X-A, Ong C.W., Tsang Y C , Choy C L and Chan P W . J. Vac. Sci. Technol. A 15 (1997) 99-106.
[7] García JA, Rodríguez R,Sánchez R,Martínez R,Varela M,Cáceres D,Muñoz A,Vergara I, C. Ballesteros. Vacuum 67 (2002) 543-550.
[8] García JA, Fuentes GG, Martínez R, Rodríguez R J, Abrasonis G, Riviere JP, Rius J. Surface & Coatings Technology 188-189 (2004) 459-465.

FINITE-SIZE EFFECTS IN THE ELECTRICAL RESISTANCE OF SINGLE BISMUTH NANOWIRES

T.W. Cornelius[1], M.E. Toimil-Molares[1], S. Karim[2], R. Neumann[1]
[1]Gesellschaft für Schwerionenforschung (GSI), Planckstr. 1, 64291 Darmstadt, Germany
[2]Fachbereich Chemie, Marburg University, Hans-Meerwein-Str., 35032 Marburg, Germany
th.cornelius@gsi.de

Objects whose size becomes comparable to intrinsic length scales, i.e., the electronic mean free path l_e and Fermi wavelength λ_F, classical and quantum size effects are expected [1]. In the semimetal bismuth both are large compared to conventional metals, making it an ideal material for studies on the nanoscale. In particular, the classical size effects cause an increase of the electrical resistivity originating from electron scattering processes from the wire surface [2] as well as from grain boundaries [3]. In order to separate both processes, it is necessary to fabricate a series of nanowires, their structure varying from poly- to single-crystallinity.

Bismuth nanowires are deposited electrochemically in ion track-etched polycarbonate membranes [4]. Single wires are prepared in single-pore membranes and subsequently contacted electrically while left embedded in the template [5]. The specific electrical resistivity ρ is affected by the fabrication conditions of the wire. The wires are constructed by smaller grains when deposited at lower temperatures T and higher potentials U. Due to the increased density of grain boundaries for such wires, ρ increases for wires created at lower T and higher U (Fig. 1). The wire resistance is a non-monotonic function of the temperature (Fig. 2). It rises, passes through a maximum, and declines when cooling from room temperature down to 20 K. The resistance maximum shifts to higher T for diminishing diameter and the maximum becomes the higher the smaller the mean grain size is. The non-monotonic $R(T)$ behaviour originates from the saturation of l_e caused by finite-size effects, in contrast to bulk bismuth where it increases from 100 nm to 400 µm when cooling down from 300 to 4 K [6].

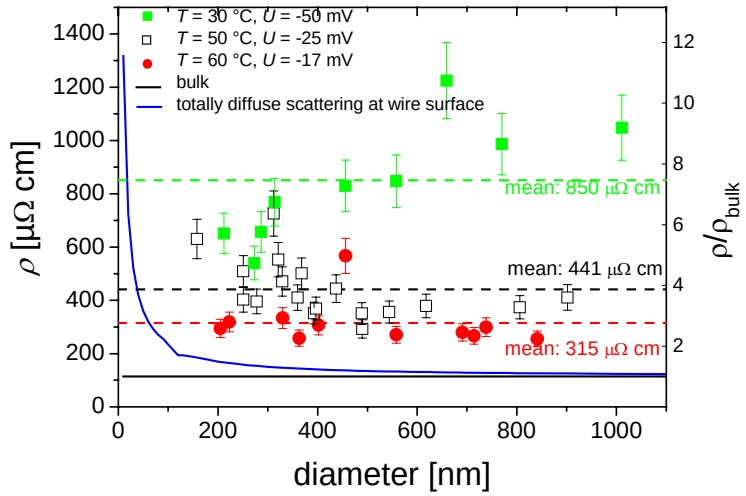


Fig. 1: Specific electrical resistivity as a function of diameter of single bismuth nanowires prepared under three different conditions.

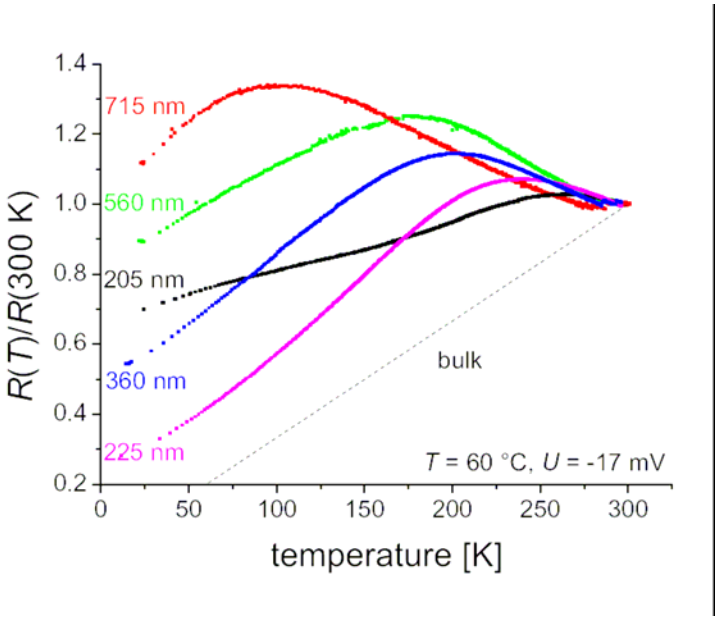


Fig. 2: Electrical resistance of single bismuth nanowires with different diameters as a function of temperature.

References

[1] V.B. Sandormirskiĭ, Sov. Phys. JETP **25** (1967) 101
[2] R.B. Dingle, Proc. R. Soc. London A **201** (1950) 545
[3] A.F. Mayadas, M. Shatzkes, Phys. Rev. B **1** (1970) 1382
[4] T.W. Cornelius, J. Brötz, N. Chtanko, D. Dobrev, G. Miehe, R. Neumann, M.E. Toimil-Molares, Nanotechnology **16** (2005) S246
[5] M.E. Toimil-Molares, N. Chtanko, T.W. Cornelius, D. Dobrev, I. Enculescu, R.H. Blick, R. Neumann, Nanotechnology **15** (2004) S201
[6] S.B. Cronin, Y.-M. Lin, O. Rabin, M.R. Black, J.Y. Ying, M.S. Dresselhaus, P.L. Gai, J.-P. Minet, J.-P. Issi, Nanotechnology **13** (2002) 653

MAGNETIC PROPERTIES OF NICKEL-ZINC FERRITE NANOPARTICLES SYNTHESIZED BY COPRECIPITATION

V. Corral-Flores[a], D. Bueno-Baqués[a], F. Paraguay-Delgado[a], C. E. Botez[b], R. Ibarra-Gómez[a], R. Ziolo[c]

[a] Centro de Investigación en Materiales Avanzados, S. C., Miguel de Cervantes 120, Chihuahua, Mexico

[b] University of Texas at El Paso,500 West University av., El Paso, USA

[c] Centro de Investigación en Química Aplicada, Blvd. Enrique Rayna 140, Saltillo, Mexico

veronica.corral@cimav.edu.mx

Nickel-zinc ferrite is a soft magnetic material having low magnetic coercivity and high resistivity values, which makes it an excellent choice as a core material for power transformers [1]. Eventhough zinc ferrite is paramagnetic, Zn substitutions on inverse spinel ferrites, e.g. nickel, cobalt or manganese ferrites, enhance the magnetic properties, being the reason of the technological importance of mixed ferrites in today's market [2].

When the particle size of the ferrite becomes very small, in the order of a few nanometers, the magnetic characteristics are strongly affected due to the influence of thermal energy over the magnetic moment ordering, originating the superparamagnetic phenomenon [3]. Wet chemical routes of synthesis can fulfill the requirements of single phase, single domain nanometer ferrite particles production, while being suitable for the synthesis of mixed ferrites [4].

The influence of zinc substitution on nickel ferrite was studied in this work. $Ni_{1-x}Zn_xFe_2O_4$ (x = 0, 0.25, 0.50 and 0.75) system was synthesized by the coprecipitation technique, using aqueous solutions of constituent ions. A digestion step at 90°C was performed to crystallize the spinel cubic phase, avoiding the sintering process, which could lead to a substantial increase in the particle size.

Single phase spinel structure was confirmed by x-ray diffraction. Transmission electron microscopy images revealed a particle size ranging from around 3 to 10 nm, increasing with the content of Zn, which is consistent with the crystallite size estimated from x-ray pattern pick width. To investigate the magnetic properties of the nickel-zinc ferrite system, hysteresis, AC susceptibility and FC/ZFC thermoremanent measurements have been made using a SQUID magnetometer. The magnetization was measured at low and room temperature, finding almost the same values at 2, 6 and 10K. All compositions showed ferromagnetic behavior at 2K, while only the sample $NiFe_2O_4$ (x=0) showed superparamagnetism at 60 and 295K.

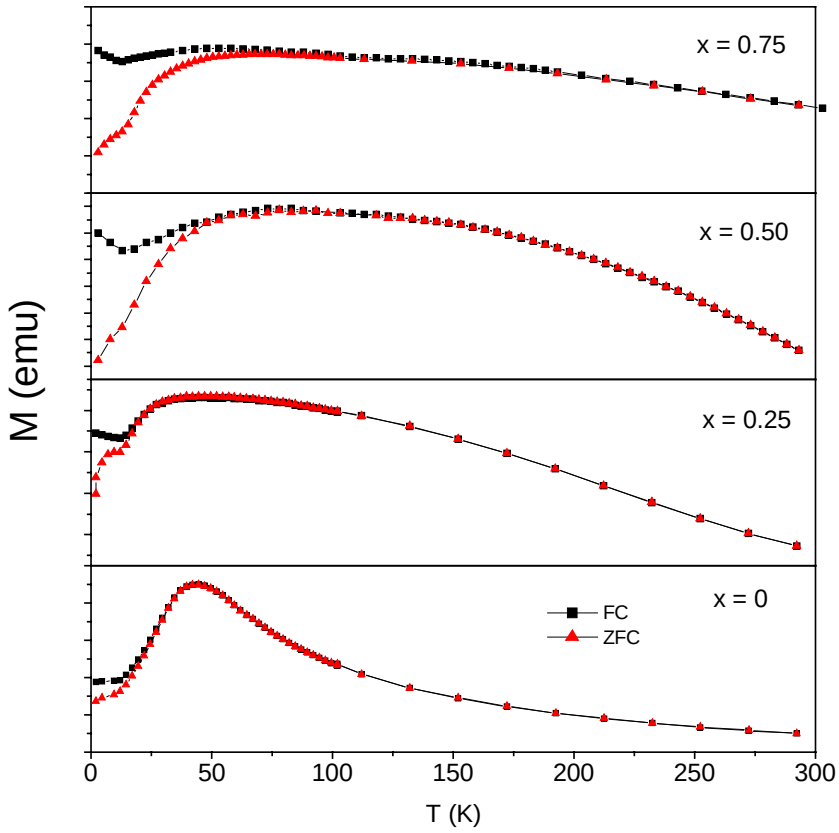
Fig. 1 shows the FC/ZFC curves measured at a DC field of 150 Oe. This curves revealed a typical superparamagnetic behavior for samples with a low content of Zn ferrite, with broad peaks which is an indicative of a width particle size distribution. The blocking temperature (T_B) increases with the increment on Zn content. This was confirmed by the AC susceptibility measurements. The increase of T_B in samples with a larger Zn content could be related to the presence of collective switching-over regions, as a result of a broad grain size distribution or the formation of nanoparticles clusters [5]. This magnetic behavior is discussed in detail.

References:

[1] Authors, Journal, **Issue** (Year) page.
[1] S. K. Date, P.A. Joy, P.S. Anil Kumar, B. Sahoo, W. Keune. Phys. Stat. Sol. (c) **1** 12 (2004) 3495-3498
[2] R. A. McCurrie. Ferromagnetic materials, structure and properties. (Academic Press, 1994), p. 137
[3] Joong-Hee Nam, Sang Jin Park and Won Ki Kim. IEEE Trans. on Magn. **39** 5 (2003) 3139-3141
[4] Candace T. Seip, Everett E. Carpenter, Charles J. O´Connor, Vijay T. John and Sichu Li. IEEE Trans. on Magn. **34** 4 (1998) 1111-1113
[5] P. Podar, H. Srikanth, S.A. Morrinson, E.E. Carpenter, J. magn. Magn. Mat. **288** (2005) 443-451

Figure 1:

Figure caption: Magnetization as a function of temperature of $Ni_{1-x}Zn_xFe_2O_4$ samples. Both field cooled (FC) and zero field cooled (ZFC) modes were measured at 150 Oe.



CURRENTS IMAGING IN OPEN QUANTUM DOTS IN THE INTEGER QUANTUM HALL TRANSPORT REGIME

Alessandro Cresti
NEST-CNR-INFM and Scuola Normale Superiore
Piazza dei Cavalieri 7, I-56127 Pisa, Italy
cresti@df.unipi.it

Open dots represent a prominent class of quantum interferometers, due to their accurate realization in high mobility AlGaAs/GaAs-based two-dimensional electron gases. Experimentally, open dots have the advantages of nearly open constrictions that cancel Coulomb blockade effects; moreover the geometric width of the region where electrons flow can be easily tuned by the gate potentials.
In the integer quantum Hall transport regime, the current is supported by states located at the edges of the wire. When this current reaches the first constriction of the open dot, it is partially transmitted and partially reflected. Sailing along one edge of the dot, electrons reach the second constriction. Part of them is transmitted while the other comes back on the other edge of the dot. The path enclosed by the current inside the dot is threaded by a magnetic field and generates Aharonov-Bohm oscillations [1]. Their frequency depends on the effective area encircled by the edge states, which is in principle regulated by the gate potential, the surface electron density and the magnetic field.
In the present theoretical analysis, I simulate the above outlined phenomenology, evidencing the presence of Aharonov-Bohm oscillations (Fig.1), and providing maps of local microscopic currents (Fig.2) and local density-of-states (Fig.3). The direct visualization of the path followed by electrons allows to gain information on the flux linkage, and, at least in principles, to design properly shaped open dots.
The simulations are based on the Keldysh Green's function formalism [2], that permits to obtain the local currents, the local density-of-states and density-of-occupied-states, and the local chemical potential. I adopt the tight-binding framework in order to have an accurate description of the geometric shape of the device and of its potential profile; this choice allows us to exploit the decimation-renormalization technique [3], that greatly reduces the cumbersome numerical calculations.

References:

[1] F.E. Camino, W. Zhou, and V.J. Goldman, Phys. Rev. B, **72** (2005) 155313.

[2] A. Cresti, R. Farchioni, G. Grosso, and G. Pastori Parravicini, Phys. Rev. B, **68** (2003) 075306.

[3] G. Grosso, S. Moroni, and G. Pastori Parravicini, Phys. Rev. B, **40** (1989) 1238.

Figures:

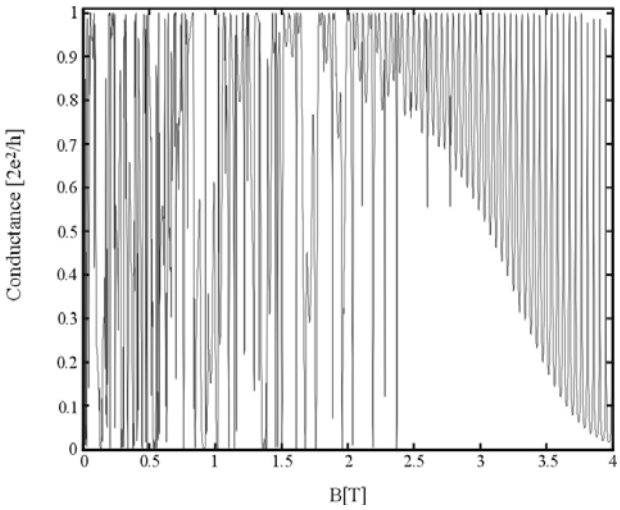


Fig.1: Conductance of the open quantum dot as a function of the magnetic field intensity, for a fixed gate potential. Notice the presence of an irregular region on the left and of a regular region with periodic Aharonov-Bohm oscillations on the right side of the figure.

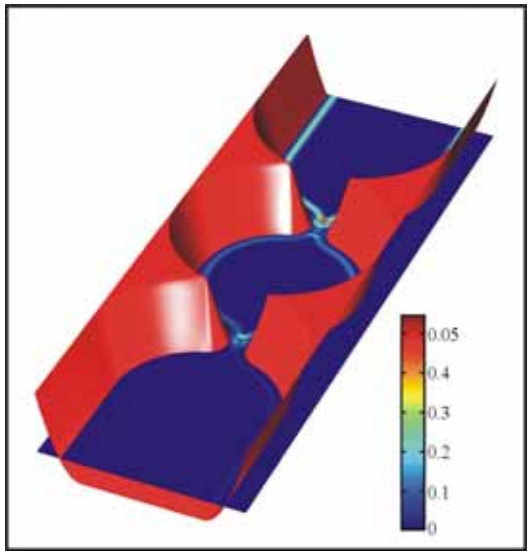


Fig.2: Map of local spectral transport currents for B=2 T. Electrons follow a closed circular path inside the dot, thus giving rise to Aharonov-Bohm oscillations. The unit on the color scale is the quantum of spectral current i_0=2e/h.

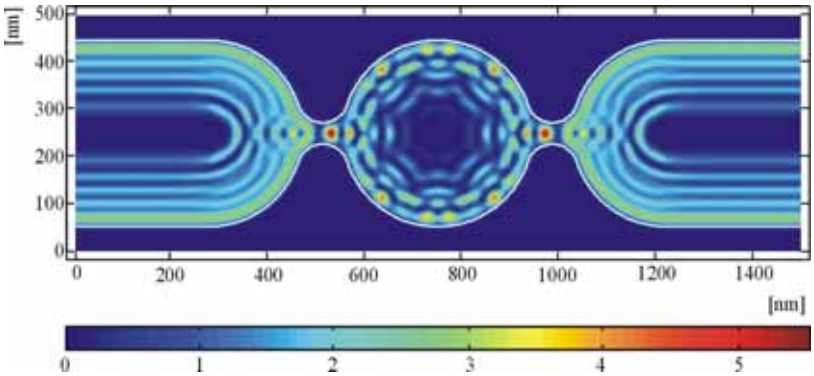


Fig.3: Local density-of-states in the irregular region (left part of Fig.1), for B=1T. Inside the open dot a spread, field dependent state is clearly visible. On the leads several edge states are present. The unit on the color scale is eV^{-1}.

Poster

FABRICATION OF NANO OBJECTS USING FOCUSED ION BEAM INDUCED DEPOSITION.

Hervé Dallaporta, Frédéric Bedu

CRMC-N-CNRS 163 Avenue de Luminy case 901 13288 Marseille Cedex 9 France,

dallaporta@crmcn.univ-mrs.fr

1 – Introduction

We will show that using the local decomposition of molecules induced by focused ion beam (FIBIB), it is possible to constructed nanostructures on surfaces. The demonstration of these possibilities has been done using the decomposition of phenanthrene molecules ($C_{14}H_{10}$) in a dual beam machine for which we have developed our own electronic beam command. Various shape objects can be obtained like auto support carbon films, dot nets, sharp tips, nanoinjector, tubes….

2 –Experimental setup:

Focused Ion Beam Induced Deposition (FIBID) is a techniques that allow the local decomposition of a precursor absorbed on the surface. The nanofabrication station is a commercial scanning electron microscope coupled with a Ga^+ ion column. The SEM provide electrons from a tungsten filament (V=3kv to 30kV Ip = 1 to 10nA). The ion column provides Ga+ ions at 30 Kv with a resolution of 10nm. To get a deposit, one need first the injection of gas (precursor) in the area of the beam focus point keeping the pressure in the workstation chamber compatible with the electron and ion guns. This is obtained by using a temperature control reservoir coupled to a line ended by capillary. The position of the capillary is computer control by a 3 axis microstage. The precursor we used for the construction is the phenanthrene ($C_{14}H_{10}$). The phenanthrene is a powder at room temperature with a vapor pressure at 1.13 hPa at 118°C. It has been used by different authors for the building of nanoobjects (Matsui, Raith..). To construct objects of different shapes one needs a way of driving the beam on the surface. It is known that in FIBID the ion beam needs to be scanned at relative high frequency to prevent the milling by the high energy impinging ions and to allow the replacement of the absorbed molecules of precursor on the surface. To get a versatile beam command that allows the driving of the beam, we have designed our own computer command. This application relies on a commercial hardware data acquisition board with 2 analog outputs at 1.25 Mech./s , 8 digital Inputs/outputs and 8 analog inputs at 1,25Mech./s. This board is driven by a software written in graphical language so that it can be easily adapted to future needs. It has been designed to allow the modification of the beam command in real time. Since it is possible to observe with the SEM the construction of the object during FIBID, we can modify the parameters during the deposition process to get the shape we want.

3 **Results:**

To illustrate the possibility of this technique we give few examples on the figures bellow. The first example is a FIBID carbon film deposited over a hole going through the support on which we have deposited thin FIBID W wires Fig N°2 (a). The image obtained by TEM demonstrated that both deposits are transparent toward high energy electrons. It could be a nice way to get heated supports for TEM. Figure N°2 gives the SEM image of a dot network obtained by FIBID in 10mn. The dots are 150nm wide separated by 75nm. It possible with this to created on few square micrometers a structuration of the surface by object around hundred nanometers. Figure N°4 give the possibility offered by this technique to design a mask on auto supported carbon membrane by FIB milling. We are able to make grooves of 50nm width separated by 80nm.

3 – Conclusion

These results open a wide range of applications like nanostructuration of surfaces, new support for TEM, tip for proximal probe, mold for microfluidic or nano imprint. We think that diamond like carbon has many interesting properties (tribologic properties, biocompatibility, mechanical properties, hardness…). Nanoobjects made of carbon like diamond can be used in very different applications in nanoscience.

References:

[1] Claudia Menozzi, Gian Carlo Gazzadi, Andrea Alessandrini and Paolo Facci *Ultramicroscopy, 104, Issues 3-4, October 2005, 220*

[2] A. Perentes, A.Bachmann, M. Leutenegger, I. Utke, C. Sandu and P. Hoffmann *Microelectronic Engineering, 73-74, June 2004, 412*

[3] J. Fujita, M. Ishida, T. Ichihashi, Y. Ochiai, T. Kaito and S. Matsui *Nuclear Instr. and Meth. in Phys. Res. B: Beam Interactions with Materials and Atoms, Volume 206, May 2003, Pages 472-477*

Figures:

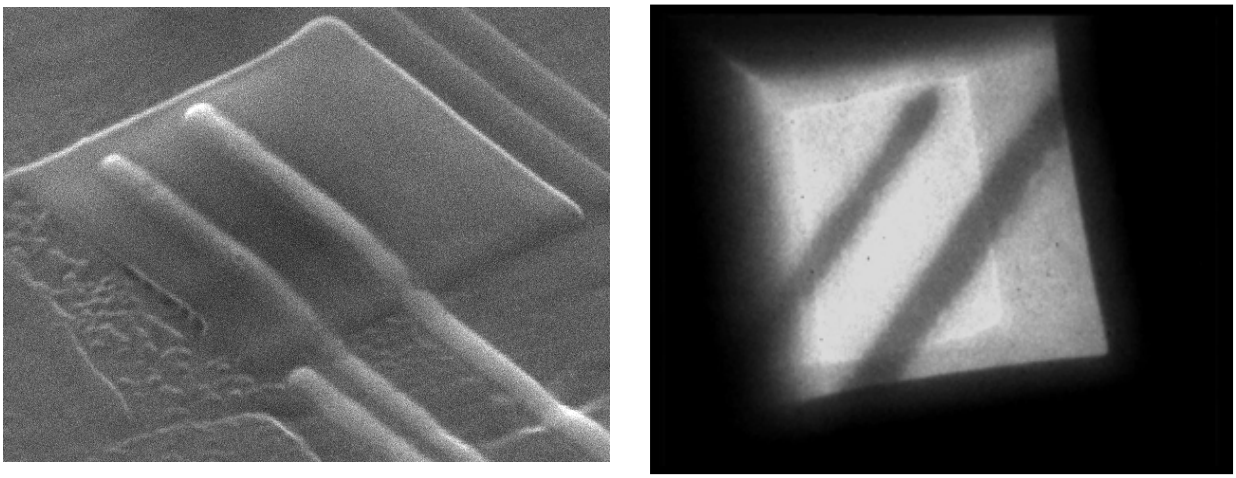


Fig N°1 :(a) SEM image and (b) TEM image of FIBID deposits

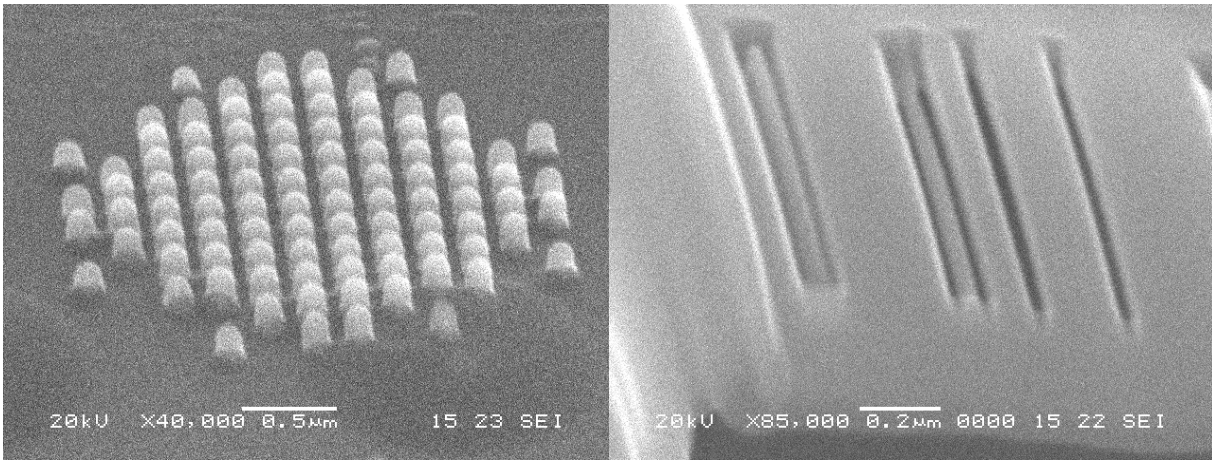


Fig N°3 Network of dots

Fig N°4 Mask designed by FIB milling of a carbon membrane

THE ACOUSTICAL ANALOG OF THE GIANT MAGNETORESISTANCE EFFECT IN MAGNETIC SANDWICHES

L.V. Dekhtyaruk,
Sumy State University, R. Corsakova Str., 2, Sumy, 40007, Ukraine
dekhtyaruk@mail.ru

The magnetic "sandwiched" structures (MS) consisting of magnetic layers separated by the ultrathin non-magnetic spacer exhibit the giant magnetoresistance (GMR) effect: the electrical resistance changes essentially when the magnetic field is applied to the sample. The GMR effect is due to the spin-dependent electron scattering at the interface and in the bulk of the sample. The same scattering mechanisms will play an essential role for other kinetic effects, e.g., under the electron absorption of ultrasonic waves that propagate along the interlayer interface. In this communication we investigate theoretically the effect which is the acoustical analog of the GMR effect in the magnetic "sandwich". The semi-classical approach within a two-current model was used. The model describes the longitudinal electron transport in magnetic layers within the assumption that both the interlayer electron scattering and the bulk electron scattering are spin-dependent. Within this model we obtain the general formula for the coefficient of acoustic energy absorption, Γ, at an arbitrary ratio between the thicknesses of the layers assuming that the total magnetization of the magnetic layers is vanishing. We found that the non-monotonic dependence of the $(\Gamma(0)-\Gamma(H))/\Gamma(H)$ as function of the ratio between layer thicknesses is due to the spin dependency of the electron scattering. The effect increases either with increasing of the specular reflectivity of the interlayer interfaces or with increasing of their transparency. The decreasing of the thicknesses of the layers also leads to the increasing of the effect.

EVIDENCE OF GOLD ON LATERAL SURFACES OF GOLD CATALYZED SILICON NANOWIRES

M.I. den Hertog[1], J.L. Rouviere[1,] F. Dhalluin[2, 3], P. Gentile[1], P. Ferret[3], T. Baron[2]
(1)DRFMC/SP2M, CEA/DRFMC (2)LTM, CNRS UMR 5129 (3)LETI/DOPT
(1,2,3)CEA-Grenoble, 17 rue des Martyrs, 38052 Grenoble Cedex 9, France
martien.den-hertog@cea.fr

Silicon nanowires have attracted a lot of interest recently, as they are regarded as key building blocks of future electronic and opto-electronic devices. Recent publications have clarified a great deal about the role of the gold catalyst particle and its influence on the final shape of the wires [1, 2, 3].
Hannon et al [2] already showed convincing indirect evidence that gold, diffusing from the catalyst particle, is also present on the lateral sides of the wires and the substrate. Here we present direct evidence of gold on the lateral sides of the wires by means of STEM (Scanning Transmission Electron Microscopy) images in combination with EDX (Energy Dispersive X-ray) analysis measurements (fig.1) and SEM (Scanning Electron Microscopy) images.
Silicon nanowires were grown by the Vapour-Liquid-Solid (VLS) mechanism using gold as the catalyst and silane as the precursor. Measurements were realized on a FEI TITAN microscope working at 300kV.
Kodambaka[4] et al showed that the diffusion of gold during growth depends strongly on the presence of oxygen. The present results seem to be specific to the Au-catalyzed VLS growth system without the presence of oxygen. As we do not work under UHV conditions, we can not exclude the possibility of traces of oxygen present during growth, however it is clear that the amount is insufficient to block the diffusion of gold over the wire surface. An approximate calculation shows that the nanowire sidewalls are covered by one monolayer of gold during growth. After growth has finished, de-wetting of the monolayer occurs and a pattern of homogeneously sized gold nanoparticles is formed. This implies a constraint on the nanowire length and a tapered shape, as the volume of the catalyst particle decreases during growth. Furthermore, the presence of gold on the nanowire sidewalls will undoubtedly have an effect on the optical and electrical properties.

References:

[1] Ross, F. M.; Tersoff, J.; Reuter, M. C.; *Physical Review Letters*, **95** (2005) 146104
[2] Hannon, J. B.; Kodambaka, S.; Ross, F. M.; Tromp, R. M.; *Nature*, **440** (2006) 69
[3] Schmidt, V.; Senz, S.; Gösele; U.; *Applied Physics A*, **80** (2004**)** 445
[4] Kodambaka, S.; Hannon; J. B.; Tromp, R. M.; Ross; F. M.; *Nano Letters*, **6** (2006**)** 1292

Figures:

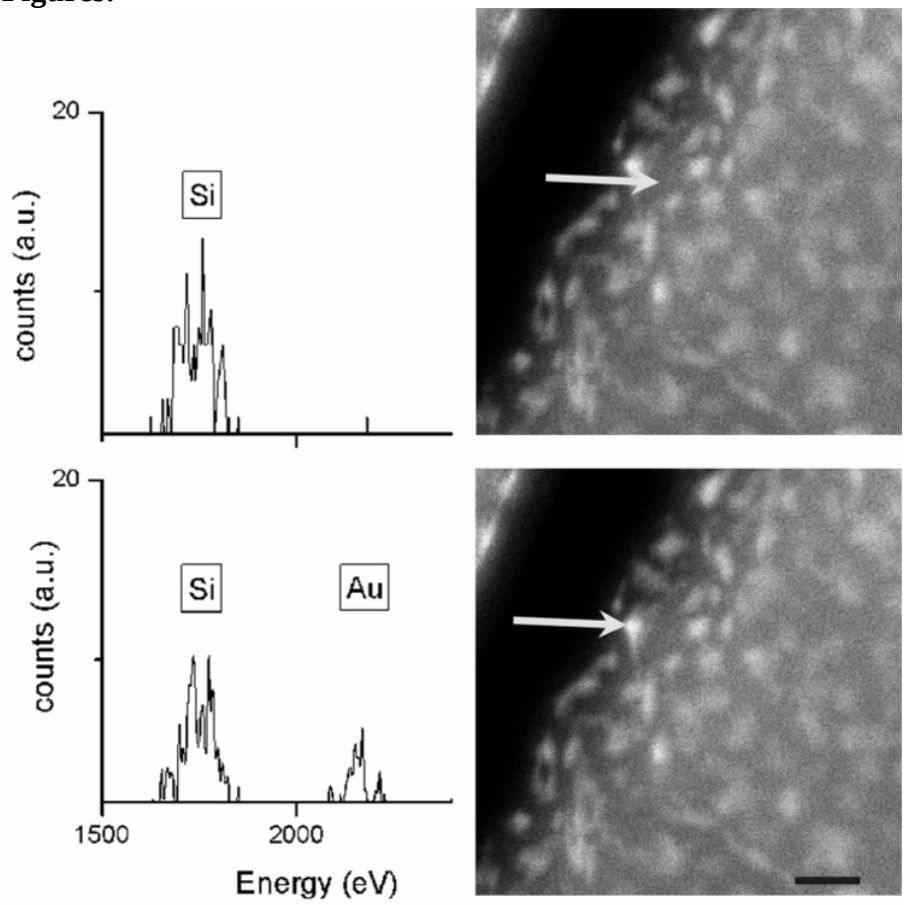


fig.1 EDX spectra and STEM images of a silicon nanowire. An arrow indicates where the EDX spectrum has been taken. The brighter particles are unambiguously gold rich clusters, as three typical gold lines appear in the EDX spectrum around 2200 eV. The scale bar is 10 nm..

KELVIN FORCE MICROSCOPY WITH SIMULTANEOUS NON-CONTACT TOPOGRAPHY IMAGING - INTERACTION BETWEEN THE TWO INVOLVED CANTILEVER RESONANCES

Heinrich Diesinger, Thierry Mélin, Dominique Deresmes, and Didier Stiévenard
Institut d'Electronique de Microélectronique et de Nanotechnologie, CNRS-UMR 8520, AvenuePoincaré, F-59652 Villeneuve d'Ascq, France

heinrich.diesinger@isen.iemn.univ-lille1.fr

Kelvin force microscopy (KFM)[1] consists in eliminating the contact potential difference (CPD) between an AFM tip and the sample surface and mapping the surface potential of the sample. It can reveal potential drops on circuits under operation, detect charge storage and perform dopant profiling at a nanometer scale.

KFM imaging is performed in an Omicron ultrahigh vacuum scanning probe microscope by electrostatically exciting the cantilever at its second resonance, simultaneously with non-contact topography imaging using frequency detection on the fundamental mode, in a setup comparable with the one proposed by Sommerhalter et al. [2]. This setup has a good surface potential sensitivity, allows simultaneous topography and surface potential imaging, and fast acquisition speed. In a first approach, it should be expected that the simultaneous operation makes the topography and surface potential imaging benefit from each other, since the non-contact topography feedback loop maintains the resonance frequencies constant while the KFM loop eliminates any contact potential difference between tip and sample, assuring pure Van der Waals type interaction and thus preventing surface potential variations from causing topography artifacts.

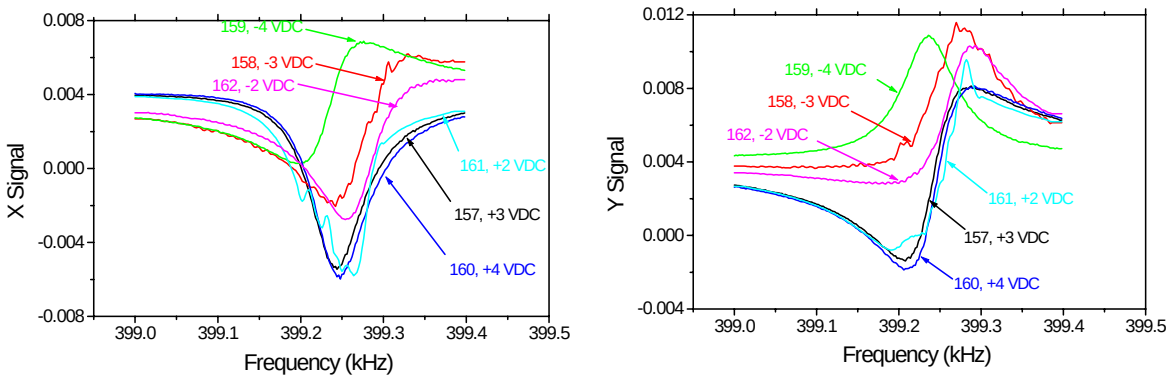


Fig. 1: Electrostatic excitation resonance curves of a non-fundamental cantilever frequency, at different contact potential difference DC components. Mechanical tip excitation at the fundamental frequency and non-contact distance regulation loop were active during the acquisition. An apparent rotation of the drive phase is observed as the DC component is modified, showing that parasitic capacitive coupling of the electrostatic excitation signal into the force feedback circuit introduces an excitation at a drive phase different from the direct electrostatic force applied to the tip.

On the other hand, since the cantilever is part of a self-oscillating force feedback loop as the pendulum of a clock, any excitation (even at higher order resonance) applied to it concerns the loop as a whole. In particular, we show that parasitic coupling between the electrostatic kfm excitation signal and any other part of the loop has to be considered as an excitation source by itself and cannot be corrected by simply subtracting a constant offset beyond the loop. Moreover, the direct electrostatic force acting on the tip and the one due to parasitic

coupling have different drive phases, making the overall drive phase rotate as the electrostatic contribution varies (fig.1). We propose an active compensation of parasitic excitation within the foce feedback loop.

Another phenomena often encountered is a fluctuation between the ratio of the two resonance frequencies: if the KFM feedback is switched off and a CPD is applied, the fundamental mode frequency is kept constant by the topography feedback while the higher order frequency drifts away, leaving a typical Lorentzian signature in the amplitude vs. CPD curve.

References:

[1] M. Nonnenmacher, M. P. O'Boyle, and H. K. Wickramasinghe, Appl. Phys. Lett. **58** (1991) 2921

[2] Ch. Sommerhalter,a) Th. W. Matthes, Th. Glatzel, A. Jager-Waldau,, Appl. Phys. Lett. **75** (1999) 286

GAUSSIAN QUANTUM DOTS OF TYPE II IN IN-PLANE ELECTRIC FIELD

J. Krasnyj[2], M. Tytus[1], W. Donderowicz[1], W. Jacak[1], A. Chuchmała[1]

[1]Institute of Physics , Wrocław University of Technology, Wyb. Wyspiańskiego 27, 50-370 Wrocław, Poland,
[2]Institute of Mathematics, University of Opole, Oleska 48, 45-051 Opole, Poland
e-mail: wojcich.donderowicz@pwr.wroc.pl

Abstract

The growing interest is now focusing on electrically defined quantum dots, which in opposition to presently most popular self-assembled dots, trap electrons simultaneously repulsing positively charged holes (or oppositely), and are thus classified as quantum dots of type II [1]. These dots are especially interesting, as they offer more flexible parameters (allowing dynamic modelling of dot characteristics with applied pattern of external electric field) in comparison to self-assembled dots, and due to continuous improvement of electrode preparation techniques [2] are very promising in terms of practical applications. Although empty QD of type II attracts one type of carrier, and repulses the other, it is however possible for it to capture electron-hole pair (X exciton) due to electrical attraction of carriers. As shown earlier [3] with good correspondence with the experimental results, an unusually rich PL structure observed in this type of quantum dots (up to four PL peaks for higher levels of activation and in the presence of external magnetic field) may be well explained by the existence of metastable (against inter-band far-infrared dipole transition) states of exciton and multi-particle exciton-complexes (X^- and X^+ trions) [4] localized in the QD, due to interplay of bare confinement and geometry sensitive Coulomb e-h interaction. Application of additional in-plane electric field causes further modification of the effective confining potential shape, and so – allows to adjust the PL characteristics and modify them in a real-time. In the current paper a theoretical study for an exciton in semiconductor quantum dot of type-II in the presence of external in-plane electric field is presented. The dependence of the photoluminescence spectrum on the dot size and in-plane electric field is analysed within the Hartree approach for planar Gaussian confinement. The wave function of the ground state and a red-shift of the exciton energy is found as a function of the electric field and the dot size.

[1] R. C. Ashoori et al., Phys. Rev. Lett. **71**, 613 (1993); D. Meurer et al., Phys. Rev. Lett. **68**, 1371 (1992)
[2] N. B. Zhitenev et al., Science **285**, 715 (1999); M. Macucci et al., Superlatt. Microstruct. **27**, 359 (2000)
[3] L. Jacak et al., Phys. Rev B **57**, 9069 (1998)
[4] L. Jacak et al., Phys. Low-Dim. Struct., **11/12**, 71-84 (2003) (2004)

ALUMINIUM CHLORIDE GRAFTED ON SILICA MESOPOROUS MOLECULAR SIEVES AS ALKYLATION CATALYSTS

D. Dubé[a], F. Béland[b] and S. Kaliaguine[a*],

[a]Department of Chemical Engineering, Laval University, Ste Foy, Québec G1K 7P4, Canada;
[b]Silicycle inc. 1200 Ave., St. Jean Baptiste, Suite 114, Que., Canada G2E 5E8. *E-mail: serge.kaliaguine@gch.ulaval.ca

Introduction For decades sulfonated linear alkylbenzenes (LABs) have been among the most important detergents. The LABs synthesis is carried out by Friedel Craft alkylation of benzene by linear olefins using hydrogen fluoride or aluminium chloride as catalyst. The use of these catalysts presents severe problems. For example, aluminium chloride is difficult to separate after reaction and produces a large amount of waste effluent. To solve these problems, attempts have been made to chemically support aluminium chloride on the surface of silica mesoporous molecular sieves (MMSs) [1]. Products can be easily separated and the catalyst can be recycled. This study deals with the characterisation of the $AlCl_{(x)}$ supported on different surfaces of MMSs and their catalytic activity in alkylation of benzene with 1-dodecene. Compared to homogeneous $AlCl_3$, $AlCl_{(x)}$MMSs increase selectivity to monoalkylation.

Experimental Four samples of Aluminium chloride supported on four mesostructured silicates (2 hexagonal and 2 wormhole like with different pore diameters) were prepared by post synthesis reaction in dry conditions (Schlenk technique).The physico-chemical properties were monitored by N_2 adsorption, XRD, atomic absorption, ^{29}Si and ^{27}Al MAS NMR and surface OH density measurements. The acidity data were obtained by TPD NH_3, and FTIR of adsorbed pyridine. The alkylation of benzene by 1-dodecene was conducted in a Schlenk tube under dry conditions: catalyst weight 0,5g, 5mL benzene, 5mL 1-dodecene (molar ratio 2,5:1), at 80°C. Products were analysed by GC-MS.

Results and discussion As shown in Table 1, specific surface area of each catalyst decreases with aluminium loading. The analysis of acidity by TPD NH_3 shows an intense signal at 190°C and a smaller one at 250°C in Fig.1. This indicates the presence of two types of Lewis acid sites. At 190°C, the aluminium chloride is grafted at two Si-OH groups and the second peak at 250°C corresponds to aluminium chloride grafted at one Si-OH on the MMS walls. A small signal around 400°C indicates the presence of a low amount of Brönsted acid sites. In dry conditions, the amount of NH_3 desorbed is high. Thus the density and strength of surface Lewis acid sites are very high. In the presence of moisture the amount of NH_3 desorbed decreases dramatically. The moisture neutralizes the aluminium chloride to form an aluminium oxide with very low content of Lewis acid sites. These results are also confirmed by ^{27}Al MAS NMR, in Fig 2, that shows two types of Lewis acid sites at 85 and 70 ppm. This Lewis acidity is further confirmed by catalytic tests in the alkylation reaction of benzene by 1-dodecene (1-Dd). As shown in Table 1, a better selectivity to monoalkylate products is obtained over $AlCl_{(x)}$ grafted on MMSs compared to $AlCl_3$ in homogeneous solution. This behaviour is believed to be associated

to the highly polar MMS support, which allows a fast out ward diffusion of the monoalkyl product, thus limiting the secondary alkylation.

Table. 1. Physico-chemical properties and catalytic activity for the benzene alkylation reaction of $AlCl_{(x)}$ grafted on hexagonal and wormhole like MMS.

Catalyst	Loading (mmol Al/g)	S_{BET} (m^2/g)	P. Size (Å)	OH density (mmol OH/g)	Ratio Bz : 1 Dd	%Mono	%Di
$D_{1\text{-}0}$	----------	1018	33	2,33	--------	----------	----------
$D_{2\text{-}0}$	----------	874	26	2,15	--------	----------	----------
$D_{1\text{-}1}$	2,00	654	30	0,62	2,5 :1	81,5	18,5
$D_{2\text{-}1}$	2,30	675	23	0,25	2,5 :1	69,6	30,4
$AlCl_3$	----------	----------	----------	----------	2,5 :1	52,8	47,2

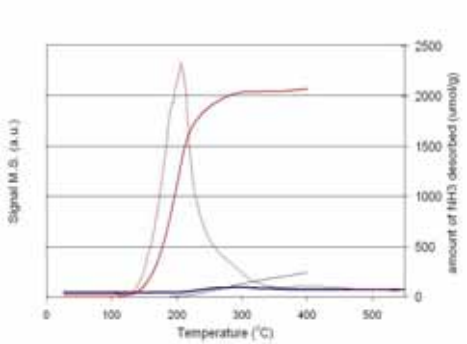


Fig. 1. TPD-NH_3 on $D_{1\text{-}1}$ – Ramp = 10K/min in 20mL/min He.

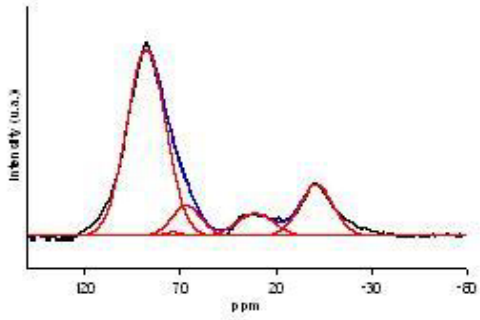


Fig. 2. ^{27}Al MAS NMR. spectra on $D_{1\text{-}1}$.

References

[1] D. Trong On, D. Desplantier-Giscard, C. Danumah, S. Kaliaguine, Appl. Catal. A:General, 222 (2001) 299.

STM induced molecular dynamics of biphenyl on Si(100) : a theoretical analysis.

Mathieu Dubois[1], Christophe Delerue[2] and Angel Rubio[3]

1. CEA / DRFMC / SPrAM (UMR 5819) / LEMOH, 17 rue des Martyrs, 38054 Grenoble Cedex 9, France
2. Institut d'Electronique, de Microélectronique et de Nanotechnologie (UMR 8520), Département ISEN, 41 boulevard Vauban, F-59046 Lille Cedex, France
3. Departamento de Fìsica de Materiales, Facultad de Quìmicas Universidad del Paìs Vasco, Centro Mixto CSIC-UPV, and Donostia International Physics Center (DIPC), E-20018 Donostia-San Sebastian, Spain

contact : *mathieu-j.dubois@cea.fr*

Since its invention in the mid 80's, Scanning Tunneling Microscopy (STM) has become a powerful tool to explore structural and electronic properties of materials at the nanoscopic scale. It has, then, widely been used in surface science as well as in studying single adsorbed molecules, carbon nanotubes or supramolecular organic assemblies. Another of its striking features is the possibility to manipulate individual objects (atoms or molecule). The STM tip can be used to mechanically move these objects, but electronic excitation is emerging as a new promising way to control the molecular dynamics at picometer scale inside a single molecule.

In this context, the work of M. Lastapis et *al.* [1] on individual biphenyl molecules adsorbed on a silicon (100) surface has demonstrated that different reversible molecular movements can be selectively activated by tuning the electron energy injected by the STM tip and by selecting precise locations for the excitation inside the molecule. From a theoretical point of view, no study has been performed on this subject but the investigation of the possible adsorption's configuration of the biphenyl on Si(100). However, the experimentally observed one is still uncertain and electronic excitations mechanisms responsible for the molecular movements remain unclear.

In this work, we present a theoretical analysis of the electronic structure, STM images and STS spectra of a biphenyl molecule adsorbed on Si(100). We chose to study a dissociated twisted biphenyl adsorption (one hydrogen atom dissociates) as it appears to be energetically favourable and to increase switching yields [2,3]. We performed *ab initio* calculations to relax the structure of the system and STM simulations have been performed using our well established model [4,5]. The electronic structure of the system (the chemisorbed molecule + a silicon cluster) has been calculated using the tight binding density functional theory code DFTB [6].

Calculated STM images present a good agreement with experimental data validating the adsorption's configuration. Moreover, local STS spectra have been calculated over both the so-called fixed and mobile parts of the molecules (Figure). Very different results have been obtained which confirms the experimental explanation for the excitation of different electronic states at a precise location inside the molecule, responsible for different dynamics. Simulations allow to clearly identify these electronic states [7].

References:

[1] M. Lastapis et *al.*, Science, **308** (2005) 1000.
[2] M. Mamatkulov et *al.*, Phys. Rev. B, **73** (2006) 035321
[3] M. Martin et *al.*, to be published
[4] M. Dubois et *al.*, Phys. Rev. B, **71** (2005) 165435
[5] M. Dubois et *al.*, accepted for publication in J. Chem. Phys (2006)
[6] T. Frauenheim et *al.*, Phys. Stat. Sol. B, **217** (2000) 41
[7] M. Dubois, C. Delerue and A. Rubio, submitted

Figures:

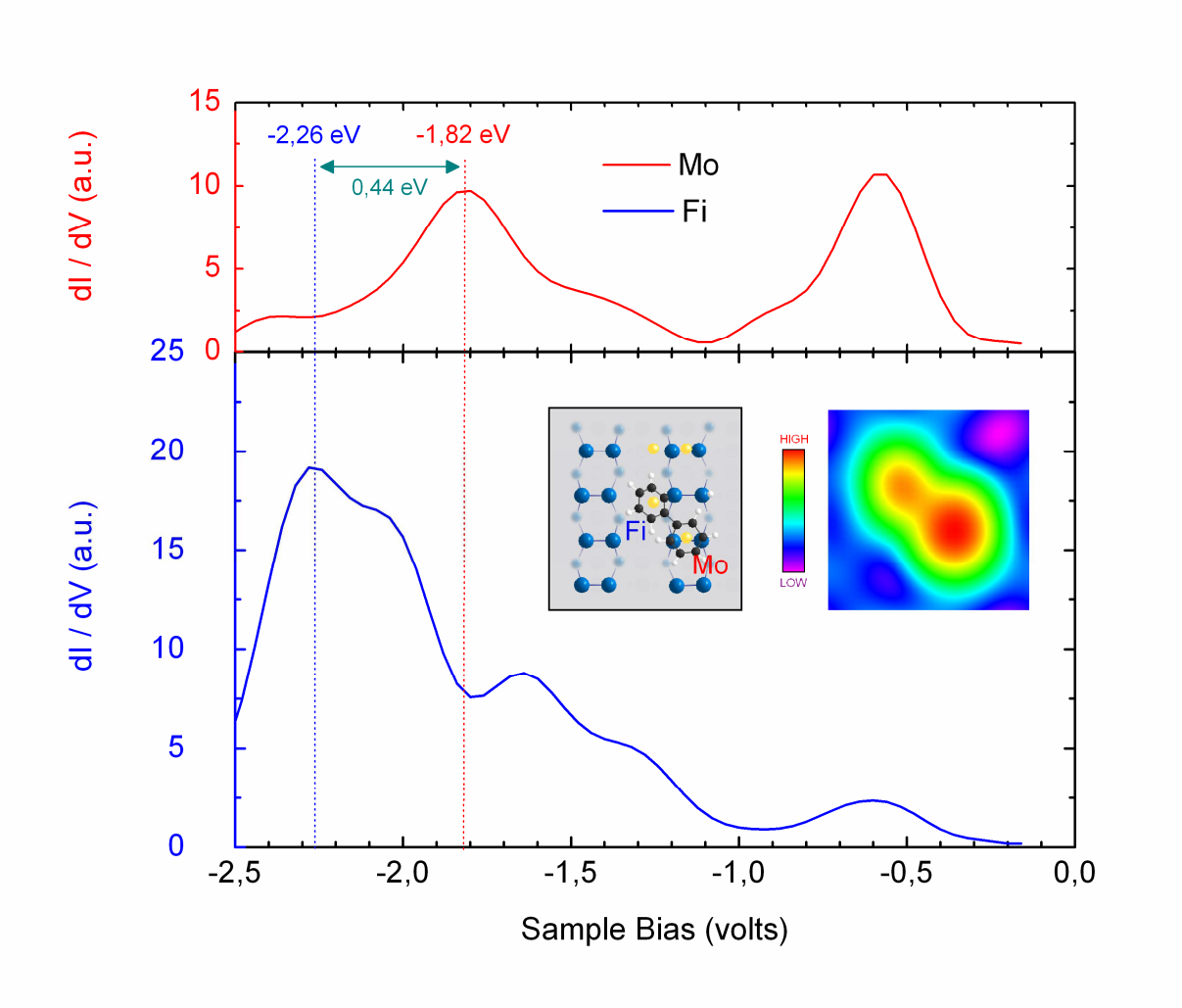


Figure :

Calculated STS spectra over the "fixed" part of the molecule (blue) and over the "mobile" one (red). Insets : positions of the STM tip used for the calculations of the STS spectra, and calculated STM image (applied bias = -1.5 V, current = 0.12 nA)

PORPHYRINS FOR MOLECULAR ELECTRONICS

L. Dubois[a], A. Fateeva[a], M. Claeys-Bruno[b], J.C. Marchon[a] and P. Maldivi[a]

[a] DRFMC/SCIB, CEA-Grenoble, 17, avenue des Martyrs, 38054 Grenoble Cedex 9, France (e-mail : lionel.dubois@cea.fr)

[b] Université Paul Cézanne, Faculté des Sciences et Techniques, Laboratoire de Méthodologie de la Recherche Expérimentale UMR 6171, Avenue Escadrille Normandie Niemen 13397 Marseille, France.

lionel.dubois@cea.fr

Porphyrins possess unic properties like stability, possibilities of a wide range of modifications, redox activity etc... In our laboratory, we want to develop the use of these molecules in the field of molecular or hybrid electronics [1], and more especially for information storage devices.

For that, we try to develop the synthesis of a new kind of chiral porphyrin **1** and **2** derived from cycloxexene carboxaldehyde or erythruronic acid. We think that this kind of porphyrins can be easily functionalized to associate different functionality like bistability, fluorescence etc.. These properties are important and can be used to store and read information in molecules.

In this poster, we present the results we have obtained in these two fields at the moment.

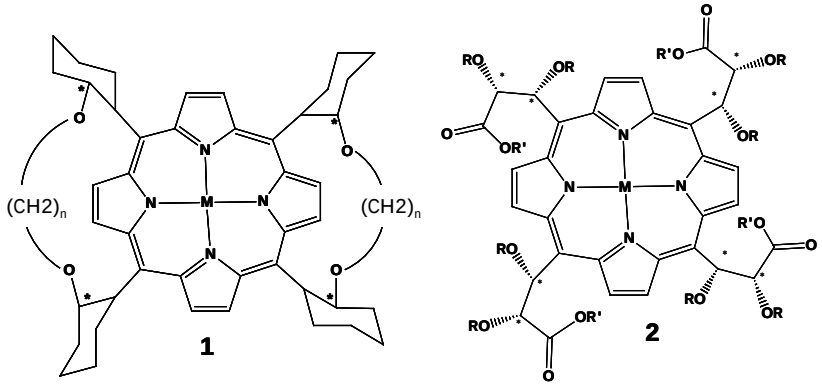


Figure 1: structure of the different systems studied.

REFERENCES

1. Kuhr WG, Gallo AR, Manning RW, and Rhodine CW. *Material Research Society Bulletin.*, **11 (**2004), 838-842.

2. Veyrat M, Ramasseul R, Turowska-Tyrk I, Scheidt WR, Autret M, Kadish KM and Marchon JC. *Inorg. Chem.*, **38** (1999), 1772-1779.

TAILOR-MADE METALLOPORPHYRINS FOR HYBRID MOLECULAR ELECTRONICS

Florence Duclairoir[a], Kai Huang[b], Guillaume Delapierre[b], Tiziana Pro[c], Barbara De Salvo[c] and Jean-Claude Marchon[a]

[a] *DRFMC, LCIB, CEA-Grenoble, 17 rue des Martyrs, 38054 Grenoble, France*

[b] *LETI/DTBS, CEA-Grenoble, 17 rue des Martyrs, 38054 Grenoble, France*

[c] *LETI/D2NT, CEA-Grenoble, 17 rue des Martyrs, 38054 Grenoble, France*

duclairo@drfmc.ceng.cea.fr

A few examples of metalloporphyrins used as discrete storage media in hybrid electronic devices are found in the literature [1, 2]. Redox molecules are particularly interesting because it is believed that they could allow the fabrication of devices with low write/erase voltage and smaller dimensions. Moreover, the ability of metalloporphyrins to reversibly convert between two redox states could be exploited to tune the different electrical states of the transistor. Such an approach is actively followed in our laboratories.

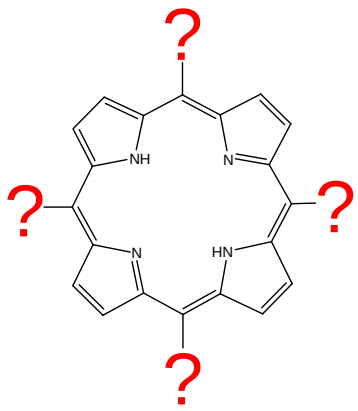
One of our current research projects is to anchor metalloporphyrins on Si by covalent Si – C bonding for the fabrication of specifically designed silicon-based devices. The different steps of the development of these devices can be divided in three major areas: (i) molecular chemistry, (ii) surface chemistry and (iii) microelectronic technology. Indeed, it is first necessary to synthesise the redox active molecules (i) and to build the base of the device (iii), and then the charge-storage elements are grafted on the device (ii).

So far our design of the molecules has been governed by two criteria: the first one is the capability of the molecule to exist in different redox states, and the second one is its ability to be grafted on the Si surface. During this project we have developed a very efficient indirect grafting technique based on a “click-chemistry” reaction [3,4]. The molecule we synthesize must therefore bear appropriate functions to undergo this grafting. In this poster the requirements regarding the porphyrins design will be presented.

References:

[1] Li C, Ly J, Lei B, Fan W, Zhang D, Han J, Meyyappan M, Thompson M and Zhou C, J. Phys. Chem. B, **108** (2004) 9646.
[2] Misra V, Bocian DF, Kuhr WG and Lindsey JS. *US Pat*. No. 2003/0111670 A1.
[3] Kolb HC, Finn MG and Sharpless KB, Angew. Chem. Int. Ed., **40** (2001) 2004.
[4] Delapierre G, Duclairoir F and Marchon J-C. *French Pat*. Application No 2005/0510987.

Figures:



GROWTH OF Si AND SiGe NANOWHISKERS BY MOLECULAR BEAM EPITAXY; X-RAY SCATTERING AND ELECTRON MICROSCOPY INVESTIGATIONS

R. Dujardin, V. Poydenot, T. Devillers, P. Gentile, V. Fabre Nicolin , A.Barski
CEA Grenoble DRFMC/SP2M/ SiNaPS, France
andre.barski@cea.frT

Metal, ceramic and semiconductor nanowhiskers and nanowires are of increasing interest due to their potential applications in nanotechnology devices [1]. Growths of silicon nanowires by chemical vapor deposition, using the vapor-liquid-solid (VLS) mechanism, have been reported by many authors. In the VLS growth mechanism, the nanowire grows from a gold/silicon catalyst droplet located on the top of the wire. The VLS mechanism can be also used in order to grow silicon nanowires by molecular beam epitaxy as reported recently by Schubert et al [2]. However, a very limited number of papers describe the growth of SiGe nanowires or nanowhiskers [3].

In our contribution we will show how to grow silicon and silicon/germanium nanowhiskers by molecular beam epitaxy on silicon (111) and discuss structural properties of our nanowhiskers as determined by X-ray scattering and electron microscopy observations. X-ray scattering experiments have been performed at the ESRF on ID01, BM02 and BM32 beamlines.

The growth procedure of silicon nanowhiskers by molecular beam epitaxy is relatively simple. After silicon oxide thermal desorption and growth of a silicon buffer layer, 50 nm thick, a thin gold film is deposited on reconstructed 7x7 silicon surface at room temperature. In order to cover the surface of silicon by gold droplets, a thermal treatment of the gold film is performed at 500°C. The size and the density of droplets depend on the thickness of the gold film and on the temperature and time of thermal treatment. After droplets formation silicon surface is exposed to a silicon flux. This induces the growth of nanowhiskers. In figure 1(a) we show a scanning electron microscopy (SEM) image of silicon nanowhiskers grown by the described above procedure. The mean diameter at the basis of whiskers is about 100nm and their length can reach 1 micron. The growth of whiskers results from the difference of the silicon growth rate under the gold droplet and between droplets. Each whisker is surrounded by a deep inclusion (see figure 1 (a)) which may correspond to the mass transport from the silicon surface to the top of the whisker where is located the silicon reach gold droplet.

Silicon whiskers have a very complex structure. From the SEM image shown in figure 1 (b), one can deduce that the walls of whiskers are not flat but built by two families of facets [4]. The presence of these two families of facets was also confirmed by grazing incidence x-ray scattering (GISAX) measurements. In figure 2 we show GISAX observations made in the <-1-1 2> direction. The same image was observed be rotating the sample by 60°. This indicates the hexagonal shape of our nanowhiskers. In figure 3 (a) and 3 (b) we show transmission electron microscopy (TEM) image of the silicon whisker with few germanium layers. In order to grow germanium layers silicon deposition has been interrupted and the sample was exposed to a germanium flux.

From the TEM image shown in figure 3 (a) and in figure 3 (b) we determined the growth rate difference between the area around the whiskers and inside the whiskers. The silicon growth rate inside the whiskers is 5.5 times faster than the growth rate of the bulk silicon. However this growth rate difference may depend on the shape, diameter of nanowhiskers and on the growth conditions (i.e. growth temperature and/or silicon flux). The thickness of the germanium layers between the whiskers (see figure 3 (b)) is about 3 monolayers which indicates that in this area germanium layers are composed of almost pure germanium. Inside the whiskers, the thickness of germanium layers is much higher thus

indicating a very high intermixing of germanium with silicon. We can propose the following mechanism inducing this silicon germanium intermixing. During germanium deposition silicon is “provided” by the gold droplet. Inside the whisker, below the droplet, does not grow a pure germanium but silicon germanium alloy. This will be discussed in our contribution on the basis of our results from anomalous x-ray diffraction performed at the Ge and Au absorption edges. Germanium/ silicon lattice parameter distribution inside the nanowhiskers, composition of the germanium/ silicon layers inside the whiskers, composition inside the droplets and gold diffusion into silicon and germanium will be also discussed.

Acknowledgements
The authors would like to acknowledge T.U. Schulli and G. Renaud on BM32, T.H. Metzger and M.I. Richard on ID01 and H. Renevier on BM02 for their help in data acquisition and very helpful discussions during synchrotron experiments on their beamlines.

References:

[1] Y. Cui, C. M. Lieber, Science 291(2001) 851.
[2] L. Schubert et al., Appl. Phys. Lett. 84, (2004) 4968.
[3] Lincoln J. Lauhon, Mark S. Gudiksen, Deli Wang and Charles M. Lieber, Nature 420(2002) 57.
[4] F.M. Ross, J.Tersoff and M.C. Reuter, Phys. Rev. Lett. 95, (2005) 146104.

Figures:

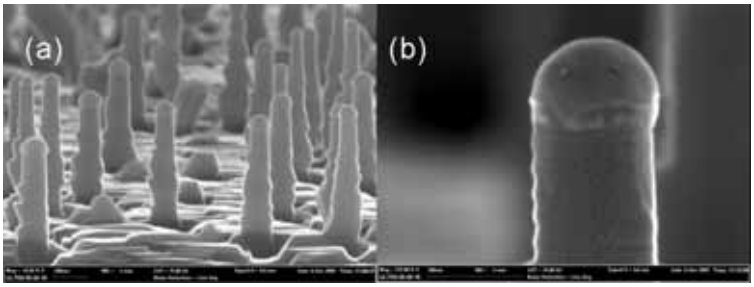


Figure 1: SEM images of (a) an assembly of silicon nanowhiskers and (b) the top of a silicon nanowhisker with a periodic faceting.

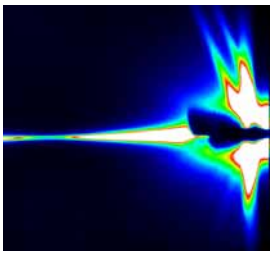


Figure 2: GISAXS pattern in the <-1-1 2> direction showing two facets at 11.2° and 23.5° from the <111> direction

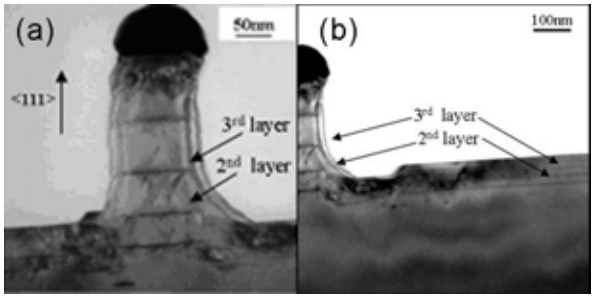


Figure 3: TEM observations of (a) the Ge layers into a silicon nanowhisker and (b) the Ge layers between nanowhiskers

NANO-SCALE RECONFIGURABLE CHIPS FOR IMAGE PROCESSING[1]

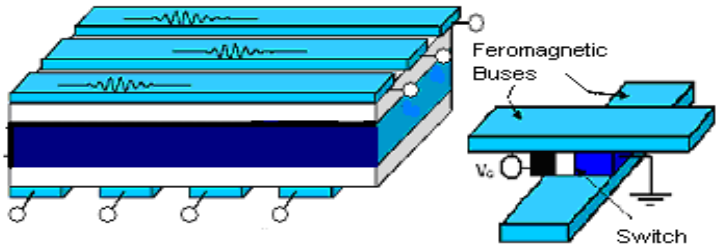
M. M. Eshaghian-Wilner, Alex Khitun*, Shiva Navab, Kang Wang*

***MARCO Focus Center on Functional Engineered Nano Architectonics (FENA)**

Department of Electrical Engineering
University of California at Los Angeles

Over the past few decades, several mesh-based parallel architectures such as mesh-connected computer, mesh-of-trees, pyramid, reconfigurable meshes, systolic meshes, and optical meshes have been considered for performing low and intermediate-level computer vision tasks. This is due the fact that a two dimensional image can be mapped in a straightforward fashion onto a two-dimensional mesh. In particular, reconfigurable meshes have been shown to be attractive computational engines due to the flexibility that the reconfigurable bus offers.

Here, we study a nano-scale reconfigurable mesh that is interconnected with ferromagnetic spin-wave buses for image processing. In this architecture, as shown in the figure below, a set of column spin-wave buses at the bottom and a set of row spin-wave buses on the top are connected via the spin-wave switches. Each switch is placed at the grid point of the mesh. Basically, except for the spin-wave buses, the nano-scale reconfigurable mesh with spin-wave buses is similar to the standard reconfigurable mesh. However, in a spin-wave architectures data is transmitted over waves, and logic can be performed using the phase of waves.



Our nano-scale spin-wave-based architecture, while requiring the same number of switches and buses as regular reconfigurable meshes, is capable of simultaneously transmitting multiple waves on each of the spin-wave buses. Furthermore, this design is fault tolerant because if there is a failure in one of the channels, any of the other channels can be reconfigured to transmit the data. Because of these feature, very fast and fault-tolerant algorithms can be designed for this architecture. The actual physical implementation of spin-wave reconfigurable mesh is currently underway at UCLA, and we have a preliminary prototype version in which we are able to detect spin-waves at nano-scale.

One of the most attractive properties of spin-waves is superposition. This property suggests that the resultant disturbance at any point in a medium is the algebraic sum of the separate constituent waves. Hence, it enables many optical signals to pass through the same point in space at the same time without causing mutual interference or crosstalk. We employ this characteristic to allow concurrent writes if all the requesting processors want to write a *"1"*. This leads to constant running time of the following geometric algorithm, under the assumption that broadcasting of O(log N) bits can be done in unit time:

[1] Authors are listed Alphabetically

Given an $N^{1/2} \times N^{1/2}$ image, using a N× N Spin-Wave reconfigurable mesh, in O(1) time, for a single figure, its nearest neighbor, convex hull and a smallest enclosing box can be found. For multiple figures, we present the following image processing algorithms illustrating the potential of our proposed spin-wave reconfigurable mesh.

Labeling of Multiple Figures on Spin-Wave Mesh

Identifying figures in an image is an early step in intermediate-level image processing. In a *0/1* picture, the connected 1's are said to form a figure. Thus, associated with each PE is a label, which is the unique *ID* of the figure to which the PE belongs. An N× N digitized picture may contain more than one connected region of black pixels. The problem is to identify to which figure (label) each *"1"* belongs.

We show that even given an N× N image, using a N× N Reconfigurable Mesh with Spin-Wave Buses, in a systolic fashion with inputs coming from left and leaving from the right, each figure can be labeled with O(1) steps per systolic cycle. This result is also an O (log N) time faster than the best known solution for systolic reconfigurable mesh. Basically the improvement is possible because of the fact that multiple labels can be simultaneously transmitted over the buses using multiple waves at different frequencies. Therefore there is no need to rotate the figure or slow down the entire process to avoid conflicts.

Furthermore, in a non-systolic fashion the same algorithm can be solved in O (log N) time. This is done by each node immediately setting the buses over the connected region and then the minimum label over each connected region to be computed by O (log N) bits. Once the figures are labeled then we can associate a different frequency to each of the figures to continue with other image computations such as the convexity problem shown below.

Convex Hull of Multiple Figures on Spin-Wave Mesh

To find the convex hull of multiple O(N) figures in an image size of O(N) using a spin-wave reconfigurable mesh of size NxN, we will find the extreme points on each of the figures. To do this, we basically find the convex hull of each figure using a different frequency on the spin-wave mesh. Therefore, before starting this algorithm, we first do a labeling of figures as discussed above and then associate to each label a distinct frequency. Now using each frequency we find the right most and left most points of each figure, and then find if they would have to be eliminated or not. A left most or a right most figure is eliminated if it is not an extreme point. An extreme point is one that makes an angle less than 180 degrees with respect to all the right most points and left most points above it and below it. This can be done in O(1) time for N figures in parallel. This is possible because the computations are done in parallel for N figures on each column using a different frequency for each of the N figures. Also, previously on the Mesh-of-Trees this was possible in O (log N) time, but only for one figure at a time. Here using the spin-wave mesh it is possible to process N figures at the same time.

Nearest Neighbors of Multiple Figures on Spin-Wave Mesh

Finding the nearest neighbor to each of the figures is relatively a simpler problem because the nearest neighbor to each point can first be found, and then the result can be propagated to each of the figures, but all in parallel. This can be done in O (log N) time, but due to space limitations the details are not shown. Similarly, for a smaller image size of N, this problem can be solved in O (1) time.

FREE CHARGE CARRIER NANOCOMPOSITE PHOTOGENERATORS AS PROMISING PHOTOCATALYTIC MATERIALS: WHICH PARAMETERS TO EVALUATE AT FIRST?

Alexis Evstratov, Cristian Chis
Ales School of Mining, 6 avenue de Clavieres, 30319 Cedex, Ales, France
alexis.evstratov@ema.fr

The materials which are capable to provide at their surfaces free charge carriers (FCC), electrons and positive holes, under UV or visible light irradiation, can be considered as Free Charge Carrier Photogenerators (FCCP). Some similar terms exist also in modern scientific literature [1, 2].
Theoretically, all the FCCP materials, both in free state and in supported form (composite species), could manifest an interest for the photocatalytic applications. The best performances are usually expected from nanometric scale FCCP because of surface attendance facilities for the free charge carriers generated in extremely small active aggregates.
However, experience shows that it is not the case: some FCCP nanocomposites can not be utilized in photocatalysis. Selecting a product which presents a potential interest as an efficient heterogeneous photocatalyst from a large range of FCCP materials remains so a problem to resolve.
At the same time, not only well known crystalline semiconductors (titanium and zinc oxides, cadmium and zinc sulphide, etc.) dispose photocatalytic capacities. It was proved [3-5] that the disordered structures can also assure the photocatalytic phenomenon.
Excepting a good activity, a promising material for photocatalytic application must conserve its initial catalytic capacity for an important period of time in order to guarantee the process steady state during all the service period.
What is the principle cause of the heterogeneous photocatalyst surface deactivation? We believe that in the case of volatile organic compound (VOC) photoxidation process, the active surface degradation is always caused by parasite acid-base reactions taking place at the same time as target reactions. In the previous example, the products of parasite reactions are represented by surface oligomer compounds formed over Lewis acid centres (acceptor cationic sites) from the VOC precursors having a strong Lewis base behaviour. Moreover, the target reactions aim to the VOC complete oxidation occurring often over the same active sites. For any FCCP, the parasite reaction domination over its surface excludes this species from a potential application as an efficient photocatalytic agent.
In order to be considered as a promising photocatalyst, a FCCP sample has to possess, at least, the following proprieties:

- maximum quantity of photogenerated FCC reaching the active surface;
- limited FCC recombination intensity;
- optimal FCC repartition at its surface (positive hole domination [6]);
- important physical adsorption capacity;
- low Lewis acid reactivity (less parasite reactivity potential);
- important photocatalytic activity in steady state process.

When faced with a novel FCCP product supposed to be applied as photocatalyst in a stedy state process, it is useful to define a mini-list of parameters to be controlled (see the table below). Getting to their states or levels advised in the table, assures good perspectives of the material's use.

Table: Basic parameter set to be controlled for the FCCP identification as efficient photocatalyst

Lot	N°	Parameter	Advised state / level
Fundamental parameters	1	Free charge carrier repartition at the active surface	Hole domination
	2	Quantum yield	Maximal
	3	Free charge carrier lifetime	Maximal
Reactivity parameters	4	Photocatalytic activity	Maximal
	5	Physical adsorption capacities	Optimal
	6	Acid-base reactivity under lighting (UV-A / sunlight)	Minimal
Other characteristics	7	Surface morphology and active aggregate dimensions	Nanosized aggregates
	8	Crystallinity rate of active components	No strict restrictions
	9	Oxidation rate of active component surface cations	Minimal
	10	Average widths of the optical forbidden zones (for crystalline products)	Optimal

The properties of Degussa P25 (reference photocatalytic product) and of an amorphous TiO_2 silica based nanocomposite material supposed to be applied as heterogeneous photocatalyst are presented and discussed in the paper. The experimental methods and techniques used for the parameter evaluation are also cited.
The mini-list presented above needs to be completed with the kinetic characteristics. Each parameter already cited in the table could be detailed for a more pertinent characterisation of a FCCP material sample as a potential heterogeneous photocatalyst.

References:

[1] A. Jain, A. Kapoor, A new approachto study organic solar cell using Lambert W-function, **Solar Energy Materials & Solar Cells 86** (2005) 197–205.
[2] T. Barfels, H.J. Fitting, A. Gulans, J. Jansons,M. Springis, H. Stolz, I. Tale, A. Veispals, Luminescence and electron transport properties of GaN and AlN layers, **Radiation Measurements 33** (2001) 709–713.
[3] L. Zang, W. Macyk, C. Lange, et al., Amorphous microporous titania modified with metal chloride as photocatalysts for detoxification and charge generation by visible light, H. **Kinch Chem. Eur. J.,** vol.6 (2000) 379-384.
[4] A. Evstratov, C. Chis, P. Gaudon, B. Ducourant, P. Jouffrey, Structures composites nanométriques en état amorphe en tant que photocatalyseurs d'une nouvelle génération, **Récents Progrès en Génie des Procédés**, 92-2005, L-14 (2005) 1-8.
[5] C.J. Lin, J. Chen, S.L. Suib et al., Recovery of bromine from methyl bromide using amorphous MnO_x photocatalysts, **J. of Catalysis**, vol. 161, N°2 (1996) 659-666.
[6] A. Evstratov, C. Chis, J.M. Taulemesse, P. Gaudon and F. Peirano, Revealing of a Particular Physical Mechanism of Disordered Photocatalytic Structure Functioning, **9th Intern. Congress NSTI Nanotech-2006, Proceedings,** vol. 1 (2006) 9-12.

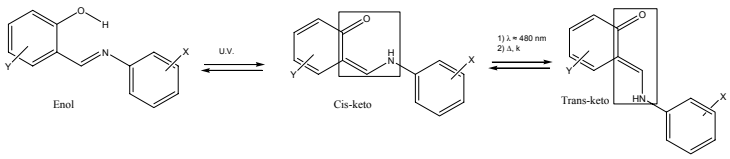
SYNTHESIS AND CHARACTERIZATION OF ELECTROPOLYMERIZABLE DERIVATIVES OF N-SALICYLDENE (ANIL) FUNCTIONALIZED BIS EDOT-CARBAZOLE

I. Fabre-Francke, K. Nakatani[a], S. Sadki[1]

UMR5819-SPrAM (CEA-CNRS-UJF) DRFMC, CEA Grenoble, 17 rue des Martyrs, 38054-Grenoble, France
[a]PPSM, UMR CNRS 8531, Ecole Normale Supérieure de Cachan, 61 avenue du Pt Wilson, 94235 Cachan, France

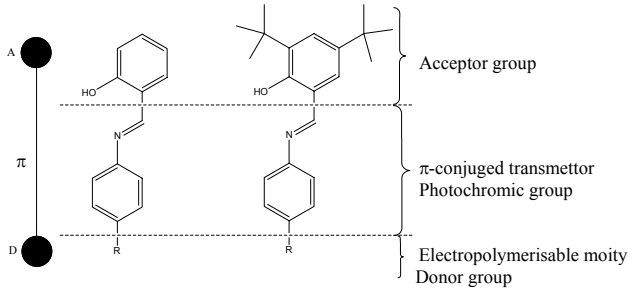
isabelle.fabre-francke@cea.fr

A great deal of attention has been focused on conjugated polymers due to the broad range of applications for which they are potentially useful.[1] Photovoltaic devices, LED's, field effect transistors, electrochromic devices, and various types of sensors are under investigation by numerous researchers around the world. As such, the search for new functional and responsive conjugated polymers exhibiting electrochromism, photochromism or NLO properties are especially sought after for use in such applications as display technology or data storage. Preparation of conjugated photochromic polymers leads the development of original materials which are good candidates for optical switches and storage devices. In designing a photochromic conjugated polymer, several can be taken. In the simplest approach the photochrom can be attached as a pendant group to the polymer backbone through a nonconjugated linkage. In the second approach a fully conjugated polymer is synthetized in which the conjugation of the photochrom is continuous with the backbone by either incorporating the photochrom directly in the backbone or using a fully pendant group. Such fully conjugated polymers are especially interesting because of the possibility for a cooperative interaction between the polymer and the photochrom due to the continuous electronic conjugation.[1]
Because of their interesting physical properties under irradiation of their photochromic groups, molecules based of carbazole-anils and EDOT-carbazole-anils derivatives are investigated. Anils (salicylidenes-anilines) are interesting class of photochrom. The mechanism for the photochromism is based on a tautomerization reaction as shown in scheme 1.



Sheme 1: Tautomerization of anils

The enol form is colorless, but upon irradiation with UV light the colored keto form is produced.[2]
Optimized synthesis of anil-carbazole monomers in one pot permits to obtain some derivatives whose substituant effect were studied.



Scheme 2: New photochromic monomers

These monomers are deposed on a glass substrate as a solid film to be studied under irradiation. It is shown that the photochromic character of these molecular films is exalted by addition of tertiobutyl groups on the phenolic ring.
A reversible photo-commutation is then possible. Monomers CzAnil **1** (Z = H) and CzAnil **2** (Z = tBu) were electropolymerized by cyclic voltamperometry and chronopotentiometry in nitrobenzene TBAP 0.1 M (Figure 1 a). Conducting polymer films are obtained on platinum and ITO electrodes.

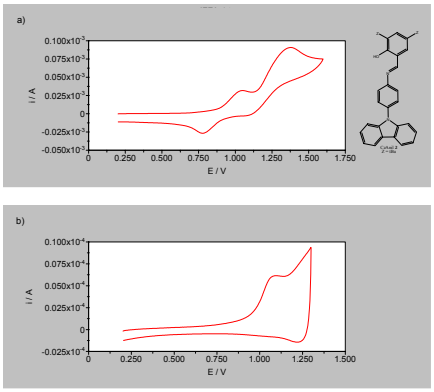


Figure 1: Electrosynthesis (a) and characterization (b) of poly (CzAnil **2**)

These new polymers films were electrochemically characterized by cyclic voltamperometry in nitrobenzene TBAP 0.1 M (Figure 1 b) from neutral to conducting state.
The potential applied to the polymer-coated electrode was sequentially increased to higher potentials to oxidize the polymer while monitoring the creation of the charge carriers. An evolution of polymer redox process is observed at $E_{1/2}$ = 1.12 V vs Fc/Fc^+ for poly-(Cz-Anil**1**) and $E_{1/2}$ = 1.15 V vs Fc/Fc^+ for poly-(Cz-Anil**2**).
Furthermore polymerization study of EDOT-carbazole-EDOT derivatives is also under investigation to obtain resistant polymers films with attractive photonic and electronic properties.[3]

References:

[1] : Skotheim, T. A.; Elsenbaumer, R. L.; Reynolds, J. R. *Handbook of Conducting Polymers*, ed. Dekker, (1998).
[2] : P. Audebert ; S. Sadki ; F. Miomandre ; P. Hapiot ; K. Chane-Ching, New J. Chem., **5** (2003), 798.
[3] : Qiu, Y.; Reynolds, J. R. *J. Electrochem. Soc.*, **17**, (1990), 900.

Conductance, surface traps and passivation in doped silicon nanowires

M. V. Fernández-Serra, Ch. Adessi and Xavier Blase

Abstract

By means of *ab initio* simulations, we investigate the structural, electronic and transport properties of p- and n-type doped silicon nanowires. We find that impurities always segregate at the surface of unpassivated wires, reducing dramatically the conductance of the surface states. Upon passivation, we show that for wires as large as a few nanometers in diameter, a large proportion of dopants will be trapped and electrically neutralized at surface dangling bond defects, significantly reducing the density of carriers. Important differences between *p*- and *n*-type doping are observed[1]. Impurities located in the core of the wire induce a strong resonant backscattering at the impurity bound state energies. Upon trapping at such surface sites, impurities become electronically inactive, yielding neither a free carrier nor inducing a significant drop of conductance. This effect is also observed for isolated surface dangling bond defects.

References

[1] M. V. Fernández-Serra, Ch. Adessi and Xavier Blase, Phys. Rev. Lett. **96**, 166805 (2006).

HALL EFFECT IN LAYERED CRYSTALS WITH THE SCATTERING OF CHARGE CARRIERS BY PHONONS

S.R.Figarova,
Baku State University, 23, Z Khalilov st., Baku, Az1143, Azerbaijan,e-mail:figarov@bsu.az
and
V.R.Figarov,
Institute of Physics, Academy of Sciences, Azerbaijan, 31, H.Javid av., Baku, Az1148, Azerbaijan, e-mail:figarov@physics.ab.az

Keywords : Hall effect, layered crystals, phonon scattering, magnetic field.

In the last few years, highly anisotropic and low-dimensional electron systems attract particular interest. The proposed paper deals with a theoretical investigation of quasi-two-dimensional and two-dimensional electron gases in a magnetic field. It is under study the Hall effect in layered crystals with a sine dispersion law with the scattering of charge carriers by phonons over the whole area of classical magnetic fields. It has been shown the Hall coefficient is anisotropic. Depending on the sense of the magnetic field, the Hall coefficient changes the sign. When a magnetic field is directed to the layer plane, the Hall coefficient is opposite in sign to the carrier charge; the magnetic field involves the reduction in the absolute value of the Hall resistance. In the pure two-dimensional case the Hall coefficient in both strong and weak magnetic fields is solely dictated by the charge-carrier concentration. In the quasi-two-dimensional case in the direction normal to the layer plane electrons behave like holes and as the magnetic field increases the longitudinal Hall coefficient declines. The field dependence of the Hall coefficient is completely caused by dimensionality of the electron gas. Such a behaviour of the Hall coefficient is due to features of the electron dynamics in the miniband and to the anisotropy of the electron motion, which is associated with the effective mass anisotropy and with the scattering of charge carriers by phonons Results obtained in the paper can find an application on explaining novel phenomena disclosed in heterostructures.

Field emission energy distributions from nanodiamond-covered single wall carbon nanotubes

A. Fiori[1], , M. L. Terranova[1], S. T. Purcell[2], P. Vincent[2], A. Ayari[2]

[1]Dept. of Chemical Science and Technologies, University of Rome Tor Vergata, 1 via della Ricerca Scientifica 00133 Rome, Italy and Micro and NAano System laboratory (MINASlab)
[2]Laboratoire de Physique de la Matière Condensée et Nanostructures, Université Lyon 1; CNRS, UMR 5586, Domaine Scientifique de la Doua, F-69622 Villeurbanne cedex; France

angelamaria.fiori@uniroma2.it

Carbon materials have recently gained a leading position among the ever increasing family of novel cold cathode materials [1]. After the first experimental works of the early 90s [2-4] demonstrating low threshold field emission, different forms of diamond have been shown to have excellent qualities as field emission sources. As a consequence, much effort has been focussed on both the synthesis of diamond nanostructures to increase the field enhancement factor [5-7] and on understanding the emission mechanism in these nominally insulating materials. Different hypotheses have been proposed to explain the controversial experimental data, which varies widely between different sample types [8-14], but so far very few reports of field emission energy distribution supporting or discarding them have appeared [4, 12-14].
Carbon nanotubes, on the other side, exhibit an unrivalled advantage in field enhancing due to their high aspect ratio and have shown very high field emission metallic performances [1]. Covering nanotubes with nanodiamond would represent a way of getting nanometer-sized diamond grains on nanoscale protrusions in order to benefit from the field enhancement in a reproducible way.
By means of a modified Hot Filament Chemical Vapor Deposition apparatus, we recently set-up a method for growing, in one synthesis step, nanodiamond-covered Single Wall Carbon Nanotube (SWNT) bundles [15]. Careful morphological and structural characterization of both phases has been carried out by means of Scanning Electron Microscopy (SEM), Raman spectroscopy and Reflection High Energy Electron Diffraction (RHEED) [15]. In short these studies showed that the nanograins are high quality crystalline diamond.
The field emission investigation involved the recording of the emission patterns, current stability and the total energy distributions (TED) at different applied voltages.
Due to the field enhancing effect of the SWNT bundles, the emission came from numerous localised sites spread over the 2 mm^2 emission zone. The emission was very stable over the meaurement cycles of several of hours.
The Fowler-Nordheim plot of the total current was shown to be rather straight leading one to assume semimetallic behaviour. However, an extremely original and remarkable feature of the emission was the displacement of the energy spectra of emitted electrons from the Fermi level which measures the voltage drops created by the passing emission currents. The spectra consisted of many separate peaks from the different emitters spread over 20 to 500 Volts below the Fermi level. The higher value is more than two orders of magnitude larger than previously reported for other diamond emitters. This remarkably large shifting is a clear sign of the highly insulating nature of our nanodiamond.
Successive spectra taken as a function of applied voltages shift from the Fermi level with a nonlinear behaviour. We propose that this is due to both a resistive drop and field penetration. Moreover, an x-y map of the TEDs of the sample demonstrated that the peaks are related to precise zones of the sample and so to different emitters or groups of emitters.
Further work including a measure of the current coming from an individual emitter, temperature dependent measurements, laser illumination and simulations are needed to clarify the details of the electronic transport leading to such spectacular TEDs.

References:
[1] N. S. Xu, S. Ejaz Huq, Materials Science and Engineering R, **48** (2005) 47
[2] C. Wang, A. Garcia, D. C. Ingram, M. Lake, M. E. Korfesch, Electron. Lett. **27** (1991) 1459
[3] Ken Okano, Kimihiko Hoshina, Masamori Iida, Satoshi Koizumi, and Tadao Inuzuka, Appl. Phys. Lett. **64** (1994) 2742
[4] N. S. Xu, Y. Tzeng, R. V. Lantham J. Phys. D: Appl. Phys. **27** (1994) 1988
[5] Y. Ando, Y. Nishibayashi, A. Sawabe, Diamond Relat. Mater. **13** (2004) 633
[6] H. Masuda, T. Yanagishita, K. Yasui, K. Nishio, I. Yagi, Y. N. Rao, A. Fujishima, Adv. Mater. **13** (2001) 247
[7] Y. K. Chih, C. H. Chen, J. Hwang, A. P. Lee, C. S. Kou, C. S. Diamond Relat. Mater. **13** (2004) 1614
[8] M. W. Geis, N. N. Efremow, K. E. Krohn, J. C. Twichell, T. M. Lyszczarz, R. Kalish, J. A. Green, M. D. Tabat, Nature **393** (1998) 431
[9] A. V. Karabutov, V. D. Frolov, V. I. Konov, Diamond Rel. Mat. **10** (2001) 840
[10] J. B. Cui, , J. Ristein, L. Ley, J. Phys. Rev. B **60** (1999) 16135
[11] J. Y. Shim, H. K. Baik, K. M. Song J. Appl. Phys. **87** (2000) 7508
[12] R. Schlesser, M. T. McClure, B. L. McCarson, Z. Sitar J. Appl. Phys. **82** (1997) 5763
[13] C. Bandis, B. B. Pate Appl. Phys. Lett. **69** (1996) 366
[14] O. Gröning, L.-O. Nilsson, O. Grönong, L. Schlapbach, Solid-State Electronics **45** (2001) 929
[15] M. L. Terranova, S. Orlanducci, A. Fiori, E. Tamburri, V. Sessa, M. Rossi, A. S. Barnard, Chem. Mater. **17** (2005) 3214-3220

Figures:

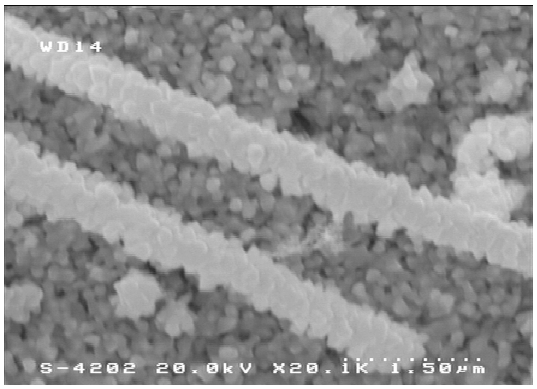


Fig. 1 A SEM image of two SWNT bundles covered by nanocrystalline diamonds

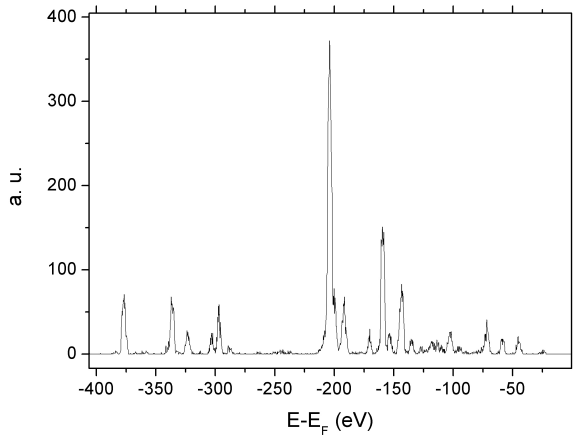


Fig. 2 A typical TED obtained by the investigated sample

ELECTRON-PHONON INTERACTION IN CARBON-NANOTUBES: A FULL MANY-BODY TREATMENT

Luis E. F. Foa Torres and Stephan Roche
CEA/DSM/DRFMC/SPSMS/GT, 17 avenue des Martyrs, 38054 Grenoble, France
luis.foa-torres@cea.fr

The effect of scattering by phonons in the electronic transport through carbon nanotubes has been a very active area of research during the last years. At high bias (when the electrons gain enough energy to emit either optical or zone boundary phonons) the experimental evidence [1-3] signals e-ph coupling as the source of current saturation. This limits their exceptional properties as ballistic conductors observed at low bias. Therefore, it is of utmost importance to include the e-ph interaction in the modeling and simulation of nanotubes based devices.

While there have been many theoretical studies aimed to tackle this problem [4-10], a clear and complete picture has not yet emerged and many fascinating new directions open up in this rapidly evolving field. The theoretical approaches used to tackle this problem include: the use of the Boltzmann transport equation [6-7], the Fermi Golden Rule [8], a diagonal self-consistent Born approximation [5] and the Kubo method [9-10]. Here, we present a full many-body treatment of electronic transport through carbon nanotubes in the presence of electron-phonon interaction with optical phonons [11]. This allows us to unveil novel quantum effects [11] which are beyond the regime of applicability of the Fermi Golden Rule.

References:

[1] Z. Yao, C. L. Kane, and C. Dekker, Phys. Rev. Lett. **84** (2000) 2941.
[2] J. Park et al, NanoLetters **4** (2004) 517.
[3] A. Javey, J. Guo, M. Paulsson, Q. Wang, D. Mann, M. Lundstrom, and H. Dai, Phys. Rev. Lett. **92** (2004) 106804.
[4] M. Georghe, R. Gutierrez, N. Ranjan, A. Pecchia, A. Di Carlo, and G. Cuniberti, Europhys. Lett. **71** (2005) 438.
[5] A. Svizhenko and M. P. Anantram, Phys. Rev. B **72** (2005) 085430.
[6] V. Perebeinos, J. Tersoff and Ph. Avouris, Phys. Rev. Lett. **94** (2005) 086802.
[7] M. A. Kuroda, A. Cangellaris and J. P. Leburton, Phys. Rev. Lett. **95** (2005) 266803.
[8] M. Lazzeri, S. Piscanec, F. Mauri, A.C. Ferrari and J. Robertson, Phys. Rev. Lett. **95** (2005) 236802.
[9] S. Roche, J. Jiang, F. Triozon and R. Saito, Phys. Rev. Lett. **95** (2005) 076803.
[10] S. Roche, J. Jiang, F. Triozon and R. Saito, Phys. Rev. B **72**, (2005) 113410.
[11] L. E. F. Foa Torres and Stephan Roche, unpublished.

CONDUCTANCE OF A ONE-DIMENSIONAL WIRE WITH STRONG RANDOM IMPURITIES

M. M. Fogler, S. V. Malinin,[*] T. Nattermann[†]
University of California San Diego, Department of Physics, 9500 Gilman Drive, La Jolla, California 92093, USA
[*] *Wayne State University, Department of Chemistry, Detroit, Michigan 48202, USA*
[†]*Institut fur Theoretische Physik, Universitat zu Koln, D-50923, Germany*

Email: *mfogler@ucsd.edu*

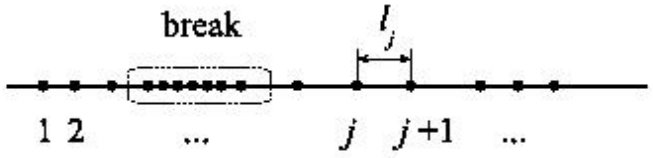
The problem of electron transport in one-dimensional (1D) conductors, such as nanotubes, nanowires, and nanofibers, continues to draw much attention. It has become a source of interesting and challenging questions for basic research and, at the same time, a vital area of emerging nanotechnology. From both standpoints, it is very important to understand how conducting properties of 1D systems are affected by unavoidable impurities and defects. Here we address this question for the case of 1D metals - systems whose electron energy spectrum is gapless in the absence of disorder. The disorder is expected to diminish their conductance. Interestingly, for many of such 1D "metals" the suppression is very strong and a markedly insulating behaviour is observed: the conductance drops by orders of magnitude as either temperature T or the bias voltage V is reduced. It has been a question of both fundamental and practical interest to determine what barriers to transport are responsible for such phenomena, what conduction mechanisms enable electrons to overcome those barriers at finite V and T, and whether one can develop a quantitative theory to describe them.

In order to shed light on these issues we analyze a model in which a 1D wire contains a finite concentration of randomly positioned strong impurities. The impurities effectively divide the wire into a chain of weakly-coupled quantum dots. We show that the conductance of such a system is dominated by the Coulomb blockade and exhibits a rich dependence on voltage V and temperature T due to the interplay of sequential and co-tunnelling. The conductance of a long wire is always limited by the "breaks": randomly occurring clusters of quantum dots with a special length distribution pattern that inhibits the transport no matter how the activation and tunnelling are combined. We find a broad range of parameters where the conductance exhibits an approximately algebraic dependence on T and V with *unequal* exponents, which resembles the behaviour experimentally observed in long nanowires. At lower temperatures the conductance crosses over to stretched exponential laws typical of the variable-range hopping.

References:

[1] M. M. Fogler, S. V. Malinin, T. Nattermann, cond-mat/0602008.
[2] M. M. Fogler and R. S. Kelley, Phys. Rev. Lett. **95** (2005) 166604.

Figure 1: Illustration of the theoretical model. Dots symbolize strong random impurities.



SYNTHESIS OF GADOLINIUM OXIDE NANOPARTICLES AS A CONTRAST AGENT IN MRI

Marc. A. Fortin, R.M Petoral Jr., F. Söderlind, P.O. Käll, M. Engström, K. Uvdal
IFM, Linköpings Universitet SE-58183, Sweden.
fortin@ifm.liu.se

Contrast agents are used on a common basis in clinical MRI since they can influence the MR signal by locally affecting relaxation parameters in the tissues (T1 and T2). Small-molecule contrast agents made of chelated paramagnetic gadolinium ions are known to affect T1 and can diffuse to the extracellular space . Those agents are quickly eliminated through the urinary tract. On the other hand, intravenously injected superparamagnetic iron oxide nanoparticles can stay in the blood for longer times, and are therefore used as blood pool contrast agents. Iron oxide nanoparticles are generally more effective for T2 enhancement. This work reports on the synthesis, preparation and functionalization of gadolinium oxide nanoparticles developed as contrast agent in MRI. Appropriately capped and prepared in aqueous suspensions, Gd_2O_3 nanoparticles could serve as an interesting T1 blood-pool imaging agent, complementary to existing T2-enhancing nanoparticle-based contrast agents. As a complement to MRI, gadolinia nanoparticles could also be used for neutron capture therapy in oncology, since gadolinium has the highest thermal neutron absorption cross section of all elements. In our studies, we synthesized through a chemical way Gd_2O_3 nanoparticles similar in size to commercial superparamagnetic iron oxide nanoparticles. The particles are capped in order to prevent leakage of the toxic Gd^{3+} ions from the crystal core. The compound is then dialyzed either in water or in aqueous buffers at stable pH in order to reproduce physiological conditions. Magnetic resonance relaxation parameters T1 and T2 will be presented and discussed for different products, and correlated to the particle size distribution, type of capping and type of buffer used during the preparation of the agent

SINGLE MOLECULE FLUORESCENCE DECAY RATE STATISTICS IN NANOSCOPIC ENVIRONMENTS

LS. Froufe and R. Carminati
Laboratoire EM2C, CNRS, Ecole Centrale Paris, 92295 Châtenay-Malabry, France.

J.J. Sáenz
Departamento de Física de la Materia Condensada,
Universidad Autónoma de Madrid, 28049 Madrid, Spain.

Several powerful optical imaging techniques are based on molecular fluorescence. Single emitters are also key elements in nanophotonics devices. Since the pioneering work of Purcell [1], it has been known that the spontaneous decay rate of a dipolar emitter (atom, molecule, Qdot) is dramatically affected by its environment. When a fluorescent molecule is placed in a complex environment (e.g., cluster, biological system), measurement of *statistical* properties can provide relevant information. This issue has been partially addressed in the literature [2]. In nanoscopic systems (e.g. clusters of nanoparticles) two important contributions are expected: (1) local field effects due to near-field interaction between the emitter and its environment; (2) absorption, which can substantially modify the statistics of the decay rate. In particular, the statistics of the radiative and non-radiative rates are expected to behave differently in the presence of absorption [3].

In this work, we study the fluorescence-rate statistics in a finite size (nanoscopic) random medium (cluster), made of small spherical particles. For a given configuration of the system, we calculate numerically the Green tensor of the system. We deduce the spontaneous decay rate Γ, as well the radiative and the non-radiative contributions. Repeating the calculation for the configuration distribution and performing ensemble averages allows to compute the full statistics (probability density, average value, standard deviation). These numerical experiments are used as a basis for a physical discussion.

We focus on the regime in which the statistics is determined by near field interactions, with negligible multiple scattering. The decay rate statistics is influenced by the local environment of the emitter (i.e. the interaction with the surrounding particles). In particular, we show that for moderate absorption, the non-radiative contribution is proportional to the imaginary part of the dielectric of the particles. The radiative decay rate statistics is almost independent on the level of absorption. In this regime, and for particles with uncorrelated positions (random cluster), a simple analytical model describes the average decay rates and the standard deviation within a wide range of parameters.

In summary, we study the statistics of the spontaneous decay rates in disordered nanoscopic clusters using both numerical simulations and a simple analytical model. Our results show that such statistics carry useful information about the local structure of the environment at the nanometer scale, even in the presence of absorption. This paves the way towards new imaging techniques.

[1] E.M. Purcell, *Phys. Rev.* **69**, 681 (1946).
[2] W. Guo, *Phys. Rev. A*, **69**, 043802 (2004).
[3] R. Carminati *et al*., *Opt. Comm*. **261**, 368 (2006).

Magnetic response of micro-SQUIDs containing a semifluxon

M. Gaaß, A. Bauer, and C. Strunk
Institut für Experimentelle and Angewandte Physik,
Universität Regensburg, D-93025 Regensburg, Germany

S. Nadj-Perge and Z. Radović
Department of Physics, University of Belgrade,
P.O. Box 368, 11001 Belgrade, Serbia and Montenegro

M. Aprili
CSNSM-CNRS, Bât. 108, Université Paris-Sud, 91405 Orsay Cedex, France

(Dated: June 9th, 2006)

It is predicted that the current-phase relation (CPR) of weakly coupled superconductors can differ substantially from a simple sine form. This is due to higher Andreev-reflection processes in the high transparency case. The current-phase relation of Josephson-junctions is commonly investigated by embedding the junction in a superconducting ring resulting in a rf-SQUID-geometry.

We present measurements of the magnetic response of such samples. In order to measure the magnetic response of a superconducting loop with an embedded Josephson junction, we deposited the loop onto the active area of a Hall-sensor (Fig. 1a).

For the sample fabrication we are using a mask system employing shadow evaporation technique consisting of a sacrificial layer of polyethersulfone, a polymer that is highly stable under thermal stress. To match the special needs for evaporation of refractory metals like Niobium we use Si_3N_4 as mask material that is deposited by PECVD. As top layer standard PMMA for electron beam lithography is used in order to pattern the Si_3N_4. After the pattern transfer to the Si_3N_4 by reactive ion etching (RIE) an isotropic oxygen-plasma is used to create an undercut of up to 1 μm.

Upon sweeping an external magnetic field, the phase difference across the Josephson-junction can be controlled owing to the fact that the superconducting ring together with the junction needs to obey flux quantization. In order to do so, in general a circulating supercurrent that corresponds to the phase difference across the junction will flow. This

circulating current can be detected via its magnetic signal by means of Hall-magnetometry. When we measure the magnetic response of the ring for one of our samples where the angle adjustment during the shadow evaporation resulted in a parallel arrangement of both, a SFS- and a SNS-junction. In these samples we see an additional substructure in the switching behavior of the loop for a certain range of the external magnetic field. A typical measurement consists of up- and down-sweep over a range of ±2mT. At the point where the critical current of the junction is reached, one quantum of magnetic flux can enter the loop which can be seen as a sharp jump in the Hall-voltage yielding a sawtooth-like pattern. Upon increasing the external magnetic field further, more flux quanta enter the loop one after another. At a certain value of the external field, depending on the temperature at which we measure, a substructure starts to evolve (Fig. 1b). An additional peak arises upon increasing the external field while the original peak gets smaller and smaller. Finally the new peak superimposes the original sawtooth giving the same switching behavior as before. We interpret this as an effect of the magnetic coupling between the superconducting loop and a semifluxon that is supposed to form at the boundary between the two different parts of the junction. A numerical simulation with realistic parameters can fully reproduce our experimental results.

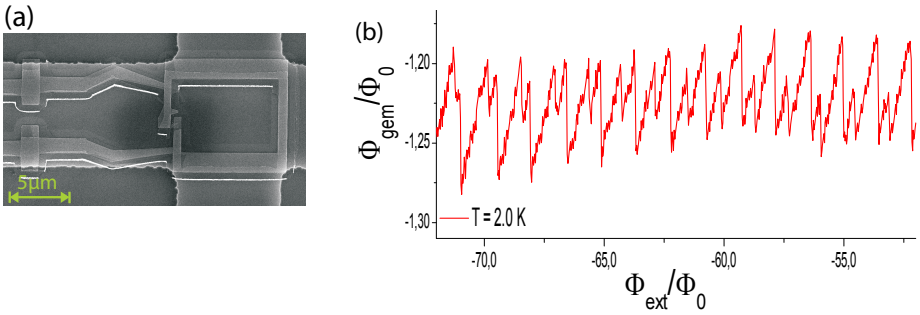


Abbildung 1: (a) Electron micrograph of the sample setup. The superconducting ring sits on top of the active area of a Hall-sensor. (b) Magnetic moment vs. external flux. The additional substructure encountered in our double junctions is clearly visible.

NANODOT PATTERNING OF SILICON SURFACES BY ION BEAM SPUTTERING

R. Gago,[1] L. Vázquez,[2] J.A. Sánchez-García,[2] O. Plantevin,[3,4] T.H. Metzger,[4] J. Muñoz-García,[5] M. Castro,[6] R. Cuerno[5], J.M. Albella[2], A. Redondo[1] and A. Climent-Font[1]

[1] Centro de Micro-Análisis de Materiales, Universidad Autónoma de Madrid, Spain
[2] Instituto de Ciencia de Materiales de Madrid, CSIC, Madrid, Spain
[3] Centre de Spectrométrie Nucléaire et de Spectrométrie de Masse, Orsay, France
[4] European Synchrotron Radiation Facility (ESRF), Grenoble, France
[5] Departamento de Matemáticas and GSIC, Universidad Carlos III de Madrid, Spain
[6] Grupo de Dinámica no lineal and GSIC, Universidad Pontificia de Comillas, Madrid, Spain
raul.gago@uam.es

The actual tendency of many technological processes requires the implementation of functional structures in the nanoscale range. In order to achieve defined structures with such dimensions, the use of self-organisation processes is gaining much attention recently. Among the "bottom-up" self-organized process, ion beam sputtering (IBS) has been shown to be a promising alternative [1]. In particular, ripple morphologies and regular arrays of dots can be produced on the irradiated surface, as those shown in Figure 1. Ripple morphologies are attained for off-normal ion irradiation whereas nanodots result under normal or isotropic ion incidence. The nanodot formation has been reported on several semiconductor systems such as GaSb, InP, Si, InAs and InSb [2]. While the formation of ripple patterns has been investigated experimentally and theoretically for a long time, the formation of regular dot arrays has gained attention only recently and is not yet fully understood [3].

Here, nanodot patterns were produced on Si(001) and Si(111) surfaces by low-energy (0.5-1 keV) Ar^+ ion bombardment at normal incidence. The resulting surface morphology was studied by means of atomic force microscopy (AFM), transmission electron microscopy (TEM), Rutherford Backscattering Spectrometry (RBS) in the channelling mode and surface-sensitive x-ray techniques at the European Synchrotron Radiation Facility (ESRF). These measurements provide complementary information about morphology, ordering and strain of the evolving nanostructures. The temporal evolution of the morphological features during the sputtering process, as well as the influence of the sputtering parameters on the pattern characteristics is addressed. Special attention is devoted to the crystallinity of the nanostructures and the role of the surface amorphous layer on the pattern formation. The results obtained not only have technological implications regarding the control over the pattern characteristics but also provide relevant information to contrast the existing theories of pattern formation by IBS. In particular, the introduction of a continuum 'hydrodynamic' model exploiting the analogy with aeolian sand dunes formation is highlighted [4].

References:

[1] U. Valbusa *et al.*, J. Phys. C **14** (2002) 8153;
[2] S. Facsko *et al.*, Science **285** (1999), 1551 ; F. Frost *et al.*, Phys. Rev. Lett. **85** (2000) 4116 ; R. Gago *et al.*, Appl. Phys. Lett. **78** (2001) 3316 ;
[3] M. A. Makeev, R. Cuerno and A.-L. Barabási, Nucl. Instr. and Methods in Physics Research B **197** (2002) 185 ; S. Facsko *et al.*, Phys. Rev. B **69** (2004) 153412 ; M. Castro *et al.*, Phys. Rev. Lett. **94** (2005) 16102.
[4] M. Castro, R. Cuerno, L. Vázquez and R. Gago, Phys. Rev. Lett. **94** (2005) 16102; M. Castro, *ibid.* **94** (2005) 139601; J. Muñoz-García, M. Castro, and R. Cuerno, *ibid*. **96**, (2006) 86101.

Figures:

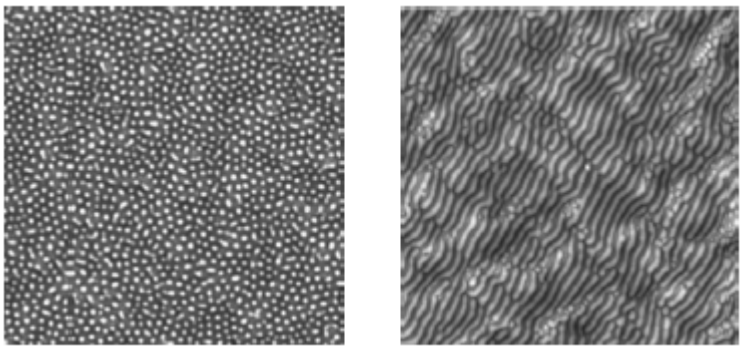


Figure 1: AFM images (2x2 μm^2) of Si(100) nanostructured surfaces after 5 min of Ar^+ ion sputtering under normal (left, nanodots) and off-normal (right, nano-ripples) ion incidence.

NANOWIRES AND SUSPENDED ATOMIC CHAINS FROM Au-Ag ALLOYS

J. Bettini[1], F. Sato[2], P. Z. Coura[3], S. O. Dantas[3], D. S. Galvão[2], D. Ugarte[1,2]
[1]Laboratório de Luz Síncrotron, 13084-971, Campinas-SP, Brazil
[2]Instituto de Física, UNICAMP, 13081-970, Campinas-SP, Brazil
[3]Departamento de Física, UFJF, 36036-970, Juiz de Fora-MG, Brazil

galvao@ifi.unicamp.br

In recent years a large amount of theoretical and experimental work has been carried out on the subject of atomic-size pure metal nanowires (NWs) generated by mechanical stretching [1]. However, it is essential to extend these studies to metal alloy NWs in order to gather information on the mechanical and electrical properties of alloy nanosystems. At the moment rather limited results have been obtained for these structures.

In this work we have used time-resolved high resolution transmission electron microscopy (HRTEM) and molecular dynamics simulations to study the atomistic aspects of the mechanical stretching of Au-Ag NWs of different compositions.

Metal NWs were produced *in situ* in the HRTEM (JEM-3010 URP 300 kV, 0.17 nm point resolution) using the methodology proposed by Kondo and Takayanagi [2]. The Au-Ag alloy thin films (10-30 nm in thickness) were prepared by thermal co-evaporation of both metals in a standard vacuum evaporator (10^{-7} mbar). A quartz crystal monitor was used to set the evaporation rate of each metal source and, subsequently, to measure the equivalent thickness of the alloy films.

In order to obtain more insights on the atomistic aspects associated with the structural evolution of metal alloy NWs, we have also carried out tight-binding molecular dynamics simulations using second-moment approximation (TB-SMA). This methodology has recently proved to be very efficient to study NWs [3,4].

In general terms our studies of metal alloy NWs revealed that, unlike pure metals, structural defects (mainly twins and stacking faults) are sometimes present at the apexes and very close to the narrowest wire constriction, or even in the NW themselves. Similarly to pure NWs we have observed the occurrence of linear atomic suspended chains (LACs) (Fig. 1). These are the first experimental evidences that LAC formation is possible from metallic alloys. HRTEM data analysis suggests that these atomic chains are composed of atoms of different types (Au and Ag). Molecular dynamics simulations also present these configurations (Fig. 2).

Another interesting aspect inferred from experiments and simulations is that the atomic-size Au-Ag alloy NWs exhibit a spontaneous gold enrichment of the nanojunction region during the wire thinning process. This leads to a dominant gold-like behavior, even for alloys with minor gold content. This can allow the spontaneous generation of organized Ag core-Au shell structured nanowires or even, in some cases, pure Ag surface enclosing a gold mono-atomic wire (Fig. 3). These phenomena open new opportunities to control the stability or length of the atomic chains by a suitable alloy composition.

Work supported in part by CAPES, CNPq, FAPESP, FAPEMIG, and SAMNBAS.

References:

[1] N. Agraït, A. L. Yeyati and J. M. van Ruitenveek, Phys. Rep. **377** (2002) 81.
[2] Y. Kondo and K. Takayanagi, Phys. Rev. Lett. **79** (1997) 3455.
[3] P. Z. Coura, S. B. Legoas, A. S. Moreira, F. Sato, V. Rodrigues, S. O. Dantas, U. Ugarte, and D. S. Galvão, Nano Lett. **4** (2004) 1187.
[4] J. C. González, V. Rodrigues, J. Bettini, L. G. C. Rego, A. R. Rocha, P. Z. Coura, S. O. Dantas, F. Sato, D. S. Galvão, and D. Ugarte, Phys. Rev. Lett. **93** (2004) 126103.

Figures:

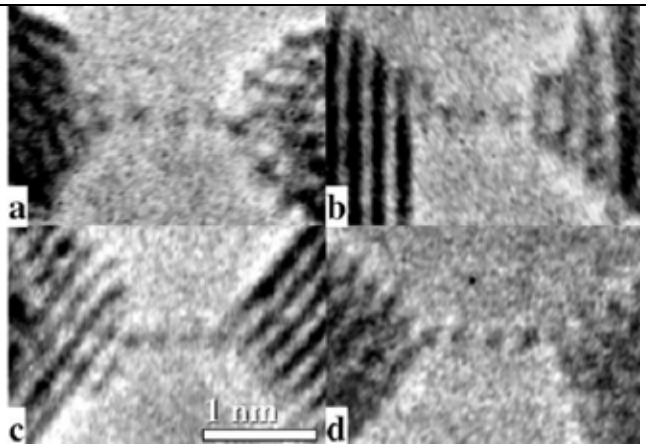


Figure 1 – Atomic resolved HRTEM snapshots of suspended atomic chains generated from different alloy compositions $Au_{1-x}Ag_x$, for x=0.2, 0.4, 0.6, and 0.8, respectively. Atomic positions appear dark.

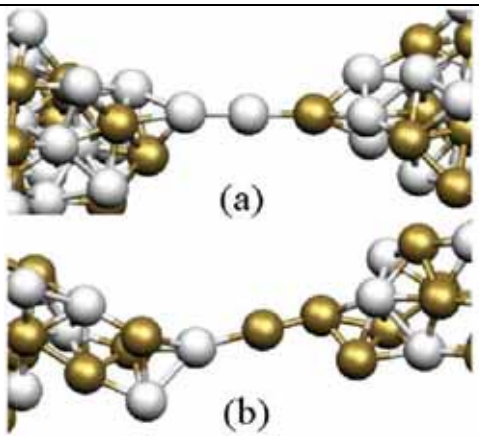


Figure 2 – Snapshots from the molecular dynamics simulations showing the formation of mixed linear suspended atomic chains from metal alloys. Yellow (gray) indicate gold (silver) atoms.
(a) $Au_{40}Ag_{60}$;
(b) $Au_{60}Ag_{40}$

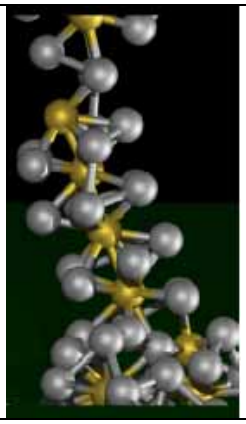


Figure 3 – Example of a configuration of pure Ag surface enclosing a gold mono-atomic wire obtained from molecular dynamics simulation for Au-Ag metal nanowire.

Study of Dynamic Magnetization Reversal Process in Ni Nanowires

A. A. Gandhi, I. Z. Rahman, Thomas Lynch, S. Belochapkine, K. M. Razeeb, M. A. Rahman*

Materials and Surface Science Institute (MSSI) & Department of Physics, National Technological Park University of Limerick, Limerick, Ireland
** Tyndall National Institute, University College Cork, Lee Maltings, Prospect Row, Cork, Ireland*

Contact: I. Z. Rahman, E-mail: zakia.rahman@ul.ie

This paper reports on the investigation of dynamic magnetization reversal process in Nickel nanowires by employing nanosecond magnetic pulse. Magnetization reversal process is characterized in terms of switching fields and time (ns to ps). If an external magnetic field of sufficient strength is applied parallel to a magnetic sample, the magnetization direction reverses in a characteristic way. The time required for a complete magnetization reversal of a magnetic material under the magnetic field called dynamic relaxation or switching time. The experimental techniques to measure magnetization reversal are described in this paper.

Nickel nanowires are grown by electrodeposition technique through the pores of nanochannel alumina (NCA). A detail description of the fabrication process of nickel nanowires inside porous alumina template has been reported in ref. [1]. The nanowires are examined by X-ray diffraction (XRD) for crystallographic analysis and surface analysis is carried out with atomic force microscopy (AFM), scanning electron microscopy (SEM) and Focused Ion Beam (FIB) technique. Magnetic properties of the nanowires grown inside the NCA templates are investigated using the Vibrating Sample Magnetometer (VSM). Figure 1 shows structural analysis of the nanowires grown inside the NCA templates by FIB technique.

Two different techniques are used to determine the nanosecond magnetization reversal in the nanowires: Magneto-Optic Kerr Effect (MOKE) described in Figure 2 and nanosecond pulsed field magnetometer. In both techniques, a co-planar waveguide, shown in Figure 2(b), is used as a source of nanosecond magnetic field and is generated using 0-200 V, 2-200 nanosecond pulse generator and a Helmholtz pair has provided the saturating and bias fields required for both techniques. Results of dynamical behavior as a function of several variables such as applied magnetic bias field, magnetic pulsed field amplitude and width are described in detail using both techniques. A computer simulation package called Object Oriented Micro-Magnetic Framework (OOMMF) has been used to simulate the magnetic domain patterns of the samples. These simulated domain patterns are compared with the experimental results based on MOKE images of magnetic domain patterns. In this paper a discussion of the dependence of magnetization reversal on the nanostructure that has evolved from the electrodeposition conditions will be presented.

References:

1) I. Z. Rahman, K. M. Razeeb and M. A. Rahman, Fabrication and characterization of nickel nanowires deposited on metal substrate, J. Magn. Magn. Mater. 262(1) (2003) 166.

Figures:

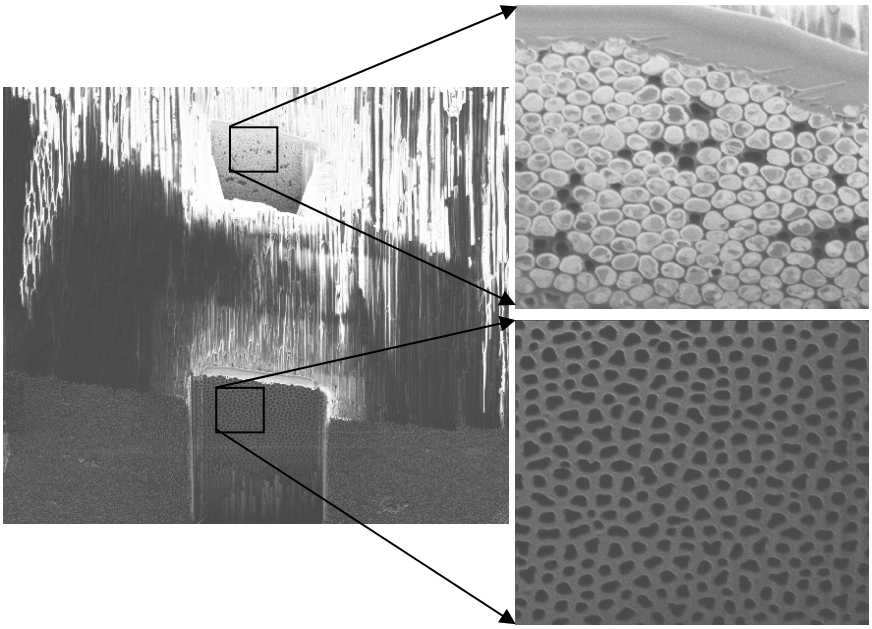


Figure 1: Focused Ion beam images of nano wire array grown inside NCA template. Top part shows the NCA pore filled with nickel nanowires and bottom part shows NCA nano pore without any fillings.

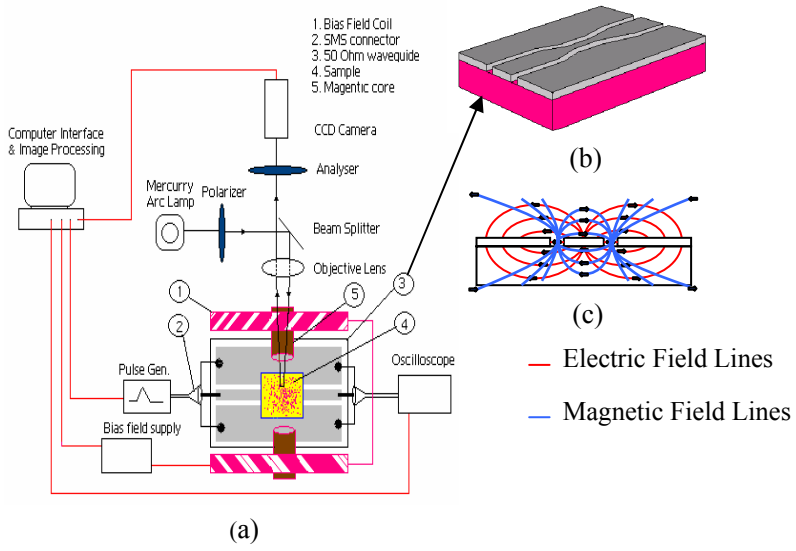


Figure 2: (a) Experimental set-up of longitudinal MOKE **(b)** Fabricated Co-Planar Waveguide (CPW) 3D view **(c)** Electric and magnetic field distribution in CPW

Poster

ELECTRONIC TRANSPORT THROUGH MOLECULAR BRIDGES WITHIN AB-INITIO METHODOLOGIES

Yamila García,[1] E. Louis,[1] and J. J. Palacios[1]

[1] *Departamento de Física Aplicada, Universidad de Alicante, San Vicente del Raspeig, Alicante 03690, Spain.*

Theoretical control of electron flow at the nanoscale will be only supported by a description at the quantum level, since atomic- and molecular-level information on structures in nanosized regions is needed[1–3]. Presumably, these basic informations will be attained within *ab-initio* methodologies[4]. This work is intended to shed light in the *ab-initio* methodology used in our group to describe quantum transport[5].

The discussion will be centered on three points:

- Electronic structure of Molecular Bridges. The electronic problems derived from the Shrödinger equation for the infinite system must be simplified in order to compute a numerical solution.

  It is currently admitted that a Density-Functional Theory (DFT) is the only manageable tool in this respect, regarding a compromise between accuracy and computational cost. The DFT success is based, for the most part, on the existence of manageable approximations to the local- exchange and correlation- potentials, local-v_{xc}, within Kohn-Sham formalism (DFT-KS methods)[6]. Concerning atomic-structure calculations, which relies on total-force-calculations, the DFT-KS success relies on the existence of manageable approximations to the exact local-v_{xc}. Concerning electronic-response calculations, which are supported on the calculation of the Green's functions[7], the applicability of DFT-KS is not well supported *a priori* [8]. In this respect, Todorov and di Ventra[9], showed that attempts to improve the DFT-KS description of an electronic transport problem could be done within Time-Dependent DFT. In this line, some recent theoretical works, formally establishes the non-existence of an exact Time-Dependent DFT-KS, (TDDFT-KS), for the characterization of electrical response [10, 11]. In addition, they formally stated, that the addition of non-local corrections to v_{xc} in the TDDFT-KS methodology is a necessity, for an exact formulation of electrical response, (**TDCDFT**).

  With all these premises, we propose a route to correct DFT-KS methodologies but remaining within mean-field methods. Numerically, we suggested that a DFT formulation of electronic response must be managed with the introduction on non-local dependences in v_{xc}. The influence of these non-local dependences is studied updating the spirit of Becke's works labeled as **Hybrid-DFT** [12]. The amount of the non-local corrections to v_{xc} is proposed through a parameter-free route[13]. Remarkably, our numerical **Hybrid-DFT** results, are closer to the experimental measurements of electronic conductance in molecular bridges than those reported within DFT-KS methodologies. The same level of agreement is being notice when comparison between **TDCDFT** and TDDFT-KS are performed at the zero-frequency limit[11].

- Chemistry-based Molecular Electronics. There are no doubts that the electronic transport measurements through molecular bridges strongly depends on the atomic arrangements in the region which connect this *finite* system to the *infinite* metallic nanocontacts. These nanojuntions exhibit radically new properties that cannot be anticipated from the behavior as finite clusters or in the bulk. These changes open up the possibility of exploring novel ideas. Nevertheless, to place this capacity in perspective, research is needed in a new field labeled Chemistry-Based Molecular Electronics. So far, we are *transporting* the capabilities of the traditional Molecular Chemistry and Condensed Matter, to this novel field. Therefore, to characterize the molecular bridges chemically, we start using standard topographical concepts like reaction bonds, self-assembly, and atomic configurations. Besides, we are assuming the existence of energetically well-defined molecular orbitals which are employed throughout the analysis of the density of states in the zone to be chemically studied[14].

- Statistical analysis of Conductance measurements.

  The characterization of Molecular Bridges is necessarily carried out through a statistical analysis of the low-bias conductance with what is called conductance histograms[2, 3]. Within this work we approach this statistical description, based on the existence of a distribution function for the electronic conductance measurements $f \equiv f(G)$. The parameters needed in the model for $f(G)$ such as, the number of the accessible microstates, the value of the conductance in those positions, and the estimation of deviations is done within the *ab-initio* methods describe in the two sections above.

To conclude, we present numerical results for some well-know samples in the context of Theoretical Molecular Electronics and in close relation to recent experimental measurements[2, 3]. The systems selected range from a single Hydrogen to carbon-based molecules like benzene dithiolate, placed between Platinum and Gold nanocontacts (see Figure 1).

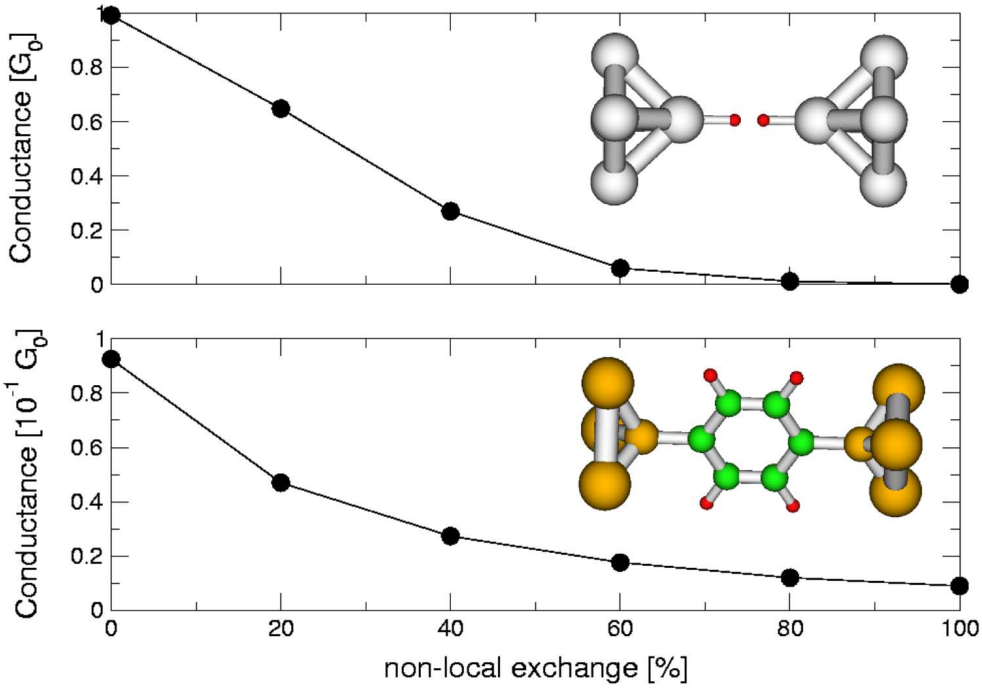


FIG. 1: **Reduction of the conductance** due to the progressive substitution of the local DFT-KS potential by a non-local contribution, Hybrid-DFT ($G_0 = 2\frac{e^2}{h}$).
Up: Hydrogen bridging Pt nanocontacts.
Down: Benzene dithiolate bridging Gold nanocontacts.

[1] A. Aviram and M. A. Ratner, Chem. Phys. Lett. **29**, 277 (1974).
[2] R. H. M. Smit, Y. Noat, C. Untiedt, N. D. Lang, M. C. van Hemert, and J. M. van Ruitenbeek, Nature (London) **419**, 906 (2002).
[3] X. Xiao, B. Xu, and N. J.Tao, Nanoletters **4**, 267 (2002).
[4] A. W. Ghosh and S. Datta, J. Comp. El. **1**, 515 (2002).
[5] E. Louis, J. A. Vergés, J. J. Palacios, A. J. Pérez-Jiménez, and E. SanFabián, Phys. Rev. B **67**, 155321 (2003).
[6] W. Kohn, Reviews of Modern Physics **71**, 50 (1999).
[7] S. Datta, *Electronic transport in mesoscopic systems* (Cambridge University Press, Cambridge, 1995).
[8] R. M. Martin, *Electronic Structure. Basic Theory and Practical Methods* (Cambridge University Press, 2004).
[9] M. D. Ventra and T. N. Todorov, Journal of Physics: Condensed Matter **16**, 8025 (2004).
[10] G. Vignale and W. Kohn, Phys. Rev. Lett. **77**, 2037 (1996).
[11] N. Sai, M. Zwolak, G. Vignale, and M. D. Ventra, Phys. Rev. Lett. **94**, 186810 (2005).
[12] A. D. Becke, J. Chem. Phys. **98**, 5648 (1992).
[13] Y. García, J. Sancho-García, E. SanFabián, J. A. Vergés, E. Louis, and J. J. Palacios (to be published).
[14] J. J. Palacios, A. J. Pérez-Jiménez, E. Louis, E. SanFabián, J. A. Vergés, and Y. García, in *Computational Chemistry: Reviews of Current Trends*, edited by J. Leszczynski (World Scientific, Singapore-New Jersey-London-Hong Kong, 2005), vol. 9, in press.

SEMICONDUCTING - METALLIC TRANSITION IN DOPED SINGLE WALLED CARBON NANOTUBE (SWCNTs)

Dr.V.Gayathri and R.Geetha

Department of Physics, Thiagarajar College of Engineering, Madurai – 625 015

Email: drvg2004@rediffmail.com

The versatile material Carbon nanotubes familiarly called CNTs has tremendous potential applications due to its unique structure dependent properties [1]. Based on the type of nanotube such as armchair, chiral and zigzag it could exhibit different behaviour in the presence of external perturbations. The size of carbon nanotube falls in the region of low dimensional systems, and so it can be considered as quantum wire [2]. Here in this paper we are interested in analyzing the electrical properties of single walled nanotube with and without doping [3].

Doping mechanism in semiconductor [4], especially with N-type impurities is a well-studied topic and the main purpose of such a kind of doping is for increasing the conductivity of the materials. As the Carbon nanotubes has high conductivity even without doping, not much work is done on this aspect. But apart from the conductivity there are several other properties, which can be improved by doping, like transition and field emission.

Experimentally it was observed that the dopants like nitrogen could change the chemical and electrical properties considerably even for small amount as < 0.5 % [5]. In this work, treating CNTs as quantum wires the ionization energies are calculated by using suitable wave function [6] for various values of impurity concentrations. The results show that the ionization energies decrease as the concentration ('n' per cm^2) increases. We could observe a transition from semiconducting to metallic, approximately for the critical value of 'n' of the order of $10^{12}/cm^2$. The estimated values of ionization energies, as a function of impurity concentration will be presented to show the transition. Effect of the diameter of SWCNT on the critical concentration will also be discussed. This result is significant for the fabrication of CNT based nanodiodes and transistors [7].

References:

1. R. Saito, G. Dresselhaus and M. S. Dresselhaus, Physical Properties of Carbon Nanotubes, Imperial College press (2003)
2. S. J. Tans et al., Nature, 386 (1997) 474
3. Andriy H. Nevidomskyy, Ga´bor Csa´nyi, and Michael C. Payne, Phys.Rev.Lett., 91 (2003) 105502
4. Introduction to Solid State Physics, Charles Kittel, 7/e (John Wiley & Sons, Inc.) (1979)
5. http://www.pcpm.ucl.ac.be/themes/TRANSPORT_NT.php
6. M.K.Kostov, M.W.Cole and G.D.Mahan, Phy.Rev. B, 66 (2002) 075407
7. K. Efsarjani, A. A. Farajin, Y. Hashi, Y. Kawazoe, Appl. Phys. Lett., 74 (1999) 79

GROWTH AND STUDY OF SILICON NANOWIRES BY CATALYST ASSISTED LPCVD.

P. Gentile[1], F. Dhalluin[3], P. Ferret[2,] T. Baron[3], T. David[1], K. Aissou[3], D. Buttard[1]
[1] CEA-DRFMC, [2] CEA-LETI , [3] LTM-CNRS, Grenoble France.

Silicon nanowires (SiNWs) are promising materials for some of the basic building blocks in microelectronics (interconnects, transistor channel, nanoelectrodes, etc.) as well as the emerging application areas of photonics, chemical sensing, and solar cells.

Silicon nanowires (SiNWs) are grown on silicon (111) and (100) substrates in a Low Pressure Chemical Vapour Deposition (LPCVD) reactor. Silane is used as a reactive gas diluted in hydrogen. Catalysts are obtained by gold film dewetting or by colloidal gold deposition on silicon surfaces. With the dewetting method is difficult to obtain small diameter nanowires, typically less than 50 nm, to reach this dimension gold colloid is used. Experimental parameters such as growth temperature, SiH_4 partial pressure, and substrate orientation were investigated with different catalysts.. The temperature dependence of growth rate is measured in the 450°C – 700°C range, showing activation energy of 71 KJ/mole for NWs diameters between 50 and 500 nm. For NWs less than 50 nm we have observed that the NWs length are limited by increasing growth temperature. TEM and SEM are used to probe crystalline quality and shape of the SiNWs. TEM images are obtained on SiNWs dispersed on copper TEM grid. In a effort to add a higher level of organization to NWs growth, the metal catalyst was organised using the self-assembled properties of copolymer diblocks and porous alumina as a deposition mask.

MONOPOLE-DIPOLE INTERACTION MODEL FOR CARBON ONIONS

N. Geuquet[1], R. Langlet[1], A. Mayer[1], L. Henrard[1] and Ph. Lambin[1]
[1]*Laboratoire de Physique du Solide, Facultés Universitaires Notre-Dame de la Paix, rue de Bruxelles 61, 5000 Namur, Belgium*
nicolas.geuquet@fundp.ac.be

We have modelled the dielectric response of fullerenes and carbon onions with a regularized monopole-dipole interaction model, which takes into account itinerant charges of the carbon sp^2 network [1]. The model has three adjustable parameters that were fitted to reproduce the measured polarizability values of isolated C_{60}, C_{70} and C_{84} molecules, essentially [2]. This model allows us to deal with the metallic behaviour of some carbon nanosystems. It yields a fairly good behaviour of the polarizability of fullerenes of various sizes and shapes. Calculations of static polarizability of hyper-fullerenes were performed with this model, for both single-shell and multi-shell nested hyper-fullerenes. This work aimes at characterizing the dielectric properties of nanocomposites materials embedding onions and onion-like carbons. (NATO Sciences for Peace Project 981051)

References

[1] A. Mayer, Appl. Phys. Lett. **86** (2005), 153110
[2] A. Mayer, Ph. Lambin and R. Langlet, Phys. Rev. Lett., submitted for publication (2006)

NANO-FABRICATION WITH FOCUSED ION BEAMS - WHERE ARE THE RESOLUTION LIMITS?

J. Gierak[a], A. Madouri[a], A. L. Biance[a], E. Bourhis[a], G. Patriarche[a], C. Ulysse[a], X. Lafosse[a], L. Auvray[b], L. Bruchhaus[c], R. Jede[c] and Peter Hawkes[d]

[a] *Laboratoire de Photonique et de Nanostructures Route de Nozay, F-91460 Marcoussis*
[b] *MPI, Université d'Évry Val d'Essone, Bd. François Mitterrand, F-91025 Évry Cedex*
[c] *Raith GmbH, Hauert 18, Technologiepark, D-44227 Dortmund, Germany*
[d] *CEMES/CNRS, 29 rue Jeanne Marvig, F-31055 Toulouse*
Contact: jacques.gierak@lpn.cnrs.fr

The interactions between energetic ions and solids lead to well-known processes that are widely used to modify the topography, crystallography or electronic properties of the irradiated target. These effects are widely exploited in microelectronics like ion etching and doping applications. Focused Ion Beam (FIB) is a technology that is extending these capabilities. Nowadays FIB instruments combining etching and deposition have become indispensable in such fields as failure analysis, transmission electron microscope (TEM) sample preparation.

We will describe our specific iterative effort started under the Nano-FIB EC project combining developments in liquid metal ion source geometries and research in ion optics specifically for high-resolution applications, together with ion induced damage fine characterisation. Our objective was to demonstrate that the Focused Ion Beam technique could be a challenging technique for nanotechnology. We were anticipating that lateral patterning of structures having one nanometre-sized dimension (thickness) with FIB would no longer rely on sputtering effects with high local incident dose ($> 10^{16}$ ions/cm²), but rather on local defect injection and surface modifications of high crystallinity substrates [**1**].

We will present our work aiming to explore the nano-structuring potential of a highly focussed pencil of ions. We will show that Focused Ion Beam technology (FIB) is capable of overcoming some basic limitations of current nano-fabrication techniques and to allow innovative patterning schemes for nanoscience. In this work, we will first detail the very high resolution FIB instrument we have developed specifically to meet nano-fabrication requirements. Then we will introduce and illustrate some new patterning schemes we have proposed for next generation FIB processing. These patterning schemes are ranging from Nano-engraving to local defect injection via the functionalisation of substrates to selective epitaxy of semiconductors. Thus demonstrating that FIB patterning is fully compatible with "bottom-up" or "organisation" processes [1].

Finally we will present the potential of our instrument now capable to fabricate **directly** nano-pores with diameters below **5 nm**. To our knowledge this performance is defining a new state of the art in direct removal of particles using a focused charged particle beam.

[**1**] Exploration of the ultimate patterning potential achievable with high resolution focused ion beams, J. Gierak , D. Mailly, P. Hawkes, R. Jede, L. Bruchhaus, L. Bardotti, B. Prével, P. Mélinon, A. Perez, R. Hyndman, J.-P. Jamet, J. Ferré, A. Mougin, C. Chappert, V. Mathet, P. Warin, J. Chapman: Appl. Phys. A, 10.1007/s00339-004-2551-z (2004)

ENGINEERED ORIENTATIONAL AND CHIRAL ORDER IN ORGANIC MOLECULAR FILMS

Nick Gislason, Calvin Murphy, and David Patrick
Department of Chemistry, 516 High Street, Western Washington University, Bellingham, WA 98225-9150

It has been previously noted that for certain classes of organic thin-films, the molecular organization in the film is strongly correlated to its optical, electronic, and chemical properties, therefore it is of great interest to understand how molecular organization can be controlled in thin-films.[1] With respect to physisorbed self assembled monolayers (pSAM's), other groups have studied the effects of substrate, solvent, and intermolecular interactions on the molecular order/organization in the films.[2,3,4,5] Our group has successfully used thermotropic liquid crystal (LC) solvents to rationally instill long range orientational and chiral molecular order on pSAM's, a process we call liquid crystal imprinting (LCI). Current studies seek to determine the mechanism by which order can be communicated to a pSAM during LCI.

[1] E.A. Silinsh, V. Capek, "Organic Molecular Crystals Ineraction, Localization, and Transport Phenomena", AIP Press, New York (1994)
[2] De Feyter, S., Schryver, F.C.D. *J. Phys. Chem. B.* **2005,** *109*, 4290-4302.
[3] Mamdouh, W.; Uji-I, H.; De Feyter, S.; et al. "Solvent Controlled Self-Assembly at the Liquid-Solid Interface Revealed by STM." *JACS*, **2006**, *128*, 317-325.
[4] Shao, X.; Luo, X.; Hu, X.; Wu, K. "Solvent effect on self-assembled structures of 3,8-Bis-hexadecyloxy-benzo[*c*]cinnoline on HOPG" *J. Phys. Chem. B.* **2006**, *100*, 1288-1293.
[5] Giancarlo, L.C.; Fang, H.; Rubin, S.M.; Bront, A.A.; Flynn, G.W. *J. Phys. Chem. B.* **1998**, *102*, 10255-10263.

OPTICAL FORCES IN PLASMONIC SYSTEMS

R. Gómez-Medina, and O. J. F. Martin

Nanophotonics and Metrology Laboratory, Swiss Federal Institute of Technology, 1015 Lausanne, Switzerland
raquel.gomezmedina@epfl.ch

In spite of the development of laser, our potential to manipulate small particles at a distance is much more limited than our ability to control the motion of the electrons. The interest to develop a powerful, nonmechanical, nondestructive and highly precise technique to manipulate and control small particles has developed a no end researchers in many areas of physics, chemistry and biology. The idea that light may affect the motion of matter has been known since the 17th century when Kepler conjured that comets tails were repelled by a solar light pressure, nevertheless it was Petrus Debye [1] who convinced the scientific community of the possibility to induce important radiation pressure forces on objects such as spheres, when a Mie resonance is tuned. Since 1970 when Ashkin and co-workers demonstrated levitation and trapping of micrometric particles [2], much effort has been devoted to exploring new techniques for trapping and manipulating all kinds of particles. By fashioning proper optical field gradients it is possible to trap and manipulate small particles with optical tweezers or create atomic arrays in optical lattices [3]. Using the evanescent field as the propagating wave it is possible to create an atomic mirror [4], manipulate Mie dielectric and 0.5 m gold particles in the evanescent region of a prism or along channelled waveguides [5]. Although far from the particle resonances light forces are, in general, very small, when the fields are confined in quasi one-dimensional waveguide structures, the coupling of the scattered dipolar field with the waveguide modes leads to a resonant state close to the threshold of a new propagating mode [6] that produces an enhanced resonant radiation pressure [6, 7] and also unusual strong optical interactions between particles [8].

Recently, another type of resonant optical system has caught a lot of attention: namely plasmonic systems, where the free electrons in a metal can be resonantly excited at optical frequencies. This resonant excitation creates extremely strong and confined electromagnetic fields, which can in turn enhance specific chemical interactions such as Raman scattering or fluorescence [9]. Quite surprisingly, optical forces are not very well known in plasmonic systems. This is probably due to the fact that the fabrication of such systems has only been mastered very recently with the advances of nanofabrication. Indeed, plasmonic systems – being it particles of films – have usually dimensions in the sub-100nm range. Plasmonic systems are also extremely sensitive to the illumination wavelength, and the field distribution they produce can dramatically change, depending whether the illumination wavelength corresponds to that of the plasmon resonance or not. Furthermore, by altering the surface, i.e., modifying size, shape and/or the environment of the metal, the conditions for plasmonic resonances can by tailored at will.

The objective of the present contribution is to study some specific effects related to optical forces in plasmonic systems. These include the fact that the strength of optical forces can be changed by tuning slightly the illumination wavelength , as illustrated in Fig. 1. This figure shows that the optical environment around a sub-wavelength cylindrical particle can be dramatically changed by tuning the illumination wavelength at the vicinity of the plasmon resonance of the system. Out of resonance, the field is strongly inhomogeneous, with a minimum just below the particle (Fig. 1.a). When the illumination field excites a surface

plasmon on the metallic film, the particle becomes immersed in a strong and homogeneous field (Fig. 1.b)

The interplay between the particle and the metallic interface is actually very subtle. Indeed, for a perfectly flat interface, no surface plasmons can be excited on the metallic film, since the dispersion relation of the surface plasmon is located below the light cone. No free-space propagation vector can therefore excite the surface plasmon. The light scattered by the particle however, creates many different wave vectors, including those required to excite the surface plasmon. This effect is mainly a near-field effect though, and the coupling between the particle and the metallic film strongly decreases as their separation increases.

References

[1] P. Debye, *Ann. Phys*. **30**, 57, 1909.
[2] A. Ashkin, *Phys. Rev. Lett*. **24**, 156 (1970).
[3] A. Ashkin, *Science* **210**, 1081 (1980); K. Svodova and S. M. Block, *Opt. Lett.* 19, 930 (1994); D.G. Grier, *Nature* **424**, 810 (2003); P. Verkerk et al., *Phys. Rev. Lett.* **68**, 3861 (1992); P. S. Jessen et al., ibid. **69**, 49 (1992).
[4] R. J. Cook and R. K. Hall, *Opt. Commun*. **43**, 258 (1980).
[5] S. Kawata and T. Sugiura, *Opt. Lett*. **17**, 772 (1992); S. Kawata and T. Tani, *Opt. Lett*. **21**, 1768 (1996).
[6] R. Gómez-Medina et al., *Phys. Rev. Lett.* **86**, 4275 (2001).
[7] P. Horak, P. Domokos, and H. Ritsch, *Europhys. Lett*. **61**, 459 (2003).
[8] R. Gómez-Medina and J.J. Sáenz, *Phys. Rev. Lett.* **93**, 243602 (2004).
[9] J. P. Kottmann and O. J. F. Martin, *Phys. Rev. B* **64**, 235402, (2001). J. P. Kottmann et al., *Opt. Express* **6**, 213 (2000).

Figures:

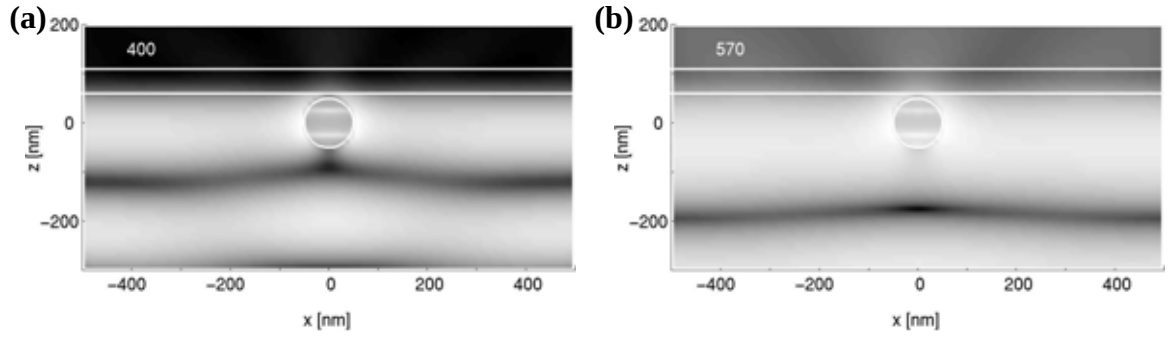


Fig. 1: Electric field intensity distribution of a dielectric particle (index n=1.5, diameter d=100nm) located 10nm below a gold film (thick 50nm) under planewave normal illumination from underneath (electric field in the plane of the figure). (a) Out of resonance (λ=400nm), (b) when a surface plasmon-polariton is excited on the golf film (λ=570nm).

FINITE SIZE EFFECTS ON THE OPTICAL RESONANCES OF NANOCYLINDER ARRAYS

R. Gómez-Medina and O. J. F. Martin
Nanophotonics and Metrology Laboratory, Swiss Federal Institute of Technology, 1015 Lausanne, Switzerland

S. Albaladejo, M.Laroche and J. J. Sáenz
Departamento de Física de la Materia Condensada and Instituto "Nicolás Cabrera" Universidad de Madrid, 28049 Madrid, Spain
raquel.gomezmedina@epfl.ch

The study of light scattering from periodic structures has been a topic of interest during the last century. Already in 1902, Wood [1, 2] reported remarkable effects (known as Wood's anomalies) in the reflectance of one-dimensional (1D) metallic gratings. Two different types of anomalies were definitely identified by Fano [3]. One is associated to the discontinuous change of intensity along the spectrum at sharply defined frequencies and was already discussed by Rayleigh [4]. The other is related to a resonance effect. It occurs when the incoming wave couples with quasi-stationary waves confined in the grating. The nature of the confined waves depends on the details of the periodic structure [5] and is usually associated to surface Plasmon polaritons in shallow metallic gratings, standing waves in deep grating grooves [5] or guided modes in dielectric coated metallic gratings [6].

In an infinite array of sub-wavelenght cylinders, the coupling of the scattered dipolar field with diffraction modes may induce dramatic resonant effects close to the onset of new propagating modes even in absence of particle resonant modes, i.e. when the cross-section of a single non-resonant nanocylinder is extremely small [7].

As we can see in Fig. 1, at the lowest resonance frequency, and in the absence of absorption, the wave is perfectly reflected even for vanishingly small cylinder radii. These sharp resonances, so-called geometrical resonances, with typical Fano line shapes, present a strong dependence with the angle of incidence and could play an important role in the design of chemical and biological sensors. However, for practical applications, finite size effects must be considered.

Here we present a multiple scattering analysis of the reflectance of a finite array of sub-wavelength cylinders. The finite array, made of N parallel infinite cylinders separated by a distance d, is illuminated by a Gaussian beam of width W_0 ($W_0<N_d$). As we will show, the shape and strength of the resonance depend mainly on the width of the Gaussian beam (i.e. on the number of cylinders under illumination).

References

[1] R.W. Wood, *Proc. R. Soc. London A* **18**, 269 (1902).
[2] R.W. Wood, *Phys. Rev.* **15**, 928 (1935).
[3] U. Fano, *J. Opt. Soc. Am.* **31**, 213 (1941).
[4] Lord Rayleigh, *Proc. Roy. Soc. (London) A* **79**, 399 (1907).
[5] A. Hessel and A. A. Oliner, *Appl. Opt.* **4**, 1275 (1965)
[6] M. Nevière, D. Maystre, P. Vincent, *J. Opt. (Paris)* **8**, 231 (1977).
[7] R. Gómez-Medina, M. Laroche and J.J. Sáenz, *Opt. Express*. **14**, 3730 (2006).

Figures:

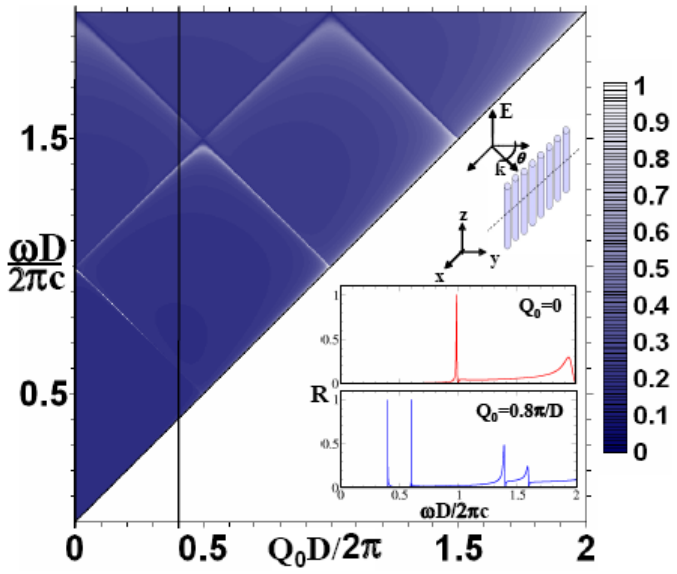


Fig. 1: (s-polarization) Reflectance of a infinite array of sub-wavelength cylinders in a frequency ω versus in-plane wave number $Q_0 = (\omega/c)\sin(\theta)$. The reflectance along the vertical lines is shown in the inset.

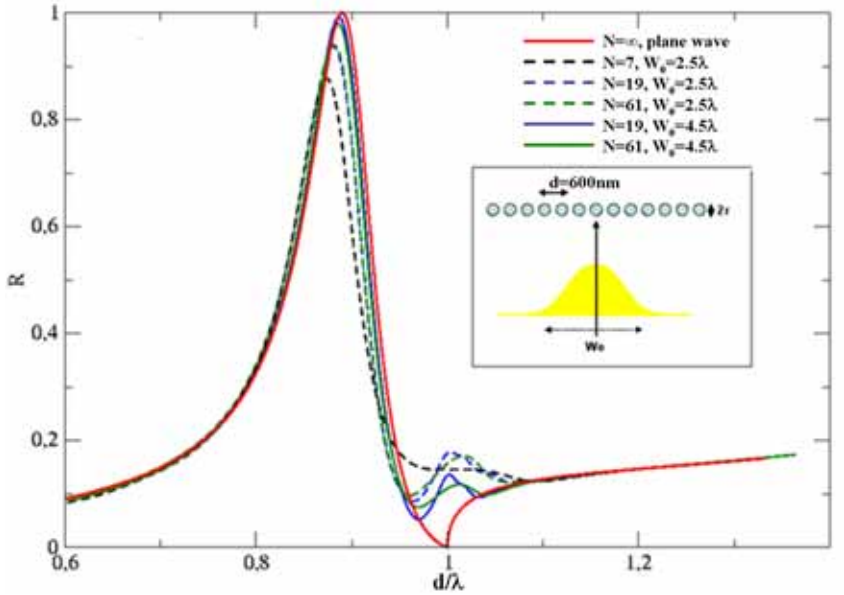


Fig. 2: Reflection coefficient for a set of parallel Si cylinders (ε=11.9, r=45nm) versus d/λ for different beam widths and cylinder numbers.

Poster

NITRIDED FeB AMORPHOUS THIN FILMS FOR NANO ELECTROMECHANICAL SYSTEMS (NEMS)

I. Fernández, M. S. Martín-González, R. González-Arrabal,R. Álvarez, J. L. Costa-Krämer, and F. Briones
Instituto de Microelectrónica de Madrid C/ Isaac Newton, 8. Tres Cantos. Madrid. E-28760 (Spain)
Kramer@imm.cnm.csic.es

Amorphous alloys present high electrical resistivity, good mechanical properties, improved corrosion resistance, soft magnetic response, high magnetic moment and Curie temperatures, and great ability to tailor their magnetic properties with continuous composition variations over a broad range. Previous experiments performed in Fe-based primary alloys have demonstrated the strong dependence of their magnetic properties on the Fe-partner concentration. It is well known the dependence of the magnetic properties of amorphous Fe_xB_{100-x} [1-3] and of crystalline Fe_yN_x [4-7] films on the boron and on the nitrogen concentration, respectively. Moreover, some studies have been done in Fe-B-N ternary alloys in which boron and nitrogen have been implanted in pure Fe films at different fluencies [8], in amorphous Fe-B-N alloys grown by co-sputtering onto a BN and a pure Fe target [9] and in crystalline Fe-B-N films prepared by reactive RF magnetron sputtering [10]. These studies show the variation of structural, electrical and corrosion resistance properties as a function of the nitrogen concentration for amorphous films, as well as, the dependence of the magnetic properties on the nitrogen concentration for crystalline films with a concentration of Fe higher than 80 at%.

The objective of this paper is to study the dependence of the magnetic and magnetoelastic properties of Fe-B-N ternary alloys on the Nitrogen concentration. Fe-B-N amorphous films have been grown by DC sputtering of a $Fe_{80}B_{20}$ target in a mixture of Argon and Nitrogen atmospheres for different nitrogen partial pressures on glass and on <100>Si substrates. For comparison an amorphous Fe-B film was also grown. It is demonstrated that nitrogen incorporates into the amorphous lattice while preserving the amorphous structure, modifying their composition and magnetic properties. The amount of nitrogen that incorporates into the amorphous structure is measured to scale approximately linearly with the nitrogen partial pressure during growth. X-Ray Diffraction data show that for low deposition times (t<10 min) all the samples are amorphous while for longer deposition time a crystallization of the structure is observed due to the heating during the deposition. XPS data reveal that N preferentially bond to B, giving rise to B_xN_y and an iron-rich $Fe_{80}B_{20}$ films. The atomic percentage of B_xN_y increases with increasing the nitrogen concentrations.

A ~20% increase of both the saturation magnetization and the saturation magnetostriction constant are found for the composition $Fe_{0.74}$ $B_{0.18}$ N_x, when x is around 7 to 9%, when compared to pure $Fe_{80}B_{20}$ amorphous films. These films are grown at moderated ~2-3% nitrogen partial pressures by triode DC sputtering.

Because their high magnetostriction coefficient and their magnetic softness, these materials offer great potential for the incorporation into micro and nano magneto mechanical devices as actuators.

References:

[1] N. A. Blum, K. Moorjani, T. O. Poehler, and F. G. Satkiewicz, J. Appl. Phys. **53** (1982) 2074-2076
[2] A. S. Dehlinger, J. F. Pierson, A. Roman, P. Bauer, Surf. Coat. Techn. **174-175** (2003) 331-337
[3] C. L. Chien and D. Musser, E. M. Gyorgy, R. C. Sherwood, and H. S. Chen, F. E. Luborsky and J. L. Walter, Phys. Rev. B **20** (1979) 283–295
[4] P. Schaaf, C. Illgner, M. Niederdrenk, K. P. Lieb, Hyper. Inter. **95** (1995) 199-225
[5]E. Andrzejewska, R. Gonzalez-Arrabal, D. Borsa, and D. O. Boerma, Instr. Meth. B **249** (2006) 838-842
[6] C. Sánchez-Hanke, R. Gonzalez-Arrabal, J. E. Prieto, E. Andrzejewska, N. Gordillo, D. O. Boerma, M. Mitra, J. Skuza and R.A Lukaszew , J. Appl. Phys. **99** (2006) 709-712
[7] J.L. Costa-Krämer, D.M. Borsa, J.M. García, M.S. Martín-González, D.O. Boerma, and F. Briones Phys. Rev. B. **69**, 2004, 144402(1:8)
[8] V. V. Uglov, J. A. Fedotova, J. Stanek, Surf. Coat. Techn. 128-129 (2000) 351-357
[9] H. Karamon, T. Masumoto, Y. Makino, . Appl. Phys. 57 (1985) 3527-3532
[10] K. H. Kim, J. H. Jeong, J. Kim, S. H. Han, H. J. Kim, J. Magn Magn. Mater. 239 (2002) 487-489

Figures:

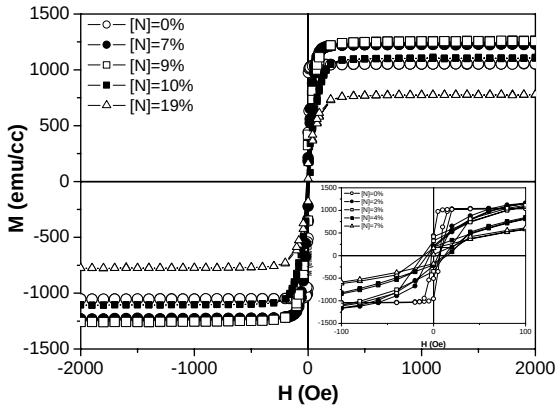


Figure 1. Magnetization measurements using a SQUID magnetometer for a Fe-B reference sample (open dots) and for Fe-B-N samples with different nitrogen concentration: [N]=7% (filled dots), [N]=9% (open square), [N]=10% (filled square), [N]=19% (open triangles).

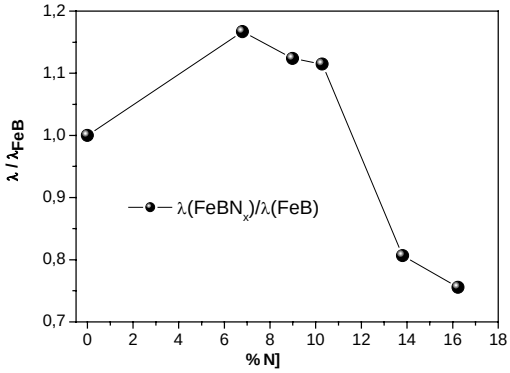


Figure 2. Magnetostriction values for Fe-B-N samples with different nitrogen concentration normalized to the magnetostriction value for a Fe-B film versus the nitrogen concentration in the samples.

GaN/ALN NANOSTRUCTURES FOR INTERSUBBAND OPTOELECTRONICS AT TELECOMMUNICATION WAVELENGTHS

F. Guillot (1), E. Bellet-Amalric (1), E. Monroy (1), M. Tchernycheva (2), L. Nevou (2), L. Doyennette (2), F. H. Julien (2), E. Baumann (3), F. Giorgetta (3), and D. Hofstetter (3)

(1) Equipe mixte CEA-CNRS-UJF Nanophysique et Semiconducteurs, DRFMC/SP2M/PSC, CEA-Grenoble, 17 rue des Martyrs, 38054 Grenoble Cedex, France.
(2) Action OptoGaN, Institut d'Electronique Fondamentale, Université Paris-Sud, UMR 8622 CNRS, 91405 Orsay Cedex, France.
(3) University of Neuchâtel, 2000 Neuchâtel, Switzerland.
fabien.guillot@cea.fr

Nitride semiconductors, with a large conduction-band offset (~1.8 eV for GaN/AlN), are promising materials for intersubband (ISB) optoelectronics in the near infrared. To develop nitride ISB devices, the growth of quantum well (QW) and quantum dot (QD) superlattices has to be precisely controlled. In particular, to operate at optical fiber telecommunication wavelengths (1.3 µm, 1.55 µm), QWs and QDs thickness should be reduced to ~1 nm. In this work, we present a study of the growth of GaN/AlN QW and QD infrared photodetectors by plasma-assisted molecular-beam epitaxy.

From the QW superlattice point of view, we have analyzed the effect of Ga and In as a surfactant during growth, as well as the effect of growth interruptions at the AlN/GaN interfaces. Best structural and optical results are obtained on samples grown with Ga as a surfactant during the deposition of both GaN and AlN, leading to an interface roughness at the monolayer scale [1]. On the other hand, Si doping is required in order to populate the first electronic level in the QWs. We have demonstrated that incorporation of Si up to 10^{20} cm^{-3} has no effect on the structural quality of the QW superlattice. From the optical viewpoint, Si doping broadens the emission and absorption spectra and introduces a blue shift due to the screening of the internal electric field. These results are independent on the Si doping location: barrier, QW, or delta doping.

GaN/AlN QW superlattices display *p*-polarized ISB absorption lines that can be tuned in the 1.33-1.91 µm wavelength range by varying the QW thickness from 4 ML to 10 ML [2]. The absorption spectra exhibit Lorentzian shape with a typical FWHM of 70-100 meV in Si doped samples, whereas a line width as small as 40 meV have been measured from undoped samples, which establishes a new state-of-the-art for nitride epitaxial growth. This complete study of the growth of AlN/GaN MQWs for ISB devices has made possible the fabrication of high-performance nitride-based QWIPs operating at 1.4 µm at room temperature [3].

Regarding QD superlattices, we have demonstrated QD densities in the 10^{11} to 10^{12} cm^{-2} range with a height (diameter) around 1-1.5 nm (10-40 nm) depending on the growth conditions (the amount of GaN deposited, the substrate temperature and the growth interruption time after each GaN layer) [4]. No effect of Si-doping on the QD morphology is observed. HRXRD based simulation suggests the superlattices are fully strained on AlN. Strong and narrow (FWHM ~ 70-150 meV) *p*-polarized ISB absorptions peaked at wavelengths ranging in 1.38-1.67 µm are observed at room temperature. These results allowed the fabrication of the first QDIP prototypes operating at telecommunication wavelengths [5].

Financial support by IST FP6 NitWave STREP 004170 program is acknowledged.

References:

[1] E. Sarigiannidou, E. Monroy, N. Gogneau, G. Radtke, P. Bayle-Guillemaud, E. Bellet-Amalric, B. Daudin, and J. L. Rouvière, Semicond. Sci. Technol. **21**, (2006) 912.
[2] M. Tchernycheva, L. Nevou, L. Doyennette, F. H. Julien, E. Warde, F. Guillot, E. Monroy, E. Bellet-Amalric, T. Remmele, and Albrecht, Phys. Rev. B **73**, (2006) 125347.
[3] D. Hofstetter, , E. Baumann, F. R. Giorgetta, M. Graf, M. Maier, F. Guillot, E. Bellet-Amalric, and E. Monroy, Appl. Phys. Lett. **88**, (2006) 121112.
[4] F. Guillot, E. Bellet-Amalric, E. Monroy, M. Tchernycheva, L. Nevou, L. Doyennette, F. H. Julien, Le Si Dang, T. Remmele, M. Albrecht, T. Shibata, and M. Tanaka, submitted to J. Appl. Phys.; M. Tchernycheva, L. Nevou, L. Doyennette, A. Helman, R. Colombelli, F. H. Julien, F. Guillot, E. Monroy, T. Shibata, and M. Tanaka, Appl. Phys. Lett. **87**, (2005) 101912.
[5] L. Doyennette, L. Nevou, M. Tchernycheva, A. Lupu, F. Guillot, E. Monroy, R. Colombelli, and F. H. Julien, Electron. Lett. **41**, (2005) 1077. A. Vardi, N. Akopian, G. Bahir, L. Doyennette, M. Tchernycheva , L. Nevou, F. H. Julien, F. Guillot, and E. Monroy, Appl. Phys. Lett. **88**, (2006) 143101.

Figures:

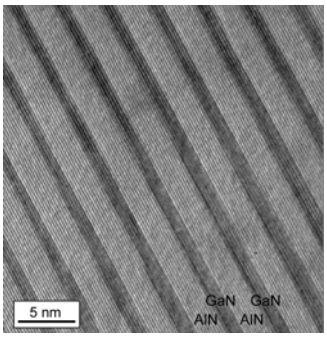


Fig. 1: HRTEM image of the active region of a QWIP structure.

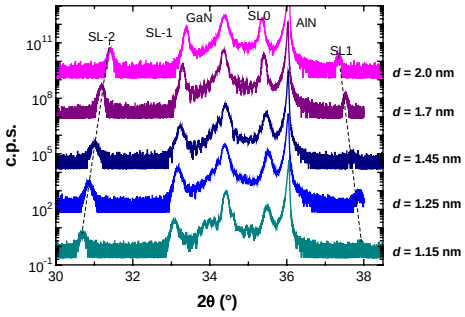


Fig. 2: HRXRD θ–2θ scans of the (0002) reflection of QWIP structures with various QW thicknesses (*d*) in the 1.15-2 nm range.

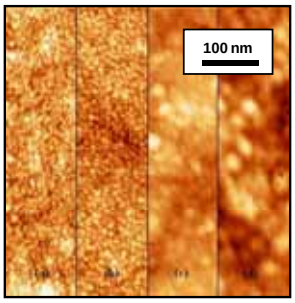


Fig. 3: AFM images of QDs deposited with the following growth interruptions: (a) 0s, (b) 15s, (c) 60s and (d) 120s

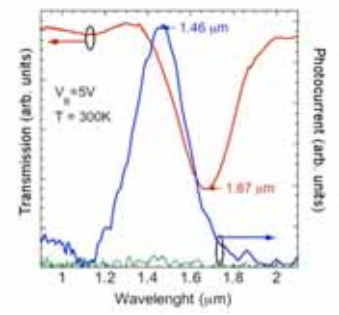


Fig. 4: Room temperature transmission (red line) and photocurrent response (blue line) of a QDIP based on lateral transport.

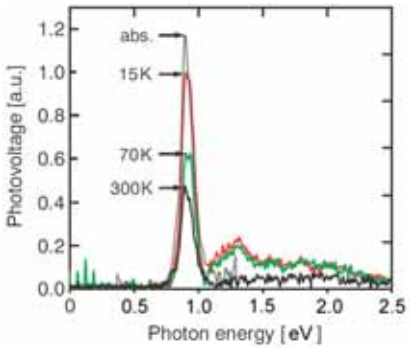


Fig. 5: Temperature-dependent photovoltage measurements from a QWIP, for *p*-polarized light. The absorbance spectrum is shown as dashed line for comparison.

TRENDS IN ELECTROSPINNING OF NATURAL NANOFIBERS

A.K. Haghi and M. Akbari
The university of Guilan, P. O.Box 3756, Rasht, Iran
Haghi@Guilan.ac.ir

Abstract- An emerging technology of manufacturing of thin natural fibers is based on the principle of electrospinning process. In conventional fiber spinning, the mechanical force is applied to the end of a jet. Whereas in the electrospinning process the electric body forces act on elements of charged fluid. Electrospinning of natural fibers offers unique capabilities for producing novel natural nanofibers and fabrics with controllable pore structure. Current research effort has focused in understanding the electrospinning of natural fibers in which the influence of different governing parameters are discussed.

Keywords: Electrospinning, natural nanofibers, process parameters, characterization.

NEW AMPLIFICATION STRATEGY FOR ELECTROCHEMICAL DETECTION OF DNA USING CATIONIC POLYMERS AGGREGATES

Harding Lepage, P.; Le Floch, F. and Leclerc, M.
Département de chimie, Université Laval, Québec, Qc, CANADA, G1K 7P4
patricia.harding@chm.ulaval.ca

The detection of DNA hybridization is of central importance to the diagnosis and treatment of genetic diseases, for the detection of infectious agents, and for reliable forensic analyses. Such DNA sensing applications require approaches that allow sensitive and specific transduction of a recognition event. Moreover, facile approaches can lead to the conception of miniaturized, portable and affordable devices. Electrical detection of DNA has shown great promise for this purpose and has been the subject of intense research activities. Strategies based on conjugated polymers for the transduction of hybridization events into an electrical signal have been reported [1-3], but they present a low signal-to-noise ratio caused by the steadily presence of the polymer, and they usually rely on a decrease of the electrical signal.

We previously reports a new promising solid-state electrostatic approach based on neutral peptide nucleic acid (PNA) capture probes and an electroactive, cationic, water-soluble polythiophene transducer bearing one ferrocene (Fc) moiety per monomer unit [4]. This simple and rapid methodology allows room temperature detection of 3×10^{9} unmarked DNA targets in a volume of 10μL, or 5×10^{-10}M.

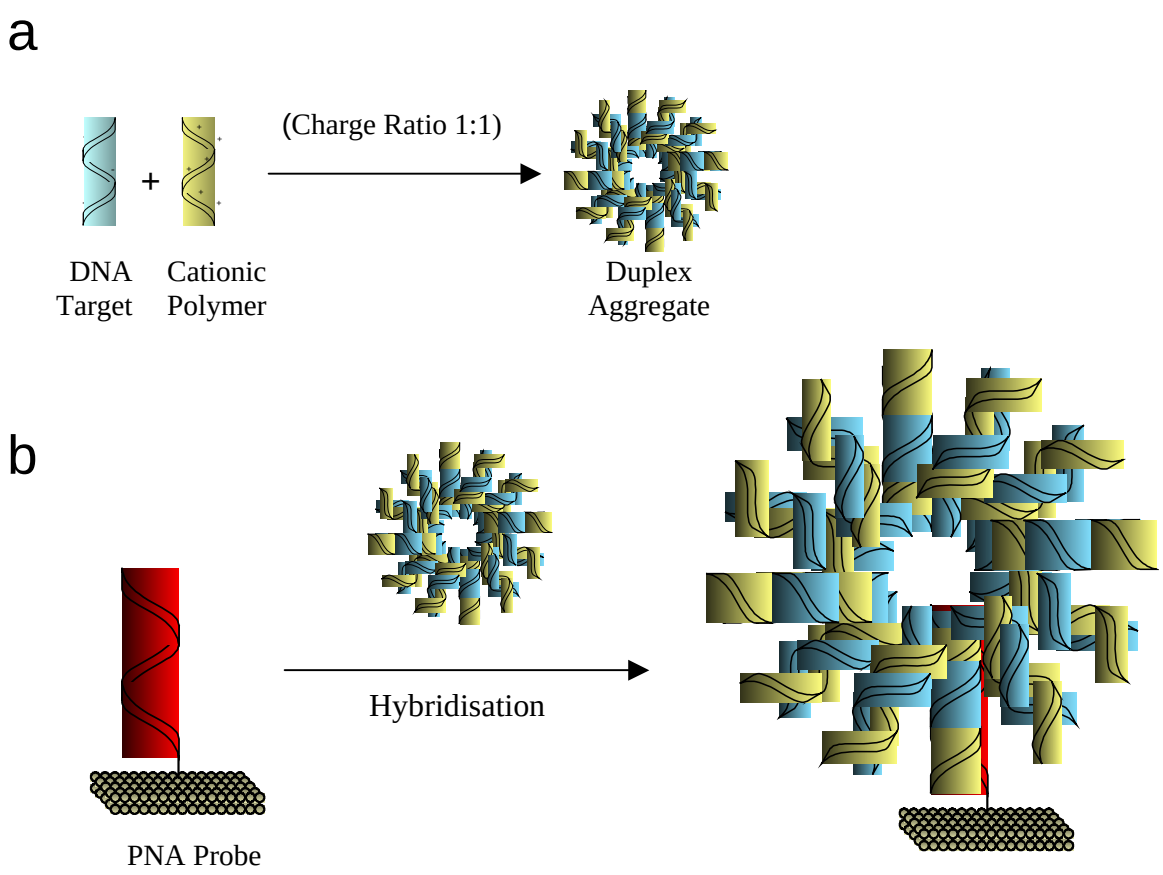
In order to understand the electronic transfer between remote Fc moieties and the gold electrode, different Fc-functionalized cationic polymers were synthesised. Cyclic voltammetry studies with those molecules discard a molecular wire-like mediation by the conjugated polymer backbone. Each ferrocenyl groups undergoes reversible oxidation but the global current measured per hybridisation event is limited by the distance of the markers to the surface.

To take advantage of the large number of Fc moieties indebted to the polymeric nature of our transducer, we propose a double surface amplification strategy using aggregates composed of polymer and single strand of DNA target (duplex). Hybridization is performed at one surface addressing specific PNA capture probe and electrochemical detection is done at an electrode nearby. Owing to the unique DNA recognition capabilities of cationic polythiophenes in the duplex form [5, 6], this strategy leads to signal amplification, coupled to an effective discrimination against non-complementary nucleic acids.

References:

[1] Korri-Youssoufi, H., Garnier, F., Srivastava, P., Godillot, P. and Yassar A., *Journal of the American Chemical Society* ***119*** (1997) 7388.
[2] Bäuerle, P., Emge, A. *Advanced* Materials ***10*** (1998) 324.
[3] Thompson, L.A, Kowalik, J., Josowicz, M. and Janata, J. *Journal of the American Chemical Society* ***125*** (2003) 324.
[4] Le Floch, F. Ho, H.-A., Harding-Lepage, P., Bédard, M., Neagu-Plesu, R., Leclerc, M. *Advanced Materials* ***17*** (2005) 1251.
[5] Ho, H.-A., Boissinot, M., Bergeron, M.G., Corbeil, G., Doré, K., Boudreau, D., Leclerc, M. *Angewandte Chemie International Edition* ***41*** (2002) 1548.
[6] Doré, K., Dubus, S., Ho, H.-A., Lévesque, I., Brunette, M., Corbeil, G., Boissinot, M., Boivin, G., Bergeron, M.G., Boudreau, D. and Leclerc, M. *Journal of the American Chemical Society* ***126*** (2004) 4240.

Figures:



EFFECT OF EXPERIMENTAL PARAMETERS ON THE MORPHOLOGY AND CRYSTAL STRUCTURE OF $MgCl_2$/EtOH

Fariba Hashemi
Department of Chemistry, Faculty of Scince, Alzahra University, Tehran, Iran
shashemi@alzahra.ac.ir

The use of $MgCl_2$–alcohol adducts as catalytic supports has attracted a great deal of attention both for the preparation of conventional Ziegler–Natta catalysts [1] and for the heterogenisation of metallocenes [2]. The main goal of the use of these adducts has been to control the morphology of the resulting polymer and to enhance the activity. Active species of catalyst system that supported on spherical $MgCl_2$ adducts have made spectacular progress in controlling polymer morphology as spherical particles. The control of morphology is achieved by the replica phenomenon, whereby the polymer formed takes the shape of the catalyst particles [3], whilst increased activity is achieved by generating longer-lived titanium centre.

The critical producer in preparing the catalysts is controlling the morphology and texture of the support. In this work, we extended our study to investigate the effect of varying reaction condition during the synthesis of adducts. Spherical $MgCl_2$ adducts, as support, were prepared by fast quenching method and ethanol was used as solvent for $MgCl_2$.The effect of molar ratio of $C_2H_5OH/MgCl_2$, (n), speed of agitation on shape (morphology), size and crystalline phase of particles were investigated. It was found that molar ratio is affected morphology and crystalline phase of adducts; although, with increasing speed of stirring and n (molar ratio of $C_2H_5OH/MgCl_2$), better spherical particles could be achieved. The particle size of supports decreased with increasing speed of agitation and n. $MgCl_2$ adducts were converted to support through the elimination of ethanol molecules from adducts by freeze drying method. The supports were characterized by X-ray diffraction and BET surface area methods.

Table 1 show the influence of the degree of dealcoholation and ethanol content on surface area of the support prepared with freeze drying and dealcoholation of $MgCl_2$.nEtOH adducts. It was observe that this method for dealcoholation is a strong influence on the porosity and surface area of the supports. These results indicate that the surface area of the supports was large when the amount of alcohol in $MgCl_2$ adducts were decreased.
The support that prepared from adducts with n=3 and stirring speed=1800 rpm, shows a lower alcohol content, higher surface area and higher porosity relative to other supports. This support presented a BET surface area of 12.2 m^2/g, porosity of 0.12 cm^3/g and average pore diameter equal to 165Å.

References:

[1] D.N. Taveira Magalhaes, O. Do Coutto Filho, F.M.B. Coutinho, Eur. Polym. J. 27 (1991) 827.
[2] Z. Guan, Y. Zheng, S. Jiao, J. Mol. Catal. A: Chem. 188 (2002) 123.
[3] A. Parada, T. Rajmankina, J. Chirinos, Polym. Bull. 43 (1999) 231.

Table 1. Surface area of supports after dealcoholation

EtOH/$MgCl_2$ (molar ratio)	Stirring speed (rpm)	Surface area (m^2/g)
2.5	1800	5.7
3.0	1800	12.2
3.0	500	10.1
3.0	800	8.9
3.0	1300	4.3

CHARGE CARRIERS IN FEW LAYER GRAPHITE

Sylvain Latil, Luc Henrard
Laboratoire de Physique du Solide, Facultés Universitaires Notre-Dame de la Paix.
Rue de Bruxelles, 61. 5000 Namur. Belgium
Luc.henrard@fundp.ac.be

The recent transport measurements on monocrystalline graphite containing only few layers (few layers graphite or FLGs) have demonstrated the potential technological importance of pure graphitic materials in semiconductor applications. Indeed, the possibility of switching from electron to hole transport was demonstrated experimentally by Hall measurements. FLGs have also been shown to behave like mixed carriers semimetallic systems, with a domain of coexistence of electrons and holes [1]. However, the exact thickness and staking order of the graphitic thin film was not unambiguously determined.

Differently to the three dimensional graphite bulk structures, electrons in FLGs are confined along one crystallographic direction, offering a genuine 2D character of its electronic response. However, the linear dispersion of the electronic bands near the Fermi level that appears in monolayer graphene is lost, as a consequence of the interaction between layers. The resulting complex dispersion relations and overlap between electron and hole bands leads to the experimentally observed coexistence of different type of carriers. The experimental data indicate an overlap in the 4 to 20 meV range.

In the present communication we report the detailed investigation of the electronic structure of FLG with 2 to 4 layers by *ab-initio* technique (ABINIT code). The different energetically favoured possible stackings of FLG that we studied are : AB, ABA, ABC, ABAB, ABCA, ABAC (identical to ABCB) .

We have demonstrated how the number of layers and of the geometry-dependence of the interlayer interaction influence the nature of the charge carriers in FLGs. Indeed, amongst 3 and 4-layer films, ABAC is found to be a narrow gap semiconductor (Eg=8.8 meV) and is then exclude to be the experimentally grown morphology. The other stacking exhibit metallic behaviour with various characteristic : The rhombehedral family (ABC, ABCA) demonstrates or very small (< 3 meV) overlap between electrons and holes bands. The Bernal family (ABA, ABAB) presents overlaps in agreement with experimental observations (from 5 meV to meV)

In conclusion, we have shown that field effect behaviour of FLG observed by Novoselov et al. is intrinsic properties of the systems and that Bernal family ABA and ABAB stacking could explain the experimental data.

Further details on the present communication can be found in [2]

References:

[1] K.S. Novoselov et al., Science **306** (2004), 666.
[2] S. Latil, L. Henrard. Phys. Rev. Lett. Accepted (2006)

INSULATING PROPERTIES OF OIL BASED MAGNETIC LIQUIDS

F.Herchl[1], P.Kopčanský[1], K.Marton[2], L.Tomčo[3], M.Timko[1], M.Koneracká[1], I.Potočová[1]
[1]Institute of Experimental Physics SAS, Watsonova 47, 043 53 Košice, Slovakia
[2]Faculty of Electrical Engineering and Informatics, Technical University, Letná 9/A, 041 20 Košice, Slovakia
[3]Faculty of Aeronautics, Rampová 7, 041 21 Košice, Slovakia
herchl@saske.sk

Magnetic liquid is a suspension of very fine magnetic particles of the order of 10 nm. Oil based magnetic fluids enable better cooling of transformers than pure transformer oils. The presence of foreign particles in liquid dielectric has a great effect on its breakdown withstand. The particles tend aggregate in the region of higher electric field if they have higher permitivity than the surrounding liquid. This can lead to breakdown. Even though, the impulse breakdown voltage in magnetic fluid was found higher than that in pure transformer oil [1]. Duxbury and Leath investigated breakdown field strengths in metal-loaded dielectric materials. According to theoretical predictions [2], breakdown field distribution $F_d(E)$ should have the following form (1)

$$F_d(E) = 1 - \exp\left[-cd^3 \exp(-)\right] \quad (1),$$

where k is constant depended on particle volume concentration Φ, d is electrode distance, E is breakdown field and c is constant, or the Weibull form (2)

$$F_d(E) = 1 - \exp\left(-cd^3 E^m\right) \quad (2),$$

where m is constant. Equation (1) correspondes to the average initial breakdown field E (3)

$$E = \frac{1}{A + B \cdot \ln(d)} \quad (3),$$

where A and B are constants depended on particle volume concentration. Equation (2) correspondes to the average initial breakdown field E (4)

$$E = \frac{1}{d^{3/m}} \quad (4).$$

The aim of this work is to investigate the DC and AC breakdown voltage distribution of magnetic fluid and compare it with theoretical model of Duxbury and Leath.

The measurements were carried out using electrodes of a uniform gap of electric field – Rogowski profile in transformer oil (Technol US 4000 and ITO 100) based magnetic liquids with magnetite particles of the average diameter of 8.6 nm coated with oleic acid. The time dependences of the breakdown development were measured with help of an inductive probe and an oscilloscope with its own memory.

It was found, that addition of certain amount of magnetic particles into transformer oil improves its breakdown withstand also by DC voltage. The boundary between better and worse breakdown properties has occured at particle volume concentration Φ=0.01 corresponding to saturated polarisation I_s=4mT [3]. Magnetic field (up to 31mT) oriented parallel and perpendicular to applied electric field increases dielectric breakdown strength. Dielectric breakdown strength of magnetic liquid with particle volume concentration Φ=0.0025 is comparable with that in pure oil at AC conditions. The DC breakdown followed immediately after appearing of initial partial discharges appear. The development of discharge lasts about 200ns. The number of partial discharges preceedes AC breakdown. They were observed long before detection of the complete breakdown occurred. The duration breakdown was in the range 200ns. Measured dependences of breakdown fields as a function of electrode distances do not allow to determine the best breakdown field distribution in magnetic liquid (Fig.1) because correlation coefficients of approximation (3) R=0.975 and approximation (4) R=0.979 are almost the same. We have attempted to approximate an AC breakdown strength distribution on the base of functions (1) and (2). In Fig. 2 is shown the probability function of

dielectric breakdown strengths corresponding to Duxbury-Leath model and Weibull approximation in comparison with Gauss approximation. The correlation coefficients of these functions are 0.990, 0.986, 0.997. It is not possible to decide which approximation is more suitable for the describing of measured distribution.

We can conclude, that magnetic fluid with particle volume concentration $\Phi<0.01$ has better dielectric properties at DC voltage and comparable but not worse dielectric properties at AC voltage. The experimental data could be described by both Duxbury-Leath and Weibull distribution functions and it is not possible to decide which function is more suitable for expression of the statistical character of dielectric breakdown strength.

References:

[1] V.Segal, K.Raj, Indian J. Eng. Mater. Sci. **5** (1998) 1410.
[2] P.D.Beale, P.M.Duxbury, Phys. Rew. B **37** (1988) 2785.
[3] P.Kopčanský, L.Tomčo, K.Marton, M.Koneracká, M.Timko, I.Potočová, JMMM 289 (2005) 415.

Figures:

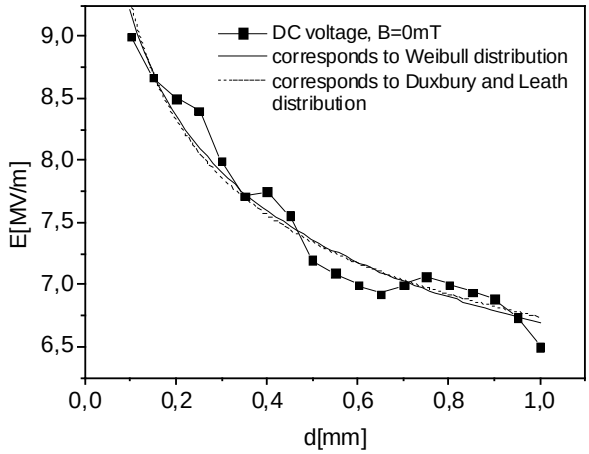


Figure 1: The DC dielectric breakdown strength as a function of electrode distance for magnetic fluid with particle volume concentration $\Phi=0.0025$, $I_s=1$mT.

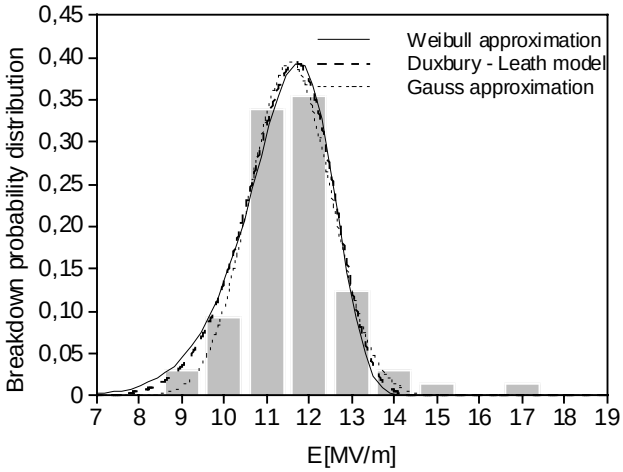


Figure 2: The AC breakdown probability distribution for magnetic fluid with particle volume concentration $\Phi=0.0025$, $I_s=1$mT.

A DFT STUDY ON ZIRCONIA OLIGOMERS AND THE INFLUENCE OF CU-DOPING.

Bárbara Herrera[a], *Francisco Gracia*[b], *Paulo Araya*[b] *and Alejandro Toro-Labbé*[a]
[a]*QTC, Departamento de Química Física, Facultad de Química, Pontificia Universidad Católica de Chile, Casilla 306, Correo 22, Santiago 6094411, Chile .*
[b]*Departamento de Ingeniería Química, Centro de Investigación Interdisciplinaria Avanzada de Ciencias de Materiales(CIMAT), Universidad de Chile, Av. Blanco Encalada 2008, Santiago, Chile.*
atola@uc.cl

A theoretical study of Zirconia-based linear oligomers $(ZrO_2)_n$ (n=1-5) has been performed in order to compare its intrinsic reactivity with the number of ZrO_2 units and the adsorption of Cu atoms. DFT-based indexes such as chemical potential (μ), hardness (η), Fukui (FF) and the dual Fukui (DF) functions were used with the aim of characterize the intrinsic reactivity on the studied clusters. B3LYP/6-31G** calculations with Lanl2dz pseudopotentials on metallic centers indicate that the ability to charge transfer and reactivity increases with the number of ZrO_2 units.

The Fukui function and the dual Fukui descriptor indicates that the nucleophilic character resides at the oxygen atoms and the electrophilic character is centered at Zr atoms. $Cu(ZrO_2)$ and $Cu(ZrO_2)_2$ clusters were analyzed and compared to (ZrO_2) and $(ZrO_2)_2$, it is found that while the nucleophilic character resides at Cu atoms being larger than at copper-free clusters, the electrophilic character remains centered at the Zr atoms.

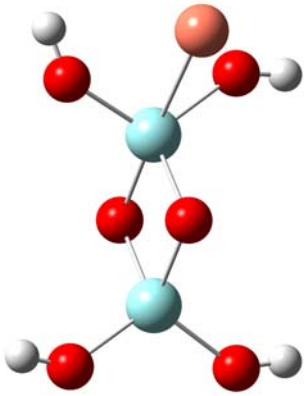


Figure1: $Cu(ZrO_2)_2$ Cluster.

This work was supported by FONDECYT through project No. 1060590, and Proyecto Bicentenario en Ciencias y Tecnología de Inserción en la Academia (PBCT#8). The authors also wish to thank MECESUP through projects PUC-0004 and Red Química UCH-0116.

Poster

NOVEL METHOD TO CONSTRUCT A TWO-DIMENSIONAL MOLECULE-NANOPARTICLE NETWORK BY ORGANOMETALLIC COMPLEX FORMATION

D. Hobara, S. Kondo, M. Choi, Y. Ishioka, S. Hirata, M. Murata, K. Azuma, and J. Kasahara
Fusion Domain Laboratory, Materials Laboratories, Sony Corporation, Okata, Atsugi-shi, Kanagawa, 243-0021 Japan
Daisuke.Hobara@jp.sony.com

Reliable formation of metal/molecule/metal junctions is important for investigation of molecular devices. There have been only a few experimental works that showed gate effects with high reproducibility despite considerable efforts to form the junction by fabricating nanometer-scale electrodes. This is due to the low yield of working devices [1]. To avoid the difficulty in the device fabrication, a nanoparticle array interconnected by organic linker molecules [2] can be used because such an array of the metal/molecule/metal junctions spontaneously forms by simply immersing the array into the solution of the linker molecule [2]. We have previously reported that a molecular device consisting of a two-dimensional array of gold nanoparticles interlinked by several dithiol molecules shows different gating behaviour depending on the nature of the molecules used [3]. The fabrication of this device is simple and highly reproducible, but the reliable formation of the junction was limited to the relatively short molecules.

In the present study, we report a novel method to construct a molecule-gold nanoparticle network array by forming organometallic complexes. Prior to the nanoparticle array formation, terpyridine ligands having thiol end group (Fig. 1a) are adsorbed on the surface of gold nanoparticles. Introduction of Fe^{2+} leads to the formation of iron bis(terpyridine) complex (Fig. 1b). As a result, the nanoparticles can be interlinked regardless of the length of the ligand molecules. This method provides more reliable formation of the junctions than that based on double-ended molecules such as dithiols. This is critical for the observation of the gate effect in the three-terminal device.

Thiophene terpyridine (Fig. 1a) was synthesized by coupling of alkyl-substituted terthiophene with 4-chloro-terpyridine under Stille condition. Gold nanoparticles (average diameter, 4.7 ± 1.1 nm) were modified with thiophene terpyridine by mixing nanoparticle and thiophene terpyridine solutions at room temperature for at least 24 h. After removing unreacted thiophene terpyridine molecules, the Au nanoparticle array was formed by Langmuir-Blodgett method and transferred onto the Si/SiO_2 substrate with Au electrode patterns formed in advance. The substrate was subsequently immersed in a $Fe(BF_4)_2$ solution for the complex formation. A densely-packed nanoparticle array was demonstrated by SEM measurements.

Formation of iron bis(terpyridine) complex was confirmed by UV-Vis spectroscopy. UV-Vis spectra of the terpyridine-modified gold nanoparticle array on a quartz substrate were measured before and after the introduction of Fe^{2+}. The difference spectrum between them showed peaks at 330 nm and 480 nm which are attributed to the bis(terpyridine) complex. The observation of red shift of the plasmon absorption peak also supports the molecule-nanoparticle network formation.

Fig. 2 shows two-terminal *I-V* measurements of the gold nanoparticle array before (Fig. 2a) and after (Fig. 2b) the introduction of Fe^{2+}. After the introduction of Fe^{2+}, two-terminal current measurements typically exhibited an about 30-fold increase. Such a large difference in

current is originated from different charge transport mechanisms, *inter*- against *intra*-molecular charge transport before and after the complex formation, respectively.

The three-terminal measurements with applying the gate voltage to the devices (W_g/L_g = 8.8 mm/50 μm; 150 nm thick SiO_2 as a gate insulator) exhibited only negligible gate modulation before the complex formation. On the other hand, p-type gating behavior with transconductance on the order of 0.1 nS was reproducibly observed after the complex formation. These results probably reflect the importance of the intra-molecular charge transport to the gating effect.

Acknowledgement

We thank Qiaoshu Hu, College of Chemistry, Peking University, for the synthesis of the thiophene terpyridine molecule.

References:

[1] J. O. Lee *et al*., Nano Lett., 3 (2003) 113.
[2] R. P. Andres *et al*., Science, 273 (1996) 1690.
[3] S. Kondo *et al*., 2005 MRS Spring Meeting Abstracts, J17.4 (2005) 274.

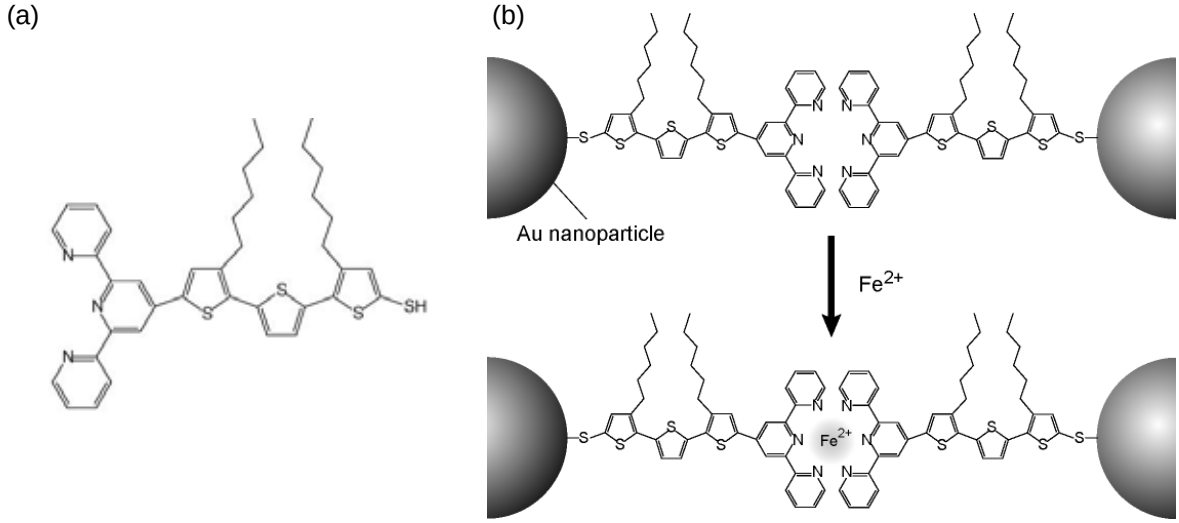


Fig. 1 (a) Thiophene terpyridine molecule, (b) Schematic representing the formation of the complex.

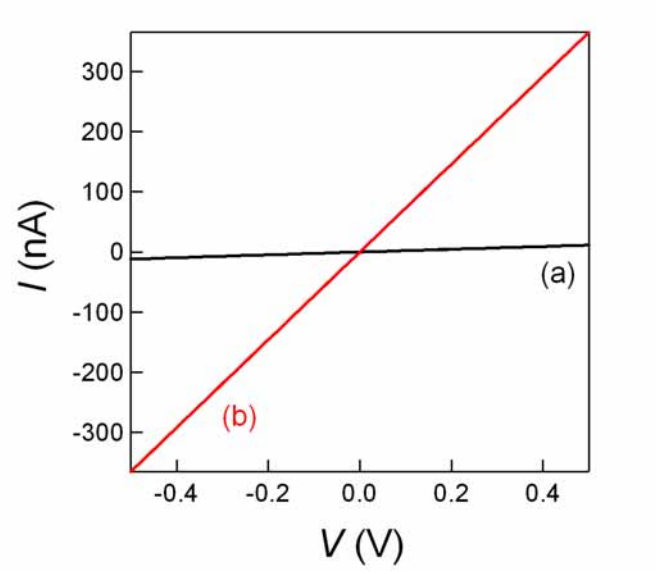


Fig. 2 Two-terminal *I-V* measurements (a) before and (b) after the introduction of Fe^{2+}.

PERCOLATION IN 2D NANOPARTICLE FILMS FROM COLLOIDAL SELF-ASSEMBLY

Ching-Ling Hsu[1], *C. T. Shih*[2], *Yi-Rong Yang*[1]
[1]*Department of Physics, Chung Yuan Christian University, Chung Li, Taiwan*
[2]*Department of Physics, Tunghai University, Taichung, Taiwan*
chsu@phys.cycu.edu.tw

Using evaporation of colloidal suspension nanoparticle droplets on flat substrates is a common method to form 2D nanostructured films. Despite the simplicity of the treatment, the nanoparticle self-assembly is a non-equilibrium process and creates a variety of spatial patterns, including well-ordered superlattices, percolated networks, fractal-like aggregates, and distinct islands. Competing effects from nanoparticle diffusion and solvent dewetting lead to this complexity. We perform electrical and topographic measurements on Au nanoparticle films on glass substrates with atomic force microscopy. In general cases, percolation phenomena emerge as the nanoparticle concentrations increase to appropriate values. The non-ohmic characteristics of the disordered films, as shown in Figure 1, can be approximately interpreted by a quasi-1D percolation path of tunnel junctions [1].

While percolation and self-assembly both play important roles in transport through nanoparticle films, particularly near phase transitions, the studies focused on their relation were surprisingly rare. Compared with the “classical” percolation due to entirely random particle occupancies, the percolation affected by self-assembly shows different critical points because of different cluster-forming dynamics. We use a two-dimensional lattice gas model to simulate the nanoparticle aggregation patterns and percolation during solvent evaporation with Monte Carlo dynamics [2]. The Hamiltonian contains the nearest neighbor (particle-particle, particle-solvent, and solvent-solvent) interactions and the chemical potential for the solvent evaporation. This model shows not only strong agreement with the observed patterns in experiments, but also gives us an insight into the emergence of the percolation under the effect of the self-assembly. Figure 2 shows an example pattern from the simulation.

This project is financially sponsored by Taiwan National Science Council (grand no. NSC 94-2112-M-033-004).

References:

[1] P.-E. Trudeau, A. Escorcia, and A.-A. Dhirani, J. Chem. Phys., **199** (2003) 5267.

[2] E. Rabani, D.R. Reichman, P.L. Geissler, L.E. Brus, Nature, **426** (2003) 271.

Figures:

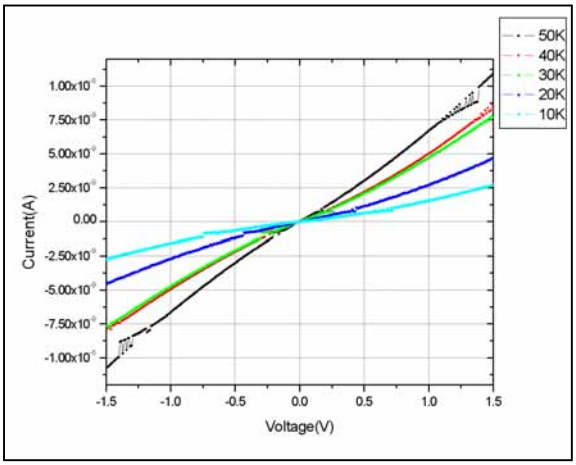


Figure 1. Typical non-ohmic behaviors observed in disordered Au nanoparticle films.

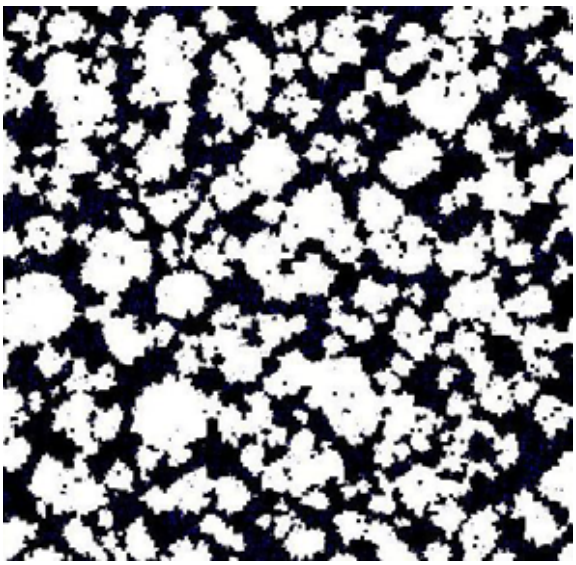


Figure 2. The dark dots represent nanoparticles. Even in lower surface coverage, self-assembly may make percolation happen.

Poster

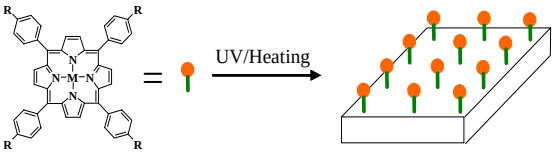
SYNTHESIS OF MOLECULAR MEMORY USING METALLPORPHYRINS MONOLAYER ON SILICON SURFACE

Kai HUANG, [1] Guillaume DELAPIERRE, [1] Florence DUCLAIROIR, [2] Tiziana PRO, [3] Barbara DE SALVO, [3] Jean-Claude MARCHON, [2] and Françoise VINET [1]

[1]*LFCM, Département des microtechnologies pour la biologie et la santé, CEA-DRT-LETI ;*
[2]*SCIB, Département de recherché fondamentale sur la matiére condensée, CEA-DSM;*
[3]*LNDE, Département des Nanotechnologies, CEA-DRT-LETI;*
CEA/Grenoble, 17, rue des Martyrs 38054 Grenoble Cedex 9, France
Kai.huang@cea.fr

1. Introduction. During the past decade there has been intense interest in developing molecular-based electronic materials for use in both memory architectures and circuit elements.[1] Recently, a new approach, the self-assembled monolayers (SAMs) of redox-active porphyrinic molecules attached to an electroactive surface serves as the active storage medium, and information is stored in the discrete redox states of the molecules has been established.[2] The objective of this research is to fabricate molecular memories using metallporphyrins monolayer on silicon surface by different linkers to form uniform and dense active storage medium (**Scheme 1**). One of our current research projects is to anchor metalloporphyrins on Si wafers by covalent Si – C bonding for the fabrication of specifically designed silicon-based devices. To this end we have recently developed a very efficient indirect grafting technique that we are currently optimising.[3]

Scheme 1



2. Experiments. The metallporphyrins were synthesized at SCIB/DSM/CEA. The metal-porphyrins SAMs was synthesized by different linkers or directly grafted on silicon surface use heating method through different processes and examined by XPS, FTIR, and cyclic voltammetry. The electrode fabrication will be made at LNDE/LETI/CEA and electron-transfer rates and charge-retention time will be determinate.

3. Result. The metallporphyrins SAM was formed by reaction of TEPPs with azidealkyl monolayer on silicon substrate by "click" chemistry,[4] and the XPS result (**Figure 1**) shows that N% was increased from 1.46% to 5.29%. At N core-level spectra, the N signal of metallporphyrins at 398.3 eV can be observed compared with N*-N-N* and N-N*-N signals of azidealkyl at 401 and 404.7 eV, respectively. It suggested that the metallporphyrins SAM was grafted on silicon substrate successfully. The cyclic voltammograms for ZnAB3P monolayer grafted on Si(100) surface by "click" chemistry was determined. The cyclic voltammograms work is in process in our laboratory.

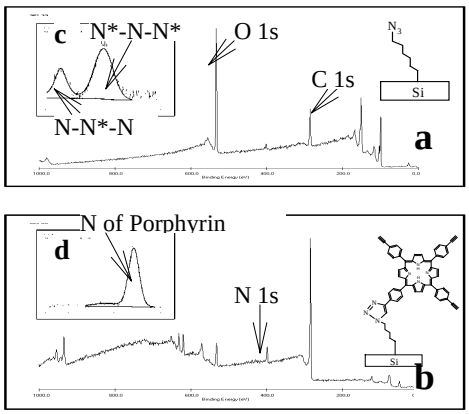


Figure 1. XPS spectra before (**a**) and after (**b**) "click" chemistry and the N core-level spectra of azidoalkyl (**c**) and porphyrin (**d**) monolayer.

References:

[1] R. L. Carroll, C. B. Gorman, *Angew. Chem. Int. Ed.* 2002, 41, 4378.
[2] Z. Liu, A. A. Yasseri, J. S. Lindsey, D. F. Bocian, *Science* 2003, 302, 1543.
[3] G. Delapierre, F. Duclairoir, J-C. Marchon *French Pat.* Application No 2005/0510987.
[4] H. C. Kolb, M. G. Finn, K. B. Sharpless *Angew. Chem. Int. Ed.* 2001; **40**: 2004-2021.

Strain distributions in core-multi-shell nanowires with nonuniform cross-sectional composition profiles

*H. L. Duan[1], X. Yi[2], B. L. Karihaloo[*1], J. Wang[2]*
[1]School of Engineering, Cardiff University, Queen's Buildings, The Parade, Cardiff CF24 3AA, UK
[2]LTCS and College of Engineering, Peking University, Beijing 100871, P. R. China
KarihalooB@Cardiff.ac.uk

Nanowires are cylinders of elliptical or circular cross-sectional shape with uniform or nonuniform composition in the radial direction. They can have a core surrounded by concentric multi-shells of the nanometer size [1-3]. In the multi-shell nanowires, the mismatch of the thermal expansion coefficients and/or lattice constants between neighbouring shells induces stress/strain fields in the core and shells, which in turn affect their physical properties and/or the properties of the composites containing them. Most works analyzing the elastic strains of nanostructures by atomistic simulations and continuum mechanics approaches have neglected the non-uniformity of the composition profile in the nanostructures and thus a comprehensive analysis of the strain fields in core-shell nanowires of nonuniform compositions is still lacking [4-6]. In this paper, the strains in embedded and free-standing nanowires with uniform and nonuniform cross-sectional compositions are studied in detail. It is found that the strains in the nanowires can be modified by adjusting their compositions and multi-shell structures. The results are useful for the band structure engineering of semiconductor nanowires.

We first calculate the elastic strains in free-standing and embedded core-multi-shell nanowires. The elastic strains $\boldsymbol{e}^k(\boldsymbol{x})$ in the core (k=1), the outer shells shells (k=2,3,...,M), and the surrounding embedding matrix (k=M+1) are

$$\boldsymbol{e}^k = \boldsymbol{S}_I^k : \boldsymbol{e}_I^* - \boldsymbol{e}_k^*, \qquad (I \in (1,M),\ k \in (1,M+1)) \qquad \text{embedded} \qquad (1)$$

$$\boldsymbol{e}^k = \boldsymbol{S}_I^k : \boldsymbol{e}_I^* - \boldsymbol{e}_k^* + \boldsymbol{E}^k(t, P_{ex}), \qquad (I \in (1,M-1),\ k \in (1,M)) \qquad \text{free-standing} \qquad (2)$$

$\boldsymbol{S}_I^k$ is the Eshelby tensor in the kth phase, which relates the uniform eigenstrains $\boldsymbol{e}_I^*$ prescribed in the Ith phase to the strain induced in the kth phase [7]. Thus the repeated subscript I in Eqs. (1) and (2) indicates summation from 1 to M (or M-1). The procedures to obtain $\boldsymbol{S}_I^k$ can be found in the work of Duan et al. [8]. Eigenstrains $\boldsymbol{e}_I^*$ are induced by the mismatch in the lattice constants ($\boldsymbol{e}_I^* = e_{m0}^* \boldsymbol{I} = \boldsymbol{I}(a_{in} - a_{ex})/a_{ex}$) or thermal expansion coefficients ($\boldsymbol{e}_I^* = e_{tm0}^* \boldsymbol{I} = \boldsymbol{I}(a_{in} - a_{ex})\Delta T$). Here, a_{in}, a_{ex} and a_{in}, a_{ex} are the lattice constants and the thermal expansion coefficients of the interior and exterior phases, respectively, ? T is the temperature difference and $\boldsymbol{I}$ is the second-order symmetric identity tensor in two-dimensional space. $\boldsymbol{E}^k(t, P_{ex})$ is the elastic strain tensor in the core and shells due to an isotropic surface stress t and an external hydrostatic pressure P_{ex} on the outermost free-standing shell.

Next, we calculate the elastic strains in the embedded and free-standing nanowires with nonuniform composition. We assume that a nanowire has a circularly symmetric composition, i.e., $\boldsymbol{e}^*(r) = e_m^*(r)(\boldsymbol{e}_r \otimes \boldsymbol{e}_r + \boldsymbol{e}_f \otimes \boldsymbol{e}_f)$, where $\boldsymbol{e}_r$ and $\boldsymbol{e}_f$ are the *local* unit base vectors in the cylindrical coordinate system. According to Vegard's law [9], $e_m^*(r) = x(r) e_{m0}^*$, $e_m^*(r) = x(r) e_{tm0}^*$, where x is the fraction of the ingredient at radial location r [7]. From the theory of elasticity of infinitesimal deformation, the only non-vanishing eigen-displacement $u_r^*(r)$ in a free-standing core is obtained from $C_{ijkl}(u_{k,lj}^* - e_{kl,j}^*) = 0$, where C_{ijkl} is the elastic

stiffness tensor of the core. When the nonuniform core is embedded in the surrounding medium, the displacement fields in the core (superscript 1) and the matrix (superscript 2) are $u_r^1 = F_1 r$, $u_r^2 = G_2 / r^2$, respectively. The constants F_1 and G_2 are determined from the interface condition $u_r^2 = u_r^1 + u_r^* |_{r=r_{co}}$ and traction condition across the interface, as shown in the work of Duan et al. [8]. Therefore, the elastic strains $\boldsymbol{e}^1$ and $\boldsymbol{e}^2$ in the nonuniform core and the uniform matrix due to $\boldsymbol{e}^*(r)$ can be obtained. For the free-standing nanowire, elastic strains $\boldsymbol{E}^k(t, P_{ex})$, $(k = 1,2)$ due to t and P_{ex} have also been calculated [8].

Fig. 1 shows the normalized elastic strain e_{xx}/e_{m0}^* in the $In_xGa_{1-x}As/GaAs$ structure (r_{co}=9 nm, $x(r) = 0.8 - 0.4r / r_{co}$) in the xy plane normal to the longitudinal axis of the cylindrical core. It is seen that the non-uniformity of composition greatly changes the elastic strain in and around the nanowire; nonuniform composition induces non-uniformity of elastic strains in the core. Fig. 2 compares the normalized elastic strain e_{xx}/e_{m0}^* in the uniform nanowire with multi-shells CdS/ZnS/CdS (M=3, r_{co1}=6nm, r_{sh1}=9nm, r_{sh2}=12nm) with that in the nonuniform nanowire $Zn_xCd_{1-x}S$ (r_{co}=9nm, r_{sh}=12nm, $x(r) = b_0 + b_1 r / r_{co}$, b_0 and b_1 are two constants). $e_{m0}^* = -7.0\%$ for the ZnS(core)/CdS(shell) structure. We consider two composition variations for $Zn_xCd_{1-x}S$: Case A: b_0=1, b_1=-0.4; Case B: b_0=1, b_1=0. Case B corresponds to a uniform nanowire. It can be seen that the elastic strains are strongly dependent on the compositions and structures of the nanowires, and are different for CdS/ZnS/CdS (M=3) and $Zn_xCd_{1-x}S$. Note that the elastic strain in the core (-0.667=z=0.667) of CdS/ZnS/CdS is uniform, whereas the strain in the core (-1=z=1) of $Zn_xCd_{1-x}S$ is nonuniform.

References:

[1] L. J. Lauhon, M. S. Gudiksen, C. L. Wang, and C. M. Liebe, Nature, **57** (2002) 420.
[2] N. Skold, L. S. Karlsson, M. W. Larsson, M. E. Pistol, W. Seifert, J. Tragardh, and L. Samuelson, Nano Lett., **5** (2005) 1943.
[3] R. N. Musin, and X. Q. Wang, Phys Rev. B, **71** (2005) 155318.
[4] V. G. Stoleru, D. Pal, and E. Towe, Physica E, **15** (2002) 131.
[5] J. Rockenberger, L. Troger, A. L. Rogach, M. Tischer, M. Grundmann, A. Eychmuller, and H. Weller, J. Chem. Phys., **108** (1998) 7807.
[6] H. J. Chu, and J. Wang, J. Appl. Phys., **98** (2005) 034315.
[7] J. D. Eshelby, Proc. R. Soc. Lond. A, **241** (1957) 376.
[8] H. L. Duan, J. Wang, Z. P. Huang, and B. L. Karihaloo, Proc. R. Soc. Lond. A, **461** (2005) 3335.
[9] L. Vegard, Z. Physik, **5** (1921) 17.

Figures:

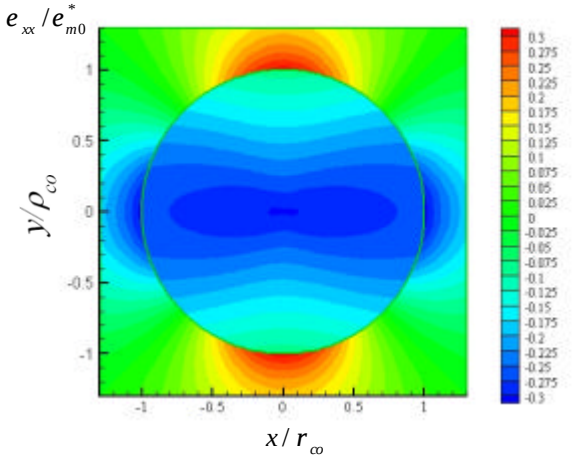


Fig. 1 e_{xx}/e_{m0}^* in the embedded nanowire $In_xGa_{1-x}As/GaAs$ structure due to $\boldsymbol{e}^*$.

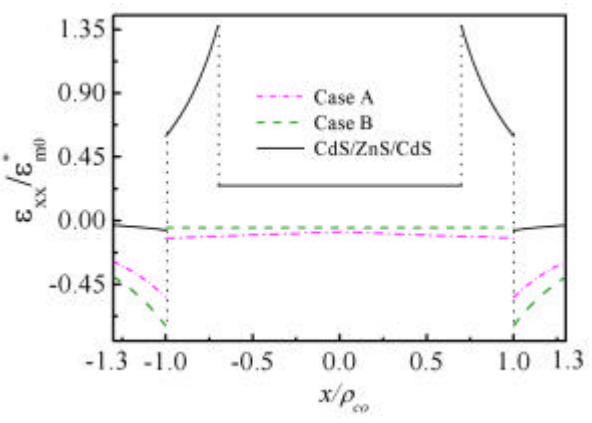


Fig. 2 e_{xx}/e_{m0}^* in the free-standing nanowire $Zn_xCd_{1-x}S$ and CdS/ZnS/CdS due to $\boldsymbol{e}^*$ and t (=1N/m).

Probing single molecule transport with superconducting electrodes

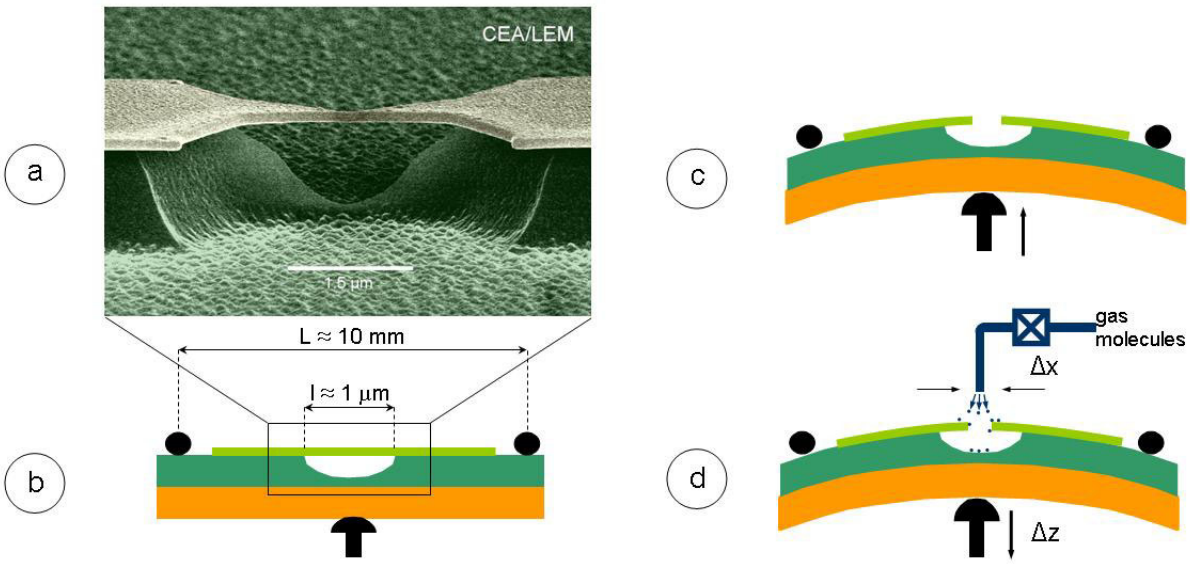
A. Isambert[1], M. F. Goffman[1], J. P. Bourgoin[1] and C. Urbina[1]
S.Wohlthat[2], F. Pauly[2] and J. C. Cuevas[2,3]
[1]LEM, Service de Physique de l'Etat Condensé (CNRS URA 2464), DSM/DRECAM/SPEC, CEA Saclay, 91191 Gif sur Yvette Cedex, France
[2]ITF, Universität Karlsruhe, 76128 Karlsruhe, GERMANY
[3]UAM, E-28049 Madrid, SPAIN
marcelo.goffman@cea.fr

Elucidating the physics of transport through single molecules is a challenging quest that needs approaches complementing the usual transport measurements with normal metal electrodes. We investigated electronic transport through diatomic molecules attached to superconducting electrodes using the break-junction technique (see Figure) at low temperatures. As was recently demonstrated in atomic-size contacts, the richness of electronic transport in the superconducting state [1] allows to make evident the direct relation between the number of conduction channels through a single atom and its chemical valence [2]. Experiments on different diatomic molecules reveal the conduction channels through the metal-molecule-metal structure and allow a quantitative comparison with theoretical calculations. In particular, depending on the molecule, it is shown that conduction is enhanced or decreased.

References:

[1] E. Scheer et al., Phys. Rev. Lett., **78** (1997) 3535. M. F. Goffman et al., Phys. Rev. Lett., **85** (2000) 170. R. Cron, M. F. Goffman, D. Esteve and C. Urbina, Phys. Rev. Lett., **86** (2001) 4104.
[2] E. Scheer et al., Nature, **394** (1998) 154.

Figures:



(a) SEM colorized picture. A metallic bridge with dimensions ~100 nm is fabricated on an insulating elastic substrate, using conventional e-beam technique. (b) & (c) Using a bending mechanism consisting of 2 side counter-supports and a centred pushing rod, the bridge is elongated until it breaks. (d) The distance between the resulting electrodes is controlled at atomic scale, allowing to connect a single molecule.

EFFECTIVE SYSTEM OF NUCLEIC ACIDS (DNA) ADSORPTION BASED UPON COMPOSITE NANOPARTICLES

Ivanchuk I.I., Pershina A.G., Sazonov A.E., Petorva I.V., Freidin M.B., Itin V.I., Terekhova O.G., Magaeva A.A., Ogorodova L.M.

During the last decade, the investigations of a possibility of use of non-organic nanomaterials with ferromagnetic capacity for immobilization of biological molecules are actively carried out. The extraction of genetic material from biological objects for biotechnology and scientific research in molecular biology is a supreme methodological task which is being solved, at the present time, by laborious and expensive techniques which effectiveness not always complies with the required one. An advantage of use of ferromagnetic nanomaterials as a selective sorbents for nucleic acids is their low toxicity, high surface capacity, and stable magnetic properties, which allows to carry out the highly specific manipulations by external magnetic field including easy separation of biological molecules from reacting mixture. The development of nano-bearers with immobilized short fragments of DNA (olygonucleotides) directed on the regulation of pathological target genes function is a promising prospect of this research field.

The aim of this work was the analysis of adsorption activity of composite nanomaterials with magnetic properties in respect to nucleic acids (DNA).

The following nanopaticles with ferromagnetic properties were used: a mixture of Fe_2O_3+ Fe_3O_4, $CoFe_2O_4$, SnO_2. They were obtained from saline systems by mechanochemical synthesis. The effectiveness of nanopaticles to adsorb/desorb the nucleic acids was estimated by fluorimeter with use of intercalating dye Sybr-Green. IR-spectroscopy was used to the analysis of chemical interaction character in complexes of activated nanopaticles and nucleic acid.

As a result of the investigation it was found that native nanoparicles weakly tie together with DNA molecules, therefore, systems of activation of adsorption capacity of nanomaterials were selected. Maximal DNA adsorption capacity (94.8%) was shown for the nanoparticles activated by Lithium salts. Desorption of DNA measure after elution by solvent was at least 75%. It was found that the dependence of quantity of combined DNA molecules on the nanopowder concentration is non-linear. It was estimated that buffer capacity for nanocomposite/DNA is 1:20. The increase of quantity of activated nanopaticles gives no significant elevation of adsorption effectiveness. The excess of nanopowder in the system results to decrease of subsequent desorption of DNA. It was suggested that activated nanoparticles are able to make two types of links with DNA molecules: 1 – irreversible firm chemical link and 2 – a link that arises after saturation of the 1st type of link due to coordination interactions. This second dissociates under influence of the solvent.

This suggestion is supported by the results of IR-spectroscopy which showed that the treatment of composite nanopowder SnO_2 by the Lithium salts results to dehydroxylation of the material surface and appearance of Lewis acid sites which can coordinate with molecules owning free electron pair.

Tin oxide nanoparticles showed high sorption activity were successfully used as a sorbent for DNA extraction with subsequent PCR. It was shown that the investigated nanoparticles did not inhibit PCR if added to the reacting mixture. Moreover, in several cases, we observed the increase of PCR effectiveness and elevation of PCR-product yield up to 15%. Probably, this is because of stabilizing action of nanopowders on nucleic acids synthesis enzymes.

Thus, is was found that magnetoactive nanoparticles (SnO_2, Fe_2O_3+Fe_3O_4, $CoFe_2O_4$) activated by Lithium salts effectively and reversibly bind the DNA molecules. The maximal effectiveness of adsorption/desorption was registered for activated tin oxide (98%).

Magnetic anisotropy changes induced by high energy ion bombardment

M. Jaafar[(a)], A. Asenjo[(a)], R. Sanz[(a)], J. Jensen[(b)], R. Schäfer[(c)] y M. Vázquez [(a)]

[(a)]Instituto de Ciencia de Materiales de Madrid, Cantoblanco, 28049 Madrid, Spain.
[(b)]Division of ion physics, Angstrom Laboratory, Uppsala University, Uppsala, Sweden
[(c)]IFW-Dresden, Desdren, Germany
m_jaafar@icmm.csic.es

In the last years, a great effort has been done in the miniaturization of the magnetic systems. Of vital importance is to study the properties of this systems, called micro or nanomagnets because they present a novel magnetic behaviour associated to low – dimensional effects that can be used in a variety of applications such as magnetic storage, semiconductor industries, ultrasmall magnetic field sensors, etc.

In particular, in the magnetic storage, it has been necessary the development of thin multilayers, nanoparticles systems and ordered magnetic nanostrucures. Several methods have been developed to fabricate such systems, like self-organization of nanoelements [1] , electron beam lithography [2] or high energy ion irradiation [3]. The candidates to be used as materials for magnetic storage devices are FePt, FePd and CoPt alloys because they present high anisotropy and superparamagnetic limit at small dimensions.

The aim of this work is study the changes in the structural and magnetic properties of the thin films due to the irradiation with high energy ions. The sample is polycrystalline FePt thin film (35nm thick) growth by sputtering onto Si (100) at 400ºC with a buffer layer of 28nm of Pt (111). From the hysteresis loops measured by VSM we know the anisotropy in mainly in plane, however, the sample presents a component out of plane.
Due to the irradiation with different ions (Br^{+} y Cl^{2+}), energies and doses, the in plane or out of plane anisotropy is favored [4]
Moreover, since the irradiation has been done through a micrometric mask we have obtain a magnetic thin film patterned at the micrometer scale.
The structural changes have been studied by X- ray diffraction and TEM (Transmission electron Microscopy).

The magnetic characterization has been done by different techniques. The volume hysteresis loops are measured by VSM (Vibrating Sample Magnetometer). In order to compare the behavior between the irradiated and no irradiated areas we use surface techniques like Magnetic Force Microscopy (MFM) and Kerr Effect Microscopy (MOKE). The MFM data are in good agreement with the VSM measurements. We can observed the out of plane component of the magnetic moment, called dense stripe domains in the non irradiated area, and different magnetic behavior in the irradiated areas as a function of the irradiation parameters. In particular, in figure 1 we can observed the two areas: the no- irradiated region presents dense stripe domains and the irradiated area presents in plane domains.
We have also measured the Kerr effect in both regions. From the local hysteresis loops obtained with this technique, we note that the Hc (in plane direction) decreases due to the irradiation.
In addition, the in plane domains have been studied by Kerr effect microscope. The images are obtained applying the magnetic fields in different in plane directions (see figure 2.)

References:

[1] S. P. Ahrenkiel, S. H. Xin, P. M. Reimer, J. J. Berry, H. Luo, S. Short, M. Bode, M. Al-Jassim, J. R. Buschert and J. K. Furdyna, Phys. Rev. Lett. 75, 1586 (1995).J. Tersoff, C. Teichert, and M. G. Lagally, Phys. Rev. Lett. 76, 1675 (1996).
[2] J. F. Smyth, S. Schultz, D. R. Fredkin, D. P. Kern, S. A. Rishton, H. Schmid, M. Cali, and T. R. Koehler, J. Appl. Phys. 69, 5262 (1991)
[3] C. Chappert et al. Science 280, 1919 (1998)
[4] M. Jaafar et al. in preparation.

Figures:

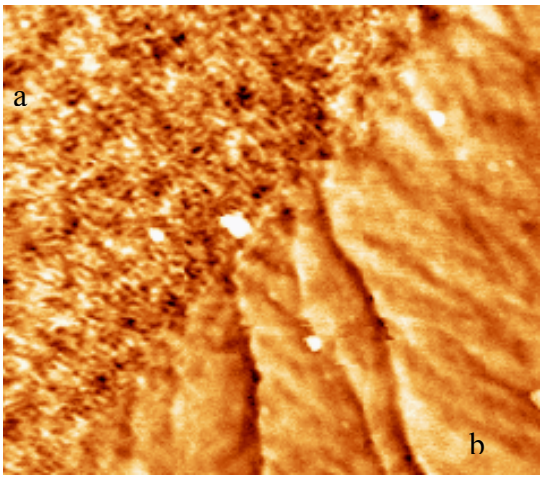


Figure 1- MFM data of the different regions (a) no irradiated, with the dense stripe domains and (b) irradiated with in plane domains. Image size: 65 μm x 65 μm

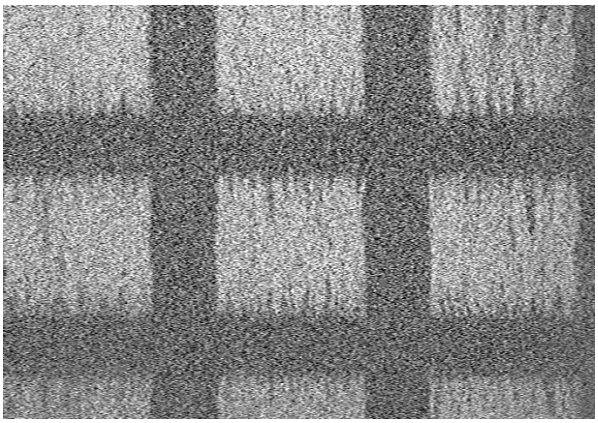


Figure 2- Magnetic domains image by Kerr Effect Microscopy. Image size: 170 μm x 130 μm

Effect of water and hydrolysis catalyst on the morphology and crystal structure of TiO_2 photocatalyst prepared by sol-gel method

Kannikar Juengsuwattananon[1], Angkhana Jaroenworaluck[2], Thammarat Panyathanmaporn[2], Supatra Jinawath[1] and Sitthisuntorn Supothina[2]*
[1]Department of Material Science, Faculty of Science, Chulalongkorn University, Phayathai Rd., Pathumwan, Bangkok, Thailand
[2]National Metal and Materials Technology Centre, 114 Thailand Science Park, Paholyothin Rd., Klong Luang, Pathumthani, Thailand
[*]sitthis@mtec.or.th

Titanium dioxide (TiO_2) is one of the most popular materials. It is widely used in many industrial applications such as, cosmetics, fillers, pigments, as well as photocatalyst. TiO_2 is present in three natural forms; anatase, rutile and brookite. Previous reports [1] suggested that the transition behavior from amorphous-to-anatase and anatase-to-rutile phase of TiO_2 photocatalyst is dependent on the synthetic conditions such as water content and amounts of hydrolysis catalyst. In this study, the TiO_2 powders were synthesized by sol-gel method and the effect of synthetic conditions on the crystal structure and morphology were examined by using X-ray diffraction (XRD) analysis and transmission electron microscope (TEM). The preparation method of the TiO_2 sol was modified from the previous work of Baolong [2]. A 0.5 M of $Ti(OBu)_4$ was dissolved in anhydrous ethanol. Then the mixture of distilled water anhydrous ethanol and hydrochloric acid was slowly added under constant stirring at room temperature for 3 hours. The composition of H_2O: EtOH: HCl was varied to 1:3:1, 1.5:1.5:2, 2:2:1 and 3:1:1. To collect the TiO_2 powders, the volume of the TiO_2 suspension after 40 days of aging time was reduced by rotor-evaporation and finally dried at 50^oC for 1 day. The appearance of TiO_2 precursors prepared with various amounts of H_2O and HCl addition aged for 40 days are shown in table 1. The letters TP, TC, M and P denote transparent, translucent, milky, and precipitating appearances, respectively. With increasing amount of H_2O (comparison of series A, C and D), the sol formation as visually seen by the milky appearance took place in series D followed by series C and A, respectively. In the case of series B, which had high amounts of both H_2O and HCl, the hydrolysis was very fast and the precursor became white precipitation. According to the above result, the sol formation was found to be greatly dependent on the amounts of H_2O and HCl addition. Fig. 1 shows the XRD patterns of the as-synthesized powders obtained from these precursors, which indicated that all samples were made of an amorphous together with fine crystals. Increasing the amounts of H_2O and HCl resulted to more anatase-to-rutile transformation, as well as crystal growth of both anatase and rutile that was observed by the sharper of XRD peaks. Moreover, the TEM results (Fig. 2) also supported the XRD analysis that the as-synthesized samples contained very fine crystals along with an amorphous phase of either the titanium oxide or organic residue. The direct observation from TEM images confirmed that the anatase-to-rutile transformation was undertaken by the increase of H_2O content. Note that the presence of anatase and rutile crystals of Sol-A was not clearly identified in this TEM image (Fig. 2(a)). As shown in Fig. 2(b), the irregular shape of rutile crystals having average size of 10 nm-wide and 60 nm-long were clearly observed.

References:

[1] Terabe K, Kato K, Miyazaki H, Yamaguchi S, Imai A, Iguchi Y, Journal of materials Science, **29** (1994) 1617-1622.
[2] Baolong Z, Baishun C, Keyu S, Shangjin H, Xiaodong L, Zongjie D, Kelian Y, Applied catalysis B: Environmental, **40** (2003) 253-258.

Table 1 Visual observation of TiO_2 sol aged for 40 days from the Ti precursor having various volume ratios of H_2O: EtOH: HCl.

Samples	Concentration of $Ti(OBu)_4$ (M)	H_2O: EtOH: HCl (Volume ratio)	Visual observation
Sol-A	0.5	1:3:1	M
Sol-B		1.5:1.5:2	TP + PPP
Sol-C		2:2:1	M
Sol-D		3:1:1	TC + PP

TP: transparent, TC: translucent, M: milky, and P: precipitated

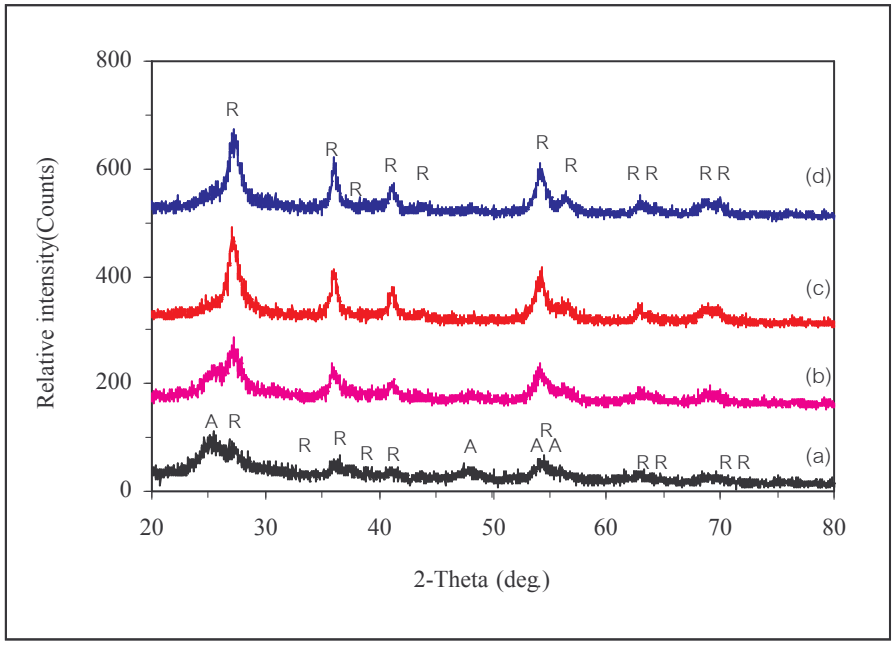
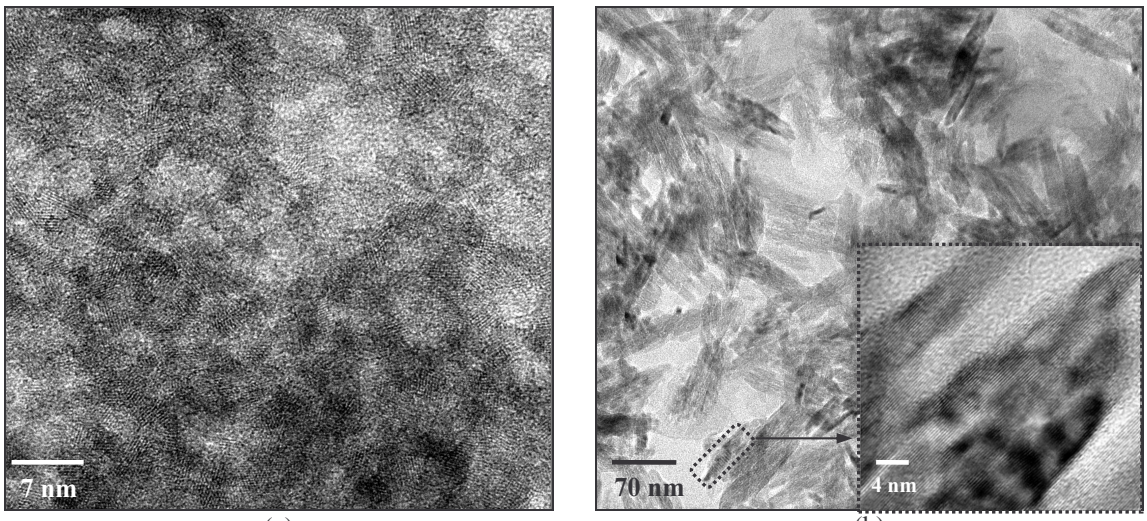


Figure 1 XRD patterns of the as-synthesized powders obtained from TiO_2 precursors, having different ratio of H_2O:EtOH:HCl, aged for 40 days; (a) Sol-A (1:3:1), (b) Sol-B (1.5:1.5:2), Sol-C (2:2:1) and Sol-D (3:1:1); A = Anatase, R = Rutile



(a) (b)

Figure 2 TEM images of the as-synthesized TiO_2 powders obtained from; (a) Sol-A (H_2O:EtOH:HCl = 1:3:1) and (b) Sol-C (H_2O:EtOH:HCl = 2:2:1) aged for 40 days

MICRO- AND NANO-SCALE TUBULAR OXIDE STRUCTURES

[1]Martin Järvekülg, [1,2]Valter Reedo, [2]Uno Mäeorg
[1]Institute of Physics, University of Tartu, Riia 142, 51014 Tartu, Estonia
[2]Institute of Organic and Bioorganic Chemistry, University of Tartu, Jakobi 2, 51014 Tartu, Estonia
martinj@fi.tartu.ee

Nano- and microscale tubular structures have exceptional properties and have great potential as the building blocks of nano- and microdevices systems of high efficiency. For that this kind of structures have been the subject of intensive research. Since the discovery of carbon nanotubes [1] there has been active interest in exploring other layered and nonlayered materials that form tubular structures. Many different methods of obtaining various materials in nanotube form have been reported and summarized in reviews [2].
TiO2, ZrO2 and HfO2 are wide band gap materials of great interest since they can be used in sensorics, photocatalysis, electronics and solar cells. Metal oxide nanotubes have been obtained through various sol-gel related methods, in both basic and acidic conditions and different synthesis temperatures. The suggested formation models are often complemented or corrected afterwards [3]. Obviously, exploring different possibilities for obtaining tubular nano- and micro-sized materials and explaining their formation is of great importance in order to establish correct theories and be able to synthesize materials with desired properties.
In present work we report a novel phenomenon and mechanism of low-dimensional tubular oxide structure formation. Microtubes of hafnium oxide were obtained by rapid vaporization of solvents from prepolymerized hafnium butoxide sols at relatively low temperatures (~ 100 °C) whereas the pre-polymerization was carried out by adding a solution of water and hydrochloric acid in butanol to the alkoxide. This kind of treatment led to the formation of microtubular oxide structures. Experiments were carried out using titanium and zirconium butoxides in a similar way, the different amounts of hydrochloric acid were added and various vaporization programs were used.
Obtained micro- and nanostructures were characterized by electron microscopy. The crystal structure was investigated by XRD. Most of the tube-like structures observed were 20-200 μm in length and 2- 10 μm in diameter. SEM images indicated that the oxidic structures have have a nature of rolled-up nanosheets. Some possible tube-forming mechanisms are also presented to explain the formation of observed structures.
This work has been supported by ETF6537, ETF6660, ETF6163, SF0382149s02, Estonian Nanotechnology Competence Center and European Science Foundation programs Nanotribo and Molsim.

References:

[1] Iijima, S. Helical microtubules of graphitic carbon. Nature, **354** (1991) 56.
[2] Remškar, M., Adv. Mater. **16 (**2004) 1497
[3]Kukovecz, A., Hodos, M., Horvath, E., Radnoczi, G., Konya, Z., Kiricsi, I. Oriented Crystal Growth Model Explains the Formation of Titania Nanotubes. J. Phys. Chem. B, **109** (2005) 17781-17783.

Figures:

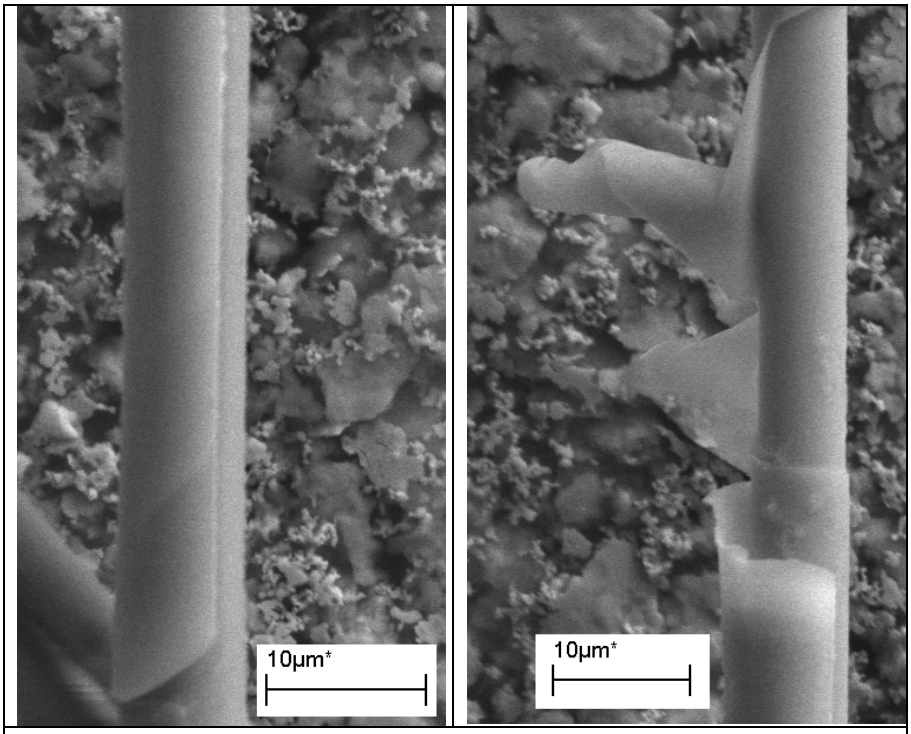


Fig. 1 SEM images of rolled-up HfO_2 structures

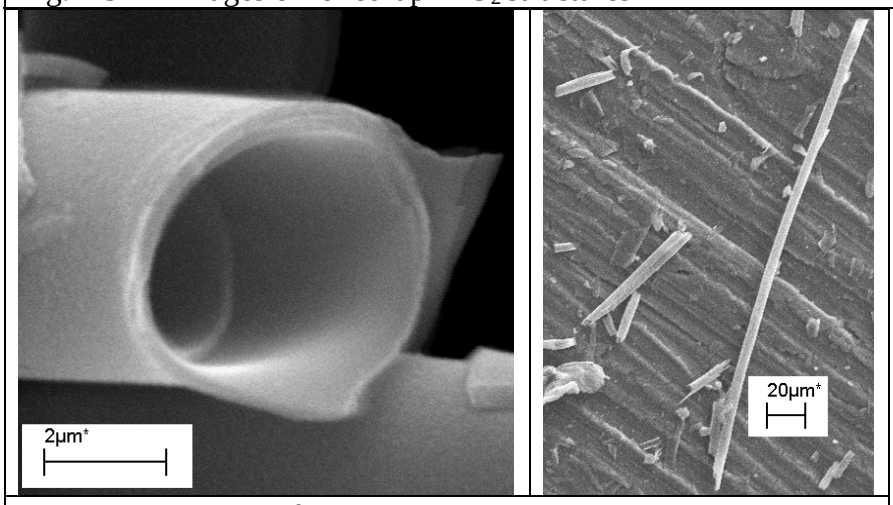


Fig. 2 SEM images of tubular ZrO_2 structures.

PHYSICS-BASED MODEL OF DISILICIDE/SILICON NANOWIRE HETEROSTRUCTURE TRANSISTORS

D. Jiménez[a], M. Dubois[b], and S. Roche[b]
[a]Departament d'Enginyeria Electrònica (Universitat Autònoma de Barcelona), Spain
[b]DSM/DRFMC/SPSMS (Commisariat à l'Energie Atomique), France
Contact: david.jimenez@uab.es; mathieu-j.dubois@cea.fr; stephan.roche@cea.fr

Silicon nanowire field-effect transistors (NW FETs) are being the subject of very intense research as building blocks for the bottom-up approach to nanoelectronics, owing to the potential control of physical and chemical characteristics during synthesis, providing a unique electronic structure and reduced carrier scattering caused by one-dimensional quantum confinement effects [1-4]. Very promising materials for defining source-drain contacts of the NW FETs are disilicides, such as $NiSi_2$, $CoSi_2$, and $FeSi_2$, due to the extremely low mismatch between their (111) surface and the silicon (111) one [5].

At present, an important issue is to dispose of a physics-based model of the current-voltage characteristics of FETs based on disilicide/silicon nanowire heterojunctions, in order to interpret experimental results at this early stage of development, guide the design and project NW FET performances. In this work we propose a simple model that accounts for the relevant physics phenomena, such as: (a) thermionic and tunnel emission over a Schottky barrier; (b) ambipolar conduction; (c) ballistic transport; (d) multimode propagation; and (e) electrostatics dominated by the nanowire capacitance. Fig. 1 illustrates the transfer characteristic of an hypothetical NW FET computed by the proposed model. The strong point of the model is an accurate treatment of the disilicide/silicon interface, accounting for quantum reflections in reciprocal space due to wavevector mismatches between incoming and outgoing states. The exact electronic structure of each disilicide is taken into account, allowing the calculation of the energy dependent current distribution at the interface (Fig. 2). In this way, we can include, in our model, the influence of the chosen material on the performance of the nanodevice.

References:

[1] Y. Cui, Z. Zhong, D. Wang, W. U. Wang, and C. M. Lieber, "High performance silicon nanowire field effect transistors", *NanoLetters*, vol. 3, no. 2, 149 (2003)
[2] Y. Wu, J. Xiang, C. Yang, W. Lu, and C. Lieber, "Single-crystal metallic nanowires and metal/semiconductor nanowire heterostructures", *Nature*, vol. 430, 62 (2004).
[3] G. Zheng, W. Lu, S. Jin, and C. M. Lieber, "Synthesis and fabrication of high-performance n-type silicon nanowire transistors", *Adv. Mater*., vol. 21, 1890 (2004)
[4] J. Xiang, W. Lu, Y. Hu, Y. Wu, H. Yan, and C. M. Lieber, "Ge/Si nanowire heterostructures as high-performance field-effect transistors", *Nature*, vol. 441, 489 (2006).
[5] G. Malegori and L. Miglio, "Elastic properties of $NiSi_2$, $CoSi_2$ and $FeSi_2$ by tight-binding calculations", *Phys. Rev. B*, vol. 48, 9223 (1993).

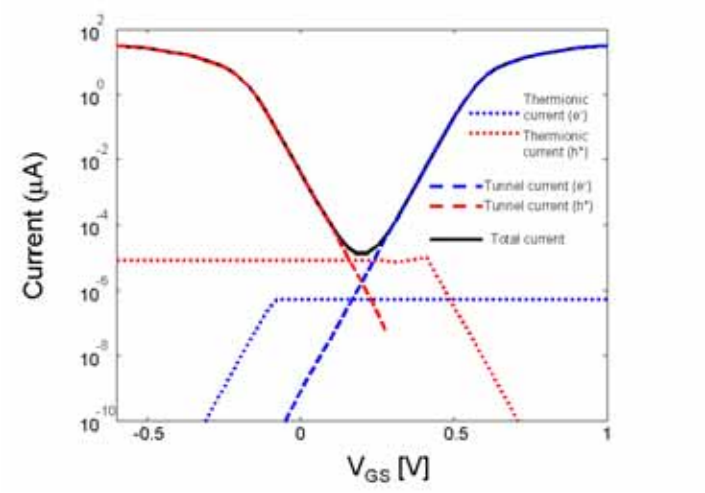


Figure 1. Transfer characteristic at room temperature of a coaxially-gated NW FET with a diameter of 1.42 nm, and silicon oxide thickness of 2 nm, showing ambipolar conduction (left branch: dominated by tunneling of holes through the Schottky barrier to the valence band; right branch: due to tunneling of electrons through the Schottky barrier to the conduction band). A Schottky barrier height of 0.65 eV, and V_{DS}=0.4 V were assumed.

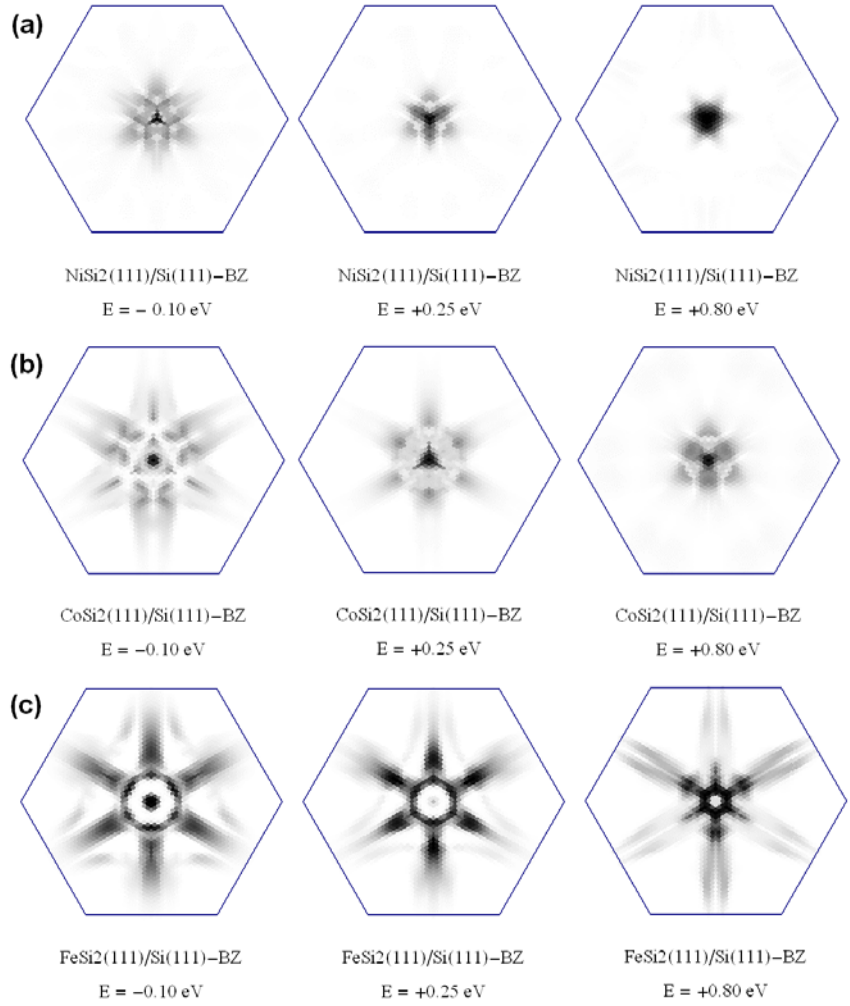
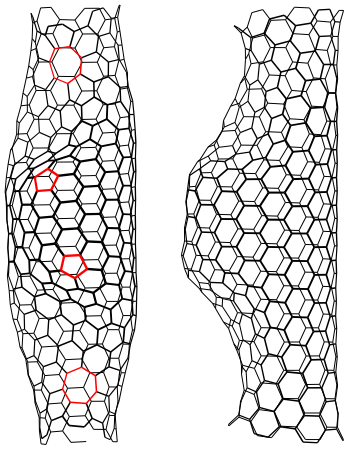


Figure 2. Energy dependence of the computed reciprocal-space current distribution, at the heterojunction interface, for $NiSi_2$ (a), $CoSi_2$ (b) and $FeSi_2$ (c). Energies are referred to the Fermi level of the disilicide set to 0 eV

Electronic Transport in Nanotubes with Resonant Cavities.

Esther Jódar and Antonio Pérez–Garrido.
Dpto. Física Aplicada, Antiguo Hospital de Marina, Campus Muralla del Mar. UPCT, Cartagena 30202 Murcia, Spain.

We investigate the properties of nanotubes sandwiched between other nanotubes with different geometry. This structure is shown in the Figure below. We use structures $(n,n)/N(m,m)/(n,n)$. Nanotubes with this kind of geometry are armchair. In the case $m > n$ this structure has, in its central part, a number of channels for transmission larger or equal to the number of channels in the leads. Henceforth, we refer to the central part of this structure as the cavity. This cavity behaves as a resonant box with quasi-bound states producing resonances and anti-resonances in transmission. This behavior is a consequence of the different band structures for nanotubes forming the cavity. Other authors have made similar studies but with another kind of structures: Sim *et al.* [1] worked with flattened-deformed nanotubes. Chico and Jaskolski [2] estudied a similar structure but with a conductance gap. In our study we employ metallic nanotubes with no gap in transmission in the whole range of energies, although dips in transmission arose due to the existence of quasi-bound states in the cavity.



In our calculations we employ a tight-binding model which only takes into account one π-orbital per atom. The overlap energy between nearest neighbors is taken as $t = -2.66$ eV where second-neighbor interactions are neglected. Curvature effects are not considered, as they are only significant when the diameter of the tube is small.

We calculate properties of our nanotube structures, as density of states and transmission function using the Green's function method [3], using the standard expression $\hat{G}(E) = \left(E\hat{I} - \hat{H}_n - \hat{\Sigma}_L - \hat{\Sigma}_R\right)^{-1}$, and the formalism developed by López Sancho *et al.* [4]. The latter has the advantage that converges very fast. We also calculate the eigen-energies E_n and eigen-functions Ψ_n, in order to obtain the participation number P_n: $P_n^{-1} = \sum_m |\Psi_n(m)|^4$, which gives a measure of the wavefunction extension and help to find out the localized or extended nature of an electronic state.

With the formalism developed above we show that transmission functions of nanotubes with cavities ($m > n$) show resonances and anti-resonances. Differences between the band structures of the nanotubes forming the whole structure are responsible for this behavior. Anti-resonances in transmission are related to quasi-bound states formed inside the cavity, as it is shown by the peaks of the LDOS that coincide with dips in Transmission. These anti-resonances are produced by interferences between bound states of the central part of the nanotube and extended states along the leads. Resonances are produced by superposition of channels weakly scattered at the boundaries of the cavity, which modulate the transmission function even in the absence of quasi-bound states. We show that in the other hand, when the cavity has less transmitting channels than the leads ($m < n$), there are not anti-resonances in transmission because of the lack of quasi-bound states inside the cavity, but transmission is slightly larger due to tunneling between leads.

We make also a deep extensive study of the behavior of the cavity as we modify its geometry. In this sense we show that 1) The larger N the less pronounced resonances in transmission while the number of peaks and valleys increases with the *length* of the cavity. 2) Increasing the *width* of the cavity makes transmission present more resonances and antiresonances. This effects are due to the interferences produced between waves weakly reflected at the boundaries of the cavity, as the number of possible energies that gives rise to interferences increases with the size of the system. Finally, properties of nanotubes with several cavities have been also studied.

References

[1] H.-S. Sim, C.-J. Park, and K. J. Chang, Phys. Rev. B **63**, 073402 (2001).

[2] L. Chico and W. Jaskolski, Phys. Rev. B **69**, 085406 (2004).

[3] S. Datta *Electronic Transport in Mesoscopic Systems* (Cambridge University Press, Cambridge 1995)

[4] M. P. López Sancho, J. M. López Sancho, and J. Rubio, J. Phys. F: Met. Phys. **14**, 1205 (1984).

Poster

Magnetism at nanoscopic scale : numerical simulation and applications

Thomas Jourdan, Alain Marty, Frédéric Lançon

CEA Grenoble / DRFMC / SP2M
17 avenue des Martyrs
38054 Grenoble Cedex 9, France

thomas.jourdan@cea.fr

Introduction Magnetisation reversal in thin layers plays a key role in magnetic recording and has recently attracted much attention, particularly for materials exhibiting high magnetocrystalline anisotropy.

Among these materials, FePt in its $L1_0$ phase is a promising candidate for high density magnetic recording systems with giant anisotropy of about 5.10^6 J.m^{-3}.

Magnetisation reversal is often linked to domain wall displacement in the layer. This motion can be influenced by the interaction with structural defects such as antiphase boundaries or extended defects called micro-twins, which appear preferentially in ordered FePt[1].

Modelling In order to correctly simulate domain wall pinning, the atomic structure has to be taken into account. We have developed an algorithm that minimizes magnetic energy using the Heisenberg model. Energy terms taken into account are exchange energy, anisotropy, dipolar energy and energy due to an applied field.

The correct handling of the anisotropy in structural defects was carried out by using Néel's model, which considers the anisotropy of an atomic site as the result of its close environment.

The computation of the dipolar term is the real bottleneck in atomistic simulations given that it is a long range interaction. Therefore, without any approximation, computing this term requires a time proportional to $\mathcal{O}(n^2)$ where n is the total number of spins.

In order to speed up the calculation of this term, we adapted a Fast Multipole Method (FMM) [2] to atomic magnetism. This kind of method is based on the multipolar expansion of the potential (coulombic, gravitational, etc.) to gather particles. It can achieve the computation in a time proportional to the number of atoms with a precise control on the error made by truncating the expansion.

Results This algorithm was used to study the pinning of a domain wall by a micro-twin (figure 1). Computations have shown a strong pinning by this type of defect : for a micro-twin constituted of 6 atomic layers, the depinning field is about 2.5 T.

In fact, once the domain wall is pinned into the micro-twin, the application of a field to move the wall on the left or on the right shows that depinning is easier in the opposite direction of the propagation ($B = 1.9$ T, whereas a field of 2.8 T is necessary in the other direction). Therefore the configuration is asymmetric and the depinning field of a domain wall in a given direction gives us information on the direction of propagation before the wall reaches the defect.

References

[1] J. P. Attané et al., *Magnetic Domain Wall Propagation unto the Percolation Threshold across a Pseudorectangular Disordered Lattice*, Phys. Rev. Lett., **93**, 2004

[2] H. Cheng, L. Greengard and V. Rokhlin, *A Fast Adaptative Multipole Algorithm in Three Dimensions*, J. Comp. Phys., **155**, 1999

Figures :

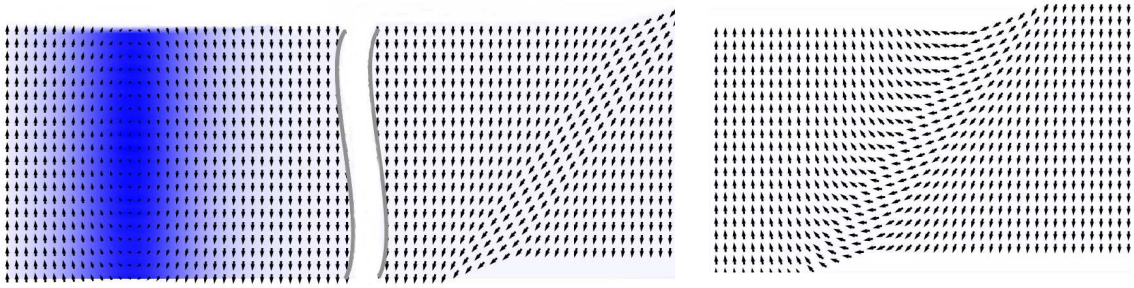


Figure 1: *Domain wall far from the micro-twin (left) and pinned into this defect (right); the system is invariant along the normal of the figure's plane.*

NEW DIAZONIUM SALTS OF METAL COMPLEXES FOR ELECTROCHEMICAL MODIFICATION OF CARBON NANOTUBES.

Bruno Jousselme [a], Cédric Goyer [b], Martial Billon [b], Stéphane Guillerez [b], Gérard Bidan [c], E. Abou Hamad [d], Christophe Goze-Bac [d], Jean-Yves Mevellec [e], Serge Lefrant [e]

[a] RTB «Post CMOS moléculaire 200mm», LETI / DIHS / LIMN;
[b] DRFMC / SPrAM / LEMOH, UMR 5819;
[c] DRFMC / DIR,
CEA-Grenoble, 38054 Grenoble cedex 9, France.
[d] LCVN, University of Montpellier II, 34095 Montpellier, France.
[e] IMN / University of Nantes, 44322 Nantes, France.
bruno.jousselme@cea.fr

Carbon nanotubes (CNTs) present remarkable electronic, mechanical, optical and chemical properties, which open a way to future applications of these nanoobjects as materials for molecular electronics, energy storage, sensors, new composites etc... Covalent or non covalent functionalizations of CNTs are more and more used in materials science with the goal to improve their solubility and the ease of their deposition in forms suitable for various electronic devices. More specifically, appropriate functionalization of CNTs may prevent form undesirable phenomena such as phase separation etc. This, in turn, facilitates their insertion into polymer matrices frequently used for the fabrication of specific electronic, optical or biological sensors. Different ways have been developed to covalently functionalise CNTs,1 involving chemical, photochemical and electrochemical processes. Electrochemical methods present two main advantages as compared to the two others. First, electrochemical phenomena proceed via electrical addressing, thus they enable selective functionalization of those nanotubes are incorporated into the electrochemical circuit2. Second, the current of electrografting is directly correlated with the density of electrons generated onto the nanotubes surfaces which allows a control of the functionalization rate. In view of new applications of CNTs in optoelectronics there exists a strong demand for the development of electrochemically active systems containing chromophore groups. We present here a promising family of such compounds, namely new diazonium salts of metal complexes which combine electrochemical activity with strong absorbtion in the visible part of the spectrum. In particular, we describe the synthesis of diazonium salts of bipyridine or terpyridine metal complexes. The electrochemical depositions of these compounds are first tested on a vitrous carbon electrode and then extended to CNTs.

References:

[1] (a) A. Hirsch, *Angew. Chem. Int. Ed.* **41** (2002) 1853; (b) D. Tasis, N. Tagmatarchis, V. Georgakilas, M. Prato, *Chem. Eur. J.* **9** (2003) 4000; (c) S. Banerjee, T. Hemraj-Benny, S.S. Wong, *Adv. Mater.* **1** (2005) 17; (d) K. Balasubramanian, M. Burghard, *Small*. **1** (2005) 180. D. Tasis, N. Tagmatarchis, A. Bianco, M. Prato, *Chem. Rev.* **106** (2006) 1105.
[2] S. E. Kooi, U. Schecht, M. Burghard, K. Kern *Angew. Chem. Int. Ed.* **41** (2002) 1353.

Dimension Dependence of Subthreshold Swing for Sub-20nm Double Gate MOSFETs

Hakkee Jung

School of Electronic and Information Engineering, Kunsan National University, Kunsan, Jeonbuk 573-701, Korea

hkjung@kunsan.ac.kr

The double-gate MOSFET (DGMOSFET) is a particularly promising candidate for ultimate CMOS scaling due to its better control of short channel effects (SCEs) such as subthreshold swing(SS) [1]. This intimate coupling between the gates and the channel makes DGMOSFET technology the most scalable of all FET designs. The DGMOSFET is electrostatically stronger than a single-gate MOSFET because two gates are used to control the channel from both sides, thus allowing for additional gate length scaling by nearly a factor of two. In addition, ballistic transport of carriers can be achieved with DGMOSFETs, due to low doping in the channel and the double-gate features. The challenge lies in obtaining suitable threshold voltages for high-speed logic devices, while controlling the extrinsic resistance. However, for DGMOSFET with gate length of sub-20nm, the SCEs such as degradation of subthreshold swing become very important issues that cannot be neglected.

The aim of this work is to analyze the dimension dependence of subthreshold swing using analytical model for the subthreshold characteristics of sub-20nm DGMOSFETs that includes the contribution of both thermionic emission and quantum tunneling to the subthreshold current. In the new model, the approximation of exponential functions is not used when modeling the potential in the channel because this term is not negligible in the case of devices with gate lengths L_g below 20nm.[2] The tunneling probability is obtained from the Wentzel-Kramers-Brillouin (WKB) approximation, which is used to obtain the gate-length and -voltage dependent tunneling currents.

This symmetric structure is characterized by two identical polysilicon gates with no overlap with the source/drain extensions, as shown in Fig. 1. A very thin lightly p-type doped silicon channel thickness t_{Si} of under 10 nm, thin gate oxide of thickness t_{ox}, and channel length L_g under 20 nm are the geometric parameters. The doping level of the p-type silicon channel is $N_A = 10^{16}$ cm^{-3}. The n-type source and drain regions are uniformly doped at the level of 10^{20} cm^{-3}. The poly-gate is uniformly doped p-type with doping concentration of 10^{20} cm^{-3}. Figure 2 shows the variation of subthreshold swing as a function of gate length. It can be seen that the analytical results from the proposed model in this paper agree well with 2D numerical simulation[3]. For shorter channels, the subthreshold-swing degradation is larger because the quantum tunneling is more pronounced. Figure 2 also shows subthreshold swings as a parameter of gate oxide thickness with $t_{ox} = 1, 2, 3nm$. The thermionic emission has been found as the main mechanism of carrier transport for channel lengths above 12 nm. On the other hand, quantum tunneling is dominant in DGMSOFETs with gate lengths below 12 nm, and it significantly influences the device scaling, especially in the sub-10nm region. We know the variation of the gate oxide thickness is negligible in the region of sub-10nm gate length, in which the tunneling current is more pronounced and subthreshold swing degradation is larger.

Reference:

[1] T.Schulz, W.Rosner, E.Landgraf, L.Risch and U.Langmann, Solid-State Electronics, **46**(2002), pp.985-989.
[2] H.K.Jung and S.Dimitrijev, IEEE Trans. Electron Devices, **53**(2006), pp.685-691.
[3] D.Munteanu and J.L.Autran, Solid-State Electronics, **47**(2003), pp.1219-1225.

Figures :

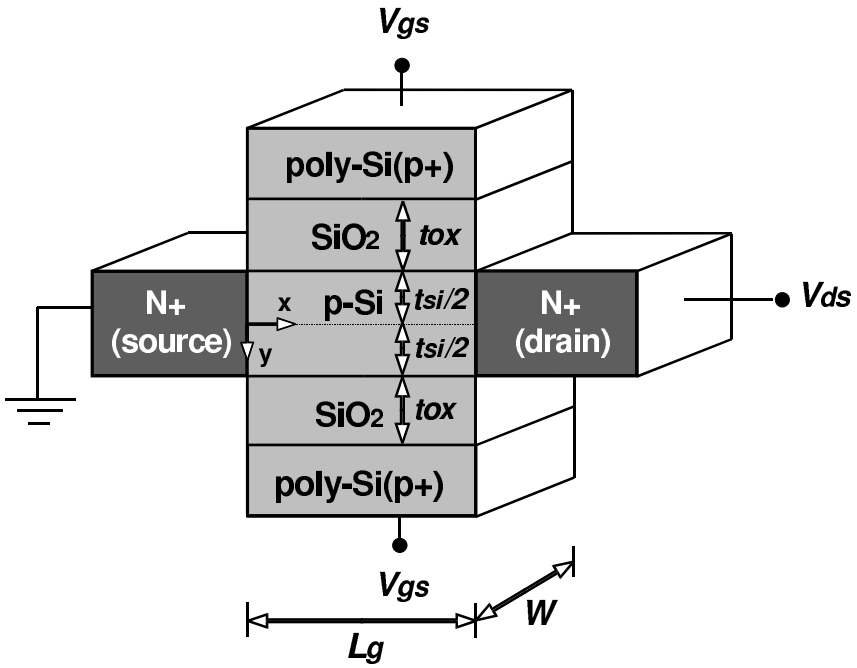


Figure 1: Schematic diagram of double gate MOSFET.

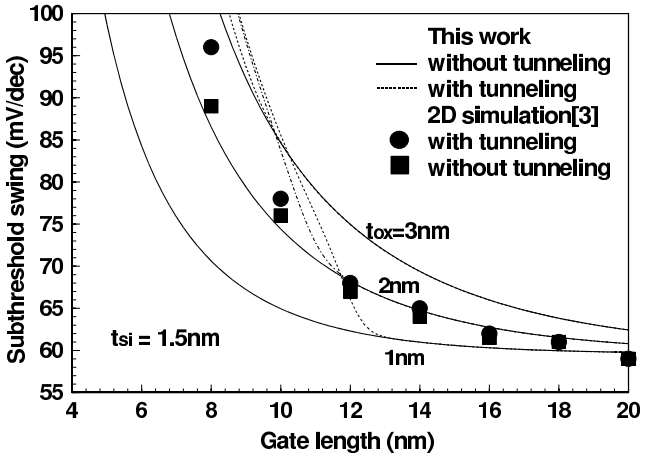


Figure 2: Subthreshold swing as a function of the channel length for DGMOSFET.

PHOTOINDUCED INTRAMOLECULAR ELECTRON TRANSFER WITHIN A NOVEL SYNTHESIZED DONOR-ACCEPTOR SYSTEM IN THE PRESENCE OF TIO_2 NANOPARTICLE

Suman Kalyan Pal, Tapan Ganguly
Department of Spectroscopy, Indian Association for the Cultivation of Science, Jadavpur, Kolkata-700032, India
pal_suman1@rediffmail.com

Photoinduced intramolecular electron transfer have been investigated in a rigid donor-acceptor system 7MTCA (7-Methoxynaphtho[1,2-*b*]thiophene-2-carboxylic acid) containing the donor moiety 7MNT (7-methoxynaphtho[1,2-*b*]thiophene) and the acceptor carboxylic acid (COOH) group [1] in chloroform ($CHCl_3$) in absence as well as the presence of nanosized (~2 nm) TiO_2 particle. Formation of charge transfer complex both in the ground state and in the excited state was apparent from both steady state absorption and fluorescence measurements of 7MTCA. The change of absorption of 7MTCA with TiO_2 concentration at a fixed wavelength was analyzed by using the Langmuir adsorption isotherm [2, 3] and an association constant of $K_a = 5 \times 10^4$ M^{-1} between 7MTCA and TiO_2 nanoparticle was observed. The observed high association constant along with the spectral changes indicate a strong interaction between the DA system and the TiO_2 nanoparticle in the ground state and the formation of ground surface complexes between the two. The formation of charge separated species through photoinduced intramolecular electron transfer reactions between the donor and acceptor groups of DA system with an efficiency of 51% and a rate constant of 1.5×10^9 s^{-1} was apparent from time resolved spectroscip measurements [4]. Transient absorption measurements by nanosecond laser flash photolysis technique demonstrate the formation of triplet ion-pair for the present DA system in the absence as well as the presence of TiO_2 nanoparticle. Analysis of the time profile of the absorbance of the anionic species of the molecule shows that formation of ground surface complexes with TiO_2 nanoparticle, enhance the survival duration of charge separated species [5] from 1.5 μs to 2 μs for the present DA system. The observed phenomenon of slowing down of charge recombination process is due to stabilization of the radical ions against destructive charge recombination process in the presence of TiO_2 nanoparticle.

References:

[1] S. K. Pal, T. Sahu, T. Misra, T. Ganguly, T. K. Pradhan, A. De, J. Photochem. Photobiol. A: Chem., **174** (2005) 138.

[2] J. Pan, G. Benkö, Y. Xu, T. Pascher, Li. Sun, V. Sundström, T. Polivka, J. Am. Chem. Soc., **124** (2002) 13951.

[3] M. Hilgendorff, V. Sundström, J. Phys. Chem. B, **102** (1998**)** 10505.

[4] L. P. Zang, B. Chen, L. Z. Wu, C. H. Tung, H. Cao, Y. Tanimato, J. Phys. Chem. A, **107** (2003) 3438.

[5] T. Misra , T. Bhattacharya , S. K. Pal, A. De , R. D. Saini , T. Ganguly , Chemical Physics Letters, **382** (2003) 167.

Figures:

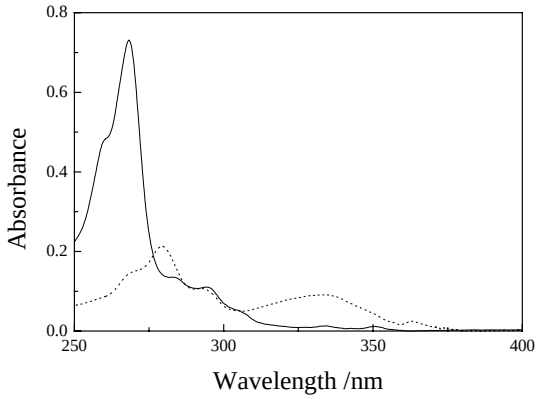


Fig. 1

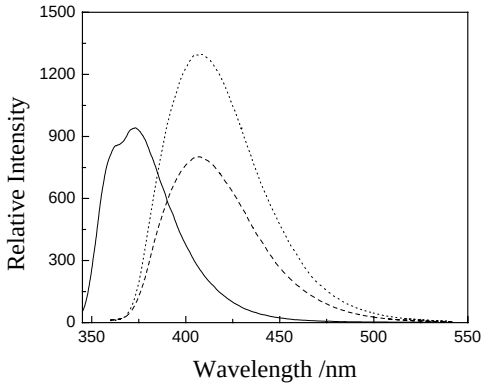


Fig. 2

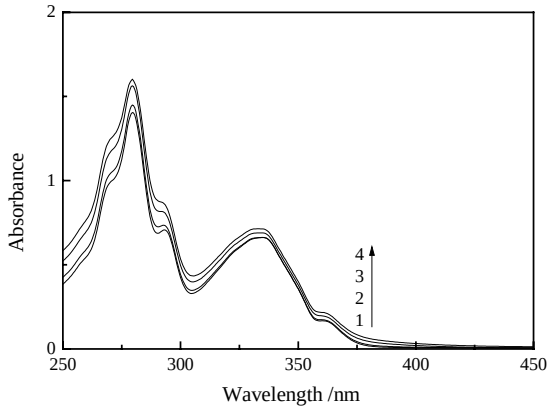


Fig. 3

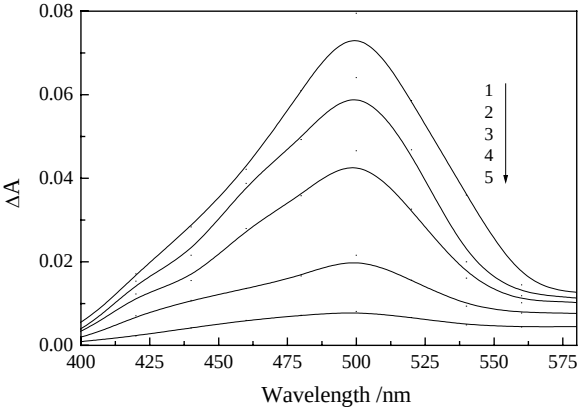


Fig. 4

Figure captions:

Figure 1. Steady state absorption spectra of 7MNT (solid line) and 7MTCA (dotted line) in chloroform.

Figure 2. Fluorescence emission spectra of 7MNT with excitation wavelength ~305 nm (solid line), 7MTCA with excitation wavelength~305 nm (dashed line) and 340 nm (doted line) in chloroform.

Figure 3. Absorption spectra of 7MTCA in chloroform in the presence of TiO_2 nanoparticles:(1) 0, (2) 1.34×10^{-5}, (3) 3.98×10^{-5}, (4) 5.29×10^{-5} mol dm^{-3}.

Figure 4. Transient absorption spectra of 7MTCA (excitation wavelength ~355 nm) at the ambient temperature at delay times: (1) 4 μs; (2) 5 μs; (3) 6 μs; (4) 8 μs; (5) 12 μs; measured in $CHCl_3$.

EXPERIMENTAL STUDY ON THE RAYLEIGH INSTABILITY OF GOLD NANOWIRES

S. Karim[1], M.E. Toimil-Molares[2], A.G. Balogh[3], W. Ensinger[3], T.W. Cornelius[2], and R. Neumann[2]

[1]*University of Marburg, Department of Chemistry and Materials Science Center, Hans-Meerwein-Str., D-35032, Marburg, Germany*
[2]*Gesellschaft für Schwerionenforschung (GSI), Planckstr. 1, D-64291 Darmstadt, Germany*
[3]*Darmstadt University of Technology, Institute of Materials Science, Petersenstr. 23, D-64287 Darmstadt, Germany*
s.karim@gsi.de

Research on the physical and chemical properties of metallic nanowires has attracted increasing interest due to potential applications of such wires in many future nanodevices [1]. In particular, a reliable thermal stability of nanowires is necessary for their implementation as either building blocks or interconnects in nanoscale devices. Models predicted that due to the high surface-to-volume ratio, nanowires become unstable particularly at elevated temperatures when the mobility of atoms by diffusion is higher [2]. Recently, it has been demonstrated experimentally that Cu nanowires with diameter 30-50 nm fragment due to the Rayleigh instability when exposed to temperatures as low as 400 ^{o}C [3]. Further, it is expected that even thinner nanowires exhibit instabilities already at room temperature [4, 5]. Similarly, large low-frequency resistance fluctuations of metallic nanowires were reported recently that occur above a certain temperature due to morphological instabilities [6]. All these findings raise concern under which conditions metal nanowires can be used as interconnects. In addition, thermal annealing is often used to improve desired physical properties of nanowires [7]. Therefore, a sound knowledge of thermal stability is thus necessary, not only for the industrial implementation where higher temperatures are required for both production and performance, but also for an optimized production of defect-free nanowires by thermal annealing.

In this work, we have systematically investigated the instability of Au nanowires annealed isothermally at different temperatures. We show that the wires driven by Rayleigh instability undergo various configurational changes and finally break up into a chain of spheres at temperatures well below the bulk melting point (Figure 1). We observed how the final morphology is influenced by the three parameters: wire diameter, temperature, and annealing time. Both the average diameter of the nanospheres formed after decay and the spacing between adjacent spheres are larger than that predicted by linear stability analysis for materials with isotropic surface energy, indicating a stabilization effect due to surface energy anisotropy.

In addition, a reliable control over this instability process can provide an effective, powerful, and economical technique for producing self-assembled nanosphere chains on a relatively large scale by using Au nanowires as starting point. This kind of structures has unique properties for many promising applications such as plasmon waveguides

where near-field coupling between surface plasmon-polariton modes of neighboring particles is used to guide light below diffraction limit [8]. The fabrication technique can also be extended to different materials and substrates.

References:

[1] Y. Xia, P. Yang, Y. Sun, Y. Wu, B. Mayers, B. Gates, Y. Yin, F. Kim, and H. Yan, Adv. Mater. **15**, 2003, 353.

[2] F.A. Nichols and W.W. Mullins, Trans. Metal. Soc. AIME, **233**, 1965, 1840.

[3] M. E. Toimil Molares, A. G. Balogh, T.W. Cornelius, R. Neumann, and C. Trautmann, App. Phys. Lett. **85**, 2004, 5337.

[4] Y. Sun, B. Mayers and Y. Xia, Nano Lett. **3**, 2003, 675.

[5] C. Brechignac, Ph. Cahuzac, F. Carlier, C. Colliex, J. Leroux, A. Masson, B. Yoon, and U. Landman, Phys. Rev. Lett. **88**, 2002, 196103.

[6] A. Bid, A. Bora and A. K. Raychaudhuri, Phys. Rev. B, **72**, 2005, 113415.

[7] C.S. Hsieh, G. Wang, D.S. Tsai, R.S. Chen, and Y.S. Huang, Nanotech. **16**, 2005, 1885.

[8] S. A. Maier, P. G. Kik, H. A. Atwater, S. Meltzer, E. Harel, B. E. Koel, and A. A.G. Requicha, Nat. Mater. **2**, 2003, 229.

Figure:

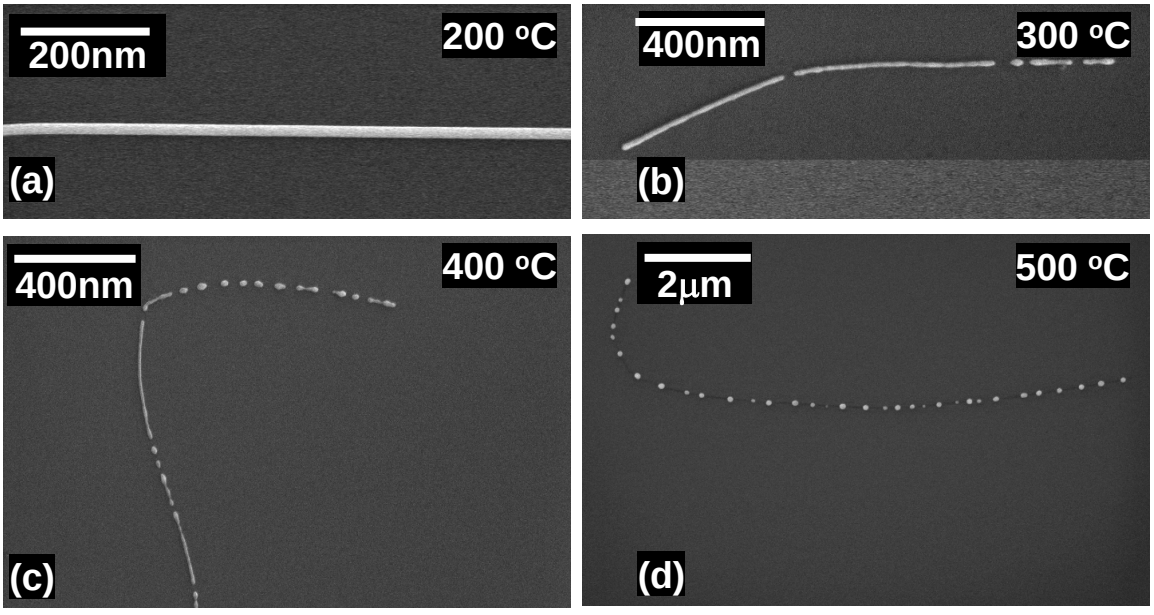


Figure 1. HRSEM images of 25 nm gold wires after annealing at different temperatures. Annealing time was in all cases fixed to 30 min. (a) A Wire preserve its shape after annealing at 200 ^{o}C. (b) At 300 ^{o}C, perturbations are developed resulting in fragmentation (c) At 400 ^{o}C, a wire decay into much shorter section. (d) Finally, at 500 ^{o}C wires transform into chains of nanospheres.

SYNTHESIS AND CHARACTERIZATION OF Dy-Ni-Fe ALLOY THIN FILMS USING ELECTRODEPOSITION TECHNIQUE

M. V. Khaddem-Mousavi, I. Z. Rahman and A. Gandhi

Materials and Surface Science Institute (MSSI) & Department of Physics, National Technological Park University of Limerick, Limerick, Ireland

Contact: I. Z. Rahman, E-mail: zakia.rahman@ul.ie

Abstract

Recently there is a great interest shown for growing nanoscale thin films of transition metals and their alloys using electrodeposition technique due to several out standing advantages over vacuum systems. Ultra thin ferromagnetic films on metallic substrates have become the subject of many investigations for its application potentiality in information technology. RE-TM alloy thin films are known to show perpendicular magnetic anisotropy, which is attractive for potential application in data storage.

In this paper we report on synthesis and characterization of Ni, Fe, and Dy to investigate the magnetic and nano structural properties of thin films using electrodeposition technique. An inorganic bath sulphate bath has been used to deposit the samples on aluminium substrates. The solubility degree of $Dy_2(SO_4)_3$ is found to be almost 100% when started with Dy_2O_3 that has been chemically treated to obtain the sulphates followed by heat treatment. The SEM, and AFM techniques are used to analyse the surface morphology (see figure 1) and XRD and EDAX are carried out to determine the crystal structure and the composition of the element in the films (See Figure 2). The magnetic properties are determined using Vibrating Sample Magnetometer. In all cases the film structure is found to be affected by deposition parameters such as pH, and temperature consequently having an influence on the magnetic properties of the films. In addition to that depending on the concentration of RE-content the deposited films structure varies from crystalline to amorphous that influences magnetic properties as well.

Figures:

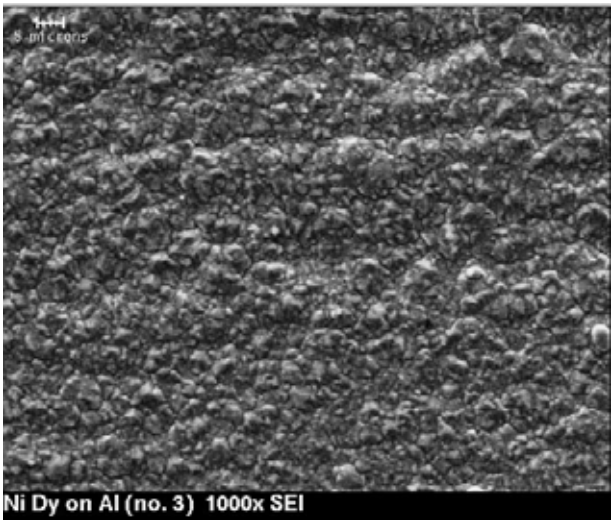


Figure1: SEM micrograph of Ni Dy electrodeposited at 50 ^{o}C, deposition time of 60 mins and pH 3.4 on Al substrate.

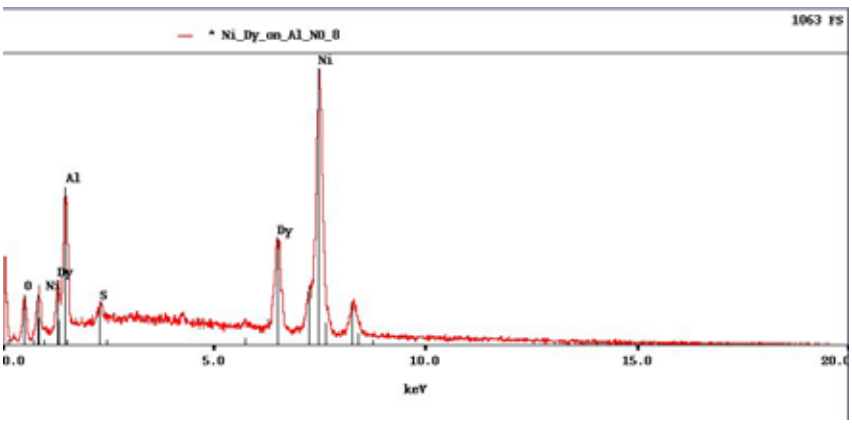


Figure 2: The EDAX result of Ni–Dy sample electrodeposited at 50 ^{o}C, deposition time of 60 minutes and pH 3.4 on Al substrate shows at weight of Dy and Ni at 3 0.6% and 32.39% respectively.

ELECTRONIC STRUCTURE OF HEXAGONAL WO_X AND CUBIC MoO_X NANOPARTICLES: EXPERIMENTAL STUDIES AND BAND-STRUCTURE CALCULATIONS

O. Yu. Khyzhun, V. L. Bekenev, Yu. M. Solonin
Frantsevych Institute for Problems of Materials Science, National Academy of Sciences of Ukraine, 3 Krzhyzhanivsky Str., Kiev UA-03142, Ukraine
khyzhun@ipms.kiev.ua

Tungsten trioxide synthesizes in a monoclinic form at room temperature (m-WO_3). However, at least five modifications of tungsten trioxide have been detected when temperature changes from 900 °C to –180 °C. The following sequence of changes of the crystal structure was observed with decreasing temperature: tetragonal D_{4h}^7 → orthorhombic D_{2h}^{16} → monoclinic D_{2h}^5 → triclinic C_i^1 → monoclinic C_s^2 [1, 2]. Structures of the above modifications of WO_3 are based on a m-WO_3-related structure and differ from each other only by distortions of the [WO_6] octahedra linked by corner sharing. In m-WO_3 each W atom is surrounded by six O atoms in an octahedral coordination. In the unit cell of m-WO_3, every four [WO_6] octahedra are slightly tilted with respect to one other. As a result, the structure of m-WO_3 is less symmetrical as compared with that of cubic ReO_3-type. The hexagonal form of tungsten trioxide, h-WO_3, was synthesized by Gerand et al. [3] due to dry heating of the $WO_3 \cdot 1/3 \cdot H_2O$ hydrate. The structure of the hexagonal form of WO_3 differs essentially from that of m-WO_3: every six [WO_6] octahedra linked by corner sharing form hexagonal channels oriented along the *c* axis in h-WO_3. The h-WO_3 compound was found to be a very prospective material for positive electrodes of rechargeable lithium batteries [4]. However, on the initial stage of hydrogen reduction of h-WO_3 the nonstoichiometric h-$WO_{2.8}$ phase with the structure belonging to UO_3 type was synthesized very recently [5]. The h-$WO_{2.8}$ compound was found to be a prospective sensor material possessing good electrochemical properties.

Molybdenum trioxide, MoO_3, crystallizes in a layered structure belonging to orthorhombic symmetry. MoO_3 can be rather easily reduced and at least eight stable Magnéli phases, namely $Mo_{18}O_{52}$, $Mo_{17}O_{47}$, Mo_9O_{26}, Mo_8O_{23}, Mo_7O_{20}, Mo_6O_{17}, Mo_5O_{14} and Mo_4O_{11}, have been synthesized in the intermediate region between MoO_3 and MoO_2 [6]. Structures of all the phases belong to orthorhombic, monoclinic or triclinic symmetry. However, a new nonstoichiometric cubic MoO_x phase was obtained when heating molybdenum hydrogen bronze, H_xMoO_3, in hydrogen at temperatures 300 to 400 °C. The composition of the cubic MoO_x phase under study corresponds to $MoO_{1.9\pm0.1}$ [7].

The hexagonal WO_3 and $WO_{2.8}$ and cubic $MoO_{1.9}$ phases studied in the present work were found to be nanocrystalline materials with particle sizes being in the range from 60 to 80 nm [5, 7]. The aim of the present work was to fulfil a complex study of the electronic structure of the mentioned tungsten and molybdenum oxides nanoparticles using X-ray photoelectron spectroscopy (XPS), X-ray emission spectroscopy (XES) and X-ray absorption spectroscopy (XAS). For comparison, monoclinic WO_{3-x} and orthorhombic MoO_3 oxides were also investigated. For the mentioned compounds, XPS valence-band spectra and XES O Kα bands (O 2p-like states) were obtained as well as the XAS W L_{III} and O K edges were measured and compared on a common energy scale. Band-structure calculations were made for the nostoichiometric cubic molybdenum oxide employing a full-potential linearized augmented plane wave (FLAPW) method with the WIEN97 program [8].

The formation of an additional near-Fermi sub-band *B*, which is absent in the both monoclinic and hexagonal forms of tungsten trioxide, was detected on the XPS valence-band spectrum of h-$WO_{2.8}$ (Fig. 1). The similar near-Fermi sub-band is also detected on the XPS valence-band

spectrum recorded for the cubic $MoO_{1.9}$ nanoparticles. The creation of this sub-band is caused by the W 5*d*- and W 6*s*-like states taking part in the formation of the M-M bonds in the h-$WO_{2.8}$ compound (Mo 4*d*- and Mo 5*s*-states in the case of cubic $MoO_{1.9}$). Energy positions of the centres of gravity and of the main maxima *c* of the O Kα band remain constant for all the compounds studied (as an example, Fig. 2 shows the XES O Kα spectra for the molybdenum oxides under study). Increasing the half-width of the O Kα band when going from m-WO_x to h-WO_x can be explained by the fact that two types of oxygen atoms are distinguished in the structures of h-WO_x: the atoms belonging to the hexagonal planes and those between the planes [9]. As a results, the O 2p-states originating from the atoms in the hexagonal planes dominate in the low-energy part of the O 2p-like band, while the states originating from the atoms between the planes dominate the top of the band. The effective positive charge on the tungsten (molybdenum) atoms decreases somewhat in the sequences h-WO_3 → h-$WO_{2.8}$ and MoO_3 → $MoO_{1.9}$; nevertheless charge states of the oxygen atoms remain constant for all the tungsten and molybdenum oxides studied. Results of the present experimental studies of the electronic structure of molybdenum oxides are in good with the theoretical FLAPW band-structure calculations for the compounds.

References:

[1] B.O. Loopstra, H.M. Rietveld, Acta Cryst. B, **25** (1969) 1420.
[2] E. Salje, K. Wiswanathan, Acta Cryst. A, **31** (1975) 356.
[3] B. Gerand, G. Nowogrocki, J. Guenot, M. Figlarz, J. Solid State Chem., **29** (1979) 429.
[4] W. Han, M. Hibino, T. Kudo, Solid State Ionics, **128** (2000) 25.
[5] Yu.M. Solonin, O.Yu. Khyzhun, E.A. Graivoronskaya, Cryst. Growth Des., **1** (2001) 473.
[6] V.E. Henrich, P.A. Cox, The Surface Science of Metal Oxides, Cambridge University Press, Cambridge, 1994.
[7] O.Yu. Khyzhun, T. Strunskus, Yu.M. Solonin, J. Alloys Compd., **320** (2001) 1.
[8] P. Blaha, K. Schwarz, P. Sorantin, S.B. Trickey, Comput. Phys. Commun., **59** (1990) 399.
[9] O.Yu. Khyzhun, Yu.M. Solonin, V.D. Dobrovolsky, J. Alloys Compd., **320** (2001) 1.

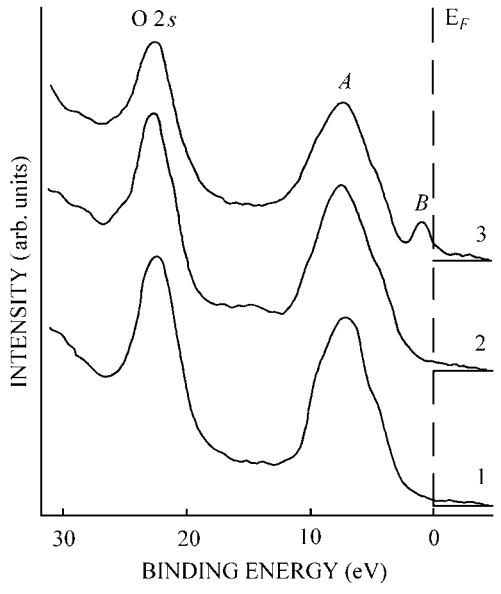


Fig.1. XPS valence-band spectra of:` (1) m-WO_3, (2) h-WO_3, and (3) h-$WO_{2.8}$

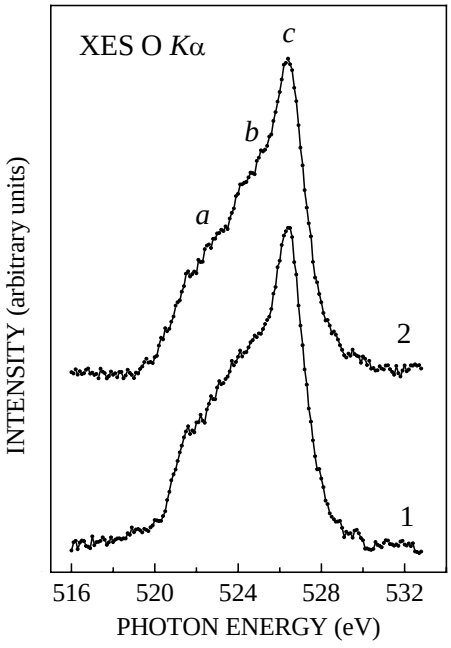


Fig. 2. XES O Kα emission bands of: (1) orthorhombic MoO_3, (2) cubic $MoO_{1.9}$

FIRST-PRINCIPLES STUDY OF THE CONDUCTIVITY OF SMALL DNA JUNCTIONS

Yong-Hoon Kim
Korea Institute for Advanced Study, 207-43 Cheongnyangni 2-dong, Dongdaemun-gu, Seoul, 130-722 Korea
yhkim@kias.re.kr

Performing large-scale density-functional and matrix Green's function calculations, we study the coherent charge transport characteristics of trimers of poly(G)-poly(C) and poly(A)-poly(T) DNA base pairs sandwiched between Au(111) electrodes. We find (i) in both cases their intrinsic electronic transport properties are dominated by the highest-occupied molecular orbitals (HOMOs), (ii) their HOMOs are originated from A and G for poly(GC) and poly(AT) , respectively, (iii) poly(GC) HOMO is located closer and higher to the Fermi level than the poly(AT) counterpart, (iv) their HOMO-originated transmissions are close to 1 due to the efficient π-π tunnelling. The results are consistent with the recent experiments that characterized dry DNAs as semiconductors or insulators.

References: [1] Authors, Journal, Issue (Year) page.

PREPARATION OF CNT ELECTRODES FOR ENHANCED ELECTROCHEMICAL PROPERTIES

Hyun-Ju Kim, Dong-Yoon Lee, Bo-Kun Koo, Won-Jae Lee and Jae-Sung Song
Electric & magnetic devices group of Korea Electrotechnology Research Institute (KERI), 28-1 Sungju-dong, Changwon-city, Gyungnam-do, Korea 641-120
dylee@keri.re.kr

There is great interest in novel carbon nanotubes(CNT)-based electrode materials for fabricating future nanoelectronic applications, including displays, interconnects, memories and sensing devices, since it provides remarkably good electrical, physical and chemical properties; good electrochemical stability, low resistivity, large surface area, etc.[1]. In order to use such good physical and chemical properties, we consider to apply CNT to the electrochemical devices like a dye-sensitized solar cells(DSSCs). Here, we may expect it to be superior to conventional grapite in electrochemical catalytic properties. Upto now, the use of CNT electrodes was mainly considered for electron emission in display, for electrical capacitor in storages and for electrodes in fuel cells. However, remarkable enhancement on electrochemical behaviors has been not reported.

In this respect, we need to improve preparation process of CNT electrode for realsing electrode potential of electrochemical cells. In order to enhance electrochemical properties of CNT electrode, we prepared CNT paste, using CNT powder, Carboxyl Methyl Cellulose(CMC) and D.I. water. CNT electrodes were fabricated as follow method [2]; CNT powder was prepared by Carbon Nanotech Co. using Fe catalyst by thermal chemical-vapor process. CNT has multi-wall type having diameter of 10~20nm and length of about 5 ㎛. First, CNT powder, de-ionized water and CMC (Carboxyl Methyl Cellulose) for paste manufacturing are prepared. Mixture of these was mechanically ball-milled for 24hrs. CNT electrodes as working electrode for electrochemical properties measurement were coated on the F-doped SnO_2 (FTO) glass by doctor-blade methode, following drying and heat-treatment.

We carried out TGA analysis of CNT paste in order to understand chemical dissociation of CMC and water. CNT paste was prepared by Dr blade, following 80^{o}C conventional heat treatment. In this case, we expect to avoid disadvantage reaction between water residual and Iodine-embedde electrolyte of DSSCs. For eliminating disadvantage of CMC and residual water in CNT electrode, we carried out heat traetment in the range of 80 to 390^{o}C on the basis of TGA. It was heat-treated at various temperatures in air; 80^{o}C, 230^{o}C, 260^{o}C, 290^{o}C and 390^{o}C. Also, we measured electrochemical properties of heat-treated CNT samples for optimising heat-treatment conditon of CNT electrode.

Fig.1 shows result of TGA on CNT pastes having CMC and water. The dissociation and carbonization temperature of CNT pasted was observed. On the basis of such results, we dicided condition of CNT heat-treatmenet temperature.

Cyclic-voltammetry (CV) and electrochemical impedance spectroscopy (EIS) measurement of test cells having CNT electrodes were investigated. Here, CNT electrodes prepared from various heat-treatment were used in order to understand performance of novel CNT electrodes for DSSCs. Fig. 2 shows cyclic-voltamogram of electrochemical cells having CNT and Pt electrodes. In this electrochemical cell, CNT electrode is a working electrode and Pt plate is a counter and reference electrode. As we can see in this fugure, we can compared to degree of electrode reaction, current density, electrode potential, and interfacial resistance, etc in our samples. In conclusion, it was understood that enhanced electrochemical properties of CNT electrodes was obtained via optimal heat treatment temperature, 230^{o}C for 1hr. on the basis of TGA, CV and EIS measurements.

References:

[1] A. Bachtold, P. Hadley, T. Nakanishi, C. Dekker, Science 294 (2001) 1317
[2] H.J.Kim, D.Y. Lee, B.K. Koo, W.J. Lee, and J.S. Song, KIEEME, Vol.17 (2004) 1090

Figures:

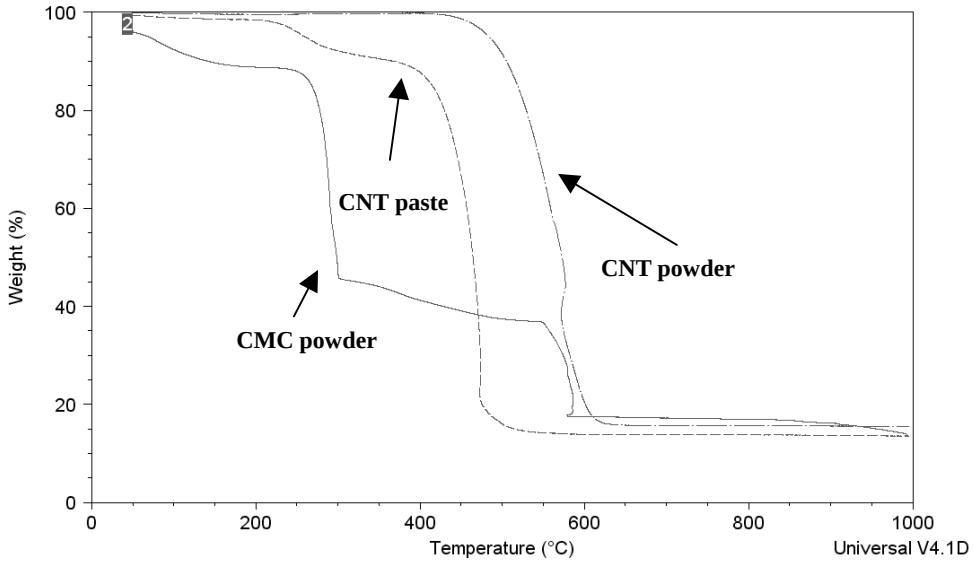


Fig. 1. TGA graphs of CNT paste, CNT powder and CMC powder.

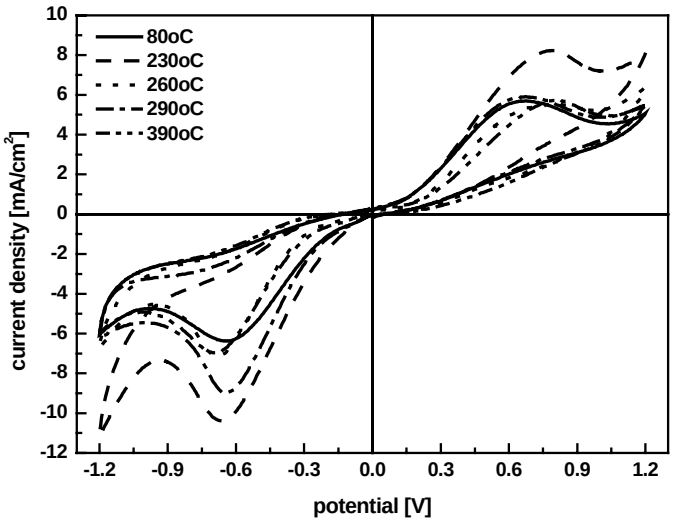


Fig 2. CV graphs of redox reaction of electrolyte on the CNT electrodes heated at the various temperature conditions.

SWNTS AND SnO2 COMPOSITE AS A HIGH PERFORMANCE AMMONIA GAS SENSOR

*Nguyen Duc Hoa, Nguyen Van Quy, Yousuk Cho, Dojin Kim**
School of Nano Science and Technology, Chungnam National University, Daejeon, Korea
dojin@cnu.ac.kr

A new ammonia gas sensor structure of single-walled carbon nanotubes (SWNTs) and SnO2 composite was developed. Thin Sn layer of ~100 nm thickness was deposited on SiO2/Si substrate followed by in-situ SWNTs deposition in an arc-discharge chamber. SWNTs/SnO2 nanocomposite was formed by annealing of the substrate at 500 oC in N2 and following oxidation at 450 oC in air. Interdigitated device structure was patterned with Pt/Ti electrodes. The SWNT quality was examined by Raman spectra, field emission scanning electron microscopy, and transmission electron microscopy. The electrical and gas sensing properties of the device were investigated. The nanocomposite revealed a semiconducting property, or decreasing electrical resistance with temperature. It showed a non-linear I-V curve due to tunneling between the semiconducting SWNTs. The electrical resistance of the nanocomposite sensor rapidly increased with exposure to ammonia gas. The sensor could detect an extremely low concentration of NH3 down to ppb level at room temperature. The sensitivity of the composite gas sensor increased linearly with NH3 concentration. The sensor also exhibited a very fast response of less than 100 seconds with reproducible sensing and recovery cycles. The recovery time was a few minutes.

Keywords: Single-walled carbon nanotubes, SnO2, nanocomposite, ammonia gas sensor

*Corresponding author: dojin@cnu.ac.kr

NANOCRYSTALIZATION OF CALCIUM CARBONATE IN MAGNETIC FIELD.

Cefalas, A. C. [(1)], Kobe, S. [(2)], Sarantopoulou, E. [(1)], Kollia Z. [(1)]. Stražišar, J. [(3)], Meden, A. [(4)]

[(1)]National Hellenic Research Foundation, TPCI, Athens, Greece.
[(2)]Department of Nanostructured Materials, Jozef Stefan Institute, Ljubljana, Slovenia
[(3)]Department for Geotechnology and Mining, University of Ljubljana, Slovenia
[(4)]Faculty of Chemistry and Chemical Engineering, University of Ljubljana, Slovenia

Abstract.

The crystallographic point symmetry group of precipitating particles on flow surfaces during the initial stage of nucleation depends besides other factors on the intensity of external magnetic fields and the state of flow during the initial stage of nucleation. Scanning electron microscopy and quantitative X-ray analyses verify that Ca^{2+} and CO_3^{2-} ions in water flow systems and under constant magnetic field of ~ 1.2 T, precipitate as $CaCO_3$ crystals with the ratio of aragonite-vaterite to calcite higher than ~ 7 (Fig. 1). The experimental data can be explained with the application of a quantum mechanical model, which predicts that magnetic fluctuations inside the flow of ionic liquids can be amplified to high values by taking energy from an external magnetic field through the angular momentum of the rotating water molecules. Results are in agreement with recently developed macroscopic magneto-hydrodynamic models of nano-crystallization [1,2].

References.

[1]Kobe, S.; Dražić, G. ; Cefalas, A. C.; Sarantopoulou, E.; Stražišar, J.; *Cryst. eng.* **2002** 5, 243-253.

[2] Kobe, S.; Dražić, G.; McGuiness, P. J.; Meden, A.; Sarantopoulou, E.; Kollia, Z.; Cefalas, A.C.; *Mater. sci. eng., C, Biomim. mater., sens. syst.* **2003**, 23, 811-815.

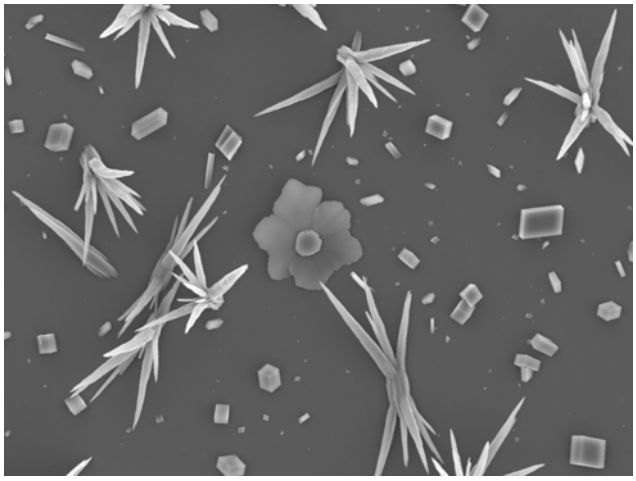


Figure 1. SEM image of precipitated crystals from water treated with the magnetic field.

NANOPARTICLE DISPERSIONS OF ORGANIC LUMINESCENT AND SEMICONDUCTING MATERIALS

Stefan Köstler, Andreas Rudorfer, Anja Haase, Georg Jakopic, Volker Ribitsch

Institute for chemical process development and control, Joanneum Research, Steyrergasse 17, Graz, Austria
Institute of chemistry, University Graz,Heinrichstrasse28, Graz, Austria
Institute for nanostructured materials and photonics, Joanneum Research, Franz-Pichler Strasse 30 , Weiz, Austria

stefan.koestler@joanneum.at

In the last few years research on different kinds of organic nanoparticles is steadily increasing. In the past, inorganic particles in the size range of a few nanometres were found to show size dependent optical and electronic properties. Organic nanoparticles recently were also found to show some size dependent optical and nonlinear optical properties even in a rather big size range between 100 to 200 nm. Especially polycyclic aromatic hydrocarbons are a very interesting class of materials. They show a very broad range of interesting properties like intensive colour, fluorescence, photoconductivity, semiconducting properties and a very special chemical and photochemical behaviour. Therefore, these materials are often used for pigments and dyes, fluorescent probes, etc. and they are promising materials for sensors, bioprobes and organic electronic devices like field effect transistors. The substances selected as model substances in this study, pentacene, tetracene and rubrene, are taken from this class of materials.

While there is abundant literature on the preparation and applications of inorganic semiconductor particles, reports on organic nanoparticles are relatively scarce. A frequently used process to prepare pure organic nanoparticle dispersions is the so called re-precipitation method. [1]. Here a solution of the organic material in a good solvent is added into an excess of a poor or non-solvent under vigorous stirring. The material precipitates and submicron sized particles are formed depending on temperature, concentration, stirring and other parameters. Another method, based on laser ablation of organic crystals dispersed in a liquid has recently been introduced by Tamaki [2]. Here, a coarse powder or large crystals of an organic material are dispersed in a solvent or surfactant solution by vigorous stirring. Then, intense laser light is shone into the dispersion and strikes the crystal of organic material. Above a certain laser fluence threshold material evaporates from the surface of the crystals by a laser ablation mechanism and subsequently condenses in the surrounding liquid phase to form submicron or nanometre sized particles.

We report on different methods for the preparation of stable nanoparticle dispersions of small molecule organic semiconductors. Some of them were prepared by the re-precipitation method from solution. Also the laser ablation method has been very recently applied to this type of materials [3] and results are compared with respect to dispersion and particle properties and preparation efficiency. A novel, especially efficient technique for the preparation of highly concentrated dispersions is introduced. This direct condensation method allows the preparation of stable dispersions in high amounts and concentrations by avoiding most of the disadvantages of existing techniques. The particles were characterized regarding particle size and shape, dispersion stability and optical and spectroscopic properties. Particle size was usually about 100 nm, and the dispersions showed structured absorbance bands in the visible region typical for the respective substances (see Figures 1 and 2). Rubrene and tetracene particles gave characteristic luminescence spectra. Many different film forming and structuring methods can be applied for further processing of the nanoparticle dispersions.

They were shown to be compatible with spin coating, spray coating, dip coating, electrostatic self assembly and ink-jetting techniques. Therefore, they are very well suited for the fabrication of functional devices in organic electronics and optical sensor technology.

Results as well as advantages and drawbacks of the different organic nanoparticle formation methods are compared and discussed with respect to material properties and implications for subsequent device fabrication.

References:

[1] H. Nakanishi, H. Oikawa: *Reprecipitation Method for Organic Nanocrystals*, in: H. Masuhara, H. Nakanishi, K. Sasaki (Eds.) *Single Organic Nanoparticles* (Springer, Heidelberg 2003).
[2] Tamaki Y., Asahi T., Masuhara H., Appl. Surf. Sci., **168** (2000) 85-88.
[3] Köstler S., Rudorfer A., Berghauser R., Jakopic G., Ribitsch V., Mater. Sci. Forum, **514-516** (2006) 1235-1240.

Figures:

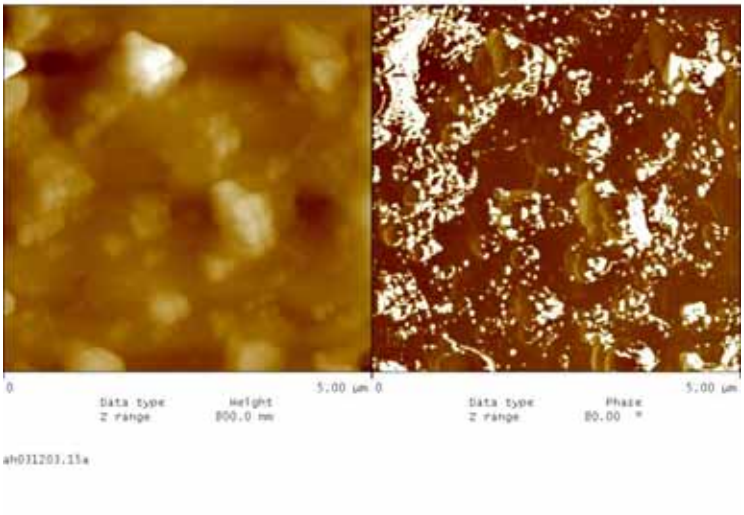


Figure 1: AFM height and phase image of pentacene nanoparticles prepared by laser ablation.

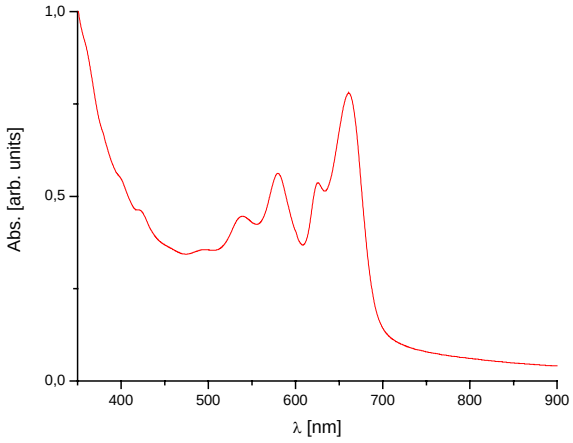


Figure 2: UV-Vis absorption spectra of a pentacene nanoparticle dispersion prepared by laser ablation.

Poster

LOCALIZED SPIN REVERSAL BY SPIN INJECTION IN A SPIN QUANTUM DOT: A MODEL CALCULATION

Satoshi Kokado, Kazumasa Ueda, Kikuo Harigaya, and Akimasa Sakuma
Shizuoka University, Hamamatsu 432-8561, Japan
AIST, Tsukuba 305-8568, Japan
Tohoku University, Sendai 980-8579, Japan

tskokad@ipc.shizuoka.ac.jpT

Magnetization reversal by spin injection, in which the magnetization of a ferromagnet (FM) is reversed by injecting a spin-polarized current into the FM, is one of the most interesting topics in spin-electronics. Recently, such phenomena have been experimentally observed in FM/non-magnetic film/FM junctions [1], and those have been analyzed by using theoretical models, where the magnetization of the FM is described by classical spins [2]. On the other hand, theoretical studies for quantum spin reversal by spin injection have scarcely been reported so far.

In this paper, we theoretically studied the quantum spin reversal by spin injection in a dot having a quantum spin (a spin quantum dot). Consequently, we derived the spin reversal time of the quantum spin and the transmission rate of the conduction spin.

As shown in Fig. 1(a), we consider a model, in which the quantum spin S with a uniaxial anisotropy energy showing a bistable potential is contacted by two electrodes with antiparallel spin-polarization. Many conduction spins flow from the left electrode (L) to the right electrode (R) one by one [3]. Here, the L has an energy level of up spin, while the R has N energy levels of down spin. Note that N levels of R are set by considering inelastic processes of conduction spins giving and taking energies with the quantum spin (the localized spin).

The interaction Hamiltonian obtained from the second order perturbation is written by,

$$V=|J|\sum_{R}\left(c^{+}_{R\downarrow}c_{L\uparrow}S_{+}+c^{+}_{L\uparrow}c_{R\downarrow}S_{-}\right),$$

where $c^{+}_{i\sigma}$ ($c_{i\sigma}$) is the creation (annihilation) operator of an electron with σ-spin (↑ or ↓) at the ith electrode (L or R), and $S_{\pm}=S_x\pm iS_y$. Furthermore, J represents the exchange interaction between the conduction spin and the localized spin. This interaction acts while each conduction spin runs through the dot. Also, it is assumed that the localized spin canted by the conduction spin is not rapidly relaxed, and it interacts with the subsequently injected conduction spin.

On condition that the initial state of the localized spin is $S_z=-S$, we solve a time dependent Schrödinger equation. From the time dependence of the probability density, the spin reversal time t_{SR} is obtained as $t_{SR}=\sum_{Sz=-S}^{S-1}\Delta t_{Sz}$,

$$\Delta t_{Sz}=\frac{h}{4|J|\sqrt{N(S-S_z)(S+S_z+1)}},$$

with h being the Planck constant, where Δt_{Sz} denotes time to transform the localized spin from S_z to S_z+1 , and also it is the transmission time of one conduction spin. Figure 1(b) shows S dependence of $t_{SR}\times\sqrt{N}|J|/h$. With increasing S, $t_{SR}\times\sqrt{N}|J|/h$ monotonically increases and comes close to $\pi/4$, which is obtained in the classical spin limit. We believe

that the spin reversal is realized when a relaxation time of the localized spin τ_{spin} satisfies the relation of $\tau_{spin} > t_{SR}$.

In addition, we investigate the transmission rate of the conduction spin $1/\Delta t_{Sz}$ for S=10, 20, 30 in the case of N =100. In Fig. 1(c), $1/\Delta t_{Sz}$ is plotted for the elapsed time $t_{Sz}\left(=\sum_{i=-S}^{Sz}\Delta t_i\right)$, where t_{Sz} means the total time to transform the localized spin from $-S$ to S_z+1. The transmission rate $(1/\Delta t_{Sz})\times h/|J|$ for each S exhibits a single peak. At each $t_{Sz}\times|J|/h$, $(1/\Delta t_{Sz})\times h/|J|$ becomes large with increasing S.

References:

[1] E. B. Myers, D. C. Ralph, J. A. Katine, R. N. Louie, and R. A. Buhrman, Science **285** (1999) 867.

[2] For example, see C. Heide, P. E. Zilberman, and R. J. Elliott, Phys. Rev. B **63** (2001) 64424.

[3] For example, see M. Eto, T. Ashiwa, and M. Murata, J. Phys. Soc. Jpn. **73** (2004) 307.

Figures:

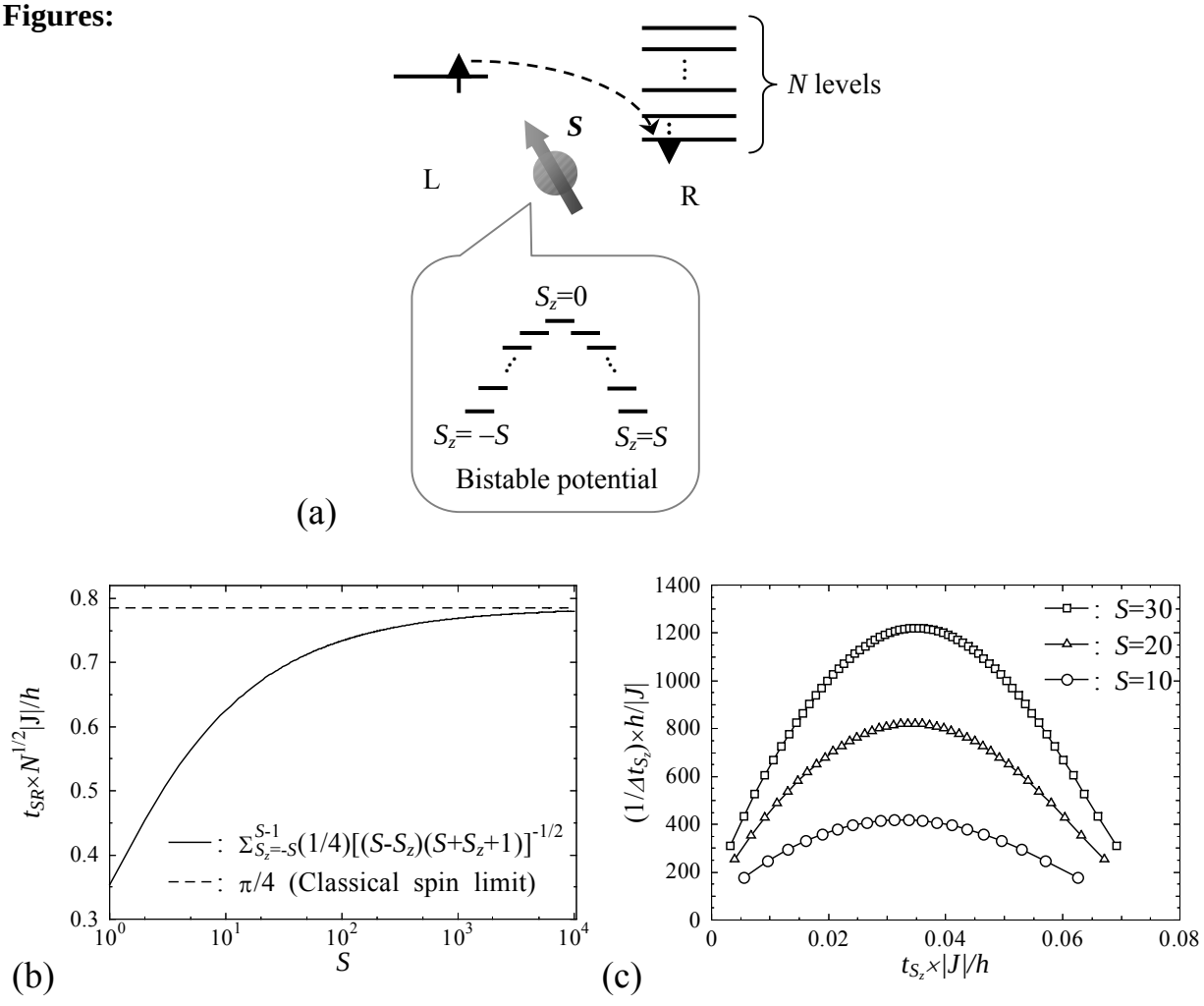


Figure 1 (a) A model of the spin quantum dot. (b) Spin S dependence of the spin reversal time t_{SR} [for convenience, $t_{SR}\times\sqrt{N}|J|/h$ vs S]. (c) The elapsed time t_{Sz} dependence of the transmission rate $1/\Delta t_{Sz}$ [for convenience, $(1/\Delta t_{Sz})\times h/|J|$ vs $t_{Sz}\times|J|/h$] for S=10, 20, 30 in the case of N =100.

HIEHARCHICAL SELF-ASSEMBLED STRUCTURES FROM BLOCK COPOLYMER/METAL NANOPARTICLES HYBRID MATERIALS INDUCED BY VUV LIGHT

E. Sarantopoulou, K. Gatsouli, Z. Kollia , S. Pispas
Theoretical and Physical Chemistry Institute, National Hellenic Research Foundation,
48 Vass. Constantinou Ave., 11635 Athens, Greece
S. Kobe
Department of Nanostructured Materials, Jozef Stefan Institute, Ljubljana, Slovenia

Thin films of block copolymer/iron metal nanoparticles hybrid organic-inorganic materials were prepared by a combination of wet chemistry, involving metal nanoparticle formation in block copolymer micellar templates and physical processing via casting or spin coating and laser illumination in the far VUV region. A variety of self-assembled structures in the nanometer to micrometer scale were observed by imaging techniques, including TEM, SEM and AFM. Investigations show a closely related hierarchy of the structures formed in the different length scales. These self-assembled structures hold a large potential for nano-technological applications.

INVESTIGATION OF NANOCRYSTALLINE SILICON THIN FILMS, DOPED BY RARE EARTH ELEMENTS

V. M. Koval, O. M. Shmyryeva

National Technical University of Ukraine "KPI", 37, Pr. Pobedy St., 03056, Kiev, Ukraine. E-mail: nanosi@list.ru

For the last decades, different kinds of silicon have investigated. The nanocrystalline silicon is just one of such new materials. It is intermediate form between amorphous silicon and monocrystalline one, because it consists of nanocrystallites, embedded in amorphous matrix. The presence of these crystallites provides improved electrical and optical properties of nanocrystalline silicon. Besides, thin films, which contain rare earth elements, are very promising from view-point of their optical properties [1, 2].

Nanocrystalline silicon is obtained either by the same way as amorphous one, but in another deposition conditions, or using recrystallization of amorphous silicon. Laser irradiation is one of the possible methods for material crystallization. It lies in the forming of crystallites in film under influence of laser radiation. Moreover nanocrystalls can appear during crystallization from liquid or solid phase. The first case is observed, if density of laser radiation reaches 120 mJ/cm^2. But films, obtained during liquid phase recrystallization, have essential drawback. They are non-planar. That is why crystallization from solid phase is preferable [3]. The appearance and growth of crystallites depend on number of pulses of laser radiation.

In this work electrical and optical properties of nanocrystalline silicon thin films, doped by rare earth elements, are investigated. They depend on composition, substrate temperature and number of laser pulses. The films were deposited by electron beam evaporation on the oxidized silicon substrates. Then the experimental samples were irradiated by semiconductor laser with wavelength 356 nm. The density of laser energy in one pulse was 80 mJ/cm^2, the duration of pulse was 20 ns.

The dependence of film conductance on number of pulses can be explained by percolation theory (fig.1). Under the low level of crystallinity the percolation cluster does not appear and the current flows in amorphous phase. When the crystalline volume fraction reaches threshold value (>50%), in film percolation cluster arises. As a result, the current flows in crystalline part of film, conductivity of which is higher than of amorphous one. The next decrease of current is caused by change of geometric form of cluster.

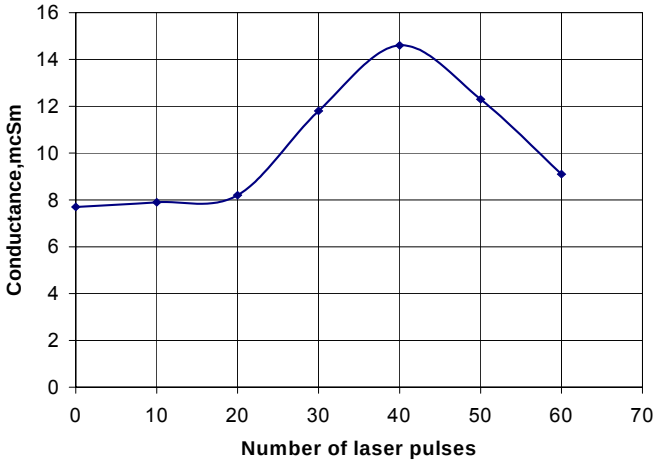


Fig. 1. Dependence of nc-Si:Y thin film conductance on number of laser pulses

The deposited films have demonstrated sensitivity in visible and ultraviolet spectral ranges. For example, for nanocrystalline silicon thin films, doped with Y, the following dependences were got (fig. 2, 3). The photosensitivity with rise of crystallinity is determined by contributions of two competing processes: increasing the carrier movement through crystalline phase, value of which much exceeds the carrier movement through amorphous

phase, and capture of photocarriers by crystallite surface defects. The changing of predominant mechanism determines behavior of this dependence.

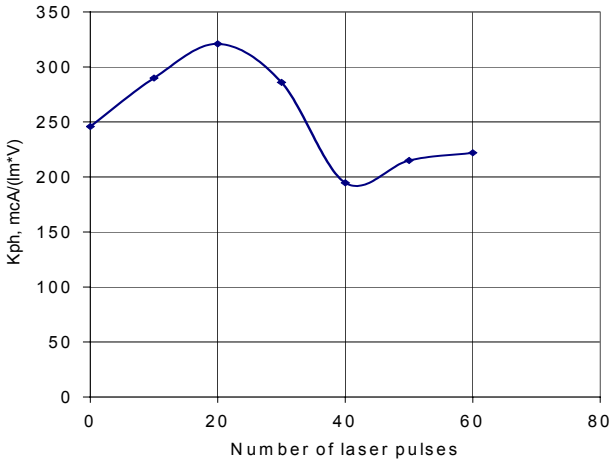


Fig. 2. Dependence of photosensitivity on number of laser pulses

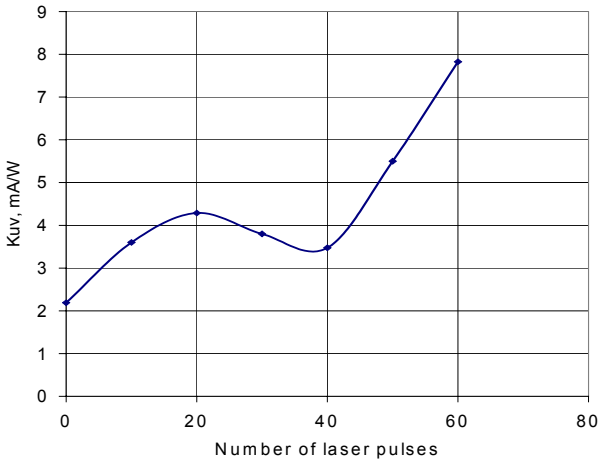


Fig. 3. Dependence of ultraviolet sensitivity on number of laser pulses

The reason of given behavior of ultraviolet sensitivity coefficient is different from photo sensitivity one. It is known that the film structure determines the band gap of material and accordingly the sensitivity to ultraviolet. The laser irradiation causes appearance of small crystallites, leading to the widening of energy gap and the increasing of ultraviolet sensitivity. But with the rise of pulse number crystallites grow mainly, that drops coefficient of ultraviolet sensitivity.

Besides, the temperature dependences of photo- and ultraviolet sensitivity and as well as of resistance were measured.

The given films were used for fabrication of heterostructure converters. They consist of monocrystalline substrate of p- or n-type with deposited on it film of nc-Si:Y. These converters characterize the large rectifying. The heterostructure converters on the base of nc-Si:Y thin films demonstrate better sensitivity to radiation in visible and ultraviolet ranges of spectrum, than film converter. This result can be explained, obviously, widening of absorption spectrum in heterojunctions in comparison with films.

So, it was obtained the new photosensitivity material with controllable semiconductor properties and heterostructure converters on it base.

References:

[1] M.-B. Park, K.-H. Han, J.-H. Shim, C. Namgung, N.-H. Cho, Applied Surface Science, **234** (2004) 78.
[2] M. Losurdo, M. F. Cerqueira, E. Alves, M. V. Stepikhova, M. M. Giangregorio, G. Bruno, Physica E, **16** (2003) 414.
[3] M. D. Efremov, V. V. Bolotov, V. A. Volodyn, Fizika i Tekhnika Poluprovodnikov **36** (2002) 109.

LASER ACTION IN ELECTRICALLY DRIVEN QUANTUM DOT MATRIX

J. Krasnyj[2], A. Chuchmała[1], W. Jacak[1], M. Tytus[1], W. Donderowicz[1]

[1]Institute of Physics , Wrocław University of Technology, Wyb. Wyspiańskiego 27, 50-370 Wrocław, Poland, [2]Institute of Mathematics, University of Opole, Oleska 48, 45-051 Opole, Poland
e-mail: jacak@if.pwr.wroc.pl

The lasing system based on a matrix of quantum dots is proposed. The laser action is obtained by a rapid changes of in-plane electric field as a pumping force. Numerical analysis of a kinetics of electron-photon system is done for various electric fields and temperatures. For parabolic type of confinement in quantum dots a convenient amplification of contribution from several levels is indicated. Calculation utilizes exact solution of Cauchy problem for an infinite chain of linear differential equations with constant coefficients.

NANOCOMPOSITE Ta-,Ti-SiN THIN FILMS: SYNTHESIS, PROPERTIES, AND APPLICATIONS IN HIGH TEMPERATURE ELECTRONICS

A.V. Kuchuk, V.P. Kladko, and A. Piotrowska[1]
V. Lashkaryov Institute of Semiconductor Physics, National Academy of Sciences of Ukraine, Pr. Nauky 41, 03028 Kyiv, Ukraine
[1]Institute of Electron Technology, Al. Lotnikow 32/46, 02-668 Warsaw, Poland
E-mail: kuchuk@isp.kiev.ua

Studies of the thin films of the type transition metal (Ta, Ti, W, Mo)-silicon-nitrogen have both scientifically interesting and practically useful [1-3]. A major interest has an application in the areas of aerospace, automobile, high temperature/power electronics, micro-electro-mechanics etc. The exceptional combination of properties, like a high melting point, good chemical stability, high electric conductivity, excellent diffusion barrier performance and hardness, makes them a widely used. However, those properties depending on many factors: a) fabrication technologies; b) chemical composition; c) structure-property relationships; d) post-deposition treatment etc. Therefore, in this work, we have investigated the effect of deposition parameters and post-deposition heat treatment on the material properties, and performance of Ta(Ti)-Si-N diffusion barriers in Au-based metallization of GaAs or GaN.

Binary Ta-,Ti-Si and ternary Ta-,Ti-SiN thin films were prepared by reactive RF (13,56 MHz) magnetron sputtering of Ta_5Si_3 (P = 200 W) and Ti_5Si_3 (P = 450 W) targets, in a pure Ar and various Ar/N_2 gaseous mixture, respectively. To determine the properties of investigated films, structures of the type Ta-,Ti-SiN/GaAs(GaN) and with Au-overlayer was prepared. In order to characterize the thermal stability, the samples were annealed up to 1000^{o}C for 3-5 min. in Ar ambient. The chemical and phase composition, electrical resistivity, mechanical stress, microstructure, surface morphology as well as diffusion barrier performances have been investigated using four-point probe sheet resistance measurements, stress measurement optical system, X-ray diffraction (XRD), secondary ion mass spectrometry (SIMS), Rutherford backscattering spectrometry (RBS), transmission electron-, and atomic force- microscopy (TEM, AFM).

For reactive sputtering of Ta-,Ti-SiN thin films, increasing of N_2/Ar flow ratio from 0 to 10%, results in increases of the N concentration into the films, electrical resistivity and change of mechanical stress (Table) [4]. These effects may be explained by incorporation of reactive nitrogen into the film during the sputtering process, and change of films microstructure. Indeed, all Ta-,Ti-Si films in the as-deposited state, exhibit broad X-ray diffraction "halo" characteristic of an amorphous material [5]. With increasing nitrogen content into the films, the position of the diffraction peak shifts to low angles and peak with at half maximum increase, indicating a structural differences in the amorphous state of the films [5]. These results indicating a change of the shot-range order of the Ta, Ti and Si atoms, due to the N suppression the reaction between Ta, Ti and Si atoms, by passivating the Ta-,Ti-silicides grain boundary with N atoms. Increase of the "degree of amorphism", which agrees well with change of chemical composition and an increase of Ta-,Ti-SiN films resistivity, is result of silicon nitride SiN_x (nonconducting/amorphous) fraction rises into the films, and of transition metal nitride TaN_x or TiN_x (conducting/polycrystalline) decreases. Nanocomposite Ta-,Ti-SiN films may be viewed as a mixture of transition metal nitride imbedded in a silicon nitride amorphous matrix. This model explains the structure-property relationships and high temperature crystallization (1000^{o}C) of optimal Ta-,Ti-SiN thin-film diffusion barriers [6].

As shown in Fig. 1 and 2, the optimal amorphous Ta-,Ti-SiN diffusion barriers have excellent thermal stability (up to 800^{o}C) preventing the metallurgical interaction in $Au/Ti_{26}Si_{17}N_{57}/Au/Pd/GaN$ and $Au/Ta_{34}Si_{25}N_{41}/GaN$ contact structures.

This work was partially supported by the NATO, under the grant No. NUKR.RIG-981275.

References:

[1] M.-A. Nicolet, P.H. Giauque, Microelectronic Engineering, **55** (2001) 357.
[2] M.-A. Nicolet, Vacuum, **59** (2000) 716.
[3] H. Zeman, J. Musil, P. Zeman, J. Vac. Sci. Technol. A, **22** (2004) 646.
[4] A.V. Kuchuk, J. Ciosek, A. Piotrowska et al., Vacuum, **74** (2004) 195.
[5] A.V. Kuchuk, V.P. Kladko, V.F. Machulin et al., Metal Physics and Advanced Technologies, **27** (2005) 625.
[6] A.V. Kuchuk, E. Kaminska, A. Piotrowska et al., Thin Solid Films, **459** (2004) 292.

Figures:

Table. Chemical composition, electrical resistivity, mechanical stress and phase composition of reactively sputtered Ta-,Ti-SiN thin films, in dependences of nitrogen content in sputtering plasma

N_2/Ar %	Composition (at.%)		Resistivity (μΩcm)		Stress (GPa)		Structure (by XRD)
	Ta-Si-N	Ti-Si-N	Ta-SiN	Ti-SiN	TaSiN	TiSiN	
0	$Ta_{67}Si_{33}$	$Ti_{62}Si_{28}$	295	312	-1.0	-0.7	nanocrystalline
4	–	$Ti_{27}Si_{20}N_{53}$	–	1012	–	-1.3	amorphous
5	$Ta_{53}Si_{20}N_{27}$	–	359	–	-1.5	–	amorphous
8	$Ta_{40}Si_{24}N_{36}$	$Ti_{26}Si_{17}N_{57}$	416	7527	-1.1	-1.4	amorphous
10	$Ta_{34}Si_{25}N_{41}$	$Ti_{25}Si_{16}N_{59}$	810	26600	-1.1	-1.4	amorphous

Fig. 1. The 2 MeV He^+ RBS spectra from as-deposited and annealed up to 800°C (Ar/3min) contact structure p-GaN/Pd/Au/$Ti_{26}Si_{17}N_{57}$/Au.
Thickness of the films:
Pd - 20nm;
Au - 130nm;
$Ti_{26}Si_{17}N_{57}$ - 100nm;
Au-overlayer - 100nm.

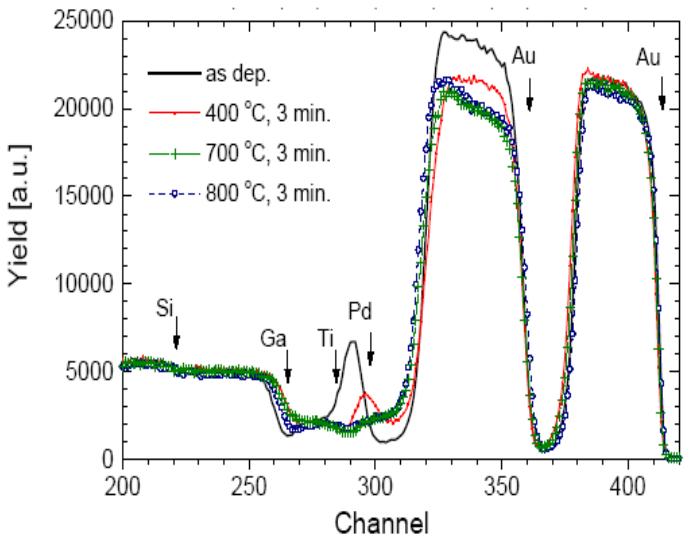
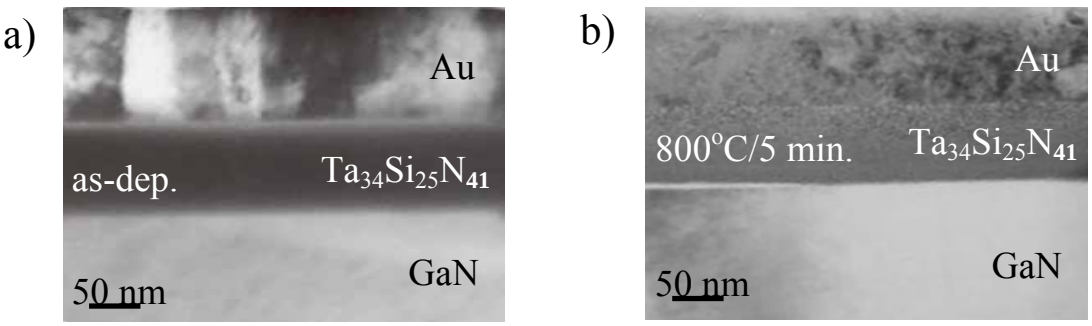


Fig. 2. Cross-sectional TEM micrographs of the GaAs/$Ta_{34}Si_{25}N_{41}$/Au samples: (a) as-deposited; (b) annealed at 800°C in Ar ambient for 5 min.



EVIDENCE OF STRONG C-H···O BONDS IN 2D ASSEMBLIES

Marc-Andre Laliberte, Stéphane Lavoie, Gautier Mahieu and Peter H. McBreen
Université Laval, G1K 7P4, Quebec (QC) Canada
chmmla@hermes.ulaval.ca

The necessity for continued miniaturization of devices underpins the study of atomic and molecular nanostructural engineering at surfaces. The approach of the present research is to understand and exploit intermolecular interactions for the formation of nanostructured assemblies on surfaces. The targeted assembly is a prochiral dimer on a Pt(111) surface. Metal surfaces are not intrinsically chiral. One approach to bestow chirality on surfaces is to add a chiral modifier[1]. Through subtle intermolecular interactions the modifier may guide substrate molecules towards face-specific reactions. This type of face-specific assembly is probably the most demanding form of 2D self-assembly.

The system presented in this poster shows H-bonded prochiral assemblies formed between aromatic chiral modifiers and carbonyl substrates on Pt(111)[2,3]. In particular, we isolate the intermolecular interactions between the coadsorbed aromatic and carbonyl functions[4,5]. Scanning tunneling microscopy (STM), reflectance FTIR (RAIRS) and thermal desorption studies show that chemisorption activates aromatics towards H-bond donation. Molecularly resolved STM images show that double H-bond donation occurs (Figure 1). That is, the carbonyl group of the substrate molecules docks between adjacent CH bonds of the aromatic. In this way 10:1 carbonyl-aromatic assemblies are formed. These nanostructures are stable under ultrahigh vacuum conditions at room temperature (Figure 2). The structures of the assemblies may be tuned through judicious substitution of the aromatic (Figure 3).

In summary a new type of strong (~2-4 kcal/mol) and strongly directional non-covalent interaction is demonstrated. This new interaction may be used in the design of 2D assemblies and in the design of new chiral catalysts.

References:

[1] Raval, R., CATTECH, **5** (2001**)** 12.

[2] Lavoie, S.; Laliberté, M.-A.; McBreen, P. H., J. Am. Chem. Soc., **125** (2003) 15756.

[3] Lavoie, S.; Laliberté, M.-A.; McBreen, P. H., Cat. Lett., **97** (2004) 111.

[4] Lavoie, S.; McBreen, P. H., J. Phys. Chem. B, **109** (2005) 11986.

[5] Lavoie, S.; Laliberté, M.-A.; Temprano, I.; McBreen, P. H., J. Am. Chem. Soc., **128** (2006) 7588.

Figures:

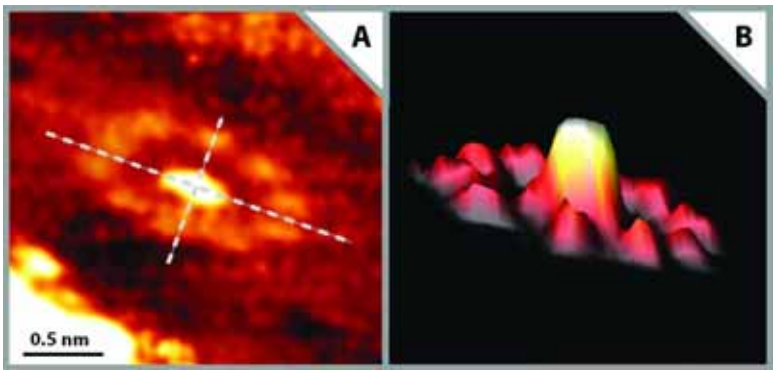


Figure 1

a) 10:1 carbonyl-aromatic assembly imaged by STM at low temperature (150 K), b) 3D representation

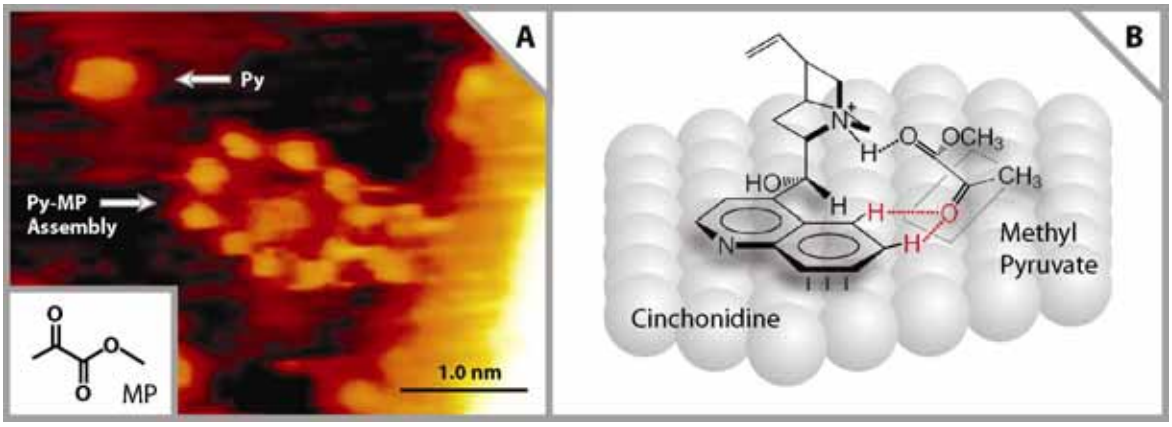


Figure 2

a) 10:1 carbonyl-aromatic assembly imaged by STM at room temperature, b) chiral assembly between a chiral modifier (cinchonidine) and a carbonyl compound (methyl pyruvate)

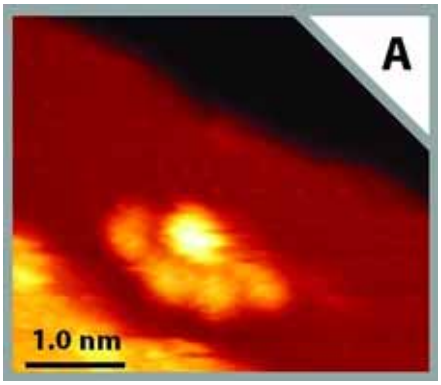


Figure 3

4:1 assembly with a substituted aromatic imaged by STM at low temperature

CHARACTERIZATION OF InAs QUANTUM WIRES ON (001) InP : TOWARD THE REALIZATION OF VCSEL STRUCTURES WITH A STABILIZED POLARISATION

J-M.Lamy, C. Levallois, A. Nakhar, P. Caroff, C. Paranthoen, O. Dehaese, A. Le Corre, A. Ramdane and S. Loualiche*
UMR C6082 FOTON - INSA de Rennes, 20 Avenue des Buttes de Coësmes, 35043 Rennes, France
**Laboratoire de Photonique et Nanostructures, CNRS UPR20, Route de Nozay, 91460 Marcoussis, France*
jean-michel.lamy@ens.insa-rennes.fr

Vertical cavity surface emitting lasers (VCSELs) operating at 1.55µm are of great interests in optical telecommunication applications. Their circular, spectral and spatial single mode laser beam is essential points for an efficient fiber coupling and high frequency modulation. Moreover, their low-cost production and the possibility to test each laser directly on the wafer represent great advantages for production applications. In contrast with edge emitting lasers, VCSEL present an important polarization instability [1], which may increase the bit error rate in data transmission. Different solutions have been proposed for controlling the polarization, from patterning the output mirror or by using a birefringent material on top of the mirror, which do complicate the device technology [2-4]. In this contribution, we propose to use a gain material presenting an important polarization anisotropy like quantum wires in order to fix the polarization of the emitting VCSEL.

InAs quantum wires (QWires) have been grown by molecular beam epitaxy (MBE). The optimization of the growth enables the achievement of uniformly sized nanostructures in a high density. QWires dimension have been estimated by atomic force microscopy to be 2.5 nm high, 50nm wide and 0.5-1 µm long (figure 1). Figure 2 is a photoluminescence spectrum of samples containing a single and several layers of optimized QWires. They present a photoluminescence (PL) peak centred at 1.48 µm, close to the 1.55 µm optical telecommunication wavelength. As QWires present a clear anisotropy in dimensions (length is ten times higher than the width), the optical emission is expected to be strongly polarized. Polarization PL experiments have been carried out on conventional quantum wells (QWs) structure and on optimized QWires (figure 3). QWires PL appears to be highly polarized in the [1-1 0] crystallographic direction (polarization factor (PF) as high as 50%), when QWs present a slight difference (PF lower than 10%). QWires efficiency has also been tested by processing wide stripe longitudinal cavity lasers. Excellent properties have been deduced, low infinite threshold current density (90 A/cm² per layer), low temperature wavelength dependence (0.35 nm/K at room temperature).

Apart from the gain region, the realization of VCSEL structures needs to have highly efficient mirrors. As InP based materials present poor performances in terms of reflectivity and thermal conductivity, dielectric materials have been used for the realization of both Bragg mirrors [5]. The dielectric materials used are amorphous silicon and amorphous silicon nitride deposited with a magnetron sputtering system. The active region is made up of lattice matched InGaAs/InGaAsP QWs (or InAs QWires) on (001) InP. The epitaxial layer thickness has been carefully optimised using simulations in order to increase the absorption of the optical pump excitation and to place the QWs (Qwires) to the maximum stationary field. The lower Bragg mirror of 6 periods is deposited directly on the active region. An Au-In eutectic bonding is employed to transfer the sample on a silicon substrate. The InP substrate is removing by mechanical polishing and chemical etching. The process ends by a fine tuning of the cavity, and the deposition of the upper Bragg mirror.

YAG laser optical excitation is used. CW laser emission has been demonstrated when QWs are used for the gain region. The CW lasing operation up to 35°C has been obtained at 1.578µm. The figure 4 shows the lasing spectra at room temperature with a maximum output power of 380µW and a threshold power of about 40kW.cm^{-2}. Like shows in the figure 3, this QWs VCSEL structure presents a randomly oriented and unstable polarisation on the whole samples. When QWires are used for the gain region, very last result do not present yet laser emission, but the VCSEL spontaneous emission is clearly polarized as previously observed with PL.
Those last results are very promising for the realization of a polarization control laser emitting VCSEL for telecommunication applications.

References:

[1] J. Martin-Regalado, F. Prati, M. San Miguel, and N. B. Abraham, IEEE J. Quantum Electron., **33** (1997) 765.

[2] T. Yoshikawa, H. Kosaka, M. Kajita, K. Kurihara, Y. Sugimoto and K. Kasahara, Electron. Lett,. **31** (1995) 1573.

[3] Y.L. Okuno, J. Geske, K.G. Gan, Y.J. Chiu, S.P. DenBaars and J.E. Bowers, Appl. Phys. Lett,. **82** (2003) 2377.

[4] T. Mukaihara, N. Ohnoki, Y. Hayashi, N. Hatori, F. Koyama, IEEE J. Sel. Topics Quantum Electron,. **1** (1995) 667.

[5] C. Levallois, A. Le Corre, S. Loualiche, O. Dehaese, H. Folliot, C. Paranthoen, F. Thoumyre, and C. Labbe, J. Appl. Phys., **98** (2005) 043107.

Figures:

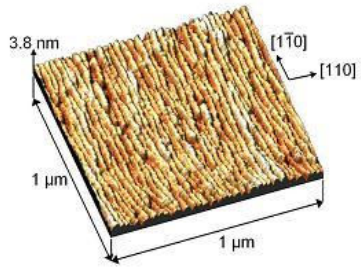


Figure 1 *Atomic force microscopy of InAs QWires on (001) InP*

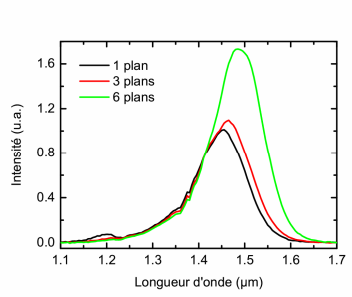


Figure 2 *PL at 1.48µm for different number of InAs QWires layers*

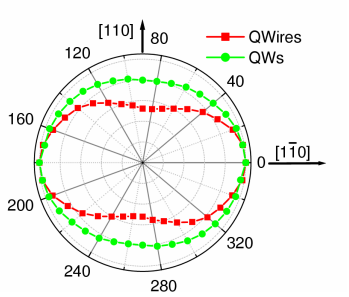


Figure 3 *PL polarised of QWs and QWires*

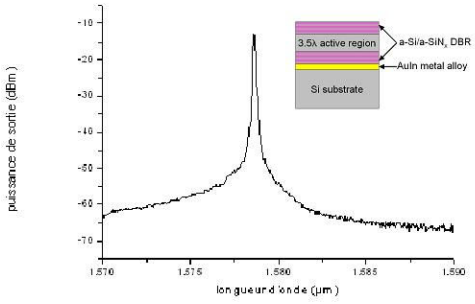


Figure 4 *VCSEL structure reported on silicon and CW laser emissionat RT of a VCSEL with an active region made of QWs.*

UNCONVENTIONNAL MAGNECONDUCTANCE OSCILLATIONS IN QUASI-BALLISTIC MWCNTs.

B. Lassagne, S. Nanot, B. Raquet, J-M. Broto.
Laboratoire National des Champs Magnetiques Pulsés ,Toulouse, France.

R. Avriller, S. Roche.
Commisariat à l'énergie atomique , DRFMC, Grenoble, France.

Lassagne@lncmp.org

Carbon nanotubes (CNT) are unique mesoscopic systems to probe quasi-1D behaviour of electrons. Moreover, thanks to their cylindrical geometry, they are ideal to explore magnetic field induced quantum oscillations like Aharonov Bohm (AB) and Al'tshuler, Aronov, Spivak effects in the weak localization regime (AAS). In CNT, AB effect appears in parallel configuration (B parallel to the tube axis). It has been shown [1] that the additional magnetic electronic wave phase modifies the available states in reciprocal space. As a consequence, the CNT is predicted to oscillate between the metallic and semi-conducting states with a quantum flux period Φ_0. AAS effects in a tubular geometry exhibit conduction oscillations with a $\Phi_0/2$ period and a decrease of their magnitude due to the field induced coherence length reduction.
We investigate quantum transport in carbon nanotubes by combining high magnetic pulsed field (up to 60T), necessary to induce a quantum of flux in a small cylinder (52T for a diameter of 10nm), with an electrostatic gate tuning of the Fermi energy to control the conduction regime [2, 3].
We will present magnetonconductance (MC) results obtained on arc discharged MWCNTs. Three diameters are investigated. First, a 10nm diameter tube in a quasi ballistic regime exhibits giant gate dependent MC oscillations at 120K with a 50 T period which matches with the AB period of the outer shell. This is the first experimental evidence of the field induced gap modulation in the ballistic regime and at high temperatures. However, assuming that transport only takes place in the outershell nanotube in presence of an homogeneous Anderson disorder and an effective coupling to the gate fails to explain conductance spectra as a function of magnetic flux, suggesting open questions concerning the role of electrostatics and intershell coupling in MWCNTs in a quasi ballistic transport regime.
The two other MWCNTS we probed with larger diameters exhibit, in the parallel configuration, MC oscillations superimposed to a monotonous positive MC, still present at room temperature. The perpendicular configuration reveals a large positive MC (50% at 35T) with no hint of saturation. Interpretations relying on a complex interplay between weak localisation effects and field induced DoS modifications are not straightforward. Results will be discussed in the frame of the existing theories.

References:

[1] *"Aharonov-Bohm spectral features and coherence lengths in carbon nanotubes"*
S.Roche, G. Dresselhaus, M.S. Dresselhaus, R. Saito, Phys. Rev. B, **62**, 16092, (2000)
[2] *"Gate-Dependent Magnetoresistance Phenomena in Carbon Nanotubes"*
G. Fedorov, B. Lassagne, M. Sagnes, B. Raquet, J.-M. Broto, F. Triozon, S. Roche, E. Flahaut, Phys. Rev. Lett. **94**, 66801, (2005).
[3] *"Energy dependent transport length scales in strongly diffusive carbon nanotubes"*
B. Lassagne, B. Raquet, JM. Broto, J. Gonzalez,.J. Phys. Cond. Mat. **18**, 1-7, (2006).

Poster

COLLOIDAL GOLD NANOPARTICLES PRODUCTION BY LASER ABLATION IN LIQUIDS

S.C.Laza[1], F.Giammanco[1], P.Marsili[1], E.Giorgetti[2], A.Giusti[2]
[1]Physics Department, University of Pisa, Largo Bruno Pontecorvo n3, 56127 Pisa-Italy
[2] Istituto dei Sistemi Complessi ISC-CNR, Via Madonna del Piano n10, 50019 Sesto Fiorentino, Firenze-Italy
simona.laza@df.unipi.it

The colloidal metallic nanoparticles are of great interest due to their plasmon resonances [1,2], which make them suitable for a large range of applications specially in the production of nanostructured materials with tailor made properties to be used in the field of medicine[6], energy technology (fuel cells and solar cells), in information technology (new memories and processors) and in environmental technology (materials cycles and disposal).

The production of nanomaterials by physical methods, in the last decade, started to represent an alternative to the chemical ones, which could be inconvenient for certain applications owing to the contamination of the resulted nanomaterials. Another important advantage of the physical metods is the possibility of a better control over the growth environment.

We present the production of gold colloidal nanoparticles by pulsed laser ablation [3] using the fundamental (1064nm) and the second harmonic (532nm) of an Nd-YAG laser with 25ps pulse length, 10Hz repetition rate and a maximal energy of 100mJ/pulse, in water, Figure 2 and 3, aqueous solution of pamam dendrimer, Figure 1, and aqueous solution of sodium dodecyl sulfate [4].

For the characterisation of the produced colloidal nanoparticles we employ the on-line monitoring of the transmited and scattered light, the off-line TEM analysis and absorption spectra. The use of LIBD is a future project for the determination of the colloidal nanoparticles size distribution and number density [5].

Our aim is to succeed in controlling the size of the nanoparticles and their size distribution and in estimating their number concentration in the colloidal solution.

References:

[1] W.Ekardt *Phys. Rev. B* Vol.**31**, No.10 (1985) 6360-6370

[2] S.Link, Mostafa A.El-Sayed *J. Phys. Chem.B* **103** (1999) 8410-8426

[3] J.-P. Sylvestre, A.V. Kabashin, E. Sacher, M. Meunier *Appl. Phys. A* **80**, (2005) 753-758

[4] F.Mafuné, J.Kohno, Y.Takeda, T.Kondow, H.Sawabe *J. Phys. Chem. B* **105** (2001) 5114-5120

[5] T.Bundschuh, R.Knopp, R.Winzenbacher, Jae II Kim, R.Köster *Acta hydrochim. Hydrobiol*. **29** (2001) 1, 7-15

[6] Jing Yang Ye, L.Balogh, T.B.Norris A*ppl. Phys. Lett.* Vol.**80**, No.10 (2002) 1713-1715

Figures:

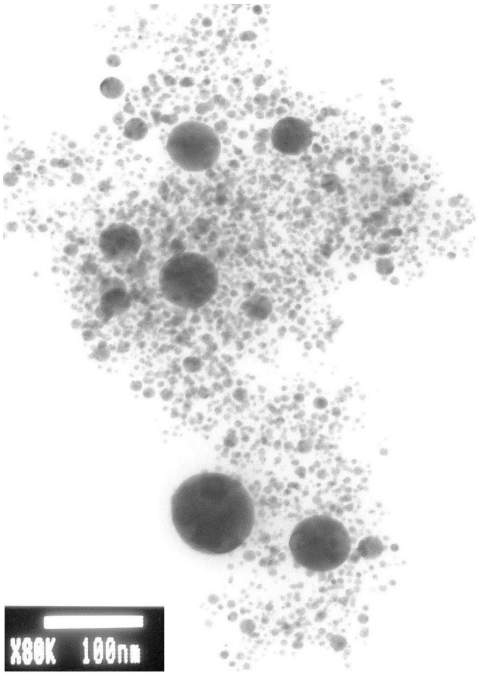


Fig.1. TEM image of gold nanoparticles in dendrimer aqueous solution.

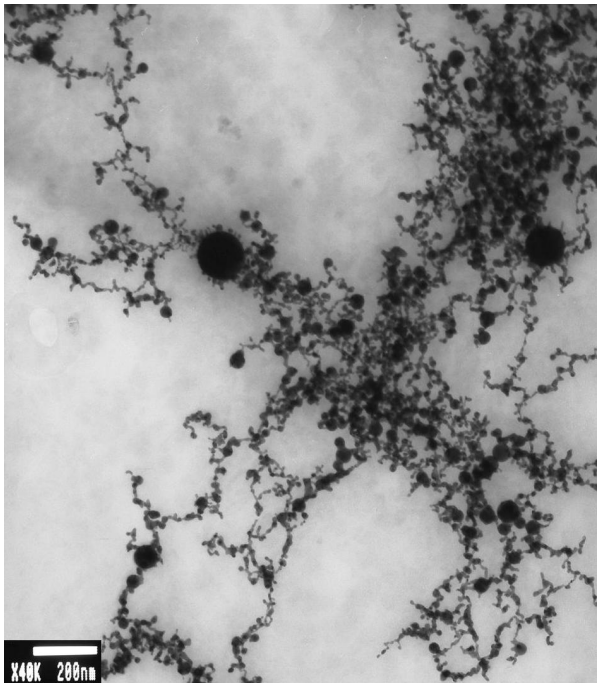


Fig.2. TEM image of gold nanoparticles in water after 24 hours.

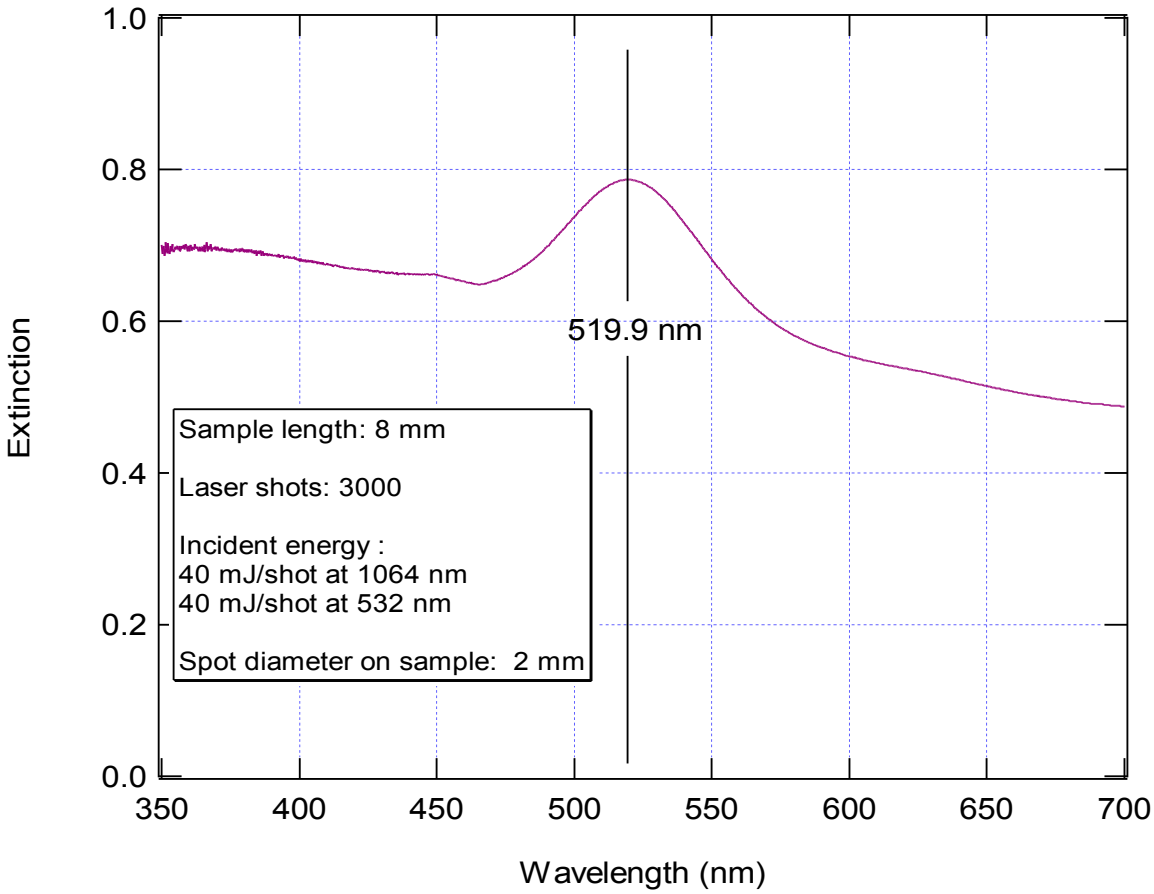


Fig.3. Extinction spectra of colloidal solution of gold nanoparticles in water.

Electronic structure and vertical transport in GaN/AlN/GaN single-barrier structures

S. Leconte, E. Sarigiannidou, and E. Monroy
Equipe mixte CEA-CNRS-UJF Nanophysique et Semiconducteurs, DRFMC/SP2M/PSC,
CEA-Grenoble, 17 rue des Martyrs, 38054 Grenoble cedex 9, France
sleconte@cea.fr

III-nitride semiconductors have experienced an astonishing evolution in the last decade, leading to the commercialization of nitride-based devices like UV-blue-green light emitters, UV photodetectors and high electron mobility transistors. The combination of the outstanding electronic, optoelectronic and piezoelectric properties of these materials renders them suitable for a broad variety of applications and provides unexplored tools for the device designer. For instance, nitride semiconductors, with their large conduction-band offset −about 1.8 eV for GaN/AlN−, are promising candidates to develop intersubband (ISB) devices operating in the near-infrared, and resonant tunneling diodes with high values of peak-to-valley ratio.

First reports of unipolar devices based on vertical electron transport (resonant tunneling diodes and quantum well infrared photodetectors) are controversial because of the scarcity and irreproducibility of the published data [1]. Current instabilities are admitted, and their assignation to resonant tunneling or trapping is under debate. Furthermore, the current densities and peak-to-valley ratios do not correspond to the values predicted by standard tunneling models. These anomalies are due to two critical factors in III-nitride technology:

- The presence of a strong internal electric field in heterostructures grown along the (0001) axis, due to the high piezoelectric constants of III-nitride materials and the difference in spontaneous polarization, which can lead to the presence of two-dimensional electron gases (2DEG) at the heterointerfaces when dimensions are reduced to the nanometer scale.
- The high density of dislocations in these materials, still in the 10^8 cm^{-2} range in high-quality substrates.

Understanding the contribution of these two factors to the vertical electron transport in III-nitride heterostructures is a priority in order to address the design of quantum devices, such as resonant tunneling diodes, quantum well infrared photodetectors or quantum cascade lasers.

In this work, we investigate the vertical electron transport through GaN/AlN/GaN single-barrier structures with different AlN barrier thickness, grown by plasma-assisted molecular-beam epitaxy. The barrier thickness was varied from 2 monolayers (ML) to 20 ML (0.5 nm to 5 nm). High-resolution and energy-filtered TEM measurements demonstrate that the GaN/AlN interfaces are chemically abrupt with a roughness of <1 ML [2]. The results of electrical characterization are interpreted by comparison with simulations of the electronic structure using a self-consistent Schrödinger-Poisson equation solver.

Capacitive measurements indicate that the internal electric field induces a partial or complete depletion of the GaN cap layer −depending on the layer thickness−, and the formation of a two-dimensional electron gas (2DEG) at the bottom interface of the AlN barrier, even for a barrier thickness as small as 0.5 nm (2 ML of AlN) [3]. This band distortion is further confirmed by low temperature photoluminescence, where the recombination from the 2DEG to the top of the valence band in the upper GaN/AlN interface was clearly identified. Conductive atomic force microscopy images of these samples display a density of leakage current spots in the 10^7 cm^{-2} range, i.e. a third of the dislocation density in these layers, which reveals that not all the dislocations contribute to the leakage current, which is significantly lower than the dislocation density (~5×10^8 cm^{-2}). For a barrier thickness of 5 nm, we observe a degradation of the electrical performance with presence of trap-induced phenomena and an enhancement of the leakage current, which is attributed to the relaxation of the AlN layer. These results are promising for the fabrication of nano-scale resonant tunneling diodes.

References:

[1] A. Kikushi et al., Appl. Phys. Lett., **81**, (2002) 1729. C. T. Foxon et al., phys. stat. sol. (c), **0**, (2003) 2389. M. Hermann et al., phys. stat. sol.(c), **1**, (2004) 2210. S. Golka et al., Appl. Phys. Lett., **88**, (2006) 172106.

[2] E. Sarigiannidou, E. Monroy, N. Gogneau, G. Radtke, P. Bayle-Guillemaud, E. Bellet-Amalric, B. Daudin, and J. L. Rouvière, Semicond. Sci. Technol., **21**, (2006) 912.

[3] S. Leconte, F. Guillot, E. Sarigiannidou, and E. Monroy, submitted to Appl. Phys. Lett.

Figures:

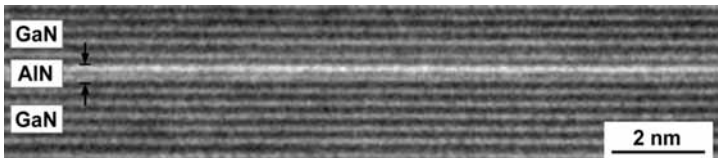


Fig. 1 : HRTEM image of a 0.5 nm barrier of AlN in GaN showing (0002) lattice fringes. The growth axis is directed upwards.

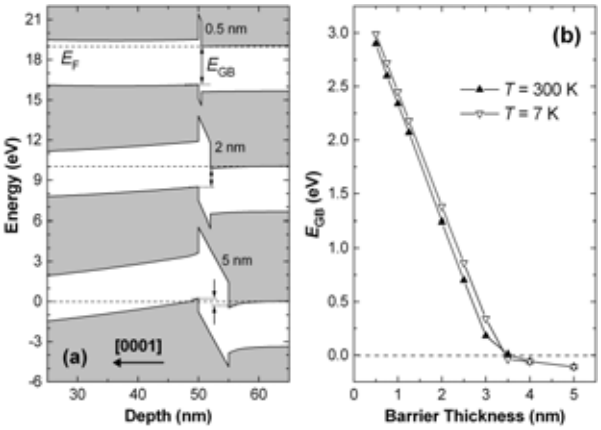


Fig. 2 : (a) Band diagram of single barrier structures with different AlN barrier thickness. The arrows indicate the energy band gap through the barrier, E_{GB}. (b) Evolution of E_{GB} with the barrier thickness, calculated at a temperature T = 7 K and T = 300 K.

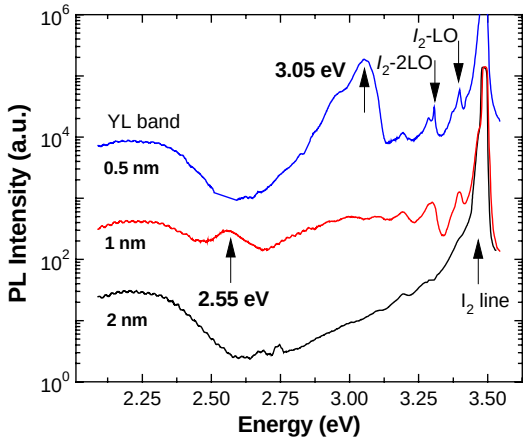


Fig. 3 : Low temperature (T = 10 K) photoluminescence spectra of GaN/AlN/GaN single barrier structures with different barrier width located 50 nm deep in the GaN matrix. The spectra are vertically shifted for clarity.

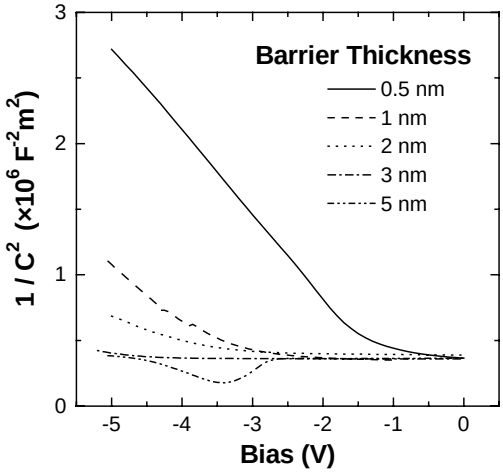


Fig. 4 : 1/C^2-V measurements of Ø = 400 µm mesas in samples with a GaN cap of 50 nm and an AlN barrier thickness from 0.5 nm to 5 nm.

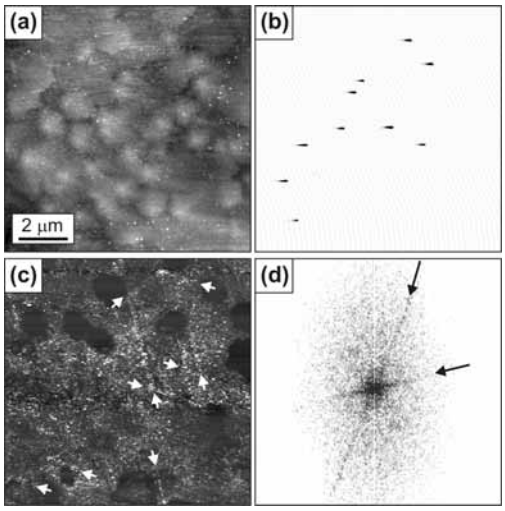


Fig. 5 : (a) AFM topographic image of the GaN(50 nm)/AlN(5 nm)/GaN structure. (b) C-AFM image under +4 V bias. (c) C-AFM image under -3 V bias. (d) 2D FFT of image (c) showing preferential orientations with a 6-fold symmetry.

NEW APPROACH OF THERMAL IMPRINT TECHNOLOGY FOR THE PRINTED CIRCUIT BOARD INDUSTRY

Choonkeun Lee, Sangmoon Lee, Jung-Woo Lee, Seunghyun Ra
Samsung Electro-Mechanics, 314, Maetan 3-Dong, Suwon, Gyeonggi-Do, S. Korea
ck1107.lee@samsung.comT

Recently, high performance microelectronic devices are designed in multi-layer structure in order to make dense wiring of metal conductors in compact size. This leads to a constant need to develop more highly integrated printed circuit board (PCB). So, there have been numerous studies by many chemists and engineers in patterning processes [1]-[3]. Imprint technology have received significant attention due to an alternative technology for photolithography on such devices.

In this study, vacuum hydrolic pressure type imprinting system is used for the delivery of uniform pressing force. As the mostly well known thermo-set polymer composite, epoxy resins reinforced with silica (SiO_2) fillers were imprinted with polymer stamp. The feature size of the stamp is 9.5/10.5 μm of line/space and 17 μm in line height, 60μm of via pad, 30μm of via and 45μm of via height. Polymer stamp and epoxy resin sheet were loaded and vacuumed in chamber. The temperature and pressure profiles of the imprinting process as a function of time are shown in Figure 1.

As shown in Figure 2, in order to understand imprinting mechanism of the epoxy resins, the rheological behaviors such as viscosity changes at elevated temperature and time of the epoxy resins were observed using rheometer (ARES, TA, USA). All of imprinted patterns such as line, space, depth and via were measured using SEM (S3000N, Hitachi, Japan) and confocal microscope (NT1100D, Veeco, USA).

SEM micrographs of the polymer stamps and the micro patterned epoxy sheets imprinted are given in Figure 3. According to the SEM micrographs, via and line patterns of the stamp were perfectly transferred to epoxy resin sheet.

After curing, copper electroplating is used for metallization on the imprinted patterns. To remove excess copper layer mechanical and chemical methods is used (Figure 4). As shown in Figure 5, all of copper line and via patterns were successfully realized in the thermo-set matrix for PCB.

Therefore, compared to conventional patterning methods, thermal imprinting method is good candidate for micro patterning on PCB industry.

References:

[1] S.Y. Chou, P.R.Krauss and P.J. Renstrom, Applied. Phys. Lett. 67 (1995) 3114-3116.
[2] Clivia M. Sotomayor Torres: Alternative lithography unleashing the potentials nanotechnology, Kluwer Academic Publishers; 1st ed. (2003) 70.
[3] K. Y. Suh, Y. S. Kim, and H. H. Lee, Adv. Mater. 13 (2001) 1386.

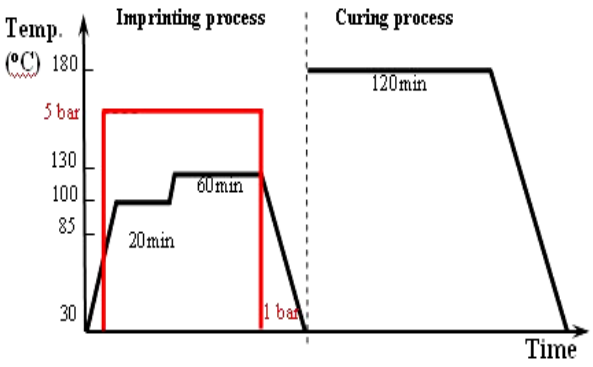


Figure 1: Trace of imprinting temperature and pressure as a function of time.

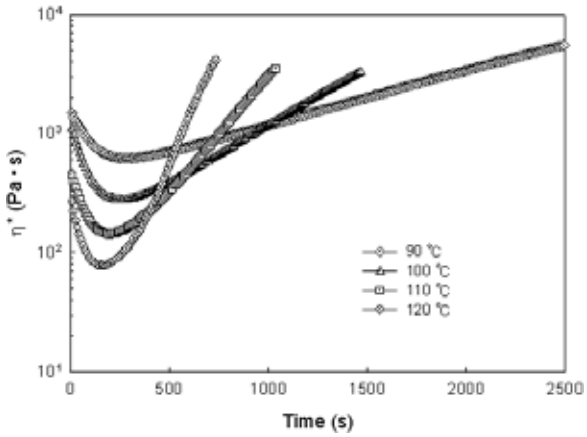


Figure 2: Viscosity changes of epoxy resin at various temperatures

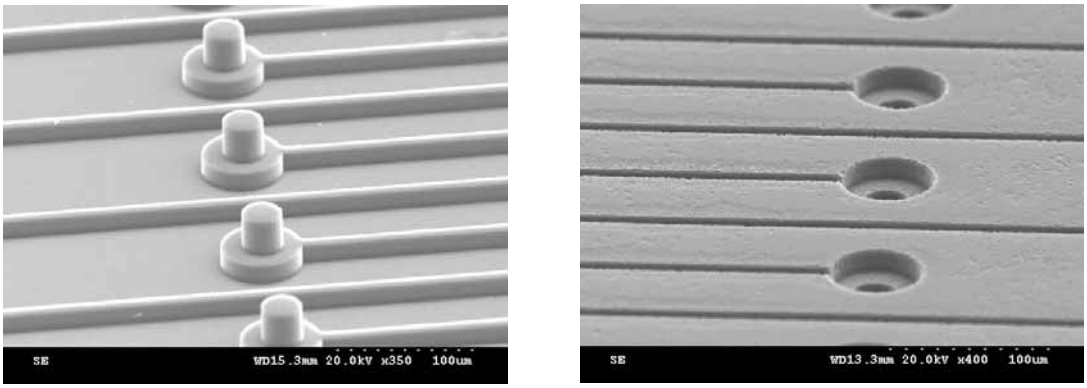


Figure 3: SEM images of the polymer stamp and imprinted epoxy patterns

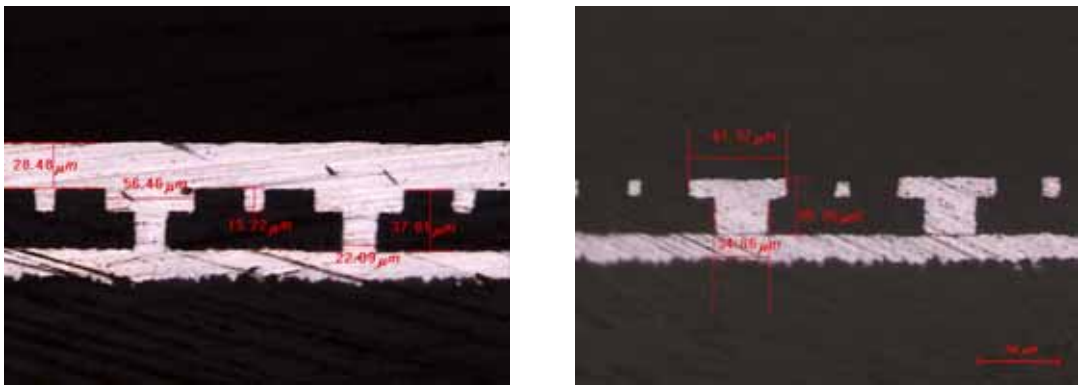


Figure 4: Cross-sectional optical micrograph of imprinted patterns after copper plating and planarization.

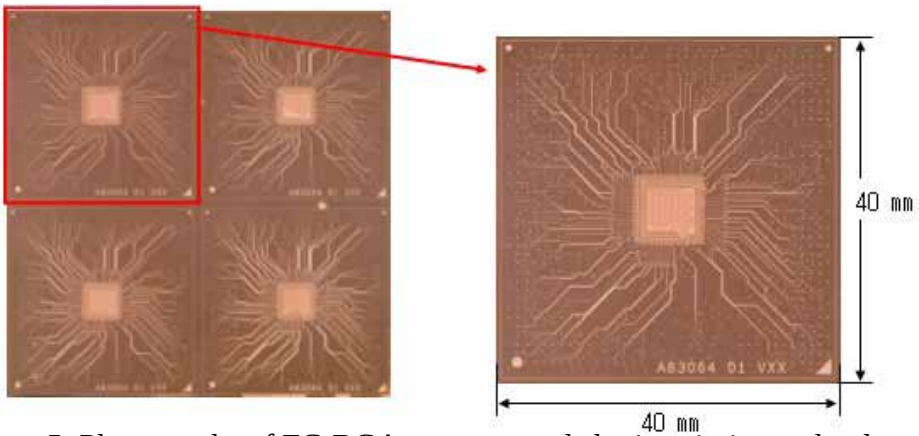


Figure 5: Photographs of FC-BGA patterns made by imprinting technology.

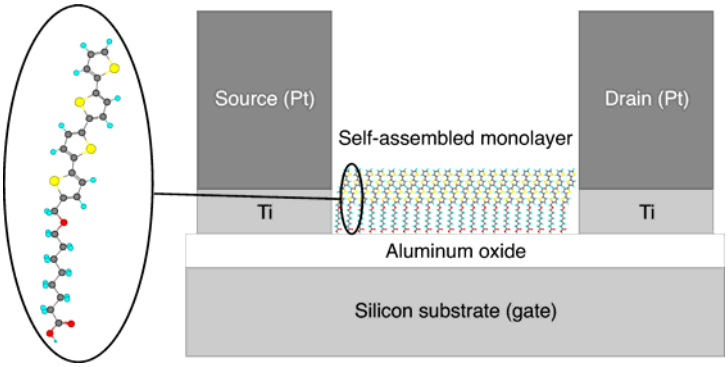
ORGANIC TRANSISTORS BASED ON SELF ASSEMBLED MONOLAYERS

S. Lenfant[2], M. Mottaghi[1], P. Lang[1], F. Rodriguez[1], A. Rumyantseva1[1], A. Yassar
G. Horowitz[1], D. Tondelier[2], D. Vuillaume[2]
[1] ITODYS, CNRS-UMR 7086, University Denis-Diderot
1 rue Guy de la Brosse, 75005 Paris, France
[2] IEMN, CNRS-UMR 8520,
Avenue Poincaré, 59652 Villeneuve d'Ascq, France

stephane.lenfant@iemn.univ-lille1.fr

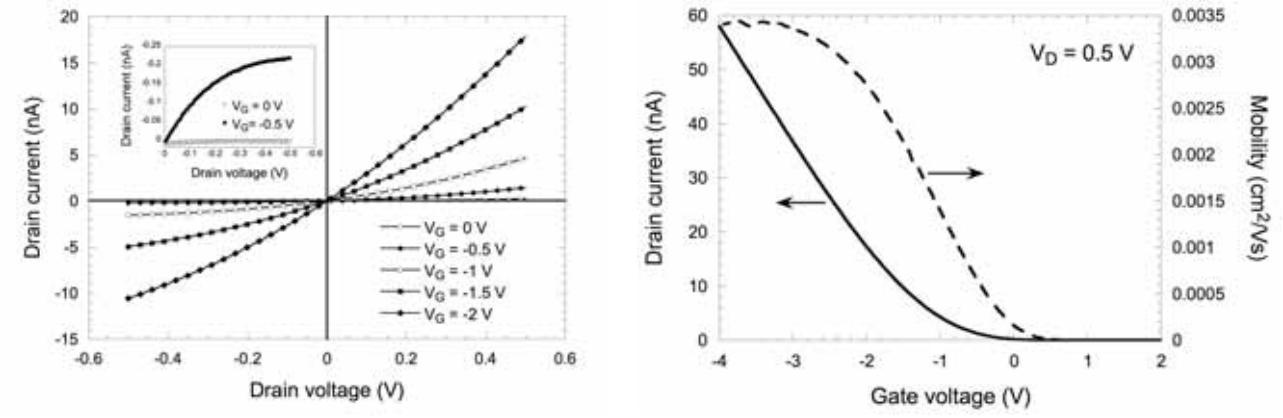
The tendencies in organic thin film transistor (OTFT) are the reduction of size of the device, for the lateral dimension (source- drain distance) but also for the thicknesses of the semiconductor and the insulator. This reduction opens the way to devices operating at low bias [1].

To reduce the thickness of the organic semiconductor, we use organic self assembled monolayer (SAM) grafted on the gate insulator (100nm alumina or 10nm silicon dioxide). The molecules used for the SAM formation are formed by an alkyl part (8 or 10 carbon atoms) linked to a moiety rich in π electrons (terthiophene or quarterthiophene). The molecules react with gate insulator by a -$SiCl_3$ moiety for the silicon dioxide, or a -COOH moiety for the alumina. Source drain electrodes (either top or bottom contact configuration) were patterned by e-beam lithography, with channel length ranging comprise between 16 and 1000nm, and a width to length ratio of 100. The scheme of the device (bottom configuration) is presented below.



The structure of the SAMs was characterized by atomic force microscopy (AFM), infrared spectroscopy, ellipsometry, contact angle to validate the synthesis. Some electrostatic force microscopy (EFM) measurements were done to analyze the distribution and concentration of injected charges in the SAM.

For the electrical characterization in most cases, ill-defined I-V curves were recorded, which we attribute to a poor electrical contact between platinum and the oligothiophene moiety. Most of the devices did not give any signal (*i.e.* current less than 8pA corresponding to a very low leakage current through the insulator).
However, a few devices offered well-defined curves (see figures below) with a clear saturation, thus allowing us to estimate a mobility of 0.0035 cm2/Vs for quaterthiophene and $8x10^{-4}$ cm^2/Vs for terthiophene. In the first case, the on-off ratio reaches 1800 at a gate voltage of -2 V.



The field effect behavior was only obtained with negative bias, thus indicating that only injection of holes could be achieved. The non-linearity of the current voltage curves and absence of saturation are attributed to the poor quality of the contacts.
Interestingly, the device operates at room temperature and very low bias, which may open the way to applications where low consumption is required.

References:

[1] G. S. Tulevski, Q. Miao, M. Fukuto, R. Abram, B. Ocko, R. Pindak, M. L. Steigerwald, C. R. Kagan, C. Nuckolls, J. Am. Chem. Soc. **126** (2004), 5048.
[2] Mohammad Mottaghi, Philippe Lang, Fernand Rodriguez, Anna Rumyantseva, Abderrahim Yassar, Gilles Horowitz, Stéphane Lenfant, Denis Tondelier, Dominique Vuillaume, Adv. Funct. Mater. (2006) *Accepted*.

TOWARDS CMOS COMPATIBLE: INTEGRATION OF IN-SITU GROWN INDIVIDUAL VERTICAL CARBON NANOTUBES INTO FIELD EMISSION DEVICES.

H. Le Poche, J. Dijon, P. Nicolas, Y. Gobil and P. Pantigny
CEA Grenoble / LITEN-LETI, 17 av. des Martyrs 38054 Cedex 9, GRENOBLE, FRANCE
helene.lepoche@cea.fr

Because of their high aspect ratio, carbon nanotubes (CNTs) are recognized as ideal candidate materials for field emission (FE) applications [1]. The aim of this work was to harness the in-situ growth of individual and vertical CNTs into submicron gated FE devices (**figure 1**) and demonstrate the feasibility of an electron source manufactured on 200mm silicon wafers. This technology will pave the way to maskless lithography; massively parallel electron beams could be generated by an array of CNT electron sources individually driven by embedded CMOS electronics. The main challenges ahead were the development of a CNT growth process compatible with the following requirements: self aligned single CNT gated electron sources, highly selective growth process to avoid parasitic electrical short-circuits and low thermal budget.

A state of the art review of CNT in-situ growth techniques reveals that they do not comply with all these requirements. Contrary to thermal Chemical Vapor Deposition (CVD), Plasma Enhanced CVD (PECVD) is adopted by most of the authors as the growth process enabling vertical orientation of individual CNT, with a suitable reactor configuration, due to field alignment [2,3,4]. Moreover, PECVD appears as the most promising technique for growth at low temperatures. However, vertical alignment of the CNTs is most commonly achieved by direct current (DC) PECVD techniques [2,3], which is known for creating CMOS circuit breakdown by plasma induced arc discharge phenomena. At last, standard PECVD requires a delicate tuning of gas composition to limit the intrinsic formation of a non catalytic carbon layer that may short the device metal layers.

In this respect, an innovative “CMOS friendly” radio-frequency PECVD growth process using a solid carbon source (CS RF-PECVD) was developed during this study [5]. As Tseng et al. [4], an alternative RF plasma source was preferred to overcome the DC drawbacks. Moreover, in order to limit the carbon supply and thus create a very selective growth process with no detrimental parasitic carbon layer, the graphite RF polarized sample holder was used as the unique carbon source, without any additional hydrocarbon feedstock gas. The process was developed on unpatterned Si wafers, with a 3 nm Ni thin film catalyst, deposited on a 60 nm TiN barrier layer. At 560°C, under a pure H_2 atmosphere, the catalyst film is first reduced and splits into nano-droplets by a sintering treatment; then a RF plasma glow discharge is ignited and a forest of vertical carbon tubular structures grows from the catalyst droplets. SEM (**figure 2**) and TEM characterizations evidenced tip growth mode of vertically field aligned carbon nanofibers, as commonly observed with standard PECVD processes. A statistical study enabled us to correlate the height of the tubes to their diameters, directly related to the dimensions of the Ni seed droplets. Furthermore, the low CNTs growth rate achieved (a few $nm.min^{-1}$) allows a very tight control of the height of the tubular structures, which is a key asset for CNT device integration.

In order to integrate ‘CS RF PECVD’ grown individual CNTs into the gated FE devices, the first issue arose from the localization of a less than 100nm diameter Ni dot into each electrons source cavities (**figure 1**). That was readily achieved without e-beam lithography, by means of a lift-off technique commonly used in FE flat panel display, but a lot of work was required to find out a lift-off layer stripping process, that let the Ni nano-dot compatible with the growth of only a single nanotube. In addition, some parameters of the growth process, such as the plasma power and the growth time had to be adjusted to demonstrate the growth of individual CNTs into their cavities with a good reproducibility **(figure 3)**.

Electrical **(figure 4)** and optical characterizations carried out on the individually addressable CNT electron sources pointed out promising results: driving voltage compatible with high voltage CMOS circuits and good angular emission. The key role of the interface between the CNT and the cathode electrode on the electrical contact was evidenced by the test of samples, where the interlayer dielectric was etched by either a dry process or a wet process prior to Ni catalyst deposition. Indeed, no stable measurements or CNT burn out were exhibited on wet etched devices, whereas stable emission characteristics were displayed with a good yield on dry etched devices.

Acknowledgments: This work was supported by the Micro and Nanotechnology Program from French Ministry of research under the grant Basic Technology Research, « maskless nanolithography ».

[1] J. Dijon et al., J. Soc. Information Display, **12** (2004): 373
[2] L. Gangloff, E. Minoux et al., Nano Lett., **4** (2004): 1575
[3] M.A. Guillorn, X. Yang et al., J. Vac. Sci. Technol. B, **22** (2004): 35
[4] S.C. Tseng, C.H. Li et al., Diamond Relat. Mater., **14** (2005): 2064
[5] J. Dijon, H. Le Poche, T. Goislard de Monsabert, French patent, FRA0407529 (2004)

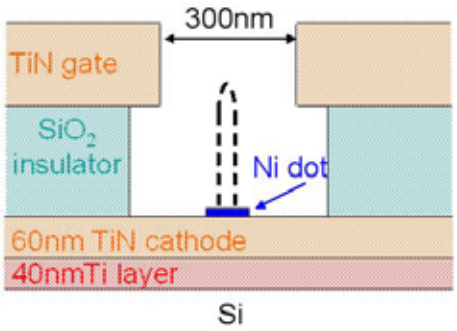


Figure 1: Cross section schematic of the gated FE submicron cavity with a single vertical CNT used as electrons emitter.

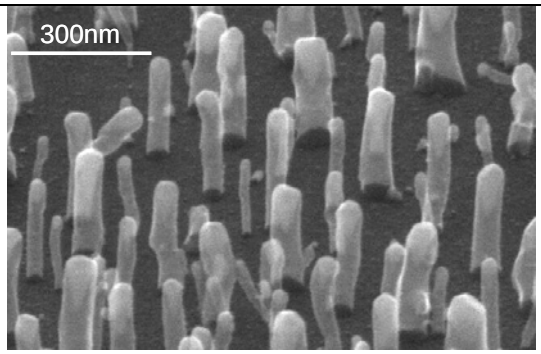


Figure 2: SEM characterization of vertically aligned carbon nanofibers obtained on unpatterned substrate after a 1h growth process under 300W H_2 plasma at 560°C (45° tilted sample).

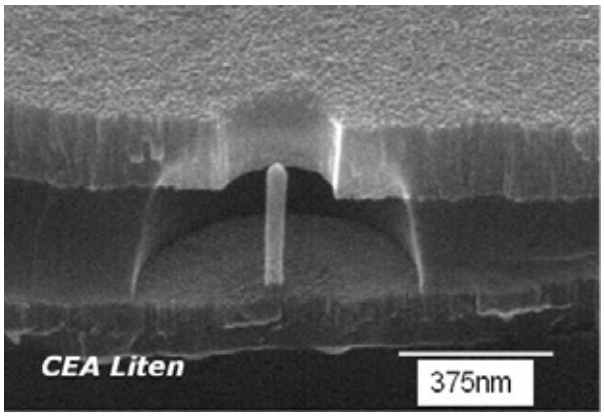


Figure 3: SEM image of a single free standing 45nm diameter CNT in-situ grown in a FE gated cavity by 'CS RF PECVD' growth process (45° tilted sample).

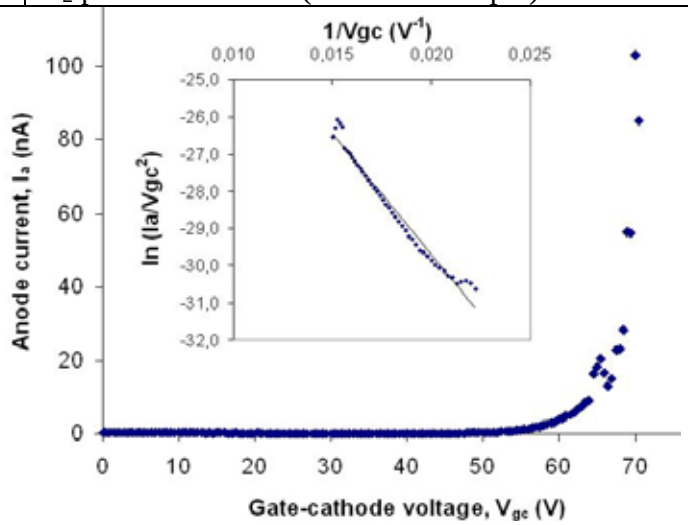


Figure 4: FE measurements obtained from an individual CNT grown in a gated cavity, where the SiO_2 insulator was dry etched. Collected current on the anode (1kV, 3mm distant from the cathode) versus gate-cathode voltage and Fowler-Nordheim plot (inset).

ULTRAFINE-GRAINED AND NANO–STRUCTURE ALUMINIUM ALLOYS PRODUCED BY CYCLIC EXTRUSION COMPRESSION

Beata Leszczyńska, Maria Richert
AGH University of Science & Technology, Faculty of Non-Ferrous Metals, Krakow, Poland
bleszcz@uci.agh.edu.pl

Aluminium alloys are very popular materials using for production of ultrafine-grained and nano-materials produced by Severe Plastic Deformation (SPD) methods [1,2]. They characterize relatively low hardening which allow exerting very large strains necessary for transformation of common structure into the nanostructure. Till now in aluminium alloys, only sometimes it was possible to obtain mean grain size below 100 nm and it also depended to the using SPD method. Good results were obtained in High Pressure Torsion (HTP) deformation [1] (Fig.1A). A lot of results connecting with the production of ultrafine-grained materials and near nanocrystalline materials come from Equal Channel Angular Pressing (ECAP) investigations (Fig.1B). Cyclic Extrusion Compression (CEC) method belongs to the SPD processes that allow obtained arbitrarily large deformations with the preservation of the initial shape of the sample. The method was invented in 1979 (Fig.1C) [3]. The high hydrostatic stresses exerted during the CEC process prevent the sample cracking.

Three aluminium alloys were deformed by CEC do the true strain $\varphi = 16$. The investigations show that only in AlMgSi alloy after the $\varphi = 16$ the nanostructure appears in about 70% of sample volume. In other alloys the ultrafine-grained structure with the mean grain size 125nm (AlCu4Zr) and 157 nm (AlMg) has bee found. Fig.2 shows the examples of the structures observed in the deformed aluminium alloys. The misorientation between the nanograins and surrounds is shown by figures. The large misorientation proofs, that the observed nanovolumes have features of grains. The microtexture is shown in the left upper corner of Fig.2A. The results indicate that the obtained grain size depends not only on the value of the exerted strain but also on the kind of the deformed material.

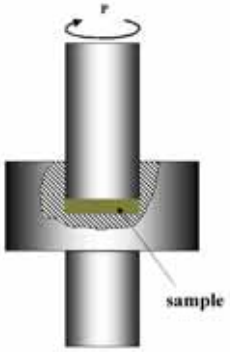
The Hall Petch relation was determined for the investigated alloys (Fig.3). It was found that the inclination of the diagrams depends on the kind of the alloy. It is characteristic that the slope of the AlMgSi diagram to the axis is largest than the other alloys. On the other hand the AlMgSi alloys as only contains 75% of the nanostructure. It could be suggested that the additional mechanism of deformation appears in this alloy [4]. However on the other hand it is also possible that the material softening appears due to the more intensified progress in the recovery processes.

The obtained results indicate that using the CEC method, the nanocrystalline materials with the mean size dimension of nanograins below 100 nm can be produced.

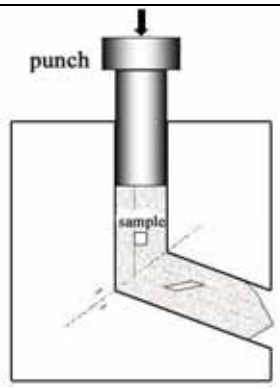
References:

[1] R.Z.Valiev, R.K.Islamgaliev, I.V.Alexandrov, Progres in Mat.Sci**. 45** (2000) 103-189.
[2] M.Richert, Archives of Materials Science, **26, 4** (2005) 235-261.
[3] J.Richert, M.Richert; Aluminium, **62, 8**, (1986) 604-607.
[4] K.S.Kumar, H.Van Swygenhoven, S.Suresh, Acta Materialia, **51, 19** (2003) 5743-5774.

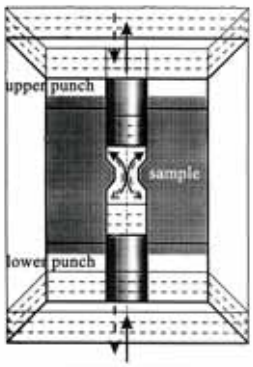
Figures:



A) High Pressure Torsion

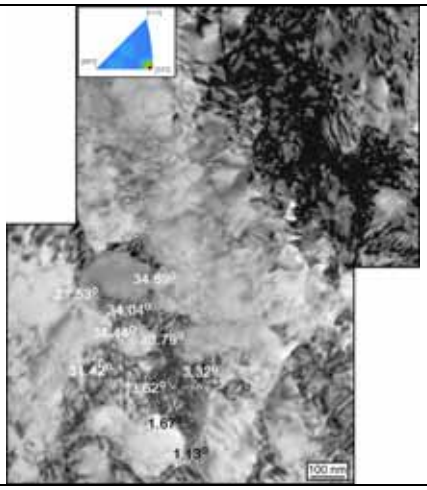


A) Equal Channel Angular Pressing

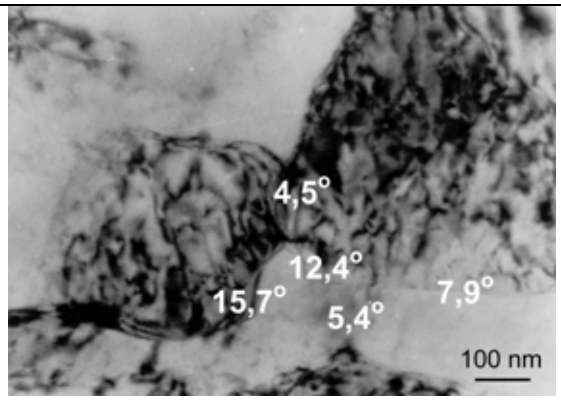


C) Cyclic Extrusion Compression

Fig.1. Scheme of different SPD methods



A) nanograins in AlMgSi after the φ = 16



B) nanograins in AlCu4Zr after φ = 14

Fig.2. Nanograins with the large misorientation in aluminium alloys

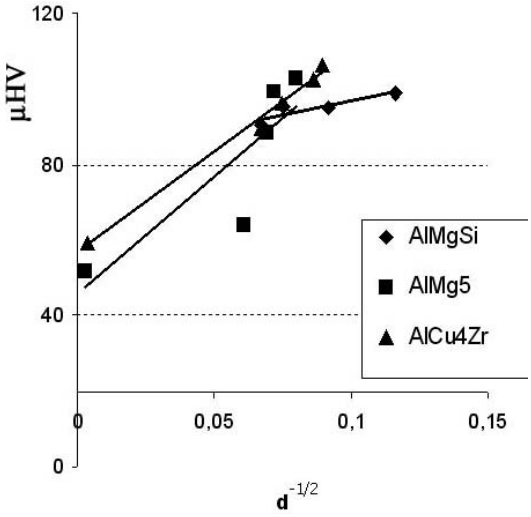


Fig.3. Hall-Petch relation of the aluminium alloys deformed by the CEC

Full-band Self-Consistent Monte Carlo Methodology for Strain Induced Effects Study in Nano-MOSFETs

Erping Li[1], Kai-fu Chang[1], Ping Bai[1], Chee Ching Chong[1], and Ganesh S Samudra[2]
[1]Institute of High Performance Computing, Singapore
[2]National University of Singapore, Singapore
eplee@ihpc.a-star.edu.sg

Scaling the conventional MOSFET to a nanoscale regime leads to explore many new materials and novel device structures. Among these approaches, the use of strained-Si as a choice of material for the FET channel is an attractive option to improve the performance of the device and has drawn great attention in recent years [1]. We present a full-band self-consistent Monte Carlo methodology for the analysis of strained Si MOSFET and its impact on the electronic transport properties. In proposed method, the strain distribution in the channel of MOSFET is simulated with TCAD simulations and tuned by experiment measurements. Numerical band structures of strained Si associate with the strain distribution are calculated and tabulated as inputs to a full band self-consistent Monte Carlo device simulator to calculate the performance of the strained Si MOSFET.

Biaxial tensile strain is introduced in Si <100> and <010> direction (in-plane) and the lattice constant in the <001> direction is computed using the elasticity theory. The strain-altered band structures of silicon are calculated using the first principle method density functional theory (DFT) with spin-polarized generalized gradient approximation (SGGA) [2]. Figure 1 and 2 shows the calculated band structures and density of states (DOS) of strained Si and unstrained Si. It is observed: (a) four (in-plane) of the six conduction band valleys are shifted upwards in energy and, (b) the heavy hole band moves away from the valence-band edge and hence break the degeneracy between the heavy and light hole bands. The lift-up of conduction bands would result in reduced intervalley or interband scattering. Together with the break-up of degeneracy between heavy and light holes, it could result in having the charge transport properties determined by the small transverse electron mass and the light hole mass mainly, and hence provide a performance boost [3]. The DOS plot shown in Fig. 2 also shows a slight upward shifting in the conduction band at the high-energy tail, which also indicates the reduced interband scattering as implied by the lift-up of conduction bands.

A two-dimensional Monte Carlo device simulator with numerical band structures, self-consistently calculated scattering rates, and quantum corrections is developed based on MOCA [4] to get the distribution function from the solution of the Boltzmann transport equation (BTE). Acoustic and optical phonon scattering rates are calculated from the full-band structures. Impact ionization, ionized impurity scattering and surface roughness scattering are also modeled. The full-band calculations also allow for consideration of strain-induced degeneracy breaking and the associated variations in scattering rates.

A strained-Si-on-insulator n-MOSFET with 25 nm gate length is built based on the scaled version device in [5] and simulated with the proposed method. Figure 3 shows the drain current-voltage characteristics for strained Si compared to unstrained Si. The drain current is significantly enhanced in strained Si. The effects of various source/drain dopant concentrations are shown in Fig. 4 & 5. It is observed that dopant concentration at 10^{20} cm^{-3} offers the largest electron velocity due to excess carriers available for injection into the channel. Reduction of the source/drain doping by one order of magnitude leads to a large decrease in drain current is observed. The preliminary calculation results agree with published data and proposed method will be further verified with experiments which are on going.

References

[1] M.L. Lee et al, "Strained Si, SiGe, and Ge channels for high-mobility metal-oxide-semiconductor field-effect transistors", *J. Appl. Phys.*, vol 97, pp. 011101-1-27, 2005.
[2] M. Brandbyge, et al, "Density functional method for nonequilibrium electron transport", *Phys. Rev. B,* 65, 165401 (2002).
[3] F. M. Bufler, *Full-Band Monte Carlo Simulation of Nanoscale Strained-Silicon MOSFETs*, Hartung-Gorre Verlag Konstanz, 2003.
[4] A. Duncan, et al, "Full-band Monte Carlo investigation of hot carrier trends in the scaling of metal-oxide-semiconductor field-effect transistors," *IEEE Trans. Electron Devices*, vol. 45, pp. 867–876, 1998.
[5] K. Rim et al, "Fabrication and mobility characteristics of ultra-thin strained Si directly on insulator (SSDOI) MOSFETs", *IEDM Technical Digest*, pp. 49-52, 2003.

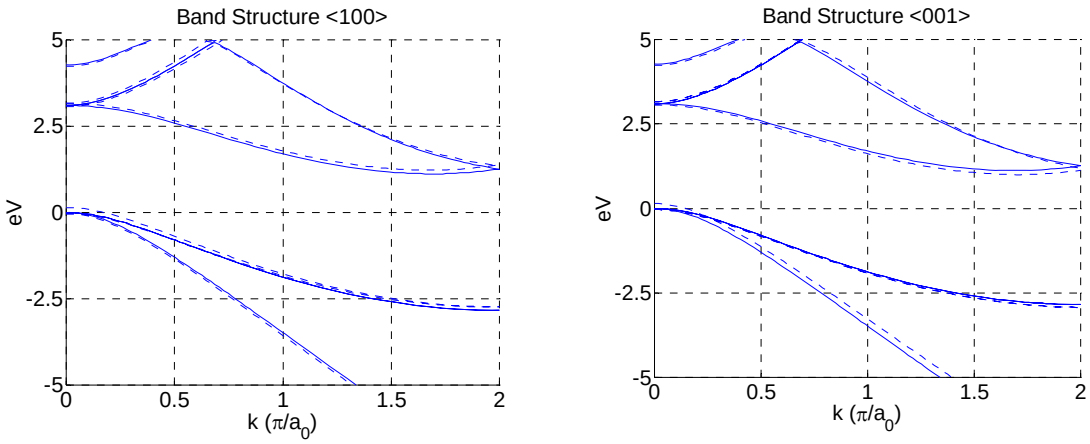


Fig. 1 Bandstructure (Γ-X) for (a) in-plane direction ; (b) the <001> direction. The solid line is for the unstrained silicon, while the dotted line represents the strained silicon.

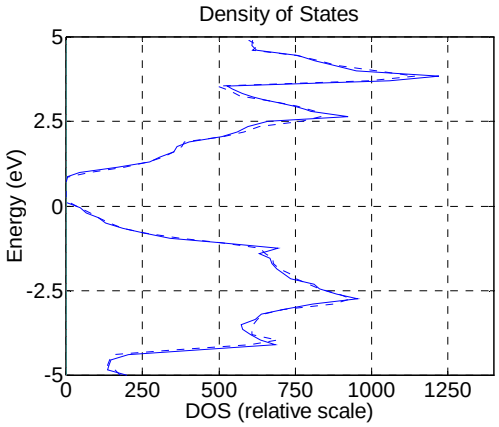


Fig. 2 The Density of States. The solid line is for the unstrained silicon, while the dotted line represents the strained silicon.

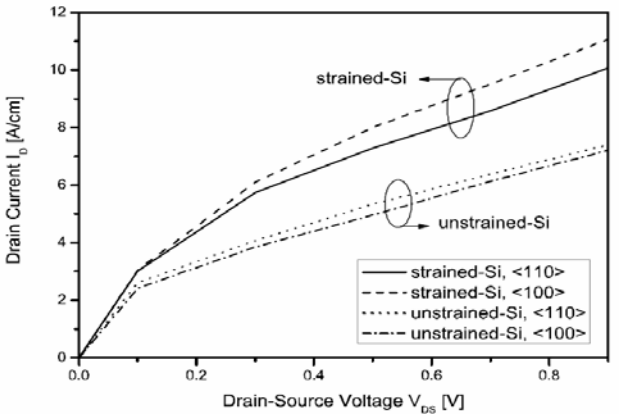


Fig. 3 Drain current-voltage characteristics for strained Si with <110> and <100> channel orientations in comparison to unstrained-Si.

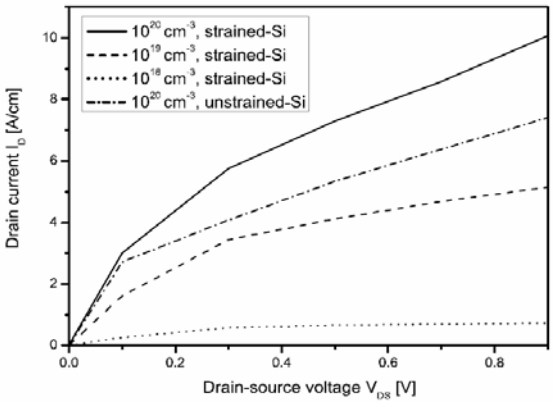


Fig. 4 Drain current-voltage characteristics for doping concentrations of 10^{20}, 10^{19}, and 10^{18} cm^{-3}.

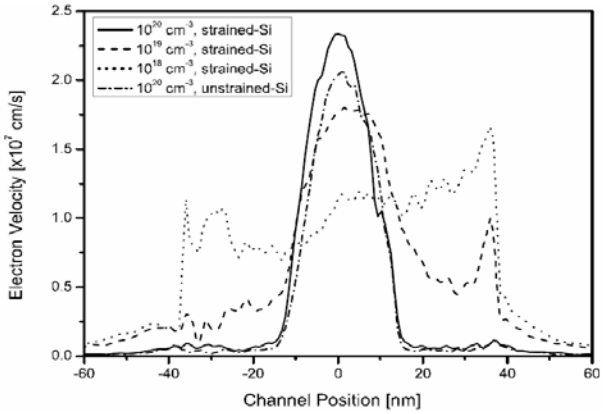


Fig. 5 Electron velocity profiles along the channel for doping concentrations of 10^{20}, 10^{19}, and 10^{18} cm^{-3}.

FORMATION OF Ni-Cu-Ag TERMINATION USING METALLO-ORGANIC DECOMPOSITION (MOD) TECHNOLOGY AT LOW-TEMPERATURES

Hong-Ching Lin[a#], *Pang Lin*[a]
[a]*Department of Materials Science and Engineering, National Chiao Tung University, 1001 Ta Hsueh Road, Hsinchu, Taiwan 300, Repubic of China.*
linsc@itri.org.tw

Chun-An Lu[b], *Ying-Chang Hung* [b], *Tzeng Ya-Chung*[b]
[b]*Materials Research Laboratories, Industrial Technology Research Institute, Bldg. 77, 195 Section 4, Chung Hsing Road, Chutung, Hsinchu, Taiwan 310, Repubic of China.*

Sea-Fue Wang[c,]
[c]*Department of Materials and Mineral Resources Engineering, National Taipei University of Technology, 1, Sec. 3, Chung-Hsiao E. Rd., Taipei, Taiwan 106, Repubic of China.*

Ni metal electrode was widely used as internal electrode for BME MLCCs. The terminations of the BME MLCCs can be formed by coating a Cu layer and subsequently a Ag layer. The purpose of the Cu layer is to enhance the adhesion between the internal Ni electrode and the external Ag termination, by forming the Ni-Cu alloy at high temperatures (800-900°C). However, the high temperature process generally develops internal stress, which leads to the formation of inner cracks and physical defects. In this research, the Ni-Cu-Ag alloy was formed using a low temperature process from the paste containing nano-size Ni metal powders, metallo-organic decomposition (MOD) agent of copper 2-ethylhexanoate, and silver oxalate. During the heat treatment at 300°C, a large quantity of heat released from the thermal decomposition of silver oxalate, which causes the thermal decomposition of copper 2-ethylhexanoate and the melting of Ni nano-powders, and subsequently results in the formation of Ni-Cu-Ag alloy. The thermal decomposition and crystallization behavior of the MOD composite were investigated in this study. Microstructure of Cu-Ni-Ag alloy was characterized using TEM, TEM-EDX, and XRD analysis. Thermal behaviors of the pastes were obtained by DTA and TGA analysis. The TEM diffraction pattern indicates an extra diffraction point and EDX analysis shows the existence of Cu, Ag, and Ni elements in the same grain. The (111) peak in the XRD patterns shifts slightly after thermal decomposition of MOD-Cu and $Ag_2C_2O_4$ at 300°C.

References:

[1] Hansen M., Constitution of binary alloys., New York, McGraw Hill., 1958.
[2] C.J. Shih, S.J. Shih, H.C. Lin, H.H. Yeh and Y.C. Hung., Nanotechnology, 14(2003), 1014-1018.
[3] J. Feng, C.P. Zhang., J. Colloid. Interface. Sci, 293(2006), 414-420.

Figures:

[1] (a) TEM morphology of Ni-Cu-Ag Alloy after the decomposition of MOD-Cu and $Ag_2C_2O_4$, and (b) the corresponding TEM diffraction pattern (extra diffraction point for arrow indicated).

[2] (111) peaks of the XRD pattern obtained from (a) pure Ni powder, (b) Ni powder with MOD-Cu agent addition after heat treatment at 300 in N_2, (c) Ni powder with the additions of MOD-Cu agent and $Ag_2C_2O_4$ after heat treatment at 300 in N_2.

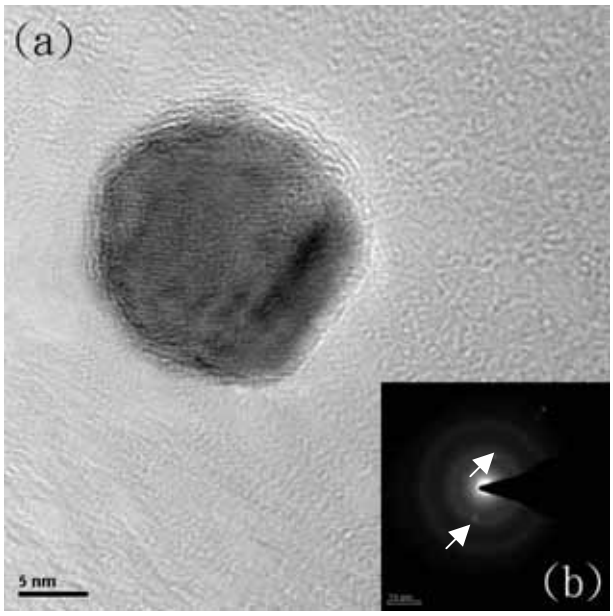


Figure 1

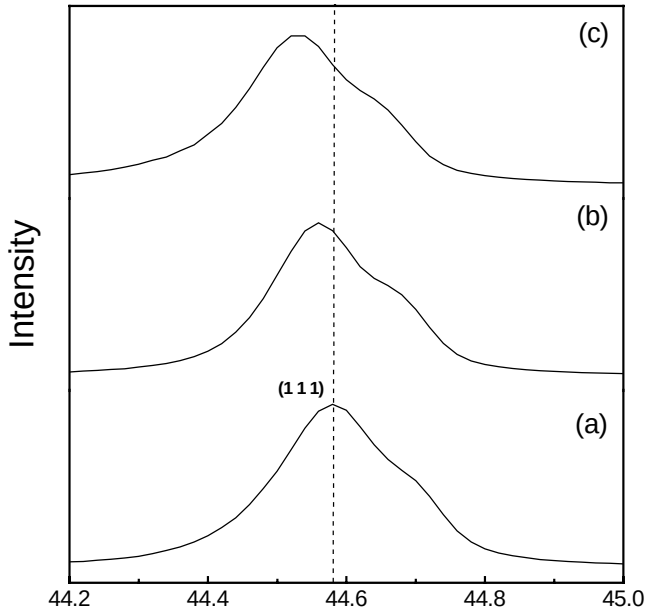


Figure 2

THE EFFECTS OF SILVER OXALATE AND NANO SILVER POWDER ADDITIONS ON THE PERFORMANCES OF THE METALLO-ORGANIC DECOMPOSITION SILVER PASTE

Hong-Ching Lin[a#], *Pang Lin*[a]

[a]*Department of Materials Science and Engineering, National Chiao Tung University, 1001 Ta Hsueh Road, Hsinchu, Taiwan 300, Repubic of China.*

linsc@itri.org.tw

Chun-An Lu[b], *Ying-Chang Hung* [b], *Tzeng Ya-Chung*[b]

[b]*Materials Research Laboratories, Industrial Technology Research Institute, Bldg. 77, 195 Section 4, Chung Hsing Road, Chutung, Hsinchu, Taiwan 310, Repubic of China.*

Sea-Fue Wang[c,]

[c]*Department of Materials and Mineral Resources Engineering, National Taipei University of Technology, 1, Sec. 3, Chung-Hsiao E. Rd., Taipei, Taiwan 106, Repubic of China.*

In the literature, it was known that the additions of metallo-organic decomposition (MOD) agents in the silver pastes would result in the low curing temperatures and the low electrical resistivities of the films, which is beneficial for use in the flexible electronics applications. In this study, silver oxalate and silver nano-particle were added in the MOD silver pastes. Silver oxalate, which is a transparent crystal, was prepared by mixing the silver salts and the soluble oxalates in the aqueous solution. As the temperature reaches the decomposition of silver oxalate, the decomposition of the silver oxalate in the paste releases a large amount of heat, which induces the chain decomposition reaction of the MOD agent and the melting of silver nano-particles. This lowers the curing temperature of the MOD silver paste and enhances the electrical connectivity and packing density of the silver particles. The phenomena is evidenced by the DTA and TGA analysis. The electrical properties of the films were measured using four-point probe method at the curing temperature of 180°C. The results indicate that electrical resistivities of < 20μΩ-cm were obtained.

References:

[1] C.J. Shih, S.J. Shih, H.C. Lin, H.H. Yeh and Y.C. Hung., Nanotechnology, 14(2003), 1014-1018.

[2] V.V. Boldyrev., Thermochimica acta, 388(2002), 63-90.

[3] K. F. Teng and R. W. Vest., IEEE, Trans. Components, Hybrid, and Manufacturing., V CHMT-12(4)(1987), 545-549.

[4] A.L. Dearden, P.J. Smith, D.Y. Shin, N. Reis, B. Derby, P. O'Brien., Macromol. Rapid. Commun., 26(2005), 315-318.

Figures:

[1] The diagram of low temperature silver paste composes for MOD agent and low temperature induced agent addition.

[2] The figure of DTA analysis was shown the different exothermic peak for silver oxalate ($Ag_2C_2O_4$) and silver 2-ethylhexanoate ($C_8H_{15}O_2Ag$).

[3] The figure of resistively was indicated the different additions in low temperature curing silver paste.

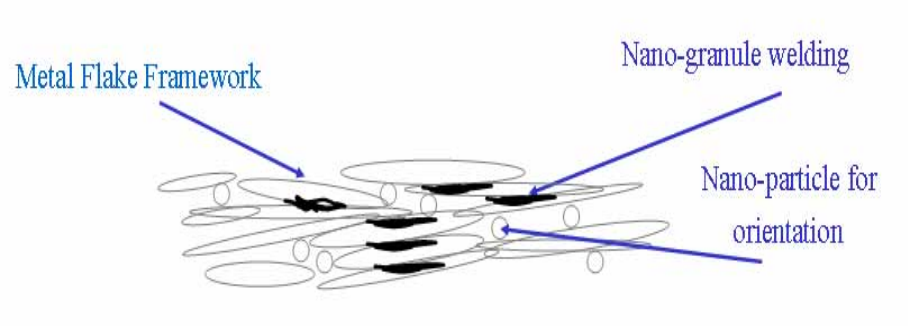


Figure 1

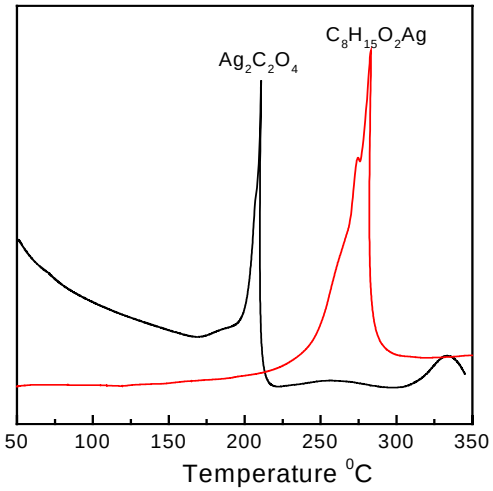


Figure 2.

Table 1

Conditions	Curing Temperature ( ) Dwell time: 10min	Resistivity (μΩ-cm)
Pure Flake Silver Paste	150	709.7
	200	15.8
Added Silver 2-ethylhexanoate	150	437.1
	200	12.1
Added Silver Oxalate	150	135.5
	200	47.1
Added Silver 2-ethylhexanoate and Silver Oxalate	150	25.7
	200	14.2

Size dependent energy level positions of InAs quantum dots determined by selective excitation photoluminescence

H. S. Ling [a)] **, S. D. Lin, S. Y. Wang, M. C. Luo, C. P. Lee**
Department of Electronic Engineering, National Chiao Tung University,
1001 Ta Hsueh Road, Hsinchu 300, Taiwan
a) karshe.ee92g@nctu.edu.tw, Tel: 886-3-5712121-54248, Fax: 886-3-5733722

Abstract:

Self-assembled quantum dots (QDs) grown on lattice mismatched material systems using Stransky-Krastanov growth mode has been widely studied in recent years. Because of the randomness of the island growth, the QDs usually exhibit a wide size distribution. In conventional photoluminescence (PL) measurement, where the excitation energy is larger than the bandgap energy of the matrix material, the emission spectrum from the QDs usually reveals a broad Gaussian shape with a FWHM around 50 meV as a result of this size fluctuation. However, if we lower the energy of the pumping photons to the range where only the QDs can absorb, i.e., an energy lower than the absorption edge of the wetting layer, we enter the resonant excitation regime [1]. Because of the property of δ-function like density of states, only certain size QDs with transition energies identical to the excitation energy can be resonantly excited. In this work, the selective excitation technique was used to probe QD samples. ***Despite the wide size distribution, we were able to obtain detailed information pertaining to individual dots. The size dependent hole level positions can be accurately deduced.***

The single InAs QD layer used in this study were grown by molecular beam epitaxy on (001) semi-insulating GaAs substrates in a Varian GEN Ⅱ reactor. The selective excitation PL spectra of the QDs were obtained with a Ti-sapphire laser pumped by an Argon ion laser. The AFM image shows that the density of the QDs is about $1x10^{11}$ cm^{-2} and the diameter is around 8 nm. The PL peak can be fitted perfectly by a Gaussian function, suggesting natural size distribution of QDs with one predominant size. With a sufficient pumping power, the peak position of this Gaussian-like PL spectrum, measured at 1.269eV, represents the transition energy of the QDs with the highest population density. Such high transition energy, due to the ultra-small size of the dots, tells us there is only one electron bound state in the QDs [2]. The selective excitation PL spectra with three different excitation energies are shown in Fig. 1. When the excitation energy E_{ex} is higher than the wetting layer energy (1.43eV determined from the PLE measurement), there is only one broad peak, the same as conventional PL. However, when E_{ex} is lower than the wetting layer energy, the PL reveals two major peaks, which correspond to the ground state transitions of two QD subgroups with different sizes [3].

The reason for the appearance of the two emission peaks when the excitation energy is low can be explained using the size dependent QD band diagram shown in Fig. 2. If there is a continuous size distribution, the energy levels of the electrons in the conduction band and the hole levels in the valence band are continuously varied. Since there is only one electron level in the conduction band, we use it as a reference. The various hole levels are shown as sloped lines. As the QDs are radiated by a pumping source, only the dots with transition energies identical to the excitation energy are excited. For example, when E_{ex} is 1.3778eV, there are two groups of QDs can be resonant-excited: one (smaller dots) with C-2Hh excitation and the other (larger dots) with C-3Hh excitation. Once the electron-hole pairs are generated in the dots, the emission, however, is all from C-1Hh ground state transition. Because the two groups have different sizes, two emission peaks are observed. When the excitation energy is changed, different dot groups with different sizes can be selectively excited. So we can basically scan the whole population of the QDs and obtain the spectral information of individual QDs. Since we know the ground state transition energy of the dots with the highest population, it is convenient to use this energy as a reference to obtain the hole energy level information for this group of dots (let's call them group A). As shown in Fig.2, photons with two excitation energies can resonantly excite group A dots. One with an excitation energy of 1.3778eV and the other with an energy of 1.3464eV. The 1.3778eV photons excite the group A dots with the C-3Hh transition and the 1.3464eV photons excite them with the C-2Hh transition. Besides the group A dots, two other groups of QDs are excited by these photons as shown in Fig.2. The emission spectra, shown in Fig.1, show the emission peaks of the two groups of dots that are excited. For the 1.3778eV excitation, besides the emission from the group A dots, we also see a peak at 1.300eV corresponding to a smaller size group. For the 1.3464eV excitation, the additional emission peak is at 1.252eV, which corresponds to a larger size group. From the diagram shown in Fig.2, we can easily deduce the separation of the hole energy levels for the group A QDs. The difference between 1.3464eV and the ground state transition energy, which is 1.269eV, gives the energy separation between 1Hh and 2Hh. The difference between 1.3778eV and 1.3464eV gives the energy separation between the 2Hh and 3Hh levels. The obtained ΔE (1Hh-2Hh) and ΔE (2Hh-3Hh) are 77.4meV and 31.4meV, respectively.

In the same way, the hole sub-level information can be obtained for QDs with other sizes. Fig.3(b) shows the deduced size dependent energy positions of three hole sub-levels. The corresponding size distribution is shown in Fig.3(c). Our experimental result, is in good agreement with the theoretical prediction given by Grundmann *et al*[2]. For the dominant size dots (group A), the deduced two excited-state hole level positions are confirmed by the result of PLE measurement, as shown in Fig.3(a)(b).

In conclusion, we have developed a selective excitation photoluminescence spectroscopy technique to probe QDs with a large size distribution and, for the first time, we are able to obtain detailed spectral information for individual QDs. The size dependent energy level positions for different hole sub-levels can be deduced.

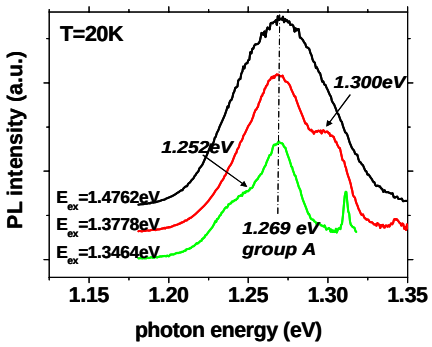


Fig. 1. Selective excitation PL spectra of InAs-GaAs QDs at 20K. Excitation energy of 1.4762eV is above InAs wetting layer, while that of 1.3778eV is below InAs wetting layer.

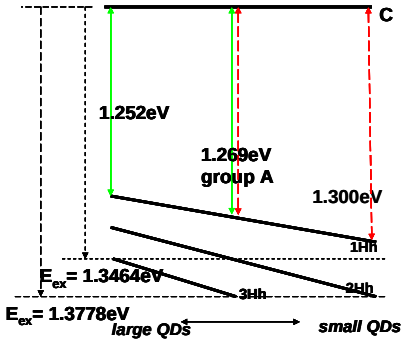


Fig. 2. Schematic size-dependent QD energy levels. The electron sub-level of different size QDs is leveled for reference.

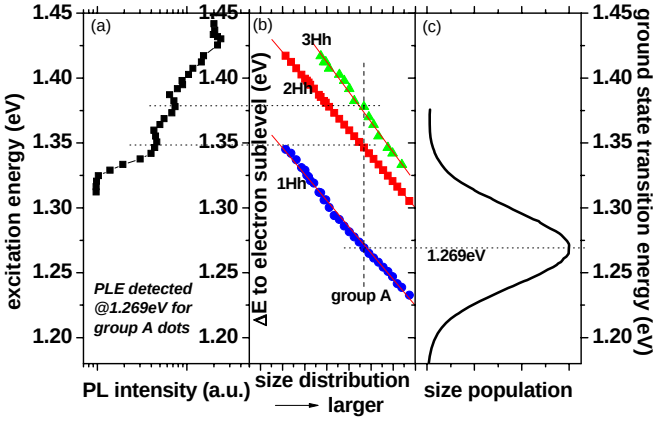


Fig. 3. Extracted hole sub-level information of individual QDs from selective excitation PL technique. (a) The PLE of dominant size QDs (group A), of which the detection energy is 1.269eV. (b) The energy difference to electron sub-level of three hole sub-levels. (c) The Gaussian-shape size population reflected by the high power PL spectrum of QD ensemble.

Reference:

[1] F. Adler, M. Geiger, A, Bauknecht, D. Haase, P. Ernst, A. Dornen, F. Scholz. J. Appl. Phys. **83** 1631 (1998)
[2] M. Grundmann, O. Stier, and D. Bimberg. Physical review B **52** 11969 (1995)
[3] S. Fafard, D. Leonard, J. L. Merz, and P. M.. Petroff. Appl. Phys. Lett. **65** 1388 (1994)

Two electron entanglement mediated by two level system

A. López and E. Medina

E-mail: alopez@ivic.ve

"We analyze the quantum entanglement induced in one dimensional scattering of a noninteracting two electron system in interaction with a two level system (qubit). It is found that transitions induced on the qubit can degrade the output entanglement induced on the two fermion system. The role of resonances is considered since it has been previously found [1] that resonant scattering modifies the quantum correlations as quantified by the concurrence [2–4]. The resulting correlations are a function of the characteristic separation between incoming fermions prepared in a antisymmetric two particle packet state. The connection to fuzzy measurements and local correlation in the Fermi sea will be discussed [5]."

---

[1] A. López, O. Rendón, V. Villalba and E. Medina, in preparation

[2] S. Hill, W. K. Wootters, *Phys. Rev. Lett.* **78**, 5022 (1997).

[3] W.K. Wootters, *Phys. Rev. Lett.* **80**, 2245 (1998).

[4] C. W. J. Beenakker and M. Kindermann, *Phys. Rev. Lett.* **92**, 056801 (2004).

[5] D. Cavalcanti, M. França Santos, M. O. Terra Cunha, C. Lunkes, and V. Vedral *Phys. Rev. A* **72**, 062307 (2005).

BIOPARTICLE MANIPULATION USING DIELECTROPHORESIS

Neophytos Loucaides

University of Cyprus

Recent progress in the fields of genomics and proteomics has accelerated the identification of genes and gene products that cause or influence numerous disease states. This increasingly molecular understanding of disease necessitates the development of novel technologies that will allow more rapid and facile molecular diagnostics, thereby enabling the benefit of this new information to be realized by a maximum number of people. Furthermore, for many applications the devices must be capable of parallel, or even continuous, measurements. Inexpensive, miniaturized, and automated devices for general molecular screening will revolutionize the diagnosis and prognosis of diseases and disease risks—even at points of care, in the home, and in environments lacking any infrastructure.

With the increasing interest in molecular nanodevices and their fabrication, techniques to handle, manipulate and attach molecules such as DNA to surfaces at specific locations, are attracting considerable research attention. Methods utilising non-uniform electric fields (Dielectrophoresis) are emerging as most promising techniques for particle manipulation as they require no moving parts and hence can be inherently scalable for massively parallel nanomanipulation. Dielectrophoresis is an electronic analogue of optical tweezers based on the same physical principle: an ac electric field induces a dipole moment on an object in solution, which then experiences a force proportional to the gradient of the field intensity. For both types of tweezers, this force must compete with thermal Brownian motion to be effective, which becomes increasingly difficult as the particle size approaches the nanometer scale.

Very promising in the development of nanomanipulation devices is the discovery and research in the properties of Carbon Nanotubes (CNT). These can be used as electrodes for sensors, with ideal electrical properties and size. Electronic methods (DEP in particular) have been proposed for separation of different types of CNTs and also for assembling CNTs and other particle networks on electrodes. These methods are considered very promising in the realisation of portable devices capable of DNA analysis and portable sensors in general and significantly reduce the time and sample required for such analysis.

The main purpose of our work is to introduce novel devices that utilise non-uniform alternating electric fields for the manipulation of nanoscale particles. These manipulation devices will be mainly used in conjunction with Carbon Nanotubes (CNTs) as electrodes in order to produce better sensor devices that offer increased sensitivity and are able to operate

with less sample input, avoiding costly preparation processes, reducing their size and enabling massively parallel analysis to be achieved. These techniques are very important for lab-on-chip systems, a furiously evolving technology which promises accurate, portable and low cost devices.

We intend to investigate the design of such devices for both their operation and fabrication. This is going to be achieved by firstly formulating a concise physical model for a system consisting of a device and a particle sample suspended in a fluid inside the device. The physical model will account for the effects of electrohydrodynamics (EHD), Dielectrophoresis (DEP), Brownian motion (which becomes increasingly important as we move from the microscale to the nanoscale), particle-particle effects and double layer effects in the operation of the device.

Our investigation will also take in account the EHD motion of the electrolyte, so that it can be used constructively in the operation of the device. Whilst this has not bee the case up to now, recent studies have indicated the possibility of using EHD to enhance the operation of the device.

Either Monte Carlo simulations or the solution of the Fokker Planck equation will be used in order to simulate the behaviour and dynamics of the above systems and to predict their behaviour. The need for these techniques arises from the stochastic nature of the system dynamics at this scale. Existing devices will be analysed in order to validate the model and then we will proceed to formulate a control problem in order to set a process for performance evaluation and optimisation of design variables for such devices.

GAS SENSITIVITY OF MODIFIED SINGLE-CRYSTAL SILICON SURFACE

A.I. LUCHENKO[1], *M.M. MELNICHENKO*[1], *K.V. SVEZHENTSOVA*[2]
[1]*Taras Shevchenko Kiev National University, 2 Prospect Glushkova, Kiev 03127, Ukraine*
[2]*Institute of Semiconductor Physics of NASU, 45 Prospect Nauky, Kiev 03028, Ukraine*
realcrystallab@univ.kiev.uaT

Modern development and application of nanotechnology stimulates intensive study of nanocrystalline materials. The example of nanocrystalline material is porous silicon, wich nanosize and ordering is defined by chemical process of etching. Thus, the presence of pores with a diameter and depth of their penetration in single-crystal silicon about several tens nanometers essentially changes geometrical, chemical, electronic and adsorptive properties of a real surface of single-crystal silicon.

As production and application of nanocrystalline silicon layers finds increasing use in microelectronics, gas and biosensor controls, the creation of new semi-conductor devices on the base of nanocrystalline silicon requires detailed study of its electronic and adsorptive properties.

In the work not polished single-crystal silicon substrate of p-type conductivity, (100) crystallographic orientation, with specific resistance 1 Ohm*cm was used. The layer of nanocrystalline silicon was created by chemical etching in a mix of acids HF and HNO_3. The thickness of a layer of nanocrystalline silicon (3 – 60 nm) during chemical modification of a surface of single-crystal silicon was supervised by preset parameters of technological process and was determined by a method of Auger electron spectroscopy.

The detailed study of chemical composition of nanocrystalline layer was carried out with the help of Auger electron spectroscopy and secondary ion mass spectrometry. The research of topography of the modified surface of single-crystal silicon was carried out by scanning tunnel microscope and scanning electron microscope. For definition of possible gas sensitivity of samples with modified surface the heterostructure (In - chemically modified silicon - single-crystal silicon – In) was used.

The contacts were received with the help of a method of magnetron dispersion of metal with use of a metal mask. In the work the research of change of parameters of the second derivative of the current-voltage characteristics of structure was carried out at change of surrounding gas environment. Gas environment was changed from a laboratory atmosphere and vacuum ($2 * 10^{-5}$ Torr) up to saturated ethanol vapor at a room temperature. The experimental research of the second derivative of the current-voltage characteristics has allowed to find out a number of features (Fig 1):

1. The presence of three resonant frequencies at which a maximum of amplitude of the second derivative is observed.

2. Different behaviour of these frequencies at change of parameters of gas environment.

3. Non-uniform frequency shift of maxima of the second derivative.

The received results are explained by features of morphology of a surface after chemical modification. These features first of all consist in existence of nanocrystallites on a surface of single-crystal silicon of two types: macro nanocrystallites about 30-40 nm and micro nanocrystallites up to 20 nm.

Latter, results in change of superficial potential of elements of a surface, which are in a different morphological environment, and consequently in change of conditions of adsorption of molecules of surrounding gas environment.

Thus, study of influence of adsorption of molecules of gas environment on properties of a material with quantum-size effects and advanced surface carried out in the work, allows to expand a circle of researched properties of semi-conductor materials with the purpose of creation on their basis of gas sensor controls.

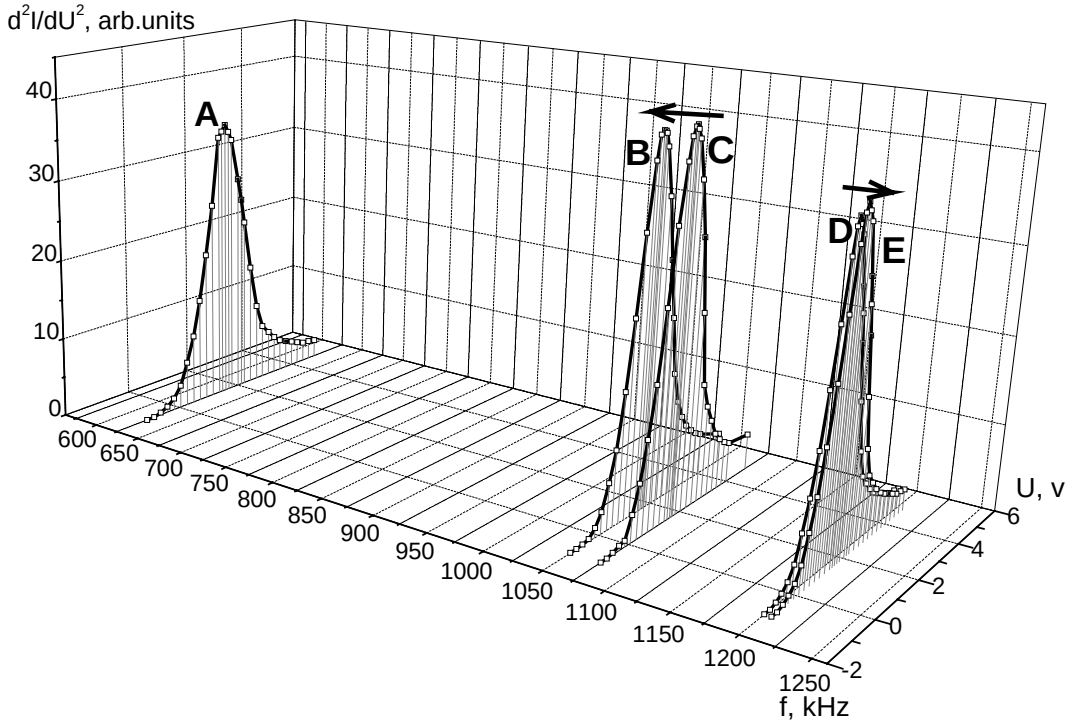


Fig. 1 d^2I/dU^2 dependence on voltage and frequency: A – in vacuum and in ethanol vapor; C, D – in vacuum; B, E – in ethanol vapor.

Photoluminescence study of high density InAs/GaAs quantum dots

M. C. Luo [1], S. D. Lin[1], S. Y. Wang[2] and C. P. Lee[1]

1) Department of Electrical Engineering, National Chiao Tung University, Hsin-Chu, Taiwan

2) Institute of Astronomy and Astrophysics, Academia Sinica, Taipei, Taiwan.

TEL : 886-3-5712121-54248, E-mail: mcluo.ee91g@nctu.edu.tw

The quantum dot (QD) based structures are of great interest in recent years due to their δ-function-like density of states and the spatial confinement of electrons and holes in artificially designed spaces.

In this work, the optical properties of high density self-assembled InAs/GaAs QD samples at low temperatures (20K) were studied. We found that the collective behavior of the high density dots has a strong influence on their photoluminescence spectra. In low density QD samples, each QD can be treated as independent and the carrier recombination time is smaller than the time needed for carriers to migrate from one to another. For high density dot samples, the situation, however, can be very different. If adjacent QDs are close enough, the carriers can tunnel from one to another before they are recombined. In this situation, the QDs can not be regarded as an ensemble of individual ones. The PL emission spectrum becomes dependent on the density of the QDs. In this study, various excitation powers from 50uW to 10mW were used. Unlike the low density samples, the high density samples showed a blue shift in the emission peak as the power is increased. The amount of shift is a strong function of the dot density.

The samples in our study were grown by molecular beam epitaxy on (001) GaAs substrates in a Varian Gen-II reactor. Two high density samples were prepared. Sample #1 was deposited with 2.4ML of InAs at a growth rate of 0.15um/hr under an As4 partial pressure of 2.8×10^{-5} Torr for the dot formation. The QDs in sample #2 was grown in an As2 environment at a partial pressure of 1.6×10^{-5} Torr. 2.6ML of InAs was deposited at a growth rate of 0.05um/hr. Both samples were grown at the same substrate temperature of 480℃. We also grew an additional QD layer with the same condition at the surface of each sample for AFM measurement. The dot density determined by AFM was $3.25\times10^{11}/cm^2$ and $3.63\times10^{11}/cm^2$ for sample #1 and #2, respectively. The average center to center distance between nearby QDs is about 17nm. To compare the results from the high density samples, we also prepared a standard low density sample (sample #3) with a dot density of $4.12\times10^{10}/cm^2$. Table 1 lists the dot density, the measured ground state energy, and the full width at half maximum (FWHM) of the PL emission from the three samples.

Figure 1 shows the position of the emission peak as a function of the pumping power for the three samples mentioned above. A blue shift of 8meV for sample #1, 4meV for sample #2, and 1meV for sample #3 were observed as the excitation power was increased. As expected, the low density sample had a very small blue shift. But a significant blue shift was observed for the high density samples. We noticed that the amount of shift, besides being a function of the dot density, is also dependent on the ground state energy of the QDs. The two high density samples, although had similar dot densities, showed different blue shift. Sample #1, which has a higher ground state energy, has a larger blue shift. For all samples, we noticed that the amount of blue shift saturates when the excitation power exceeds 5mW.

In high density QD samples, the distance between adjacent dots is very small. The excited carriers can be thermalized through the tunneling process. At low excitation power, the carrier in smaller QDs can transfer to the nearby larger ones. In this way, The PL spectrum is mainly contributed by the larger QDs. As the excitation power increases, the larger QDs are filled with carriers, which prevent further transfer of carriers from the smaller QDs to the larger dots. As a result, the PL emission comes from all of the QDs and this results in a blue shift of the PL emission peak. When the QDs are smaller, or the transition energy is higher, the tunneling probability between dots increases. This will further enhance the blue shift as the pumping power is increased.

In figure 2, we observe that FWHM also becomes larger as the excitation power increases. From the PL spectra shown in Fig.3, we notice that increase in the line width is only at the high energy side. So large QDs always contribute to PL emission while the emission from the small dots needs pumping at a higher power level. This effect is stronger for high density dots and dots with small sizes.

In conclusion, the tunneling between QDs plays an important role in the PL emission spectrum. Denser and smaller dots give a clear blue shift in the emission peak as the pumping power is increased as a result of carrier transfer among the QDs through the tunneling process.

Table 1: sample information

Sample #	Dot density (#/cm^2)	Ground state energy (eV)	FWHM (meV)
Sample #1 (200uW)	3.25×10^{11}	1.2679	57.5
Sample #2 (200uW)	3.63×10^{11}	1.1665	66.6
Sample #3 (20uW)	4.12×10^{10}	1.1632	58.3

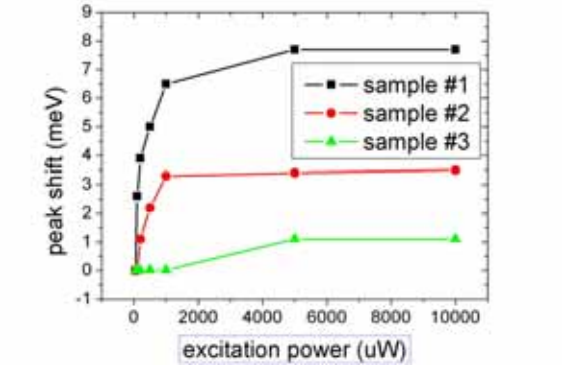


Figure 1: peak shift at different excitation power

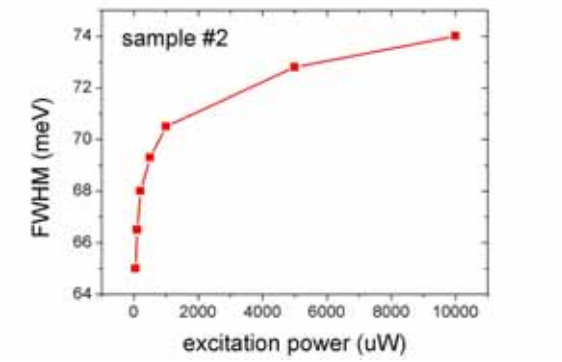


Figure2: FWHM at different excitation power.

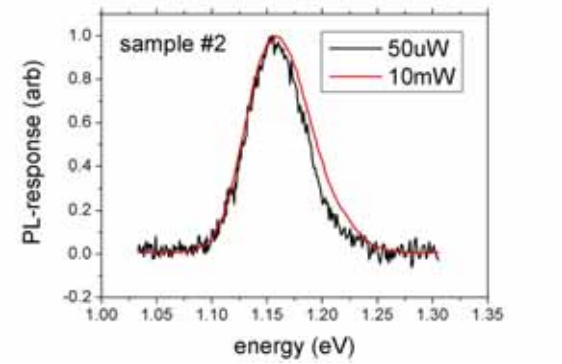


Figure3: PL spectrum at two different excitation powers

[1] C.H. Wu, Y.G. Lin, S.L. Tyan, S. D. Lin and C. P. Lee, Chinese Journal of Physics. 43, 847 (2005)

[2] Yu. I. Mazur, W. Q. Ma, Z. M. Wang, G. J. Salamo, and M. Xiao, Apply Physics Letter. 83, 987 (2003)

AFM AND SEM STUDY OF RUBRENE MICRO-CRYSTAL THIN FILM AND NANOWIRES GROWTH

Y. Luo,[a] M. Brun,[b] P. Rannou[a] and B. Grevin[a]

[a] UMR5819-SPrAM(CEA-CNRS-UJF), DRFMC CEA-Grenoble,17 rue des Martyrs 38054 Grenoble Cedex 9, France
[b] LETI-DIHS CEA-Grenoble, 17 rue des Martyrs 38054 Grenoble Cedex 9, France
yi.luo@cea.fr

Regarding organic electronic applications [1,2], rubrene ($C_{42}H_{28}$) has recently attracted attention for the extraordinary large carrier mobility (as high as 15cm^2/Vs[3]) in field effect transistors based on single-crystals. However, so far, no high performance rubrene thin film transistors have been reported. Due to complex molecular conformations[2], the fabrication of high quality rubrene thin film is indeed difficult compared with other oligoacenes.

In this communication, the growth of rubrene on Si/SiO_2 substrates under UHV conditions is presented. At room temperature, the growth of isolated amorphous islands with widths up to 300nm is observed. Temperature dependant Rubrene thin film growth has been investigated. At higher substrate temperature (85^oC) and high deposition rate, a mode of growth has been identified which results in micro-crystal rubrene domains with lengths up to 10μm (Fig1). The length of the rubrene domains is sufficient to be covered by source and drain electrode for OFET fabrication. A 80-120nm thick amorphous continuous film with holes covers the whole substrate, on which huge polycrystalline rubrene spherulite structures with widths up to 500mm are observed. From the centre of the islands, rubrene dendrites grow outwards. The nucleation and initial growth of rubrene spherulite structures has also been studied. At the initial growth, the fractal structure has been observed. Afterward, with more deposited material, the compact spherulite structure was formed.

Additionally, rubrene nanowires are observed on these spherulite islands. Studied with Scanning electron microscopy (SEM), the rubrene nanowires have lengths up to 10μm with dimensions of the range between 50nm to 150nm, as shown in Fig 2.

These results open the way for the synthesis of rubrene nanowires and high quality micro-crystal thin films. Besides, the report of thin film growth mode on a "template" amorphous layer indicated new possible strategies to be followed for the realization of rubrene-based thin film OFETs.

References

[1] Forrest, S.R. *Nature*, **2004**, *428*, 911.
[2] *Chem.Mater.*, **2004**, ***16***, pp 4381-4846. *Special issue on Organic Electronics*
[3] V.C. Sundar, *et al.*,*Science* 2004, *303,* 1644
[4] D. Käfer, *et al.*, *Phys. Rev. Lett.* 2005, *95,* 166602

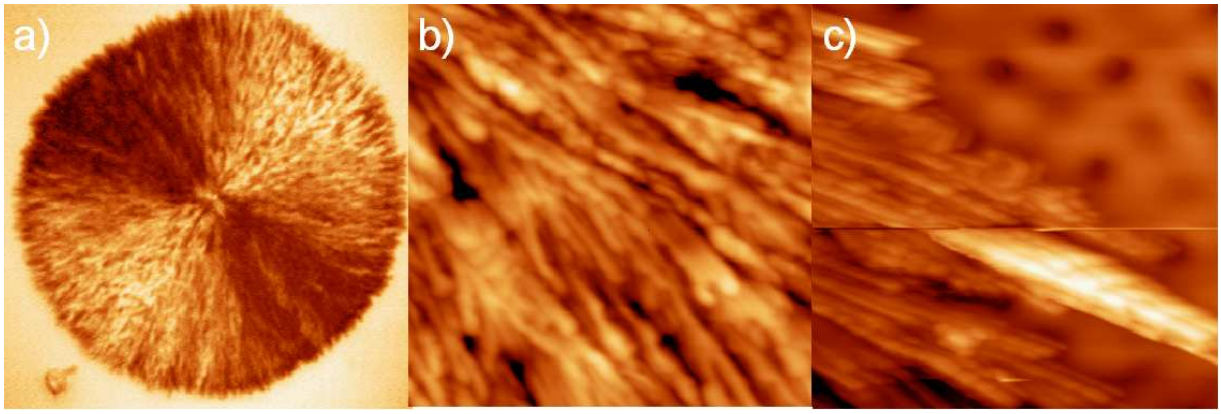


Fig 1. Morphology of rubrene thin films growth on SiO_2. a) optical micrographs of rubrene islands. b) AFM image of rubrene crystalline dendrites (3µm×3µm) c) edge of a polycrystalline island on the amorphous template layer (5µm ×5µm).

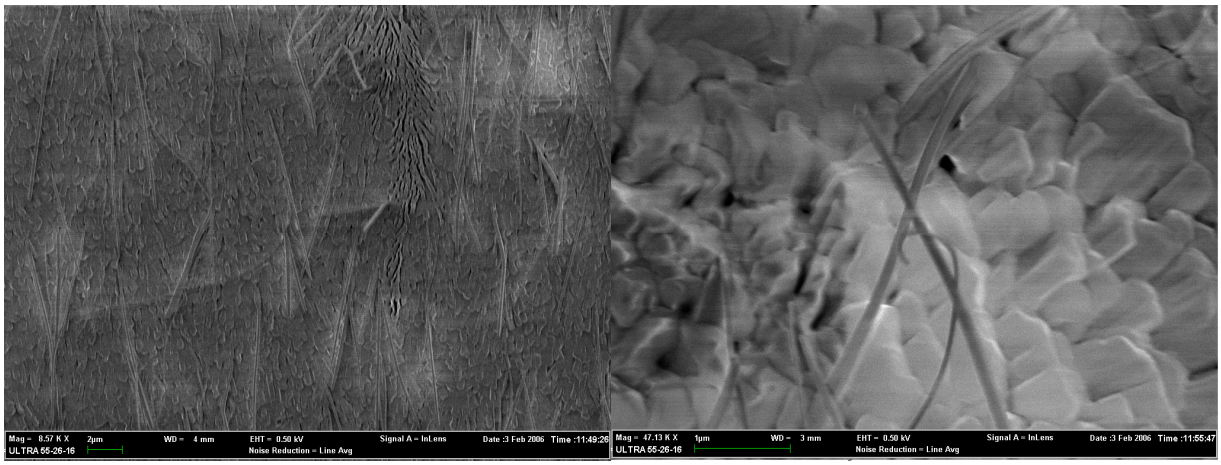


Fig 2. SEM images of rubrene nanowires grown on rubrene thin films.

Poster

PREPARATION AND CHARACTERIZATION OF METAL-POLYMER NANOCOMPOSITE MEMBRANES FOR ELECTROCATALYTIC APPLICATIONS

D.N. Muraviev[a], J. Macanás[a], J. Parrondo[b], M. Muñoz[a], S. Alegret[a] and F. Mijangos[b]
a) Analytical Chemistry Division, Department of Chemistry, Autonomous University of Barcelona, 08193 Bellaterra, Barcelona, Spain. b) Department of Chemical Engineering, University of Basque Country, Apdo. 644, 48080 Bilbao, Spain.

Jorge.Macanas@uab.es

The synthesis and characterization of Metal NanoParticles (MNP) has attracted great interest of scientists and technologists within the last years due their unique physical and chemical properties, which substantially differ from those of both bulk material and single atoms. These properties provide various practical applications of MNP including catalysis- and electrocatalysis-based processes, which occur in, for example, in fuel cells of different types or in various sensing devices (e.g. amperometric sensors and biosensors). Nevertheless, the main drawback, which still limits their wide applications, is insufficient stability of MNP dealing with their high trend for aggregation and the loos, as the result, of their special properties. Stabilization of MNPs in polymeric matrices of different types has been proven to be one of the most promising strategy to prevent their aggregation and to stabilize their properties [1]. The Polymer-Stabilized MNP (PSMNP) and the polymer-metal nanocomposite materials on their base start to find wide applications in various fields of science and technology. For example, sulfonic ion-exchange resins containing palladium MNP are used as bi-functional catalysts comprising the acid as well as the hydrogenation-active centers. Such catalysts are currently employed in at least four industrial processes.

In this communication we demonstrate that Metal-Polymer Nanocomposite Membranes (MPNCMs) containing MNP can be easily prepared in a Sulfonated PolyEtherEther Ketone (SPEEK) polymeric matrix by using the polymeric membranes as nanoreactors to both synthesize and to characterize the composition and architecture of the formed MNP [2]. Metal ions (or metal ion complexes) are first incorporated in the polymeric matrix where they undergo a reduction reaction that leads to the formation of corresponding MPNCMs. Since this technique allows for carrying out successive metal loading-reduction cycles, it appears to be possible to synthesize the core-shell MNP by changing the type of metal ion in the second or sequential loadings.

In this study MPNCM containing Pt@Cu-PSMNP were prepared and characterized by several techniques, such as TEM (see Fig.1a), SEM (see Fig. 1b), water absorption measurements (see Fig. 2a), impedance spectroscopy (see Fig. 2b) and some others. Some characteristics of MPNCM e.g., water absorption and conductivity) appear to depend on the thickness of platinum shell. The electrocatalytic activity of Pt@Cu-PSMNP has been shown to also depend on this parameter.

References:

[1] A.D. Pomogailo, G.I. Dzhardimalieva, A.S. Rozenberg, D.N. Muraviev, J. Nanoparticle Res., **5** (2003) 497-519.
[2]. D.N. Muraviev, Contributions to Science, 3(1) (2005) 17-30.
[3] D.N. Muraviev, J. Macanás, M. Farre, M. Muñoz, S. Alegret, Sensors & Actuators, (2006) in press.
[4] J. Macanas, M. Farre, M. Muñoz, S. Alegret, D. N. Muraviev, Phys. Stat. Sol. (a), 203, **6**, (2006) 1194-1200.

Figures:

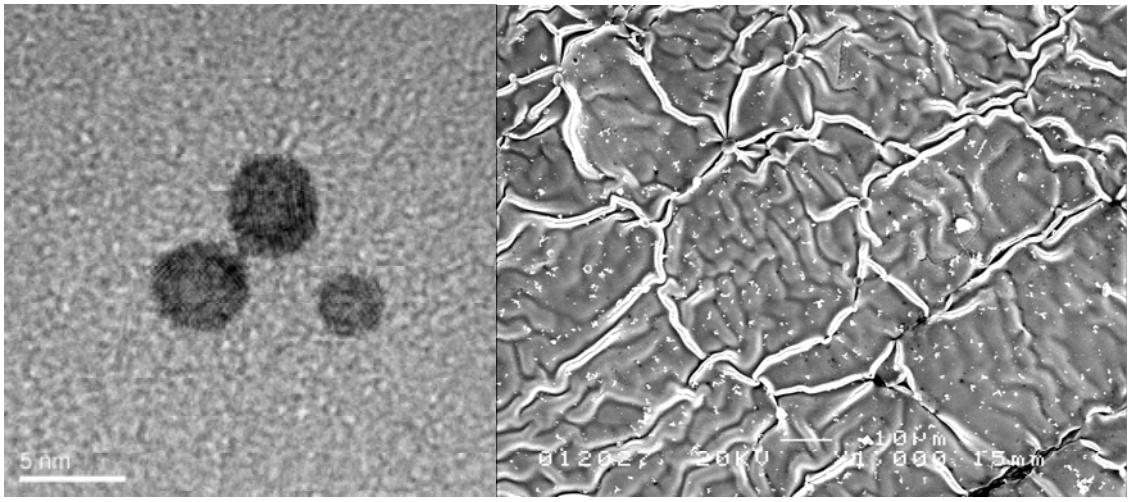


Fig. 1: *Typical TEM images of MPNCMs containing Pt@Cu-PSMNPs (a) and typical SEM micrographies of MPNCMs surface.*

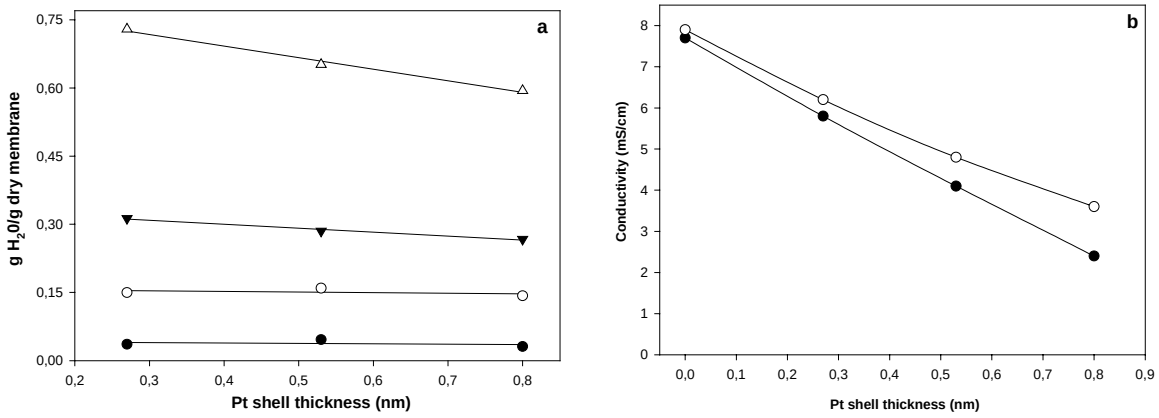


Fig. 2: *Pt-MNP shell thikness influences both (a) the membrane water absortion and the membrane ionic conductivity (b). Water absorption was measured at different values of Relative Humidity (RH): ● 59%, ○ 83%, ▼ 93% and △ 100%. Ionic conductivity was determined by impedance spectroscopy of (○) Pt@Cu-SPEEK and (●) Pt@Cu-SPEEK:SPEEK 1:1 samples.*

USE OF NANO-SCALE ZERO-VALENT IRON FOR GROUNDWATER REMEDIATION

Christian Macé, Florin Gheorghiu; Michael Pupeza; Wei-xian Zhang
GOLDER ASSOCIATES, 1951 Old Cuthbert Road, 08034 Cherry Hill, NJ,USA

Zero-valent iron has been used to remediate many organic contaminants, which can be completely reduced to non-toxic compounds such as ethene and ethane. Nano-scale zero-valent iron (NZVI) particles have been shown to be more reactive and extremely effective by virtue of their increased surface area compared to granular coarser iron particles and the ability to distribute the particles directly into contaminant plumes.

Initially, Golder Associates implemented this technology at a pharmaceutical facility in Research Triangle Park, North Carolina. The results of this application showed rapid treatment of chlorinated solvents to below drinking water standards. Golder Associates has since conducted numerous in-situ pilot tests in fractured bedrock and porous media aquifers. Results have demonstrated the ability to rapidly reduce contaminant mass while concurrently conditioning the aquifers for more effective bioremediation. The rapid reaction rate and small particle size facilitates expeditious primary treatment in source areas and dissolved plumes, thereby substantially shortening overall remediation timeframes for otherwise recalcitrant groundwater plumes. This presentation will provide a review of the theory behind zero-valent iron remediation, case studies, and the viability of nano-scale zero-valent iron application to expedite redevelopment and reuse of Brownfields sites.

References:

Christian Macé, 2006, "Controlling Groundwater VOCs, Do Nanoscale ZVI Particles Have Any Advantage Over Microscale ZVI or BNP?" Pollution Engineering, April 2006, p. 24-28

Christian Macé, Steve Desrocher, Florin Gheorghiu, Allen Kane, Michael Pupeza, Miroslav Cernik, Petr Kvapil, Ramesh Venkatakrishnan, and Wei-xian Zhang, 2006, "Nanotechnology and groundwater remediation: a step forward in technology understanding", Remediation, volume 16, number 2, spring 2006, p. 23-33, Wiley editor.

Florin Gheorghiu, Christian Macé, Ramesh Venkatakrishnan and Wei-xian Zhang, 2005, "In-Situ Treatment Using Nano-Scale Zero-Valent Iron Implemented in North America and Europe", proceedings of the USEPA workshop on Nanotechnologies for Site Remediation, State of the Science, Washington DC, USA, 20-21 October 2005.

Florin Gheorghiu, Christian Macé and Wei-xian Zhang, 2005, "Field Testing of Nano-Scale Zero-Valent Iron and Bimetallic Nano-scale Particles, Case studies and Conclusions" Poster presentation for the first Innovative Environmental Technologies Conference, Newark, NJ, USA, 26 October 2005.

Christian Macé, 2005, "Nanotechnologies et Réhabilitations de Sites Contaminés: Etudes de Cas Utilisant les Nanoparticules de Fer Zero Valent", Géologues n° 147, p. 78-83, December 2005.

Ramesh Venkatakrishnan , Florin Gheorghiu, Robert E. Glazier, Jarrett Elsea, Lindsey Walata, and Wei-xian Zhang; Conference Proceedings Volume: Multi-Parameter Monitoring

of Nanoscale Particle Injection in Triassic Basin Bedrock, North Carolina: Petroleum Hydrocarbons and Organic Chemicals in Groundwater; 20th. NGWA Conference, California, August 2003.

Florin Gheorghiu, Lindsey Walata, Ramesh Venkatakrishnan, Wei-xian Zhang, and Robert E. Glazier, Filed Testing of Nano-Scale Zero-Valent Iron Particle Technology for in-Situ Groundwater Treatment, Florida Remediation Conference Proceedings, 2003.

Robert E. Glazier, Ramesh Venkatakrishnan, Florin Gheorghiu, Lindsey Walata, Robert Nash , and Wei-xian Zhang, 2003, "Nanotechnology," Civil Engineering Magazine, Vol 73, No. 5, May 2003.

Florin Gheorghiu, Ramesh Venkatakrishnan, Robert E. Glazier, Lindsey Walata, Robert Nash , and Wei-xian Zhang, 2003, "Hydrogeological Site Characterization for the Implementation of a Pilot Test of In-Situ Groundwater Treatment using Dual-Phase Slurry Injection In Fractured Bedrock," proceedings of the 2003 EGS-AGU-EUG Joint Assembly, Nice, France, April 6-11, 2003.

Wei-xian Zhang , Lindsey Walata , Robert Nash, Florin Gheorghiu, Robert Glazier Ramesh Venkatakrishnan, 2003, "Field Testing of Bimetallic Nanoscale Particle Technology for In-Situ Groundwater Treatment of a Fractured Rock DNAPL Zone," proceedings of the 2003 EGS-AGU-EUG Joint Assembly, Nice, France, April 6-11, 2003.

NON-COVALENT FUNCTIONALIZATION OF CARBON NANOTUBES TOWARD BIOSENSING APPLICATIONS

Nicolas Mackiewicz,[†] Séverine Padiolleau,[‡] Didier Boquet,[‡] Eric Doris,[†] and Charles Mioskowski[†]
[†]CEA-Saclay, SMMCB Bât. 547, 91191 Gif-Sur-Yvette Cedex, France
[‡] CEA-Saclay, SPI Bât. 136, 91191 Gif-Sur-Yvette Cedex, France
nicolas.mackiewicz@cea.fr

Carbon nanotubes (CNTs) are molecular wires that exhibit interesting structural, electrical and mechanical properties which make them promising material in nanotechnology. Recent development led to the setting-up of carbon nanotube-based biosensors.

Our objective is to design a sensing device directed towards specific antigens using carbon nanotubes as template. For this purpose, the grafting of a moiety which is able to selectively interact with the target is required. We chose as interacting moiety an antibody's fragment known as single-chain fragment variable (scFv).

Obtained through recombinant molecular biology techniques, scFv is the smallest entity retaining high affinity for the antigen, which makes it ideal candidate for new immunosensors. Also, scFv incorporates a poly-histidine tag which will be used for the anchoring of the fragment on the nanotube via selective interactions with nickel ions.

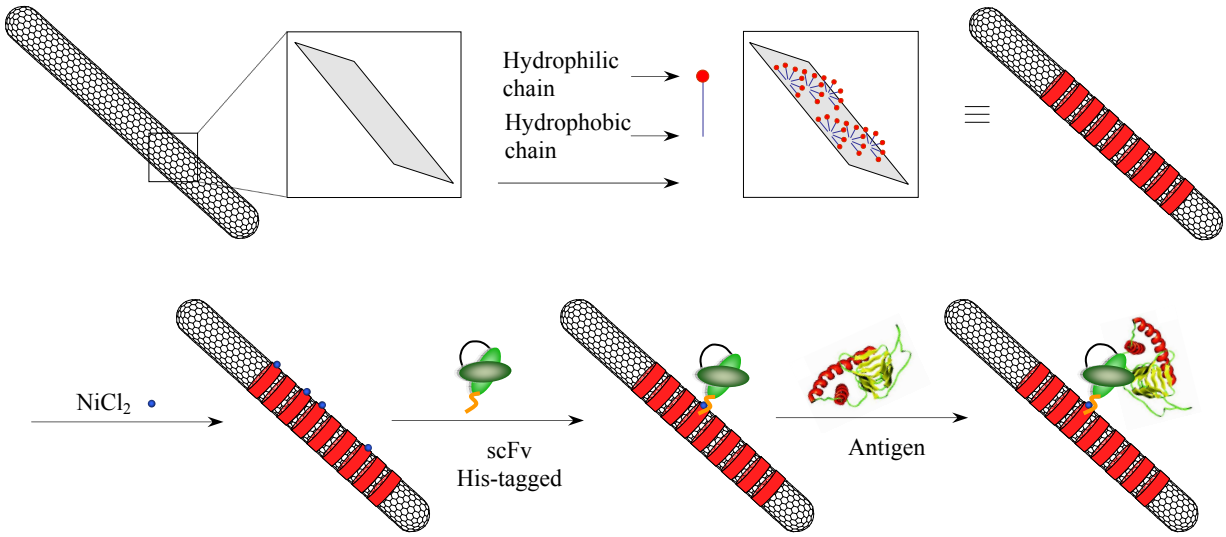
The nanotubes were first functionalized using a lipid made of a nitrilotriacetic acid (NTA) group, as a hydrophilic head, and an alkyl chain, as a hydrophobic tail. The choice of the NTA polar head was governed by the fact that NTA is also able to complex nickel.

In the presence of the nanotube, the lipids self-organize as nano-rings. This non-covalent functionalization preserves the sp^2 nanotube structure and thus the electronic properties of the tube.

The interaction between the scFv and the nano-rings is induced by the formation of a complex between NTA, nickel and the his-tag attached to the scFv. The supra-molecular assembly was characterized by immunoanalysis techniques and by electron microscopy.

Future prospects under investigation are the affinity evaluation of the scFv for the antigen and then, to build up a suitable method to test this assembly towards biosensing applications.

Figure:



OPTIMIZED TECHNIQUE FOR THE CALCULATION OF CARBON NANOTUBE DISPERSION RELATIONSHIPS

P. Marconcini, M.Macucci

Dipartimento di Ingegneria dell'Informazione, Università di Pisa

Via Caruso, 16 – I-56122 PISA

Carbon nanotubes are a very promising material for applications in many different fields, due to their small dimensions and to their remarkable physical properties. Indeed, the fact that they can have either a metallic or a semiconducting behavior, depending on their geometrical structure and on the applied magnetic field, together with the high current densities that they can handle and with their direct bandgap, makes them quite a promising material for electronics and optoelectronics. On the other hand, their large Young modulus, tensile strength and thermal conductivity, as well as their notable sensitivity to chemical interactions, make them suitable also for mechanical, thermal and chemical applications.

Since a single-wall carbon nanotube can be seen as a graphene sheet rolled up in a cylindrical shape along one of its lattice translational vectors (the chiral vector), many of its physical properties can be obtained from those of graphene, with the addition of a closure boundary condition along the chiral vector. This implies a discretization of the allowed graphene wave vectors along parallel segments of the reciprocal space; sectioning the graphene physical relations along these segments and folding them onto the nanotube Brillouin zone (located along the nanotube axis) we can obtain the correspondent nanotube relations. Such a technique (the so-called zone folding technique) is usually applied to the rectangular region of the graphene reciprocal space containing all the inequivalent graphene wave vectors and having an edge parallel to the nanotube axis and coincident with the nanotube Brillouin zone, in such a way as to easily fold the graphene relations.

Here we illustrate how this useful rectangular region, which can be taken as alternative primitive unit cell of the graphene reciprocal lattice, is related to the overall graphene reciprocal space. Since the usual unit vectors $\vec{b}_1$ and $\vec{b}_2$ in the graphene reciprocal space, corresponding to the commonly used graphene unit vectors $\vec{a}_1$ and $\vec{a}_2$ in the direct space, do not have a direct correspondence with such a rectangular region, we introduce an alternative choice of graphene unit vectors, which depends on the considered nanotube and which clarifies how the rectangular zone is repeated inside the graphene reciprocal space.

This choice of unit vectors allows to obtain, from any graphene wave vector, the equivalent vector inside the rectangular region in a computationally very inexpensive way. This can be fruitfully applied to significant graphene wave vectors, such as the ones corresponding to the graphene degeneration points. For example, when determining the nanotube dispersion relations from those of graphene through the zone folding technique, knowledge of the wave vectors equivalent to the graphene degeneration points, and located inside the rectangular zone where the zone-folding technique is applied, makes it possible to limit the computation only to the most interesting bands, thereby reducing the computational effort. In particular, we present an example of application of this technique to the computation of the graphene dispersion relations by means of the tight-binding method, with the inclusion of the contributions from up to the third-nearest neighbor atoms.

ATOMIC RESOLUTION AFM AT LOW TEMPERATURES USING THE QPLUS SENSOR

M. Maier
Omicron NanoTechnology GmbH, Limburger Str. 75, D-65232 Taunusstein, Germany
Phone: +49 6128 987 297, Fax: +49 6128 987 33 297
Email address corresponding author: m.maier@omicron.de

Over many years, low temperature STM has been established as an advanced imaging and spectroscopy tool in various scientific fields such as inelastic tunnelling spectroscopy (IETS) on single molecules or manipulation on the atomic scale. However, the creation and investigation of nano-structures on insulating surfaces gains more and more interest an thus push AFM as an alternative and complementary imaging technique. Ideally, the used AFM probe should simultaneously or alternatively work in STM and STS modes and not compromise on performance. Based on a proven LT STM platform, we have integrated a QPlus [1,2] sensor for atomic resolution AFM while maintaining ease of use and level of STM performance. Especially at low temperatures and related spatial constraints, this self-sensing AFM technique is an ideal alternative to cantilever based optical detection.

The QPlus sensor [1,2] employs a quartz tuning fork for force detection in non-contact AFM operation mode. One prong of the tuning fork is fixed while the SPM probe tip is mounted to the second prong. It thus acts as a quartz lever transforming it's oscillation into an electrical signal as a result of the piezo-electric effect. The feedback signal is based on frequency shift originating from tip-sample force interaction.

A dedicated pre-amplification technique ensures distance control based on the pure vibrational signal. Perfect separation of the tunnelling current is important when working on conducting samples, since tunnelling at the oscillation reversal point of the lever can easily dominate the feedback signal. In addition, extremely low signals require the first amplification stage to be very close to the sensor, i.e. to be compatible with low temperatures.

Measurements on Si(111) 7x7 show that tunnelling current and vibrational signal are clearly separated. We have been using wet-chemically etched tungsten tips, which allow the sensor to be simultaneously or alternatively operated in STM mode. In addition, benchmark measurements on NaCl with a typical corrugation of approx. 10pm prove that resolution on insulation samples is competitive to best cantilever based AFM results.

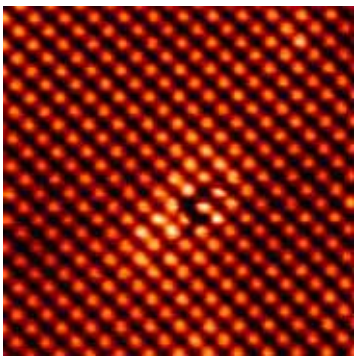


Image: Atomic resolution on NaCl(100) using QPlus force detection (no filtering applied). Lattice constant 5.65 Å (fcc), typical corrugation 10pm. Imaging parameters: scan range 6 x 6 nm^2, df = -2Hz, $f_{res} \approx 25230$Hz, Q = 36671, oscillation amplitude $\approx 1.5nm_{pp}$.

[1] Franz J. Giessibl, Appl. Phys. Lett. **73**, 3956 (1998)
[2] Franz J. Giessibl, Appl. Phys. Lett. **76**, 1470 (1998)

ULTIMATE NANOPROBING IN UHV: FOUR INDEPENDENT SCANNING TUNNELING MICROSCOPES NAVIGATED BY HIGH RESOLUTION UHV SEM

M. Maier
Omicron NanoTechnology GmbH, Limburger Str. 75, D-65232 Taunusstein, Germany
Phone: +49 6128 987 297, Fax: +49 6128 987 33 297
Email address corresponding author: m.maier@omicron.de

A major challenge in Nanotechnology is the incorporation of single nano-devices into larger integrated circuits. Device technology research requires high resolution topographical and chemical analysis with well established experimental techniques or electrical characterisation using standard probing systems.

Traditional instrumentation suffers from one fundamental issue: How to cover the dimensional range of a fully integrated circuit down to the nanometer range (or even atomic scale) of single devices and have an adequate integrated navigation system. To meet these requirements, we have established and being advancing a new approach to integrating state-of-the-art SPM technology via high resolution electron microscopy and spectroscopy: (1) Bridging dimensions and rapid navigation; (2) Combining different surface analysis methods at the very same sample area to gain complementary information; (3) Integrated position-readout of sample and probe positioning; (4) Pushing each single technology to its inherent limits.

The system facilitates four independent Scanning Tunnelling Microscopes and the UHV version of the Zeiss Gemini SEM column with ultimate resolution below 4nm for probe navigation and rapid localisation of sample features or devices. STM imaging is used to pro-actively position and contact the probe(s) on nano-devices. Using STM probe approach technology, a controlled electrical contact is ensured to finally perform a four-point measurement on the nano-scale.

Beyond navigation, SEM enables different electron spectroscopy methods to gain magnetic or chemical information on the sample area. Using SEMPA (SEM with polarization analysis) magnetic domain imaging with a resolution in the 10nm range is achieved to allow for correlation of transport properties and domain distribution. Using SAM (Scanning Auger Microscopy) chemical mapping can be achieved with 10nm resolution to correlate transport properties and material composition. Various application examples will be shown to illustrate the system capabilities.

Magnetic response in n-fold twisted Möbius strips

Santanu K. Maiti
Theoretical Condensed Matter Physics Division,
Saha Institute of Nuclear Physics,
1/AF, Bidhannagar, Kolkata 700 064, India

An important aspect in quantum mechanics is to find a relation between a global geometry of a sample i.e., the boundary conditions and its physical properties. This issue is addressed by comparing flux periodicity of persistent currents in a cylinder and in a moebius strip. Here I investigate the influence of the topology on generic features of persistent current and low-field magnetic susceptibility in n-fold twisted moebius strips both for free electrons and in the weakly disordered regime. A mesoscopic ring threaded by a magnetic flux ϕ offers one of the prime examples of quantum coherence in mesoscopic physics called, persistent current. It has been observed that in perfect one-channel mesoscopic rings current shows saw-tooth like behavior, while, in presence of impurity current gets a continuous variation with ϕ. In this case current shows $\phi_0 = ch/e$ flux-quantum periodicity. In multi-channel mesoscopic cylinders some additional kink-like structures may appear depending on the choices of chemical potentials μ or total number of electrons N_e for the systems described by fixed chemical potential (μ) or by fixed number of electrons (N_e). In these cylindrical systems also current shows ϕ_0 flux quantum periodicity like as one-channel mesoscopic rings. I describe the behavior of persistent current and low-field magnetic susceptibility in n-fold twisted moebius strips for two limiting cases. In one case electrons are unable to hop in the transverse direction, while, in other case they are allowed to hop in the transverse direction. For finite transverse hopping strength of the electrons the behaviors of the persistent current and low-field magnetic susceptibility are quite similar to the results as obtained in un-folded moebius strips. But for zero transverse hopping strength these results strongly depend on the value of n i.e., whether n is odd or even. Current shows $\phi_0/2$ flux-quantum periodicity for odd n, while, it exhibits ϕ_0 flux-quantum periodicity when n is an even integer.

DIRECTED ASSEMBLY AND TRANSFER OF SWNTs USING NANOTEMPLATES

Prashanth Makaram, Steve Ryley and Ahmed Busnaina
The NSF Nanoscale Science and Engineering Center for
High-rate Nanomanufacturing,
Northeastern University, Boston, MA 02115, USA
pmakaram@coe.neu.edu

With the new focus on utilizing nanotecnhnology for new generation of commercial products in many areas such as electronics, medical, etc., there is a need to develop developing tools and processes that will enable high-rate/high-volume bottom-up, precise, parallel assembly of nanoelements (such as carbon nanotubes, nanoparticles, etc.) and polymer nanostructures. For example, carbon nanotubes have shown enormous promise as next generation switches or interconnects in electronic applications. However, the realization of Single Walled Nanotubes (SWNT) electronics is hampered by the unavailability of tools for mass manufacturing. At the Center for High-rate Nanomanufacturing (CHN), nanotemplates are utilized to conduct fast massive directed assembly of nanoscale elements.

Electric field assisted nanotemplate are used for directed assembly of SWNTs.. SWNTs are negatively charged due to the presence of carboxylic acid groups. Under bias the negatively charged SWNTs assemble onto a templated positively charged substrate. The SWNTs assemble during Electrophoretic Deposition (EPD) [1] using nanotrench made into Poly Methyl Methacalate (PMMA) on a conductive substrate. The density of SWNTs assembled can be controlled by varying the template width and the voltage applied. The process takes 30-90 second to assemble SWNTs into 80 nm wide and 100,000 nm long trenches.

The PMMA is dissolved to expose the SWNTs assembled on the conductive substrate. The assembled SWNTs are then transferred to another patterned substrate either by using polymer such as Poly dimethyl siloxane (PDMS) [2] or by using a chemically functionalized substrate. The recipient substrate could be used as an electronic device (such as nanotube mechanical switches[3]) or other type of applications such as sensors. This technique provides an approach to mass manufacture aligned carbon Nanotubes in a very short time.

References:

[1] Van Der Biest, O.O.; Vandeperre, L.J. *Annu. Rev. Sci.* **1999** , *29*, 327-352.

[2] Meitl et. al., Nanoletters, Vol. 4, **2004,** 1643- 1647.

[3] Ward, J.W.; Meinhold, M.; Segal, B.M.; Berg, J.; Sen, R.; Sivarajan, R.; Brock, D.K.; Rueckes, T., IEEE, **2004,** 34-38.

Figures:

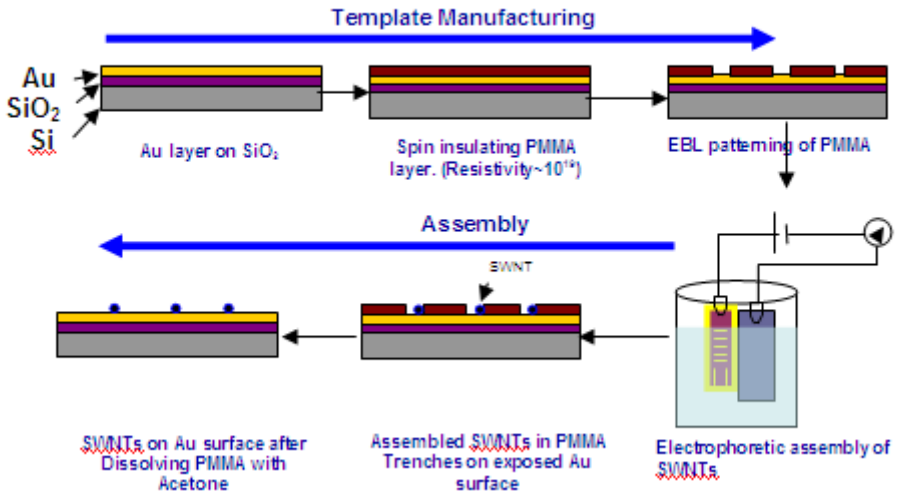


Figure 1: SWNT assembly process

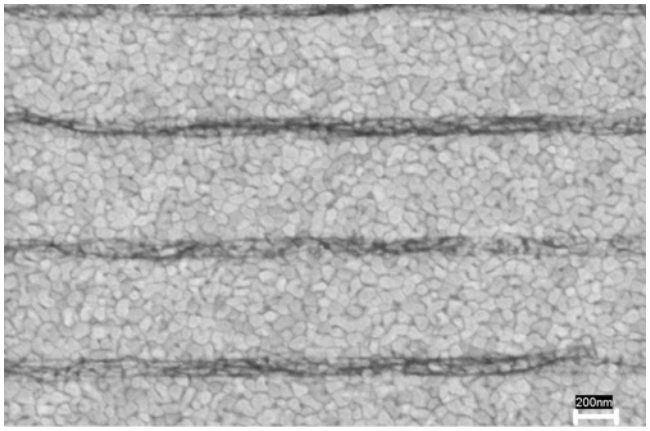


Figure 2: Assembly of SWNTs after dissolving of PMMA

COMPUTATIONAL STUDY OF THE MECHANICAL PROPERTIES OF TOBERMORITE AND JENNITE CRYSTALS IN COMPARISON WITH C-S-H GEL

H. Manzano [1], J.S. Dolado [1], A.Ayuela [2].
[1] LABEIN-Tecnalia, Parque Tecnológico de Bizkaia Edificio 700, 49160 Derio, Spain.
[2] Donosita Internacional Physics Center (DIPC), P.O.Box 1072, 20018 San Sebastián, Spain.
Hmanzano@labein.esT

Cement paste matrix is a complex multi-phase, heterogeneous and amorphous material. Among its hydration products, the so called C-S-H (Calcium Silicate Hydrate) gel is the most important one. It is responsible for the hardness and cohesion of the material, and it represents up to the 70% by volume of the cement paste

Yet intensively characterised by techniques such as SEM, TEM, XDR, NMR, etc [1], the complex and poorly organised nanostructure of the C-S-H gel has not been completely elucidated. Nevertheless certain structural features are already recognised. For instance, it is fair to say that, in essence, C-S-H gel is composed of silicate chains held together by calcium oxide layers, as schematically represented in Fig. 1. In fact, several models have been proposed so far which represent the atomic scale of C-S-H gel as a mixture of Tobermorite-like and Jennite-like structures in which these crystalline and layered species show multiple defects and imperfections [2].

At larger scales, let say from 1nm to 100 nm, the exiting descriptions of the C-S-H gel have been centred in the recognition of the colloidal and gel-like properties of the C-S-H gel. The current vision is the so called Jennings model [3], which states that certain basic (almost spherical) building blocks exist, and that they pack themselves to build up the C-S-H structure. According to this model, two kinds of C-S-H gels arise, the high-density (HD) C-S-H gel and low density (LD) C-S-H gel, depending on the packing efficiency of the basic building blocks. Interestingly, both varieties (LD and HD) exhibit dissimilar mechanical properties, as recently shown by nanoindentation experiments [4,5].

Thus, important technological applications in the construction sector are clearly envisaged provided the appearance HD C-S-H gels could be somehow favoured. To this end, it is clear that a closer linkage between the layered morphologies addressed in the structural models and the rounded basic building blocks proposed in Jennings model colloidal is clearly needed.

This work precisely attempts to shed light on this issue from a theoretical viewpoint. By means of ab-initio calculations with SIESTA code [6] and semiempirical calculations with GULP code [7], the mechanical properties of both Tobermorite and Jennite crystals and suggested smaller pieces of them will be assessed and compared with the existing experimental data. Special emphasis will be also paid to the establishment of linkages between the structural and colloidal viewpoints.

References:

[1] Ramachandran, V. S., Beaudoin, J. J. *Handbook of Analytical Techniques in Concrete*. (William Andrew Publishing, New York, 2001).

[2] I.G. Richardson, *Cement and Concrete Research*, **34** (2004) 1733-1777.

[3] Hamlin M. Jennings, *Cement and Concrete Research*, **30** (2000) 101-116.

[4] G. Constantinidis and F.-J. Ulm. *Cement and Concrete Research* **34** (2004) 67-80.

[5] C. Plassard, E. Lesniewska, I.Pochard, A Nonat, Ultramicroscopy, **100** (2004) 331-338.

[6] J.M. Soler, E. Artacho, J. Gale, A. García, J. Junquera, P, Ordejón, D. Sánchez-Portal, *Journal of Physics-Condensed Matter*, **14** (2002), 2745-2779.

[7] J. Gale, *Journal of the Chemical Society, Faraday Transactions*, 93 (1997) 629-637.

Figures:

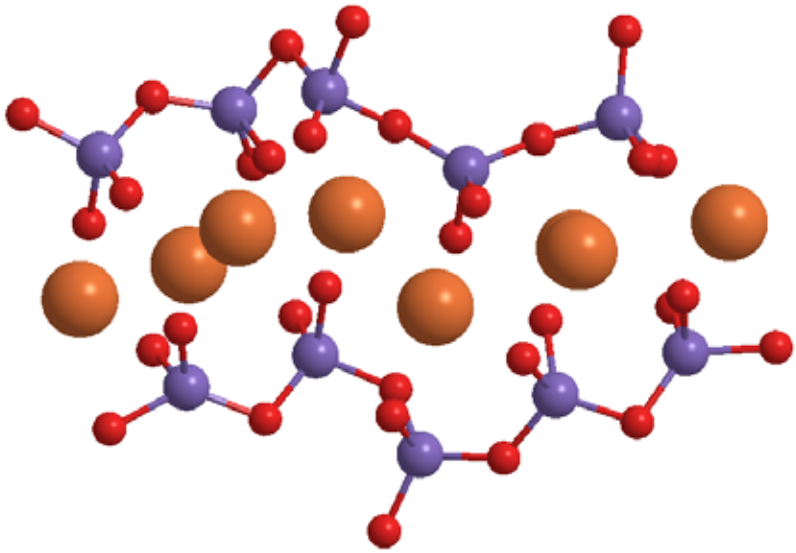


Fig 1. Schematic representation of the C-S-H gel.

RELAXOR-BASED THIN FILMS MEMORIES AND THE DEPOLARIZING FIELD PROBLEM.

Manuel I. Marqués and Carmen Aragó

Dpto. de Física de Materiales, C-IV, Universidad Autónoma de Madrid, Spain

ABSTRACT

Thin film memories based on ferroelectric materials are a topic of main interest in the computer industry. Nanomemories consisting on a few layers of ferroelectric materials such as $BaTiO_3$ could be a promising solution to the problem of miniaturization. However, when a ferroelectric memory is written by inducing a polarization different from zero in the thin film, a depolarizing field spontaneously appears, due to the existence of uncompensated charges at the substrate. If the width of the memory is very small (down into the range of nanometres) the depolarizing field increases to a value large enough to cancel the polarization [1].

In a simple first neighbour model we have found a mathematical relation between the lateral size of the memory (L), the width (D), the screening of the charges at the substrate (S) and the strength of the ferroelectric interaction (J) by considering the different energetic contributions to the system. We find that in order to obtain a polarization different from zero (not cancelled by the depolarizing field) the width of the ferroelectric memory must be $D > SL/2J$. So, miniaturization to a single layer is usually forbidden for a given set of (L, S, J) values.

On the other hand, new kinds of materials named relaxors elicited more and more attention from the ferroelectricity researchers during last years. Relaxors are materials with an intrinsic disorder [2**]**. This intrinsic structural disorder seems to result in the existence of nanodomains that persist even at high temperatures. Using the Random Field Ising Model, we consider that each nanodomain is affected by a different random electric field. The behaviour of these random fields when polarizing the relaxor has been studied lately in some detail [3].

In this paper we propose a possible mechanism to cancel the effect of the depolarizing film in thin film memories based on the use of relaxor nanolayers. Under the hypothesis of an internal organization of the random fields inside the nanolayer we show analytically how it should be possible to miniaturize the memory to a width as small as D=1 for any value of L, J and S. Further numerical and experimental work is in progress in order to test the viability of this theoretical proposal.

REFERENCES

[1] J. Junquera, P. Ghosez : Nature 422, 506 (2003)
[2] L.E. Cross, Ferroelectrics : 76, 241-267 (1987)
[3] M.I. Marqués, C. Aragó : Europhysics Letters 71 (1)**,** 124-130 (2005)

X-ray excited optical luminescence in InAs-based nanostructures: preliminary results

G. Martinez-Criado,[1] B. Alen,[2] A. Homs,[1] D. Fuster,[2] J. M. Ripalda,[2] A. Labrador,[1]
R. Steinmann,[1] J. Susini[1], L. González,[2] Y. González,[2] and J. M. García[2]
[1]European Synchrotron Radiation Facility, 38043-Grenoble, France
gmartine@esrf.fr
[2]Instituto de Microelectrónica de Madrid (CNM-CSIC), 28760-Tres Cantos, Madrid, Spain

Because of their versatile applications, the past decades have witnessed rapid growth in research and development of luminescent materials.[1] However, further progress towards advanced optical devices with higher efficiencies, lower costs, and longer lifetimes are based on nanotechnology (e. g., nanopowders, nanostructures, quantum wells/wires/dots, nanoparticles, etc.).[2] All together requires a better understanding of the role played by confining effects, interfaces and surfaces, defect formation on the optical properties. As a result, there have been strong motivations for the application of new optical characterization techniques using several probes like photons, electrons, ions, and also x-rays. Many studies have been carried out in almost all the fields: photoluminescence, cathodoluminescence, electroluminescence, thermoluminescence, bioluminescence, among others.[3] New optical phenomena in known materials have become possible to observe: induced dichroism, depolarization of luminescence with increasing excitation power, two-photon absorption, luminescence at forbidden transitions, hot luminescence, biexcitonic emissions, electron-hole drops, ultrafast processes, self-focusing of light, non-linear phenomena, etc.[4] The range of luminescent compounds has been also broadened owing to the production of complex systems, and often, materials that do not exist in nature at all, i.e., artificial atoms, biomolecular electronic compounds, quantum structures, stressed layers and superlattices.[1]

However, there are still new light detection strategies to overtake the next generation of advanced optical devices. In the present work, we propose a new experimental approach based on the simultaneous application of different non-destructive techniques at the hard X-ray microprobe of the European Synchrotron Radiation Facility (ESRF).[5] This alternative system is designed for parallel collection of multiple signals: scanning μ-X-ray fluorescence, X-ray absorption spectroscopy (XANES/EXAFS) and scanning μ-X ray-dispersive photoluminescence. The synchronous detection of different emission processes on the sub-micron scale provides valuable insights into the elemental composition of the crystal lattices and defects contained within the nanostructures.[6] Accordingly, a mini-cryostat has been specially designed with optimal optical access, broad temperature range (11-300 K), excellent thermal stability ($\Delta T/T \leq 2.3 \times 10^{-2}$ at 12 K) and extremely short working distances (4.5 mm).[7] Given the ID22 beamline capabilities with achromatic micro-focusing optics (up to 18 keV), multi-element Si(Li) detector and high photon flux (10^9 - 10^{12} ph/s), a wide range of excitation/relaxation pathways could be explored and a few elemental monolayers probed. We have applied this new technique to the optical study of molecular beam epitaxy (MBE) grown heterostructures: InAs quantum wires (1.6 ML thick) on (001) InP substrates and InGaAsSb quantum dots (2.5 ML thick) on (001) GaAs substrates. Their luminescence, basically in the near IR optical range, presents astonishing properties due to quantum size effects, which potential applications in optical fiber telecommunications or as single photon emitters or resonant tunneling structures for high-frequency. By exciting with the X-ray microbeam we are able to collect not only quantum luminescence but also optical signal from the barrier material and substrate. Through the latter, no heating induced by higher X-ray photon flux is

observed on the different samples. In fluorescence detection mode, EXAFS spectra from the InAs quantum wires at the As K-edge are detected with orientation-selective excitation (the electric field vector of the synchrotron radiation parallel and perpendicular to the quantum wires).

In summary, the development of the X-ray excited optical luminescence technique within the framework of the hard X-ray microprobe offers unique and complementary information on the short/long-range order and electronic structure of crystalline nanostructures directly involved in the light emission processes. In contrast to conventional XANES and EXAFS analyses, we will be not only element selective but also site selective since the wavelength of the luminescence may depend on the elemental local environment. By measuring in both fluorescence and luminescence yield modes at the same time, different sample depths can be probed due to the shorter attenuation length of the visible photons.

References:

[1] *Handbook of luminescence, display materials and devices,* ed. by Hari Singh Nalwa, Lauren Shea Rohwer (American Scientific Publisher, 2003).
[2] *Optical Materials,* ed. by Joseph Simmons, Kelly S. Potter (Academic Press, 2000).
[3] *Luminescence of Solids,* ed. by D. R. Vij (Plenum Press, 1998).
[4] *Advanced Luminescent Materials and Quantum Confinement,* ed. by M. Cahay, J. P. Leburton, David J. Lockwood, S. Bandyopadhyay, N. Koshida, M. Zacharias (Electrochemical Society, 2002).
[5] A. Somogyi, R. Tucoulou, G. Martinez-Criado, A. Homs, J. Cauzid, P. Bleuet, S. Bohic, A. Simionovici, J. Synchrotron Rad., **12** (2005) 208.
[6] G. Martinez-Criado, C. R. Miskys, A. Cros, O. Ambacher, A. Cantarero, M. Stutzmann, J. Appl. Phys., **90** (2001) 5627.
[7] R. Steinmann, P. Van der Linden, *Miniature Continuous Flow Helium Cryostat*, Proceedings of the International Workshop on Mechanical Engineering Design of Synchrotron Radiation Equipment and Instrumentation 2006, Egret Himeji, Japan (to be published).

SYNTHESIS AND CHARACTERIZATION OF POLYMER-EMBEDDED $CoPt_3$ NANOPARTICLES FOR BIOANALYTICAL APPLICATIONS

Manuel A. Martins[1], Márcia C. Neves[1], Ana Catarina C. Esteves[1], Penka I. Girginova[1], António J. Guiomar[2], Vítor S. Amaral[3] and Tito Trindade[1]

[1]Department of Chemistry, CICECO, University of Aveiro, 3810-193 Aveiro, Portugal
[2]Department of Biochemistry, FCT, University of Coimbra, 3001-401 Coimbra, Portugal
[3]Department of Physics, CICECO, University of Aveiro, 3810-193 Aveiro, Portugal
msilva@dq.ua.pt

The recent developments in the synthesis and characterization of nanomaterials afforded new means to produce functional nanoparticles, at a size scale comparable to those of important biological systems. These functional nanostructures are expected to have a great impact in medicine. For example, there has been great interest in magnetic nanoparticles for biomedical applications which include magnetic cell separation and labelling, drug targeting, hyperthermia treatments and magnetic resonance imaging agents [1].

For biological applications however, the use of magnetic nanoparticles produced by colloidal routes is limited by their lack of biocompatibility. To overcome this drawback, different surface modification strategies have been developed. The most popular is the encapsulation of magnetic nanoparticles in a protective shell, which can be inorganic (e.g. silica) [2] or organic (e.g. polymer) [3]. The protective shell also enables further surface modifications and protects from particle aggregation and nonspecific binding to the cells. Polymer based magnetic nanoparticles seemed especially versatile materials since they can be tailor to fulfill the requisites of biocompatibility and biofunctionality, necessary for medical applications [4].

We have been interested in investigating strategies to develop colloidal systems for bioanalytical applications, including the magnetic separation of cells. Our previous studies showed that hydrophobic inorganic nanoparticles can be embedded in polymer matrices using the miniemulsion polymerization technique [5]. This led us now to investigate in more detail the preparation of organically capped magnetic nanoparticles (e.g. $CoPt_3$).

Here we present our results concerning magnetic functionalized latexes prepared by the encapsulation of organically capped $CoPt_3$ magnetic nanoparticles via *in situ* radical miniemulsion polymerization of *tert*-butyl acrylate (*t*BA) (Figure 1-1). The magnetic $CoPt_3$/P(*t*BA) nanocomposites contain surface protected polyester groups that can be readily removed by hydrolysis, rendering the surface with carboxylic functionalities to improve aqueous stability and to promote bioconjugation. As a proof of concept, the bioconjugation of antibodies to the nanoparticles surfaces have been demonstrated (Figure 1-2) and the application of this strategy to other bio-functional nanomaterials will be discussed.

This work was funded by the University of Aveiro (Project 3.64.33.7/NANOENG/CTS15). We also thank the assistance provided by Dr A. Barros-Timmons (UA) in the polymerization work.

Figure

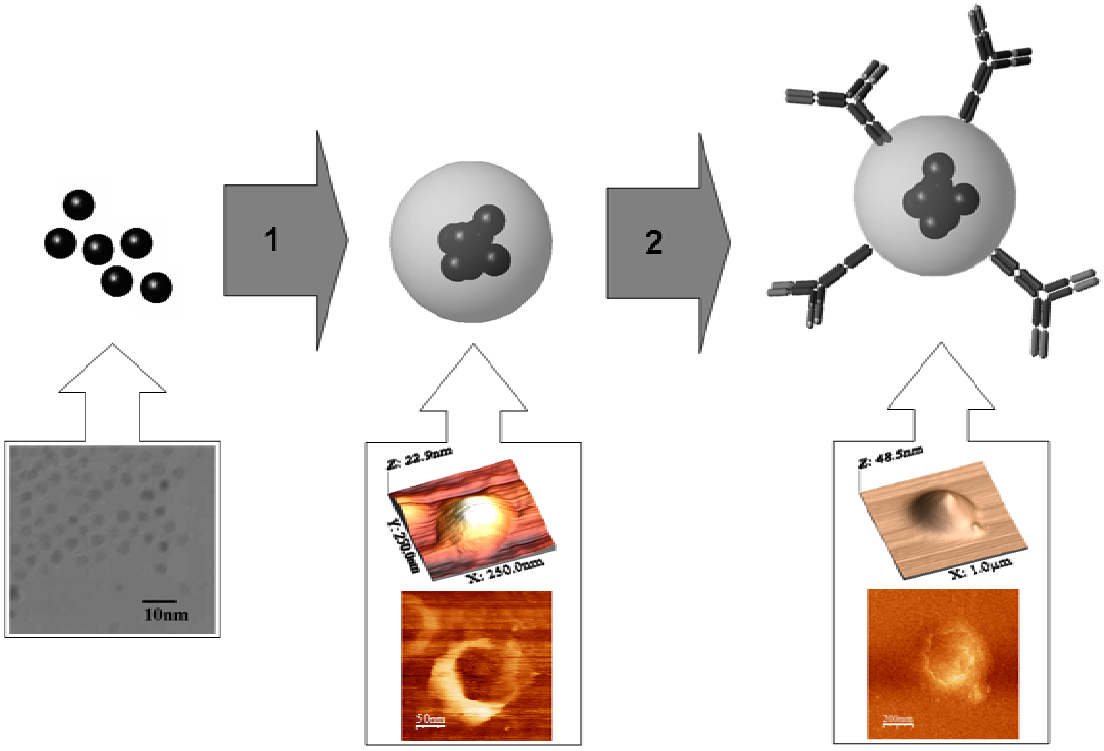


Figure 1. Surface modification of magnetic nanoparticles and antibody conjugation: 1) the organically capped $CoPt_3$ nanoparticles were encapsulated into P*t*BA; 2) the surface polyester groups of P*t*BA were removed by hydrolysis to produce surface carboxylic groups which were used to anchor antibodies. (a) TEM image of organically capped $CoPt_3$ nanoparticles (b) AFM images of the $CoPt_3$/P*t*BA nanocomposite (topography and phase modes) (c) AFM images of an antibody attached to the surface of a $CoPt_3$/P*t*BA nanoparticle (topography and phase modes).

References

[1] Q. A. Pankhurst, J. Connolly, S. K. Jones and J. Dobson, J. Phys. D: Appl. Phys. **36** (2003) R167.
[2] Y. Kobayashi, M. Horie, M. Konno, B. Rodríguez-González, and L. M. Liz-Marzán, J. Phys. Chem. B **107** (2003) 7420.
[3] A. Elaissari, e-Polymers, **28** (2005) 1.
[4] P. Tartaj; M. P. Morales, S. Veintemillas-Verdaguer, T. González-Carreño, and C. J. Serna, *J. Phys. D: Appl. Phys.* **36** (2003) R182.
[5] A. C. C. Esteves, A. Barros-Timmons, T. Monteiro, and T. Trindade, *J. Nanosci. Nanotech.* **5** (2005) 766.

CHARGE INJECTION MECHANISMS IN MULTIWALLED CARBON NANOTUBES

T. Mélin[1], M. Zdrojek[1,2],T. Heim[3], H. Diesinger[1], W. Gebicki[2], D. Stiévenard[1], L. Adamowicz[2]
1. Institut d'Electronique, de Microélectronique et de Nanotechnologie, CNRS UMR 8520, Avenue Poincaré, F-59652 Villeneuve d'Ascq, France
2. Faculty of Physics, Warsaw University of Technology, Koszykowa 75, 00-661 Warsaw
3. Institut de Recherche Interdisciplinaire, IRI, CNRS FR 2953, c/o IEMN Avenue Poincaré, F-59652 Villeneuve d'Ascq, France

In this talk, we will review charge injection and electric force microscopy (EFM) experiments in carbon nanotubes. Individual single-walled and multi-walled nanotubes are deposited on insulating layers and charged from a biased atomic-force microscopy tip. We will describe the phenomenological behaviors observed upon CNT charging: charge delocalization, charge stability and instability associated with defects points along the nanotube, charge emission to the insulating substrate with enhanced emission patterns at the nanotube cap [1].

The issue which will then be addressed is the charging mechanisms of multiwalled nanotubes. We will dissociate between capacitive charging mechanisms (in which the nanotube is put at the AFM tip bias during the charging, and the charge is stored in the nanotube outer shells), and inner-shell charging associated with intershell tunneling processes.

To do so, we first perform a dedicated analytical modeling of EFM signals in a realistic tip-nanotube-substrate geometry. This extends our previously published work on the modeling of charge states of nanoparticles deposited on conductors [2] by first considering the dielectric layer on which the CNTs are deposited, and then taking into account the one-dimensional character of the charged nanostructure. Results will be compared with three-dimensional finite element numerical calculations.

From the quantitatively measured linear CNT charge densities as a function of the CNT radius, we will then discuss capacitive versus inner-shell charging mechanisms. Cases where the injected charge is mostly stored in the CNT and cases where the observed injected charge is mostly found as emitted from the CNT onto the oxide surface [3] will be presented, and the linear charge densities shown to shown to follow similar variations as a function of the CNT diameter. Linear charge densities will be compared to cylinder-plane capacitance, and analyzed quantitatively.

References:

[1] M. Zdrojek, T. Melin, C. Boyaval, B. Jouault, M. Wozniak, W. Gebicki, A. Huczko, D. Stievenard and L. Adamowicz, Appl. Phys. Lett. **86** 213114 (2005).

[2] T. Mélin, H. Diesinger, D. Deresmes and D. Stiévenard, Physical Review B 69, 035321 (2004).

[3] M. Paillet *et al.*, Phys. Rev. Lett. **94** 186801 (2005) ; M. Zdrojek *et al.*, Phys. Rev. Lett. **96** 039703 (2006); M. Paillet *et al.*, Phys. Rev. Lett. **96** 039704 (2006).

NOVEL HYBRID METHOD FOR THE DYNAMIC PROPERTIES OF AFM CANTILEVERS AND THE CALIBRATION OF THEIR SPRING CONSTANTS

David-A. Mendels[1#], Martin Lowe[1], Alexandre Cuenat[1], Markys G. Cain[1], Elena Vallejo[2], David Ellis[2], François Mendels[3]

1: National Physical Laboratory, Hampton Road, Teddington TW11 0LW, UK
2: IDAC Ltd, Airport House, Purley Way, Croydon CR0 0XZ, UK
3 : Cognoscens, 35 Crs d'Herbouville, 69004 Lyon, F

A hybrid method is introduced for the calibration of the spring constants of atomic force microscopy cantilevers. It is based on the minimisation of the difference between the modelled and experimentally determined full-field displacement maps of the surface of the cantilever in motion at several resonant frequencies. The dynamic mechanical response of the cantilever to periodic motion is measured in vacuum by means of a scanning vibrometer. Given the dimensions of the cantilever, the obtained surface displacements together with analytical or numerical models are used to resolve the physical unknowns of the probe. These are the elastic properties of the cantilever, and the residual stress state built up during the deposition of the reflective coating on the backside of the cantilever. The scanning vibrometry experiment allows the precise determination of the first ten resonant frequencies and the modes associated. After optimisation of the elastic properties and the surface stress, the relative agreement between all resonant frequencies is better than 1% with the finite element model and 2% with the Timoshenko beam equation. The agreement between surface displacements is also excellent when the damping constant of the system has been determined, except for the first lateral mode, which exhibits strong coupling to a reflection of the first torsional mode. Because all the displacements at resonance are known, it is possible to decouple these modes, and the result is shown to compare well with the model. The cantilever being fully characterised (geometry, materials, residual stress state and boundary conditions), it is straightforward to deduce all its spring constants, in the linear and non-linear elastic regimes.

[#] to whom correspondence should be addressed

Poster

ALTERATION OF SUPERCONDUCTIVITY OF SUSPENDED CARBON NANOTUBES BY DEPOSITION OF ORGANIC MOLECULES

M. Ferrier, A. Yu. Kasumov, V. Agache, L. Buchaillot, A-M. Bonnot, C. Naud, V. Bouchiat, R. Deblock, M. Kociak, M. Kobylko, S. Gueron, H. Bouchiat

LPS, Orsay, France
IEMN, Lille
LEPES,Grenoble

We have altered the superconductivity of a suspended rope of single walled carbon nanotubes, by coating it with organic polymers. Upon coating, the normal state resistance of the rope changes by less than 20 percent. But superconductivity, which on the bare rope shows up as a substantial resistance decrease below 300 mK, is gradualy suppressed. We correlate this to the suppression of radial breathing modes, measured with Raman Spectroscopy on suspended Single and Double-walled carbon nanotubes. This points to the breathing phonon modes as being responsible for superconductivity in carbon nanotubes. [1]

References:

[1] *Ferrier et al*, cond-mat/0508518.

Figures:

Poster

SWIFT HEAVY ION INDUCED DISSOLUTION OF GOLD NANOPARTICLES EMBEDDED IN SILICA MATRIX GROWN BY CO-EVAPORATION

Y. K. Mishra[1]*, D. Kabiraj[1], J. C. Pivin[2] and D. K. Avasthi[1]

[1]Inter University Accelerator Centre, Post Box No. 10502, New Delhi 110067, India.

[2]CSNSM, IN2P3-CNRS, Batiment 108, F-91405, Orsay Campus, France

ykmishra@nsc.res.in

Abstract: Gold nanoparticles embedded in silica matrix (~100nm) that were prepared by co-evaporation technique. After deposition, the samples were annealed at different temperatures in inert environment for 30 minutes. UV visible absorption measurements of as-deposited and annealed samples were performed. No signature of nanoparticle formation was found in case of as deposited 10 atomic % Au in silica, whereas signature of nanoparticles was evident by SPR peak at ~ 520 nm in the case of as-deposited 20 atomic % Au in silica. Decrease in full width at half maximum (FWHM) in the absorption spectra with increase in annealing temperature indicated the agglomeration of Au nanoparticles. The size of nanoparticles was estimated using Fermi velocity formula. The annealed films were irradiated with 100MeV Ag ions at different fluences. UV-visible absorption measurements of pristine and irradiated films showed a clear signature of dissolution with ion flux. Rutherford Backscattering (RBS) spectrometry was used for quantification of gold. X-ray diffraction (XRD) measurements showed that Au nanoparticles are in face centred cubic (FCC) face.

NANO SIZED COPPER CLAY BASED HYBRID MATERIALS

Nirendra M. Misra and Tanushree Choudhury

Indian School of Mines, Department of Applied Chemistry, Dhanbad, INDIA

nirendra_m@hotmail.com

Properties of hybrid inorganic-organic materials depend to a great extent on the dispersion and interaction of the inorganic material with the organic matrix. The present work is aimed to prepare an antibacterial composite materials using clay. Cu-montmorillonite based material functionalised by sol-gel process using Ti-isopropoxide as precuror. Exfoliation of clay has been attempted using natural dispersants. The material was characterized using SEM, DSC, XRD and FTIR. SEM results, fig. 1, indicate formation of microstructure in the case of Cu-montmorillonite functionalised by sol-gel process when compared to Cu-montmorillonite using natural dispersant. These functionalised materials have a promising future in protective coatings and water purifiers.

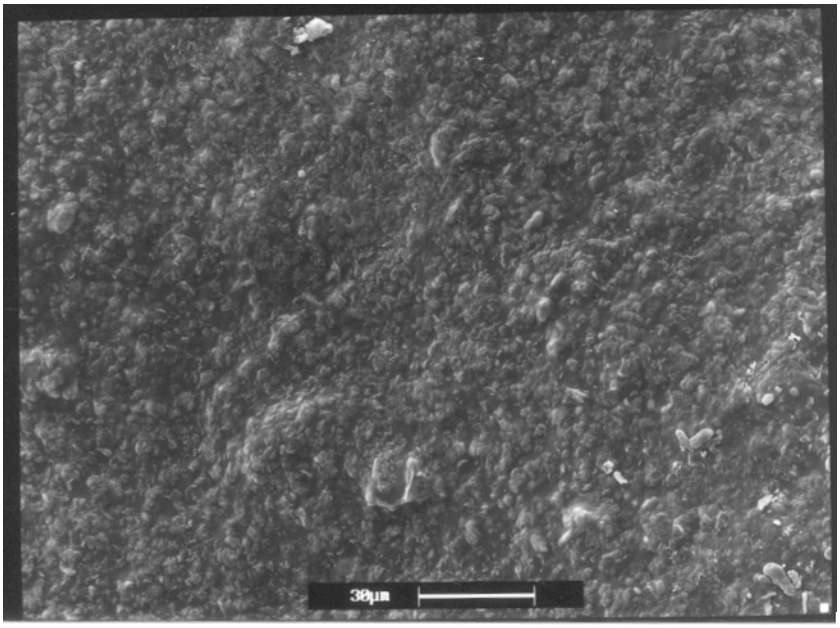


Fig. 1 SEM of Cu-clay functionalised with Ti-isopropoxide

Reference:
[1] Gomez-Romero, Pedro and Sanchez, Clement (eds.), *Functional Hybrid Materials*, Wiley-VCH, Germany, 2004
[2] Nassar, E.J., Neri, C.R., Calefi, P.S., Serrra, O.A., Functionalised silica synthesized by sol-gel process, Journal of Non-Crystalline Solids, 1999, 247, pp. 124-128.

ADSORPTION SITE-DEPENDENT DIFFUSION OF AZOBENZENE ON Cu(110)

J.A. Miwa[1], S. Weigelt[2], H. Gersen[2], F. Besenbacher[2], F. Rosei[1], T.R. Linderoth[2]
[1]Institut National de la Recherche Scientifique – Énergie, Matériaux et Télécommunications, Université du Québec, Varennes, Quebec, Canada, J3X 1S2
[2]Interdisciplinary Nanoscience Center and Department of Physics & Astronomy, University of Aarhus, DK-8000 C Aarhus, Denmark
miwaj@emt.inrs.ca

The adsorption of molecules on surfaces plays an important role in bottom-up nano-fabrication. It is therefore essential to understand the influence of the surface on fundamental chemical processes, such as conformational changes and reactions [1]. Studies of azobenzene and derivatives thereof are particularly interesting for nano-electronics since these molecules are considered as model-systems for molecular switches, based on light induced reversible *trans-cis* isomerizations. However, the study of these prototypical molecules under well-defined ultra-high vacuum (UHV) conditions are only just emerging [2-4]. These findings could greatly enhance our knowledge on the transferability of the switching properties that these single molecules undergo when adsorbed at surfaces.

Here we present our recent findings on the adsorption site dependent diffusion of azobenzene on the Cu(110) surface [2]. The *trans*-isomer was observed and found to occupy two adsorption geometries – an energetically stable and a metastable state. We show for the first time that the *trans*-isomer spontaneously adopts a metastable adsorption geometry. Diffusion occurred along the closed-packed direction of the surface and the diffusivity for the two adsorption states was found to differ by approximately one order of magnitude.

Moreover, our results demonstrate a moderately strong molecule-surface interaction [3] in this system, suggesting that the copper surface could be a highly relevant substrate for future studies into the photo-isomerization of adsorbed azobenzene.

References:

[1] R. Otero, F. Rosei, F. Besenbacher, Ann. Rev. Phys. Chem. **57** (2006) 17.1.
[2] J.A. Miwa, S. Weigelt, H. Gersen, F. Besenbacher, F. Rosei, T. R. Linderoth, J. Am. Chem. Soc. **128** (2006) 3164.
[3] A. Kirakosian, M.J. Comstock, J. Cho, M.F. Crommie, Phys. Rev. B. **71** (2005) 113409-1.
[4] J. Henzl, M. Mehlhorn, H. Gawronski, K.-H. Rieder, K. Morgenstern, Angew. Chem. Int. Ed. **45** (2006) 603.

Figures:

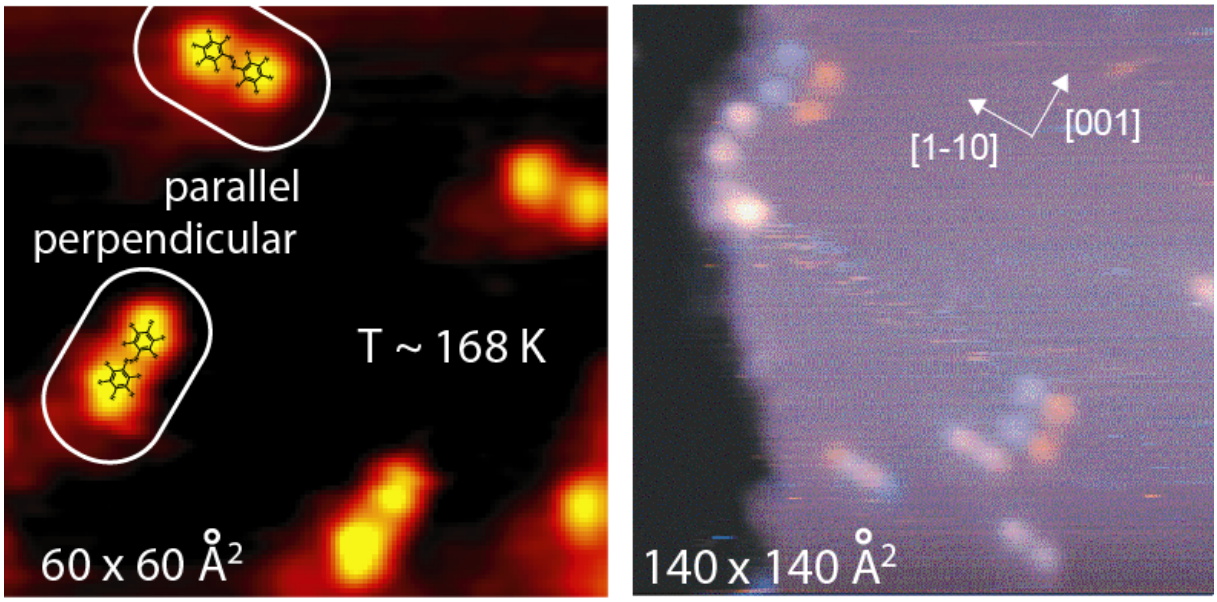


Figure 1 Both the energetically stable (parallel) and metastable (perpendicular) adsorption geometries of azobenzene (left) are shown. Two time-lapsed superimposed STM images demonstrate diffusion of both adsorbed species along the [1-10] direction (right).

MELTING BEHAVIOR OF GaN NANOWIRES : MOLECULAR DYNAMICS STUDY

Won Ha Moon, Hyun Jun Kim, Chang Hwan Choi
Samsung Electro-Mechanics Co., LTD, Suwon, Korea
wonha.mun@samsung.com

GaN is a promising semiconductor material that exhibits many outstanding physical and chemical properties in high-temperature, high-power, and high-frequency devices. One-dimensional GaN nanowires have also attracted much interest due to their significant potential for nanoscale electronics. Recently, many experimental investigations have been reported for the synthesis and the physical property of GaN nanowires [1,2]. In this paper, we investigate the structure and the melting behaviour of hexagonal GaN nanowires using the molecular dynamics (MD) simulations based on the Stillinger-Weber potential for GaN [3].

We first calculate the optimized structure of hexagonal GaN nanowires with the [0001] growth direction. Figure 1 shows the optimized structure of the GaN nanowire with the diameter of 28.67 Å. The hexagonal GaN nanowires are enclosed by six side (10-10) facets, shown in Fig. 1 (b). Figure 2 shows the cohesive energy of GaN nanowires as a function of diameter. As expected, the cohesive energy of GaN nanowire decreases as $1/D^2$ (D is the nanowire diameter) with increasing diameter.

The melting behavior of GaN nanowires is also investgated. We calculate the variation of the cohesive energy of GaN nanowires as the temperature is increased. The overall melting temperatures of GaN nanowires are much lower than that of bulk GaN and increase when the diameters of the nanowires are increased. These results are agreement with the trend for other nanowires.

To our knowledge, MD simulations for GaN nanowires using the empirical potential have not been reported so far. These theoretical calculations will provide considerable information about the possibility of GaN nanowires.

References

[1] J. C. Jhonson et al., Nature Mater., **1** (2002) 106.
[2] C. Y. Nam et al., Nano Lett., **6** (2006) 153.
[3] A. Bere and A. Serra, Phys. Rev. B, **65** (2002) 205323.

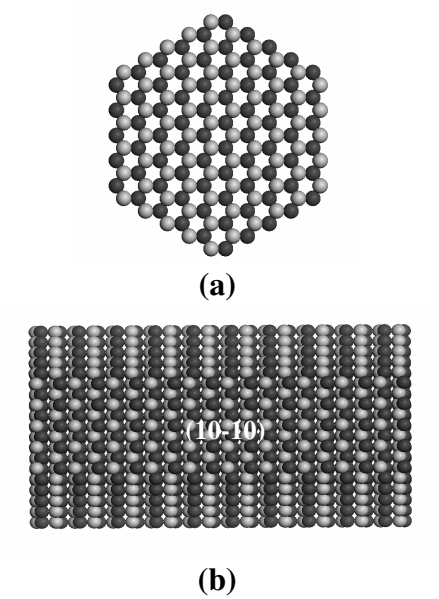


Figure 1. Optimized stuructre of GaN nanowire with the diameter of 28.67 Å. (a) Top view along the [0001] growth orientation. (b) Side view

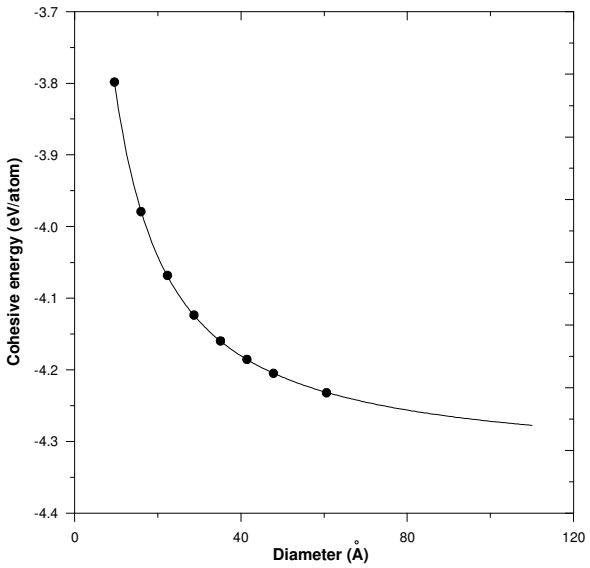


Figure 2. Cohesive energy of GaN nanowires as a function of diameter. The solid line is obtained by the least squares fit of data.

THE BIOCOMPATIBILITY MICROORGANISMS-CARBON NANOSTRUCTURES FOR APPLICATIONS IN MICROBIAL FUEL CELLS

Adina Morozan, L. Stamatin[*], F. Nastase, A. Dumitru, S. Vulpe, C. Nastase and I. Stamatin
3 Nano-SAE Research Centre, University of Bucharest, P.O. Box MG-38, 077125, Bucharest-Magurele, Romania
[*]Longhin Scarlat Hospital, Microbiology Laboratory, Serban Voda 94, Bucharest, Romania
adina.morozan@gmail.com

In the broadest sense, biofuel cells would be defined as devices capable of directly transforming chemical to electrical energy via electrochemical reactions involving biochemical pathways. Biocatalysts, either protein, enzyme or whole organism, can also offer cost advantages over metallic catalysts, although this is not likely to be the case until the consumption of the enzyme is sufficient to merit large scale production. For long time, biofuel cells have been under research eye either as a curiosity but have recently reborn due to a series of bizarre applications already devised for future decades. Their study will enlarge our knowledge of the electrochemistry of the human body - where micro and nano microbial fuel cells (MFCs) can work in a cooperative way. A microbial fuel cell mimics a biological system which can be viable for sustained time. When incorporated into a MFC design, a colony of microorganisms nicely solves the hydrogen supply problem. Current efforts to improve the efficiency of such fuel cells are limited by the lack of knowledge about the microbial ecology of these systems: (i) to elucidate whether a bacterial community, either suspended or attached to an electrode, can evolve in a microbial fuel cell to bring about higher power output, and (ii) to identify species responsible for the electricity generation [1, 2]. Likewise, the need to have the highest conductivity and active surface area for carbon electrodes, combined with biocompatibility for working microorganisms in MFCs is one of biggest challenges for these devices. Thus, power generation depends of microorganisms and, biologically the potential losses can be resolved by the selection of adapted bacteria.

In this context, the study of the interaction between the carbon nanostructures and the biological systems represents a new and interesting research domain of bionanotechnology to the investigation of the process of growing for microorganisms. Fluorescent probe have been widely used to study the complexity of biological interactions in a variety of media. A new demand in bio-labeling is to be able to measure many biological indicators simultaneously in live cells. Quantum dots (QDs), by their unique light emitting properties are starting to attract considerable attention as novel luminescent probes [3, 4].

This work is focused on the evaluation of biocompatibility of *Escherichia coli* and *Staphylococcus aureus* with different species of nanocarbons in terms of their incorporation into a MFC anodic design. Thus, some types of bionanocomposites (BNC) were designed. The fluorescent QDs are used for labeling and rapid identification for colonies developed. The preliminary results entry by testing of nanocarbon with turbostratic structure synthesized by laser pyrolysis, in terms of biocompatibility with *Staphylococcus aureus* (Figure 1 shows optical microscopy for colonies developed on bionanocomposites with this type of nanocarbon), prove the prospective experiments with different types of CNTs from SWNT to MWNT with various morphologies and structures synthesized by the novolac pyrolysis with different adds of ferrocene.

Novolac (phenol-formaldehyde condensation resin) is one of the good graphene source giving pyrolysis structures with different aspects. The carbon nanotubes resulted in this systems have thick walls with large variation in the inner diameter, with relatively small defects, ropes and disordered carbon (Figure 2). Electrodes of carbon foam based on nanotubes resulted from polymer pyrolysis with ferrocene should be used with good results in MFC, being very well known that one of the major areas of CNT research is the field of

biosensors, biomedical materials and devices [5, 6]. Also, our CNTs were used before and after purification to investigate and the role of iron content in microorganisms' growing.

References:

[1]. K. Rabaey, N. Boon, S. D. Siciliano, M. Verhaege, W. Verstraete, Applied and Environmental Microbiology, 70 (9) (2004) 5373–5382
[2]. K. Rabaey, W. Verstraete, Trends in Biotechnology, 23 (6) (2005) 291-298
[3]. S. Ravindran, S. Kim, R. Martin, E.M. Lord, C.S. Ozkan, Nanotechnology, 16 (2005) 1-4.
[4]. A. J. Sutherland, Current Opinion in Solid State and Materials Science, 6 (2002) 365-370.
[5]. S.K. Smart, A.I. Cassady, G.Q. Lu, D.J. Martin, Carbon, 44 (2006) 1034–1047
[6] Y. Lin, S. Taylor, H. Li, S.K.A. Fernando, L. Qu, W. Wang et al., J. Mater. Chem., 14(4) (2004) 527–41

Figures:

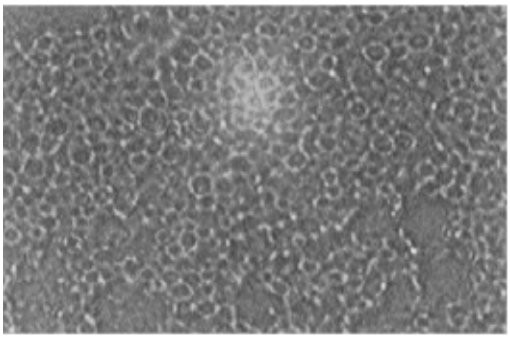


Figure 1. BNC with *Staphylococcus aureus*

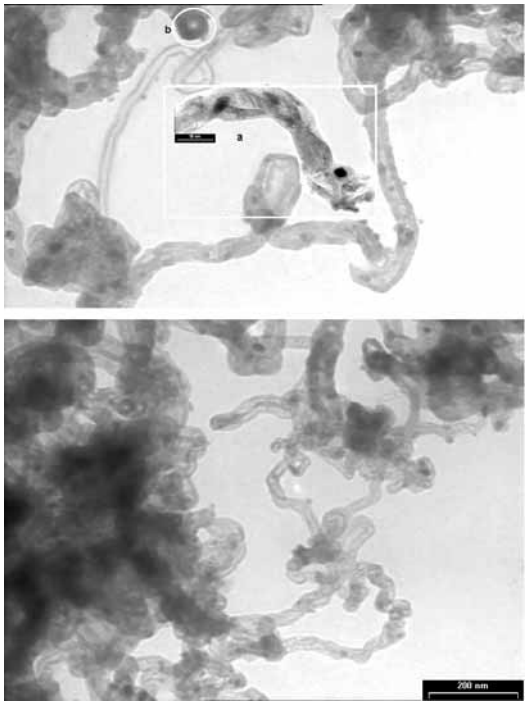


Figure 2. TEM image of a large amount of nanotubes and ropes random intercalated: in (a) is shown the rope morphology and in (b) a Fe_3C nanoparticle ending a nanotube.

ELECTROSPINNING OF FIBRINOGEN NANOFIBERS

Tatjana Morton[1], Lila Nikkola[2], Nurredin Ashammakhi[2], Martijn van Griensven[1], Heinz Redl[1]
[1]Ludwig Boltzmann Institute for Experimental and Clinical Traumatology, Vienna, Austria
[2]Tampere University of Technology, Institut of Biomaterials, Tampere, Finland
nureddin.ashammakhi@tut.fi

Electrospinning has been recognized as an efficient technique for the fabrication of polymer nanofibers. It uses an eletric field to control the deposition of polymer fibers onto a target substrate. This electrostatic processing strategy can be used to fabricate fibrous polymer mats composed of fiber diameter mostly between 100 nm and 3 µm. In this study we describe electrospinning of fibrinogen nanofibers in an attempt to create biomimicking tissue in vitro for use as a tissue scaffold.

We have used lyophilized human fibrinogen of the product Tisseel® VH (Baxter AG, Austria) to demonstrate fibrinogen electrospinning. Fibrinogen dissolved in 1,1,1,3,3,3-hexafluoro-2-propanol and sodium chloride solution was eletrospinned under various conditions. Electrospun fibers of fibrionogen were processed for scanning electron microscopy (SEM) evaluation and analyzed by native gelelectrophoresis.

The SEM evaluation showed that formed fibers were flat and had large diameter distribution from 120-1000µm resulting in approximate fiber diameter of 550µm. With some conditions bead formation occurred.

The efficacy of this process, as well as the final fiber product, are affected by many factors, including, but not limited to solution polymer concentration, viscosity of solution, voltage between solution and ground electrode, the distance between the Taylor cone and the ground electrode, and environmental conditions such as humidity and temperature. Nano fiber similarity in size to native extracellular matrix components and the 3-dimensional structure allows cells to attach to several fibers in a more natural geometry. In summary, the electrospinning process is a simple and efficient technique for the fabrication of 3D structures composed of fibrinogen fibers.

CONTROLLED DEPOSITION OF CARBON NANOTUBES BY DIELECTROPHORESIS

S. A. Moshkalev, J. Leon, C. Veríssimo, M. B. de Moraes
CCS, UNICAMP, C.P. 6061, CEP 13083-870, Campinas, SP, Brazil
stanisla@led.unicamp.br

For fabrication of carbon nanotubes (CNTs) based devices, it is necessary to deposit or grow individual CNTs in a controlled way between micro ou nano-electrodes. A number of approaches has been utilized for directional deposition of nanotubes: alingment using a gas flow, deposition using chemical funcionalization with nanotemplates, and electric field assisted growth of CNTs. A relatively simple method is a dielectrophoresis [1], which utilizes a nonhomogeneous electric field, created between two micro-electrodes, which attracts and orients the nanotubes. This method permits deposition of both individual CNTs and films of single or multy-walled nanotubes (SWNTs and MWNTs) [2, 3].

In the present work, MWNTs with diameters in the range of 10-30nm, lengths of 5-15 μm, and 90% purity were used. Aqueous solution with sodium dodecilsulfate (SDS) as a surfactant was prepared by sonication during 30 minutes. Immediately after the sonication, the suspension was centrifuged at 15000 rpm for 10 minutos, in order to remove big flocs. The MWNTs suspension stabilized in a surfactant had a mass concentration about 0.5-10 μg/ml. A set of 30nm-Ti/70nm-Au (or Pd) thick micro-eletrodes was fabricated for the nanotubes deposition. The metal deposition was made using a lift-off technique and standart optical lithography on *n* type silicon wafers covered by 400 nm thick thermal oxide layers. Distances between the pairs of electrodes were in the range of 3 to 10 μm and the eletrodes width was 10μm. For a dielectrophoresis process, a small (volume of ~1μl) drop of the suspension was put above the region of the inter-eletrode gaps. Then, a signal from a frequency generator with AC peak-to-peak voltage ranging between 2 and 10V and frequency in the range from 10Hz to 10MHz was applied between the electrodes. After the process, a drop was dried softly by a flow of nitrogen. Finally, the samples were washed with deionized water and methanol. The experiments were carried out at a normal temperature and atmospheric pressure. The nanotubes deposited over the gap were observed by a SEM (JEOL JSM-5410). An eletrical parameters analyser (HP4145B) coupled with a micro-manipulator (Signatore Co. Inc., model 6000) with tungsten probes was used for measurements of the *I-V* characteristics.

Analysis of SEM images of samples with MWNTs deposited between the electrodes under different process conditions (amplitudes and frequencies of the AC field) shows that there is orientation of the deposited tubes along the direction of the field. More intense deposition apparently occurs at the corners of the electrodes where the field is less uniform. The powered electrode attracts more nanotubes that the grounded one. It is important to note that the degree of orientation and the deposition density strongly depend on the frequency and on the amplitude of the field applied. For

higher frequencies the degree of orientation is much higher. For the same frequency, the higher is the AC amplitude, the more intense deposition is observed. For very low frequencies (10 Hz), the deposition is relatively weak and the tubes are not oriented. Some observations also indicate that nanoparticles (originated from contaminations) are deposited more under low frequency conditions. The alignment of the tubes can be attributed to the electrical polarization induced in the tubes by the field. If the electric field is not uniform, its interaction with the induced dipole results in a force, which is different for two ends of the alongated object, thus moving the particle. For the case of AC field, the alternating of the field direction is accompanied by the alternating of the dipole direction so that the force (and the net movement) direction does not change. Due to a structural anisotropy of the nanotubes, the dipolar moment induced along the tube axis is much stronger than that in the perpendicular direction. This results in a preferential orientation and movement of the nanotubes along the field direction. On the other hand, the impurity particles present in a solution have more isotropic dipole moments and thus respond more slowly to the AC field than the nanotubes.

Characteristics I-V measured for the samples deposited under different conditions, just after the process, show that lower resistivities are achieved for higher frequencies and high AC amplitudes. The resistivities were measured to range from 100KΩ to 3MΩ and from a few KΩ to 1MΩ for the V_{p-p} = 2 and 10 V, respectively. The lower resistivities obtained for higher frequencies are likely due to higher degree of the nanotube orientation. The I-V curves show basically the metallic behavior of the nanotubes used in the experiment. For longer depositions, denser films of nanotubes were obtained. With a dilution of a suspension, it is possible to deposit a few or individual nanotubes. For the lowest concentration of MWNTs used here (0.5μg/ml), the current through the gap was less than 1 μA. At low voltages, the curves show non-linear behavior probably due to high resistance of the contact nanotube-metal. For higher density of the deposition, linearization of the I-V curves is observed.

In order to obtain better contacts between CNTs and metal electrodes, two methods of additional metal deposition above the CNTs/electrodes have been used. The first method employes liquid metal Ga, which expands over the electrodes under elevated temperature coinditions and finally covers the nanotubes. This process is performed at temperatures of 150° C in an inert atmosphere. The second method employs the electroless deposition. Both methods proved to be useful for fabrication of the CNT-based devices. Detailed comparison of the methods will be presented.

References:

[1] R. Krupke, F. Hennrich, H.B. Weber, D. Beckmann, O. Hampe, S. Malik, M.M Kappes, H.V. Löhneysen, Appl. Phys. A **76** (2003) 397.
[2] M. Dimaki, P Boggild, Nanotechnology 16 (2005) 759.
[3] R.H.M. Chan, C.K.M. Fung, W.J. Li, Nanotechnology 15 (2004) S672

SYNTHESIS OF Si/SiGe NANOWIRES FOR APPLICATION IN THERMOELECTRIC SYSTEMS

MOUCHET Céline, Emmanuelle ROUVIERE, Marc PLISSONNIER, Frederic GAILLARD
CEA Grenoble DRT/LITEN/DTNM/LCH,
17 rue des Martyrs, 38054 GRENOBLE Cedex 9, France
celine.mouchet@cea.fr

Miniaturized electronics systems are more and more used in the new technological objects both in civil and military fields (Micro drones, biological sensors, micro-electro-mechanical systems (MEMS), power suppliers…). Thermoelectric microgenerators supply electric energy for microsystems from thermal energy conversion. Thermoelectric converters are light, reliable and wireless. So, they are a good alternative to micro-batteries, micro fuel cells and micro-turbines and give the advantage to use a renewable energy. The nanowires-based thermoelectric generators will address energy needs of wireless microsystems. They should also solve thermal problems in microelectronics (solution to low thermal dissipation in chips vias). [1]

Efficient energy converters are based on Peltier effect for cooling and Seebeck effect for energy production. Materials with high Seebeck coefficient, high electric conductivity and low thermal conductivity are required. Theoretical [2] and experimental studies [3] evidenced that nanowires and nanostructured materials as superlattices have a high potential in thermoelectricity. The use of those materials increases ZT value, the factor of merit which characterizes a thermoelectric material, and consequently, increases the converter efficiency. This augmentation results from two physical phenomena: high phonons scattering in superlattices interfaces which lowers the thermal conductivity, and charge carrier confinement, which modifies transport properties. Thanks to their structures, Si/SiGe multi-layers nanowires take advantage of the two physical phenomena.

The aim of the study is to use chemical vapor deposition technique to perform Si/SiGe nanowires for high efficiency thermoelectric converters (>10%). Silane and germane gases are decomposed in a thermal CVD reactor. N type or p type nanowires are obtained by mixing dopant gas with precursor gas. Si and SiGe nanowires have been first synthesized before to carry out Si/SiGe multi-layers nanowires. In thermal CVD, silicon nanowires growth is attributed to the VLS mechanism (Vapor-Liquid-Solid) developed by Wagner in 1964 [4]. For each nanowires type, a accurate morphological study is done thanks to SEM (Scanning Electron Microscopy). A growth parametric study will be perform in order to investigate the influence of each parameter on growth and to obtain specific nanowires for thermoelectric measures.

Acknowledgments: This work is supported by DGA, French general delegation for army, of French defense ministry under a PhD grant from october 2005 to september 2008.

References:

[1]: F. J. DISALVO, Thermoelectric cooling and power generation, *Science, 1999, 285 (5428), 703-706*
[2]: L. D. HICKS, M. S. DRESSELHAUS, Thermoelectric figure of merit of a one-dimensional conductor, *Physical review B, 1993, Vol.47, N°24, 16631-16634*
[3]: R. VENKATASUBRAMANIAN, Thin-film thermoelectric devices with high room-temperature figures of merit, *Nature, 2001, Vol.413, 597-602*
[4]: R. S. WAGNER, Vapor-liquid-solid mechanism of single crystal growth, *Applied physics lett., 1964, Vol 4, N° 5, 89-90*

Figures:

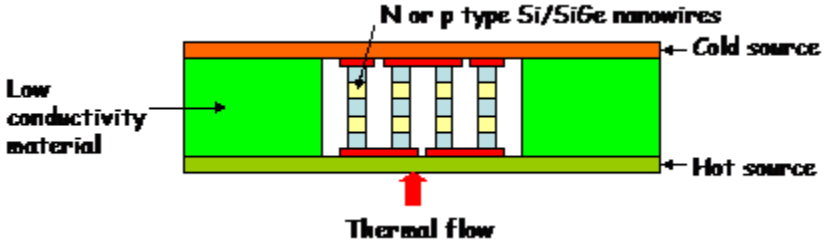


Figure 1: Concept of thermogenerator

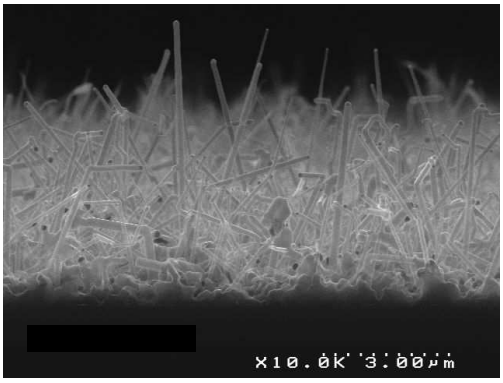


Figure 2: Silicon nanowires made in CVD reactor

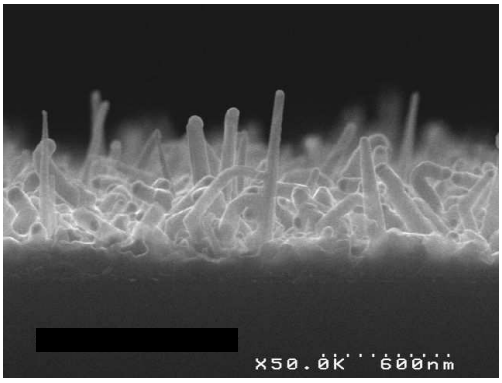


Figure 3: SiGe nanowires made in CVD reactor

Simple Route for Intermatrix Synthesis of Polymer Stabilized Core-Shell Metal Nanoparticles for Sensor Applications

D.N. Muraviev, J. Macanás, M.J. Esplandiu, M. Farre, M. Muñoz and S. Alegret
Analytical Chemistry Division, Department of Chemistry, Autonomous University of Barcelona, 08193 Bellaterra, Barcelona, Spain.
Dimitri.Muraviev@uab.es

The use of nanometer-sized metal particles (MNP) in sensor and biosensor construction can substantially improve their performance and therefore increase their applications in clinical, biomedical, and environmental research fields. MNP are objects of great interest in the modern chemical research due to their unique physical and chemical properties, which are distinct from both those of the bulk metal and those of isolated atoms and molecules. The main drawback of MNP is their high trend for aggregation. Without stabilization MNP fuse together, losing their special shape and properties. The development of Polymer-Stabilized MNP (PSMNP) is considered to be one of the most promising solutions to the MNP stability problem [1]. In many instances the sensor and biosensor constructions are based on the use of noble MNP as sensing element due to their unique electrocatalytic properties. One of the most important problems in this case is the decrease of the noble metal loading without dramatic change of the performance of sensing element. One of the possible solution of this problem is the use of core-shell PSMNP, which are composed of a cheap metal core covered with a thin noble metal shell.

In this presentation we report the novel simple route for the inter-matrix synthesis and characterization of PSMNP with core-shell structure. The proposed approach is based on the use of functionalized polymeric membranes (FPM) as a nanoreactor for both to synthesize and to characterize the composition and architecture of PSMNP. The desired functionalization is achieved by the chemical grafting of functional groups to the polymeric matrix or by using the physical immobilization of metal-selective extractants inside the polymer. The optimal degree of functionalization provides, on one hand, insolubility of the polymer in water and, on the other hand, its solubility in some organic solvents (e.g., DMF). Due to the presence of functional groups, the polymer matrix is able to chemically fix metal ions or complexes (metal loading stage) prior to their reduction, which results in the formation of PSMNP. After metal reduction the functional groups of the functional polymer appear to be prepared for the next metal loading-reduction cycle. The first cycle permits to form the core-PSMNP of desired size, while the second cycle leads to the coverage of pre-shaped core with the second metal forming the shell.

The proposed approach is illustrated by the results obtained by studying the intermatrix synthesis of Cu-Pt and Cu-Pd core-shell PSMNP of different compositions in the sulfonated poly(etherether ketone) (SPEEK) membranes. MNP-containing SPEEK membranes were characterized by SEM, AFM and TEM (see Fig. 1) techniques to evaluate the morphological changes of the membrane structure and to estimate the MNP size.

The core-shell-MNP loaded membranes were also deposited on the surface of graphite-epoxy composite electrodes [2] to study the electrochemical properties of polymer-PSMNP composites and to estimate their applicability in sensor constructions. The electrochemical response of amperomtric sensors has been shown to increase with the loading of the second (shell-forming) metal (see Fig. 2). The preliminary results shown in Fig. 2 demonstrate that the presence of Pt@Cu-PSMNC inside the membrane not only substantially improves the

electric conductivity of the polymer, but also testifies to manifestation of clearly pronounced strong electrocatalytic activity of Pt@Cu-PSMNC towards analyte under study (H_2O_2).

References:

[1] A.D. Pomogailo. Uspekhi Khimii (Russ. Chem. Rev.), **66** (1997) 679.
[2] A.D. Pomogailo, G.I. Dzhardimalieva, A.S. Rozenberg, D. Muraviev, J. Nanoparticle Res., **5** (2003) 497.
[3] F. Cespedes, E. Martinez-Fabregas, S. Alegret. Trends Anal. Chem., **15** (1996) 296.

Figures:

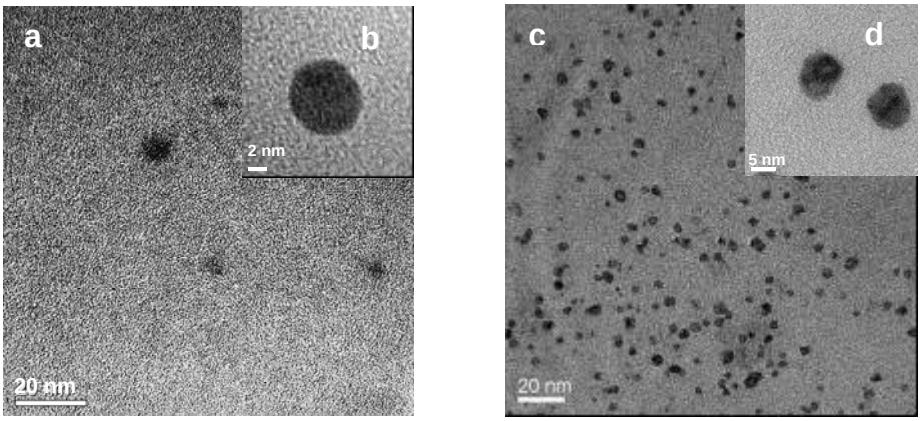


Figure 1. Typical TEM (a, c) and HRTEM (b, d) images of Cu-core PSMNP (a, b) and Pt@Cu-core-shell PSMNP (c, d) for sample with platinum loading of 45 mg/g of initial SPEEK membrane. Diameters of both Cu- and Pt@Cu-PSMNP lie within 5-7 nm range and particles demonstrate quite narrow size distribution.

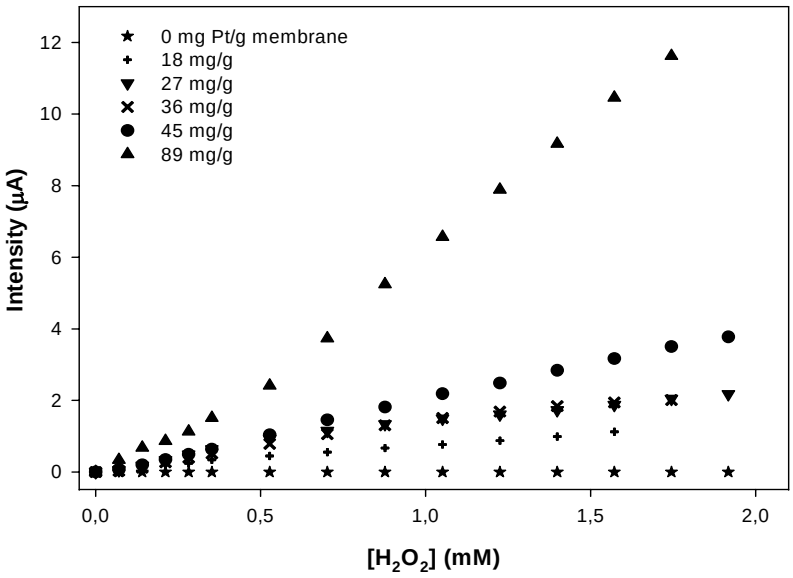


Figure 2. Calibration curves of amperometric sensors prepared by modification of graphite-epoxy composite electrodes with Pt@Cu-PSMNP-SPEEK membranes at different values of platinum loading. Conditions: potential: -250 mV; 0.1 M KCl in 0.1 M acetate buffer, pH = 7.0.

ELECTROSPUN BIODEGRADABLE NANOFIBERS AS A TISSUE ENGINEERING CANDIDATE

[1]A Ndreu, [2]L Nikkola, H Ylikauppila[2], N Ashammakhi, [1]V Hasırcı

[1]BIOMAT, Middle East Technical University, Department of Biological Sciences, Biotechnology Research Unit, Ankara 06531, Turkey
[2]Institute of Biomaterials, Tampere University of Technology, Tampere, Finland
nureddin.ashammakhi@tut.fi

Tissue engineering is an outgrowth of the biomaterials field and involves producing tissue substitutes from a combination of biodegradable polymers and cells specific for the tissue whose structural characteristics and function need to be restored. The most challenging step in tissue engineering is the design of an appropriate scaffold that would mimic both biological functions and structure of natural extracellular matrix (ECM). Since ECM components are in nanometer range, design of scaffolds in this range has become more attractive in the last decade. Scaffolds can be prepared in the film, foam or fibrous forms. It has been observed that cells attach and organize well on fibers with a diameter smaller than that of cells. A variety of processes have been utilized to manufacture nanofibers. In electrospinning process, a high voltage is applied to a polymeric solution and as the voltage overcomes the surface tension of the solution, fibers are ejected in the form of a jet. This process needs to be optimized in order to obtain an appropriate scaffold that can enhance adhesion, and proliferation of cells. The aim of the present study is to construct a nanofibrous scaffold of a biological polyester with the ultimate aim of using it as a tissue engineering scaffold.

Different concentrations of biodegradable poly(3-hydroxy butyrate-co-3-hydroxy valerate) (PHBV8), containing 8% of 3-hydroxyvalerate, and its four blends were prepared in chloroform or a 96:4 mixture of chloroform/N,N-dimethyl formamide (DMF) to investigate the influence of solvent, concentration, and polymer type on the properties of the nanofiber formed. Parameters such as solution concentration, voltage, distance from collector to syringe tip and the effect of some BTEAC salt on fiber structure and morphology were also studied. The resultant nano- and microfibers were collected onto a metal substrate as an interconnected, non-woven mat. Alignment of fibers was also attempted using a rotating collector in place of the static plate collector. The morphology of the electrospun fibers was studied by Scanning Electron Microscopy (SEM) and their diameter was measured via an Image J analyzer program.

SEM analysis demonstrated that increase in solution concentration results in an increase in fiber diameter and a change in bead formation and shape. Addition of salt resulted in bead-free fibers but in this case some fiber fusion occurred due to decreased solvent evaporation. Furthermore, addition of a solvent with a higher dielectric constant (DMF) to chloroform improved the electrospinning conditions and more uniform, bead-free nano- and microfibers were obtained. Fiber diameters ranged from 284 nm to 2.2 μm depending on the conditions used. Diameter of the aligned fiber was not significantly different than the random ones.

It was possible to produce nano- and microfibers using PHBV8 and its blends. Conductivity of the polymer solution was an important parameter and it was improved by addition of DMF as solvent. All blends showed varying fiber structure and morphologies. Furthermore, alignment of the nanofibers was possible using this biopolyester.

Acknowledgements: This study was supported by TUBITAK Project NanoBioMat and the EU FP6 NoE Project (EXPERTISSUES) are greatly appreciated.

WURTZITE CADMIUM TELLURIDE NANOWIRES GROWN BY PULSED LASER DEPOSITION

S.Neretina[1], *R.A. Hughes*[2], *N.V. Sochinskii*[3], *J. Preston*[1,2], *and P. Mascher*[1]

[1] Department of Engineering Physics, McMaster University, Hamilton, Ontario, Canada

[2] Brockhouse Institute for Materials Research, McMaster University, Hamilton, Ontario, Canada

[3] Instituto de Microelectronica de Madrid – CNM – CSIC, Madrid, Spain

neretis@mcmaster.ca

Deposition of ordered arrays of semiconductor nanowires on commercially available substrates is an area of great interest. One of the most promising methods to achieve such structures has been the production of nanowires derived from catalytically driven processes accessible through the formation of metal droplets on a substrate's surface. One material that has received little attention in this regard is the II-VI semiconductor Cadmium Telluride (CdTe). Presented here is a report describing the deposition CdTe nanowires on C-plane sapphire substrates.

Pulsed laser deposition was used to deposit the CdTe nanowires as well as the catalytic material. Nanowire formation falls within a relatively narrow window of processing parameters. Nevertheless, wires produced in this manner can show a high degree of size uniformity and a complete absence of the 2-dimensional background layer that often grows simultaneously in other semiconductor systems. Figure 1 shows a scanning electron microscope (SEM) image of the CdTe nanowires randomly distributed on the substrate's surface. Growth dynamics limit the wire height to approximately 350 nm. Images showing the top view (Figure 2) indicate that the nanowires are highly faceted with a hexagonal geometry. The orientational relationship between the faceting directions relative to the underlying substrate is identical for all nanowires; a clear indication of an epitaxial relationship between the wire and substrate. X-ray analysis indicates a strong wurtzite signature instead of the zincblende crystal structure normally associated with bulk CdTe. The analysis indicates that a small amount of the zincblende phase is present, but it is likely attributable to the small number of tetrahedron structures found on the surface (Figure 3).

Thus far, no attempts have been made to produce periodic arrays of these nanowires. An encouraging observation in this regard, however, is the existence of long lines (>100 um) of nanowires that are infrequently observed on the substrate's surface (Figure 4). These lines likely originate from the nucleation of nanowires at a structural defect in the substrate. Such a mechanism may facilitate the formation of CdTe arrays. Progress in this regard will also be reported.

This work is funded through the Ontario Research and Development Challenge Fund (ORDCF), the Ontario Photonics Consortium (OPC) and the Natural Science and Engineering Research Council (NSERC) of Canada.

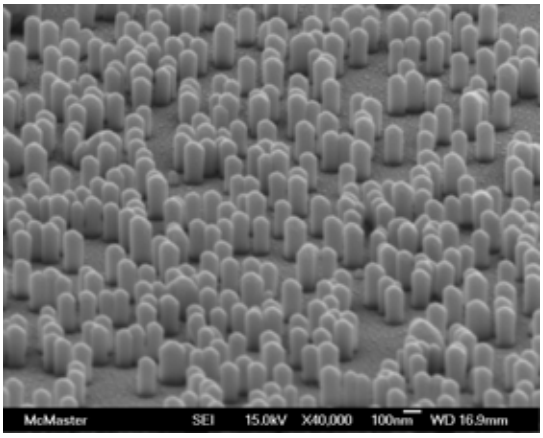


Figure 1

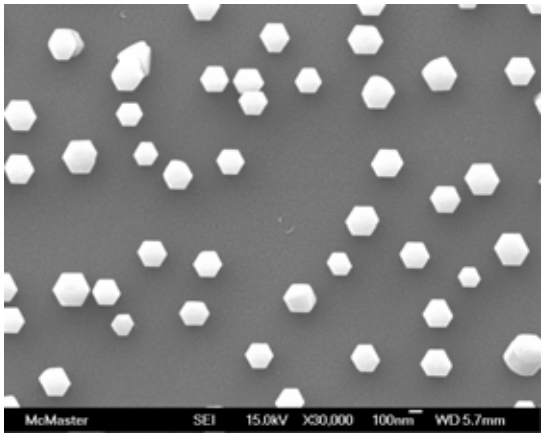


Figure 2

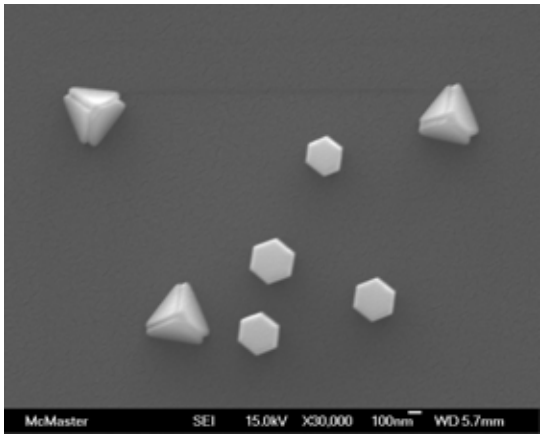


Figure 3

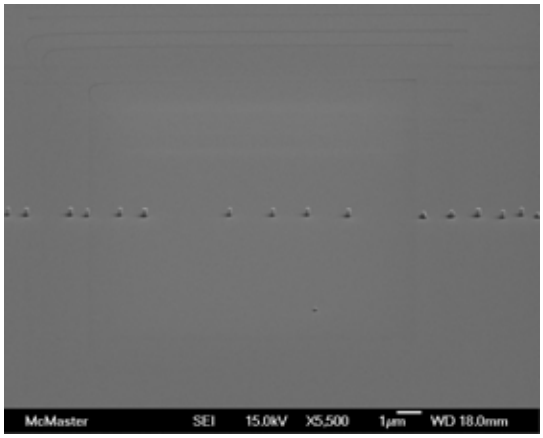


Figure 4

Figure Captions:

Figure 1: SEM image of CdTe nanowires deposited on a C-plane sapphire substrate.

Figure 2: SEM image showing the top view of CdTe nanowires deposited on a C-plane sapphire substrate.

Figure 3: SEM image showing the presence of both hexagonal and tetrahedral CdTe structures.

Figure 4: SEM image showing the nucleation of CdTe nanowires in a line that extends well over 100 um in length.

RF PERFORMANCE OF MULTIPLE-CHANNEL CARBON NANOTUBE TRANSISTORS

Kaoru Narita, Hiroo Hongo, and Masahiko Ishida, Fumiyuki Nihey
NEC Fundamental and Environmental Research Laboratories,
34, Miyukigaoka, Tsukuba, Ibaraki, 305-8501, Japan
nihey@cd.jp.nec.com

Carbon nanotube field effect transistors (CNTFETs) are high-mobility devices and expected to operate at very high-speed. Theoretical analyses suggest that the cutoff frequency (f_T) of an ideal CNTFET is from 800 MHz to 1.3 THz when the gate length is 0.1 μm [1][2]. However, measuring the RF performance of CNTFETs, especially their cutoff frequencies, is generally difficult because their output impedances (~10^5 Ω) are high enough compared with the impedance (50 Ω) of the measurement system using the network analyzer. This large mismatch hinders us from measuring accurate S-parameters and determining the cutoff frequencies of the devices. In this paper, we show the successful results of measuring the RF performance of CNTFETs. This was achieved by a newly developed multiple channel CNTFET structure whose output impedance is much lower than the usual single channel CNTFET, and a de-embedding scheme that removes existing errors in measured S-parameters.

As shown in Fig.1, the evaluated CNTFET was fabricated on SiO_2 insulator on the high-resistive Si substrate. By the CVD method, approximately 200 CNT channels were grown from catalyst (Fe) islands that were patterned by electron-beam lithography. The gate oxide was SiO_2 with the thickness of 40 nm. The top gate structure (L=0.2 μm) was used to reduce parasitic capacitances. The drain and source electrodes were formed by evaporation of Au, and made ohmic contacts with CNT channels. Using high-frequency probes, 2-port S-parameters of the device were measured by the network analyzer. Even using the multiple channel structure, the device impedance was still higher compared with usual RF transistors. Therefore, we applied the calibration method with which the parasitic error matrix can be effectively eliminated and the S-parameters of only the transistor part can be extracted using open-short-through standards on wafer (Fig.2).

Resulting current gain ($|h_{21}|$) and power gain (maximum stable gain) as a function of frequencies are shown in Fig.3. Determined cutoff frequency is 10.3 GHz, and the maximum stable gain is +3.8 dB at 10 GHz. These values are ones of the highest among the previously published papers[3][4][5]. To verify consistencies, we analyzed an equivalent small-signal circuit model of the CNTFET (Fig.4). From this model, the cutoff frequency was derived and approximately represented as;

$$f_T = \frac{g_m'}{2\pi C_g} \quad \text{where} \quad C_g = C_{g-cnt} + C_{gs} + C_{gd}\,, \quad g_m' = \frac{g_m}{1+(R_s+R_d)g_d}\,,$$

g_m' and g_m are measured and intrinsic transconductance respectively. Cg is gate capacitance which consists of gate-CNT capacitance (Cg-cnt) and parasitic capacitance between the gate and source (or drain) electrodes (Cgs + Cgd). g_m' is obtained by DC measurement, Cg-cnt can be calculated by the theoretical concern[1] and Cgs + Cgd can be estimated by the geometry. It was found that our result of f_T is quite reasonable value when we substitute g_m' = 226 μS, Cg-cnt = 1.2 fF and Cgs + Cgd = 2.2 fF into the above formula (f_T[model]=10.6GHz). This implies that the equivalent circuit model is appropriate, in addition, the device RF performance can be considerably improved by increasing g_m' and reducing parasitic capacitance and resistance of the device in the future study.

References:

[1] P. J. Burke, "AC performance of nanoelectronics: towards a ballistic THz nanotube transistor," Solid-tate Electronics, 48, pp.1981-1986, 2004.

[2] S. Hasan, S. Salahuddin, M. Vaydyanathan and M. A. Alam, "High-Frequency Performance Projections for Ballistic Carbon-Nanotube Transistors," IEEE Transaction on Nanotechnology, Vol.5, No.1, pp.14-22, 2006.

[3] D.V.Singh, K.A. Jenkins, J. Appenzeller, D. Neumayer, A. Grill, and H.-S.P. Wong, "Frequency Response of Top-Gated Carbon Nanotube Field-Effect Transistors," IEEE Transactions on Nanotechnology, Vol.3, No.3, pp.383-387, 2004.

[4] S. Lee, Z. Yu, S. Yen, W.C. Tang and P.J. Burke, "Carbon nanotube transistor operation at 2.6 GHz, " Nano Letters, Vol. 4, No.4, pp.753-756, 2004.

[5] S. Kim, T. Choi, L. Rabieirad, J.-H. Jeon, M. Shim, and S. Mohammadi, "A Poly-Si Gate Carbon Nanotube Field Effect Transistor for High Frequency Applications," 2005 IEEE MTT-S International Microwave Symposium Digest, 12-17 June, pp.303 - 306, 2005.

Figures:

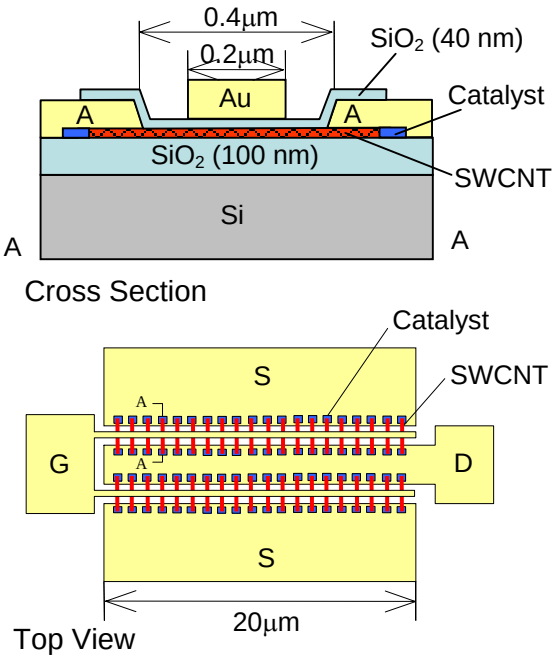


Fig.1: Multiple channel CNTFET structure

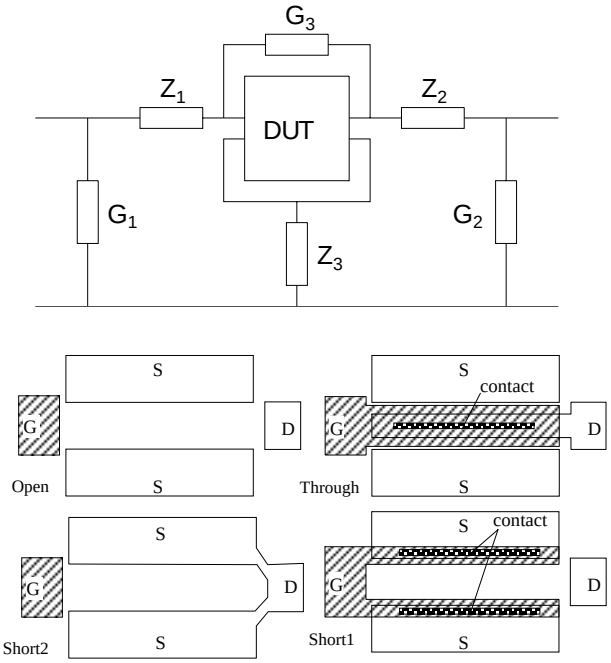


Fig.2: Parasitic errors and de-embedding standards

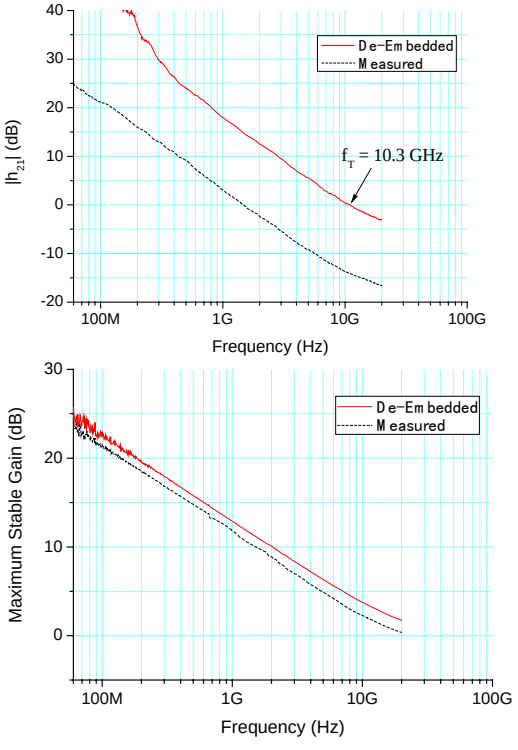


Fig.3: Current gain (|h21|) and power gain

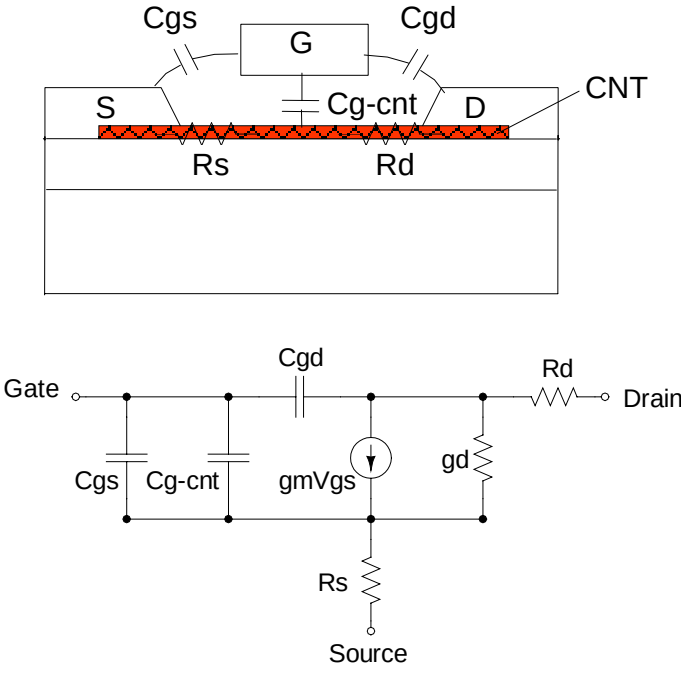


Fig.4: Equivalent small-signal circuit model

ELECTROSPUN NANOFIBROUS SCAFFOLD WITH DRUG RELEASING PROPERTIES

L Nikkola[1], K Vapalahti[1], J Seppälä[2], N Ashammakhi[1]
1. Tampere University of Technology, Institute of Biomaterials, P.O.BOX 589, 33101 Tampere, Finland
2. Helsinki University of Technology, P.O. Box 6100, FIN-02015 HUT, Finland
nureddin.ashammkhi@tut.fi

The aim of this work was to develop a nanomat with diclofenac sodium releasing properties. A bioabsrbable polymer was diluted into solvent. Diclofenac sodium was added to the solution. Nano-fibers were made by electrospinning onto substrate. Microstructure of the sheet was studied using SEM and drug release profiles with UV/VIS spectroscopy.

Thickness of spinned sheet was about 2 mm. SEM analysis showed that polymeric nano-fibers containing drug particles form very interconnected porous nano structure. The average diameter of nano-fibers was 130nm. After the high start peak of drug release as the rate was decreased after one day. More details will be presented.

The nano-fibrous porous structure made of bioabsorbable polymer loaded test drug is feasible to develop and hoped to improve biomaterial properties for analgesic release applications.

Research funds from the European Commission (EXPERTISSUES Project NMP3-CT-2004-500283), Technology Development Center in Finland (TEKES) and the Academy of Finland (Center of Excellence 73948) are greatly appreciated.

Electronic properties of strained nanowire heterostructures

Y. M. Niquet
CEA/DRFMC/SP2M/L_Sim
17, rue des Martyrs, 38054 Grenoble Cedex 9, France

yniquet@cea.fr

Semiconducting nanowires grown from metal catalysts have attracted a lot of interest in the past few years [1]. They provide new insights into the physics of one-dimensional systems, and are promising building blocks for opto- and nanoelectronics. These nanowires are very versatile. Their composition can be modulated along the growth axis, which allows the synthesis of high-quality heterostructures with embedded quantum dots or tunnel barriers. GaAs/GaP [2], InAs/InP [3], or InAs/GaAs [4] nanowires for example have shown remarkable optical and electrical properties. Nanowire-based devices such as resonant tunneling diodes [5] or single-electron transistors [6] have been sucessfully realized.

Strain is a fundamental issue in semiconductor heterostructures. The lattice mismatch between the different materials indeed limits the design of conventional, quantum well systems. The coherent epitaxy of thick lattice mismatched layers has however been demonstrated in nanowires. Their surface can actually bend to help relieving the strains. The relaxed strain distribution might however be very inhomogeneous. Moreover, the actual effect of strain relaxation on the electronic properties of the nanowires is largely unknown. Previous studies on etched nanowires suggest that the carriers might be localized (in compressed layers) near the surface where strong relaxation takes place [7,8]. This, of course, is not desirable for most experiments and applications.

In this work, we compute the structural and electronic properties of InAs/GaAs and InAs/InP nanowire superlattices, using a semi-empirical $sp^3d^5s^*$ tight-binding model. We take strains and piezoelectric fields into account. The effects of the image charges, that arise from the dielectric mismatch between the nanowire and vacuum, and of the electron-hole interaction are also included in the calculation. We show that strain relaxation is indeed efficient in nanowire heterostructures. It is, however, very inhomogeneous if the thickness of the InAs layers is much smaller than the radius of the nanowire. Strain relaxation then digs a well in the conduction band that traps the electrons at the surface (see Fig .1). This decreases the oscillator strength and might ease the capture of the electrons by nearby surface defects. We discuss in detail the electron and hole localizations as a function of the geometry of the nanowire.

This work was supported by the French “Action Concertée Incitative” (ACI) “TransNanofils” and by the European Integrated Project (IP) NODE (EU contract Nr 015783 NODE).

References:

[1] : A. M. Morales and C. M. Lieber, Science **279** (1998) 208.
[2] : M. S. Gudiksen, L. J. Lauhon, J. Wang, D. C. Smith, and C. M. Lieber, Nature **415** (2002) 617.
[3] : M. T. Björk, B. J. Ohlsson, T. Sass, A. I. Persson, C. Thelander, M. H. Magnusson, K. Deppert, L. R. Wallenberg, and L. Samuelson, Appl. Phys. Lett. **80**, (2002) 1058.
[4] : B. J. Ohlsson, M. T. Björk, A. I. Persson, C. Thelander, L. R. Wallenberg, M. H. Magnusson, K. Deppert, and L. Samuelson, Physica E **13** (2002) 1126.
[5] : M. T. Björk, B. J. Ohlsson, C. Thelander, A. I. Persson, K. Deppert, L. R. Wallenberg, and L. Samuelson, Appl. Phys. Lett. **81** (2002) 4458.
[6] : C. Thelander, T. Martenson, M. T. Björk, B. J. Ohlsson, M. W. Larsson, L. R. Wallenberg, and L. Samuelson, Appl. Phys. Lett. **83** (2003) 2052.
[7] : H. Straub, G. Brunthaler, W. Faschinger, G. Bauer, and C. Vieu, J. Cryst. Growth **159** (1996) 451.
[8] : Y. M. Niquet, C. Priester, C. Gourgon, and H. Mariette, Phys. Rev. B **57** (1998)14850.

Figures:

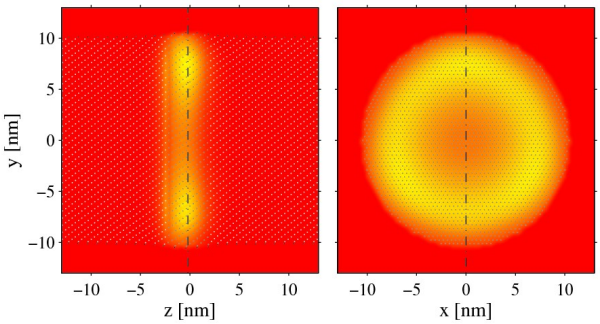


Fig. 1 : Square of the lowest electron wavefunction in an InAs/GaAs nanowire superlattice with radius R = 10 nm. The thickness of the InAs layer is t = 4 nm. It extends from z = -2 nm to z = +2 nm. The wavefunction is plotted in a plane containing the axis of the nanowire (left), and in the z = 0 plane (right). The dots are the In/Ga atoms in the plane of the plots.

Poster

THEORY AND EXPERIMENTAL VERIFICATION OF MICRO SWITCH GROUP SENSOR (MSGS)

K. Nishiyama, M.C.L Ward
School of Engineering, Mechanical Engineering, The University of Birmingham, Edgbaston, Birmingham, B152TT, UK
Tel: +44 (0)121 414 4217, Email:kxn249@bham.ac.uk

Micro system technology is having a huge impact on the design and development of sensor technology. It is now possible to produce micro sensors such as accelerometers and gyroscopes that are just a few hundreds of microns in size with integrated signal processing electronics and the feature sizes are approaching nano meter dimension [1, 2, 3] . While this is a marvellous achievement, the nature of the sensing elements and their mode of operation have changed little compared to their macroscopic origins. Because of their extremely small size, micro and nano devices inevitably suffer from Brownian motion which will introduce a source of noise into the system [4, 5, 6] and also from inherent randomness in their performance due to the technology used to manufacture them [7].

The concept is then demonstrated experimentally using an electronic system using zener diode noise source and comparators. The preliminary results obtained suggest that the MSGS may have a rate to play in future NEMS sensors.

Theory of MSGS:

Suppose there is large number of switches which has probability function $P_{on}(V_{in})$ in their conversion, where V_{in} is the input voltage. $P_{Nn}(V_{in})$, the probability of the state that n in N switches are turned on can be expressed by equation (1).

$$P_{Nn}(V_{in}) = {}_N C_n \times P_{on}(V_{in})^n \times \{1 - P_{on}(V_{in})\}^{N-n} \quad (1)$$

${}_N C_n$ is the sign of combination and given as;

$${}_N C_n = \frac{N!}{n!(N-n)!} \quad (2)$$

Then when n switches are turned on we may confer the input voltage as

$$\overline{V_{in}}(N,n) = \int_{-\infty}^{\infty} p_{Nn}(V_{in}')V_{in}'dV_{in}' \quad (3)$$

Related to (3), $p_{Nn}(V_{in})\Delta V_{in}$ is the ratio of $P_{Nn}(V_{in})\Delta V_{in}$ to the area inside of the curve, which gives the equation (4) below;

$$p_{Nn}(V_{in}) = \frac{P_{Nn}(V_{in})}{\int_{-\infty}^{\infty} P_{Nn}(V_{in})dV_{in}} \quad (4)$$

Error ranges of each state are obtained by the standard deviation of each state by the following equation;

$$\sigma_{Nn} = \left[\int_{-\infty}^{\infty} (V_{in} - \overline{V_{in}}(N,n))^2 \, p_{Nn}(V_{in})dV_{in} \right]^{\frac{1}{2}} \quad (5)$$

According to the statistical method, 95.44 percent of samples are contained in the range of $\overline{V_{in}}(N,n) - 2\sigma_{Nn} \le V_{in} \le \overline{V_{in}}(N,n) + 2\sigma_{Nn}$.

Experimental works:

In this experiment an electric circuit which has three switches affected by noise signals is built. This circuit consists of zener diode as noise generator and comparators. A range of voltage was then applied to the circuit and the performance of each of switch and the output signal are observed. The signals from each switching unit are summed up together by summing amplifier and regarded as output signal of MSGS. However in normal circumstances, the signal will be summed up as digital signal directly by using shift resistors avoiding the need for A/D converters.

Results and Discussions;

The average number of switches turned on at each of input voltages are plotted in **Fig.1**. There is a clear tendency that the number of switches turned on increases by higher input voltages. It is concluded that the input voltage and the number of switches turned on has correlation each other in agreement with the theory of the earlier section. In the output signals fluctuations of the number of switches turned on also observed as in **Fig.2** and it would affect the accuracy of measurement. It was most intense around the mean voltage of the noise signals. This phenomenon is understood by considering the fact that the noise signal is fluctuating on the time base.

Conclusion:

In this experiment, a MSGS which has three switches was made exploiting the noise generators and comparators and its output signal was observed. The result would make us to expect the potential application for the sensing device of MSGS. Sensors depending on this theory would be a core of next generation sensor exploiting nanomechanical structures.

References:

[1] Gardner, J.W., Varadan, V.K., Awadelkarim, O.O., Microsensors MEMS and Smart Devices, LTD, ISBN 047186109, (2001) pp1-8.
[2] Romig, A.D., Jr, Dugger, M.T., McWhorter P.J., Acta Material, **51**, (2003) pp5837-5866.
[3] Kloek, B., De Rooji N.F., Semiconductor Sensors, S.M. Sze, ISBN 0471546097 (1994) Chap1.
[4] Vig, J.R., Kim Y, IEEE Transactions on Ultrasonics, Ferroelectrics, and Frequency Control, **46**, (1999) pp1558-1565.
[5] Huber, D., Corredoura, P., Lester, S., Robbins, V., Kamas, L., Journal of Microelectromechanical Systems, **13**, (2004) pp732-736.
[6] Gabrielson, T.B., IEEE Transaction of Electron Devices, **40**, (1993) 903-909.
[7] Sharpe, W.N., Jr, The MEMS Hand Book, CRC Press, ISBN 0849300770 (2001) Chap38

Figures:

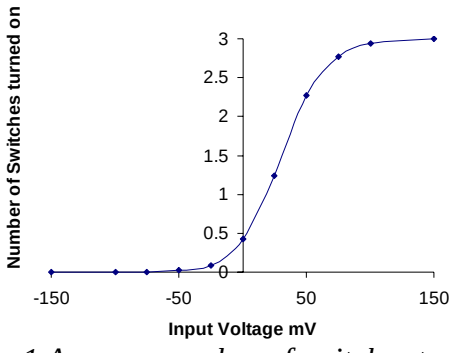


Fig.1 Average number of switches turned on

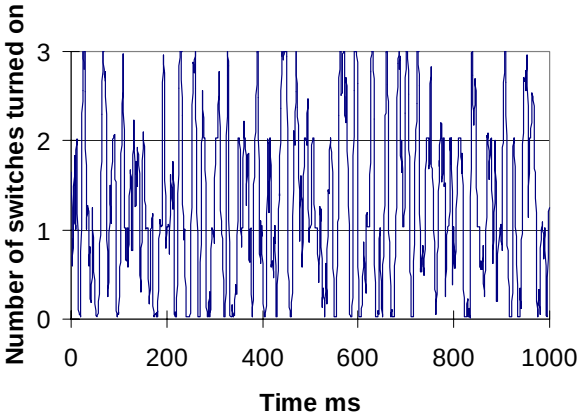


Fig.2 Output signal by input voltage 25mV

ROOM-TEMPERATURE GREEN PHOTOLUMINESCENCE OF SILICON NANOWIRES COVERED BY DEPOSITED SILICON OXIDE LAYERS

Pierre NOE, Jérémie GUIGNARD, Pascal GENTILE, Vincent CALVO, Pierre FERRET[1], Thierry BARON[2]
Laboratoire Silicium Nanoélectronique Photonique et Structure, CEA/DRFMC/SP2M, CEA-Grenoble 17 rue des Martyrs, 38052 Grenoble Cedex 9
[1] Laboratoire de Photonique sur Silicium, CEA/LETI/DOPT, CEA-Grenoble 17 rue des Martyrs, 38052 Grenoble Cedex 9
[2] Laboratoire des Technologies de la Microélectronique, CNRS UMR 5129, CEA-Grenoble 17 rue des Martyrs, 38052 Grenoble Cedex 9
pierre.noe@cea.fr

Silicon nanowires (SiNWs) due to their specific dimensions and particular shapes are promising structures for nanoelectronic [1], photonic [2], nano-mecanic, chemical [3] and biological applications. In this context we have studied room-temperature PL of SiNWs covered by silicon oxide. Silicon oxide layers have been obtained by three different deposition techniques such as Plasma Enhanced Chemical Vapor Deposition, magnetron sputtering and electron-beam evaporation.

SiNWs were synthesised by VLS mechanism on (100) and (111) Si substrates at temperatures between 450 °C and 650 °C in a low pressure chemical vapor deposition (LPCVD) reactor. Gold was used as the catalyst and silane (SiH_4) as the Si source. After growth different silicon oxide layers were deposited on the SiNWs samples by electron beam evaporation, magnetron sputtering or plasma enhanced chemical vapour deposition (PECVD). Silicon oxide layers thickness varied from 200 to 1600 nm in order to entirely cap the SiNWs. After deposition samples were annealed at 850°C for one hour under forming gas (N2+H2 95/5) or pure oxygen. SiNWs were observed by scanning electron microscopy (SEM) and by transmission electron microscopy (TEM). High resolution images confirm the crystallographic structure of the nanowires.

Photoluminescence (PL) spectra were realised at room temperature. Excitation was made with the 351 nm line of an Argon laser and PL signal detection was supplied by a silicon CCD camera coupled with a visible spectrometer. We show room-temperature PL spectra, as a function of the silicon oxide elaboration method and the annealing atmosphere. Then the origin of this PL will be discussed as compared to previously reported room-temperature visible photoluminescence from as-grown and oxidized SiNWs [4, 5]. Red, green and blue PL were observed and attributed to the quantum confinement effects and the recombination emissions from the defect centers, respectively.

References:

[1] Y. Cui and C. M. Lieber, Science **291**, 851 (2001)
[2] J. D. Holmes, K. P. Johnston, R. C. Doty, and B. A. Korgel, Science **287**, 1471 (2000)
[3] Y. Cui, Q. Wei, H. Park, and C. M. Lieber, Science, **293**, 1289 (2001)
[4] D.P. Yu, Q.L. Hang, Y. Ding, H.Z. Zhang, Z.G. Bai, J.J. Wang, Y.H. Zou, W. Qian, G.C. Xiong, S.Q. Feng, Appl. Phys. Lett., **73**, 3076 (1998)
[5] Z.G. Bai, D.P. Yu, J.J. Wang, Y.H. Zou, W. Qian, J.S. Fu, S.Q. Feng, J. Xu, L.P. You, Mater. Sci. Eng. B, **72**, 117 (2000)

Figures:

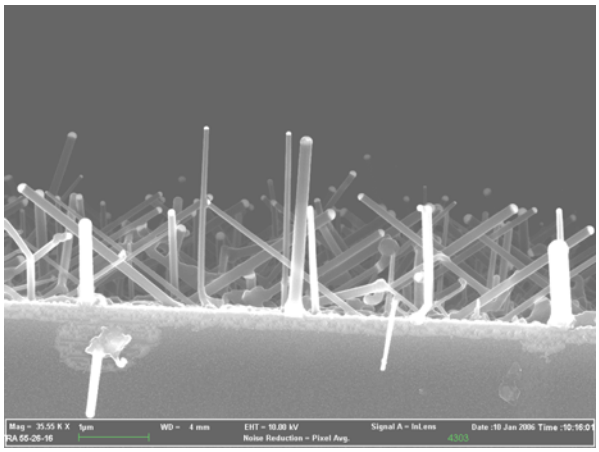


Figure 1 : SEM image of silicon nanowires grown on a (100) Si substrate

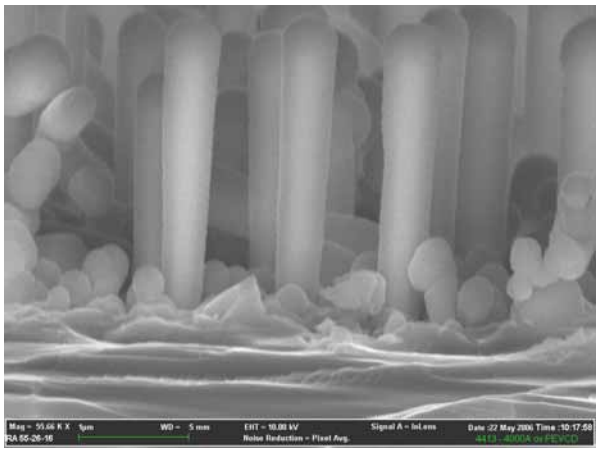


Figure 2 : SEM image of 400nm PECVD silicon oxide deposited on silicon nanowires grown on a (111) Si substrate

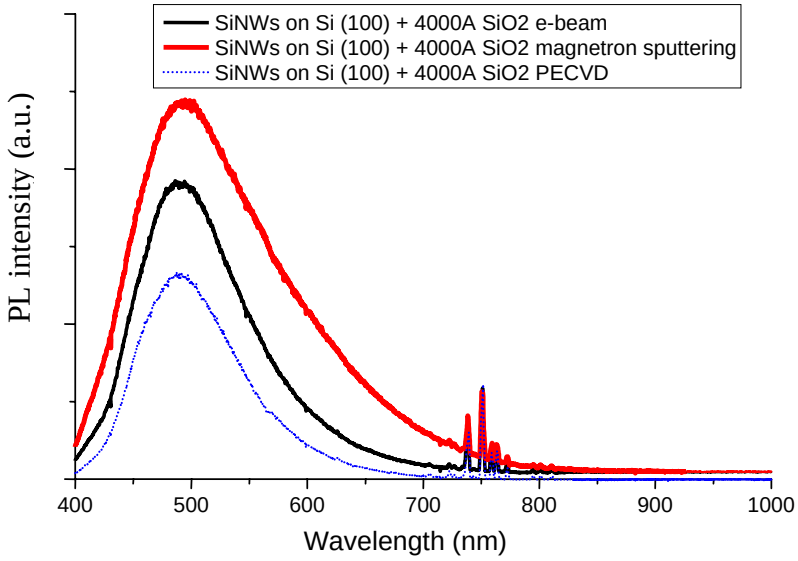


Figure 3 : PL spectrum of silicon oxide deposited on SiNWs on Si (100)

CONICAL QUANTUM DOTS SUPERCRYSTALS

Javier Francisco Nossa, Ángela Camacho
Universidad de los Andes, Cra. 1E No. 18A-10. Edificio H, *Bogotá, Colombia*
ja-nossa@uniandes.edu.co, acamacho@uniandes.edu.co,

The necessity of innovation in the nanotechnology has lead to implementation of the quantum dots as tools of interdisciplinary skills, addressing all fields of science and technology at the nanoscale. Therefore, the study of the properties of quantum dots becomes a scientific and technological necessity for the development of them. Quantum dots have several applications in different fields as optical and optoelectronic devices [1], quantum computing [2], materials for cascade lasers [3], 3D imaging inside living organism [4], etc.

In this work we calculate the energies and probability densities of a conical quantum dot of GaAs with bottom radio 5nm, height 5nm and angle of 25^{o}, embedded in a matrix of AlGaAs (Fig 1). In addition, thanks to the experimental perspectives and of simulation in the formation of quantum dots arrays [5-6], we present the electronic structure of minibands of a conical quantum dots supercrystal, by means of the tight-binding model, using the base s, p3. The study of these quantum dots supercrystals allows the implementation of new and better material with fixed properties following the trend of devices development.

References:

[1] A. J. Shields and M. P. O'Sullivan , Appl. Phys. Lett. 74, (1999) 735-737 .
[2] Daniel Loss and David P. DiVincenzo, Phys. Rev. A 57,(1998) 120–126
[3] N. Ulbrich, J. Bauer, G. Scarpa, R. Boy, D. Schuh, and G. Abstreiter , Appl. Phys. Lett. 83, (2003) 1530-1532.
[4] X. Michalet, et. al**.,** Science, 28 (2005) 538 - 544.
[5] P. Liu, Y.W. Zhang and G. Lu, Appl. Phys. Lett. 80, (2002) 3910-3912.
[6] C.s. Lee, B. Kahng and A. L. Barabasi, Appl. Phys. Lett. 78 , (2001) 984-986.

Figures:

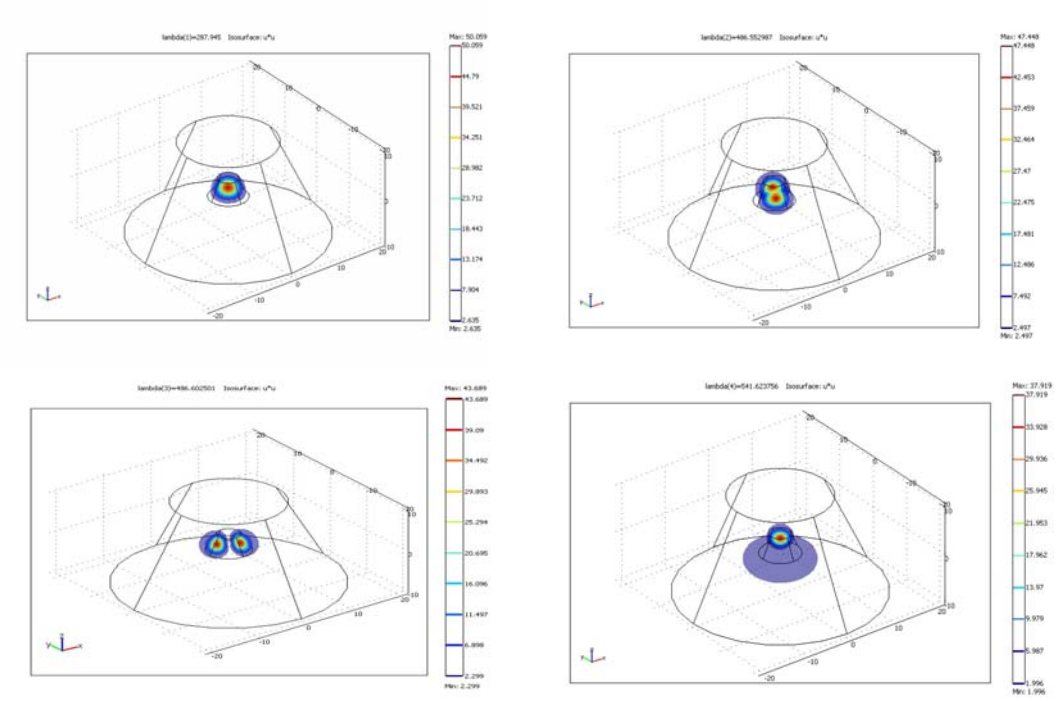


Figure 1. Probability densities and energies for a conical quantum dot.
Lambda=Energy [meV], $u^{*}u$ = Probability density

Quantum Confinement Effects in Si Nanowires

Seán O'Callaghan, Michael Nolan, James C. Greer and Giorgos Fagas

Tyndall National Institute, University College, Cork, Ireland

sean.ocallaghan@tyndall.ie

As device dimensions approach atomic diameters, silicon nanowires (SiNWs) are expected to play a major role in future nanoelectronics and possibly optoelectronics, both as devices and interconnects [1]. For example, the FinFet, a leading contender to replace the MOSFET, utilises a long Si channel as the connector between source and drain, through which the transistor action takes place via an overlying gate.

With decreasing cross-section ($\sim$nm), quantum confinement induces subband formation and effectively restricts propagating states to one dimension along the wire axis. Using first-principles methods, we show that the resulting electronic structure for small diameter wires exhibits a much larger direct bandgap (E_g) compared to the indirect $\Gamma - \chi$ gap in bulk Si. In agreement with experimental results [2] and previous calculations [3], E_g falls monotonically with increasing dimension for hydrogen passivated surfaces (wires) as shown in fig. 1.

Allowing for different surface preparation, we identify a novel chemical mechanism that allows for band gap engineering [4] with either blue or red shift for a fixed diameter. Transport properties are also investigated via the analysis of (a) the complex band structure which determines the tunneling decay parameter in undoped wires [5], and (b) the elastic mean free paths for surface impurity scattering.

.

References

[1] L. Canham, Nature, **408** (2000) 411.

[2] D.D. Ma et al., Science, **299** (2003) 1874.

[3] Zhao et al, Phys. Rev. Lett., **92** (2004) 236805.

[4] M. Nolan, J.A. Larsson and J.C. Greer, Comp. Mat. Sci., **27(1-2)** (2003) 166.

[5] G. Fagas, A. Kambili and M.Elstner, Chem. Phys. Lett, **389** (2004) 268.

Figure

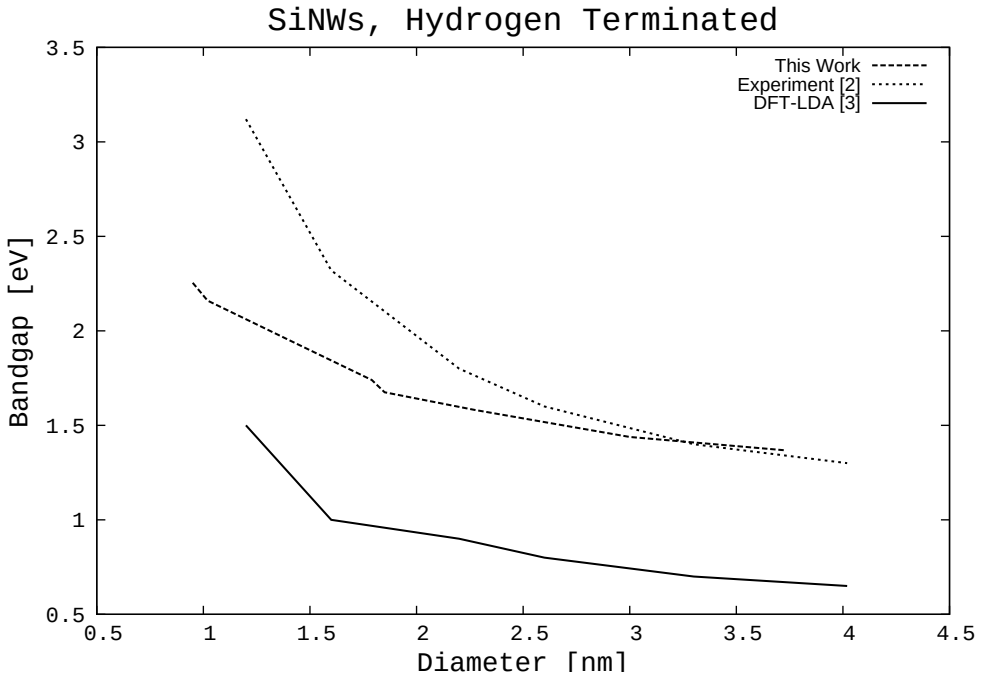


Figure 1: Bandgap vs. Diameter relation along the [110] direction compared with other studies.

ELECTRONIC STRUCTURE AND ION-ELECTRON EMISSION OF NANODIAMONDS AND CARBON NANOTUBES

A.V. Okotrub, A.V.Gusel'nikov, L.G. Bulusheva

Nikolaev Institute of Inorganic Chemistry SB RAS, pr. Ak. Lavrentieva 3, Novosibirsk 630090, Russia,

Electronic structure of various fractions of the detonation nanodiamonds (ND) and different kinds of carbon nanotubes (NT) were probed using X-ray spectroscopy and X-ray photoelectron spectroscopy. The ND particles have been extracted from the detonation soot using a gradual oxidation procedure and than separated to fractions by centrifugation in the range of G-forces 46-40000 g. X-ray absorption spectra near the K-edges of carbon and oxygen and X-ray photoelectron spectra of the samples were recorded using the Berlin synchrotron radiation facility at the Russian-German laboratory in BESSY-II. The overview X-ray photoelectron spectra of ND fractions detected a presence of nitrogen and oxygen in samples. C1s- and O1s-lines of X-ray photoelectron spectra are split, while N1s-line is presented by a single narrow maximum. The spectral splitting could be caused by the induced charging of ND particles due to oxidized surface layer. Actually, intensity of satellite lines in the C1s- and O1s-spectra was found to correlate with ND agglomerate size and composition of ND surface. The satellite lines drift depending on duration and energy of the exciting synchrotron radiation. With lowering the radiation energy up to 330 eV, the satellite lines were disappeared and C1s-spectra of the samples were interpreted in the terms of chemical shifts under the effect of oxygen-containing functional groups.

Depending on kinetic parameters the products of ND annealing consist of onion-like carbon (OLC) or sp^2/sp^3 composites, comprised a diamond core enclosed by graphitic shells. The graphite-like shells were found to begin developing at temperature above 1200 K and almost completely cover a diamond core with ND annealing in the region of 1400–1600 K. When the temperature reaches 1800 K the particles formed have an onion-like structure. The final stage of ND annealing at the temperatures higher than 2000 K yields the hollow graphitic polyhedrons. X-ray fluorescent spectroscopy investigation of the annealing products detected a significant increase of density of high energy occupied states in the OLC compared with the polyhedral particles. The electronic states of interface were separated by subtraction of the ND and graphitic polyhedron X-ray spectra from the composite ones taking into account the true density data on samples. Localization of the electrons near the Fermi level was detected both for the valence and conductance bands of sp^2/sp^3 composites. X-ray spectroscopy study on the OLC particles found the strong enhancement of density of occupied states only. To interpret the experimental data the density functional calculations on models were carried out. The fragment of diamond, graphite, diamond/graphite hybrid, and the holed C_{240} fullerene have been computed and the results were used for theoretical spectra plotting. We found the localized electronic states in the composite particles could be attributed to the three-coordinated carbon on the (111) diamond surface, while the origin of electron localization in OLC is non-bonding states of two-coordinated carbon atoms.

We recorded the ion current occurred in the result of d sorption of molecules from ND and NT surface in an electric field. A sawtooth voltage regulated the electric field with certain frequency of 0.01 - 5 Hz. The ion and electron currents and current-voltage characteristics of cathode were measured at a time. The correlations between the potential for ion current appearance and the electron emission threshold were established for different types of carbon nanostructures. The contributions in ion current from residual gas ionization and from ion emission of molecules adsorbed of nanoparticles surface were evaluated. To understand the experimental results in detail the quantum-chemical calculations on models were performed. Effect of electric field on the binding energy of various molecules adsorbed on the top and body of NT and ND was examined.

Poster

MAGNETIC PROPERTIES OF THE Co_2MnGa HEUSLER ALLOY FILMS WITH DIFFERENT CRYSTALLINE ORDER

V. A. Oksenenko[a)], *Y. V. Kudryavtsev*[b)], *V. A. Kulagin*, *J. Dubowik*[*]

Institute of Metal Physics, National Academy of Sciences of Ukraine,
36 Vernadsky str, 03142, Kiev-142, Ukraine
[*]*Institute of Molecular Physics, Polish Academy of Sciences,*
Smoluchowskiego 17, 60-179, Poznań, Poland
[a)]oksenen@imp.kiev.ua, [b)]kudr@imp.kiev.uaT

The grate progress in the injection of spin-polarized carriers from ferromagnetic layer into semiconductor stimulates a deep interest in materials with a high spin polarization at the Fermi level, E_F. It was theoretically predicted, that a significant number of Heusler alloys (HA) are half-metals [1], therefore these materials are the most perspective and efficient candidates for the spin injectors in the spintronic devices. Indeed, the full spin polarization at the E_F (or half-metallicity state) was theoretically predicted only for the HAs with an ideal $L2_1$ type of structure, characterized by the narrow gap in the minority-spin subband at the E_F [2]. The physical properties of the Mn-containing HAs directly depend on the exchange interaction between nearest-neighbor Mn atoms. Any changes in the atomic order lead to the reconstruction of the electron energy structure, influence on the magnetic behavior and, as a consequence, effect on the spin polarization of the carriers. We report the research of magnetic properties depending on the atomic order in the Co_2MnGa HA films.

Co_2MnGa alloy films were prepared by flash-evaporation method onto glass, mica and NaCl substrates kept at different temperatures (150–728 K) in a vacuum better than 2×10^{-5} Pa. Deposition of the Co_2MnGa HA films onto substrates cooled by liquid nitrogen leads to the formation of the amorphous (or disordered) structures. Microdiffraction patterns of such films exhibit a few smeared halos and the mean grain size less than the resolution limit of the transmission electron microscopy technique (< 2~3nm). The annealing of disordered films leads to the crystallization, that begins at ~400 K, and formation at 513 K and 598 K (in our case) of the ordered structure with $B2$ type of symmetry. To obtain highly ordered films with $L2_1$ type of structure the amorphous films were annealed at 728 K (see Table I).

It was revealed by using VSM and FMR techniques, that unlike another HAs, such as Cu_2MnAl [3], Ni_2MnGe [4], the Co_2MnGa alloy films in amorphous state have a nonzero magnetic moment. Thus, according to the VSM measurements, the saturation magnetization, M_s, at room temperature was about 60 G (see Fig. 1). Furthermore, out-of-plane angular dependence of the FMR spectra except of the main peak, have an additional peaks, that correspond to the para- and ferromagnetic phases in the disordered films. Effective magnetization, M_{eff}, of such films is 290 G, that may be originate from the Co clusters in nonmagnetic environment. Pointed out on the verity of this assumption also the spectral shape of the equatorial Kerr effect for such films, that is very similar to that of pure Co. The difference between M_s and M_{eff} might be explained by that the M_s is the mean volume magnetization, while M_{eff} is a local magnetization of the largest Co clusters.

The formation of $B2$-ordered structure (at T_A=513 K) results in a significant increase in M_{eff} (to 485 G) and M_s (to 253 G) (see Fig. 1). It is occured the noticeable changes in the FMR spectrum taken at the perpendicular configuration: the main absorption peak became more intense and shifted to about 0.8 T and only a weak trace of additional absorption peak at 0.32 T can be observed (see Fig. 2). Therefore, it can be concluded that crystallization of amorphous Co_2MnGa HA film results in the formation of more homogeneous magnetic ordering. The formation of $B2$-ordered structure (at T_A=598 K) results in a substantial growth in M_s of ~ 430 G nearly equal to M_{eff}. The structural transformation to $L2_1$-type of symmetry does not practically change M_s and M_{eff} of the Co_2MnGa HA films. The difference between

M_s and M_{eff} for the crystalline films may be explained by a remarkable strain-induced magnetic anisotropy of Co_2MnGa alloy [5].

References:

[1] R. A. de Groot, F. M. Mueller, P. G. van Engen and K. H. J. Buschow, Phys. Rev. Lett. **50**, 2024 (1983).
[2] R. A. de Groot, F. M. Mueller, P. G. van Engen, and K. H. Bushow, Phys. Rev. Lett. **83**, 203 (1999).
[3] Y. V. Kudryavtsev, V. A. Oksenenko, N. N. Lee, Y. P. Lee, J. Y. Rhee, and J. Dubowik, J. Appl. Phys. **97**, 113903 (2005).
[4] V. A. Oksenenko, L. N. Trofimova, Yu. N. Petrov, Y. V. Kudryavtsev, J. Dubowik, and Y. P. Lee, J. Appl. Phys. **99,** 063902 (2006).
[5] M. J. Pechan, C. Yu, D. Carr, and C. J. Palmstrøm, J. Magn. Magn. Mater. 286 (2005) 340.

Table I. The parameters of the investigated Co_2MnGa HA films and bulk specimen. T_S is the deposition temperature, T_A the annealing temperature, d_G the main grain size (using Scherrer equation), a the lattice constant, M_{eff} and M_s are the effective and saturation magnetizations, determined by FMR and VSM measurements, respectively, $\Delta(2\theta)$ is the full width at half maximum of the most intense diffraction peak (220).

Sample	T_S (K)	T_A (K/h)	d_G (nm)	Structure, a ($\mathring{A}$)	$\Delta(2\theta)$, °	M_{eff} (G)	M_s (G)
Bulk	-	680 / 6.0	---	$L2_1$, 5.7935	0.28	---	---
Disordered film	150	-	< 2~3	-	4.70	270	60
Crystalline film 1	150	513 / 0.5	238	$B2$, 5.8109	0.36	485	253
Crystalline film 2	150	598 / 1.0	215	($B2$, 5.792) + ε-Mn_3Ga and/or Mn_3Co_7	0.40	501	434
Crystalline film 3	150	728 / 1.0	175	($L2_1$, 5.7863) + ε-Mn_3Ga and/or Mn_3Co_7	0.49	533	404

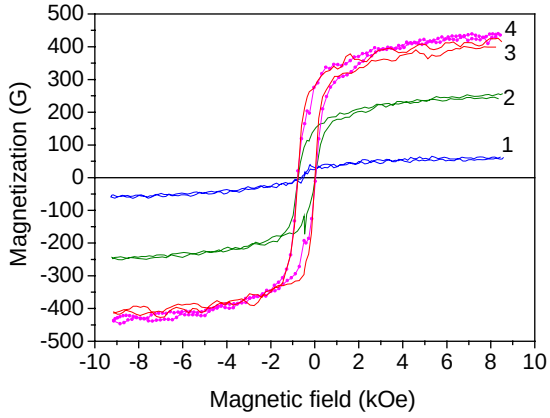


Fig. 1. Hysteresis loops for the Co_2MnGa HA films: 1 – disordered, 2 – $B2$-ordered (T_A=513 K), 3 - $L2_1$-ordered (T_A=728 K), 4 - $B2$-ordered (T_A=598 K),

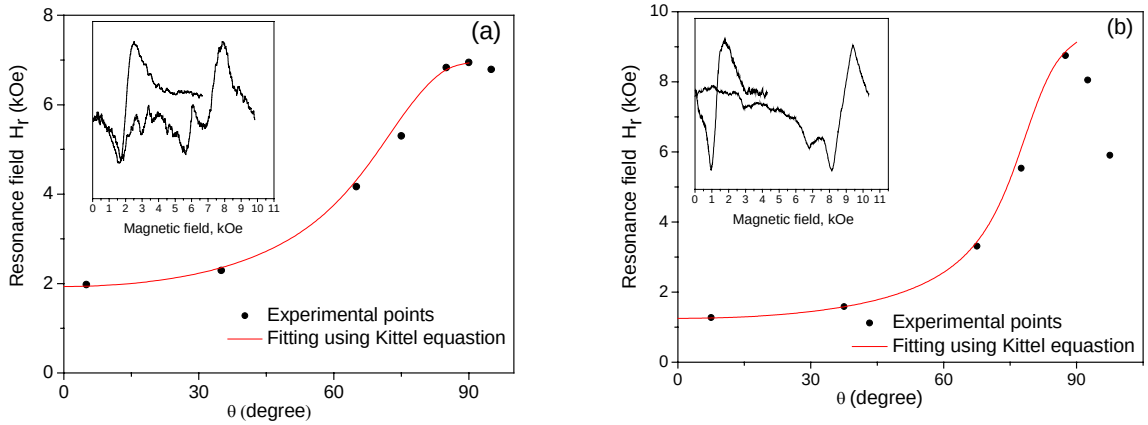


Fig. 2. Out-of-plane angular dependence of the FMR spectra for the Co_2MnGa HA films: (a) – disordered, (b) – $B2$-ordered (T_A=513 K). Insets show FMR spectra in parallel and perpendicular geometries.

STM IMAGING OF CARBON NANOTUBE POINT DEFECTS

Z. Osváth, L. Tapasztó, G. Vértesy, A. A. Koós, Z. E. Horváth, J. Gyulai, and L. P. Biró
Research Institute for Technical Physics and Materials Science, H-1525 Budapest, P.O. Box 49, Hungary
osvath@mfa.kfki.hu

Carbon nanotube defects can play important role in the applications since their presence affect mechanical [1] and transport properties [2]. Topological point defects (e.g. non-hexagonal carbon rings) can form during the nanotube growth process or they can be introduced after synthesis for example by chemical purification or irradiation. In this work we investigated nanotube point defects created by ion irradiation. Multi-walled carbon nanotubes produced by the arc-discharge method were dispersed on HOPG surface and irradiated with Ar^+ ions of 30 keV. We used a low dose of D = $5x10^{11}$ ions/cm^2 in order to create individual, non-interacting defects. The arc-grown nanotubes are generally straight tubes and they accumulate very few defects during synthesis in comparison with the catalytically grown nanotubes [1].

STM investigations revealed that the nanotube defects created by irradiation appeared as hillock-like features (Fig. 1b) similar to the hillocks observed earlier on irradiated HOPG [3]. These hillocks could not be observed on the non-irradiated nanotubes (Fig. 1a).

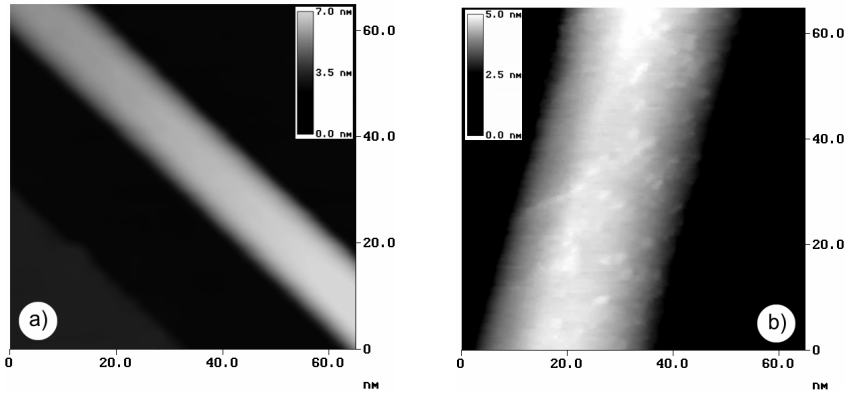


Figure 1. STM images of multi-walled carbon nanotubes before (a) and after irradiation (b). The hillock-like features in (b) are the signatures of the irradiation induced defects.

In order to study the origin of the observed hillocks, we performed both STM and contact mode AFM measurements on the irradiated HOPG substrate. The measurements showed that 100 – 105 hillocks could be imaged on an area of 100x100 nm^2 by STM (Fig. 2a), while only 9 – 10 hillocks could be detected on a same size area by AFM (Fig. 2b).

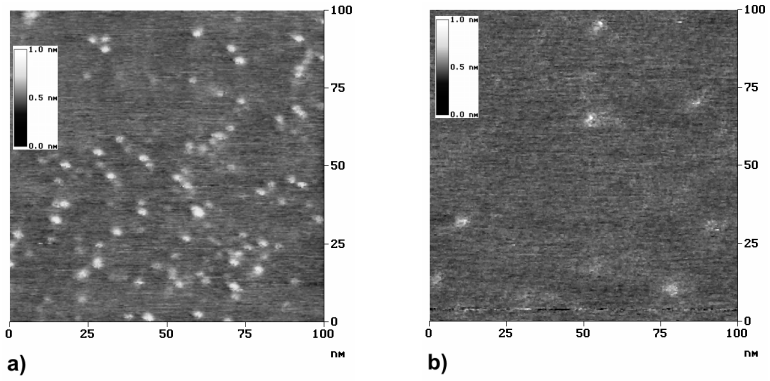


Figure 2. STM (a) and contact mode AFM image (b) of irradiated HOPG substrate.

These results show that the major part (~ 90 %) of the hillock-like protrusions seen by STM is due to the change in the local electronic density of states (LDOS), and only a small part (~ 10 %) can be attributed to clusters and deformations topographically emerging from the HOPG surface. Due to the graphitic structure of multi-walled nanotubes it is reasonable to assume a similar ratio for the hillocks observed on the nanotube surfaces. The major part of the hillocks can be ascribed mostly to vacancies, since at this ion energy the nuclear stopping dominates over the electronic stopping. Furthermore, according to simulations vacancies appear as hillocks on the STM images [4].

We observed hillock-like protrusions not only on the STM images of irradiated nanotubes but also during the STM investigation of coiled carbon nanotubes (Fig. 3b). Figure 3a) shows a coiled nanotube synthesized by the decomposition of fullerenes [5], with 3.5 nm between the coils.

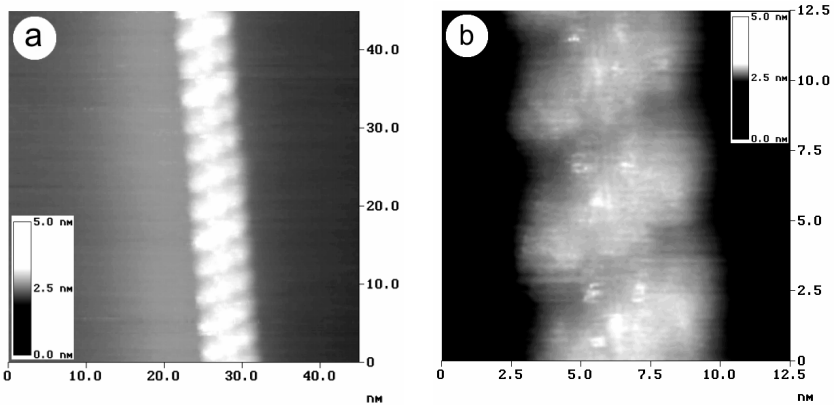


Figure 3. STM images of a coiled carbon nanotube. The image in (b) shows a magnified portion from (a). The hillock-like features in (b) are attributed to non-hexagonal carbon rings.

Figure 3b) shows a magnified portion from Fig. 3a), where one can observe the hillock-like features which appear repeatedly and in a regular way along the coils. These features are attributed to the non-hexagonal carbon rings which are responsible for the bending and coiling of the nanotubes. Theoretical works show that non-hexagonal carbon rings incorporated in a hexagonal structure also appear as hillocks, because they change the LDOS by introducing additional electronic states near the Fermi level [6, 7]. The regular appearance of the hillocks along the coils agrees well with the early model structure proposed for coiled nanotubes [8].

References:

[1] J.-P. Salvetat, J.-M. Bonard, N. H. Thomson, A. J. Kulik, L. Forró, W. Benoit, L. Zuppiroli, Appl. Phys. A **69** (1999) 255
[2] J. W. Park, J. Kim, J.-O. Lee, K. C. Kang, J.-J. Kim, K.-H. Yoo, Appl. Phys. Lett. **80** (2002) 133
[3] L. Porte, M. Phaner, C. H. de Villeneuve, N. Moncoffre, and J. Tousset, Nucl. Instrum. Meth. B **44** (1989) 116
[4] A. V. Krasheninnikov, K. Nordlund, M. Sirviö, E. Salonen, and J. Keinonen, Phys. Rev. B **63** (2001) 245405
[5] L. P. Biró, R. Ehlich, Z. Osváth, A. A. Koós, Z. E. Horváth, J. Gyulai, J. B.Nagy, Mat. Sci. Eng. C **19** (2002) 3
[6] V. Meunier, Ph. Lambin, Carbon **38** (2000) 1729
[7] D. Orlikowski, M.B. Nardelli, J. Bernholc, C. Roland, Phys. Rev. B **61** (2000) 14194
[8] S. Ihara, S. Itoh, and J. Kitakami, Phys. Rev. B **48** (1993) 5643

PHOTO-INDUCED INTERCONVERSION OF CONJUGATED AZOBENZENES ON METAL SURFACES

Giuseppina Pace [a], *Violetta Ferri* [b], *Mark Elbing* [c], *Marcel Mayor* [c,d], *Maria A. Rampi* [b], *Paolo Samorì* [a,e]

[a] *ISIS -Université Louis Pasteur, 8 allée Gaspard Monge, F-67083 Strasbourg, France*
[b] *Department of Chemistry, University of Ferrara, Via L. Borsari 46, I-44100 Ferrara, Italy*
[c] *Institute for Nanotechnology, Forschungszentrum Karlsruhe GmbH, D-76021 Karlsruhe, Germany*
[d] *Department of Chemistry, University of Basel, St. Johanns-Ring 19, CH-4056 Basel, Switzerland*
[e] *Istituto per la Sintesi Organica e la Fotoreattività, CNR, via Gobetti 101, I-40129 Bologna Italy*
gpace@isis-ulp.org

Self-assembly of thiol functionalized organic architectures on a metal electrode represents a convenient strategy for incorporating molecules into micro- and nano-electronic circuits. Photoactive molecules, as azobenzene, are attractive systems to design and assemble photoswitchable molecular devices [1]. The photo-isomerization of conjugated azobenzenes organized in self-assembled monolayers (SAMs) on metal surfaces is reported to be hampered because of the tight packing between nearest neighbor molecules in the SAM.

Previously, the endeavour has been addressed to the formation of SAMs from alkanethiol functionalized azobenzenes chemisorbed on gold [2]. However, alkanethiol derivatives are not ideally suitable as electroactive units for nanoelectronics because of the poor conductivity of the alkane chain. Here we describe the first case of fully conjugated azobenzene derivatives (AZO, Fig. 1A) exhibiting reversible *trans-cis* photo-isomerization when organized in single-component SAMs on Au(111).

Scanning Tunneling Microscopy (STM) and Near Edge X-ray Absorption Fine Structure (NEXAFS) studies have been carried out in order to characterize the molecular self-assembly across a wide range of length scales. They revealed that the AZO chains pack nearly perpendicular to the substrate, if compared to conventional alkanethiol SAMs on Au(111). The tilt angle of the molecular backbone with respect to the normal to the substrate is ~20°, allowing the maximization of the intermolecular interactions.

High-resolution STM current images showed that the AZO molecules assemble into a rectangular unit cell containing two molecules as shown in Fig. 1B; this behavior is similar to the case of simpler arenethiols SAMs [2]. We also found that molecules bind the substrate as dimer. The binding of the dimers is evidenced by the typical herringbone structure appearing in the SAM's domains (Fig. 1B).

Previous AFM and STM studies revealed two different patterning for the arenethiols and alkane-thiolated azobenzenes chemisorbed on Au(111); this observation has been explained in view of the existence of two different lattices: the pseudo-hexagonal and the herringbone [3]. Sub-molecularly resolved STM images recorded at different scan angles allowed us to rule out the existence of two different molecular lattices for our conjugated azobenzene thiolated derivatives. Upon change of the scan angle we observed that the herringbone structure becomes a pseudo-hexagonal patterning and vice versa, maintaining the identical unit cell size and geometry. Thus we conclude that the two lattices are equivalent. We attribute this scan angle dependence of the image contrast to the contribution of the frontier's orbitals of the conjugated molecules to the electron tunneling. Consequently the molecular packing within the dimer, consisting of two

aromatic chains assembled according to a herring-bone motif, is very likely to play a role. Such herringbone structure is thermodynamically favored since the face-to-face packing of two π-systems is characterized by a repulsive interaction, whereas when the π-systems glide one other or rotate away from each other the interaction becomes attractive [4].

STM measurements of the AZO SAM under UV light irradiation have been also performed. We found that both in SAM formed from solutions kept under irradiation during chemisorption and in samples incubated in the dark and post-irradiated when dried, the self-assembled monolayers mostly exhibit domains containing molecules in their *trans* conformation.

The photo-induced interconversion was also monitored by UV-Vis spectroscopy in transmission mode using transparent metal surfaces and the conductivity was measured using the drop mercury junction method [5]. The I-V characteristics of the junction, before and after irradiation through the transparent substrate, revealed changes in the electrical conduction of one order of magnitude. The current can be switched "on" and "off" several times by irradiating at different wavelengths. This proves that the conductivity of the junction can be modulated by a light driven molecular switch.

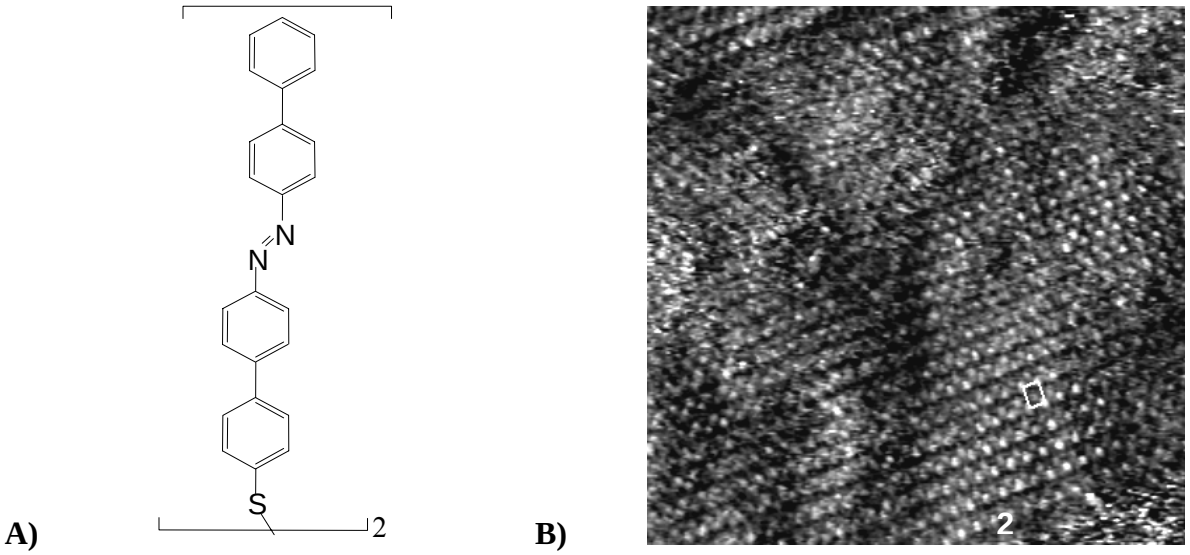


Fig. 1: A) Molecular structure of an azobenzene derivative (AZO1). B) Constant-current STM image of AZO1 SAM on Au(111) showing a rectangular unit cell containing two molecules. Unit cell parameters: a= (0.65±0.3) nm; b= (0.89±0.5) nm; alpha = (84± 3)°. Similar unit cell was reported for arenethiols SAMs on Au(111) [2].

References:

[1] N. Tamai, H. Miyasaka, Chem. Rev., 100, (**2000**), 1875
[2] S.D. Evans, R.S. Johnson, H. Ringsdorf L.M. Williams, H. Wolf, Langmuir, 14, (**1998**), 6436
[3] H. Wolf, H. Ringsdorf and collaborators J. Phys. Chem., 99, (**1995**), 7102
[4] C. A. Hunter, K. R. Lawson, J. Perkins, C. J. Urch, J. Chem. Soc. Perkin Transactions 2, (**2001**), 651
[5] E. Tran, M.A. Rampi, G.M.Whitesides, Angew. Chem. Int. Ed., 43, (**2004**), 3835
M. A. Rampi, G. M. Whiteside, Chem. Phys., 281, (**2002**), 373

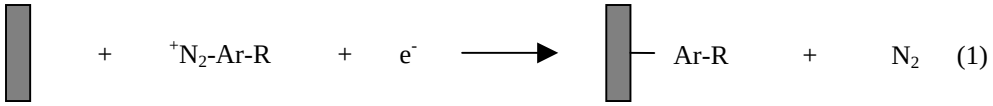
ADHESION OF ELECTROGRAFTED NITROBENZENE FILMS ON SILICON SURFACES AS A FUNCTION OF THE APPLIED POTENTIAL: AN AFM STUDY

J. Charlier, M. Laudé and S. Palacin

Chimie des Surfaces et des Interfaces, CEA-Saclay, DSM-DRECAM-SPCSI,
91191 Gif sur Yvette Cedex (France)
julienne.charlier@cea.fr

Abstract:
We report the formation of multilayer nitrobenzene films attached to silicon surfaces. Thin films are grafted to the surface via the electrochemical reduction of aryl diazonium salts. As a function of the final applied potential, the coating is more or less strongly attached to the surface as evidenced by AFM. For a final potential more cathodic than -0.8V/Ag wire in our electrolytic medium, coating can be removed from the surface by the mechanical friction of the AFM tip. A nanoscale pattern can be then obtained and the free restored surface becomes again available for a later grafting.

Diazonium compounds are known to easily form radicals in chemical reactions, and the electrochemical reduction of aryl diazonium salts on various conductive surfaces is a very effective means for generating thin films containing a wide range of chemical functionalities. Attack of the electro-generated radical at the surface leads to covalent attachment (eq 1).

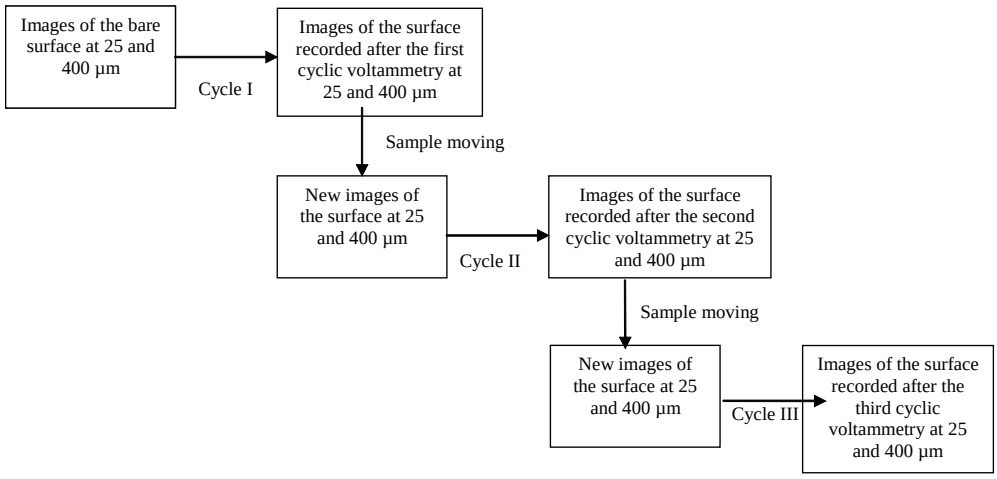


The thin film that is initially grafted does not completely impede the further reduction of diazonium ions; hence the generation of radical species and film growth may continue. The current work investigates the multilayer formation of nitrobenzene films by coupling *in situ* electrochemistry and AFM analysis. The deposition and imaging processes involve the following steps (scheme 1): (1) substrate, placed in the electrochemical cell in presence of the electrolytic solution, is first imaged in the contact AFM mode; (2) the tip is then withdrawn from the surface (5µm), and electrochemical procedure is applied (cyclic voltammetry between the open circuit voltage and the chosen final potential); (3) after electrochemical process, the resulting coating was imaged by switching to AFM contact mode; (4) after withdrawing the tip, the sample is moved (from a few mm with a micro-control plate) and a new area is imaged. At that last position, a new voltammetry cycle is applied and the resulting surface modifications are again imaged by AFM. This protocol was set up because it makes it possible to check at the same time the homogeneity and the adhesion of the coating on a large range of the sample.

When the first cyclic voltammetry occurs, the resulting organic grafting is strongly attached to the surface whatever the final applied potential. No mechanical erosion of the coating was observed when we moved the sample after the first cycle and analysed a new area. The first organic layer is thus strongly attached to the surface leading to a covalent bond between the aryl radical and the substrate.

But when the number of cycles increases, and when the final potential becomes more cathodic than -0.8V/Ag wire, a mechanical erosion of the coating by the tip is clearly observed. The images recorded at 40 µm by 40 µm clearly highlight a square of 5 µm by 5 µm formed by the precedent scanning of the tip at that same position. This phenomenon starts to be observed starting from the second cycle and is accentuated even more for the following cycles (fig. 1).

It is likely that strongly cathodic potentials promote very efficient formation of radicals from the diazonium solution. Those radicals can eventually react between them thus forming compounds which are not anchored to the surface of the sample. A polynitrophenylene multilayer film is formed which is not grafted to the surface and can be removed (or displaced), by simple mechanical effect, with the successive scans of the tip. Beyond a threshold potential (-0.8V/Ag wire in our case), one notes the drive of the matter in contact with the tip even on surfaces said "new", visible on the images by the formation of a square on the surface, corresponding in dimensions, with the preceding scanning. One can use this characteristic to structure the substrate at a sub-micronic scale.



Scheme 1: Steps of the experimental applied protocol combining in situ electrochemistry and AFM analysis

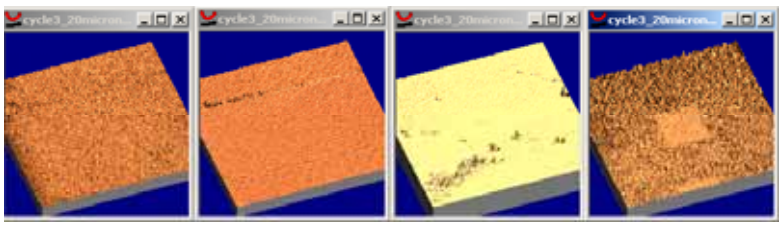


Figure 1: Images in contact AFM, 40µm by 40µm, of the coating obtained after three cyclic voltammetry as function of the final applied potential.

INTERFACIAL SIGNATURE OF THE POLYMER-TO-METAL BONDING

G. Deniau, L. Azoulay, G. LeChevallier, P. Jégou and S. Palacin*

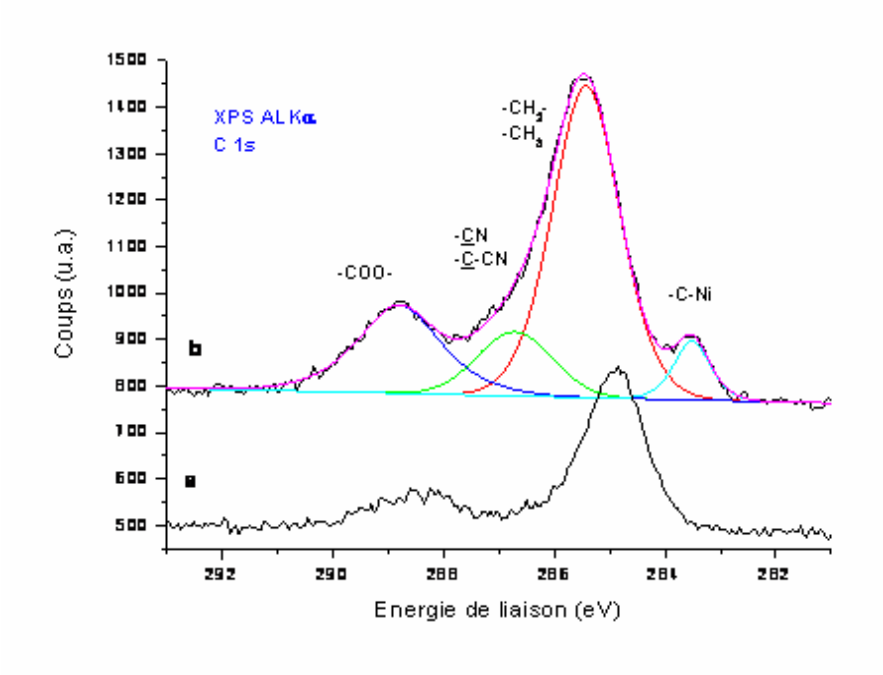
Chimie des Surfaces et des Interfaces, CEA-Saclay, DSM-DRECAM-SPCSI, 91191 Gif sur Yvette Cedex (France)
guy.deniau@cea.fr

Cathodic electropolymerization has already proven its ability to produce robust and conformal organic films chemically grafted on metallic and semiconducting surfaces used in various domains such as microelectronics, biomedical applications, soldering, chemical waste treatment or corrosion protection. (1) Contrary to the electrodeposition of semi-conducting polymers like polypyrrole or polyaniline, strong covalent bonds between the cathode and the polymer film area created during the process, as indirectly proved by numerous studies including chemical post-treatments, electrografting on rotating electrodes or mechanical measurements (1). A direct evidence can however be obtained from XPS.

Probing the chemical interface between a polymer film and a metallic substrate is very difficult. Indeed, the interface is "buried" under the polymer film and thus difficult to reach. For instance, XPS cannot probe more deeply than ca. 15 nm below the outmost surface. It is thus necessary to limit the growth of the polymeric film to be able to probe the interfacial signature.

This was done by using a redox active molecule that cannot polymerize. Indeed, with classical vinylic monomers such as acrylonitrile or methyl methacrylate, the grafting step that immediately follows the electron transfer from the cathode, gives a very unstable species bearing a negative charge very close to a negatively charged electrode. The instability is classically relaxed by the polymerization that moves away the charged species from the electrode (1).

With crotononitrile, another relaxation route is possible through a proton transfer that heals the carbanion before polymerization occurs. Hence, ultrathin grafted films are obtained. XPS analysis of the resulting films allows the direct observation of the carbon-metal bond that is buried under the grafted film and contributes greatly to its robustness. A clear and distinct peak at 283.5 eV is observed which is attributed to C-Ni bonding. (2) Its full width at mid-height is only 0.8 eV, which indicates that the bonding is probably perpendicular to the surface.



XPS spectra (C1s area) of the Nickel surface before (a) and after (b) electrografting of crotononitrile.

Spectrum (a) shows classical carbon contamination of the crude Nickel surface

References:

(1) Palacin, S.; Bureau, C.; Charlier, J.; Deniau, G.; Mouanda, B.; Viel, P.; Electrografting: "Covalent bonding at Metals and Semiconductors" *ChemPhysChem* , 2004, **10**, 1469-1481

(2) Bureau, C., Defranceschi, M., Delhalle, J., Deniau, G., Tanguy, J. and Lécayon, G.; "Theoretical monomer cluster model of a polymer-metal interface- Poly(methacrylonitrile) on a Nickel Surface". *Surf. Sci*. 1994. **311**, 349-359

Experiments on Carbon nanotubes with ferromagnetic contacts

Emiliano Pallecchi[1], Dominik Preusche[1], E. Thune[1], A. Morpurgo[2] and Ch.Strunk[1]

[1] *Institut für Experimentelle und Angewandte Physik, Universität Regensburg, Germany.*
[2] *Kavli Institute, TU Delft, Netherlands.*

Carbon nanotubes (CNTs) have unique mechanical and electronic properties, which make them a very interesting material for both fundental research and applications. Carbon nanotubes are also characterized by a very low spin-orbit coupling, so they are expected to have a very long spin flip-length, which made them a good candidate for spintronics devices.

The band structure of a SWNT is determined by the indices *(n,m)* or equivalently by the diameter d and the chiral angle θ. The knowledge of these parameters would allow a direct comparison between theoretical prediction and transport measurements. We used the selected area electron diffraction (SAED) technique to characterize the structure of CVD grown CNTs on a Si_3N_4 membranes. The membranes were previously prepared with alignment marks and slits. The first were used to locate the tube while the latter are necessary in order to have partially freestanding nanotubes (fig. 1a). This allows us to perform high resolution nanodiffraction (on the free-standing part) and transport measurements on the same sample. The background stemming from the membrane would cover the weak diffraction pattern produced by the tubes while a support is need in order to contact the CNT. By means of this technique was also possible to distinguish SWNTs, DWNTs and small bundles. Moreover, we could obtain the indices *(n,m)* of an individual CNT. For DWNT it was possible to determine the diameter and the chirality of both shells. The assignment of *(n,m)* for a given tube is done by simulating the diffraction pattern and the equatorial line for different tubes, then searching the best match between measured and calculated data. Because of the small signal (we are doing diffraction on part of a single CNT) it was not always possible to make a unique assignment of the indices, nevertheless it was still possible to restrict the choice to a few possiblities.

In order to investigate spin transport, we have chosen a palladium-iron alloy as contact

material. Palladium is known to make transparent contacts to nanotubes and by adding iron it gets ferromagnetic. Two concentrations of $Pd_0.8Fe_0.2$ and $Pd_0.6Fe_0.4$ were used. Different shapes for the two contacts lead to different coercive fields, allowing a crossover between parallel and antiparallel magnetization orientations. By sweeping an in-plane magnetic field it was then possible to control the relative magnetization of the contacts.

The magnetic properties of the contacts were studied by SQUID measurements and Lorentz microscopy. From SQUID measurements we obtained the hysteresis curves of arrays of many contacts. Lorentz microscopy allowed to explore the magnetization dynamic of the single contact, i.e. to resolve single domain.

Low temperature magnetoconductance measurements were performed on SWNTs and MWNTs with PdFe contacts. The CNTs was laying on a heavily doped silicon substrate which was used as backgate. The low-field magnetoconductance showed a hysteretic switching (fig.1b) The amplitude of the low-field magnetoconductance was found to be gate and bias dependent. The maximum switching amplitude was 4%, while for certain gate voltages it was completly suppressed. For MWNTs, the high-field magnetoconductance shows weak localization. From weak localization measurements it is possible to get a signature of the band structure and to extract the position of the Fermi energy for a given gate voltage. This should allow to relate band structure and spin transport properties of carbon nanotubes.

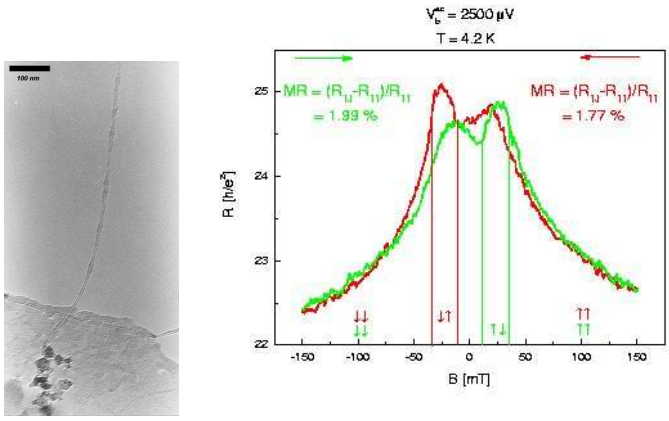


Figure 1: (a) TEM image of a SWNT. (b) Magnetoresitance of a SWNT as a function of the applied in-plane magnetic field, the change from parallel to antiparallel configuration is reflected in the jump in the resistance.

INVESTIGATION OF NANOSCALE FIELD EMISSION ELECTRON SOURCES FORMATION IN BIPOLAR POWER SUPPLY MODE

Pashkevich A.A., Popov E.O.
A.F. Ioffe Physico-Technical Institute of Russian Academy of Sciences,
Polytechnitscheskaya 26, 194021, St.-Petersburg, Russia
e.popov@mail.ioffe.ru

Despite the fantastic progress, made in the development of methods and technologies of different nanostructures production (creation) for the last 5-6 years, the future prospects of their application in vacuum devices such as unheated cathodes are still being unclear. The problems of emission current fluctuation, stability and maintainability of emitters' functioning in the technical vacuum (e. g., after spark discharge) are not solved so far, as well as the task of receiving of stably high (during the long period of time) field-emission currents, etc. The main problem lies in the limited number of really working emission centres, which is several orders less, than number of potentially created nanostructural elements.

At present there is a significant increase in experimental research (patents) devoted to emitter formation in situ. The works, aimed at creation of field emission nano- and microstructures by natural means (at least, partly), in the course of experiment (immediately in the device), are of great interest. Investigation of conditions, enabling direct relation between number of emission points, working simultaneously, and the field itself (e. g. as in case of liquid metal tips [1]) or field emission current, will result in significant stabilization of emission characteristics, long lifetime, tolerance to vacuum conditions, etc.

During our investigations significant influence of supply mode on field emission surface forming of some metal and polymeric materials [2] was discovered.

The main peculiarity of our work is carrying out the investigations in the regime of quite high field emission currents (from 1-10 mA and higher) under the influence of high-voltage low-frequency power supply pulses, and, what is most interesting, bipolar pulses. In the last case the field emission source of electrons is investigated when both electrodes are emitters.

Our experiments revealed significant influence of power supply regime on emitter action and nanostructures formation. Namely, we obtained a growth of the whisker array and a considerable increase in emission current. Formed surfaces demonstrate sufficient field emission current stability in vacuum from 1e-4 to 1e-6 Torr and good tolerance and maintainability of field emission characteristics after series of explosive emission pulses.

Obtained in the regime of bipolar power supply and high emission currents distributed emission surface, observed by scanning electron microscope (SEM), sufficiently uniform luminescence of luminescent screen, high magnitudes of emission current (5-10 mA and more), low intensities of electric field (4-5 kV/mm - magnitudes, comparable with the best samples of CNT), are evidences of simultaneous emission of a great number of emission centres.

References:

[1] Popov E.O., Pashkevich A.A., Popov S.O., Vitugov A.V. Charge Particle Source for Industrial and Research Accelerators operating at the poor vacuum conditions//EPAC'04 Proceedings, 9th European Particle Accelerator Conference, EPAC2004, 5-9 July 2004, Switzerland, Lucerne, pp.2146-2148.

[2] Ionov A.N, Popov E.O., Svetlichniy V.M., Nikolaeva M.N., Pashkevich A.A. Field Electron Emission from Flat Metal Cathodes Covered by Thin Polymer Films // Tech. Phys. Lett., Vol. 30, **Iss. 7**, 2004, pp. 566-568.

GROWTH OF MOLECULAR NANOSTRUCTURES ON Si USING SAMs OF LONG-CHAIN ALKYLTRICHLOROSILANES

Lionel Patrone [(1)], Simon Desbief [(1)], Didier Goguenheim [(1)], Dominique Vuillaume [(2)]

(1) L2MP - Laboratoire Matériaux et Microélectronique de Provence - CNRS UMR 6137 / ISEN-Toulon, Maison des Technologies, Place G. Pompidou, 83000 Toulon - France
(2) IEMN - Institut d'Electronique, de Microélectronique et de Nanotechnologie - CNRS UMR 8520, Avenue Poincaré, BP 60069, 59652 Villeneuve d'Ascq cedex - France
lionel.patrone@isen.frT

Controlling the preparation of smaller and smaller nanostructures is a key-point in nanotechnology. But today, limits of conventional lithography techniques as well as their costs are major obstacles to get over in order to go further in the integration of devices. A promising solution consists in using molecular self-assembly as a non lithographic approach for preparing nano-devices. In this communication, we report on a study of the growth behaviour of single and binary molecular self-assembled monolayers (SAMs) of long alkyltrichlorosilanes on Si/SiO_2 in order to get a better control of the preparation of nanostructures from such molecules on a technological substrate like silicon.

We first present the growth study of long chain alkyltrichlorosilane SAMs (16, 18, 20 and 30 carbon atoms chains) from a liquid phase on a Si surface covered with its natural oxide, at several temperatures and relative humidity values (RH). It is known that below a critical temperature increasing with the chain length, akylsilanes are grafted nearly perpendicular to the surface following an island growth [1] up to the complete monolayer formation. Such a growth mode is driven by van der Waals intermolecular interactions. They occur during the diffusion of the molecular species on the oxide surface, which is lubricated by the presence of a natural water thin film, before grafting. Analyzing the growth kinetics of these alkyltrichlorosilanes using atomic force microscopy (AFM), ellipsometry, and contact angle measurements, we explain the behaviour of the molecules according to the deposition conditions using a model based on Diffusion Limited Aggregation (DLA). We thus show that the C_{30} behaviour at 20°C and 40% RH is similar to that of C_{16}, C_{18} and C_{20} at 11°C and 40% RH. We have also established that the molecules diffusion coefficient increases with relative humidity, and surprisingly decreases with temperature. Another important result is the decrease of the growth characteristic time with the number of carbon atoms in the alkyl chain except for C_{30}. Such behaviour of the growth kinetics with the number of carbon atoms is interpreted by the competition between the molecular diffusion coefficient and the DLA capture radius, the first one decreasing with the chain length while the second increases.

In a second step, we report on the phase separation study between C_{30} on one hand and C_{16}, C_{18}, C_{20} on the other hand according to the deposition parameters (Fig. 1). Indeed, phase separation in such systems [2-3] is promoted by the length difference which modifies the chain to chain van der Waals interaction. In addition to the classical phase separation by islands of C_{30} in a surrounding phase of shorter molecules, we observe a demixtion involving dendritic "filaments" of C_{30} in a shorter molecules phase, regardless the couple of molecules studied. A third sort of phase separation also appears in the case of C_{30}/C_{18} and C_{30}/C_{20}: formation of holes composed of islands of the shorter molecule, in a surrounding phase of C_{30}. We interpret the possibility to obtain such a demixtion using only C_{18} and C_{20} as short molecules with C_{30} by the fact that we are working below the critical temperatures of $C_{18\text{-}30}$ molecules, which is not the case for C_{16}. To our knowledge, this is the first observation of "filaments" and "holes" structures resulting from the phase separation in a binary mixture of alkylsilanes. Furthermore, we show the composition of binary SAMs performed at low humidity (20% RH) is almost the same that the one of the silanisation solution in the case of SAMs that phase separate by islands or holes. Concerning SAMs synthesized at high

humidity (40% RH), regardless the phase separation, we note that the proportion of longer chain molecules is always lower in the SAM than in the solution. The good transfer of the solution composition to the deposition substrate at low RH conditions on one hand, and the depletion of longer chain molecules in the SAM compared to the solution on the other hand are explained within DLA growth model. Indeed, at high humidity the SAM growth is mainly driven by the diffusion coefficient, while at low humidity the deposition rate from solution is shown to be the leading parameter of the growth.

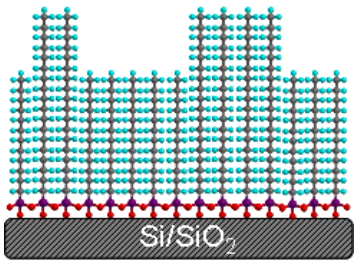
As a summary, we performed a study of the growth behaviour of long alkyltrichlorosilanes from 16 to 30 carbon atoms, in single and binary SAMs. To our knowledge, this is the first time that C_{30} alkyltriclorosilanes have been studied so extensively and that they have been used in binary SAMs. The two relevant parameters are temperature and relative humidity. We explain the growth kinetics of individual molecules within a DLA model. As for the mixture of two alkyltrichlorosilanes of different lengths, we could obtain for the first time “holes” and “filaments” demixtion patterns. We show the SAM composition can be controlled varying relative humidity, which is explained by DLA model of growth. These results are a step forwards the preparation of size controlled nano-domains acting as a pattern for building molecular devices. For instance, modifying the functionality of the domains by changing the moieties of the grafted molecules in a selective chemical way would allow building different devices such as molecular diodes [4] and nano-transistors by grafting a conjugated oligomer (channel) on top of the alkyl chains [5]. The advantage of this Si-molecules hybrid approach of nanoelectronics is to be compatible with the well-known silicon technology regarding applications.

References:

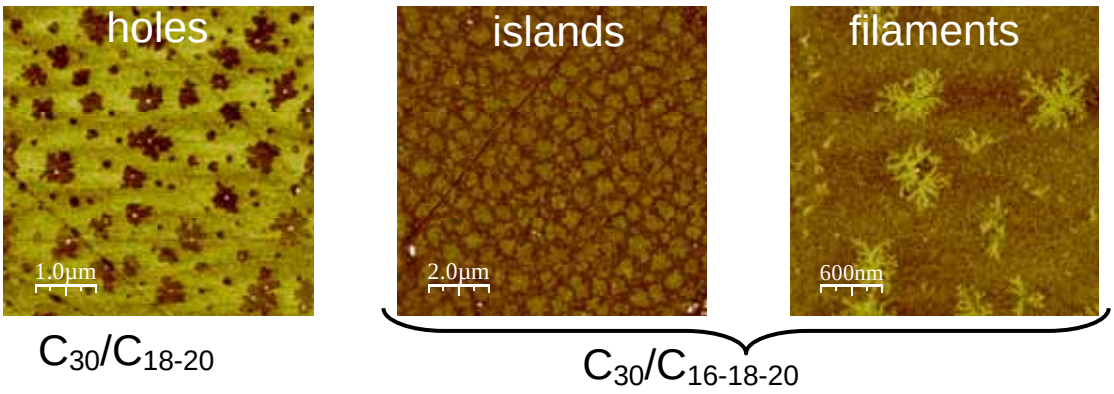
[1] C. Carraro, O.W. Yauw, M.M. Sung, R. Maboudian, J. Phys. Chem. B **102** (1998) 4441
[2] B.L. Kropman, D.H.A. Blank, H. Rogalla, Langmuir **16** (2000) 1469
[3] L. Breuil, Ph.D. Thesis, University of Sciences and Techniques Lille Flandres-Artois (2000)
[4] S. Lenfant, C. Krzeminski, C. Delerue, G. Allan, D. Vuillaume, Nano Lett. **3** (2003) 741
[5] J. Collet et al., Appl. Phys. Lett. **76** (2000) 1339

Figure 1. Binary SAMs : a) cross-section scheme, b) examples of demixtion patterns (AFM images).

a)



b)



LANTHANIDE DOPED ZnO NANOCRYSTALS: SYNTHESIS, SURFACE MODIFICATION AND OPTICAL BEHAVIOUR

Angela Sofia Pereira[a], Marco Peres[b], Sérgio Pereira[c], Teresa Monteiro[b], Tito Trindade[a]
[a] *Department of Chemistry, University of Aveiro, CICECO, 3810-193 Aveiro, Portugal*
[b] *Department of Physics, University of Aveiro, 3810-193 Aveiro, Portugal*
[c] *Department of Physics, University of Aveiro, CICECO, 3810-193 Aveiro, Portugal*
Contact: aspereira@dq.ua.pt

Quantum dots (QDs) have been extensively investigated during the past decades. Their unique optical properties due to quantum confinement effects are of interest for application in optoelectronics, such as in display monitors but also as optical biomarkers [1]. A great interest arises from the optical properties of doped semiconductor nanocrystals namely lanthanide (Ln) doped zinc oxide. While doping in bulk semiconductors is now habitual, the doping of semiconductor nanocrystals is not straightforward. The small dimensions of the colloidal QDs guides the way to new difficulties not stumbled upon in bulk materials. Once the QD doping is achieved, an additional dilemma is encountered. The dopant may is likely to diffuse towards the surface or into the solution due to thermodynamic driving forces, since the dopant atoms are always only a few lattice constants from the QDs surface [2].

Lanthanide ions are excellent candidates for luminescent centers due to their 4f intra-shell transitions, e.g. the characteristic narrow emission bands make Ln-doped materials bright colored luminescent materials. Here the incorporation of foreign ions in a host, in particular for ZnO nanocrystals, does not mean necessarily replacement of ions in the crystalline lattice. Regardless the type of incorporation of Ln ions in semiconductor nanocrystals, optical properties of nanocrystals are anticipated to be remarkably modified. However, it is also true that this task poses several challenges namely due to size and charge constrains.

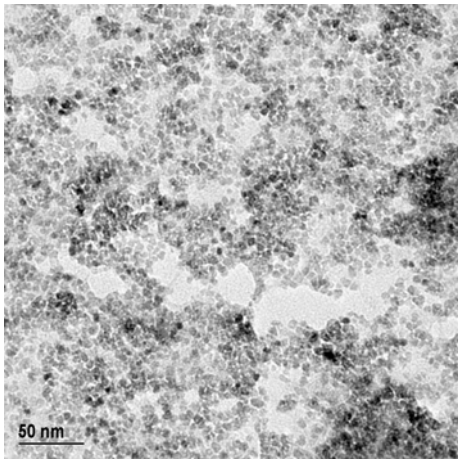


Fig.1 – TEM image of ZnO nanocrystals

We report here our attempts on the incorporation of Ln cations in ZnO quantum dots using a wet colloidal method previously applied for d-metal doping of ZnO nanostructures.[3,4] Several experimental parameters have been investigated in order to vary the morphological features of ZnO quantum dots. The average size and monodispersity of the colloids, and hence the optical band gap, could be controlled by a rigorous adjustment of the temperature of synthesis as shown in Fig.2. The spectra shown in Fig.2 are characteristic of quantum sized ZnO particles obtained in the presence of Tb^{3+} and are similar to those of pure ZnO, i.e. prepared in the absence of the lanthanide. For each temperature of synthesis, the ZnO optical bang gap is shifted to higher energies when compared to the typical bulk band gap value (Eg~ 3.3 eV at RT). Surface modification methods were investigated as the path to develop core-shell ZnO heterostructures.[4] In some cases such surface modification was surveyed to evidence the location of the foreign cations in the host. These studies were complemented with a detailed analysis of the photoluminescence properties of the starting dots and the resulting core-shell nanostructures.

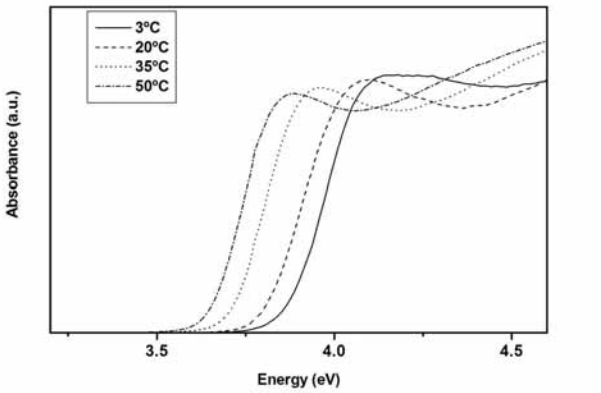


Fig. 2 - Room temperature absorption spectra of Tb^{3+} doped ZnO colloids synthesised at distinct temperatures.

Acknowledgements: ASP would like to thank FCT for her PhD grants. This work was funded by Universidade de Aveiro (Project 3.64.33.7/NANOENG/CTS15) and by Fundação para a Ciência e Tecnologia (POCTI/CTM/45236/02).

[1]S. G. Penn, L.He and M. J. Natan, Curr Opin Chem Biol, 7 (2003), 609
[2] M. Shim, C. Wang, D. J. Norris and P. Guyot-Sionnest, MRS Bulletin, **26** (2001) 1005.
[3] D.A. Schwartz, N.S. Norberg, Q.P. Nguyen, J.M. Parker, D.R. Gamelin, J. Am. Chem. Soc. **125** (2003) 13205
[4] A.S.Pereira, M. Peres, M.J. Soares, E. Alves, A. Neves, T. Monteiro, T. Trindade, Nanotechnology, **17** (2006) 834

Charge transport properties of semiconductor nanowires within the Kubo-Greenwood and Landauer-Büttiker approaches.

Martin P. Persson[1], A. Lherbier[1,2], Y. M. Niquet[1], S. Roche[3] and F. Triozon[4]
[1]CEA/DRFMC/SP2M/L_Sim
[2]LTM (UMR CNRS 5129)
[3]CEA/DRFMC/SPSMS/GT
[4]LETI/D2NT
17, rue des Martyrs, 38054 Grenoble Cedex 9, France

martin.persson@cea.fr

Semiconductor nanowires are promising building blocks for one-dimensional physics and nanoelectronics. They have indeed shown remarkable properties. Ballistic transport has for example been achieved in Si/Ge core-shell nanowires [1]. Various devices such as resonant tunnelling diodes [2], biological sensors [3] and single-electron transistors [4] have moreover been realized in just a few years using these nanowires. However, little is known about the physics of these devices. The effects of disorder for example have not yet been assessed in detail.

We are computing the transport properties of semiconducting nanowires using the Kubo-Greenwood and Landauer-Büttiker formalisms in a semi-empirical tight-binding framework. Both formalisms have previously been sucessfully applied to carbon nanotubes [5,6]. In the Kubo-Greenwood approach, a wave packet is propagated along an infinite (disordered) nanowire. The spread of the wave packet gives access to the "intrinsic" transport properties of the nanowire, such as the mean free path, the localization length and the mobility as a function of the Fermi energy. The Landauer-Büttiker approach yields the transmission through a nanowire connected to source and drain electrodes. The combination of both approaches will ultimately allow to distinguish between intrinsic and contact-related effects in the $I(V)$ characteristic of a nanowire-based transistor. We are also comparing the results of both approaches on disordered nanowires.

We are presently studying the effect of surface roughness on the transport properties of silicon nanowires. This disorder is characterized by the rms of the radius fluctuations, $<\delta R^2>^{1/2}$, and by the typical length scale L_0 of these fluctuations along the nanowire (see Fig. 1). We have computed the mean free path and mobility as a function of these parameters. We will later consider other kind of relevant disorders (trapped charges, dopants).

This work was supported by the French "Action Concertée Incitative" (ACI) "TransNanofils" and by the European Integrated Project (IP) NODE (EU contract Nr 015783 NODE).

References:

[1] : W. Lu, J. Xiang, B. P. Timko, Y. Wu, and C. M. Lieber, PNAS **102** (2005) 10045.
[2] : M. T. Björk, B. J. Ohlsson, C. Thelander, A. I. Persson, K. Deppert, L. R. Wallenberg, and L. Samuelson, Appl. Phys. Lett. **81** (2002) 4458.
[3] : Y. Cui, Q. Wei, H. Park, and C. M. Lieber, Science **293** (2001) 1289.
[4] : C. Thelander, T. Martenson, M. T. Björk, B. J. Ohlsson, M. W. Larsson, L. R. Wallenberg, and L. Samuelson, Appl. Phys. Lett. **83** (2003) 2052.
[5] : F. Triozon, S. Roche, A. Rubio, and D. Mayou, Phys. Rev. B **69** (2004) 121410(R).
[6] : F. Triozon, Ph. Lambin, and S. Roche, Nanotechnology **16** (2005) 230.

Figures:

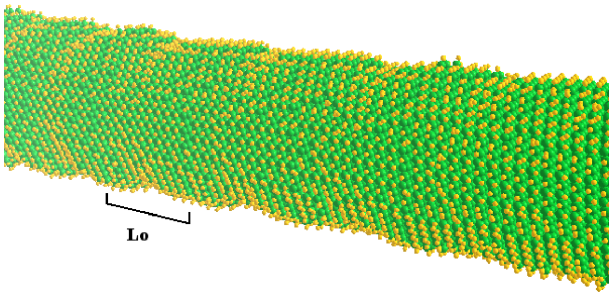


Fig. 1 : A nanowire (average radius R = 2 nm) with surface roughness.

Gold-seeded growth of Ge nanostructures inside channelled substrates by supercritical fluid-liquid-solid (SFLS) method

Nikolay Petkov, Richard Phelan, Guillame Audoit, Michael A. Morris and Justin D. Holmes
Department of Chemistry, University College Cork, Cork, Ireland
n.petkov@ucc.ie

The ability to pack high densities of memory storage and processing circuitry into specific nanoscale arrays, and utilise the unique transport properties associated with these architectures, is expected to lead to future generations of computer processors with device sizes many times smaller and faster than current silicon based processors. However, both physical constraints and economics are expected to limit continued miniaturisation of electronic and optical devices using current 'top-down' lithography based methods [1]. The necessity to develop alternative non-lithographic methodologies for fabricating mesoscopic features of integrated circuitry will soon be needed [2]. One possible approach is to use well ordered and aligned channelled architectures as hard templates to host and guide the growth of 1 D nanostructures, thereby enhancing their electrical or optical properties.

In our group we have pioneered the development of supercritical fluid (SCF) inclusion-phase techniques for forming ordered arrays of semiconductor, metal and metal oxide nanowires within the pores of mesoporous materials and columnar channels of anodic alumina membranes (AAMs) [3]. The process involves decomposition of suitable precursors at high temperatures and pressures that results in filling the porous supports but also forms undesirable blocking, surface converge and poor crystallinity of the products. On the other hand, gold-seeded SFLS has been developed and well studied for the batch production of single crystalline semiconductor nanowires [4]. In this report we present a new approach for growing Ge nanostructures "in-place" by first positioning gold-seeds inside the channelled substrates, followed by SFLS growth at temperatures slightly higher than the Au/Ge eutectic point.

Two different types of channelled supports were used in the study: (i) AAMs with nominal channel sizes of 200 and 60nm and (ii) grooved Si-wafers with thermally grown SiO_2 layer (150 nm) with a SiN (150 nm) capping layer provided by CRANN/Intel (Ireland). The alumina and silica surfaces were modified with organo-silane resulting in covalently anchored thiol or primary amine groups. In a second step colloidal gold (5-6 nm particles) were assembled on the thiol modified surfaces or 30 mM $H[AuCl_4]$ solutions were used to impregnate the amino-modified substrates. In the course of these reactions, gold seeds were introduced along the channelled substrates that were further used for SFLS growth in SC hexane at 375 ^{o}C and 1000 psi with diphenyl germane as a Ge precursor.

The deposition of the gold seeds, and the subsequent growth of the Ge nanostructures was followed by cross-sectional SEM, plan-view TEM, selected area electron diffraction (SEAD) and EDX measurements. For example, Figure 1 shows cross-sectional SEM images of the Ge nanostructures inside the 200 and 60 nm columnar channels of AAMs. 1D nanostructures are seen to protrude out of the channels, aligned along the direction of the channels. The structures appear grainy, composed of crystalline domains. The nanowires are embedded and at the same time isolated from each other inside the porous alumina matrix yielding high density, semi-ordered array of 1D nanostructures. TEM images of the isolated nanowires obtained after dissolving the alumina template in phosphoric acid showed well shaped nanowires extending for more than several microns and with diameters corresponding to the diameters of the channelled substrates. Figure 1c shows typical TEM image of one such structure where the dark spots can be attributed to the gold-seeds that are encapsulate in the

Ge matrix. Thus polycrystalline, grainy 1D nanostructures were formed that can be envisioned as chain of gold-nanoparticles connected through semiconductor Ge crystallites.

Similar approach was used when Ge nanostructres were grown "in place" along grooved Si wafers. Figure 2a shows gold seeds preferentially assembled on the SiO_2 surface that was modified with thiol functionalities. The SiN capping layer served as a coating that passivated the SiO2 surface and hindered its subsequent modification with organo-silane molecules. Thus the gold seeds were assembled only inside the trenches and gave growth to the Ge nanostructures "in place". The structures appear again grainy, composed of small crystallites filling completely the channels.

In summary, a new synthetic approach for the growth of semiconductor nanostructures is presented that relies on selective modification of channelled alumina or silica surfaces with gold seeds that guide the growth of 1D nanostructures by SFLS mechanism .

References:

[1] Timp, G. Nanotechnology; 1st ed; Springer-Verlag: New York, 1999.
[2] Heath, J. R.; Kuekes, P. J.; Snider, G. S.; Williams, R. S. *Science* **1998**, *280*, 1716.
[3] Crowley, T. A.; Daly, B.; Morris, M. A.; Erts, D.; Kazakova, O.; Boland, J. J.; Wu, B.; Holmes, J. D. *J. Mater. Chem.* **2005**, *15*, 2408.
[4] Hanrath, T. Korgel. B. A., *J. Am. Chem. Soc.* **2004**, *126*, 15466.

Figures:

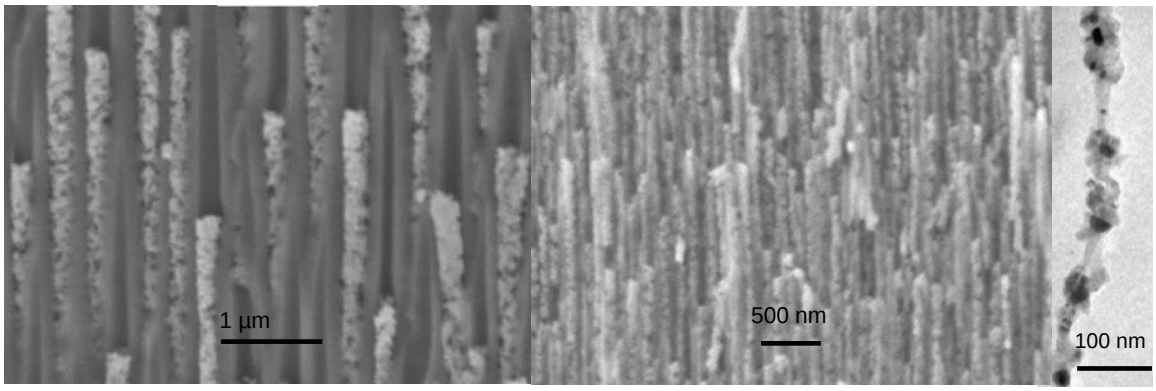


Figure 1 Cross-sectional SEM images of the gold-seeded Ge nanostructures grown inside the a) 200 and b) 60 nm channels of the AAMs, and c) TEM image of an isolated nanowire.

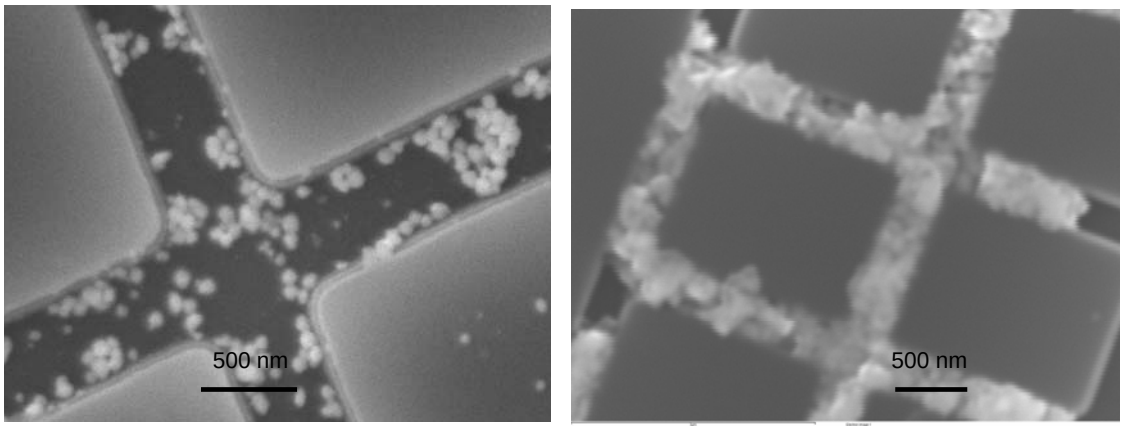


Figure 2 Plan-view SEM image of grooved substrates that were a) modified with gold-seeds and b) after SFLS growth of Ge nanostructures.

HIGH SPEED ATOMIC FORCE MICROSCOPY OF BIOLOGICAL SYSTEMS: ACHIEVING MILLISECOND TEMPORAL RESOLUTION

Loren Picco, Dave Engledew, Laurent Bozec, Mike Horton, Mervyn Miles
University of Bristol, H H Wills Physics Laboratory, Tyndall Avenue,
Bristol BS8 1TL, United Kingdom
Loren.Picco@Bristol.ac.uk

Atomic force microscopy (AFM) has proven itself to be one of the most versatile forms of scanning probe microscopy (SPM). Capable of imaging in air, liquid and vacuum using a wide range of interaction forces to provide various types of data such as surface topography, friction or electrostatics. Of particular interest is its application to the field of biological systems where its nanometre resolution and ability to image under native and physiological conditions allow for greater understanding of a whole host of intriguing systems. However it has yet to fulfil its potential in this area as such processes often occur on the millisecond timescale, which is several orders of magnitude faster than current methods can follow and means that the experimenter has to extract information from a series of time lapsed stills.

Subsequently there has been great enthusiasm and interest in improving the speed of AFM imaging and many varied approaches have been employed to try and overcome this scan-speed limitation. For example, the development of small cantilevers and the optimisation of the feedback loop, which has enabled several groups to pursue increased speed with intermittent contact mode imaging [1,2]. Arguably however both the miniaturisation of the cantilevers and the optimisation of the feedback loop are reaching their physical limits. A new and novel approach to overcoming a major hindrance of conventional AFM, the onset of mechanical resonances, has recently been demonstrated by Humphris *et al* [3]. The technique does not try to avoid such vibrations of the system, but uses a mechanical resonance to scan the tip in a plane above the surface. Combining this resonant scanning method with a high bandwidth mechanical feedback loop, high speed AFM with millisecond time resolution has been achieved [4].

The work presented here develops upon the resonant scanning method and shows it to be capable of achieving millisecond temporal and nanometre lateral resolution on biological samples. Fibres of rat-tail collagen were dried down onto glass cover slips and imaged at up to 30 frames per second with tip velocities in excess of 2.5 cm/s (Figure 1). The characteristic 67 nm banding was observed in detail (Figure 2) and the fibres were seen to be stable despite tens of minutes of imaging at such high scan rates.

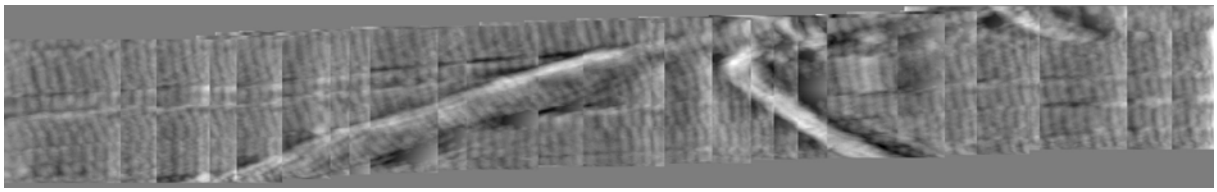
Please note:
An oral presentation is requested as well as a poster presentation as the high speed movie files created whilst imaging are capable of significantly more impact when they can be seen to be dynamically changing in a talk rather than when shown as a series of static images.

References:

[1] N. Kodera, H. Yamashita, T. Ando, Review of Scientific Instruments, **76** (2005) 053708
[2] G.T. Paloczi, B.L. Smith, P.K. Hansma, D.A. Walters, Applied Physics Letters, **73**, (1998) 1658
[3] A.D.L. Humphris, J.K. Hobbs, M.J. Miles, Applied Physics Letters, **83** (2003) 6
[4] A.D.L. Humphris, J.K. Hobbs, M.J. Miles, Applied Physics Letters, **86** (2005) 034106-1

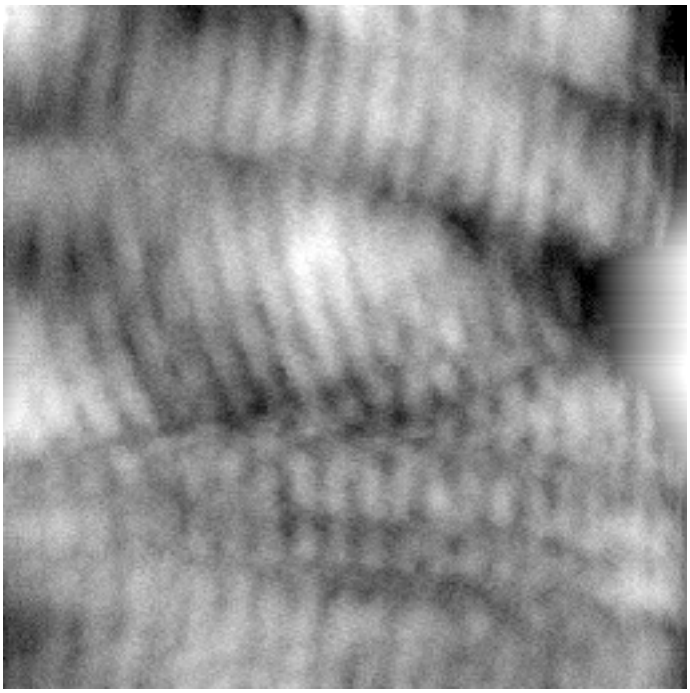
Figures:

Figure 1



A composite image of rat-tail collagen fibres showing the expected 67 nm repeat banding. The image was constructed from a high speed movie in which each 256 x 256 frame was captured in 27 milliseconds at a tip velocity of 2.7 centimeters per second. Total length of the composite image is 7.1 microns.

Figure 2



A single 256 x 256 pixel frame collected in 27 milliseconds providing a clearer image of the periodic banding running along the collagen, image size is ~ 1.4 microns.

DYNAMIC STUDY AND CONTROL OF GOLD COLLOIDAL DROP EVAPORATION

T. Pinedo*, J. Tallal, M. Gordon, D. Vempaire, C. Ternon, K. Berton and D. Peyrade.
LTM/CNRS 17 avenue des Martyrs 38052 Grenoble CEDEX 9
*tatiana.pinedo@cea.fr

Keywords : Gold colloids, Capillary force assembly, sessile drop evaporation.

One of the major technological bottelnecks of nanotechnology research is the precise localization of nanostructures to fully exploit their intrinsic properties. For example, one would like to put a Qdt[1] in the high field center of an optical cavity, position a Nc[2] between two electrodes, or use a metallic Np[3] as a catalyzer for localized wire or CNT[4] growth. Several ingenious approaches have already been developed using local capture techniques involving magnetic or electrostatic fields for single nanostructures as well as global strategies like functionalized substrates and large scale templates.

In this work, we present our results on an alternative technique **[1-3]** to localized Np from colloidal solution into lithographic patterns. This technique is based on the use of capillary forces applied on the Np at the triphasic point (vapor-liquid-substrate) when the solvant evaporates above the lithographic pattern. Pattern filling can be obtained when the capillary force is superior to thermal fluctuations (several kT). The strength and direction of this force is determined by careful control of the contact angle at the triphasic point, surface tension and contact line speed . Dynamically monitoring of the drop drying allows to show different regimes in the drop evaporation. By controlling the drop temperature, the contact line speed (CLS) can be modulated. Finally, the exponential behavior of CLS-temperature relationship has been put into evidence.

[1] A. P. Alivisatos et al., Nano Lett., 4(6), 1093-1098, (2004)
[2] A. P. Alivisatos et al., J. Vac. Sci. Technol., B22(6), 3409, (2004)
[3] Y. Xia et al., J. Am. Chem. Soc., 123, 8718-8729, (2001)

[1] Qdt : Quantum dot
[2] Nc : Nanocrystal
[3] Np : Nanoparticle
[4] CNT : Carbon Nanotube

Molecular Wires Composed of Thiophene Oligomers

Ping Bai[1], Erping Li[1], Eng Ann Ong[1], Peter Collier[2]
[1]Institute of High Performance Computing, Singapore
[2]Singapore Institute of Manufacturing Technology (SimTECH), Singapore
baping@ihpc.a-star.edu.sg

Molecular electronics, exploiting a cross-disciplinary bottom-up approach and using interconnected molecules to perform the basic functions of microelectronics, has attracted a great attention. Conjugated molecules, possessing delocalized π electrons, are pointed out being promising candidates to build new generations of electronic and photonic devices. It is essential to understand the electron conduction mechanism inside the molecules and at the interface between the molecule and electrodes. Thiophene-conjugated systems present generally higher stability than other conjugated systems and their properties can be easily chemically tailored [1]. We study the electron transport properties of molecular wires, which are composed of thiophene oligomers connecting to metal electrodes, using the first principles method [2] which is based on density functional theory and non-equilibrium Green's function. At the same time, thiophene films of dimers, tetramers and hexamers are synthesized and electron conductances of the films are measured with atomic force microscope.

To simulate the electron transport properties of thiophene oligomer based wires, we connect the thiophene oligomers to two gold (Au) electrodes to build atomic metal-molecule-metal junctions as in Fig. 1. The oligomers are connected to Au(111) surface via terminal groups which are located at Au(111) hollow site, the most energetically favored location [3]. The density of states (DOS), transmission functions (TF), and current-voltage (I-V) characteristics of the junctions are calculated to analyze their electronic properties. The effects of different substitutes, terminal groups and the wire lengths are focused.

Different alkyl substituents can modify the electronic properties of thiophene oligomers. This is done by changing the inter-ring torsional angles in thiophene oligomers. Considering the complexity in the relationship between the alkyl substituents and final conformations of the thiophene oligomers in an adsorbed film in the experiments due to the energy barriers for chain rotations, we simulate the effects of the alkyl substituents by varying the torsional angle systematically from 0 to 180 degrees instead. Figure 2 shows the simulation results of the thiophene dimers with three typical torsional angles 0, 90 and 180 degrees: DOS (Fig. 2a), TF (Fig. 2b), and I-V characteristics (Fig. 2c). Thiophene dimers with planar structures show better conductance due to better electron delocalization to the π orbitals.

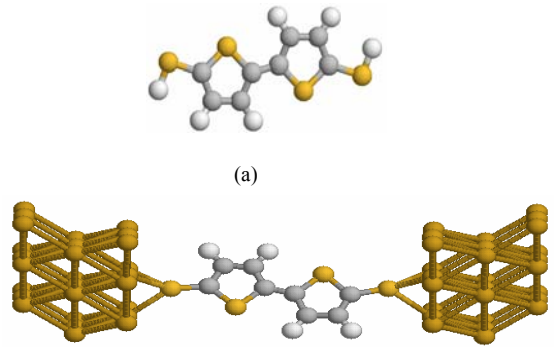
Terminal groups, which are used to build stable bonds between organic molecules and metal electrodes, will affect the electron transport of molecular systems [4]. In our experiments, S and CN have been used to connect the thiophene oligomers and Au substrates. Figure 3 shows the calculated I-V characteristics of thiophene tetramers connecting to Au electrodes with terminal group S and CN and the effects of terminal groups are clearly seen.

The resistance of molecular wires with different lengths will be fundamental for any kind of electronic wire applications. Thiophene dimers, tetramers and hexamers are synthesized and connected to Au electrodes to study the effects of the wire lengths. Figure 4 shows the simulated I-V characteristics of the dimer, tetramer and hexamer systems with torsional angle of 180 degrees. At bias less than 0.3eV (inset in Fig. 4), linear electron transport characteristics are observed in all three systems. The resistances of dimer, tetramer and hexamer wires are 16KΩ, 77kΩ, and 288 kΩ, respectively. The longer the wire is, the bigger the resistance will be.

More comprehensive analyses will be done once the measurement results come out in near term.

References

[1] J. M. Pernaut, P. Garcia and D. Delabouglise, *J. Chim. Phys.* **91**, 433 (1994).
[2] M. Brandbyge, J. L. Mozos, P. Ordejon, J. Taylor and K. Stokbro, *Phys. Rev. B,* **65**, 165401 (2002).
[3] P. Bai, E. Li, C. C. Chong and Z. Chen, "Effects of Metal-Molecule Interface Conformations on the Electron Transport of Single Molecule", *Cur. Appl. Phys.* In press.
[4] P. Bai, E. Li, Neerja, P. Collier, *IEEE T. Nanotech.,* **4(4),** 422, July 2005.



(a)

(b)

Fig. 1 Schematics of optimized thiophene dimer (torsional angle 180 degrees) with terminal group S (a) and the Au-thiophene-Au system composed of the thiophene dimer (torsional angle 180 degrees) sandwiched between gold electrodes with terminal atom S.

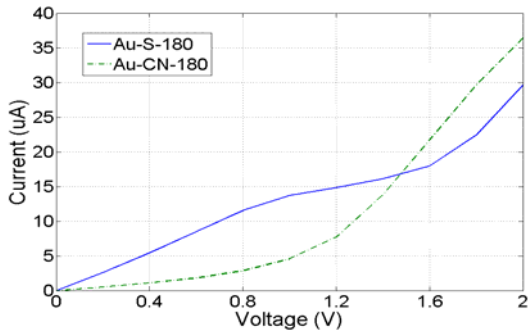


Fig. 3 I-V characteristics of thiophene tetramers (torsional angle 180) connecting to Au electrodes with terminal group S (solid) and CN (dashed).

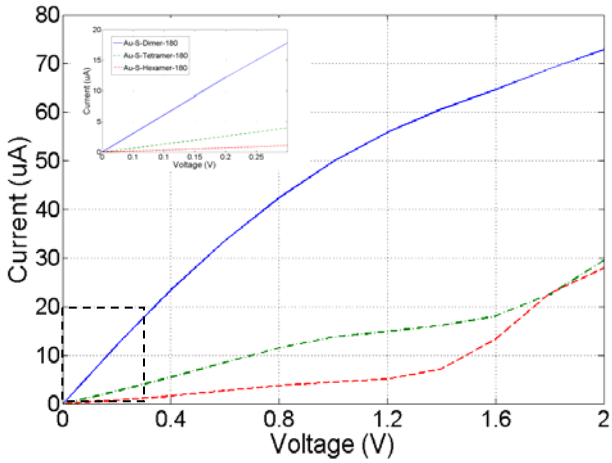
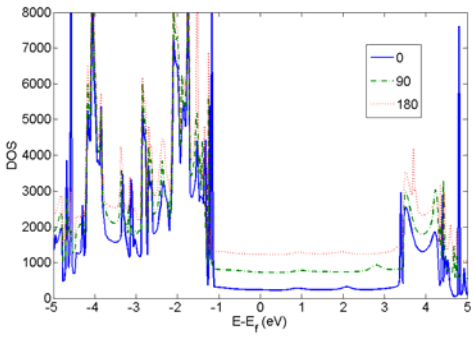
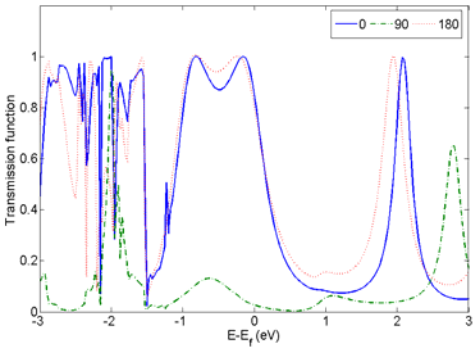


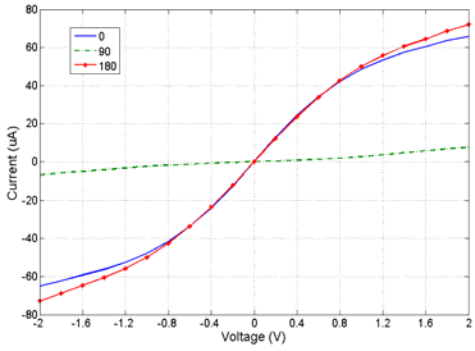
Fig. 4 I-V characteristics of the dimer (solid), tetramer (dashed), and hexamer (dotted) with torsional angle 180 connecting to Au electrodes with terminal group S.



(2a)



(2b)



(2c)

Fig. 2 Simulated density of states (a), transmission functions (b), and I-V characteristics (c) of three metal-molecule-metal junctions composed of thiophene dimers with torsional angle of 0, 90, and 180 degrees, connecting to Au (111) with terminal group S..

Poster

ANTI-INFLAMMATORY BIOERODIBLE NANOMATS

A M Piras (1), L Nikkola (2), F Chiellini (1), N Ashammakhi (2)
1 Department of Chemistry and Industrial Chemistry, University of Pisa, Pisa, Italy
2 Institute of Biomaterials, Tampere University of Technology, Tampere, Finland
Nureddin.ashammakhi@tut.fi

Pain is an unpleasant sensory experience commonly produced by damages to bodily tissues and it is one of the most significant public health problems. Pain may be treated by using polymeric drug controlled release devices that would reduce drug side effects and improve patient compliance1. The objective of the current study is to investigate the application of synthetic bioerodible polymers in the preparation of nanofibers for the controlled release of diclofenac sodium (DS). 1-butanol hemiester poly(maleic anhydride-alt-2-methoxyethyl vinyl ether) was prepared at the university of Pisa2. 5-10% polymer solutions either in ethanol or in acetic acid were prepared and 2% DS was added to half of them. The solutions were electrospun to produce nanomats that were characterised in terms of morphology (SEM and electron back scattering microanalysis), thermal properties (DSC) and drug release kinetics. The average fiber diameter of the prepared nanomats ranged from 100 nm to 1 m. It was observed that increasing polymer concentration increased the size of the fibers but reduced the number of beads. The use of DS as sodium salt induced both an increase of the charge density of the electrospun jet and of the viscosity of the solutions. These effects were correlated to the fiber diameters that resulted thinner when the increase of charge density was predominant. Electron back scattering analysis evidenced that DS was homogeneously distributed along the specimens. In general, the electrospun materials displayed a decrease in Tg attributed to the large surface to volume ratio of nanofibers with air as the plasticizer, whereas the presence of the drug led to smaller changes in Tg values. The actual drug loading level of all the investigated nanomats corresponded to the theoretical loading levels, calculated on the concentration value of each nanomat component employed in fiber preparation. The release of DS was immediate and no major difference was detected between ethanol and acetic acid specimens. These preliminary electrospinning studies evidenced the feasibility of preparing bioerodible polymeric nanofibers loaded with anti-inflammatory drugs that can have potential use in pain management. Further investigations aimed at a better control of drug release kinetics will be performed.

References:

[1] Al Malyan et al. J. Craniofac. Surg. 17(2), 2006.

[2] Chiellini et al. Macromolecular Symposia (1995), 803-24.

Synchrotron studies of solvent mediated nanocrystal thin film self-assembly.

Diego Pontoni[1], *K. Alvine*[1], *A. Checco*[2], *O. Gang*[2], *B. Ocko*[2], *P.S. Pershan*[1], *F. Stellacci*[3]

[1] Physics Department and DEAS, Harvard University, Cambridge, MA, 02138
[2] Brookhaven National Laboratory, Upton, NY, 11973
[3] Massachusetts Institute of Technology, Cambridge, MA, 02129

diego@xray.harvard.edu

Since the discovery of super-crystal formation [1] and opal nucleation from solutions of highly polydisperse gold nanocrystals [2], a growing set of experimental and theoretical studies have investigated self-assembly and ordering phenomena that occur as a consequence of solvent evaporation from metal and semiconductor nanocrystal solutions (see for example [3-6]). Initially, the experiments consisted in real-space (microscopy) characterization of the end products obtained after rapid and complete solvent evaporation [2]. Subsequent studies recognized and exploited the importance of control over the evaporation rate [5,7,8], while recent x-ray experimental developments allowed kinetic scattering studies of the micro-structural evolution during partially controlled evaporation [9]. However even in the latter case the self-assembly evolved in conditions that are far from thermodynamic equilibrium.

We have initiated a research effort aimed at the detailed investigation of the nanocrystal microstructure in states of thermodynamic equilibrium that are intermediate between those of the disordered bulk nanocrystal suspension and the completely dry, self-assembled nanocrystal thin film.

Extended monolayers of bimodal/polydisperse thiol-stabilized gold nanocrystals were prepared on a water surface using a Langmuir trough and were transferred to flat silicon substrates at a controlled surface pressure. The substrates were subsequently wet by solvent adsorption from vapours having a precisely controlled chemical potential. Solvents of different quality were probed. The method allowed in practice to stop and restart at will the solvent adsorption (or evaporation) and to control the thickness of the adsorbed solvent film with angstrom resolution over the range 1-100 Å. The corresponding equilibrium nanocrystal microstructure was probed in-situ by surface x-ray scattering and diffraction techniques. Complementary microscopy data (TEM, SEM, AFM) were acquired prior and after the x-ray/wetting experiments.

Results include: (a) hints of core size dependent effects not only in the plane of the monolayer but also in the vertical structure characterized by the nanocrystal-substrate separation; (b) monolayer expansion followed by dissolution upon adsorption of increasing amounts of a good solvent; (c) reversibility of the monolayer dissolution/assembly process upon film thickness cycling with a good solvent; (d) expansion of the monoloayer in the thin film regime regardless of the solvent quality; (e) self-assembly of oriented 3D nanocrystal aggregates in the thick film regime with a poor solvent; (f) compaction and fixation of the 3D aggregates upon poor solvent thinning and final drying. All the different structures can be reversibly obtained from the same starting sample upon choice of the correct solvent and amount of liquid adsorbed (Fig. 1).

In view of the fact that there are subtle problems associated with analysis of the measurements involving the bimodal/polydisperse size distribution there is a clear need for other investigations. On the other hand, we believe that the approach presented here can contribute

to one of the main objectives of modern nanoscience, namely understanding the fundamental mechanisms of nanocrystal self-assembly and exploiting its technological potentialities.

References:

[1] M.D. Bentzon, J.v. Wonterghem, S. Morup, A. Thoelen, and C.J.W. Koch, *Phyl. Mag. B.*, **60** (1989) 169.

[2] P.C. Ohara, D.V. Leff, J.R. Heath, and W.M. Gelbart, *Phys. Rev. Lett.*, **75** (1995) 3466.

[3] C. B. Murray, C. R. Kagan, and M. G. Bawendi, *Science*, **270** (1995) 1335.

[4] B.A. Korgel, S. Fullam, S. Connolly, and D. Fitzmaurice, *J. Chem. Phys. B*, **102** (1998) 8379.

[5] J. Tang, G.L. Ge, and L.E. Brus, *J. Phys. Chem. B*, **106** (2002) 5653.

[6] E. Rabani, D.R. Reichman, P.L. Geissler, and L.E. Brus, *Nature*, **426** (2003) 271.

[7] X.M. Lin, H.M. Jaeger, C.M. Sorensen, and K.J. Klabunde, *J. Phys. Chem. B*, **105** (2001) 3353.

[8] F.X. Redl, K.S. Cho, C.B. Murray, and S. O'Brien, *Nature*, **423** (2003) 968.

[9] S. Narayanan, J. Wang, and X.M. Lin, *Phys. Rev. Lett.*, **93** (2004) 135503.

Figures:

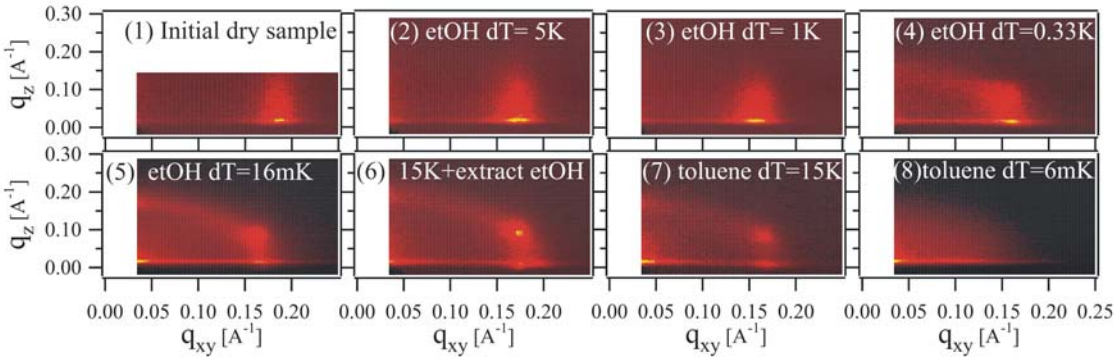


Figure 1 Grazing Incidence X-ray Diffraction patterns from a nanocrystal thin film under various equilibrium wetting conditions. (1) Initial dry monolayer. (2-3) Thin film of poor solvent: monolayer expansion. (4-5) Thick films of poor solvent: signature of oriented aggregates/superlattices. (6) Aggregate annealing and compaction by solvent thinning and drying. (7) Thin good solvent: partial aggregate disruption. (8) Thick good solvent: complete thin film dissolution.

Poster

ELECTRONIC STRUCTURE OF CLUSTERS

A.V. Popov
Altai State Technical University, Lenin st. 46, Barnaul 656038, Russia
andrey_popov@barnaul.ru

Cluster beams are often used to prepare thin films and new materials, especially those in which insertion clusters form nanostructures in the initial matrix [1]. The formation of clusters in the form of beams is convenient for both generation and applications thanks to the high rate of generation and transport to the place of destination. High rates are of importance because clusters possess high chemical activity, and the chain of processes is complex and nonequilibrium. For this reason, the output parameters of cluster beams strongly depend on the processes that accompany generation and transport and can be considerably improved by changing the procedure or even the conditions of cluster generation.

Cluster properties are intermediate between those of atoms and molecules on the one hand and condensed matter on the other. The evolution of clusters leads to the formation of either the gas or condensed phase and involves several metastable excitations. For this reason, studies of intermediate compounds are of great importance for basic research and applications (for the generation of cluster beams). In our view, the most complete and deep understanding of the processes involved in the transition from one intermediate state into another can be attained only on the basis of a theory that allows a large set of various material properties reliably substantiated by experiments to be calculated within a unique scheme. Calculations are of importance also because many values are easier to calculate than to measure. If based on a well-grounded theory, they can even now be used to obtain a fairly complete idea about the properties of a substance yet unsynthesized. Fairly accurate calculations are also of importance because phenomena and processes characteristic of cluster beams are determined by a large number of competing factors, which makes qualitative considerations insufficient. This raises the question of the selection of a method for calculations and its physical and mathematical accuracy.

The present paper reports the results of theoretical investigation of electron excitations in beryllium, magnesium, and calcium. The excitations described in terms of the Hartree-Fock method with allowance for the width of the atomic levels [2]. The Hartree-Fock method was used as the basic one, because this method is the most systematic of all one-electron methods. It provides precise formulations of all the assumptions and makes it clear how to go beyond them in order to obtain more and more exact final results.

With standard spectrum problem solving one assumes that the wave function of many-electron atom is regular and continuous by angle variables. That results in solving with integer values of orbital and magnetic quantum numbers. Method used for describing excitations of high power leads to refusal from limitations for integer values of the orbital quantum number l, considered it as complex $L=l+x+iy$, where l, as before, an integer. The domain of the complex additive $x+iy$ can be limited, e.g., by $|x|<0.5$ and $|y|<0.5$. Refusal from these limitations allows the electrons motion with orbital damping to be considered. Thus, the problem of determining the spectrum of the orbital atomic excitations is reduced to the search for the eigen values of the Schrödinger stationary equation. On trying all the possible values of $|x|<0.5$ and $|y|<0.5$ when finding self-consistent solutions to Schrödinger equation, we can deduce the spectral characteristics of an excited atom from the minima of its total energy.

This method was used for description of excitations in beryllium, magnesium, and calcium. It was shown in [2] that when the beryllium atom is excited, the 2p-states are split, unequal shift of single-electron energy levels and mixing of the 2s and 2p states at excitation energies of 10

and 14 Ry are observed, and, starting from 6.7 Ry, the atom is stabilized. In the X-ray range of excitation energies the long-living excitations were not detected. But with the help of proposed method was shown the principle possibility of forming of long-living states in beryllium, magnesium, and calcium.

Let us consider the excitation of a beryllium atom in the optical range of energies. To do this, it is sufficient to assume that electron transitions from the 1s states are forbidden. In this case, the electron occupancies of these states remain unchanged and equal to two (with allowance for the spin degeneracy). The greatest changes are found in the occupation numbers of the 2s and 2p states. The occupation numbers of the 3s states are close to zero, because the transitions 2s-3s are forbidden by the selection rules and the transitions 2p-3s are improbable in view of a small filling of the 2p states by electrons. By the increasing of the implicit part of orbital quantum number *l* the 1s state is raising up in the scale of energies. This phenomenon is treated by us as a collapse of an atom, which is intensively discussed in the work [3] in an example of a hydrogen atom. The most stable excitation in beryllium has been revealed at the distance between the atoms around 4 Bohr radii in the optical range of excitation energies [4].

To work with more heavy elements is very promising. In [5] is shown that conditions for the emergence of condensed excited states in magnesium created for any (indefinitely small) excitation fields in the optical energy range. The weaker the external field, the longer the lifetime and the shallower the potential well for the condensate of excitations. Most stable excitations in magnesium were detected at atomic distances of about 9 Bohr radii.

The calculations show that excited states in calcium can be formed at any even very small intensity of excitations [6]. Long-lived excitation states in calcium are found for interatomic distances of about seven Bohr radii. This distance is considerably larger than four Bohr radii in beryllium but is less than nine Bohr radii in magnesium. On the whole, calcium is the most perspective for the search of condensate of long-living excited states.

The above mentioned method allows calculating a finite number of discrete states. It is impossible to consider the contribution of all discrete and continuous spectrums. Let us consider the method of overcoming these difficulties and take into account the contribution of continuous spectrum. Let the clusters be in a lattice with a big value of lattice parameter, and clusters interact insignificantly. In this case the reciprocal lattice parameter would be small, so bands are consider very close. One can average over wave vectors analytically by using, for example, a basis of Gaussian-type. Such method allows to shorten the time of numerical calculations and to describe a weak interaction between clusters in a lattice.

The calculations show that the total energy of beryllium has the minimum at 4.32 Bohr radii. It corresponds to experimental value of close-packed hexagonal lattice parameter. It is shown that transition from gas phase to crystal phase is more profitable through formation of stable clusters Be_4, Be_5, Be_6 and so on. Note that, the bigger number of atoms in cluster, the bigger number of metastable states it has.

References:

[1] Smirnov B. M., Usp. Fiz. Nauk **173** (2003) 609.
[2] Popov A.V., Optics and Spectroscopy, **93** (2002) 1.
[3] Delone N.B., Kraoenov V.P., Phys. Usp. **38** (1995) 1247.
[3] Popov A.V., Plasma Physics Reports, **31** (2005) 253.
[4] Popov A.V., Journal of Experimental and Theoretical Physics, **101** (2005) 197.
[5] Popov A.V., Plasma Physics Reports, **32** (2006) 332.

NANOELECTROMECHANICAL SYSTEMS BASED ON MULTI-WALLED NANOTUBES: NANOTHERMOMETER, NANORELAY AND NANOMOTOR

Andrey M. Popov[1], Elena Bichoutskaia[2] Yurii E. Lozovik[1], Anton S. Kulish[3]
[1]Institute of Spectroscopy, Troitsk, Moscow region, 142190, Russia
[2]Cambridge University, Chemical Laboratory, Cambridge CB2 1EW, UK
[3]Moscow Institute for Steel and Alloys, Leninskii prosp. 4, 117936, Moscow, Russia
popov@ttk.ru

Unique properties of carbon nanotubes, such as easy relative sliding and rotation of the walls and metallic conductivity, allow using the walls of nanotubes as a movable element and an element of electric circuit in nanoelectromechanical systems (NEMS). An example of such application is the nanotube-based nanomotor, which has been recently realized [1,2]. A new type of NEMS based on the nanotubes, for which the relative motion of the walls is controlled by the corrugation of the interwall interaction energy surface, has been proposed in [3] as a nanodrill and in [4,5]. Here we proposed three new NEMS of this type: an electromechanical nanothermometer, a nanorelay, which can also be used as a memory cell, and a nanomotor for transformation of forward force into relative rotation of the walls.

Both the conductivity, G, and the interwall interaction energy, U, of double-walled carbon nanotubes (DWNTs) depend periodically on relative displacement of the walls, z. Thus, the probability of relative displacement of the walls can be defined as $p(z)=A\exp(-U(z)/kT)$. The total conductivity of DWNT for a given temperature, $G(T)$, can be then found by integrating $\int G(z)p(z)dz$. We propose to use the dependence $G(T)$ for elaboration of electromechanical nanothermometer. Several principal schemes of such nanothermometer are shown on Figure 1. The density functional theory (DFT) calculations of the interwall interaction energy, $U(z)$, have been performed using the (6,6)@(11,11) DWNT as an example (the details of the method can be found in [5,6]). These calculations are used to estimate the minimal length of the nanothermometer for which relative diffusion of the walls does not hinder its operation. An analytical expression for the dependence $G(T)$ is also derived.

The schematics of a nanorelay based on relative motion of the walls of DWNT are shown on Figure 2. In this nanorelay, the inner wall is pushed out of the outer wall, connected to the electrode (3), by electrostatic force F_e and attracted to the electrode (4) by Van der Waals force F_a (position 'on'). The core can be retracted into the shell by capillary force F_c (position 'off'). The friction force F_f acting between the core and the shell is also taken into account. The force F_f arises due to the corrugation of the interwall interaction energy surface. The forces F_c and F_f are calculated using DFT, whereas F_a is calculated semi-empirically. Structure of the caps of the inner wall has been obtained using the Q-Chem 2.0 *ab initio* package. The force F_e and related voltages of switching have been calculated analytically for the capacity of the system. If the electrode (4) is copper, then $F_a>F_c$. Thus, the nanorelay shown on Figure 2A can be used as a memory cell for both the external and on-line storage. If the electrode (4) is a carbon nanotube, as shown on Figure 2B, and the size of a memory cell can be considerably reduced. For such nanorelay $F_a<F_c$, thus it can only be used as a memory cell of the on-line storage, for which $F_a+F_e>F_c$. However, we found that for DWNTs with the nonchiral commensurate walls it is possible to select the length of the outer wall so that friction force is great and therefore $F_a+F_f>F_c$. In this case the nanorelay shown on Figure 2B can also be used as a memory cell of the external storage. The schematics of nanorelays with the third control electrode are also considered. The possibility of producing a gas nanosensor based on the proposed nanorelays is discussed.

We also suggest the schematic of a nanomotor based on the four-walled nanotube and intended for transformation of forward force into the relative rotation of the walls. In such a

nanomotor two inner walls are the rotational nanobearings and two outer walls have the thread-like potential relief of the interwall interaction energy, which operate as the nanobolt-nanonut pair. The theory which describes the operation of the nanomotor is presented.

References:

[1] A.M. Fennimore, T.D. Yuzvinsky, W.Q. Han, et al., Nature **424** (2003) 408.
[2] B. Bourlon, D.C. Glatti, L. Forro, and A. Bachfold, Nano Lett. **4** (2004) 709.
[3] Yu.E. Lozovik, A.V. Minogin, and A.M. Popov, Phys. Lett. A **313** (2003) 112.
[4] A.V. Belikov, A.G. Nikolaev, Yu.E. Lozovik, and A.M. Popov, Chem. Phys. Lett. **385** (2004) 72.
[5] E. Bichoutskaia, A. M. Popov, M.I. Heggie, and Yu. E. Lozovik, Phys. Rev. B **73** (2006) 045435.
[6] E. Bichoutskaia, A.M. Popov, A. El-Barbary, M.I. Heggie, and Yu. E. Lozovik, Phys. Rev. B **71** (2005) 113403.

Figures:

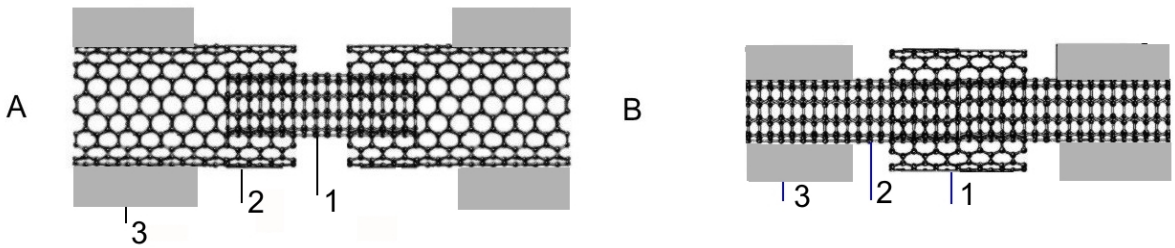


Figure 1. Schematic of electromechanical nanothermometer. A: telescopic nanothermometer with movable outer wall, B: shuttle nanothermometer with movable inner wall. The movable wall is marked off by (1), the fixed wall by (2) with the attached electrodes (3).

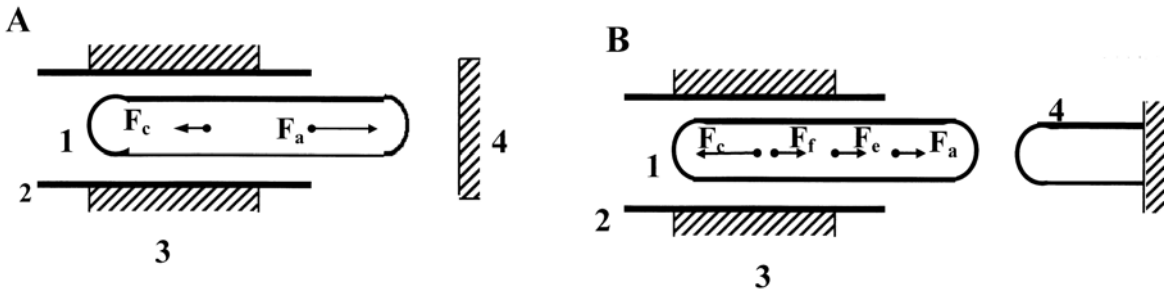


Figure 2. Schematic of double-wall nanotube-based memory cell in position 'on'. A: memory cell with flat second electrode, B: memory cell with carbon nanotube attached to second electrode. The movable inner wall is marked off by (1), the fixed outer wall by (2) with the attached electrodes (3) and (4).

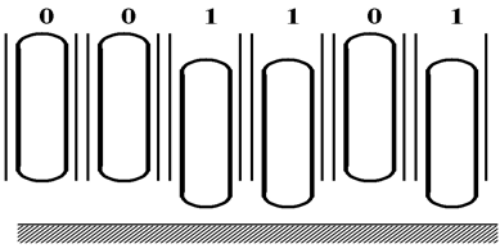


Figure 3. Example of the storage produced of nanotube-based memory cells.

NANOSTRUCTURED POROUS SILICON AS THICK ELECTRICAL INSULATOR FOR RF APPLICATIONS

A. Porcher, B. Remaki, C. Populaire and D. Barbier.

Laboratoire de Physique de la Matière (UMR CNRS-INSAL 5511)
INSA de Lyon, Bat. 502, Avenue A. Einstein
F - 69621 Villeurbanne cedex, France.

Porous silicon (PS) is a promising material for electronics and sensors devices. This material exhibits attractive properties [1-3] such as quantum confinement (silicon based photo-emitting devices), a large specific surface (chemical sensors) and insulating potentialities. As illustrated in figure 1, Meso-porous form (crystallites size around 10_/100 nm) presents columnar structure allowing thick and mechanically stable porous layer production. It is known as an electrical semi-insulator even at low porosity [4-6]. The residual electrical conduction of the porous layers is due to various electrical transport mechanisms: quasi intrinsic conduction within continuous paths of nano-crystallites at low frequencies, Space Charge Limited Currents under DC voltage bias and hopping transport on localized states in the chaotic porous structure at high frequencies. So, the electrical insulating capabilities of this material need an accurate evaluation considering the conditions of use (thickness, electrical bias, temperature, frequency,..).

In the present work, our study concern non biased thick meso-porous silicon layers with the aim of rf devices integration which require efficient thick insulating substrates. In these conditions, the electrical transport in the layers is controlled by the intrinsic and hopping bulk conduction. We have used complex impedance measurements and rf resonant circuits characteristics to determine the electrical parameters of spiral inductors /porous-Si/Si structures (see figure 1). The samples were realized on 10^{-2} Ω -cm p-type Si substrates using a well known anodic electrochemical dissolution process [7] to etch porous layers of 100µm of thickness and 50% of porosity. The impedance of the porous layers is determined in $10^2 – 10^6$ frequency range from measurements between the metallic inductor (used as an electrode) and the P^+ substrate using a HP 192 bridge in parallel mode.

As shown in figure 2, at different temperatures, for frequencies higher than 100 kHz, the capacitance part of the impedance corresponds to the geometrical value and remains constant when the conductance part increase with the frequency revealing a hopping conduction phenomena. However, the tangent loss value is 10^{-2} at 100 kHz and decreases with the frequency. This indicates clearly the capacitive nature of porous silicon at high frequencies. Rf measurements on the corresponding resonant circuit are reported below on figure 3 using the integrated inductor with external capacitance. The measurements were carried out using an Agilent E5070B network analyzer in S_{11} parameters mode (figure 3a). The extracted loss resistance is compared to numerical data obtained by mean of Femlab software simulations. We can see from a typical curve on figure 3b that moderately oxidized porous silicon exhibits a comparable value of loss resistance than efficient insulators such as glass or vacuum in a prospected frequency range of 10^5 Hz to 10^9 Hz.

1. L. T. Canham, *Appl.Phys. Lett.* , **57**, 1046 (1990)
2. G. Bomchil, A. Halimaoui, R. Herino, *Microelectr. Eng.* 8, 293 (1988).
3. See for a complete revue, *properties of porous silicon*, edited by L. T. Canham, *Emis* **18**, *Inspec*, UK (1997)
4. V. Lehman, H. Hofmann, F. Möller, U. Gruning, *Thin Solid Films*, **255**, 20 (1995)
5. I. G. Polissiki, D. Kovalev, G. Dollinger, T. Sulima, G. Koch, *Physica B*, **273**, 951 (1999)
6 B. Remaki, C. Populaire, V. Lysenko, D. Barbier, Mat. Sc. Eng. B, vol. 101, pp. 313-317, (2003).
7. A. Halimaoui, in *Porous Silicon : Science and Technology*, edited by J.-C. Vial and J. Derrien, *Springer Verlag, Berlin Heidelberg and Les Editions de Physique, Les Ulis*, 33 (1995)

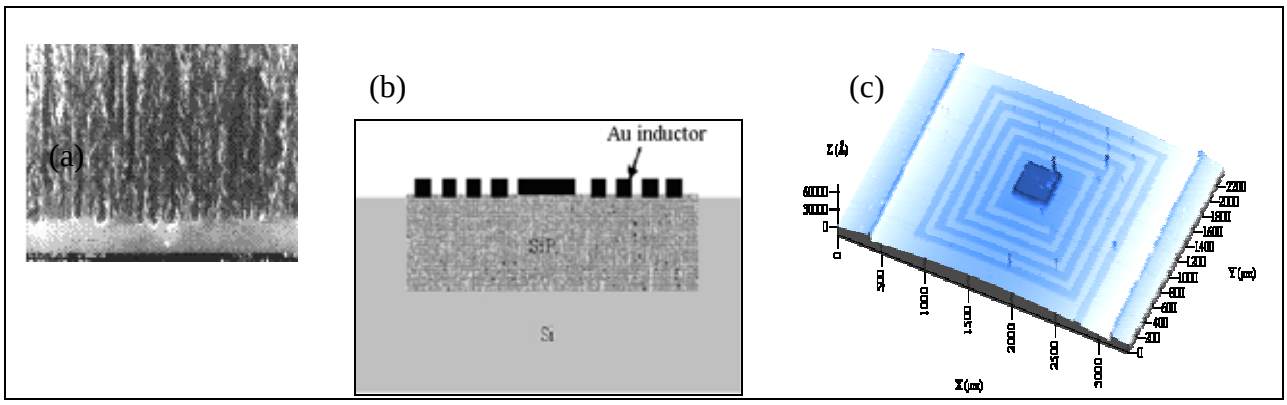


Fig. 1. Geometrical configuration of the samples: (a) morphology from cross-section SEM view (b) Au inductor /PS/p_-Si structures; (c) view of 2mmx2mm microcoils.

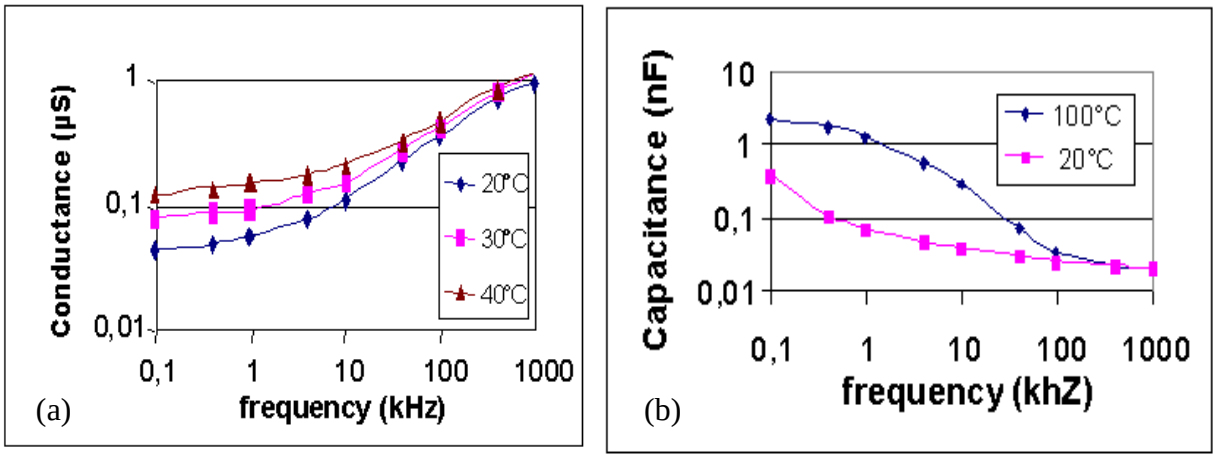


Figure 2. (a) conductance – frequency and (b) capacitance – frequency measurements of the porous layers at different temperatures.

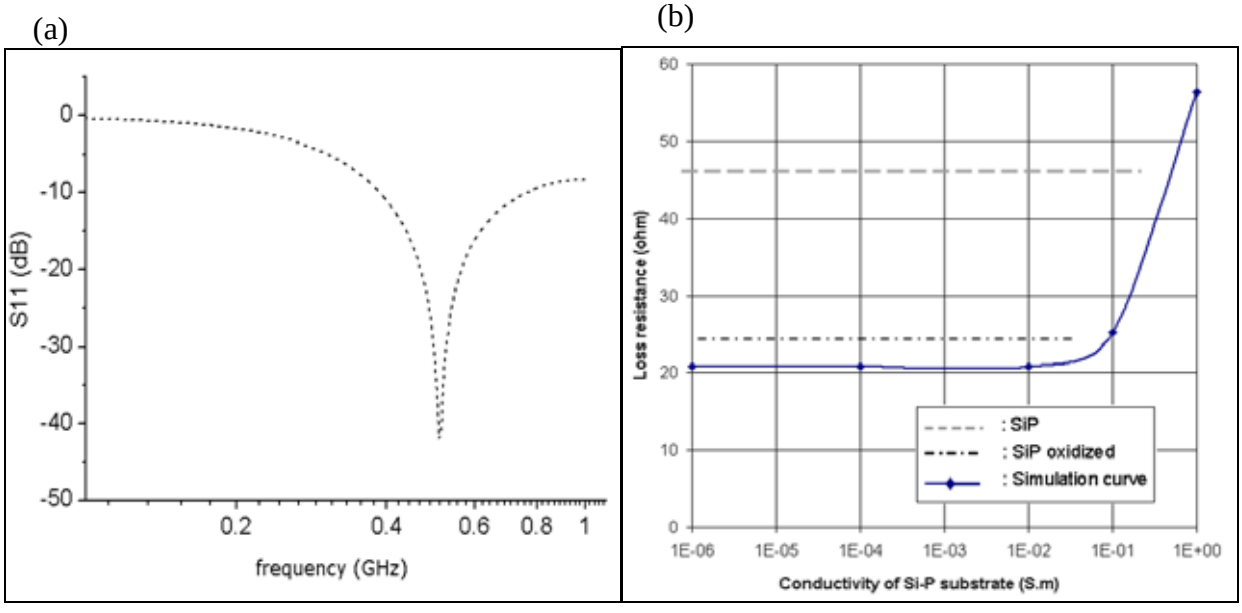


Figure 3. (a) typical spectra of the resonant circuit (b) simulated loss resistance variation with the dielectric conductivity (dashed lines: experimental data using porous silicon dielectric)

On the Effect of Electron-Phonon Interaction Parameters on the Performance of Carbon Nanotube Based Transistors

M. Pourfath and H. Kosina
Institute for Microelectronics, TU Wien, Gußhausstraße 27–29/E360, A-1040 Wien, Austria
email: pourfath@iue.tuwien.ac.at

Exceptional electronic and mechanical properties together with nanoscale diameter make carbon nanotubes (CNTs) promising candidates for nanoscale transistors. Semiconducting CNTs can be used as a channel for field-effect transistors (FETs), and metallic CNTs can serve as interconnect wires. In short devices carrier transport through the device is nearly ballistic [1].

The non-equilibrium Green's function (NEGF) method has been successfully utilized to investigate the characteristics of nanoscale Silicon transistors [2], carbon nanotube (CNT) based transistors [3, 4], and molecular devices [5]. In this work we employ the NEGF formalism to study in detail quantum transport in CNT based transistors.

Non-equilibrium statistical ensemble averages of the single particle correlation operator can be calculated using the NEGF formalism. Four types of Green's functions are defined: $G^{R,A}$ deal with the dynamics of carriers and $G^{<,>}$ with the statistics of carriers. For a steady state problem the Green's functions can be written as [6]:

$$G^{\mathrm{R,A}}_{\mathbf{r},\mathbf{r}'}(E) = [EI - H_{\mathbf{r},\mathbf{r}'}(E) - \Sigma^{\mathrm{R,A}}_{\mathbf{r},\mathbf{r}'}(E)]^{-1} \quad (1) \qquad G^{<,>}_{\mathbf{r},\mathbf{r}'}(E) = G^{\mathrm{R}}_{\mathbf{r},\mathbf{r}'}(E)\Sigma^{<,>}_{\mathbf{r},\mathbf{r}'}(E)G^{\mathrm{A}}_{\mathbf{r},\mathbf{r}'}(E) \quad (2)$$

In (1) an effective mass Hamiltonian is assumed. A recursive Green's function method is used for solving (1) and (2), see [2]. We consider the self-energies due to contacts and electron-phonon interaction, $\Sigma = \Sigma_{\mathrm{s}} + \Sigma_{\mathrm{d}} + \Sigma_{\mathrm{e-ph}}$. The self-energy due to the coupling of the device to the source and drain contacts is only non-zero at the boundaries. The self-energy due to electron-phonon interaction consists of the contributions of elastic and inelastic scattering mechanisms, $\Sigma_{\mathrm{e-ph}} = \Sigma_{\mathrm{el}} + \Sigma_{\mathrm{inel}}$. Assuming local scattering ($\Sigma_{\mathbf{r},\mathbf{r}'} = 0$ for $\mathbf{r} \neq \mathbf{r}'$) the self-energies due to electron-phonon interaction are given by:

$$\Sigma^{<}_{\mathrm{inel},(\mathbf{r},\mathbf{r})}(E) = \sum_{\nu} D^{\nu}_{\mathrm{inel}}[(n_B(\hbar\omega_\nu)+1)G^{<}_{\mathbf{r},\mathbf{r}}(E+\hbar\omega_\nu) + n_B(\hbar\omega_\nu)G^{<}_{\mathbf{r},\mathbf{r}}(E-\hbar\omega_\nu)] \quad (3) \qquad \Sigma^{<,>}_{\mathrm{el},(\mathbf{r},\mathbf{r})}(E) = D_{\mathrm{el}}G^{<,>}_{\mathbf{r},\mathbf{r}}(E) \quad (4)$$

$$\Sigma^{>}_{\mathrm{inel},(\mathbf{r},\mathbf{r})}(E) = \sum_{\nu} D^{\nu}_{\mathrm{inel}}[(n_B(\hbar\omega_\nu)+1)G^{>}_{\mathbf{r},\mathbf{r}}(E-\hbar\omega_\nu) + n_B(\hbar\omega_\nu)G^{>}_{\mathbf{r},\mathbf{r}}(E+\hbar\omega_\nu)] \quad (5) \qquad \Im m[\Sigma^{\mathrm{R}}] = \frac{[\Sigma^{>} - \Sigma^{<}]}{2i} \quad (6)$$

where ν is the phonon mode and the phonon occupation number is given by the Bose-Einstein distribution function $n_B(\hbar\omega_\nu) = 1/(\exp(\hbar\omega_\nu/k_BT) - 1)$. The electron-phonon coupling coefficients ($D_{\mathrm{el,inel}}$) depend on the chirality and the diameter of the CNT [7]. The imaginary part of the self-energy broadens the density of states and is given by (6). The carrier concentration and the current density at some point $\mathbf{r}$ of the device can be calculated as (7) and (8).

$$n_{\mathbf{r}} = -4i \int G^{<}_{\mathbf{r},\mathbf{r}}(E)\frac{dE}{2\pi} \quad (7) \qquad j_{\mathbf{r}} = \frac{4q}{\hbar}\int \mathrm{Tr}[\Sigma^{<}_{\mathbf{r},\mathbf{r}}G^{>}_{\mathbf{r},\mathbf{r}}(E) - \Sigma^{>}_{\mathbf{r},\mathbf{r}}G^{<}_{\mathbf{r},\mathbf{r}}(E)]\frac{dE}{2\pi} \quad (8)$$

The effects of the electron-phonon coupling strength and the phonon energy on the static response of CNTFETs are investigated. All simulations were performed for the structure shown in Fig. 1. To compare the effect of different scattering mechanisms, we define the ballisticity as the ratio of the current in the presence of electron-phonon interaction to the current in the ballistic case ($I_{\mathrm{Sc}}/I_{\mathrm{Bl}}$). With increasing $D_{\mathrm{el,inel}}$ the imaginary part of the self-energy increases, which adds dissipation to the Hamiltonian, and as a result the total current decreases. Fig. 2 shows the ballisticity versus $D_{\mathrm{el,inel}}$. Elastic scattering conserves the energy of carriers as in the ballistic case, but the current decreases due to elastic back-scattering of carriers. With inelastic scattering the energy of carriers is not conserved. Carriers which acquire enough kinetic energy can emit phonons and scatter into lower energy states. Fig. 2 shows that the variation of ballisticity versus D_{inel} strongly depends on the phonon energy. For a better comparison Fig. 3 shows the ballisticity versus phonon energy. With the increase of phonon energy the ballisticity increases, since scattered carriers lose more kinetic energy and the probability for back-scattering decreases [8]. As the phonon energy increases the occupation number decreases exponentially. Therefore, the self-energy decreases and the current is weakly affected even for strong electron-phonon coupling. Fig. 2 and Fig. 3 show the results for a device with a length of $50\ \mathrm{nm}$. As the length of the CNT increases the ballisticity of the devices decreases. Fig. 4 shows the ballisticity versus the device length. As one expects, the ballisticity is inversely proportional to the device length.

In general electron-phonon interaction parameters depends on the diameter and the chirality of the CNT. The calculation of these parameters is presented in [7]. In CNTs the band gap is inversely proportional to the diameter. A rough estimate is $E_{\mathrm{g}} = 0.8\ \mathrm{eV}/d_{\mathrm{CNT}}\ \mathrm{nm}$. CNTs with a diameter $d_{\mathrm{CNT}} > 2\ \mathrm{nm}$ have a band gap $E_{\mathrm{g}} < 0.4\ \mathrm{eV}$, which render them unsuitable as channel for FETs. However, the fabrication of devices with a diameter $d_{\mathrm{CNT}} < 1\ \mathrm{nm}$ is very difficult. As a result, we limit our study to zigzag CNTs with diameters in the range $d_{\mathrm{CNT}} = 1 - 2\ \mathrm{nm}$.

In CNTs elastic scattering is caused by acoustic phonons and inelastic scattering occurs due to zone boundary (ZB), optical (OP), and radial breathing (RBM) phonon modes. Considering the class of CNTs we discussed above, the energies of the these phonon modes are $\hbar\omega_{\mathrm{ZB}} \approx 160$ and $180\ \mathrm{meV}$, $\hbar\omega_{\mathrm{OP}} \approx 200\ \mathrm{meV}$, and $\hbar\omega_{\mathrm{RBM}} \approx 30\ \mathrm{meV}$ respectively [9]. The corresponding coupling coefficients are $D^{\mathrm{ZB,OP}}_{\mathrm{inel}} < 50 \times 10^{-3}\ \mathrm{eV}^2$ and $D^{\mathrm{RBM}}_{\mathrm{inel}} < 10^{-3}\ \mathrm{eV}^2$ [7, 9]. As we discussed, for short devices (less

than some hundred nano-meter) high energy phonons, such as OP and ZB phonon modes, degrade the performance only weakly, whereas the RBM phonon mode can have a detrimental effect. However, due to weak electron-phonon coupling the RBM mode has a negligible effect at room temperature. The electron-phonon coupling is also weak for acoustic phonon (AP) modes ($D_{\mathrm{el}}^{\mathrm{AP}} < 10^{-3}\ \mathrm{eV}^2$), which implies weak elastic backscattering of carriers. Therefore, short CNTFETs can operate close to the ballistic limit. Fig. 5 shows excellent agreement between simulation results and experimental data [1]. The result for the bias point $V_{\mathrm{G}} = 1.3$ V is compared with the ballistic limit, which confirms the validity of nearly ballistic transport in short CNTFETs.

Based on the NEGF formalism we investigated the effect of electron-phonon interaction on the performance of CNTFETs. For elastic scattering the electron-phonon coupling strength plays an important role. For inelastic scattering not only the coupling strength, but also the phonon energy is an important factor. In CNTs relevant for FETs, either the electron-phonon coupling is weak or the phonon energies are high. Therefore, the performance of short devices is only weakly affected.

References

[1] A. Javey *et al.*, Nano Lett. **4**, 1319 (2004).
[2] A. Svizhenko *et al.*, J.Appl.Phys. **91**, 2343 (2002).
[3] J. Guo, J.Appl.Phys. **98**, 063519 (2005).
[4] A. Svizhenko *et al.*, Phys.Rev.B **72**, 085430 (2005).
[5] W. Tian *et al.*, J.Chem.Phys **109**, 2874 (1998).
[6] S. Datta, Superlattices & Microstructures **28**, 253 (2000).
[7] G. Mahan, Phys.Rev.B **68**, 125409 (2003).
[8] J. Guo *et al.*, Appl.Phys.Lett. **86**, 193103 (2005).
[9] S. Koswatta *et al.*, cond-mat/0511723 (2005).

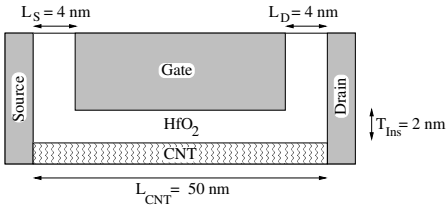


Figure 1: Sketch of the device. $T_{\mathrm{Ins}} = 2$ nm, $L_{\mathrm{CNT}} = 50$ nm and $\epsilon_{\mathrm{r}} = 15$.

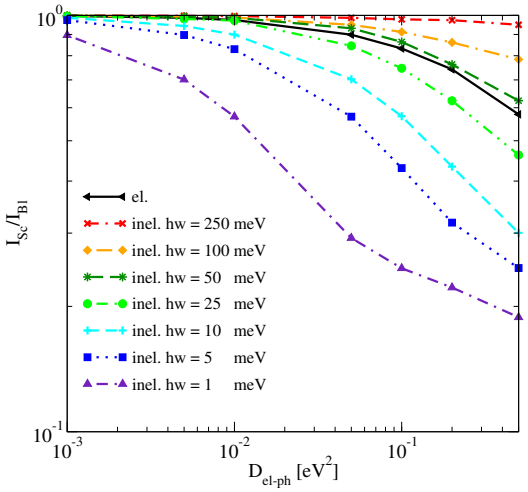


Figure 2: Ballisticity versus the strength of electron-phonon coupling ($D_{\mathrm{el,inel}}$) for elastic and inelastic scattering.

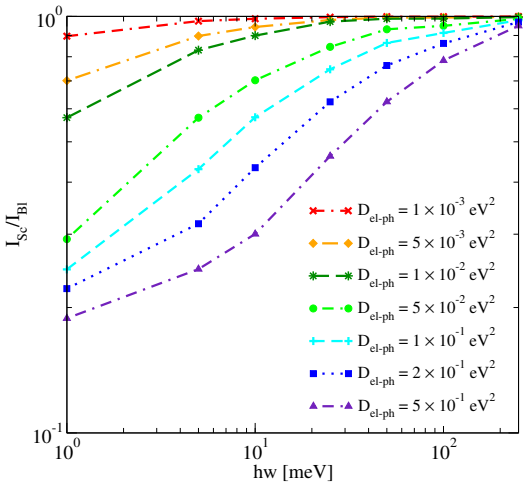


Figure 3: Ballisticity versus phonon energy ($\hbar\omega_\nu$) for inelastic scattering.

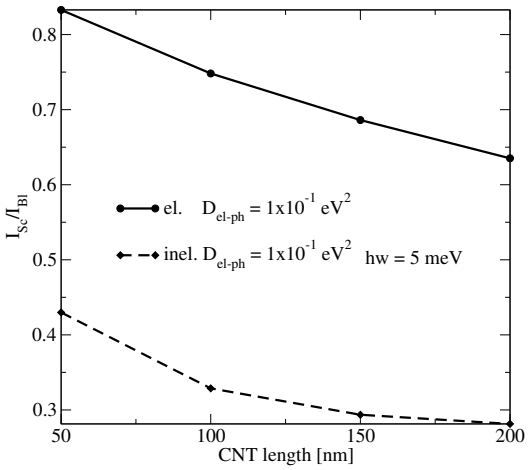


Figure 4: Ballisticity versus CNT length.

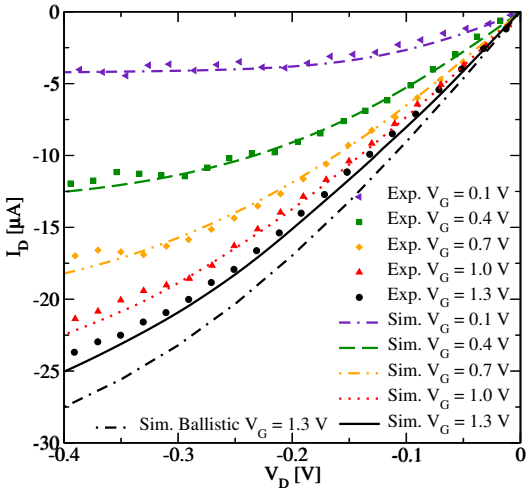


Figure 5: Comparison of the simulation results and experimental data for the output characteristics. The results for the bias point $V_{\mathrm{G}} = 1.3$ V are compared with the ballistic limit.

HIGHLY ORDERED GERMANIUM NANOSTRUCTURES GROWN BY MOLECULAR BEAM EPITAXY ON TWIST BONDED SILICON (001)

V. Poydenot[1],R. Dujardin[1], F. Fournel[2], J.L. Rouvière[1] and A. Barski[1]
[1] CEA-DSM, DRFMC/SP2M, CEA/GRE, [2] CEA-DRT-LETI - CEA/GRE,
17 Avenue des Martyrs,
38054 Grenoble Cedex 9, France

valierp@yahoo.comT

In silicon thin film bonded to silicon substrate by molecular bonding, the film rotation, in respect to the substrate, generates networks of regularly spaced screw and mixed interface dislocations, related respectively to the twist and the tilt disorientation [1]. The network of twist and tilt dislocations, modify the surface energy allowing the precise control of surface topography [2]. In this work, we investigated the germanium growth on a silicon films 10 nm thick, bonded to the silicon substrate with a standard tilt disorientation of ~0.5° and twist angle: (i) 2.2° and (ii) 20°.

For our low twist angle (2.2°) bonded silicon substrate, the interface is composed by a screw dislocation network with a period of 10 nm and an array of tilt dislocations with a period of 110 nm. In figure 1(a) we show the surface topography (AFM observations) after the deposition of 8 monolayers of germanium. The distance between adjacent lines of dots corresponds to the period of the tilt dislocation array. On the plane-view transmission electron microscopy image, figure 1(b), one can see simultaneously the screw dislocation network, the tilt dislocation array (dislocation lines), and the germanium dots. The germanium dots grow forming a linear arrangements governed by tilt dislocation lines.

For high twist angle of 20°, the strain field generated by the twist dislocation network on the surface of the bonded film is negligible. For such high twist angles, the period of twist dislocations is lower than 1 nm. Consequently, only a one dimensional array of tilt (mixed) dislocations lines, with a period of few tenth of nm, induces a strain field in the bonded film, which propagates up to the surface. The orientation of this tilt dislocation lines in respect to the main crystallographic orientation of the film can be differently choose. In Figure 2, we show AFM observations of germanium dots grown on two different substrates, A and B. For both substrates tilt and twist angles are the same but substrates differ by the orientation of tilt dislocation array: for A substrate the tilt dislocation lines is almost parallel to the [100] direction (5° misalignment) of the bonded film, while for the B substrate they are oriented close to the [110] direction (10° misalignment). On both bonded substrates, the germanium hut islands grow in highly ordered linear rows which are parallel to the interfacial dislocation arrays. Moreover, the distance between two rows of hut islands on substrate A and B is identical to the distance between two rows of tilt dislocations.

In our contribution we will show that the observed organization in germanium deposition for low and high twist angle silicon bonded substrates is due to the strain field generated on the silicon surface by interfacial tilt dislocations.

References :

[1] Q. -Y. Tong, U. Gösele, Materials Chemistry and Physics, Vol. 37 (2), 1994, p 101-127.
[2] A. E. Romanov, P. M. Petroff, and J. S. Speck, Appl. Phys. Lett., 74, 2280 (1999).

Figures:

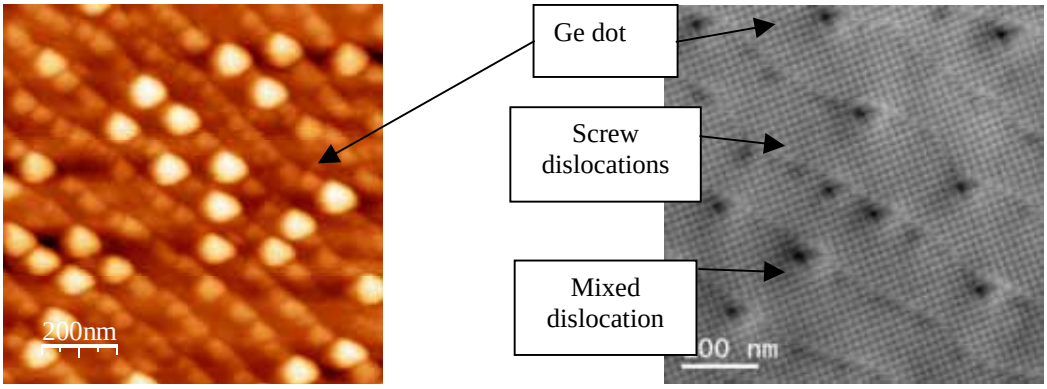


Figure 1: (a) AFM observation after growth of 8 ML of germanium. (b) Plan-view TEM observation of the same sample: one can observe the screw dislocation network, the tilt dislocation array and the germanium dots.

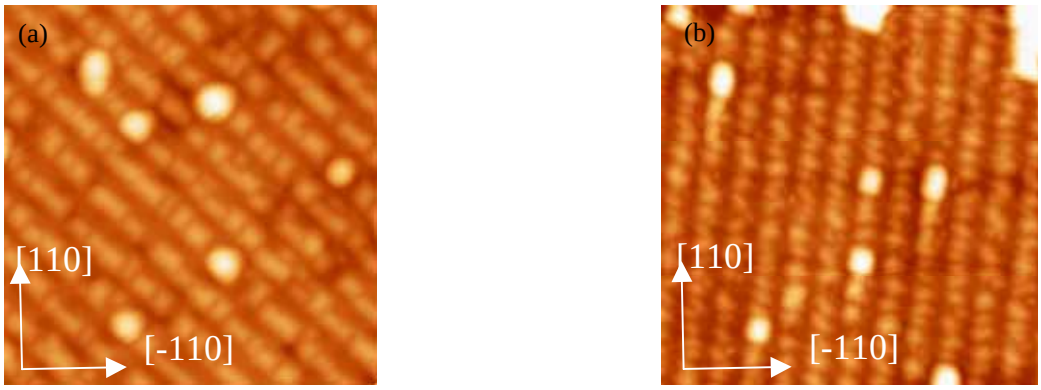


Figure 2: Atomic force microscopy observations of 8 ML of germanium grown at a substrate temperature of 600°C, on: (a) substrate A and (b) substrate B.

STUDY OF HYBRID PORPHYRIN-BASED MONOLAYER / SILICON MEMORY DEVICES

T. Pro[1], M. Gely[1], K. Huang[1], F. Duclairoir[2], G. Delapierre[1],
J. C. Marchon[2], F. Vinet[1], B. De Salvo[1] and S. Deleonibus[1]
[1] CEA/LETI, [2] CEA/DRFMC,
17 Rue des Martyrs, 38054 Grenoble Cedex 9, France, Tel. +33-438786497,
Tiziana.pro@cea.fr

Abstract

It is well recognized that in next decades, the device scaling process in traditional semiconductor technology will reach its limits. The latest conceived devices are already developed with a significant change in the basic structure. In Non-volatile memories, Single Electron Memory (SEM), like Nano-crystal memories, reduce the dimension of the device to few tenths of nanometers [1]. More recently, molecular electronics appear as a promising solution. They could offer significant advances in miniaturisation but also imply lower fabrication cost, thanks to a bottom-up manufacturing process.

In this context, our project aims to exploit molecules as charge storage media for a SEM based on a hybrid Molecule/Silicon structure. The charge storage effect can be obtained with a redox active molecule. We have chosen to use porphyrins such as H_2TEPP, H_2TAOPP and H_2AB_3P and their metal complexes (Fig. 1), which have several available redox states, either on the macrocycle or on the central metal, providing effective charge storage at the molecular level. These molecules are anchored as a monolayer on a silicon surface using combined hydrosilylation-cycloaddition reactions [2][3].

This work presents the electrical characterisation of different electronic devices. The objectives are 1- to control the redox behaviour of the various porphyrin monolayers by tuning the gate voltage, and 2- to test the charging effect of porphyrins on the device.

Furthermore, the same electrical characterization, on identical devices without porphyrin, allows us to make some comparisons.

Firstly, we will present results obtained on electrochemical cells, similar works being already presented in the literature [4]. The cells, developed in our laboratory, correspond to wells

with a Si (100) base modified with a monolayer of molecules (base surfaces varying from 1 mm^2 to 576 μm^2). The walls are made of 10.5µm-thick SiO_2 (Fig. 2) The well is then filled with electrolyte solution and C-V characterization is made.

Tests on pseudo-MOS devices will also be presented (Fig. 3), where a monolayer of porphyrins lays on the Si film (thickness varying from 30 to 100 nm). The voltage is applied to the Si bulk while the current is measured by two tips, pressed on the top surface of the Si film, and between which a voltage difference is applied. This is an important device since it operates without an electrochemical process, hence it shows that interactions between porphyrins and a silicon device are possible and even controllable.

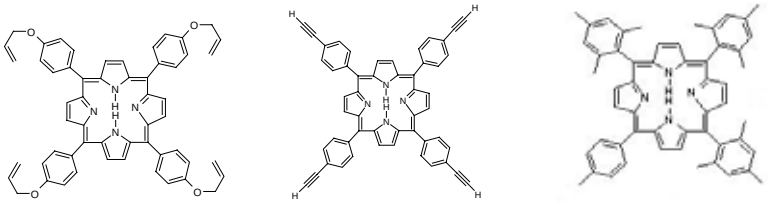


Figure 1. From left to right: free-base TAOPP, free-base TEPP, free-base AB_3P. The central H atoms can be replaced with a metal such as Mn, Fe, Co or Zn.

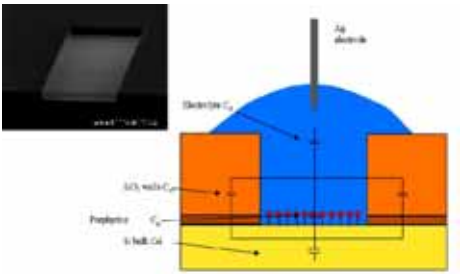


Figure 2: Scheme of the electrochemical capacitor with porphyrin SAM. On the left corner: SEM image of a cell (300µm x150µm).

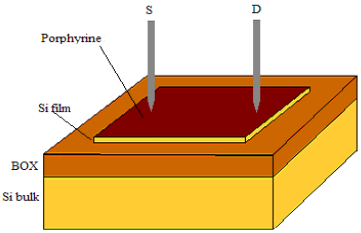


Figure 3: Scheme of a pseudo-MOS device.

[1] G. Molas et al., IEEE Transaction on Nanotechnology, Vol. 3, No. 1, p. 42, March 2004.

[2] F. Duclairoir, J.-C. Marchon, "Metalloporphyrins for memory application",TNT2005.

[3] G. Delapierre, Huang Kai, French Patent submitted N° 05 10987.

[4] Qiliang Li et at., Advanced Materials, Vol. 16, No. 2, p. 133, 2004.

ELECTROSPUN NANOFIBROUS SCAFFOLD FOR TISSUE REGENERATION

E.Chiellini[1], F.Chiellini[1], A.M.Piras[1], D.Puppi[1], H.Ylikauppila[2], L.Nikkola[2], N.Ashammakhi[2]

1. Department of Chemistry and Industrial Chemistry –University of Pisa
via Risorgimento 35- 56126 Pisa, Italy
emochie@dcci.unipi.it

2. Institute of Biomaterials – Tampere University of Technology,
Hermiankatu 12 A FI-33101, Tampere, Finland
Nureddin.ashammakhi@tut.fi

Most tissue engineering strategies adopted for creating functional replacement of tissues or organs rely on the application of temporary three-dimensional scaffolds to support and guide the differentiation, poling and proliferation of seeded cells [1]. Electrospinning is a technique that allows for the obtainment of fibers with very small diameter (down to 100 nm), able to mimic the nanometer scale of the extra cellular matrix (ECM) of native tissue, and therefore appears suited for the realization of scaffold with a widespread and interconnected porosity using various polymers [2]. Electrospinning method is flexible to control the fiber morphology and also can supply continuous fibers. Polymer concentration of the solution submitted to electrospinning is affecting the fiber diameter of choice: basically, higher polymer concentration leads to high viscosity of solution and nanofibers with larger diameter can be produced [3]. Although current nanofiber non-woven mesh produced by electrospinning can be used in many applications, with a production rate that surpasses many other nanotechnologies, more can be done to improve the quality and quantity of the nanofibers and the mesh produced.

In the present study nanofibrous meshes made of polyvinylalcohol (PVA) were prepared using the electrospinning technique and the relationship between structure and fabrication parameters, such as starting solution concentration, applied voltage and distance between needle tip and collector, was studied. To better assess the applicability of the electrospinning technology for nanofibrous meshes fabrication, three different molecular weights of PVA (37000, 67000, 130000 g/mol) were used to prepare starting water solution. Morphological properties of manufactured scaffolds were investigated. The influence of electrospinning solution concentration on the meshes structure was evaluated using various concentrations (5 ÷ 20% w/v) and studies with different applied voltages (40 and 60 KV) and needle-collector distance (15 and 25 cm) were carried out. Scanning electron microscopy (SEM) revealed a highly porous, three-dimensional structure, with very thin fibers and average fiber diameter under 1 μm for all scaffolds(Figure 1). Micrographs analysis showed also the influence of various preparation parameters on morphological properties of the electrospun meshes: dependence of fiber diameter and interfiber distance from polymer concentration, molecular weight, voltage applied and needle tip-collector distance was displayed. To develop a rational approach for the design of novel affinity-based delivery systems for growth and differentiation therapeutics in tissue engineering, human serum albumin (HSA) was added as model protein to the electrospinning solution in three different concentrations (0.5, 1 and 2% w/v). SEM analysis showed that HSA-loaded meshes structure was comparable to the structure of the unloaded one (Figure 2). Research is in progress as aimed at looking the nanofibers with active agents.

References:

[1] Dietmar W. Hutmacher,Biomaterials, **21 (**2000) 2529-2543.

[2] Chunmei Li, Charu Vepari, Hyoung-Joon Jin, Hyeon Joo Kim, David L. Kaplan, Biomaterials, **27** (2006) 3115–3124.

[3] Zheng-Ming Huang, Y.-Z. Zhang, M. Kotaki, S. Ramakrishna, Composites Science and Technology, **63** (2003) 2223–2253.

Figures:

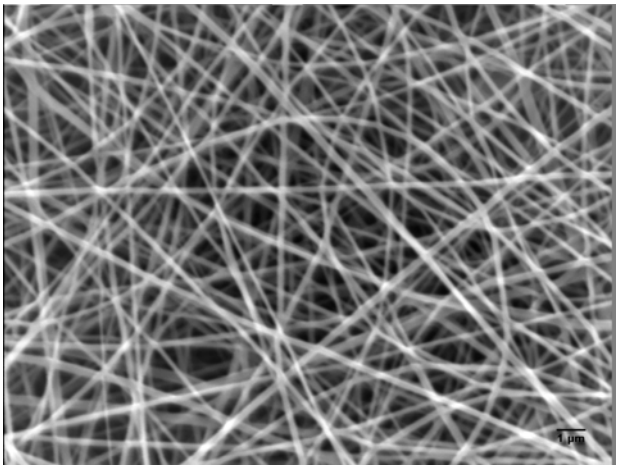


Fig. 1. SEM image of electrospun mesh made of PVA8/88 (Mw = 67000g/mol) 15% w/v in water (applied voltage = 40KV; needle tip – collector distance = 15cm)

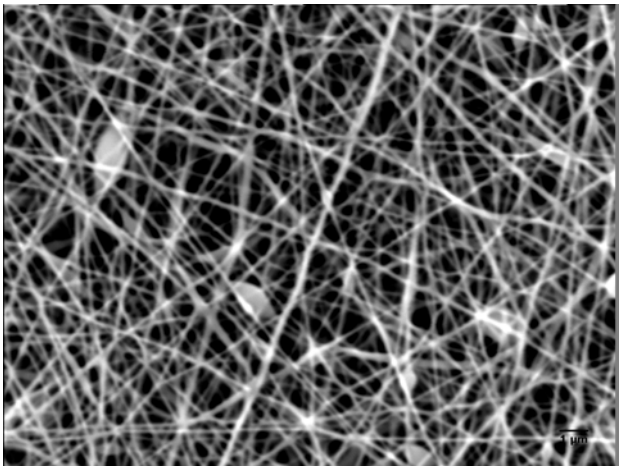


Fig. 2. SEM image of electrospun mesh made of PVA8/88 (Mw = 67000g/mol) 15% w/v, HAS 2% w/v in water (applied voltage = 40KV; needle tip – collector distance = 15cm)

DETERMINATION OF REFRACTIVE INDEX AND THICKNESS OF TIO2 NANOPARTICLE-POLYMER COMPOSITE THIN FILM COATED ON A SPUTTERED GOLD LAYER BY BROADBAND SPECTRAL SURFACE PLASMON RESONANCE SPECTROSCOPY

*Zhi-mei Qi, Hirofumi Matsuda, Itaru Honma, Haoshen Zhou**
PRESTO, Japan Science and Technology Agency (JST), Kawaguchi 332-0012, Japan;
Energy Technology Institute, National Institute of Advanced Industrial Science and Technology (AIST), Tsukuba,305-8568, Japan
Hs.zhou@aist.go.jp

Mesoporous thin films and composite layers containing either nanoparticles or nanotubes or nanowires are of great current interest because of their unique physical and chemical properties and potential applications.[1,2] Determination of refractive index and thickness of such nanomaterial films is necessary for many kinds of applications. To do these, commercial ellipsometers are used [1,2]. Such equipments are expensive and therefore not easily available in many laboratories. Here we introduce an inexpensive and simple technique, i. e., spectral surface plasmon resonance (SPR) spectroscopy, for determination of refractive index and thickness of nanomaterial layers

SPR is a well-known powerful sensing technique for detection of chemical and biological molecules [3,4]. SPR is also an effective tool for determination of refractive index and thickness of various thin films coated on the metal surfaces [5]. Popular SPR sensors operate at a single wavelength with an angular sensitivity. Different from these, a broadband, time-resolved spectral SPR sensor has been developed most recently in our group by using a polychromatic light source, a charge-coupled device detector and a 50-nm-thick gold layer sputtered on a slide glass substrate (see Fig. 1a). After covering the gold layers with the TiO_2 nanoparticle-polymer composite thin films fabricated from the ethanolic solution of polymer-stabilized TiO_2 colloids, we investigated the SPR absorption spectra of the resulting structure with either air or water in the flow cell. As shown in Fig. 1b, with water as the reference and air as the sample, the SPR peaks with air and the SPR dips with water were simultaneously observed, and these peak and dip positions are dependent on the incident angle. Note that without covering the gold layer by the TiO_2 nanoparticle-polymer composite thin film, the SPR absorption spectrum at a given incident angle consists of only a single peak (or dip). Fig. 2a and 2b show that the spectral SPR sensor is sensitive to refractive index of the aqueous sucrose solution, with both the resonant wavelength and effective refractive index being a linear function of the solution index of refraction.

By fitting the resonant wavelengths measured in Fig. 1b with numerical calculations, we determined that thickness and refractive index of the TiO_2 nanoparticle-polymer composite layer are 67.7 nm and 1.53 at λ = 786 nm. We also investigated the thickness of the composite film by atomic force microscopy (AFM). As shown in Fig. 3, the composite thin film is rather coarse relative to the sputtered gold layer due to the presence of TiO_2 nanoparticles. The height from the gold layer surface to that of the composite film is ~ 64 nm. The film thickness derived from the SPR measurements is very close to that measured by AFM, thereby accurate. The findings indicate that spectral SPR spectroscopy is applicable not only to chemical sensings but also to determination of thickness and refractive index of nanomaterial layers.

References:

[1] Z. Qi, I. Honma, M. Ichihara, H. Zhou, Adv. Funct. Mater, **16** (2006) 377.
[2] Z. Qi, I. Honma, H. Zhou, Anal. Chem. **78** (2006) 1034.
[3] J. Homola, Sens. Acutators B, **41** (1997) 207.
[4] J. S. Yuk, J. Jung, S. Jung, J. Han, Y. Kim, K. Ha, *Biosens. Bioelectron*. **20** (2005) 2189.
[5] J. J. Saarinen, E. M. Vartiainen, K.-E. Peiponen, Appl. Phys. Lett., **83** (2003) 893.

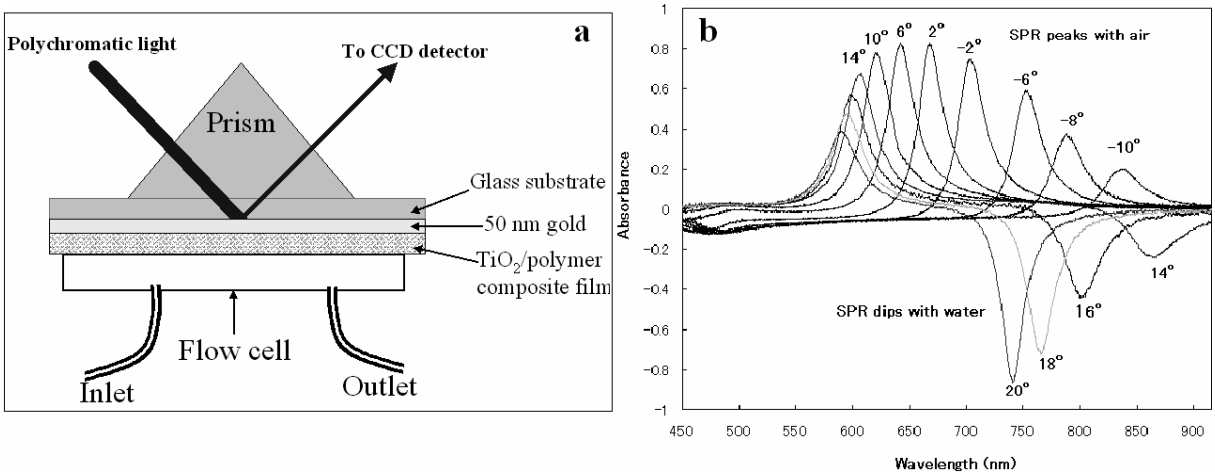


Fig. 1. (a) structure of a spectral SPR sensor coated with a TiO_2 nanoparticle-polymer composite thin film; (b) SPR absorption spectra at different incident angles

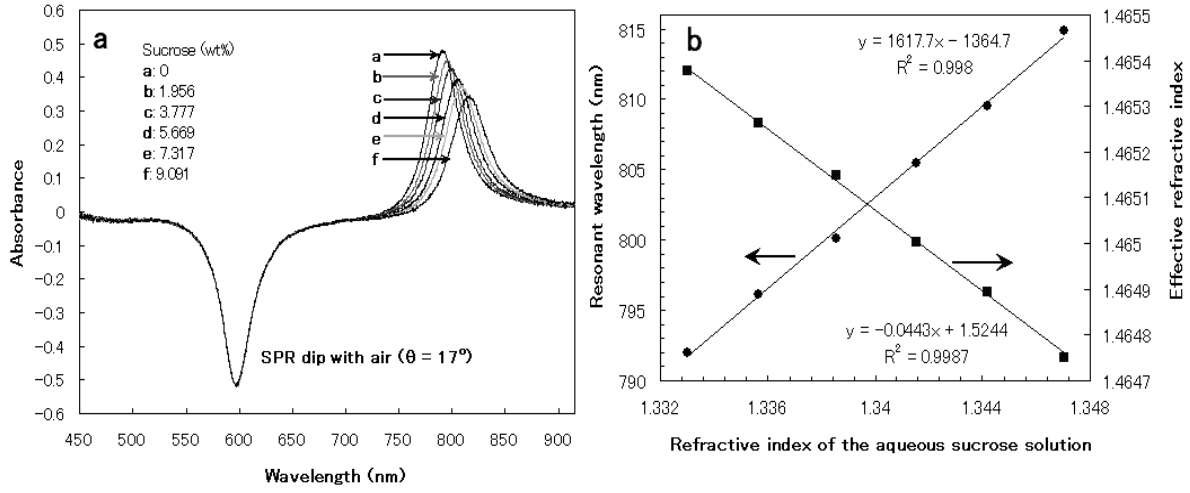


Fig. 2. (a) SPR absorption spectra measured with aqueous sucrose solutions in the cell; (b) dependences of resonant wavelength and effective refractive index on refractive index of the sucrose solution

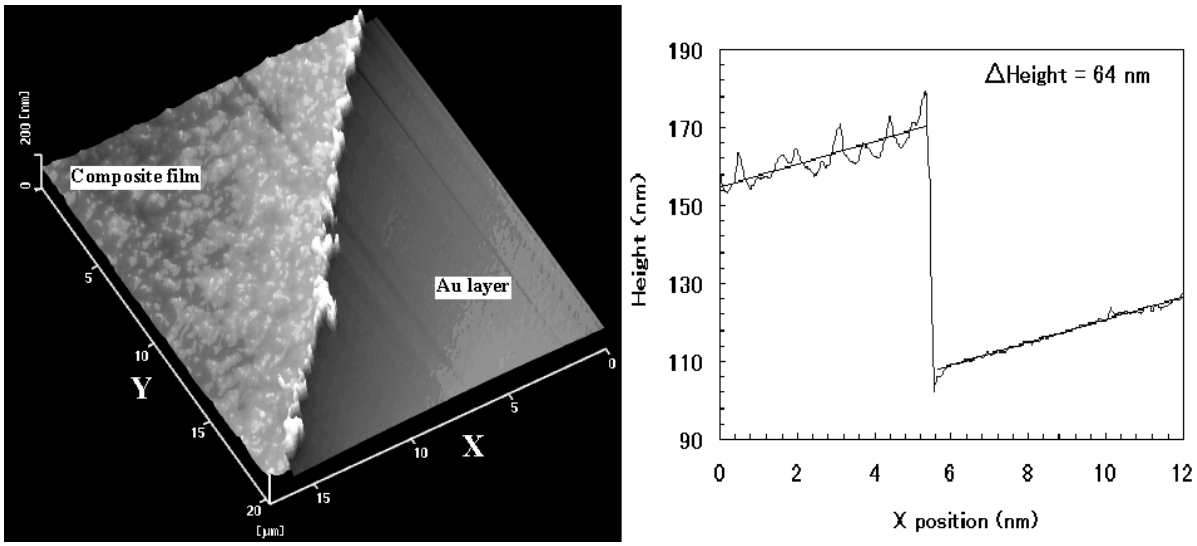


Fig. 3 Height profile of the TiO_2 nanoparticle-polymer composite thin film measured by atomic force microscopy.

Poster

INTERLAYER EXCHANGE COUPLING TEMPERATURE DEPENDENCE IN ANTIFERROMAGNETICALLY COUPLED MULTILAYERS

L. Zárate,[a] C. Quirós,[a] M. Vélez,[a] G. Rodríguez-Rodríguez,[a,b] J. I. Martín,[a] and J. M. Alameda[a]

[a] Departamento de Física, Universidad de Oviedo, Avda. Calvo Sotelo, s/n, 33007 Oviedo, Spain
[b] Instituto del Carbon (INCAR), CSIC, c/ Francisco Pintado Fe, 26, 33011 Oviedo, Spain
carquir@string1.ciencias.uniovi.es

The study of Interlayer Exchange Coupling (IEC) through non-metallic spacers has stimulated intense research, both from the experimental and the theoretical point of view. Most of the available results correspond to the Fe/Si system, where several mechanisms based on tunneling, RKKY-like exchange, interface bands and spin fluctuations have been suggested to be in the origin of the coupling. In addition, the presence of impurities in the spacer or in the interfaces has been recently suggested as a mechanism leading to the coupling observed in the Fe/Si system [1,2]. Interestingly, the temperature dependence of this type of coupling shows a decrease in strength with increasing temperature which is contrary to the predictions made by the model based on quantum interference [3]. These differences in the predicted behaviour of the temperature dependence of the coupling constant can be very useful to identify the mechanisms underlying the experimentally reported IEC through non-metallic spacers.

Although the case of Co/Si has been less studied, recently, weak antiferromagnetic exchange coupling has been reported at room temperature for amorphous Co_xSi_{1-x} / Si multilayers [4]. The presence of antiferromagnetic (AF) coupling has been confirmed by Magneto-Optical Transverse Kerr Effect (MOTKE) for compositions in the amorphous range, below 76 % atomic Co. Figure 1 shows MOTKE hysteresis loops for the case of a 2 period multilayer having the following structure (3 nm Si / 5 nm $Co_{74}Si_{26}$)$_{x\ 2}$ / 3 nm Si / Substrate. Panel (a) corresponds to the loop obtained by applying the magnetic field along the easy axis direction. The plateau observed around zero magnetic field corresponds to the formation and stabilization of the AF state. Interestingly, the switching field needed to break this state and reverse the magnetization is very low, of the order of only 2 Oe for passing from positive to negative saturation. A detailed characterization by MOTKE of the AF plateau and switching field has been done as a function of T. Interestingly, for this simple case of a 2 period multilayer, the coupling strength, J, can be easily written in terms of the H_1-H_4 fields indicated in Figure 1. This has been used to characterize the temperature dependence of J [5]. The results indicate that J decreases when increasing the temperature, in agreement with the predictions of some of the theoretical models [1,2].

This work has been supported by the Spanish CICYT under grant FIS2005-07392 and NAN2004-09087. L. Z. acknowledges support from Spanish MEC under FPU grant. C. Q. acknowledges support from the Spanish Government and the European Social Fund through the “Ramón y Cajal” program. G. R.-R. acknowledges support from MERG-CT-2004-513625.

References:

[1] M. Y. Zhuravlev, E. Y. Tsymbal, and A. V. Vedyayev, Phys. Rev. Lett. **94**, 26806 (2005).

[2] V. Tugushev, E. Kulatov, O. Navarro, Microelectr. J. **36**, 488 (2005).
[3] P. Bruno, Phys. Rev. B **52**, 411 (1995).
[4] C. Quirós, J. I. Martín, L. Zárate, M. Vélez, and J. M. Alameda, Phys. Rev. B **71,** 24423 (2005).
[5] L. Zárate, C. Quirós, J. I. Martín, M. Vélez, G. Rodríguez-Rodríguez, J. I. Martín, and J. M. Alameda, Phys. Rev. B. **74**, 14414 (2006).

Figures:

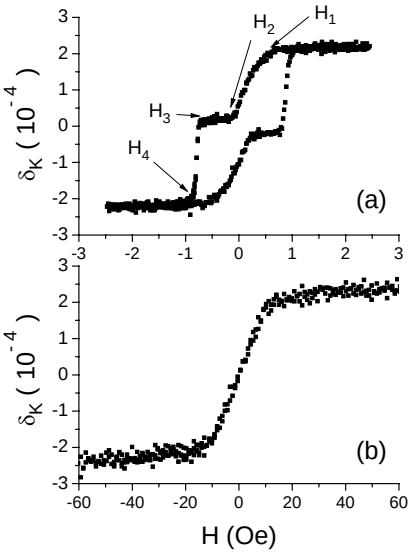


Figure 1. MOTKE hysteresis loops for a two period multilayer measured applying the magnetic field along the easy (a) or hard (b) axis direction. The plateau observed in panel (a) is characteristic of the AF coupling. Panel (b) confirms the in-plane uniaxial magnetic anisotropy of the films.

ELECTRONIC FLUCTUATIONS IN MULTI-WALLED CARBON NANOTUBES

B. Raquet, B. Lassagne, S. Nanot, J.-M Broto
Laboratoire National des Champs Magnétiques pulsés, LNCMP-UMR5147,
CNRS-UPS-INSA, 143 av. de rangueil 31400 Toulouse, France

J.-P Cleuziou, Th. Ondarçuhu, M. Monthioux
Centre d'Elaboration des Matériaux et d'Etudes
Structurales, CEMES-CNRS, UPR 8011, 29 rue Jeanne Marvig, 31055
Toulouse, Cedex 4 France

The physics and application of Carbon Nanotubes (CNTs) in nano-electronics are currently under intense studies. Most of the striking characteristics of the electronic transport in CNTs have been expressed using the time average of the conductance. However, high order statistic conductance fluctuations in nano-scale conductors are a powerful experimental tool to unveil the exceptional richness of charge carriers properties in a confined environment.
The issue of the electronic noise experiments on CNTs has to be addressed in the very specific context of their unique electronic transport properties. This implies noise measurements as a function of the Fermi energy location to probe the interplay between the electronic fluctuations and the band structure. Up to now, the very few studies on individual CNTs display a low frequency *1/f*-noise whose the magnitude ranges over four decades. The contribution of the tube alone to this noise and its structural quality dependence are opened questions.

In this work [1], we bring evidence that gas, mainly oxygen surrounding the tube, significantly contributes to the electronic fluctuations at room temperature. Under controlled atmosphere, the excess noise level and its temperature dependence are also conditional on the conduction regimes of the tubes. We demonstrate that quasi-ballistic Multi-walled Carbon Nanotubes (MWCNTs) are low noise conductors at room temperature. The *1/f*-noise behaves like a background noise independent on the number of conduction channels. In case of diffusive MWCNTs, we infer a distribution of the activation energies responsible for the intrinsic CNT noise. From multi-probes measurements, an estimate of the localized contact noise is proposed.
Finally, we give evidence that low noise MWCNTs at room temperature may exhibit huge random telegraph noise at low temperature by tuning the Fermi energy location. From the spectroscopy of the RTN, we sketch the possible contribution of impurity scattering fluctuations enhanced by quantum interferences.

[1] B. Lassagne & al., New J. Phys. 8, 31 (2006).

Poster

FORMATION OF MICRO- AND NANO-DIMENSIONAL DISK-SHAPE TiO_2 AND ZrO_2 PARTICLES AT AIR-WATER INTERFACE

Valter Reedo[1,2], Argo Lukner[1]
[1]*Institute of Physics, University of Tartu, Riia 142, 51014 Tartu, Estonia,*
[2]*Institute of Organic and Bioorganic Chemistry, University of Tartu, Jakobi 2, 51014 Tartu, Estonia*
valterre@fi.tartu.ee

Low-dimensional metal oxides (*e.g. TiO_2*) have acquired great attention as compared with the traditional materials, nano-phase materials processes unusual chemical, optical, mechanical, magnetic and electrical properties [1].

In recent decade, sol-gel techniques in relation with materials chemistry have been extensively investigated and employed to explore new approaches in obtaining transition metal oxides in form of thin film layers, fibres or colloidal particles. Controlled synthesis of wide band gap pure and rare earth ions doped TiO_2 and ZrO_2 materials are of great interest since they can be used in gas sensorics [2], photocatalysis, electronics, photonic and solar cells. In almost all of these cases the dimensions and shape of these metal oxides is an important factor affecting the performance and application of the materials.

In present work we report a novel method for preparation of nano-dimensional undoped and rare earth ions doped circular TiO_2 and ZrO_2 particles (figure 1, 2). Disk-shape metal oxide particles were obtained by dropping solution of pre-polymerized metal butoxide solution in butahanole on air-water interface. Formed particles were 0.5-10μm in diameter and 20-80nm in thickness. Undoped and rare earth ions doped TiO_2 and ZrO_2 particles where heat treated up to 1000^{o}C for crystallization of material.

Current work include:

- Characterisation of formed particles by AFM and SEM visualization.
- Observation effect of water pH and temperature for the dimensions of formed particles.
- Observation the rate of polymerization of Ti and Zr alkoxides for the dimensions of forming particles.
- Some possible disk-shape-forming mechanisms are also proposed to explain the formation of observed novel structures.
- Presentation of some novel optical gas sensing properties of prepared samples.

This work has been supported by ETF6537, ETF6660, ETF6163, SF0382149s02, Estonian Nanotechnology Competence Center and European Science Foundation programs Nanotribo and Molsim.

References:

[1] H. Gleiter, Progress in Materials Science, **4** (1989) 223-315.

[2] V. Reedo, S. Lange, V. Kiisk, T. Tätte, A. Lukner and I. Sildos, SPIE Proceedings, **5946** (2005) 5946 OD1-5.

Figures:

Figure 1. SEM image of TiO_2 disk-shape particles.

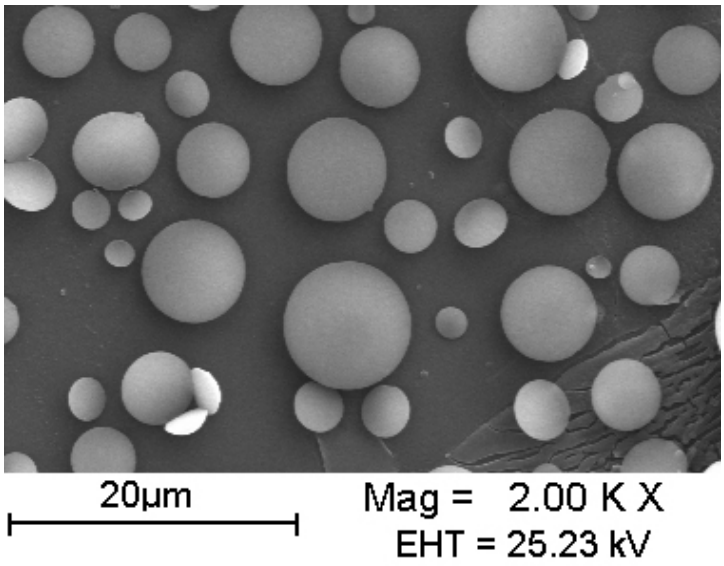
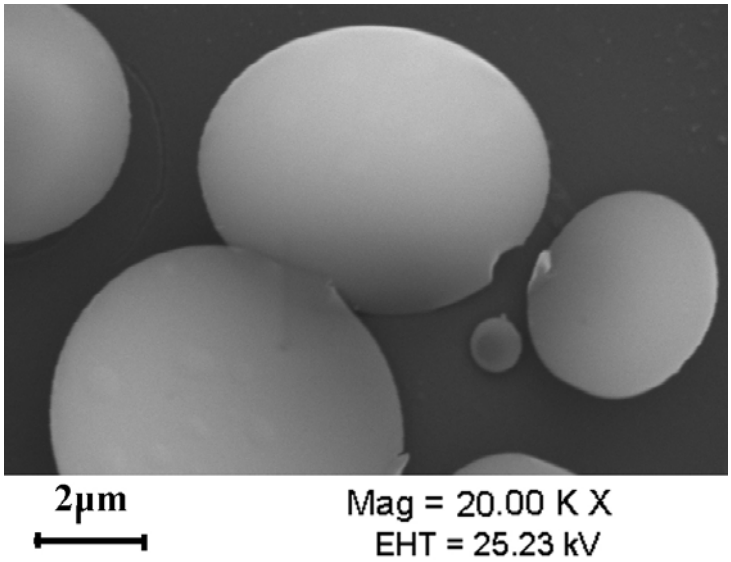


Figure 2. SEM image of TiO_2 disk-shape particles.



ANODISED TiO2 NANO-TUBES: VOLTAGE RAMP INFLUENCE ON THE OXIDE MORPHOLOGY AND INVESTIGATION OF PHASE CHANGES IN THE CRYSTAL STRUCTURE PROMOTED BY THERMAL TREATMENTS

D. Regonini[1], C. R. Bowen[1], R. Stevens[1], D. Allsopp[2] and A. Jaroenworaluck[3]

[1]Materials Research Centre, Dept. of Mechanical Engineering, University of Bath, UK

[2]Dept. of Electronic & Electrical Engineering, University of Bath, UK

[3]MTEC: National Metal and Materials Technology Center, Pathumthani, Thailand

D.Regonini@bath.ac.uk

Abstract

The generation of titanium dioxide nano-tubes (Fig.1 and 2) by anodising commercially pure (99.6%) titanium in a fluorine-based electrolyte has been studied. Experiments have been performed using an electrolyte consisting of a 1M solution of sodium sulphate, with a small amount of sodium fluorine (0.1-1%wt) added. The electrolyte pH was controlled by addition of sulphuric acid, helping reduce unwanted precipitates that partially covered the nano-layer. The use of an initial voltage ramp prior to applying a constant voltage to the cell, caused a different morphology to develop in the anodised oxide nano-structure. Changes in the thickness of the oxide layer were also promoted by use of a controlled voltage ramp. The thermal stability of the nano-tubes layer has been investigated by annealing at different temperatures, from 200 to 600°C, for 3h. Scanning Electron Microscopy (SEM) indicates the nano-tube morphology is stable up to 500°C. X-Ray Diffraction (XRD) has been performed to monitor phase changes in the crystal structure developed by the thermal treatments. The as-prepared nano-tubes are amorphous, the anatase phase start to form at 300°C whilst the rutile phase is found above 500°C. Initial results obtained by characterising the as-prepared nano-tubes with Transmission Electron Microscopy (TEM) confirm the results and clearly show the three dimensional network which forms the structure. Electron diffraction at 200kV confirms the amorphous nature of the as-formed TiO_2 film.

Figures:

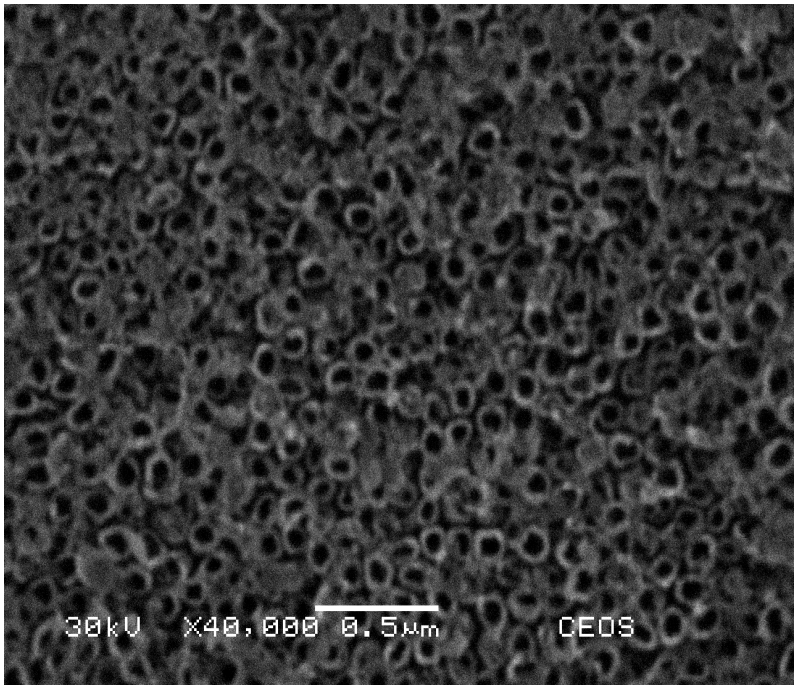


Figure 1. Top-view of a titanium dioxide nano-tubes array grown by anodisation in a fluorine-based electrolyte.

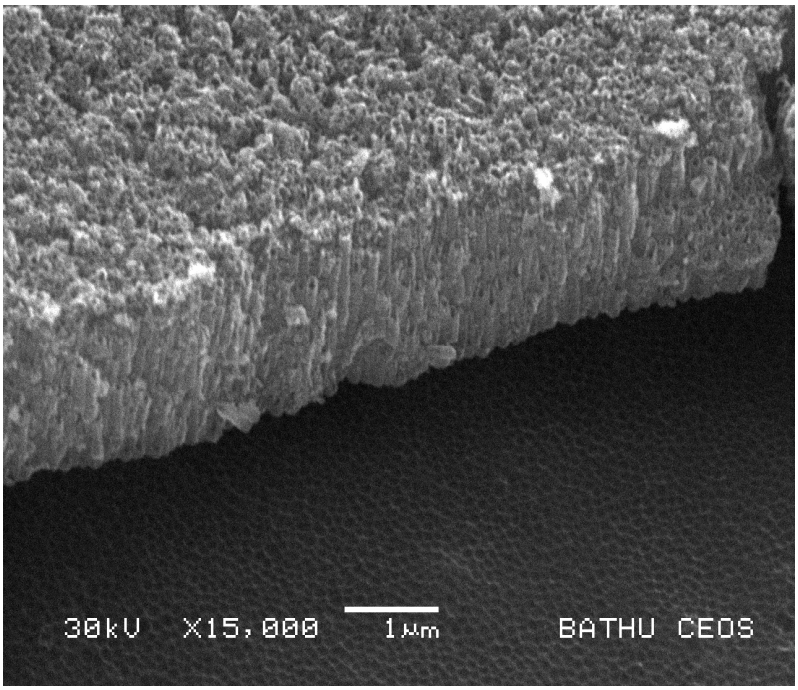


Figure 2. Cross sectional view of the nano-tubes layer. The concave-shaped layer of titanium underneath the nano-tubes is also shown.

Structural and electrical studies of tungsten nano-electrodes prepared by FIBID (focused ion beam induced deposition)

A Reguer, F. Bedu, D.Tonneau, M.Prestigiacomo*, P. Sudraud*, J.Herman** and H. Dallaporta
CRMCN, CNRS UPR 7251, 163 Avenue de luminy , Case 901, 13288 Marseille cedex 09, France
**Orsay Physics, Z.A. Les Michels, Chemin Départemental 56, 13710 Fuveau, France*
***LP3, UMR 6182 CNRS, 163 Avenue de luminy, Case 917, 13288 Marseille cedex 09, France*
reguer@crmcn.univ-mrs.fr

The use of an ion focused beam to induce the deposition of materials from metalorganic precursors has recently emerged as an important technique to fabricate nanowires and integrated circuit devices [1-3]. Focused-ion-beam-induced deposition (FIBID), based on the local decomposition of gaseous precursor by the ion beam, is a maskless direct writing technique allowing the deposition of sub-micronic patterns. We have studied the properties of electrodes (or wires) formed by FIBID from a tungsten hexacarbonyl $W(CO)_6$ precursor and subjected to an electrical treatment. These electrodes are supported on a structure also elaborated by FIBID. We present conductivity measurements and structural analysis of these electrodes before and after electrical treatment.

The experimental setup consists of a cross beam system coupling a scanning electron microscope (SEM, JEOL) and a focused ion beam (FIB, Orsay Physics), equipped with a gas injection system (GIS, Orsay Physics). Using a current–voltage (I–V) picoammeter, the electrical characteristics of the wires can be followed *in situ* during the deposition process and the electrical treatment.
The electrodes, prepared for subsequent analysis in the TEM, were deposited on a diamond like carbon (DLC) thin membrane (3x10 µm² ; thickness 50-100 nm). The carbon membranes are prepared by FIBID from a phenantren ($C_{14}H_{10}$) precursor and are used to bridge two aluminium electrodes *(Fig.1)*. These membranes are insulating (resistivity: 100 Ω.cm), very hard (Young modulus : 600Gpa) and are transparent to electrons.[4-5]

The structure and the morphology of the electrodes were characterized by atomic force microscopy (AFM) and high-resolution transmission electron microscopy (HRTEM). Their dimensions are : length 20 µm, width 45-60 nm and thickness 15-30 nm (function of the deposition time). Before electrical treatment, the microstructure of the wires shows no obvious long range order implying the deposited material exists in an amorphous like state. These nanowires are a mixture of tungsten (75%), carbon (10%) and oxygen (5%) resulting from the precursor decomposition and gallium (10%) coming from the ion beam.[6-8] During the deposition process, a constant voltage of 50 mV was applied between the aluminium electrodes and the current through the wires was measured *(Fig.2)*. We obtained electrodes with resistances between 10 and 100 kΩ for deposition time between 5 and 60s.

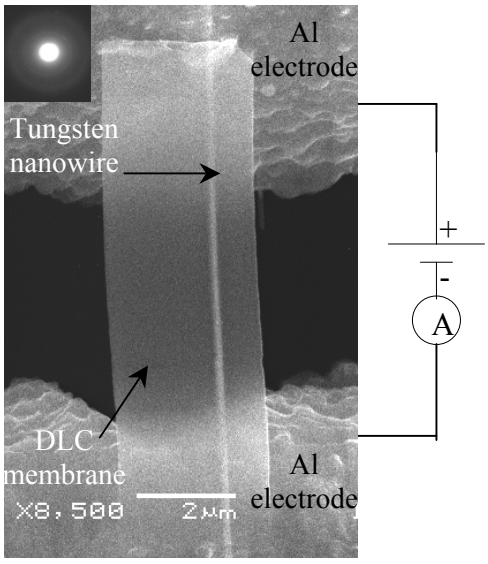


Fig-1 *:SEM view of the experimental support*

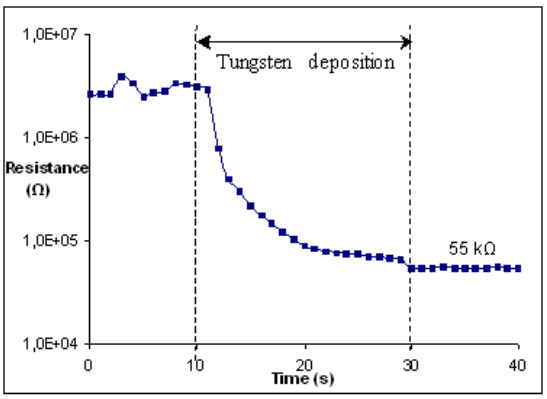


Fig-2 *: Electrode résistance during deposition process*

We have observed that simple electrical treatment can substantially improve the wire resistivity.[9] It consists in the application of voltage ramps to the wire *(Fig.3*), producing a high current density and inducing an electrical annealing. This treatment first induces a segregation of Ga atoms forming droplets. The level of impurities in the wire decreases, and the wire becomes metallic. Then, as high temperature is reached (~600°C) the Ga droplets evaporate and a reorganisation of the microstructures occurs in the Ga-free wire. Figures 4 shows high magnification SEM and TEM images for the nanowire after electrical annealing. The wavelength of the modulation in the HRTEM image is about 0.22 nm, which corresponds to the interplanar distance of (110) tungsten's lattice planes (bcc ; a=3,16Å). The associated electron diffraction pattern in the inset of the figure reveals the (110) reflections. The periodicity of both the lattice planes and the associated electron diffraction pattern indicate that the treated nanowires are crystallized (crystal 5-20nm).

Our process allows the fabrication of polycrystalline tungsten nano-electrode with low resistivity (50μΩ.cm) being able to support high density current (5.10^7 A/cm²). These results open a wide range of applications for the FIBID technology. The high resolution images presented here show the most promising application of our carbon membranes as substrates for electronic transmission microscopy. Furthermore, the nano-electrodes can be used to probe and heat nano-objets in in-situ TEM preparations.

Electrical annealing

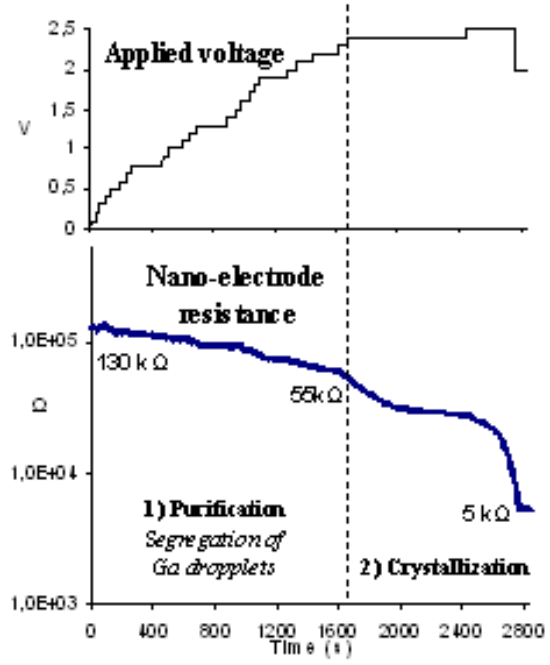


Fig-3 : *Evolution of the nano-electrode resistance during the electrical treatment*

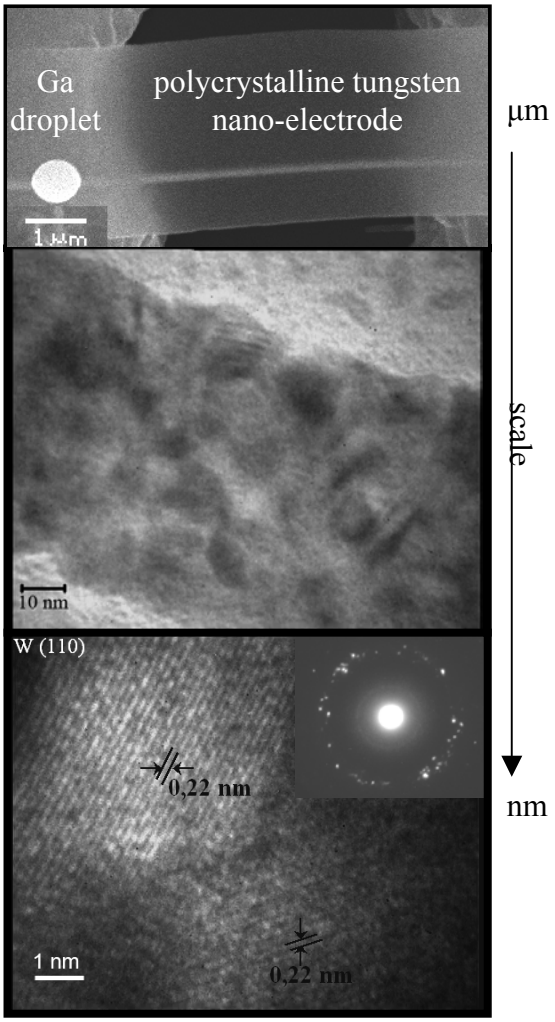


Fig-4 : *SEM, TEM , HRTEM images and diffraction pattern of the annealed nano-electrode*

Références :

[1] G. De Marzi, D. Iacopino, A. J. Quinn, and G. Redmond, J. Appl. Phys.96, 3458 (2004).
[2] E. S. Sadki, S. Ooi, and K. Hirata, Appl. Phys. Lett. 85, 6206 (2004).
[3] Thomas J. Gannon,a) George Gu, J. David Casey, Chuong Huynh,Neil Bassom, and Nicholas Antoniou, J.Vac. Sci. Technol. B 22, 3000 (2004).
[4] S. Matsui, T. Kaito, J. Fujita, M. Komuro, K. Kanda, and Y. Haruyama, J.Vac. Sci. Technol. B 18, 3181 (2000)
[5] J. Fujita, M. Ishida, T. Sakamoto, Y. Ochiai, T. Kaito, and S. Matsui, J.Vac. Sci. Technol. B 19, 2834 (2001)
[6] D. K. Stewart, L. A. Stern, and J. C. Morgan, Proc. SPIE 1089, 18 (1989)
[7] M. Ishida, J. Fujita, T. Ichihashi, Y. Ochiai, T. Kaito, and S. Matsui, J. Vac.Sci. Technol. B 21, 2728 (2003).
[8] M. Prestigiacomo, L. Roussel, P. Sudraud, F. Bedu,, and H. Dallaporta, Microelectron. Eng. 76, 175 (2004)
[9] M. Prestigiacomo, F. Bedu, F.Jandard, D.Tonneau, L. Roussel, P. Sudraud, and H. Dallaporta, Appl. Phys. Lett.86,1(2005)

IN-FLIGHT OPTICAL ANNEALING OF FePt NANOPARTICLES.

Bernd Rellinghaus, Elias Mohn, Franziska Schäffel, Christine Mickel, and Ludwig Schultz.
IFW Dresden, P.O. Box 270116, D-01171 Dresden, Germany
b.rellinghaus@ifw-dresden.de

Monodisperse fractions of FePt nanoparticles within a size range of 4-6 nm were prepared by DC magnetron sputtering in an inert gas atmosphere at elevated gas pressures of roughly 1 mbar. Subsequent ejection into high vacuum results in an increase of the mean free path of the particles and thereby in a substantial suppression of particle-particle coagulation, hence the formation of particle agglomerates can be effectively controlled. In order to prepare the chemically ordered tetragonal $L1_0$ phase without sacrificing monodispersity, the particles were subjected to in-flight thermal annealing prior to their deposition. This ordered phase is of particular interest owing to its very high magneto-crystalline anisotropy.

Since convective heating [1] is not an option in high vacuum, optical heating is necessary in order to thermally treat the particles in-flight. We have therefore developed an ultra high vacuum (UHV) compatible light furnace, in which three halogen lamps (with a total power of up to 4.5 kW) are focussed on the flight path of the particles at a length of 150 mm. The morphology and crystal structure of the deposited particles are characterized by (high resolution) transmission electron microscopy ((HR)TEM).

Inter-particle coalescence (sintering) as induced by the in-flight optical annealing was studied as function of the applied power of the light furnace. TEM investigations show that it is possible to sinter particle agglomerates down to single particles when a sufficiently high power is provided to the optical furnace. The minimum temperature of the particles during the in-flight annealing was estimated to be T = 800°C, which implies that the construction of the light furnace allows for an effective radiative heat transfer to the particles. The experimental results were corroborated by model calculations of the energy transfer based on classical electrodynamics. Investigations of particles, which were deposited at a certain distance to the principle particle flight path and thus to the focus line of the light furnace, show that particles, which do not travel completely within this focal line, experience a reduced degree of inter-particle coalescence.

(HR)TEM investigations provide evidence for the formation of the ordered $L1_0$ phase in the in-flight annealed particles, if the annealing temperature is at least T = 800°C. It is noteworthy that the $L1_0$ ordering was achieved even though the annealing times were as short as roughly one millisecond. The experimental results will be analysed with respect to the $L1_0$ ordering kinetics, and the magnetic properties of the deposited particles will be discussed.

References:

[1] S. Stappert et al., J. Cryst. Growth 252 (2003) 440-450.

Figures:

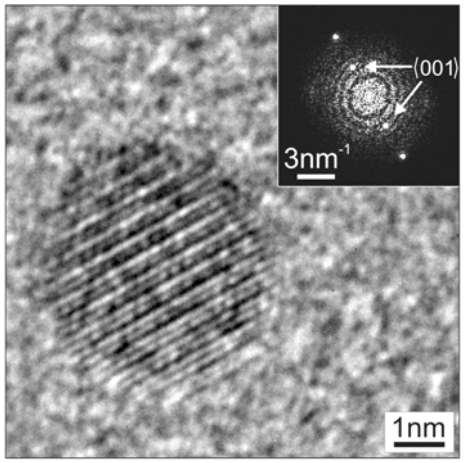


Fig. 1 HRTEM micrograph of a $L1_0$ ordered FePt nanoparticle, as obtained after in-flight optical heating. The Fourier transform of the image (insert) clearly reveals the occurrence of (001) super structure reflections.

PHONON MULTIPLEXING THROUGH 1D CHAINS

Diego Reyes, Alba Ávila

Centro de Microelectrónica
Departamento de Ingeniería Eléctrica y Electrónica
Universidad de los Andes
Carrera 1 #18A-10 Bogota, Colombia
+57(1) 3399999 Ext. 2828
Email: di-reyes@uniandes.edu.co, a-avila@uniandes.edu.co

Phonon propagation trough atomic structures have became an important study issue. The most important applications rise on the thermal field, since phonons can carry thermal and acoustic energy. The technological advantage makes possible to engineer thermal an acoustic paths as desire.

A linear numerical method was developed in order to analyze the scattering and filtering of phonons in 1D atomic structures. Only transverse propagation modes were taken into account. Bonding forces between atoms were assumed linear; also these forces were restricted to be first nearest neighbor interaction.

A simple phonon multiplexer proposed by Dobrzynski [2] was analyzed. It consists of two mono-atomic chains of atoms and a coupling structure between them which is made out of two atoms connected together. Dobrzynski´s results [2] were verified making possible to use the developed model in further analyzes. Earlier analysis of the structure did not establish a way of changing the wave length in which the phonon transfer occurs. Taking advantage on the friendly numerical methods, it was possible to establish simple rules that able us to actually select a wavelength of transmission and tune the structure by changing its constitutive parameters such as atoms masses and bonding forces. Multiplexer efficiency was also studied setting the limits of well performance of the filter. Finally frequency analysis led to obtain the energy gaps between the propagating modes. The developed method allows studying much more complex structures than the one presented here. In summary we find how the parameters of the structure allows us design phonon filters.

References:

[1] J. S. Jensen, “Phononic band gaps and vibrations in one- and two-dimensional mass-springs structures”, Journal of sound and Vibration 266 (2003) 1053-1078.

[2] L. Dobrzynski, et Alt., “A simple phonon multiplexer”, Europhys. Lett., 65 (6), pp. 791-794 (2004).

[3] Dobrzynski L., Djafari-Rouhani B., Akjouj A., Vasseur J. and Zemmouri J., Europhys. Lett., 46 (1999) 467.

Figures:

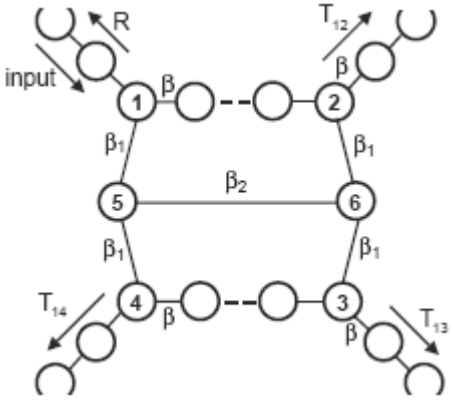
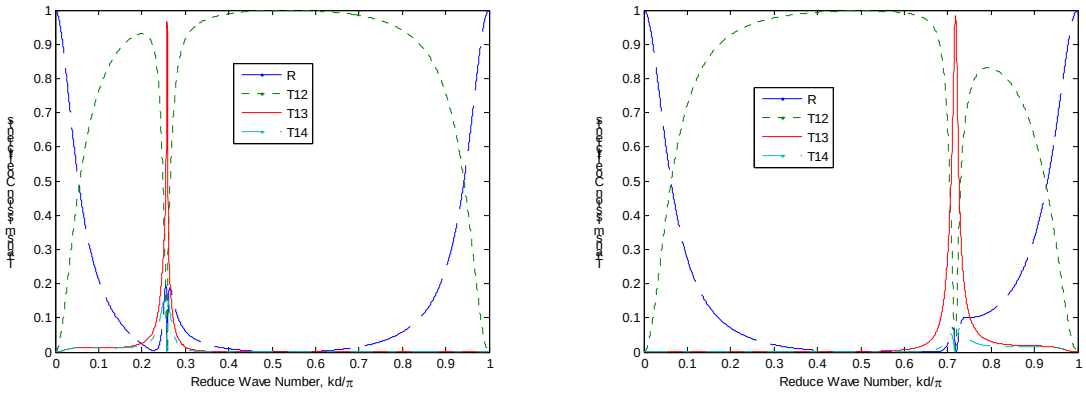


Fig.1. Phonon Multiplexer proponed by Dobrzynski [2].



(a) (b)

Fig. 2. Transmission coefficients tuned at different wavelengths.

SYNTHESIS OF PHOTOLUMINESCENT SILICON NANOCRYSTALS BY REACTIVE LASER ABLATION

Daria Riabinina, Christophe Durand, Federico Rosei, Mohamed Chaker
Institut National de la Recherche Scientifique – Energie, Materiaux et Telecommunications, Universite du Quebec, Varennes, Quebec, Canada, J3X 1S2
riabinina@emt.inrs.ca

In recent years, silicon nanoparticles have attracted considerable interest due to their remarkable light-emitting properties [1]. Si nanostructures are key elements for the integration and development of optoelectronic devices into existing silicon-based technology [2].

Pulsed laser deposition (PLD) has established itself as a very versatile method for thin film growth of almost any kind of material [3].[1] Reactive PLD (in reactive oxygen atmosphere) is an excellent method of controlling the stoichiometry of deposited films [4].[2]

In this work, for the first time, we use reactive laser ablation for synthesizing Si nanoparticles. Partial oxidation of ablated species during reactive PLD followed by thermal annealing yields the formation of Si nanocrystals embedded in a Si oxide matrix (Figure 1). The oxygen pressure was varied between 0.03 and 1.5 mTorr.

The optical and structural properties of Si nanocrystals were studied by photo-luminescence spectroscopy, transmission electron microscopy, X-ray diffraction and X-Ray Photoelectron Spectroscopy.

The nanocrystal size was linked to the concentration of non-oxidized Si in SiO_x films which is the intrinsic parameter of deposited films [5]. The variation of the Si concentration between 1 and 70 % results in variation of nanocrystal size from 13.3 to 2 nm.

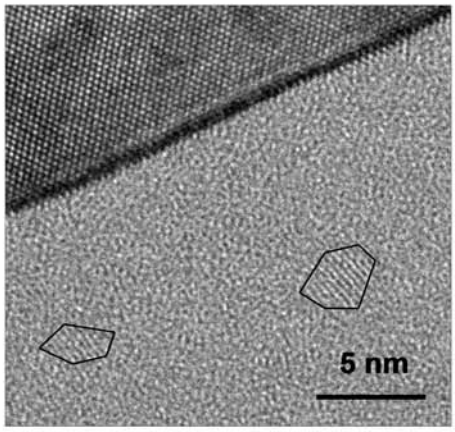


Figure 1. TEM image of Si nanocrystals embedded in Si oxide matrix produced by reactive PLD.

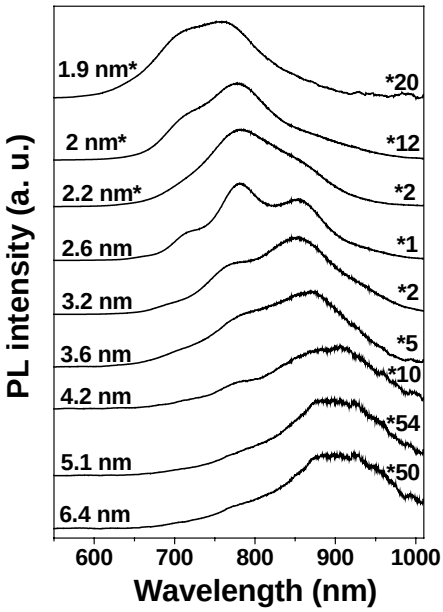


Figure 2. PL spectra of Si-nc in Si oxide.

This correlation allowed discussing the principal mechanisms of formation of Si nanocrystals in Si oxide matrix.

The samples containing nanocrystals of 2 to 6 nm in diameter exhibited a significant luminescence (Figure 2). Photoluminescence spectra were found to be dependent on the degree of oxidation of the material. Basing on structural characterization of the samples, we established a correlation between the position of photoluminescence spectra and the nanocrystal size. A detailed analysis of the origin of PL spectra was performed.

References:

[1] H. Takagi, H. Ogawa, Y. Yamazaki, A. Ishizaki, T. Nakagiri, "Quantum size effects on photoluminescence in ultrafine Si particles," Appl. Phys. Lett. **56** (1990) 2379.
[2] L. Pavesi, L. Dal Negro, C. Mazzoleni, G. Franzo, F. Priolo, "Optical gain in silicon nanocrystals," Nature **408** (2000) 440.
[3] D. Riabinina, F. Rosei, M. Chaker, "Structural properties of Ge nanostructured films synthesized by laser ablation," J. Exp. Nanoscience 1 (2005) 83.
[4] D. Riabinina, C. Durand, M. Chaker, N. Rowell, F. Rosei, "Photoluminescent germanium nanoparticles synthesized by reactive laser ablation," Nanotechnology 17 (2006) 2152.
[5] D. Riabinina, C. Durand, M. Chaker, F. Rosei, Appl. Phys. Lett. **88** (2006) 073105.

SYSTEMATIC SEARH FOR THE Si(553)-Au RECONSTRUCTION.

Sampsa Riikonen, Daniel Sánchez-Portal
Donostia International Physics Center (DIPC), Paseo Manuel de Lardizabal 4,
20018 Donostia-San Sebastián, Spain
swbriris@sc.ehu.es

Gold deposited on silicon surfaces at the monolayer regime results in a variety of reconstructions. The most peculiar ones are the (quasi-) one dimensional phases, featuring monatomic wires of gold. They promise exotic physical phenomena, such as the Luttinger liquid [1]. These wires can be grown on the flat Si(111) surface which yields three possible directions for the wires to grow [2]. Stepped silicon surfaces avoid this problem; the wires grow parallel to the step edges. These systems have been manufactured now for years [3].

We present an *ab-initio* study of the Si(553)/Au surface reconstruction using the SIESTA method [4]. Very recently the Si(553)/Au surface has been studied with growing intensity [3],[5],[6],[7],[8],[9],[10]. The reason for this is the peculiar band structure seen in the photoemission that features one half-filled and another quarter-filled band [5]. As the temperature is increased, these bands show Peierls-like distortions with different periodicities in the atomic structure [7].

Big amount of experimental information is available, including STM, photoemission and x-ray diffraction studies [5],[6],[7],[8] but an atomic structure [3],[8],[9],[10] that would give consistent results with the experiments has not been found up-to-date. We present a systematic method for searching any quasi one-dimensional surface reconstruction based on a tetrahedric coordination of both Au and Si atoms in the surface (we are able to search through all the surface reconstructions that include the most typical Si(111) building blocks: honeycomb-chains, surface-dislocations, stacking-faults, etc.). We have arrived at a model that produces the experimental band structure extremely well. The half-filled band has a strong gold-character as it should in order to feature the (spin-orbit) splitting [11] seen in the experiment [5],[7], while the quarter-filled band originates from the silicon atoms at the step-edge. The structure does not feature the honeycomb-chain structure, as proposed earlier [9] and is very different from the well-known Si(557)-Au reconstruction [11]. We present also simulated STM-images of the new structure.

References:

[1] J. M. Luttinger, J. Math. Phys. **4**, 1154 (1963)
[2] R. Plass and L. D. Marks, Surf. Sci. **380**, 497 (1997)
[3] J. N. Crain, J. L. McChesney, et.al. Phys. Rev. B. **69** 125401 (2004)
[4] J. M. Soler, E. Artacho, et. al. J. of Phys.: Cond. Mat. **14**, 2745 (2002)
[5] J. N. Crain, A. Kirakosian, et. al. Phys. Rev. Lett. **90** 176805 (2003)
[6] J. N. Crain, M. D. Stiles, et. al. Phys. Rev. Lett. **96** 156801 (2006)
[7] J. R. Ahn, P. G. Kang, et. al. Phys. Rev. Lett. **95** 196402 (2005)
[8] S. K. Ghose, I. K. Robinson, et. al. Surf. Sci. **581** 199 (2005)
[9] S. Riikonen and D. Sanchez-Portal Nanotechnology **16** 218 (2005)
[10] S. Riikonen and D. Sanchez-Portal Surf. Sci. **600** 1201 (2006)
[11] D. Sanchez-Portal, S. Riikonen and R. M. Martin Phys. Rev. Lett. **94** 146803 (2004)

INITIAL STAGE SOF THE GROWTH OF COBALT ON RU(0001) STUDIED BY LEEM

J. M. Puerta,[1] Farid El Gabaly,[2] Christof Klein,[2] Angela Saa,[2] Andreas K. Schmid,[3] Kevin F. McCarty,[4] J. I. Cerda,[1] and Juan de la Figuera[2]

[1]*Instituto de Ciencia de Materiales de Madrid, CSIC, Madrid 28049, Spain*
[2]*Dpto. de Física de la Materia Condensada and Centro de Microanálisis de Materiales, Universidad Autónoma de Madrid, Madrid 28049, Spain*
[3]*Lawrence Berkeley National Laboratory, Berkeley, California 94720, USA*
[4]*Sandia National Laboratories, Livermore, California 94550, USA*

We study the clean Ru(0001) surface and the layer-by-layer growth of cobalt on ruthenium employing a low-energy electron microscope (LEEM). By means of selected-area diffraction measurements, we have performed IV analysis for data acquired on single terraces in order to determine the corresponding surface structures.

The clean surface presents a somewhat large first interlayer contraction which is at contrast with previous experimental studies but in close accordance with theoretical predictions for a hydrogen free ruthenium surface. The first Co monolayer grows pseudomorphically following the hcp stacking sequence. The vertical lattice spacing is contracted by 4% relative to the bulk ruthenium value. Films thicker than a monolayer present a relaxed in-plane lattice spacing, as detected by the presence of satellite spots in the diffraction pattern. We identify the stacking sequence of the different films. Films thinner than three monolayers are hcp without any stacking faults. Three monolayer thick islands nucleate in two different stacking sequences, starting the evolution of the film towards an fcc structure. The different stacking sequences of the islands are reflected in their shape, as proven by comparison with selected-area diffraction data.

Keywords:

Poster

OPTIMIZATION OF THE LUMINESCENCE EMISSION IN NANOCRYSTALLINE SIGE/SIO_2 MULTILAYERS

A. Rodríguez [1], M. I. Ortiz [1], J. Sangrador [1], T. Rodríguez [1],
M. Avella [2], A. C. Prieto [2], J. Jiménez [2], A. Kling [3], C. Ballesteros [4].
[1] *Dpto. Tecnología Electrónica, Universidad Politécnica de Madrid, 28040 Madrid, Spain.*
[2] *Dpto. Física de la Materia Condensada, U. de Valladolid, 47011 Valladolid, Spain.*
[3] *Instituto Tecnológico e Nuclear, Estrada Nacional 10, 2686-953 Sacavém, Portugal.*
[4] *Dpto. Física, E.P.S., Universidad Carlos III, 28015 Leganés (Madrid), Spain.*
e-mail: andresr@etsit.upm.es

The formation of a high density of SiGe nanocrystals with uniform size, less than 5 nm, embedded in a dielectric medium has potential applications in the fabrication of electronic and optoelectronic devices which can be integrated with the Si-based electronics [1]. A weak luminescence emission in structures with nanocrystals embedded in SiO_2 fabricated by LPCVD and annealing was reported previously [2]. This work is focused on the influence of the dimensions and the annealing conditions on the intensity of the luminescence with the aim of its maximization. The samples deposition was carried out in a commercial LPCVD reactor at 390 ºC. SiGe nanoparticles with a Ge fraction around 0.3 were deposited using Si_2H_6 and GeH_4. SiO_2 was deposited using Si_2H_6 and O_2. The deposition process is described elsewhere in detail [3]. Multilayer structures with five periods of SiGe/SiO_2 were deposited to increase the area density of nanoparticles. Four samples were fabricated with two diameters of nanoparticles (d) and two thickness of the SiO_2 interlayers (l), which are labelled A (d ≈ 5 nm, l ≈ 20 nm), B (5 nm, 50 nm), C (3 nm, 20 nm) and D (3 nm, 50 nm). The crystallization of the nanoparticles was achieved by subsequent annealing of the samples in N_2 atmosphere at temperatures between 700 and 1000 ºC for times up to 120 s using a RTA unit. SiO_2 films were also deposited and annealed in the same conditions for comparison. Figure 1 shows cross-section TEM images of samples B and C. Stacks of five layers of SiGe nanoparticles separated by SiO_2 interlayers can be observed. An estimation of the average number of nanoparticles per cm^2 is 1.2×10^{12} in each layer. Figure 2 shows Raman spectra of samples A and C (different nanoparticle size). In sample A (and B), with large nanoparticles, the intensities of the three Raman bands of crystalline SiGe increase with the temperature and annealing time. No further crystallization is detected above 900 ºC for 60 s. In sample C (and D), with small nanoparticles, the Raman bands slightly increase their intensity and are narrowed as the annealing temperature increases, indicating that crystallization is taking place. The crystallization does not progress if the annealing is prolonged at a fixed temperature. As the size of the nanoparticles decreases, the annealing temperature must be increased to crystallize them. Figure 3 shows RBS spectra of samples A and B (different oxide thickness). Annealing at a temperature of 800 ºC or lower does not cause diffusion of Ge in any case. In sample A (and C), with thin oxide interlayers, annealing at 900 ºC causes diffusion of Ge that results in the degradation of the structure of the sample. In sample B (and D), with thick oxide interlayers, a slight Ge diffusion also occurs at 900 ºC but the structure of the sample is not strongly affected. Annealing at temperatures higher than 900 ºC causes the loss of integrity of the structure in all cases. Figure 4 shows cathodoluminescence spectra of sample D. The spectrum exhibits similar features in all four samples. A strong increase of the intensity of the main emission band at 400 nm (3.16 eV) takes place as the crystallization proceeds. This band is associated to the presence of the SiGe nanocrystals, since it is not present in the spectra of either the as-deposited sample or the annealed oxide. Figure 5 shows the intensity of the luminescence at 400 nm in the four samples after annealing in different conditions. The intensity increases as the nanoparticle size decreases and as the SiO_2 thickness increases. A very intense luminescence is measured in sample D, with small SiGe nanoparticles and thick oxide barriers, annealed at 900 ºC for 60 s. These conditions represent a good compromise between the appropriate crystallization of the small nanoparticles and the limited degradation of the structure by Ge diffusion due to the thick SiO_2 interlayers.

References:

[1] S. H. Huang *et al.*, Nanotechnology **14** (2003) 25.
[2] M. I. Ortiz *et al.*, Nanotechnology **16** (2005) S197.
[3] M. I. Ortiz *et al.*, Physica Status Solidi (a) **203** (2006) 1284.

Figures:

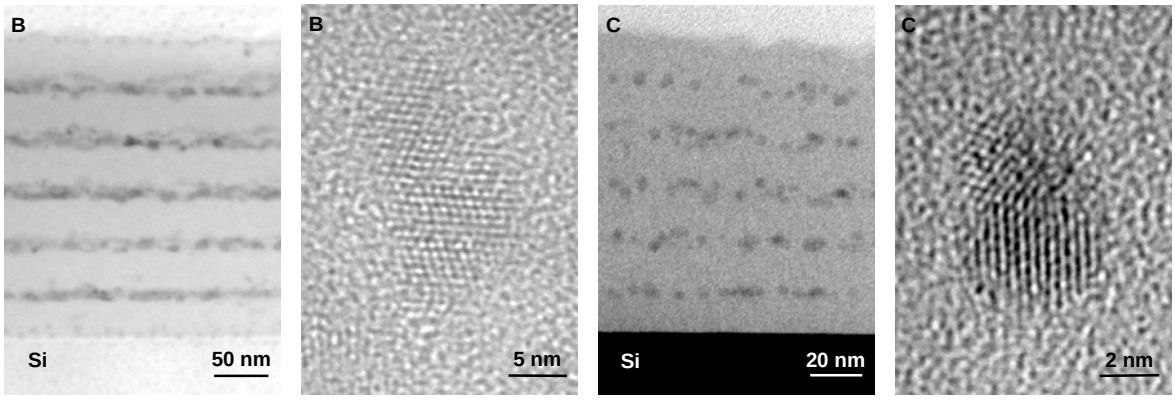


Figure 1. Cross-sectional TEM images of samples B and C annealed by RTA at 900 ºC for 60 s showing the SiGe (dark) / SiO_2 (bright) multilayers. The SiGe nanocrystals are visible in the high resolution images.

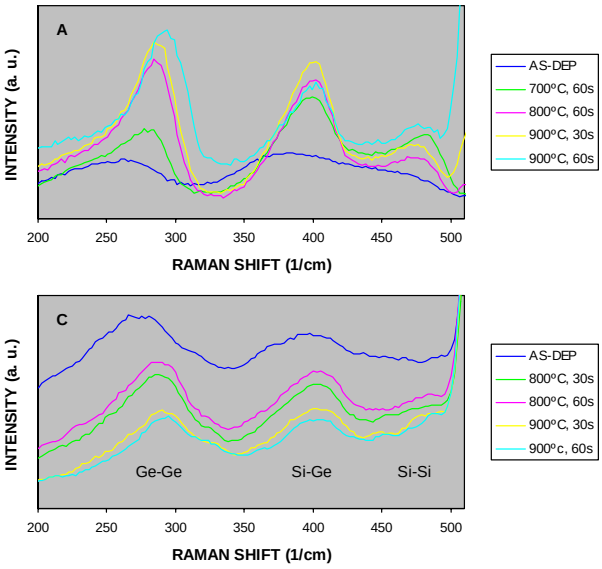


Figure 2. Raman spectra of samples A and C (different nanoparticle size).

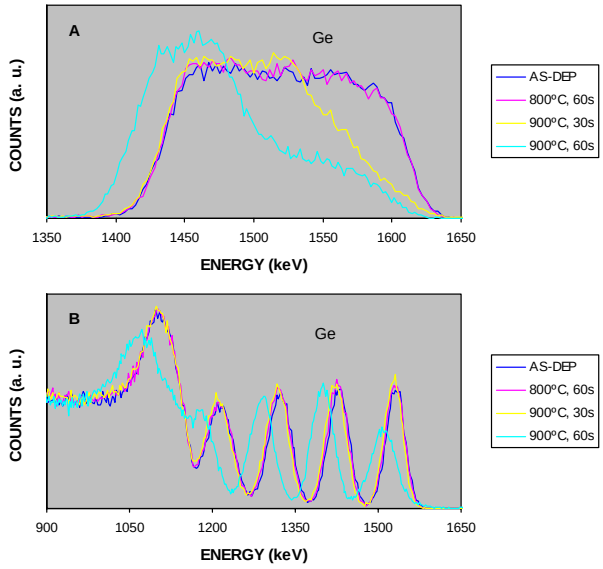


Figure 3. Ge signal of the RBS spectra of samples A and B (different oxide thickness).

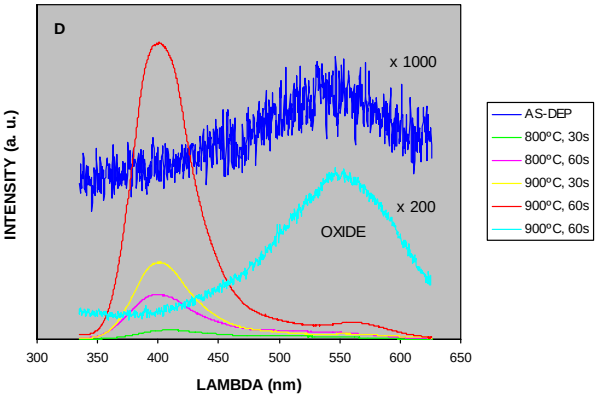


Figure 4. Luminescence spectra of sample D and spectrum of the annealed oxide.

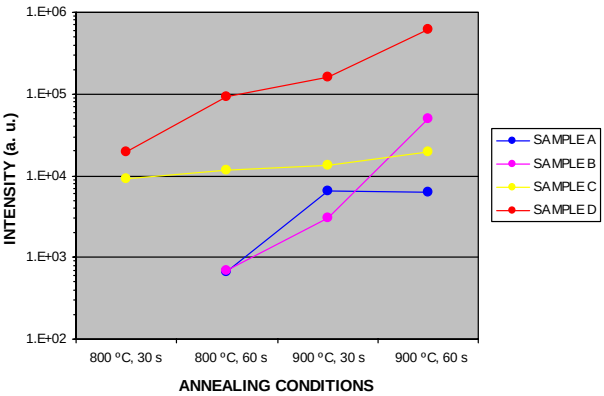


Figure 5. Intensity of the luminescence emission at 400 nm measured in samples A, B, C and D.

SYNTHESIS AND CHARACTERIZATION OF MIXED MONOLAYERS ON HYDROGEN-TERMINATED SILICON SURFACES.

Rogero C[1,2], Hong Q[2], Horrocks B[2], Houlton A[2], Mateo-Marti E[1], Briones C[1], Martín-Gago J A[3]
(1) Centro de Astrobiología (CSIC-INTA), Madrid, Spain
(2) Chemical Nanoscience Laboratories.University of Newcastle upon Tyne, Newcastle, United-Kingdom
(3) Instituto ciencia de materiales de Madrid (CSIC), Madrid, Spain
crogerobc@inta.es

Construction of self-assembled molecular layers on surfaces is one of the most important subjects not only for fundamental science but also for a wide range of applications. The most studied system is the self assembled monolayers of alkanethiols on various metals, especially on gold. It is clear, however, that deserve importance to construct ordered molecular layers on semiconductor surfaces. In this sense, Si is the most important semiconductor substrate for organic layer formation at present, because the wide range of possible applications in conjunction with the advanced silicon technology. There has been increasing interest in the molecular fuctionalization of bulk silicon surfaces through reactions with the hydrogen-terminated layer. Our work extends the range of silicon modification to include mixed monolayers controlling the immobilization process.

We focus our study on the absorption of mixed monolayers at hydrogen-terminated silicon surfaces by thermal reaction of alkenes. We have combined different silicon surfaces, porous Si and Si(111) single crystal, different molecules to mixed, octyl (C_8), undecyl (C_{11}), undecenyl aldehyde ($C_{10}CHO$), and undecanol ($C_{11}OH$), and different experimental techniques in order to fully characterize these mixed monolayers. The combination of Fourier transform infrared and Synchrotron Radiation X-ray photoelectron spectroscopies reveals that the resulting molecular films present a composition that is representative of the composition of the solution.

On the other hand atomic force microscopy gives us information about the structure and resistance for the layers prepared in every stage of the inmobilization process. AFM images show that lateral diffusion and/or desorption-readsorption of the adsorbate is very small. These well-mixed monolayers at silicon surfaces are convenient for the separation of active sites by a simple dilution method, and therefore they possibility the control of the mean spacing between reactive groups on a surface through simple solution chemistry. This procedure shows itself as a useful method for nanoscale surface design [1].

References:

[1].- Qi Hong, Celia Rogero, Sanna Hakkarainen, Bernard A. Connolly, Jeremy H. Lakey, Eva Mateo-Marti, Carlos Briones, Jose Angel Martin-Gago, Benjamin R. Horrocks, and Andrew Houlton. in press Phys.Chem.Chem.Phys.

MOLECULAR SWITCHES AND COORDINATION POLYMERS BASED ON THE CYCLAM FRAMEWORK

Guy ROYAL, Aurélien GASNIER, Christophe BUCHER, Jean-Claude MOUTET, Eric SAINT-AMAN

Laboratoire d'Electrochimie Organique et de Photochimie Redox

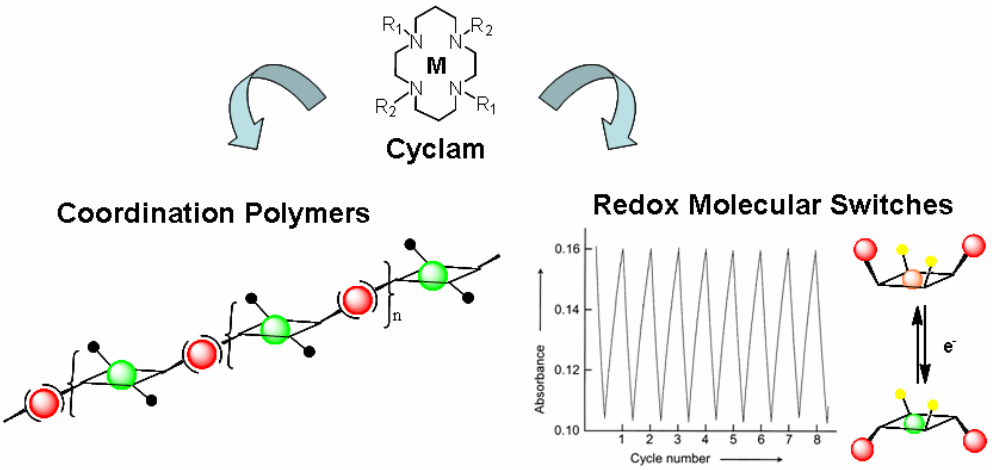
Université Joseph Fourier, Grenoble, France

Contact: guy.royal@ujf-grenoble.fr

The conception and development of molecular architectures based on inorganic and coordination complexes are of great interest due to their potential applications in catalysis, non-linear optics, molecular recognition and separations or information storage. In this context, the cyclam (1,4,8,12-tetraazacyclotetradecane) macrocycle appears to be a wonderful building block for the preparation of such molecular devices. Indeed, when cyclam derivatives coordinate to four equatorial sites of a metal cation, they can adopt five energetically distinct configurations depending on the relative orientation of the substituents on each nitrogen atom to the N4 coordination plane. Using this property, this work shows how the cyclam framework can be functionalized and assembled to generate redox-active receptors, molecular-level machines, molecular wires and coordination polymers.

References:

1. M. Ho, C. A. Mirkin, Nature **438** (2005) 651.
2. 2. C. Bucher, J.-C. Moutet, J. Pécaut, G. Royal, E. Saint-Aman, F. Thomas, Inorg. Chem., **43** (2004) 3777.
3. O. Reynes, C. Bucher, J.-C. Moutet, G. Royal, E. Saint-Aman, M. Ungureanu, J. Electroanal. Chem. **580-2** (2005) 291.
4. C. Bucher, J.-C. Moutet, J. Pécaut, G. Royal, E. Saint-Aman, F. Thomas, S. Torelli, M. Ungureanu, Inorg. Chem., **42** (2003) 2242.



LATERAL PHOTORESPONSE IN GE/SI QUANTUM DOT STRUCTURES

S. V. Kondratenko, S. L. Golovinskiy, A. S. Nikolenko and O. V. Vakulenko
Kyiv National Taras Shevchenko University, Physics Department
2 Acad. Glushkov Ave., 03022, Kyiv, Ukraine
Yu.N. Kozyrev, M.Yu. Rubezhanska, A.I. Vodyanitsky
Institute of Surface Chemistry
17 Generala Naumova Str., Kyiv 03164, Ukraine

E-mail: kozyrev@iop.kiev.ua

We studied spectral dependences of the lateral photoconductivity of Ge/Si heterostructure with strained Ge quantum dots. The photoresponse of strained structures with Ge quantum dots in Si(100) matrix was found in the range of (1.0 - 1.1) eV at T = 290 K, while photocurrent of *c*-Si substrates without Ge layers was greatly attenuated. Such a result was explained by elastic strain arising in the structure, which affects on optical absorption of the silicon material. The studied heterostructures proved to be photosensitive below 120 K in the spectral region from 0.4 to 1.1 eV, where *c*-Si was transparent. The photocurrent in this region is likely to be due to hole transitions from the ground states localized in the quantum dots to the delocalized states of the valence band.

Method for the fabrication of quantum wire arrays

Riccardo Rurali, Jordi Suñé, and Xavier Cartoixà
Departament d'Enginyeria Electrònica, Universitat Autònoma de Barcelona (UAB)
Campus de la UAB, 08193 Bellaterra (Barcelona), Spain
Riccardo.Rurali@uab.es

We propose a novel method for the engineering of one-dimensional nanostructures fabrication with no need of catalyst agents. This method would yield an ensemble of identical nanowires, grown along the same crystallographic orientation and with similar properties concerning the length and the diameter.

We present supporting density-functional calculations performed with the Siesta ab-initio package [1,2], discussing in detail the case of silicon and gallium arsenide. This method, if successfully implemented, would have the additional advantage of lending itself naturally to the fabrication of quantum dots with potential applications as light emitting devices.

References:

[1] P. Ordejón, E. Artacho and J. M. Soler, Phys. Rev. B **53** (1996) R10441.
[2] J. M. Soler, E. Artacho, J. D. Gale, A. García, J. Junquera, P. Ordejón and D. Sánchez-Portal, J. Phys.: Condens. Matter **14** (2002) 2745.

Figures:

FORMATION OF NANOTEMPLATES BY GENETICALLY ENGINEERED TRUNCATED S-LAYER PROTEINS WITH PRESERVED SELF-ASSEMBLY POTENTIAL.

P. Ryzhkov[1], K. Ostermann[1], A. Blüher[2], M. Mertig[2], G. Rödel[1]
[1]Technische Universität Dresden, Institut für Genetik, Zellescher Weg 20b, D-01217 Dresden, Germany
[2]Technische Universität Dresden, Institut für Werkstoffwissenschaft, Helmholtzstraße 7, D-01062 Dresden, Germany
pavel_m_ryzhkov@yahoo.com

Surface layer (S-layer) proteins are the outermost cell wall components, found in many types of bacteria and archaea. S-layers mostly consist of a singular type of protein, rarely of two or more different proteins [1]. These proteins form periodic ordered structures with oblique, square or hexagonal type symmetry. It is currently believed, that such structures are formed by non-covalent interactions in an entropy-driven self-assembly process [2]. The unit of the S-layer lattice is composed of 1 to 4 different proteins (p1 – p4 lattice types), thereby forming characteristic pores of 2 to 8 nm. The main factors that disrupt the formation of S-layers are changes in the pH value, changes of cultivation temperature, oxygen limitation, mechanical stress and application of different chemicals, interfering with hydrogen bonds formation (e.g. guanidine hydrochloride, urea). For a variety of S-layer proteins it was shown that the isolated protein monomers maintain the ability to form periodic self-assembly structures and recrystallize in solution, on lipid films (e.g. on the surface of liposomes [3]), or on liquid/air and liquid/solid phase interfaces. S-layer periodic structures are of high interest for different applications in nanotechnology. For example, they have been used as nanotemplates for the formation of metal clusters, for the immobilization of different reagents and as molecular sieves.

We will report on our investigations of the self-assembly potential of the *Sporosarcina* (*S.*) *ureae* S-layer protein SslA and genetically engineered derivatives. The native SslA S-layer exhibits a p4 square type symmetry and a lattice constant of 13.2 nm. Reassembled S-layer sheets have been shown to bind metal ions and to facilitate the formation of metal clusters [4]. Until recently, biotechnological work with the *S. ureae* S-layer protein was impeded by the fact that its amino acid and the corresponding DNA coding sequences were not known. We isolated and determined the DNA sequence of the *sslA* gene encoding the S-layer protein of *S. ureae* [5]. A Cys residue at the extreme carboxyl-terminal end – an unusaual feature for S-layer proteins – may explain the affinity of SslA lattices for heavy metal ions.

We constructed several truncated protein versions, expressed them heterologously in *E. coli* and analyzed their ability to self-assemble into supramolecular structures. Based on the results of multiple sequence alignments with the S-layer proteins SbsC from *Bacillus stearothermophilus* and SbpA from *Bacillus sphaericus*, for which an extensive truncation analysis was performed [6,7], it was estimated that the N- and C-terminal regions of SslA might be deleted without affecting its self-assembly properties. We constructed (i) an N-terminally truncated SslA with deletion of the first 341 amino acids, (ii) a C-terminally truncated SslA, which lacks the last 172 amino acids, and (iii) a SslA derivative with the above mentioned truncations at the both C- and N-terminal ends (see fig. 1). The respective SslA constructs were overexpressed in *E. coli*, monomerized with 5 M GuHCl after isolation, and dialysed against dH_2O for 24 to 48 hours to allow self-assembly. The native SslA was prepared from *S. ureae* cells and treated in the same way. Self-assembly products were precipitated onto the substrate surface and analysed by means of scanning (SEM) and transmission electron microscopy (TEM). Microscopy data revealed that all truncated protein versions formed nanosheets with typical dimensions in the range of 0.1-10 µm, that are similar to those formed by the native SslA protein (fig. 2). Based on the assembly studies with the native SslA protein on different surfaces (Si wafers, silanized Si wafers, glass, APTES-glass) self-assembly structures have a higher affinity to the surfaces with lower

hydrophobicity. This finding can be explained by a model, according to which the protein multilayer structures are first formed in solution at high protein concentrations, and thereafter attach with their exposed hydrophilic parts to the substrate surface.

In summary, our work shows that native as well as recombinant SslA monomers have the ability to form self-assembly structures upon crystallization in solution and on the substrate surfaces. Self-assembly into nanosheets of 0.1 to 10 µm is mediated by the central protein part and not impaired by C- or N-terminal deletions.

References:

[1] M. Sara and U. B. Sleytr, J. Bacteriol., **182** (2000) 859-868
[2] T. Candela, T. Mignot, X. Hagnerelle, M. Haustant and A. Fouet, Microbiology, **151** (2005) 1485-1490
[3] U. B. Sleytr, H. Bayley, M. Sara, A. Breitwieser, S. Küpcü, C. Mader, S. Weigert, F. M. Unger, P. Messner, B. Jahn-Schmid, B. Schuster, D. Pum, K. Douglas, N. A. Clark, J. T. Moore, T. A. Winningham, S. Levy, I. Frithsen, J. Pankovc, P. Beale, H. P. Gillis, D. A. Choutov, K. P. Martin, FEMS Microbiol. Rev., **20** (1997) 151-175
[4] M. Mertig, R. Kirsch, W. Pompe and H. Engelhardt, Eur. Phys. J. D, **9** (1999) 45-48
[5] P. M. Ryzhkov, K. Ostermann and G. Rödel, NCBI Database, acc. number AM085153
[6] N. Ilk, C. Völlenkle, E. M. Egelseer, A. Breitwieser, U. B. Sleytr and M. Sara, Appl. Environ. Microbiol., **68** (2002) 3251-3260
[7] M. Jarosch, E. M. Egelseer, C. Huber, D. Moll, D. Mattanovich, U. B. Sleytr and M. Sara, Microbiology, **147** (2001) 1353-1363

Figures:

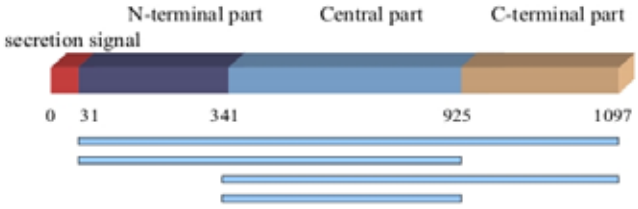


Fig.1 Schematic representation of SslA protein sequence: processed as well as truncated versions are indicated below

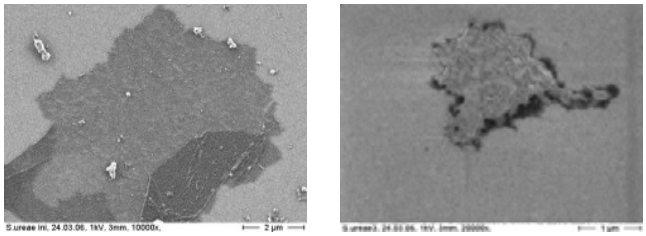


Fig.2 SEM images of self-assembly nanosheets: structures formed by the native protein (left) and the C-terminally truncated version (right) are shown as examples

ELECTROCHEMICAL STUDY OF FERROCENE FUNCTIONALIZED COLLOIDS; AN INSIGHT INTO SURFACE FRACTAL DIMENSION OF TiO_2 AND SnO_2 COLLOIDS

Sadki S[a] Miomandre F[b], Audebert, P[b]

Molecular Electronics Lab, SPrAM/UMR 5819 CEA-CNRS-UJF, 17 rue des Martyrs, 38054 Grenoble Cedex 9 (France)[a]

PPSM, Ecole Normale Supérieure de Cachan, 61 avenue du Président Wilson 94230 Cachan, cedex (France)

Said.sadki@cea.fr

There has been a large amount of research devoted to the coating of colloids with organic substrates, in order to obtain nanoparticles displaying a specific property of the substrate [1], such as fluorescence [2], conductivity (in the case of a conducting polymer) [3], or molecular recognition [4]. Recently, several groups have tried to bind ferrocenes to either nanosize colloids, or dendrimers, either to recognise specific substrates such as phosphate anions [5], or in order to perform theoretical analysis of electron transfer within the dendrimer core [6]. As the phosphonic acid group proved to be very efficient to anchor functionalized organic molecules on metal oxides surfaces [7] (such as for the preparation of highly ordered monolayers on ZrO_2 or TiO_2, or the study of supported bipyridine or terpyridine–Ru complexes on TiO_2), we used this function to covalently bind -conjugated ferrocenes to SnO_2 and TiO_2 particles (Figure 1). The grafting of phosphonic acid on metal oxides is known to be irreversible and very stable over a wide range of pH. Therefore it is possible to study the electrochemistry of such colloids, either dispersed in a suspension, or in the solid phase, which is obtained by evaporation of a drop of the colloidal suspension onto an electrode. The electrochemical response of the colloidal suspension allows us to determine the hydrodynamical diameter of the colloids, which correlates well with the diameter of the dried powder. However, the electrochemical response of the modified electrode that can be obtained from the colloidal suspension is still more informative, since the response strongly depends on the repartition of the electroactive sites at the surface of each colloid grain. When the characteristic transport length of the electrons is much larger than the grain dimension, a classical pseudo-diffusion behaviour is observed. However, when the transport length becomes in the range or smaller than the colloid dimension, an abnormal behaviour, typical of a fractal site repartition is obtained, and the analysis of the curves allows one to determine with a reasonable precision the fractal dimension of the grain surface [8].

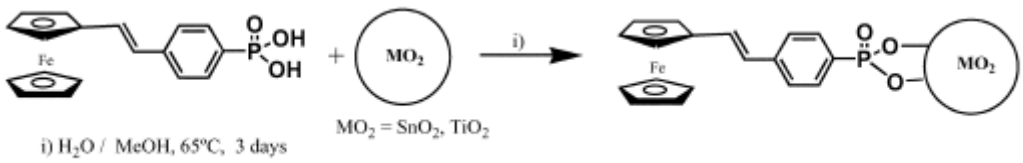


Fig. 1 functionnalisation of the colloids

We will shown in this presentation that ferrocene anchoring to metal oxide colloids via phosphate groups lead to very stable functionalized nanoparticles, which in turn allow the preparation of very stable modified electrodes. In addition, the study of the charge transfer in such electrodes was not found to follow a classical behaviour, which is indicative of the

fractal character of the colloid surface. More detailed analysis of the electrochemical data allow an estimation of the fractal dimension of these surfaces [8].

References:

1) A. N. Shipway, E. Katz and I. Willner, *ChemPhysChem*, **2000**,1, 18.
2) R.Meallet-Renault, P. Denjean and R. B. Pansu, *Sens. Actuators,B.*, **1999**, 59, 108.
3) (a) S. Maeda and S. P. Armes, *J. Colloid Interface Sci*., **1993**, 159, 257;
(b) S. Maeda and S. P. Armes, *J. Mater. Chem*., **1994**, 4, 935.
4) Y. Xiao, H.-X. Ju and H.-Y. Chen, *Anal. Chim. Acta*, **1999**, 391,73.
5) C.-O. Turrin, J. Chiffre, D. de Montauzon, J. C. Daran,A.-M. Caminade, E. Manoury, G. Balavoine and Jean-Pierre Majoral, *Macromolecules*, **2000**, 33, 7328.
6) C. Amatore, Y. Bouret, E. Maisonhaute, J. I. Goldsmith and H. D. Abruna, *ChemPhysChem*, **2001**, 2, 130.
7 (a) J. Sotomayor, G. Will and D. Fitzmaurice, *J. Mater.Chem*, **2000**, 10, 385.
8) P. Audebert, S.Sadki, F. Miomandre, F. Lanneau, R. Frantz, J.O. Duran, *J. Mat. Chem*, **2002**, 12,1-5.

Nanoscale Surface Analysis using Scanning Tunneling Microscope Coupled with Highly Brilliant Hard X-ray Micro-Beam

A.Saito[1,2,3], K.Takahashi[1], Y.Takagi[2], K.Kitamoto[2,4], K.Hanai[4], Y. Tanaka[2], D.Miwa[2], M.Yabashi[2], S.Shin[2], T.Ishikawa[2], Y.Kuwahara[1,2,3], M.Aono[3,5]

[1]Dept. of Material and Life Science, Osaka University, Suita, Osaka 565-0871, Japan.
[2]RIKEN SPring-8 Center, RIKEN Harima Institute, Sayo-gun, Hyogo 679-5148, Japan.
[3]Nanoscale Quantum Conductor Array Project, ICORP, JST, Saitama 332-0012, Japan.
[4]Dept. of Mathematical Sciences, Osaka Prefecture University, Osaka 599-8531,Japan.
[5]Nanosystem Functionality Center, National Institute for Materials Science, Tsukuba 305-0003, Japan.

Electric address: saito@prec.eng.osaka-u.ac.jp

An attempt to combine STM with X-rays appears appealing because that includes various possibilities of original and important applications. Inner-shell excitation of a specific level under the STM observation leads to analyse the elements or control the local reaction with the spatial resolution of STM. However, the number of researches to combine STM with X-rays is quite limited. To surmount a small efficiency of core-excitation by X-rays, we used the synchrotron radiation (SR) of the highest brilliance at the SPring-8 (Fig. 1). The incident beam was still focused two-dimensionally to increase the photon density. To solve difficulties derived from the high brilliance (thermal and electrical noise, damage around the STM scanner, instability of the system such as thermal drift, etc.), we developed a special STM system dedicated to the *in situ* observation under the irradiation of SR [1].

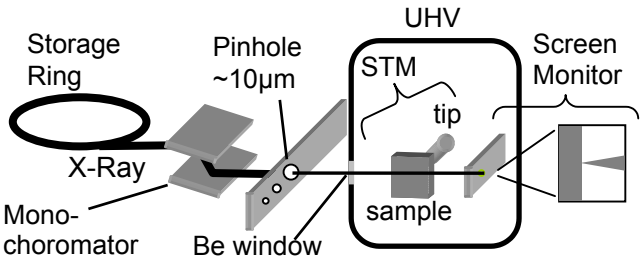


Fig.1 Schematic view of experimental setup.

Apparatus & Method The point is how to adjust the incident X-rays as small as possible at the observation point of STM in order to avoid the excessive irradiation. The *in situ* STM measurements were enabled by developing an accurate alignment system: the small X-ray beam of φ 10 μm was aligned at the STM observation point in ultra high vacuum (UHV) with accuracy of 1 μm. A system to monitor the STM tip and sample in the X-rays was specially developed to realize a prompt alignment. A detection system of the tunnelling signal was also developed to obtain high signal to noise (S/N) ratio and record a small signal [2].

In situ STM measurements with X-rays

Despite the noisy condition and radiation load around the tip, STM images were successfully obtained with atomic resolution. After thermal noise was effectively removed, the tip-current modulation was successfully obtained on Ge nanoislands on a clean Si (111) surface, by changing the incident photon energy across the Ge absorption edge. Figure 2 shows the topographic (left) and beam-induced current images (right), which were obtained simultaneously, at higher (11.114 KeV) and lower (11.090 KeV) energies than the Ge absorption edge. The tip current image at higher photon energy shows

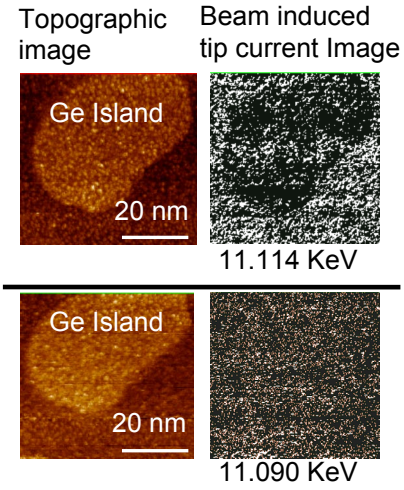


Fig.2 Energy dependence of the scanned image of the tip current (50 x 50 nm, -2 V, 0.5 nA for all).

the Ge island darker than the surrounding area. The emitted electrons cannot explain the decrease in current gap on the Ge island. This is because the emitted electrons must increase the current on the Ge island, in which the Ge atoms might be richer than in the surrounding area. The decrease of the tip current on the Ge island was not observed at lower photon energy (Fig.2), which also indicates that the dark Ge island is not an effect of the modulated tunneling gap that is based on the tip motion. The above results indicate that the difference between on and out of the Ge island was detected across the absorption edge with spatial resolution of STM.

Next step A problem remains to be solved on stability and accuracy in the experimental system. The difference of the tip current between on and out of the Ge island (Fig.2) was not stable and the value varied easily. The instability is undesirable for pursuit a principle of the elemental analysis. By improving the above experimental scheme (including the alignment system and stability of an active dumper) and trying various STM conditions, the S/N ratio was found to be a clue to obtain the stability and accuracy of the above results. Figure 3 shows energy spectra of the beam-indued tip current obtained from a tip fixed at the center of the Ge island under tunneling (a) and tip-retracted (b) conditions. The spectra show two kinds of noise: One is the current at lower energy than the absorption edge, which is normally originated from Si atoms (two broken arrows in Fig.3). Another is originated from the Ge atoms, but it is collected from wide area and damages the spatial resolution (dotted arrow in Fig.3 (b)). The signal containing local information is the component under the tunnelling condition (solid arrow), although it contains still a noise component such as dotted arrow. To obtain the local information, it is essential to increase the true signal (solid arrow) and reduce the noise (dotted and broken arrows) .To estimate the origin of the noise more precisely, a new tip composed of coaxial structure was developed (Fig.4(c)), of which the side is coated with insulator to shut the electrons coming from wide area. The new tip reduced the noise effectively, giving a hope to improve the accuracy of the elemental analysis. This SR-based STM study is in a new stage to obtain the stable and accurate results, which will lead to elucidate a principle and mechanism of the nanoscale chemical analysis based on the interaction of surface atoms and the hard X-rays. The results will serve to local reaction control with STM resolution, too.

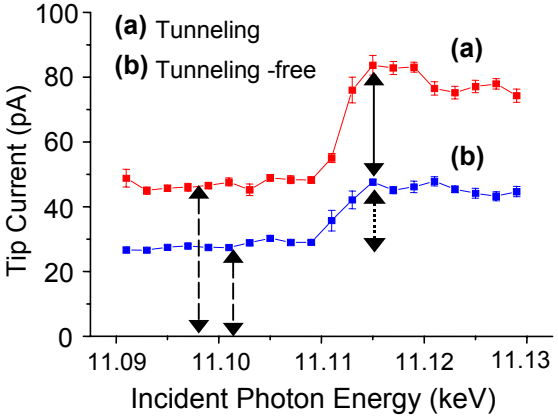


Fig.3 Energy spectra of tip current obtained on the Ge island under the tunneling condition -2 V, 0.3 nA (a), and tip-retracted condition (b).

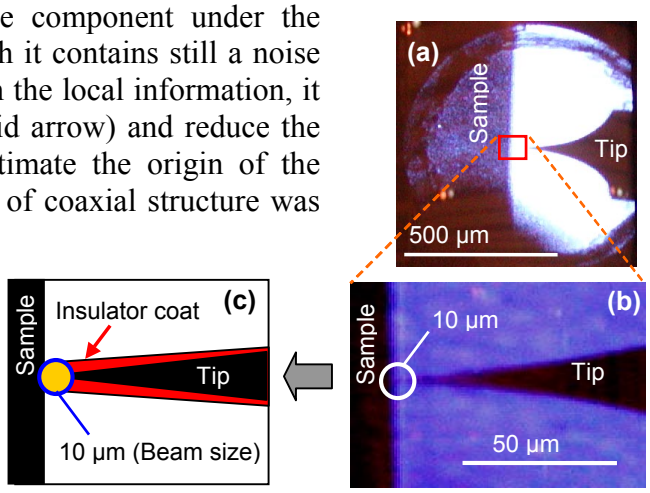


Fig. 4 Images of the tip and sample in the X-ray beam: (a) with X-rays of φ 800 μm (x 300) for coarse alignment, (b) with higher magnification, (c) Schematic image of the low-noise experimental condition with an insulator-coat tip and X-rays of φ 10 μm

References:

[1] A.Saito, S.Shin, T.Ishikawa, Y.Kuwahara, M.Aono *et al.*: J. Shynchrotron Rad. **13** (2006) 216-220.

[2] A.Saito, J.Maruyama, K.Manabe, K.Kitamoto, K.Tkahashi, M.Ishii, Y.Takagi, S.Shin, T.Ishikawa, Y.Kuwahara, M.Aono *et al.*: Jpn.J.Appl.Phys. **45**, **3B** (2006) 1913-1916.

NANOSTRUCTURED SURFACE AS EWOD COUNTER ELECTRODE FOR MATRIX-FREE MASS SPECTROMETRY ANALYSIS

B. Salhi*, **, Y. Coffinier*,**, N. Verplanck*, M. Wisztorski***, G. Piret *,**, V. Thomy*, I. Fournier***, M. Salzet***, JC. Camart*, and R. Boukherroub*,**
* Institut d'Electronique de Microélectronique et de Nanotechnologie, Vill. d'Ascq, France
** Institut de Recherche Interdisciplinaire, Villeneuve d'Ascq, France
*** Laboratoire de Neuroimmunologie des Annélides, Villeneuve d'ascq, France

keywords: EWOD, Superhydrophobic surfaces, Nanowires, DIOS-MS.

Current digital microfluidic systems are often based on the electrowetting on dielectric (EWOD), which allows fundamental droplet handling operations [1]. To date, the best EWOD results obtained for MALDI analysis concern a set up consisting of two parallel plates, a base and a cover preventing from evaporation, between which microdroplets of biological liquid are sandwiched [2]. Classically the base is made of an electrode array coated with a bilayer composed of a dielectric and an amorphous fluoropolymer plane layer. The cover, working as a counter electrode, is made of a conductive substrate (ie silicon) coated with the same amorphous fluoropolymer layer.

This paper reports on the preparation of a superhydrophobic nanostructured surface consisting of chemically modified silicon nanowires for the realisation of EWOD counter electrode and matrix-free mass spectrometry analysis. The main advantages associated with such a substrate are: (*i*) flow resistance of droplets is dramatically reduced, (*ii*) simple realisation of hydrophilic and functionalized pads in the superhydrophobic surface allowing analytes trapping and enhancement of the liquid / surface interaction, (*iii*) subsequent analysis by matrix-free desorption/ionization MS-DIOS on these pads.

The bottom plates were fabricated using standard microfabrication techniques. The bottom glass plate consists of an array of independently addressable control electrodes (1 mm²) patterned in a 10 nm thin layer of nickel, which is further coated with a SU-8 layer (2µm) as a dielectric. A hydrophobic layer of Teflon AF 1600 (20 nm) is then deposited (Fig.1, contact angle = 115°). Silicon nanowires are synthesized on silicon substrate (counter electrode) using the well-known Vapor-Liquid-Solid (VLS) technique (Fig.2-3) [3]. The formation of a superhydrophobic layer on the silicon nanowires surface was achieved by chemical derivatization with octadecyltrichlorosilane (OTS) (Fig 4, contact angle = 149°) while the DIOS pads are prepared by a simple exposure of the octadecyl-terminated silicon nanowires surface to UV-ozone through a physical mask containing 20*50 µm apertures. Thus, we can control locally the wetting properties of a macroscopic hydrophobic surface.

The gap between two plates is 300µm so that a 1µL droplet of biological liquid (Substance P amide, 5.10^{-5}Mol/L) can be moved under 68 V compared to 100 V required to displace the same droplet with a classical cover (silicon wafer coated with Teflon).

Finally, mass spectrometry analysis of the targets in the hydrophilic DIOS pads is carried out using MALDI TOF-TOF without addition of an organic matrix. We have found that silicon nanowires can successfully be used as a substrate for MS analysis without any organic matrix (Fig 5) [3].

[1] S.K. Cho, H. Moon and C.J. Kim, *J. Microelectromech. Syst*., 2003, 12, pp. 70-80
[2] A.R.Wheeler, H. Moon, C.A. Bird, R.R. O. Loo, C.J. Kim, J.A. Loo, R. L. Garrell, *Anal. Chem.* 2005, 77, pp. 534-540
[3] R. Boukherroub et al. (to be published)

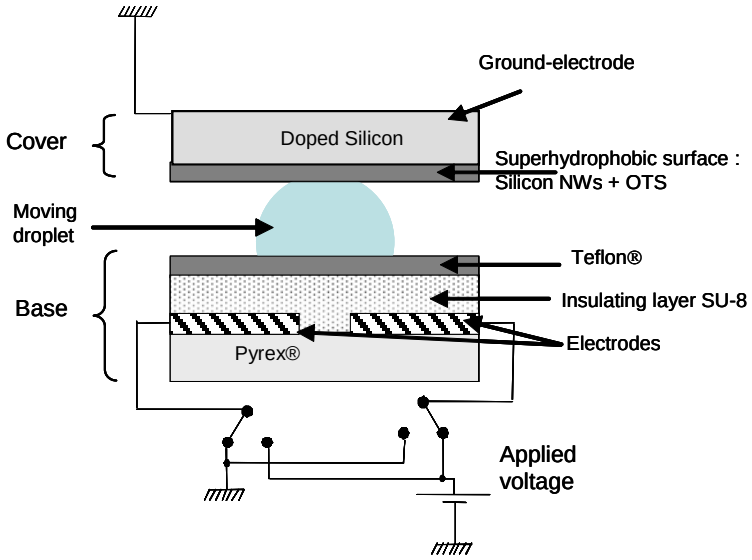


Figure 1: Setup of the EWOD platform

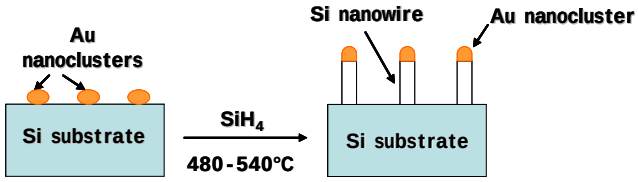


Figure 2 : Silion nanowires growth using VLS technique

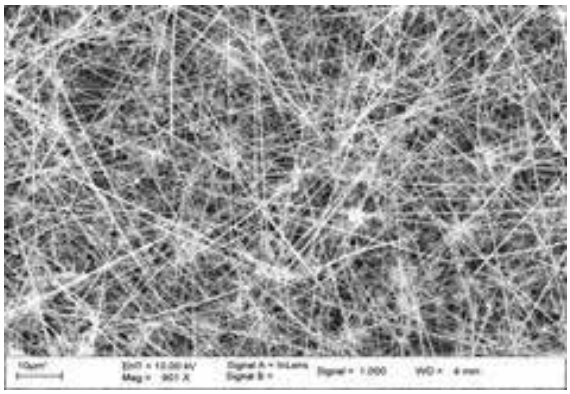


Figure 3: SEM view of silicon nanowires

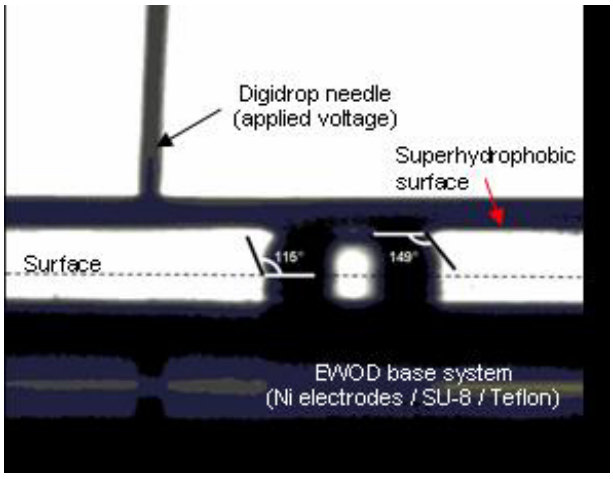


Figure 4: Droplet sandwiched between two plates system (base coated with Teflon, cover with NW / OTS)

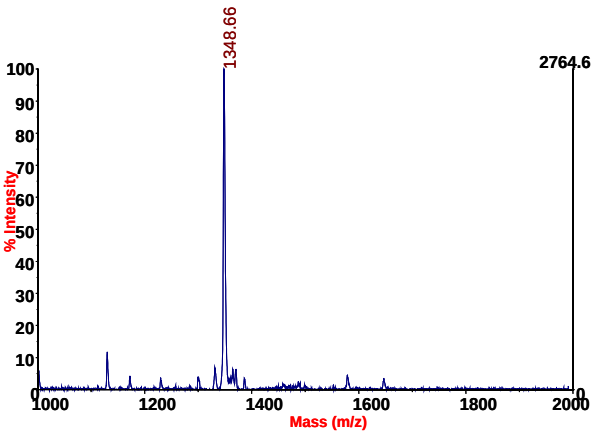


Figure 5: Mass spectrum of Substance P amide on VLS hydrophilic pads Mass

FABRICATION OF 3D SILICON NANOSTRUCTURES USING ION IMPLANTATION AND WET CHEMICAL ETCHING

Billel Salhi [1,2], Sebastien Tétin[1, 2], David Troadec[2], Gilles Patriarche[3] and Rabah Boukherroub[1,2]

[1] *Institut de Recherche Interdisciplinaire (IRI)*

[2] *Institut d'Electronique de Microélectronique et de Nanotechnologie (IEMN), UMR CNRS-8520*

Cité Scientifique, Avenue Poincaré - BP. 60069, 59652 Villeneuve d'Ascq, France.

[3] *Laboratoire de Photonique et de Nanostructures, route de Nozay, 91460 Marcoussis, France*

Control of the synthesis and manipulation of nano-objects, and their electronic and optical properties are key parameters for the development of functional devices. Several techniques are available to create nanostructures in a controlled fashion. Over the past ten years, the focused ion beam (FIB) technique has taken more and more place in the design and manipulation of nano-objects [1]. Indeed the FIB milling mode permits to remove layers from substrate allowing the imaging of a sample cross section with a high accuracy. FIB offers also the possibility for ion implantation and deposition of metal nanostructures [1]. Furthermore, the FIB enables to repair wires on a micrometer scale or making connections for electrical measurements (for example: carbon nanotubes characterization) [2].

Recently, a combination of FIB implantation and chemical wet etching was investigated for the preparation of micrometer scale nano pyramids array (NPA) approaching the 100 nm resolution [3]. The wet etchants used are strong bases (pH>12) such as KOH, TMAH or hydrazine (N_2H_4) known for their crystalline plan dependent etching.

In this paper, we report our experimental results on the synthesis of silicon 2D and 3D nanostructures of controlled shapes and sizes using focused ion beam implantation of Ga^+ ions into crystalline silicon followed by wet etching in TMAH. Ion implantation into silicon renders the implanted regions amorphous and relatively immune to chemical etchants. The difference in the dissolution rates of the implanted *vs* non implanted regions and silicon dissolution anisotropy in TMAH allows producing Si nanosctructures of various shapes and sizes in a controlled way (**Figure 1**).

FEI strata DB 235 dual (focused ion and electron) beam (FIB/SEM) system (acceleration voltage of 30 keV) was used in this study. The implanted doses were controlled by varying the current from 1pA to 300pA and exposure time from some seconds to some minutes. After ion implantation, the surface was exposed to 25% aqueous solution of TMAH at 80°C for few seconds.

The resulting nanostructures were characterized using SEM and TEM microscopies and energy dispersive X-ray (EDX) analysis. The obtained nanostructures are amorphous and EDX results showed the presence of ~ 5% of Ga^+ ions in the silicon nanostructures.

Crystallization of the nanostructures by thermal annealing is currently under investigation in our laboratory.

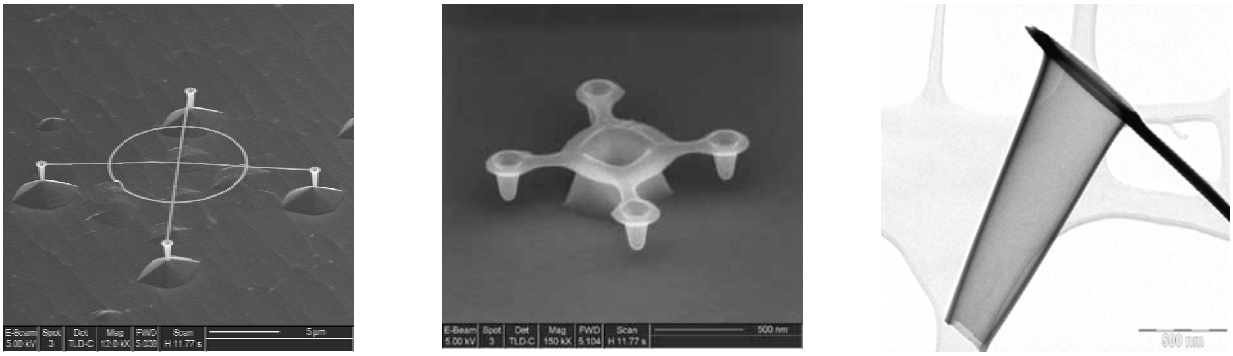


Figure 1: SEM images of 3D silicon nanostructures produced using focused ion beam and wet chemical etching in TMAH.

References

[1] Recent Developments in nanofabrication using focused ion beam.
A. A. Tseng, *Small 1 (2005) 924-939*
[2] Fabrication technique for carbon nanotube single-electron transistors using focused ion beam.
Y. Kurokawa, Y. Ohno, S. Kishimoto, T. Okazaki, S. Shinohara, T. Mizutani, *Jpn. J. Applied Phys. Vol. 43. (2004) 5669-5670.*
[3] Simple nanostructuring on silicon surface by means of focused beam patterning and wet etching.
M. Koh, S. Sawara, T. Shinada, T. Goto, Y. Ando, I. Ohdomari, *Appl. Surf. Sci. 162-163 (2000) 599-603.*

OPTICAL LOSSES CONTROL BY FINELY TUNING THE DISTANCE BETWEEN A BRAGG MIRROR AND A 2D PC.

Antoine SALOMON[1,2], *Emmanuel PICARD*[1], *Vincent CALVO*[1], *Emmanuel HADJIi*[1] .
1-DRFMC/SINAPS, CEA-GRENOBLE, 17 RUE DES MARTYRS, F 38054 GRENOBLE CEDEX 9.
2-LETI, CEA-GRENOBLE, 17 RUE DES MARTYRS, F 38054 GRENOBLE CEDEX 9.
antoine.salomon@cea.fr

We report on how the coupling of a Bragg reflector and a 2 dimensional Photonic Crystal (2D PC), by finely tuning the gap between them, can modify and enhance, the properties of the light emitted by SOI. Measurements pointed out a modulation of the extracted intensity as well as one of the quality factor (Q).

It will be very convenient to have, for future optoelectronic circuits, a light source made of crystalline silicon because of its wide use in the micro-electronic industry. But since crystalline silicon has an indirect gap it is a very poor light emitter and few report on emission from it[1]. We have studied how we can enhance the light emission properties of SOI by combining a Bragg mirror and 2D PC etched in the Si layer of a SOI wafer. The PC consists of a triangular lattice of Si rods and presents a slow group velocity mode at silicons' gap. The Bragg is made of quarter wave plate at 1.1µm. We have designed a piezo-electric set-up with which we were able to tune the coupling distance separating the Bragg and the PC at the scale of the wavelength. When we scanned this distance the recorded intensity showed periodic oscillations as depicted in figure 1. The period of these oscillations are half of the wavelength which is in agreement with 2D FDTD calculations. Results also pointed out a modulation of the quality factor of the structure as the mirror was taken away from the PCs' surface. Figure 2 shows these oscillations. The period of the Qs' oscillations is, just like for the intensity, half of a wavelength and is in accordance with 2D FDTD calculations. These two variations, with respect to the coupling distance, present the same period but are in phase opposition. When the intensity extracted is important the Q is weak as when the extracted intensity is low the Q is strong. This can be understood in terms of Fano[2] resonances as the optical mode interferes with the pseudo continuum of states of the space above the PC thus generating such resonances. As we move away the mirror we modify the pseudo continuum of states. As a consequence we change the interferences with the PCs' mode and Fano resonances. When the optical mode of the PC can couple to a Fano resonance (when interferences are constructive), losses are high, the Q is then weak and the extracted intensity important. In the other case interferences are destructive, the losses are weak, the Q is important and the extracted intensity low.

In conclusion we have designed and made a piezo-electric set-up enabling us to scan the gap between a Bragg mirror and a 2D SOI made PC at the scale of the wavelength. Results proved that by finely tuning this gap we could either enhance or deteriorate the intensity extracted from the PC as well as the quality factor. These results are in agreement with results studies on the coupling between Braggs and 2D PC[3,4].

References:

[1] B. Cluzel et al, App. Phys. Lett, **88,** accepted under publication [11] B. Cluzel et al, App. Phys. Lett, **88,** accepted under publication
[2] U. Fano, Phys. Rew.**124**, 1866(1961)
[3] X. Li, P. Boucaud,X. Checoury, M. El Kurdi, S. David, S. Sauvage, N. Yam, F. Fossard, D. Bouchier J. M Fédéli, A. Salomon, V. Calvo, E. Hadji, *App. Phys. Lett*.**88**, 01122(2003)
[4] B. Ben Bakir,a_ Ch. Seassal, X. Letartre, P. Viktorovitch, M, Zussy, ,. Di Cioccio, and J. M. Fedeli, *App. Phys Lett*.**88**, 081113(2003).

Figures:

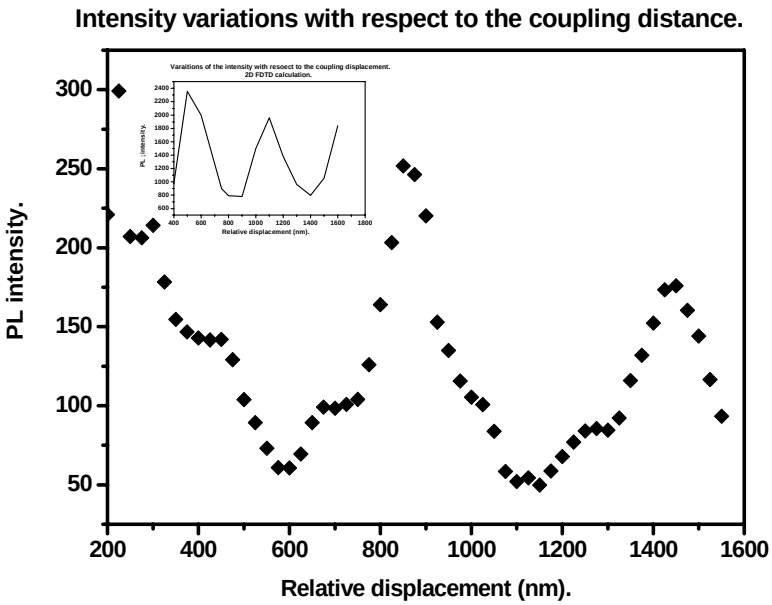


Figure 1 :Extracted intensity variations with respect to the air gap.

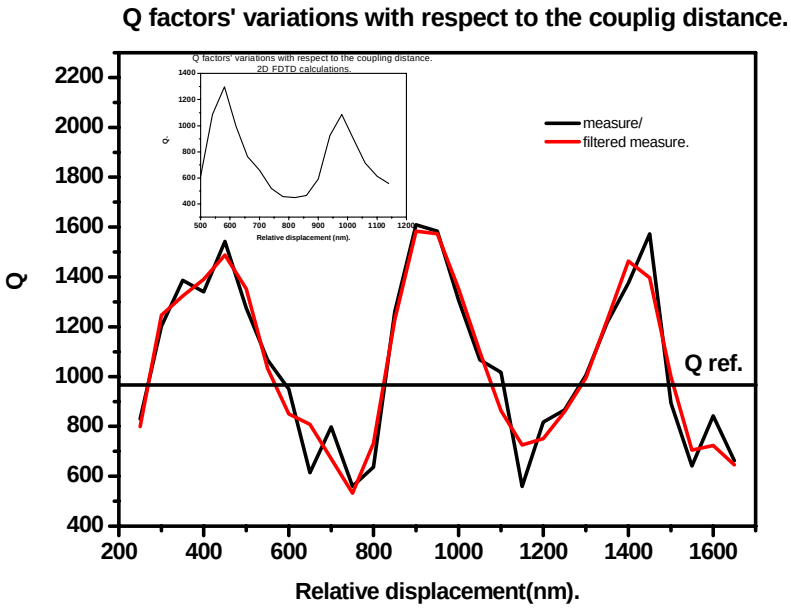


Figure 2 :Quality factor oscillations with respect to the air gap.

Poster

DNA-ASSISTED PURIFICATION AND SELF-ASSEMBLY OF SINGLE-WALLED CARBON NANOTUBES ON GOLD

Germarie Sánchez-Pomales, Lenibel Santiago-Rodríguez and Carlos R. Cabrera
Department of Chemistry and Center for Nanoscale Materials,
University of Puerto Rico-Río Piedras, PO Box 23346, San Juan, Puerto Rico 00931-3346
germarie1@prtc.net

The properties of nanotubes, as well as their applications have been the subject of many studies since the discovery of carbon nanotubes (CNTs) by S. Iijima in 1991.[1] CNTs possess outstanding structural, mechanical, and electronic properties. Nevertheless, to achieve the full potential of the CNTs, many problems still need to be solved, including the development of an easy and effective purification procedure, the design of functionalization chemistries that result in increased solubility of the CNTs in aqueous solvents without altering their properties, and the development of an easy methodology for the attachment of aligned CNTs on solid substrates that allows their integration with other circuit elements for electronic and sensing applications. DNA offers a solution to all of the previous challenges.

Recently, Zheng and coworkers reported the dispersion of single-walled carbon nanotubes (SWNTs) in aqueous solvents by the non-covalent functionalization of the tubes with DNA molecules.[2] On the other hand, the self-assembling technique has been previously used by our group to attach aligned DNA-CNT complexes on a solid substrate.[3,4] During our functionalization experiments, we found out that the methodology used leads to the DNA-assisted purification of SWNTs. The results to be presented indicate that the used method is a straightforward, easy and time-effective route for the purification of SWNTs at room temperature. The purified SWNTs will be characterized and subsequently attached to gold substrates via the formation of self-assembled monolayers (SAMs).

Briefly, aqueous solutions of DNA-CNT hybrids were prepared by a procedure similar to the one used by Zheng and coworkers [2], where as-received SWNTs were mixed with a disulfide modified-single-stranded-DNA (RSSDNA) solution and sonicated for 1 hour in an ice-bath. The mixture was diluted to prepare dispersions with different DNA concentrations and these were centrifuged to remove insoluble material (i.e amorphous carbon, catalyst particles, etc.).

Results for the characterization of the DNA-CNT hybrids are published elsewhere.[3] The individually dispersed DNA-CNT complexes had lengths smaller than 100 nm, as determined by atomic force microscopy (AFM) and transmission electron microscopy (TEM) images. The TEM results also show ropes of DNA-CNT of larger length. Additionally, the DNA-CNT complexes were analyzed with Raman, energy dispersive (EDS) and energy loss spectroscopy (EELS), and compared to as-received CNTs. Raman spectroscopy results show a decrease in the band around 1300 cm^{-1}(D-band), which corresponds to disordered carbon, for DNA-CNT in comparison to as-received CNTs. EDS results for the DNA-CNT complexes showed the absence of the bands corresponding to Fe (catalyst particles), which were present in the as-received CNTs. Additionally, the peak due to the π^* states for as-received CNT is smaller in size and is located at higher energy compared to DNA-CNT, which is consistent with a higher content of amorphous carbon, since as the sp^3 content increases, the π^* decreases in size and moves to higher energy. TEM and scanning electron microscopy (SEM) results also demonstrate a decrease in the impurities after functionalization with DNA. These results suggest that the wrapping of the CNTs by DNA might serve as a crude purification procedure.

In addition, the DNA-CNT complexes were used to form SAMs on gold. The AFM results show SAMs containing aggregates of DNA-CNT hybrids with surface coverage up to 10 % were obtained. The DNA-CNT complexes have a small length distribution (from 40 to 100

nm) and were attached to the surface at an ~20° angle from the surface normal. An overview of the results is presented in Figure 1. These results suggest that the DNA-CNT complexes might be promising materials for the design of novel nanodevices and sensors.

References:

[1] Iijima, S.; *Nature*, **354** (1991) 56.
[2] Zheng, M.; Jagota, A.; Semke, E. D.; Diner, B. A.; Mclean, R. S.; Lustig, S. R.; Richardson, R. E.; Tassi, N. G.; *Nat. Mater.*, **2** (2003) 338.
[3] Sánchez-Pomales, G.; Morales-Negrón, Y.; Cabrera, C. R.; *Rev. Adv. Mater. Sci.*, **10** (2005) 261.
[4] Sánchez-Pomales, G.; Cabrera, C. R.; *To be submitted.*

Figures:

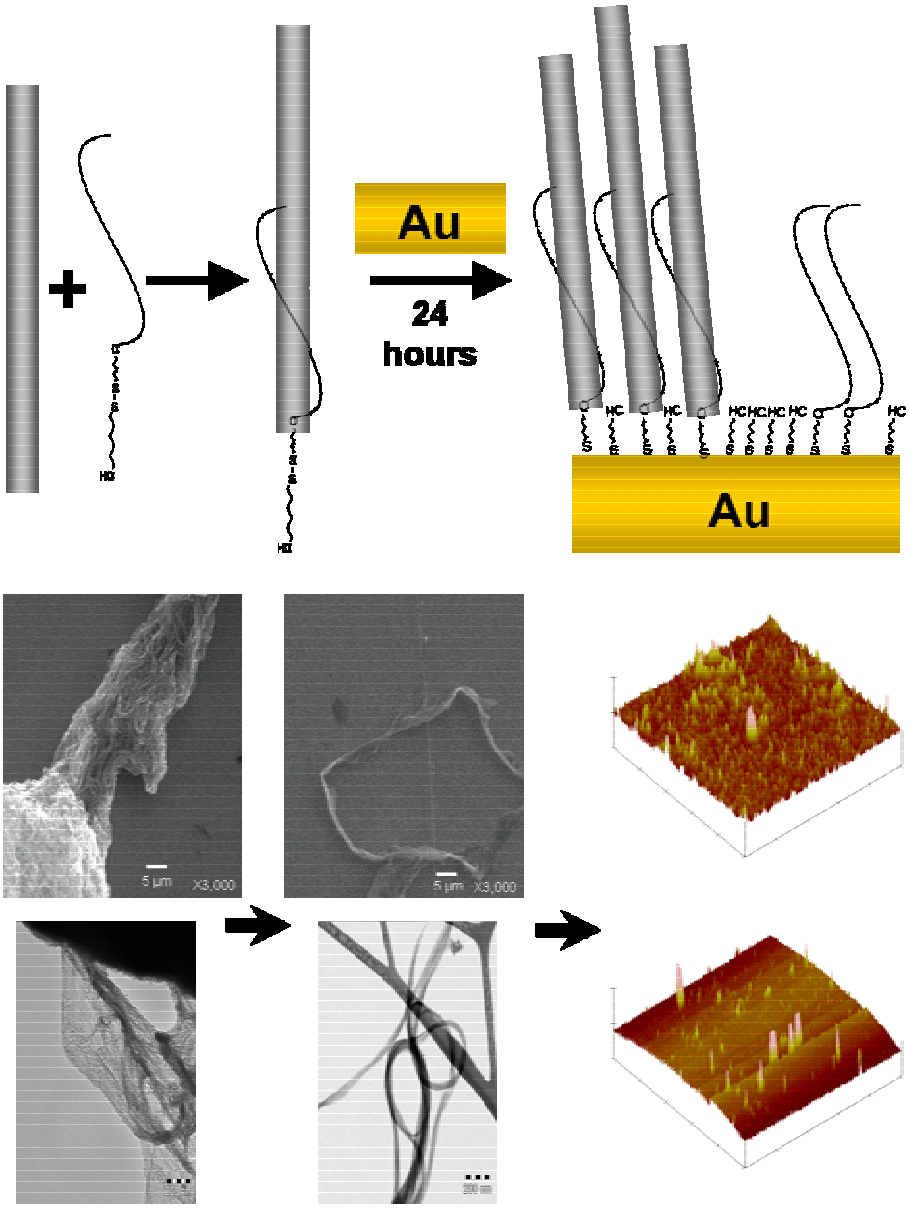


Figure 1: Overview of the methodology and the results, showing SEM and TEM images of the CNTs before (left) and after (middle) functionalization with DNA, and AFM results of the DNA-CNT SAMs on gold (right).

Poster

ON THE LATTICE PARAMETER AND HEIGHT PROFILES IN THE STRANSKI-KRASTANOV GROWTH MODE

S.N. Santalla, C. Kanyinda-Malu and R.M. de la Cruz

Departamento de Física, Universidad Carlos III de Madrid, Avenida de la Universidad 30, 28911 Leganés (Madrid), Spain
e-mails: rmc@fis.uc3m.es, ssantall@fis.uc3m.es

One of the most characteristic features of the Stranski-Krastanov (S-K) growth mode in low-dimensional heterostructures is to obtain distributions of semiconductor quantum dots (QDs) nearly homogeneous in their shapes and sizes. The uniformity of sizes and shapes could allow the fulfilment of optoelectronic devices with appropriate quality.
It is generally understood that the main mechanism of the formation of QDs in thin solid films on solid substrates is the Asaro-Tiller-Grinfeld instability that releases epitaxial elastic stresses in the film caused by the crystal lattice mismatch between the film and the substrate [1]. The faceting instability of a thermodynamically unstable surface is another mechanism that can also play an important role in the formation of surface structures during epitaxial growth [2]. Both mechanisms lead to the formation of mounds that usually coarsen, with larger islands growing at the expense of the smaller ones. In the coarsening process, the balance between the surface and elastic energies can lead to the formation of uniform-size islands as a preferred configuration having minimal energy. Additionally, mechanisms based on wetting interactions between the film and the substrate can terminate coarsening of the surface structures. Attending to the last mechanism, the boundary-layer and glued wetting-layer models are reported in the literature, where variation of -the surface energy, -misfit or -lattice parameter with the film height is considered [3-5]. Focusing on the lattice parameter variation, several dependences with the film height (coverage) are proposed [5, 6]. Due to the complexity of the above phenomena, it seems convenient to investigate the possible influence between the lattice parameter and the resultant height profile.
Then, the aim of this work is to obtain the lattice parameter and height profiles in typical semiconductor heterostructures like Ge/Si and InAs/GaAs evaluated self-consistently. With the continuum elasticity theory in linear approximation, the minimization of free energy density by Euler-Lagrange method leads to a second order differential equation for the lattice parameter variation, whose coefficients are related to the stiffness constants of the film material and the lateral size of the system. The resolution of this equation yields the lattice parameter dependence with the film coverage. Once the lattice parameter profile is obtained, the Euler-Lagrange method applied again to the free energy density leads to Poisson equation for the height function. The inhomogeneous term in Poisson equation is related to constitutive constants of the heterostructure materials and the coverage film. This term represents the geometrical curvature of the investigated systems. Within the framework of the linear approximation, only one step in the self-consistent scheme

is enough to obtain the solution convergence for both profiles. Throughout all calculations, assumption of isotropic surface energy and small slope approach are considered.

References:

[1] J. Asaro and W.A. Tiller, Metall. Trans. **3** (1972), 1789; M.Y. Grinfeld, Sov. Phys. Dokl. **31** (1986), 831.
[2] J. Stewart and N. Goldenfeld, Phys. Rev. A **46** (1992), 6505; F. Liu and H. Metiu, Phys. Rev. B **48** (1993), 5808.
[3] B.J. Spencer, Phys. Rev. B **59** (1999), 2011 and references therein.
[4] A.A. Golovin, M.S. Levine, T.V. Savina and S.H. Davis, Phys. Rev. B **70** (2004),235342.
[5] A. Sasaki, E.R. Weber, Z. Liliental-Weber, S. Ruminov, J. Washburn and Y. Nabetani, Thin Sol. Film **367** (2000), 277.
[6] See for example, S.N. Santalla, C. Kanyinda-Malu and R.M. de la Cruz, Nanotechnology **15** (2004) S15.

INFLUENCE OF INLET-GAS FLOW-RATE ON QUALITY OF MWNTs PREPARED BY CATALYTIC CVD WITH OPTIMISED GAS-MIXTURE COMPOSITION

M.G. Donato[1], G. Messina[1], C. Milone[2], S.Santangelo[*1]
[1]*Reggio Calabria University, Italy;* [2]*Messina University, Italy*
santange@ing.unirc.it

Carbon nanotubes (NTs) constitute an exciting research field, gathering enormous scientific and technologic interest. A lot of methods ***[1]*** are successfully utilised for preparing NTs with a large spread of properties, as demanded by the various application fields. Multi-walled (MW) NTs are preferred when higher rigidity and mechanical strength are required. Catalytic methods have reached the goal of high-yield MWNTs production ***[2,3]*** and ethane has been proposed as a cheap and non-toxic carbon source ***[3]***. However, high crystalline quality and phase purity remain the crucial tasks to be addressed.

The routine laboratory-diagnostics of the synthesis products, aimed at the optimisation of the preparation method, is usually performed by means of several complementary characterisation techniques, such as scanning electron microscopy (SEM), high resolution transmission electron microscopy (HRTEM) and Raman spectroscopy (RS).

In this work, the results are presented of structural and morphological analysis carried out on MWNTs prepared, by chemical vapour deposition (CVD) in optimised (1:1) ethane-hydrogen mixture, over 20%Fe/SiO_2 catalyst. The effect of the changes in gas flow-rate on the final issue of the synthesis process, in terms of reaction yield and process selectivity, is investigated.

Reaction yield increases, up saturating, with increasing the flow rate of inlet gases. However, the comparative discussion of SEM and HRTEM observations and of results of the quantitative RS analysis evidence that correspondingly the morphology of carbon deposit varies. In particular, the highest process selectivity and the best quality of reaction products are achieved using the lowest flow rate. Unfortunately, this is paid with significant Fe-nanoparticle encapsulation, responsible for catalyst deactivation and consequent low-yield achievement. As flow rate increases, catalyst inclusion progressively reduces and reaction yield improves. Conversely, the synthesis process becomes less selective and the formation of phases different from NTs intensifies.

Above results suggest that the optimisation of the preparation process actually comes out from a balance of competing factors and requires a careful tuning of the growth conditions. By carrying out preparation in a 1:1 ethane-hydrogen atmosphere, the use of a 120 sccm flow rate appears to be the best compromise among process selectivity, reaction yield and structural quality of the C deposits.

[1] M.S.Bell et al., in *"Carbon: the future material for advanced technology applications"*, G.Messina, S.Santangelo Eds., Springer's series Topics in Applied Physics, Heidelberg (2006) pp. 81-97
[2] H.J.Jeong et al., *J. Phys. Chem.* B**108** (2004) 17695
[3] B.Louis et al, *Catalysis Today* **102-103** (2005) 23

[*]Corresponding author

CHARACTERIZATION OF Ru/Pt/C NANOCATALYST PREPARED BY ROTATING DISK-ELECTRODE (RoDSE) TECHNIQUE

Diana Santiago, Miguel Cruz, Carlos R. Cabrera
University of Puerto Rico, PO Box 23346, San Juan, Puerto Rico
anaidsan@yahoo.com

Of the pure metals, platinum has shown the highest activity for methanol oxidation [1], but the poor performance of pure platinum for methanol oxidation results from the strong adsorption shown by CO on the metal. In order to overcome the blocking effect of CO on platinum, it can be alloyed with other metals to produce materials that exhibit catalysis rates considerably higher for methanol electro-oxidation than pure platinum [2]. Bimetallic Pt-Ru systems are promising electrocatalysts for methanol electro-oxidation, which afford significant current enhancements at given potentials compared to pure platinum. These systems, in high surface area form on unsupported or supported on carbon black, behave as excellent catalysts for direct methanol fuel cells. It is known that ruthenium promotes the electro-oxidation of methanol on platinum; the detailed explanation for its catalytic influence on this reaction is still a matter of discussion.

The major goal in fuel cell area is prepare catalytic with small particle size to obtain high surface area. For this I'm introducing a novel technique using rotating disk electrode called rotating disk-slurry electrode technique (RoDSE). In this investigation we used the carbon black as support. The surface area of the carbon blacks is very important in this investigation. For the ruthenium electrodeposition, we use $Ru(NO)(NO_3)_3$ and the commercial catalyst, 20% Pt-vulcan XC-72R from E-tek. The purpose of this study is to observe the Ru behavior when it was electrodeposited over the 20% Pt/C commercial catalyst at different potential with the RoDSE technique. In this study we used 200 mV, 100 mV, 0 mV, -100 mV, and -200 mV.

The TEM images demonstrate that the carbon surface has particles deposited over it, but only with the TEM imagine we can't determine if the Ru is deposited over the Pt/C surface (see figure 1). For this reason, we performed TEM-EDS analysis. Figure 2a is the EDS analysis of 20% Pt/C commercial catalyst that has the characteristics Pt peaks. Figure 2b is the EDS analysis of Pt/C catalyst after the Ru electrodeposition at constant potential of -200 mV. With this analysis we can see that the Pt/C nanocatalyst has Ru, because this EDS spectrum has an additional peak corresponding to Ru. The XPS analyses corroborate the TEM-EDS analysis when high resolution analysis for the Ru $3p_{3/2}$ peak was done (figure 3). The EDS mapping, XRD and electrochemical analysis also show the Ru presence on the Pt/C nanocatalyst. The rotating disk-slurry electrode is an appropriate technique for the metal electrodeposition, because avoid conglomeration over the catalyst support material

References:

[1] Bolivar, H.; Izquierdo, S.; Tremont, R.; Cabrera, C.R. J. Appl. Electrochem. **33** (2003) 1191.
[2] Ishikawa, Y.; Liao, M.S.; Cabrera, C.R. Surf Sci. **463** (2000) 66.

Figures:

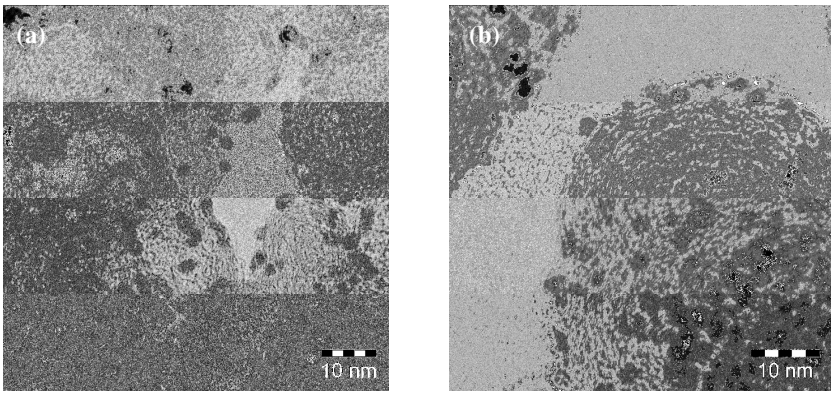


Figure 1: TEM imagine of (a) 20% Pt/C commercial catalyst, (b) Ru electrodeposited at -200 mV over 20% Pt/C commercial catalyst.

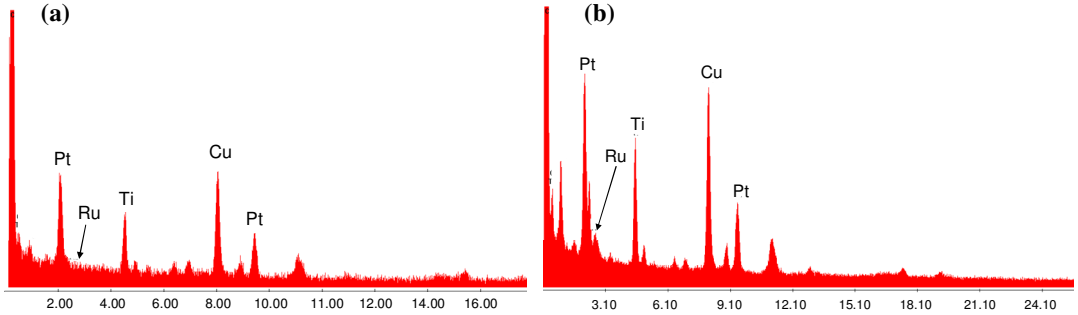


Figure 2: EDS spectrum of (a) 20% Pt/C commercial catalyst, (b) Ru electrodeposited at -200 mV over Pt/C commercial catalyst.

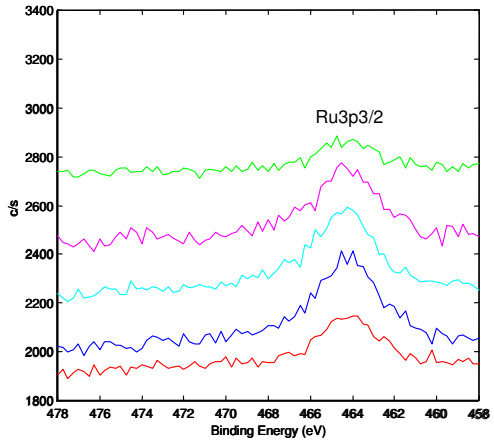


Figure 3: High resolution XPS analysis for Ru/Pt/C nanocatalyst prepared using: 200mV (red line), 100mV (dark blue line), 0 mV (light blue line), -100 mV (pink line) and -200 mV (green line).

NANO- DEPTH CONTROL OVER SELF ASSEMBLED STRUCTURES ON BIO-COMPATIBLE POLYMERIC THIN FILMS FOR BIO-ARRAY APPLICATIONS.

E. Sarantopoulou
National Hellenic Research Foundation. Theoretical and Physical Chemistry Institute, 48 Vassileos Constantinou Aven. Athens 11635, Greece.

Surface treatment and preparation of biopolymers for bio- arrays applications with lasers at 157 nm allows surface roughness depth control for optimizing surface –probe binding strength and detection sensitivity [1]. Optimization and control on the surface quality of bio-polymers, besides optimizing detection sensitivity, is accelerating hybridization time and sets the limits in relation to defect-free surface preparation from DNA immobilized strands localized on bio compatible polymer substrates. In this communication, the surface roughness from self-assembled structures on Teflon thin films was controlled with atomic resolution allowing thus optimum surface preparation for bio-array applications.

References

[1] 157 nm laser ablation of polymeric layers for fabrication of biomolecule microarrays. A. M. Douvas, P. S. Petrou, S. E. Kakabakos, K. Misiakos, P. Argitis, E. Sarantopoulou, Z. Kollia, A. C. Cefalas. *Anal. Bioanal. Chem., V381, 1027 (2005).*

CARBON NANOTUBES GROWN FROM GAS PHASE PREPARED IRON CATALYST PARTICLES

F. Schäffel, C. Kramberger, M. Rümmeli, R. Kaltofen, D. Grimm, E. Mohn, T. Gemming, T. Pichler, B. Büchner, B. Rellinghaus, and L. Schultz
IFW Dresden, P.O. Box 270116, D-01171 Dresden, Germany
F.Schaeffel@ifw-dresden.deT

An innovative technique which successfully grows carbon nanotubes (CNT) by chemical vapor deposition (CVD) using cyclohexane will be introduced. The novelty of the technique lies in the separately generated catalytic nanoparticles which are synthesized via a gas aggregation technique of the type conceived by Haberland et al. [1]. The particles grow from a supersaturated metal vapor obtained by sputtering from an iron target at pressures of 1 mbar. After nucleation and subsequent growth of the particles within an aggregation volume, they are ejected into high vacuum (10^{-5} mbar) through a double aperture system. As a consequence and in contrast to other gas phase techniques [2], further agglomeration of the particles is suppressed (Fig. 1).

If deposited onto appropriate substrates (e.g. Si with a 10 nm Al_2O_3 layer), these particles can act as individual nucleation sites for the growth of CNT. While the size of the particles templates the diameter and defines the type of the resulting CNT, their spatial distribution controls their density. The use of separately generated particles provides the advantage to control and characterize their size, morphology, spatial distribution and mutual separation. In addition size fractionation of the particles via quadrupole mass filtering (for masses as high as $4*10^6$ amu) can be employed [3]. The spatial distribution is conveniently controlled by the deposition time.

Thus far, we show that this technique can successfully grow both single wall and multi wall CNT of high quality (Fig. 2-3). Further, the technique offers significant control over the catalyst particle size and hence the type and diameter of the resulting CNT.

References:

[1] H. Haberland et al., J. Vac. Sci. Technol. A **12** (1994) 2925.
[2] S. Stappert et al., J. Cryst. Growth **252** (2003) 440.
[3] S. H. Baker et al., Rev. Sci. Inst. **68** (1997) 1853

Figures:

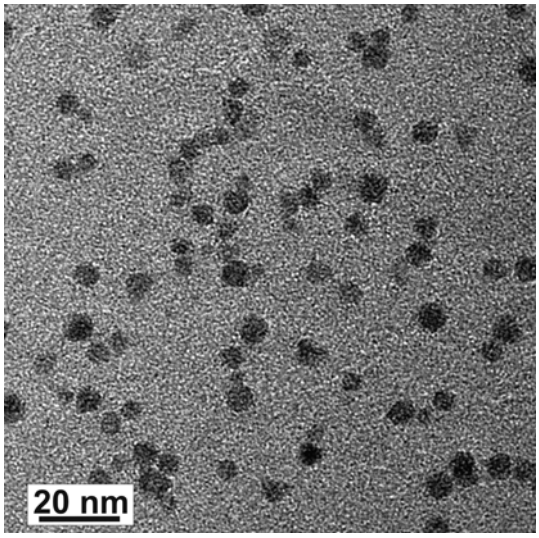


Fig. 1: TEM micrograph of the gas phase prepared catalyst nanoparticles

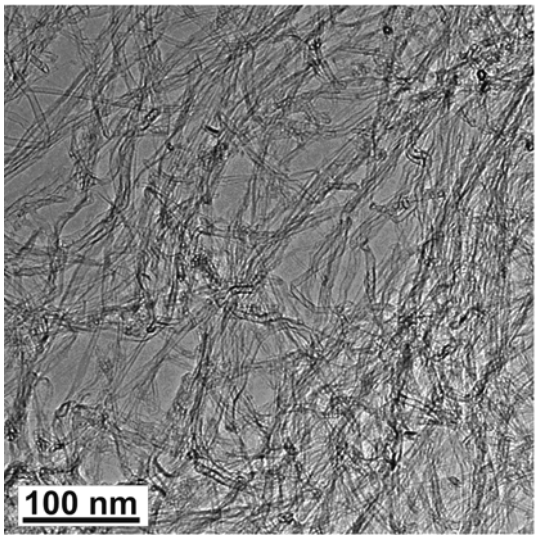


Fig. 2: Large scale overview TEM micrograph of the as grown CNT network

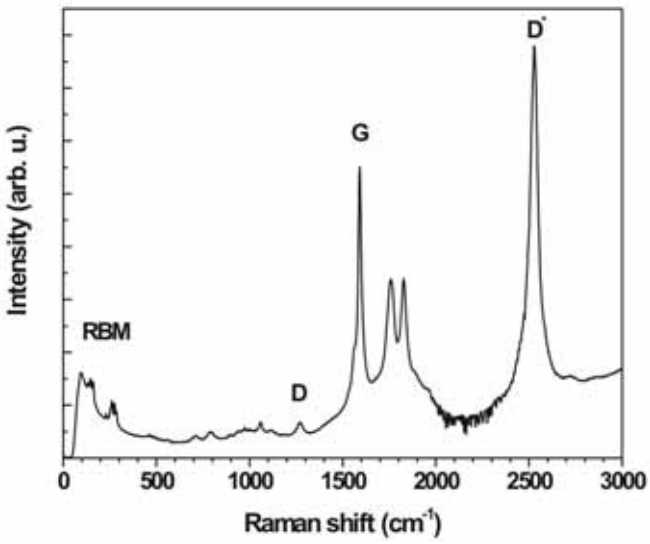


Fig. 3: Fourier Raman spectrum (1064 nm) of high quality CNT.

Poster

POTENTIAL OF ENZYMATIC SILVER DEPOSITION

Thomas Schüler, Katarina Hering*, Robert Möller, Wolfgang Fritzsche

Institute for Physical High Technology, PF 100239, 07702 Jena
*Friedrich-Schiller University, Institute for Physical Chemistry, 07743 Jena

The fast development in DNA Microarray technology is founded in the search for simple, cost effective and fast methods for the detection of biomolecules. At the moment biomolecules like DNA, proteins and others are mainly detected by marking them with fluorescence dyes. This technique is highly sensitive and broadly established but shows also disadvantages, for example photo bleaching and quenching.

In the last years metal nanoparticles showed the potential to be an alternative marker for the detection of biomolecules. Nanoparticles offer various unique properties, for this reason different approaches have been developed for the detection of nanoparticle labeled biomolecules, for example electrochemical, optical and gravimetric methods.

This work presents an electrical method for DNA detection. It is based on the electrical detection of nanoparticle-labeled DNA by the immobilization of the particles in the gap between two microstructured electrodes on the surface of a DNA chip. In case of a binding event the capture DNA immobilized in the gap binds their specific partners (target), and gold nanoparticles are bound to a special modification in the target molecule. Finally, silver is deposited on the bound gold nanoparticles. The metal enhancement step leads to a bridging of the gap between the electrodes and a decrease in the measured resistance over the gap (Fig. 1).

The main problem with this method is the increasing background at longer silver enhancement times. Therefore an alternative enhancement system was tested. In this connection an enzyme, horseradish peroxidase, replaces the gold nanoparticles. Only the enzymatic activity of horseradish peroxidase is responsible for the silver deposition. With this system we were able to improve the sensitivity and to minimize the background due to the highly specific, localized silver deposition. In order to further optimize this approach, a better knowledge is required about the kinetics of silver enhancement of gold nanoparticles and horseradish peroxidase for the quantification of our results on the electrical DNA-Chip.

For that purpose the enzyme was immobilized on mica and the growth of these enzymatically formed silver particles was analyzed with the AFM at the single particle level (Fig. 3). To give a statement about the enzyme kinetics, particles with different enhancement times were

measured. After that every single particle was characterized in height and volume to determine the enzyme kinetics. Furthermore the potential was investigated to create DNA-guided electrical pathways based on the enzymatic metal enhancement (Fig. 4).

Möller, R.; Csáki, A.; Köhler, J. M.; and Fritzsche, W. *Langmuir* **2001,** 17, 5426-5430.

Urban, M.; Möller, R.; and Fritzsche, W. *Review of Scientific Instruments* **2003,** 74, 1077-1081.

Möller, R, R. D. Powell et. al., *Nano Letters* **2005**, 5, 1475-1482

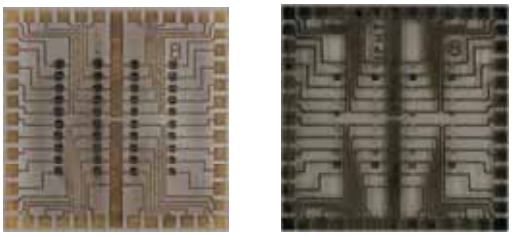


Fig. 1: screen printed chips with gold and platin structures after enzymatic silver deposition

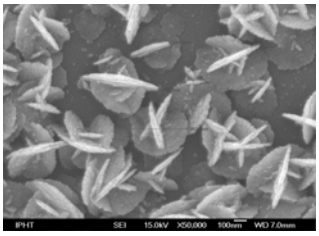
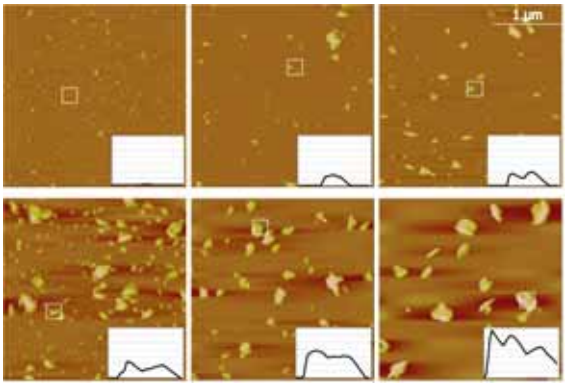


Fig. 2: SEM image, particles after enzymatic silver deposition



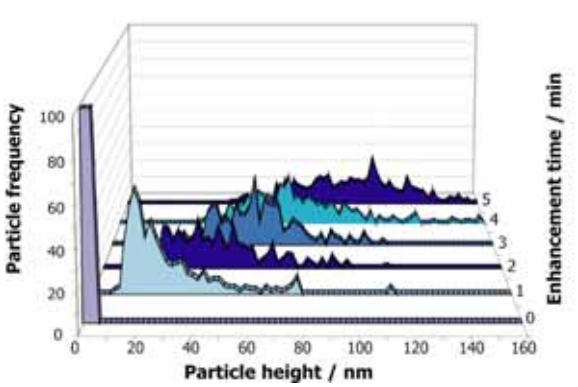


Fig. 3: Stepwise metal deposition by the enzyme in 1 min steps starts at the image on the top with the untreated enzyme complex and ends at 5 min silver enhancement shown in the image on the bottom (right), the particle height distribution is shown in the diagram

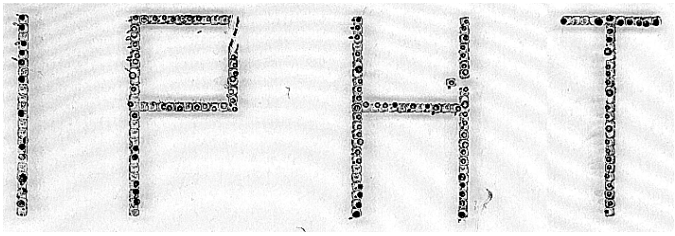


Fig. 4: slide spotted with DNA and silver enhanced by the enzyme

STM STUDY OF πCONJUGATED FLUORENONE-BASED SELF-ASSEMBLED ORGANIC SEMICONDUCTORS

Lorette Scifo[1], Renaud Demadrille[1], Fabrice Mathevet[2], Mickael Brun[2], Bertrand Donnio[3], Henry Janeczek[4], Jacques Pécaut[5], André-jean Attias[6], Patrice Rannou[1], Adam Pron[1] and Benjamin Grévin[1].

[1]LEMOH, UMR5819-SPrAM (CEA-CNRS-UJF), DRFMC, CEA-Grenoble, 17 rue des Martyrs, 38054 Grenoble Cedex 9, France.
[2]LIMN, DIHS, LETI, CEA-Grenoble, Grenoble 38054 cedex9, France,
[3]GMO, IPCMS, Strasbourg 67034, France
[4]Centre of Polymer Chemistry, Polish Academy of Sciences, Zabrze 41819, Poland
[5]SCIB, DRFMC, CEA-Grenoble 38054 cedex9, France
[6]UMR7610-Chimie des Polymères, ParisVI, Paris 75252, France.

Studying the structural organization of πconjugated architectures and supramolecular assemblies adsorbed on substrates is of considerable importance for the development of organic and molecular electronics. We report here on a LC-STM study under UHV condition on self-assembled monolayers of two πconjugated fluorenone-based organic semiconductors, B4OTF and B5OTF.

Both B4OTF and B5OTF monolayers self-assemble on HOPG to give highly organized 2D crystals. They display moreover almost identical organization due to very close molecular structure. However, we will show that the different anchoring position of the n-octyl side-chains on the thiophene heterocycle induces strain inside the monolayer resulting in a periodic relaxation along one of the crystallographic axes.

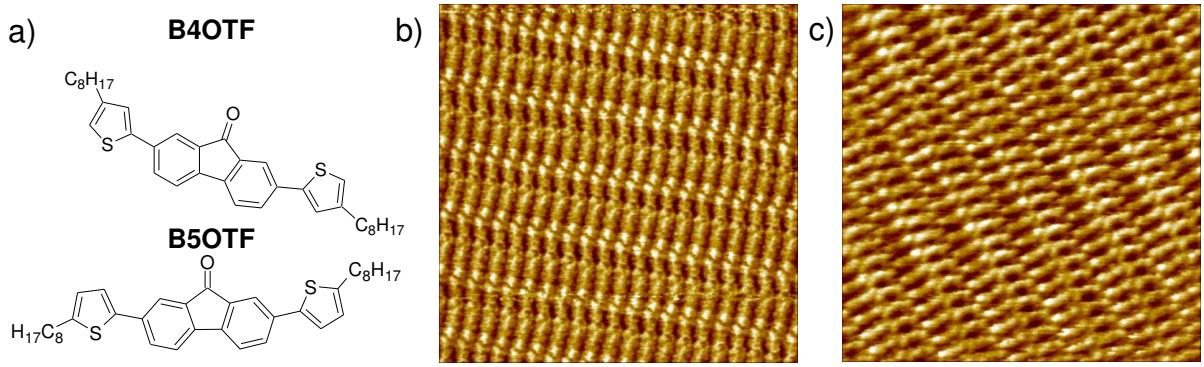


Fig1: a) B4OTF and B5OTF monomers b),c) STM (25x25 nm, 500x500 pixels) images of self-assembled monolayers B4OTF(b : I_t= 10pA, V_g=-1V) and B5OTF(c : I_t= 15pA, V_g=-1.5V).

Additionnally, we will show that, upon annealing under UHV condition, B5OTF monolayers can self-assemble into a second 2D crystalline phase. All these 2D structural organization will be discussed and analyzed and tentative 2D packing model will be proposed. These models will be compared to the 3D packing (DSC, POM and XRD) of these organic semiconductors in their "bulk" crystalline (single crystal) and liquid crystalline phases.

SYNTHESIS OF CARBON NANOTUBES, NANOFIBERS AND CARBON ENCAPSULATED NANOPARTICLES BY DECOMPOSITION OF ACETYLENE OVER PD AND Pd-Ge CATALYSTS

Rodrigo Segura[1], *Alejandra Tello*[2], *Galo Cardenas*[2] *and Patricio Häberle*[1]
[1]*Departamento de Física, Universidad Técnica Federico Santa María, Chile*
[2]*Facultad de Ciencias Químicas, Universidad de Concepción, Chile*
rodrigo.segura@usm.cl

Since their discovery, the design and study of Carbon nanotubes (CNTs), nanotubes-based materials and devices have become topics of great interest in material science. CNTs have been used as building blocks in the design of molecular electronic devices of great technological interest, as field emitters, in diodes, transistors, flat-panel displays, scanning probe microscopy tips and many others. Potential applications currently being investigated include hydrogen storage, reinforced polymers, molecular (drug) delivery and scaffolding in tissue engineering. For these applications, mass production of nanotubes play an important role. Due to this reason the discovery of new catalysts for an efficient production, remains a current topic of investigation. In this line we present results from a study of the decomposition of acetylene over alumina-supported palladium and palladium-germanium catalysts.

The catalysts were prepared by the Solvated Metal Atom Dispersion technique (SMAD).[1] This procedure is carried out by simultaneous evaporation of Palladium and/or Germanium and an organic solvent like 2-propanol to generate a frozen matrix on the walls of the metal atom reactor at 77K. After warming this matrix to room temperature, a colloid with very small and highly reactive clusters is obtained. These clusters react with acid sites of the high surface area γ-alumina, forming anchored nucleus of Pd, Ge and Pd-Ge alloys. This mixture was subsequently dried and the powder ground in a mortar before their use as catalyst. For this study we prepared γ-alumina catalysts with the following loads: Pd(1%), Pd(1%)-Ge (0.1%), Pd(1%)-Ge (0.3%), Pd(1%)-Ge (0.5%), and Ge (0.1%).

The decomposition of acetylene was carried out in a Chemical Vapor Deposition apparatus (CVD) composed of a horizontal tube furnace and gas flow lines.[2] The catalyst, was loaded in a quartz boat inside the tube reactor, heated at a rate of 20ºC/min and annealed 10 min in a Ar/H_2 stream at 800 ºC. Then, acetylene (25 ml/min) was decomposed over the catalyst for 30 min. We have chosen 800 ºC because this is the optimum temperature for synthesis of pure carbon nanotubes with the Pd(1%)/γ-Al_2O_3 catalyst.[3] The effects of Germanium loading in the final nanocarbon products were analyzed by Transmission Electron Microscopy.

When pure palladium catalyst is used carbon products consist predominantly of Multiwall Carbon Nanotubes (MWCNTs). In terms of yield, one gram of palladium produces about 110 grams of MWCNTs. When a small amount of germanium (0.1%) is added to the catalyst formula, it produces around 210 grams of MWCNTs (see Figure 1). The change in the yield could be attributed to modifications in the electronic structure of the palladium nanoparticles, which preferentially induces the production of tubular structures. When 0.3% of Germanium is added to the catalyst something different occurs. Carbon products decrease close to 20 grams per gram of palladium. TEM micrographs show the formation of carbon fibers (Figure 2). Additional amounts of germanium in the catalyst formulation (0.5%), induces the formation of carbon encapsulated Pd-Ge nanoparticles (Figure 3). Probably germanium, in this case, is blocking the active sites or producing drastic changes in the electronic structure of palladium particles, thus hindering the formation of filamentous structures. Similar effects were observed when pure germanium was used as catalyst (figure 4).

As final remarks we can conclude that adding small amounts of germanium to the palladium catalyst can improve considerably the yield toward the formation of carbon nanotubes. The formation of carbon encapsulated Pd-Ge nanoparticles by this method could also have technological interest.

1. G. Cárdenas, R. A. Segura, J. Reyes, *Colloid Polym. Sci*. **2004**, 282, 1206.
2. R. A. Segura, W. Ibáñez, R. Soto, S. Hevia, P. Häberle, *J. Nanosc. Nanotech.* **2006** (in press)
3. R. A. Segura, A. Tello, G. Cardenas, P. Häberle (unpublished)

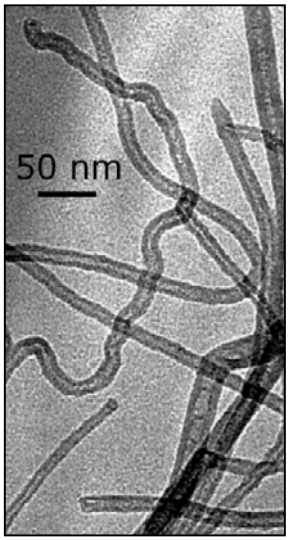


Figure 1. Multiwall Carbon Nanotubes obtained by decomposition of acetylene at 800 ºC in a Pd(1%)-Ge(0.1%)/γ-Al_2O_3. The mean diameter of nanotubes is 18 nm.

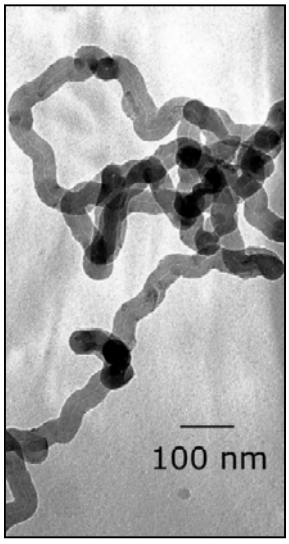


Figure 2. Carbon Nanofibers obtained by decomposition of acetylene at 800 ºC in a Pd(1%)-Ge(0.3%)/γ-Al_2O_3. The mean diameter of fibers is 38 nm.

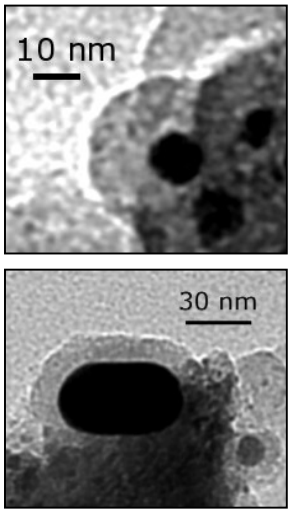


Figure 3. Carbon encapsulated nanoparticles obtained by decomposition of acetylene at 800 ºC in a Pd(1%)-Ge(0.5%)/γ-Al_2O_3.

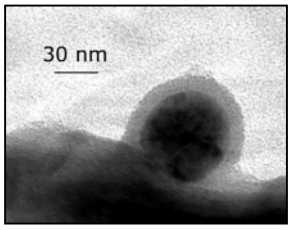


Figure 4. Carbon encapsulated germanium nanoparticle obtained by decomposition of acetylene at 800 ºC in Ge(1%)/γ-Al_2O_3 catalyst.

DESIGNING MAGNETIC NANOPARTICLES FOR PROTEIN SEPARATION – A COMPARATIVE STUDY BETWEEN FLAME SPRAY PYROLYSIS AND SOL-GEL SYNTHESIS

Cordelia Selomulya[1], *Li Dan*[2], *Wey Yang Teoh*[2], *Robert Woodward*[3], *and Rose Amal*[2]
1 Department of Chemical Engineering, Clayton Campus, Monash University, Melbourne VIC 3800, AUSTRALIA
2 ARC Centre for Functional Nanomaterials, The University of New South Wales, Sydney NSW 2032, AUSTRALIA
3 School of Physics, The University of Western Australia, Crawley WA 6009, AUSTRALIA
cordelia.selomulya@eng.monash.edu.au

The application of magnetic particles in the field of biological and biomedical science can be traced back to the 1970s where micron-sized particles were used as support material for enzyme immobilization [1] and bioaffinity adsorbents [2]. Success in synthesizing nano-sized magnetic particles has empowered a wider range of exciting bio-applications, including magnetic resonance imaging (MRI) [3], bioseparation [4], and drug delivery [5]. The ideal properties of magnetic nanostructures (depending on the specific application) would be uniform size, large surface area, fast adsorption kinetics, biocompatibility, and superparamagnetism with high magnetic strength. Often, an additional inorganic or polymeric coating layer is necessary to avoid the aggregation of magnetic cores and to improve the functionality or biocompatibility of the nanostructures. Despite ongoing research efforts in the search for reliable synthesis routes allowing the control of these properties, wet chemistry-based methods such as micro-emulsion, sonochemical, reverse micelles, and sol-gel techniques are inherently limited in scalability. On the other hand, Flame Spray Pyrolysis (FSP) has been demonstrated as a rapid, scalable and waste-free production technique with a production rate 600 g/h of nanoparticles on a pilot scale [6]. The use of FSP-synthesized magnetic particles with tailored properties for specific bio-related applications thus has great potentials.

In this study, Flame Spray Pyrolysis (FSP) was used to synthesize maghemite (γ-Fe_2O_3) nanoparticles of BET-equivalent diameter (d_{BET}) of 5nm, 13nm, and 20nm. Composite nanostructures of SiO_2/ γ-Fe_2O_3 with different Fe:Si molar ratios were also produced using either a one-step FSP method or by sol-gel coating of silica onto the FSP-produced 13nm γ-Fe_2O_3 core [Figure 1]. The physical, chemical and magnetic properties of the γ-Fe_2O_3 and SiO_2/ γ-Fe_2O_3 nanostructures were characterised and compared. The nanostructures were predominantly superparamagnetic at room temperature, with saturation magnetism decreasing with γ-Fe_2O_3 size and the thickness of silica coating [Figure 2]. To observe the potential use of these particles for protein separation, adsorption and desorption of bovine serum albumin (BSA) onto γ-Fe_2O_3 and SiO_2/ γ-Fe_2O_3 particles were studied in phosphate and formate buffers. Highest BSA binding capacity of 373$\pm$20mg/g with a dissociation constant of 0.016gL^{-1} was obtained for FSP 5nm γ-Fe_2O_3 in 10mM formate buffer [Figure 3(a)]. The binding capacity is influenced predominantly by suspension chemistry that altered the electrostatic interaction of particles surfaces and BSA, and by the particle surface properties affecting the hydrophobic interaction with BSA and the number of binding sites available as a function of specific surface area. BSA desorption was best achieved by shifting the pH of suspension from 5.3 to 9 using K_2HPO_4 [Figure 3(b)]. The substantial affinity of BSA towards the particles surface, coupled with mild desorption conditions and easy recovery under external magnetic field render these particles ideal for protein separation purposes. Furthermore, the silica layer could be functionalised for specific ligands attachment via the well established silane coupling chemistry to introduce selectivity. The synthesized particles are promising nanomaterials for efficient bioseparation.

References:

1. Robinson, P. J., Dunnill, P. and Lilly, M.D., Biotechnology and Bioengineering, **15** (1973) 603-606.
2. Dunnill, P. and Lilly, M.D., Biotechnology and Bioengineering, **16** (1974) 987-990.
3. Bomatí-Miguel, O., Morales, M.P., Tartaj, P., Ruiz-Cabello, J., Bonville, P., Santos, M., Zhao, X. and Veintemillas-Verdaguer, S., Biomaterials, **26** (2005) 5695-5703.
4. Bucak S., Jones D. A., Laibinis P.E. and Hatton T.A., Biotechnology Progress, **19** (2003) 477-484.
5. Yu, S. and Chow, G.M, Journal of Materials Chemistry, **14** (2004) 2781-2786.
6. Mueller, R., Jossen, R., Pratsinis, S. E., Watson, M. and Akhtar, M. K. Journal of American Ceramics Society, **87**(2) (2004) 197-202.

Figures:

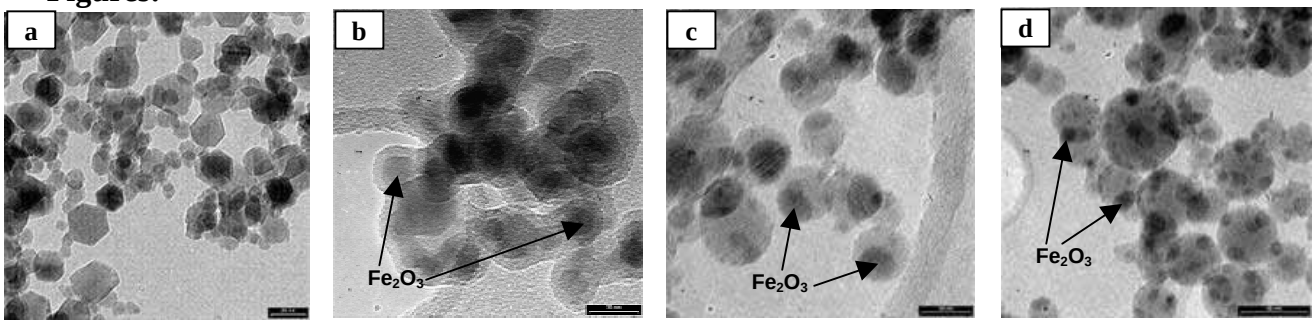


Figure 1 – FSP-synthesized γ-Fe_2O_3 of (a) d_{BET} = 20nm; (b) sol-gel coated SiO_2 on 13nm FSP γ-Fe_2O_3 with Fe:Si = 1:1; (c) one-step FSP-synthesized SiO_2/γ-Fe_2O_3 with Fe:Si = 1:2 and (d) Fe:Si = 1:5

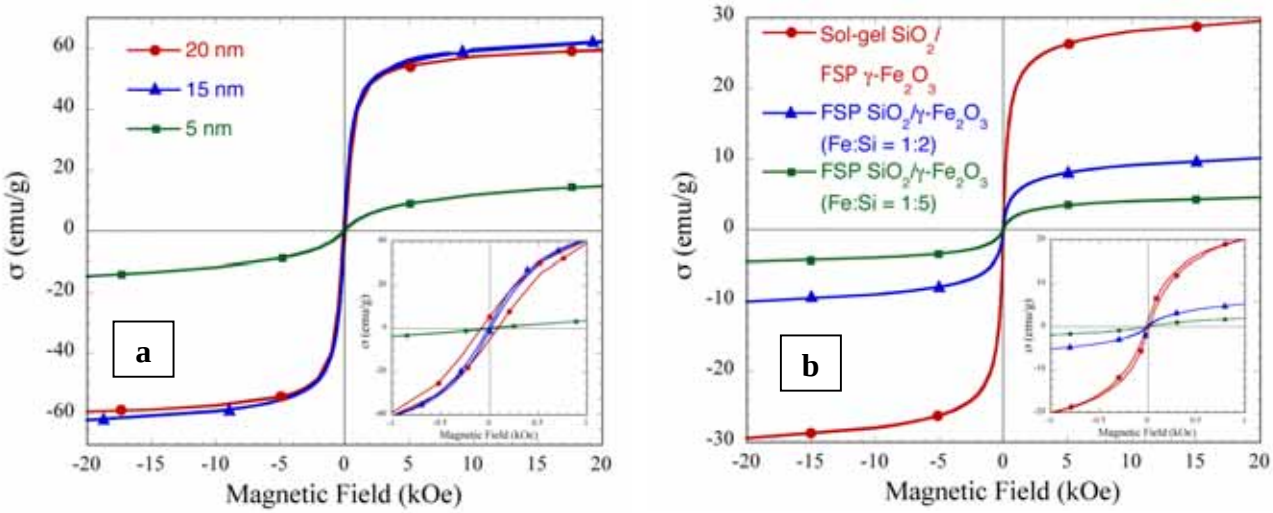


Figure 2 – Hysteresis loops at 300K for (a) d_{BET} 5nm, 13nm, and 20 nm γ-Fe_2O_3; (b) SiO_2/γ-Fe_2O_3 particles

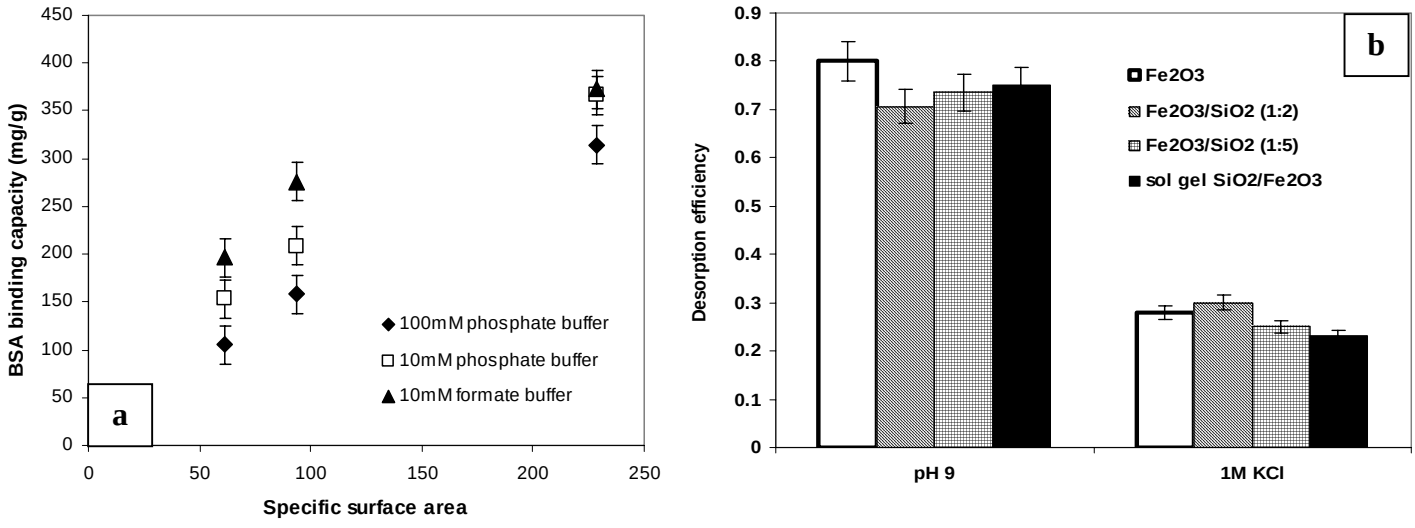


Figure 3 – (a) BSA binding capacity at 2.5±0.1g/L particle loading and room temperature after 3hr adsorption as a function of specific surface area; (b) % BSA desorbed in phosphate buffer

Poster

BIOTECHNOLOGICAL ASPECT FOR THE SYNTHESIS OF BIOACTIVE NANOPARTICLE

Sushil K Shahi* and Mamta Patra

Department of Nanotechnology, Center for Advance Research and Development

Gwalira Road, Ved Vihar, Saharanpur- 247001, India.

*Email: shahiindia@rediffmail.com

The area of nanotechnology, which spans the synthesis of nanoscale matter, understanding/utilizing their exotic physicochemical and optoelectronic properties, and organization of nanoscale structures into predefined superstructures, promises to play an increasingly important role in many key technologies of the new millennium [1,2]. As far as the synthesis of nanoparticle is concerned, there is an ever-growing need to develop clean, non-toxic and environmentally friendly (green nanochemistry) procedures. Consequently, researches in the field of nanoparticle preparation have been looking at biological systems for inspiration. The above factors, combined with academic curiosity, have lead to the development of biomimetic approaches for the growth of advance materials (bioactive materials). Many organisms, both unicellular and multicellular, are known to produces inorganic materials either intra- or extracellularly [3,4]. Even through microbes have been used with considerable success in biotechnological applications, such as remediation of toxic metals, reports on their use in the synthesis of nanomaterials are extremely limited. Mukherjee and coworker have demonstrated the formation of gold nanoparticle through *Verticillium* fungus sp [5]. In the present communication we showed that the lichen fungi (*Usnea orientalis)* synthesized the bioactive nanoparticle in culture conditions. Lichen fungi have diverse range of chemicals and produce some characteristic metabolites during artificial culture in synthetic medium [6,7,8]. During artificial culture of some lichens fungi in synthetic medium for metabolite synthesis, the lichen fungi of *Usnea orientalis* (ascomycetes fungi) found to be synthesized bioactive nanoparticle in specified medium under additional conditions. The size of the nanoparticle of almost uniforms in size, with a diameter of around 50-200 nanometer across. Such a narrow size distribution is characteristic of microbially synthesized nanoparticle. The nanoparticle become trapped both on the surface of the cell wall and on the cytoplasmic membrane. The controlled synthesis of nanoparticles of well-defined dimensions over a range of chemical compositions is an important aspect of nanomaterials engineering. Biological process are inherently accurate, and synthesis of all the particles takes place during a specific period of cell growth, most of the particle synthesized are of the same size-they have a very narrow size distribution. There is an ever-growing need to develop cleaner, non-toxic and environmentally friendly procedures for synthesizing the nanoparticles. So the research turned to biological systems for inspiration. This is first ever report of microbially synthesis of bioactive nanoparticle from lichen biomass (mycobiont) through in vitro culture. After almost exhaustion of medium after 7-8 days nanoparticles were isolated from medium through various methods before being purified. We were used Bio nanoemulsion technology for in vitro bioactivity testing of formulated nanoparticles from lichen metabolites. Detail in vitro analysis of nanoparticles was carried out against human pathogenic fungi, *Trichophyton rubrum, T. mentagrophytes, Epidermophyton floccosum, Microsporum gypseum, M. audouini,* causing fungal infection in humans and animals. Bioactive nanoemulsion was also found broad antifungal spectrum killing some other fungi,

Candida albicans, Aspergillus flavus, Microsporum nanum. For clinical investigation, we have formulated bioactive nanoemulsion, before specific analysis. Bioactive nanoemulsion was found to be stable upto two year, during this period no agglutination was observed as specific natural surface protectant was added. Nanoemulsion was found to be extremely safe and effective for controlling dermatophytoses during in vivo investigation. Thus, our study will definitely provide an effective natural nanomedicine (bio-nanoantifungal) active against dermatophytoses; in near future after successful clinical trial, which is our next step. So, in this way we can exploit the lichen biomass (mycobionts) as nanofactories for the production of raw material for nanodrugs.

References:

[1] G. Schmid, In: Clusters and Colloids. From therapy to application, Wiley-VCH, New York, (1994) (ed: A.S Edelstein, R.C Cammarata)

[2] G. Schmid, In: Nanomaterials, Synthesis, Properties and applications (ed/; A.S Eeelstein, R. C Cammarata), IP, Bristol, (1996).

[3] K. Simkiss, K.M Wilbur, In: Biomineralization, Academic Press (ed: S. Mann) New York, (1989).

[4] K. Simkiss, K. M Wilbur, In: Biomimimetic materials chemistry, VCH (ed: S. Mann) New York, (1996).

[5] P. Mukherjee, A. Ahmed, D. Mandal, S. Scnapati, S.R Sainleem, M. I Khan, R. Ramani, R. Parischa, P. V Ajayakumar, M. Alam, M. Sastry, R. Kumar. Angew Chem. Int Ed: 40 (2001) 3585.

[6] SK. Shahi, AC. Shukla, A. Dikshit and DK. Uperti, Lichenologist, **33**(2) (2001) 177-179

[7] SK. Shahi, M. Patra, A. Dikshit and DK. Uperti, Phytotherapy Research **17** (2003) 399-400.

[8] SK. Shahi and M. Patra, Review of Advance Material Science, 5 (2003) 501-509.

PROXIMITY EFFECT AND MULTIPLE ANDREEV REFLECTIONS IN GRAPHENE

A. Shailos, A. Kasumov, M.Ferrier, S. Gueron, R. Deblock, H. Bouchiat

Laboratoire de Physique des Solides, Associ´e au CNRS,
Batiment 510, Universite Paris-Sud, 91405, Orsay, France
shailos@lps.u-psud.fr

We perform transport measurement in Graphene at temperature range between 300 K and 60 mK. The device is prepared by mechanical exfoliation of graphite. A small mesa of graphene is placed on top of an aluminum oxide with a silicon substrate. With the use of FIB, deposited Tungsten wires connect the Graphene with big metallic pads. We show experimental evidence of a two dimensional carrier confinement in Graphene. In addition we observed proximity effect superconductivity due to the superconducting Tungsten wires and the formation of Andreev states as a nonlinearities in the IV characteristics.

Transport, magnetotransport and magnetic properties of composites of polymer and carbon encapsulated iron carbide nanoparticles.

S. Shekhar, V. Prasad and S. V. Subramanyam
Dept. of Physics, Indian Institute of Science, Bangalore, India 560 012
sshekar@physics.iisc.ernet.in

Polymer incorporated with ferromagnetic or superparamagnetic nanoparticles are of immense practical applications in spin polarized devices, high-density data storages to biomedicines [1]. The composites of iron carbide nanoparticles encapsulated in carbon matrix and polymer have been prepared by the dispersion of nanoparticles in host polymer (PVC) by solvent mixing method [2]. The carbon encapsulated iron carbide nanoparticles (filler) have been prepared by pyrolysis at 980^0C of ferrocene and maleic anhydride (1:2 molecular weight ratio) [3]. A low percolation threshold is observed which implies that a homogeneous dispersion is achieved. The transport properties have been studied from 300K to 1.3K. The composites obey Efros-Shklovskii variable range hopping (ES-VRH) conduction mechanism [$\rho=\rho_0 \exp(T_0/T)^{1/2}$] confirming disordered nature of the composites. The ES-VRH conduction mechanism is observed when there is a gap in density of states near the Fermi energy. This gap is produced in disordered materials due to interaction between hopped charge carriers. A new type of crossover from one ES-VRH to another ES VRH is observed nearly at 50K with different prefactor (ρ_0) and different T_0 (see fig.2). The crossover is observed for all the samples above the percolation threshold value.

The magnetoresistance [$(\rho(B)- \rho(0))/ \rho(0)$] of the composites show a crossover from negative magnetoresistance (MR) to positive MR as the magnetic field increases (fig.3). This kind of behaviour arises due to combination of various effects. The VRH gives positive MR whereas Kondo effect is responsible for negative MR and the combined effect give a crossover from negative to positive MR. Similar behaviour was reported in carbon nanotubes network [4]. The value of MR decreases with the increase in temperature.

The magnetisation measurements have been carried out on the composites containing wide range of filler varying from 1.5% to 35% in weight percentage. The zero field cooling (ZFC) and field cooling (FC) magnetization plots for one of the composite is shown in fig.4. The ZFC departs to FC curve near to 300K, attributes to very high blocking temperature. This implies that a high energy barrier exists which resists magnetic moment flipping even at room temperature. The saturation magnetization increases linearly with the filler concentration, which indicates that the contribution comes from filler and the host polymer matrix does not provide any resistance. Below 300K (blocking temperature) composites show hysteresis behavior. The ratio of remanence to saturation magnetization is nearly 0.15 at 300K, which increases to 0.33 at 10K. This value indicates the anisotropy to be non-uniaxial [5]. The coerecivity is found to be increasing at lower temperatures for a given composite whereas a filler concentration coerecivity shows a maximum for an intermediate value.

References:

[1] J. L. Wilson, P. Poddar, N. A. Frey, H. Srikanth, K. Mohomed, J. P. Harmon, S. Kotha and J. Wachsmuth, J. Appl. Phys, **95** (2005) 1439.
[2] S. Shekhar, V. Prasad, S. V. Subramanyam, Mat. Sc. Engg. B, (in review).
[3] E. P. Sajitha, V. Prasad, S. V. Subramanyam, S. Eto, K. Takai and T. Enoki, Carbon, **42** (2005) 2815.
[4] G. T. Kim, E. S. Choi, D. C. Kim, D. S. Suh, Y. W Park, K. Liu, G. Duesberg and S. Roth,

Phys. Rev. B , **58** (1998) 16 064.
[5] A Ceylan, C. C. Baker, S. K. Hasanain and S. I. Shah, Phys. Rev. B**, 72** (2005) 1441

Figures:

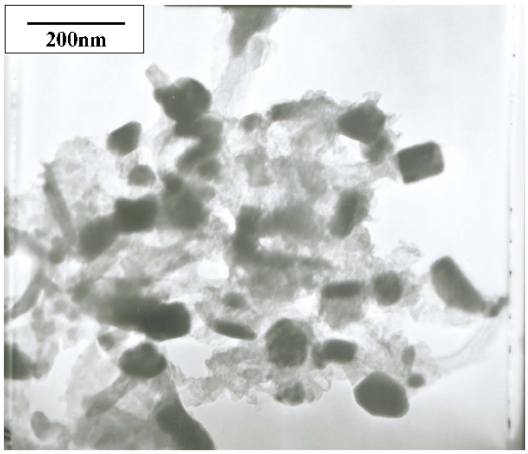


Fig. 1 TEM graph of carbon encapsulated iron carbide nanoparticles.

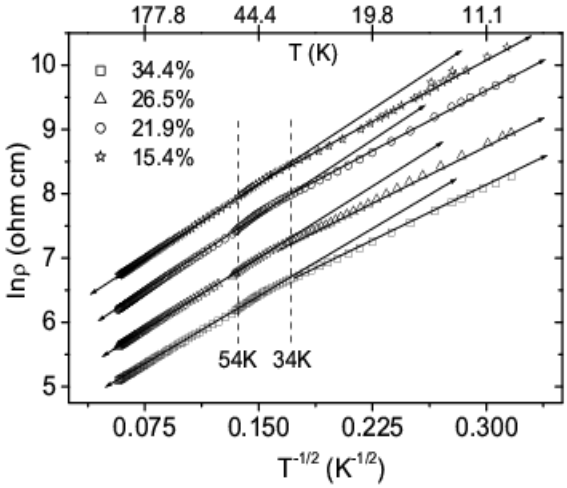


Fig. 2 Plot of lnρ vs linearly $T^{-1/2}$. lnρ varies linearly with $T^{-1/2}$. The crossover region is marked ny dotted vertical line.

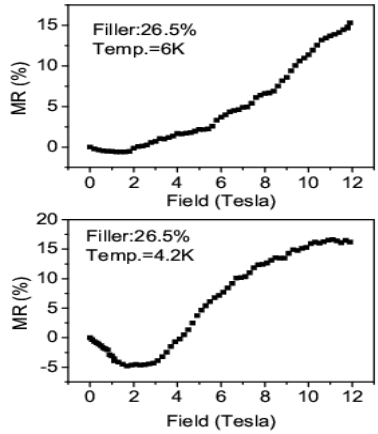


Fig.3 Plot of Magnetoresistance of composite. A crossover from negative to positive occurs.

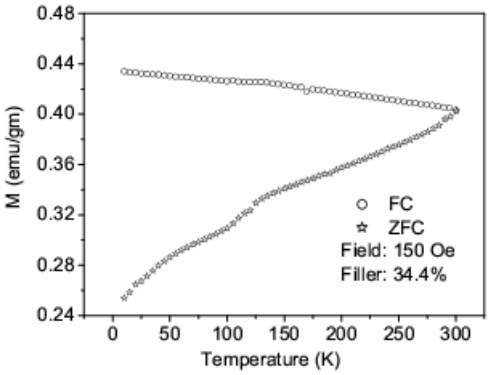


Fig.4 The FC-ZFC plot of composite from 300K-10K. High blocking temperature is observed.

SIZE AND QUALITY CONTROL OF COBALT FERRITE NANOCRYSTAL SYNTHESIS USING A MAGNETO-OPTICAL PROBE

Gabriel Shemer, Einat Tirosh, and Gil Markovich
School of Chemistry, Raymond and Beverly Sackler Faculty of Exact Sciences, Tel-Aviv University, Tel-Aviv, Israel

gshemer@post.tau.ac.il

Controlling the structure and composition of ternary compounds is a formidable task. In particular obtaining the correct phase of the same materials in the form of colloidal nanocrystal dispersion is even more difficult since the temperatures that can be applied in the synthesis of colloidal oxide nanoparticles are limited by solvent boiling/decomposition temperatures, which are usually much lower than the proper annealing temperatures required for achieving equilibrium structures in the bulk materials. At the elevated temperatures used in bulk materials synthesis the colloidal particles would agglomerate and sinter to larger crystals. Ferrites have a spinel-type crystal structure, where the lattice is constructed of a fcc structure of the oxygen ions, and two types of metal cation interstitial sites, the tetrahedrally coordinated 'A' site, and the octahedrally coordinated 'B' site. Cobalt ferrite has a partially inverse spinel structure, where the Co^{2+} ions occupy both the A and B sites and so does the Fe^{3+}.

The present study focused on developing a colloidal $CoFe_2O_4$ (cobalt ferrite) nanocrystal synthesis using magneto-optical (MO) spectroscopy as a probe of the insertion of the Co^{2+} ions into the ferrite lattice. We have developed a new cobalt ferrite synthesis using mixed types of organometallic precursors and compared to cobalt ferrite nanocrystals produced according to previously reported synthesis techniques. The standard characterization techniques (e.g., EDS, SQUID magnetometry, provided similar results for the nanocrystals prepared by the different syntheses (roughly Co/Fe ratio of 0.5), while MO spectroscopy yielded very different results for the various syntheses[1]. MO spectroscopy is a site-specific probe, since it probes localized electronic transitions at distinct crystal interstices and thus used to probe the concentration of the Co^{2+} ions in the ferrite lattice. The newly developed synthesis produced nanocrystals with a significantly higher inclusion of cobalt ions in the crystal lattice compared with other synthesis schemes published in recent years, which probably have most of the Co out of the lattice or as Co^{3+}. The second part of the study examined the influence of the addition of co-surfactant polyol type molecules on the synthesized cobalt ferrite nanocrystals. The addition of the co-surfactant was found to increase the size of the synthesized nanocrystals, while the MO spectra revealed that the size

increase was accompanied by a decrease in the concentration of the Co^{2+} ions incorporated into the ferrite lattice.

The achievement of control over cation distribution in the ferrite particles is less important in the case of tuning the magnetic properties of the nanocrystals and more important in the case of using the nanocrystals for magneto-optical applications. Moreover, this study is a significant milestone in the development of general preparation schemes of stoichiometrically and size controlled multi-cation oxide nanocrystals and in the application of suitable characterization probes.

Poster

CHIRALITY OF SILVER NANOPARTICLES SYNTHESIZED ON DNA

Gabriel Shemer,[1] Olga Krichevski[1], and Gil Markovich[1]

Tatiana Molotsky,[2] Irit Lubovitz,[2] and Alexander B. Kotlyar[2]

1)School of Chemistry,Raymond and Beverly Sackler Faculty of Exact Sciences.

2)Departmentof Biochemistry,George S.Wise Faculty of Life Sciences,

Tel Aviv University,Tel Aviv,69978,Israel

gshemer@post.tau.ac.ilT

Chiral imprinting in molecular and polymer films and enantioseparations using chiral substrates are well known phenomena.[1] It has been found that the binding of chiral molecules to a substrate lacking optical rotation has induced optical activity in the substrate. Small metal clusters have been shown to exhibit optical activity depending on their arrangement[2] or growth template. These metallic nanoparticles have usually been grown through the reduction of metallic cations using various templates (e.g., various surfactants and peptides). DNA was found to be an excellent template for the growth of metallic nanoparticles.[3] In this work we demonstrate that a DNA template induces chirality of silver nanoparticles grown in it. The silver particles were produced by reduction of Ag^+ bound to 700 base pairs poly(dG)-poly(dC). The complex between the DNA and Ag^+ ions is stable and does not dissociate during size-exclusion HPLC. Reduction of Ag^+ with $NaBH_4$ in anaerobiosis resulted in the appearance of a new band centered around 425 nm in the absorption and CD spectra of the complex. This band in the CD spectrum is associated with the plasmon of the silver nanoparticles formed on the poly(dG-)-poly(dC) scaffold. In order to understand whether or not the chirality is induced in the particles during its formation in the optically active DNA environment we have prepared silver nanocrystals separately from the DNA and complexed them with the DNA afterwards. Only the silver particles, which were grown on the DNA template, show a characteristic CD spectrum in the 350-550 nm region. Neither Ag nanocrystals in solution nor the nanoparticles absorbed to the DNA (post-synthesis) showed CD response around 400 nm (see figure below). Based on the similarity of the TEM images of the two types of DNA-Ag samples and large difference between the CD spectra of the two samples we suggest that the DNA directed asymmetric assembly of the particles from Ag atoms bound to this chiral template. The Ag nanocrystals produced in optically inactive aqueous environment by reduction of Ag^+ atoms and further complexation of the particles with the DNA lack this chirality. The passivation of small gold clusters with chiral molecules gives rise to optical activity[4]. Several explanations for this optical activity were thought of, among them the formation of a chiral metal core due to the influence of the chiral ligand

molecules on the formation of the cluster or through chiral arrangements of the ligands on an achiral metal core. We believe that in our case of the former explanation is more plausible than the latter one.

References:

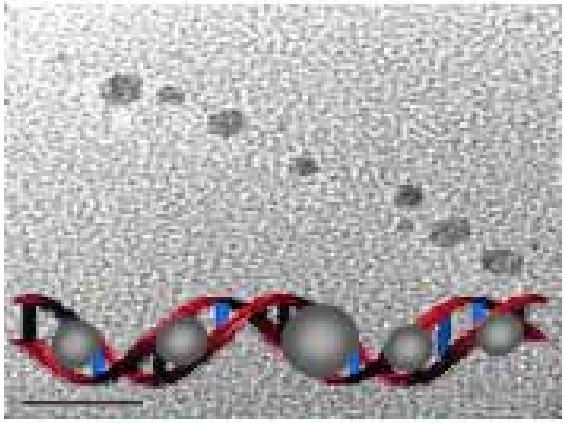
[1] S. Che, Z. L iu, T. Ohsuna, K. Sakamoto, O. Terasaki, T. Tatsumi, Nature 429(2004), 281.

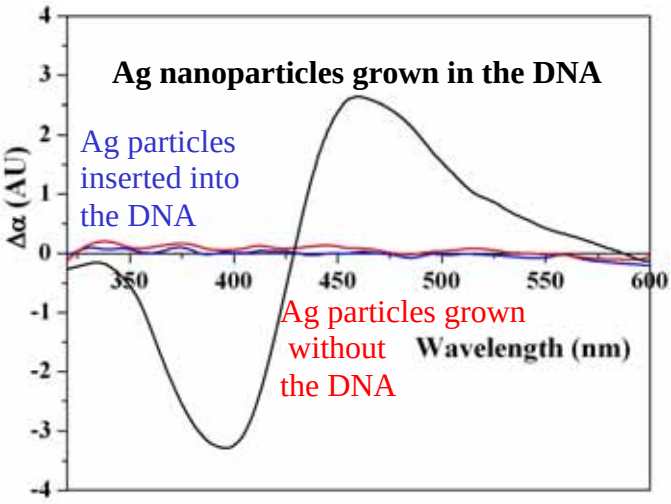
[2] V.P. Drachev, W.D. Bragg, V.A. Pdolskiy, V.P. Safanov, W.T.Kim, Z.C. Ying, R.L. Armstrong and V.M. Shalaev, J. Opt. Soc. Am. B, **18**(2001), 1896.

[3] J. Richter, Physica E, **16**(2003), 157.

[4] T.G. Schaaff and R.L. Whetten, J. Phys. Chem. B., **104**(2000), 2630.

Figures





Poster

STRUCTURE-PROPERTY RELATIONSHIPS OF POLYSTYRENE/LAYERED SILICATE NANOCOMPOSITES AS A FUNCTION OF THEIR PREPARATION

Siengchin S., Karger-Kocsis J.

Institut für Verbundwerkstoff GmbH (Institute for Composite Materials), University of Kaiserslautern, Germany

suchart.siengchin@ivw.uni-kl.de

In the past decade, polymer nanocomposites have attracted great attention because of their excellent physical-mechanical properties [1-2]. The exfoliation of layered silicate (LS) particles in thermoplastic matrices was found extremely effective to improve their thermal and mechanical properties. Note that pristine layered silicates, being hydrophilic in nature, have low interaction with polymers. Accordingly, no intercalation/exfoliation take place and the resulting material is a micro- instead of the targeted nanocomposite. In order to support the intercalation/exfoliation of LS, they have to be modified. This occurs via cation exchange in aqueous slurry using suitable cationic tensides as organophilic modifiers. This modification makes the organophilic LS to an expensive "nanofiller". The question is whether it is possible to use pristine layered silicate to produce thermoplastic nanocomposites. The basic idea is that water may serve as "modifier" for the LS as water swells them and thus increase the gallery distance between the layers. This project was aimed at producing polystyrene (PS)-based nanocomposites by various methods and compare their properties. In case of the masterbatch method pristine LS was added to a PS-latex, the resulting material dried and then melt mixed with additional PS granules in a heated kneader prior to hot pressing. For comparison propose a PS composite was produced by incorporating the LS in the PS melt (termed direct melt mixing). The mechanical and thermo-mechanical properties of the PS composites with varying LS contents were determined and the differences traced to the dispersion state of the LS.

Sodium fluorohectorite with an interlayer distance of 0.94 nm served as LS. PS latex with 50 wt% dry content was used as LS swelling agent. Granulated PS was utilized as polymeric matrix for all composite systems. A scheme of the masterbatch technique is given in Figure 1. After evaporation of the water at room temperature for 48 h and in an air circulated oven for 12 h it was introduced in the PS melt in a Brabender Plasticorder. Sheets were produced by hot press. TEM observations revealed that melt compounding did not result in delamination of the LS. On the other hand, the masterbatch technique resulted in a far better dispersion of the LS particles – cf. Figure 2. The effect of composite preparation is obvious when plotting the storage moduli of the materials as a function of temperature at various LS contents – cf. Figure 3. One can recognize that the stiffness of those composites which were prepared by direct melt compounding always inferior to those prepared by the masterbatch technique. This is due to the better dispersion of the LS in the related systems in accordance with the TEM results (cf. Figure 2). Figure 4 collates the creep compliance values for the neat PS and its composites produced by direct melt mixing and masterbatch methods. The shape of the creep curves of the nanocomposites is very similar to that of the unfilled PS, but their creep compliance values are much smaller compared to the unfilled PS. For the composites containing 4.5 wt% LS the creep compliance was reduced by ca. 40 % and 10 % compared to the neat PS when produced by the masterbatch and direct melt compounding, respectively. This creep behavior is a signature of the better intercalation/exfoliation achieved through the masterbatch technique.

In this work, we have demonstrated that pristine layered silicate (LS) can be easily and well dispersed in polystyrene (PS) by a masterbatch technique. The latter means that LS is "predispersed" in a PS latex. Improvements in the thermo-mechanical behavior (increased

stiffness, reduced creep) when compared with results achieved on direct melt compounded systems were attributed to the better dispersion of the LS. This was evidenced by TEM results.

References:

[1]Zhang, M. Q., Rong, M. Z. and Friedrich, K.: Processing and properties of nonlayered nanoparticle reinforced thermoplastic composites in *"Handbook of Organic-Inorganic Hybrid Materials and Nanocomposites"* (Ed.: Nalwa, H. S.), Am. Sci. Publ., Los Angeles, CA, 2003, Vol.2, pp. 113-150.

[2]Karger-Kocsis, J. and Zhang, Z.: Structure-property relationships in nanoparticle/semicrystalline thermoplastic composites in "*Mechanical Properties of Polymers Based on Nanostructure and Morphology*" (Eds.: Michler, G.H. and Baltá Calleja, F.J.), CRC, Boca Raton, FL, (2005), Ch. 13, pp. 553-602.

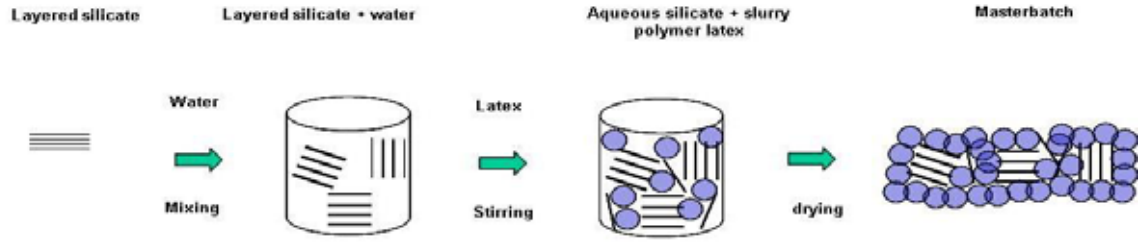
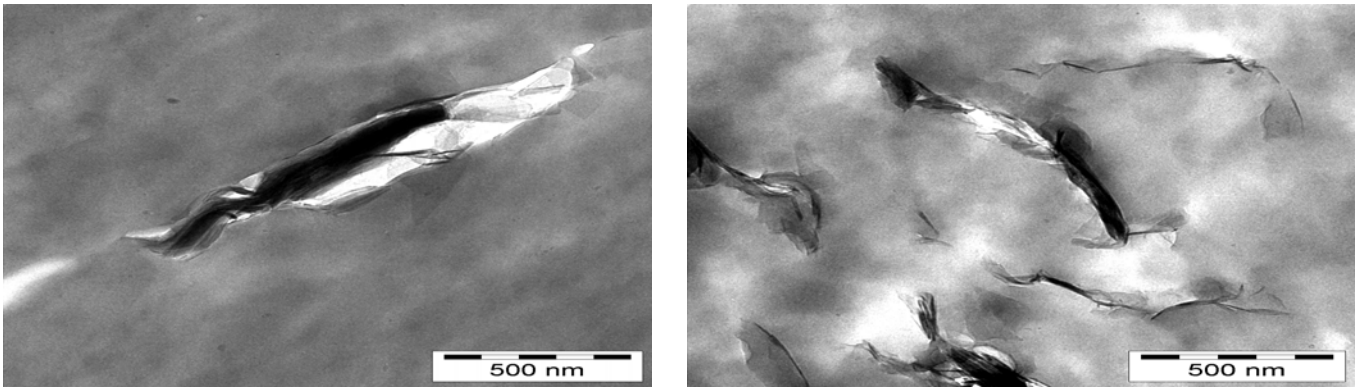


Figure 1: Scheme of PS/silicate nanocomposite preparation by masterbatch technique.



a) b)

Figure 2: TEM micrographs of PS+4.5 wt% silicate prepared by different methods a) direct melt mixing b) masterbatch technique

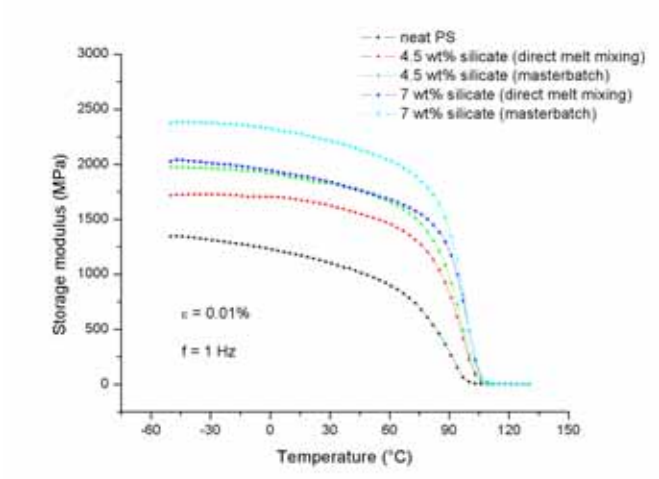


Figure 3: PS and its silicate nanocomposites prepared by different methods: Storage moduli as function of temperature.

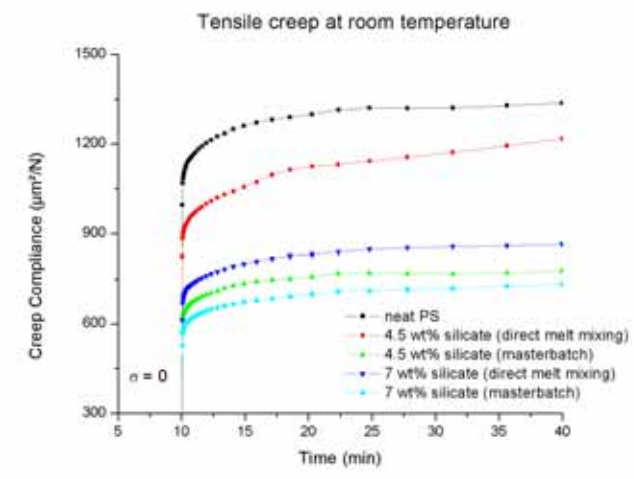


Figure 4: Creep of the neat PS and its silicate nanocomposites prepared by different methods (Notes: Stress applied at t = 10 min).

ORGANO-VERMICULITE STRUCTURE ORDERING AFTER PVAC INTRODUCTION: EXPERIMENT AND MODELING

Gražyna Simha Martynková, Marta Valášková
Institute of Materials Chemistry, VŠB-TU Ostrava, 17.listopadu 15, Ostrava-Poruba, Czech Republic
Grazyna.Simha@vsb.cz

Interactions of clay minerals with organic polymers have increasing interest from the industrial and scientific perspectives. Layered silicates, in particular clay minerals, have been used because their excellent intercalation abilities.
Natural clays, containing inorganic cation in interlayer, are hydrophilic, while exchanging an inorganic cation to certain large organic cation, the clay properties are altered and material becomes hydrophobic.

The role of surfactant molecules is to prepare more opened organophilic host material with larger interlayer spacing. The alkyl ammonium ions of surfactant are cationic exchanged for the inorganic cations in clays, a lateral bilayer or inclinated paraffin–like structure results. At higher concentration of onium ions a lipid–like structure is formed [1].This organo-clay readily accepts other neutral molecules. The combination of a nano-dimensional clay material with a polymer may yield either a microcomposite, in which the clay is acting as filler and is not dispersed at the nanometer level, or a true nanocomposite. Though vinyl acetate is water-soluble, there is not required an organophility of vermiculite; organo-vermiculite assured suitable space for monomer sorption and polymerization.

Simulation techniques become an essential adjunct to experimental techniques, since the information about the spatial arrangement of molecules within the interlayer is hard to obtain without the aid of computer simulation [2, 3].

In this study were observed:

- Changes of vermiculite interlayer space after intercalation with different quaternary ammonium salts using X-ray diffraction method.
- Changes of organo-vermiculite structure after introduction of monomer and following polymerization Fig.1.
- Molecular interaction of individual components in the modified vermiculite and nanocomposite using IR spectroscopy.
- Simulation possibilities for the nanocomposite systems Fig.2.

References:

[1] N.A.D'Souza in: H.S.Nalwa (Ed.) Encyclopedia of Nanoscience and Nanotechnology 3, Am. Sci. Publishers, 2004 253-265
[2] R.Toth, A.Coslanich, M.Ferrone, M.Fermeglia, S.Pricl, S.Miertus, E.Chiellini, Polymer **45** (2004) 8075.
[3] K.S.Katti , D.Sikdar, D.R.Katti, P.Ghosh, D.Verma, Polymer **47** (2006) 403.

Figures:

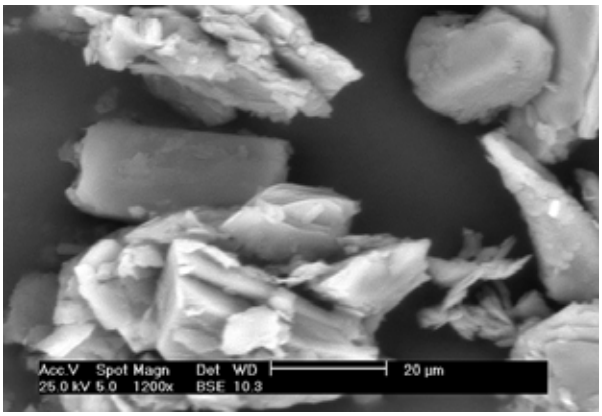


Fig.1 Scanning electron microscopy image of nanocomposite

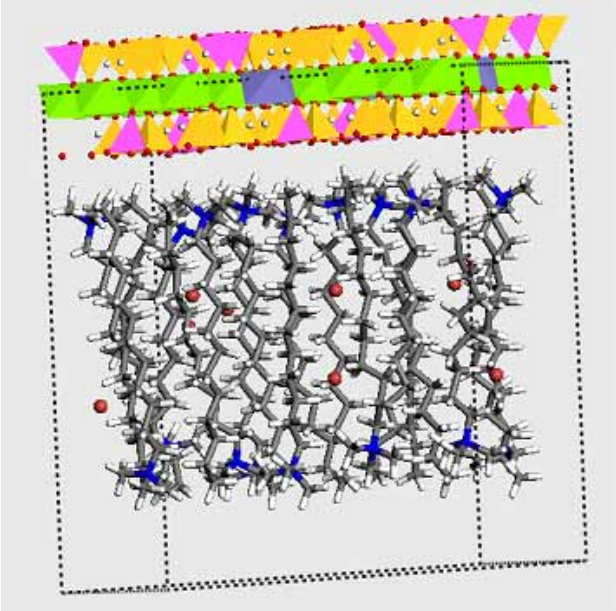


Fig.2 Structure of organo-vermiculite simulated using *MS Accelrys*

ZnO NANOCRYSTALLITES OBTAINED BY OXIDATION OF ZINC ARACHIDATE – ARACHIDIC ACID LB MULTILAYERS

Sukhvinder Singh, R.S. Srinivasa†, S.S. Talwar and S.S. Major
Department of Physics, †Department of Metallurgical Engineering and Materials Science, Indian Institute of Technology Bombay, Mumbai-400076, India
sukhvinder@iitb.ac.inT

Formation of ultrathin and homogenous metal oxide films has been reported by either direct oxidation[1] or oxidation subsequent to UV treatment of precursor Langmuir-Blodgett (LB) multilayers[2]. In the present work, the direct oxidation method has been exploited to form uniformly distributed, isolated and nearly mono-disperse nanocrystallites of ZnO on quartz and freshly cleaved mica substrates using zinc arachidate - arachidic acid (ZnA - AA) composite LB multilayers as precursors.

ZnA LB multilayers transferred at different subphase pH in the range 5.0 to 6.2 have been studied by X-ray reflection (XR) and Fourier transform infrared spectroscopy (FTIR). Fig. 1 shows the FTIR spectra in the region 1300 cm^{-1} - 1800 cm^{-1} for ZnA multilayers. These results show that as the subphase pH is lowered, there is a gradual decrease in the intensity of the carboxylate asymmetric stretching band (at ~1539 cm^{-1}) and increase in the intensity of C=O band (at ~ 1700 cm^{-1}), indicating a decrease of ZnA content with a corresponding increase of AA content in the multilayers. The X-ray reflection (XR) studies of the multilayers transferred at different subphase pH showed the presence of single phase layered structure (with bilayer period of 47 Å) in all the multilayers. However, the intensities of the Bragg peaks are found to diminish with decreasing subphase pH. These observations suggest mixing of ZnA and AA at molecular level and decrease of zinc content with decrease in subphase pH.

The precursor ZnA-AA multi-layers were oxidized in air at 400-700 °C. The XR patterns of ZnA-AA multilayers oxidized at 150 °C show the disappearance of Bragg peaks, which suggests the complete destruction of layered structure. FTIR studies of the oxidized multilayers showed that with increase in annealing temperature, the intensities of IR bands corresponding to various organic groups decrease and finally disappear in the case of the film oxidized at 400 °C. This indicates the complete removal of organic moieties at the oxidation temperature of 400 °C. UV-Visible studies of ZnA-AA multilayers at different oxidation temperatures corroborate the FTIR observations and show the appearance of absorption edge of zinc oxide subsequent to oxidation at or above 400 °C.

ZnA-AA mixed multilayers having different ZnA contents were oxidized at 700 °C and their optical absorption and surface morphology were studied by UV-Visible spectroscopy and atomic force microscopy. Typically, the ZnA multilayers transferred at a subphase pH of 6.2 on quartz substrates and oxidized above 400 °C show the absorption edge at ~ 3.2 eV, close to the bulk band gap of ZnO. The multilayers transferred at a lower subphase pH, of 5.0, with much reduced zinc content and oxidized at 700°C also show a weak absorption edge at ~ 3.0 eV (Fig. 1(b)). The AFM image of a 15 monolayer ZnA film transferred at a subphase pH of 6.2 shows the presence of ~ 2 μm clusters of nanocrystallites having size 20-40 nm (not shown here). In contrast, the AFM image of a 15 monolayer ZnA films transferred at subphase pH of 5.0 and oxidized at 700°C shows a large number of nanocrystallites of average size ~ 10 nm. In order to further decrease the ZnA content in the precursor ZnA-AA

multilayers and obtain isolated nanocrystallites, LB films with lesser number of monolayers were transferred at subphase pH of 5.0. AFM studies of these multilayers showed a decrease in spatial density and narrowing of size distribution of nanocrystallites with decreasing number of monolayers in the precursor multilayer. Fig. 2 shows a typical AFM image of a seven-monolayer LB film on mica substrate, oxidized at 700 °C. This image shows uniformly distributed isolated nanocrystallites of average size ~ 11 ± 3 nm. Most of the nanocrystallites were in a narrow size range of 10 - 15 nm. Thus, the control of zinc content of the precursor LB multilayers achieved through proper selection of subphase pH and number of monolayers is seen to result in a reduced surface density of isolated nanocrystallites with a narrow size distribution.

References:

[1] M. Parhizkar, N. Kumar, P.K. Nayak, S. Singh, S. S. Talwar, S. S. Major and R. S. Srinivasa. Colloids and Surfaces A: Physicochem. Eng. Aspects, **257–258** (2005) 445.
[2] M. Schurr, M. Seidl, A. Brugger and H. Voit, Thin Solid Films, **342** (1999) 266.

Figures:

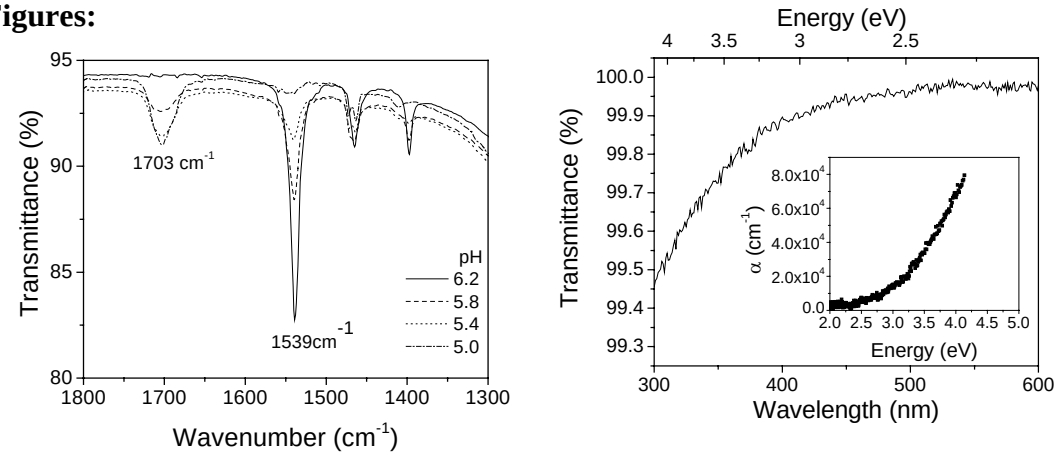


Fig. 1. (a) FTIR transmission spectra of ZnA - AA composite multilayers in the range 1300 - 1800 cm^{-1}, transferred at different subphase pH values. (b) UV-Vis. spectrum of nanocrystalline ZnO obtained by oxidation at 700°C of 15 monolayer ZnA-AA LB multilayer transferred at subphase pH 5.0.

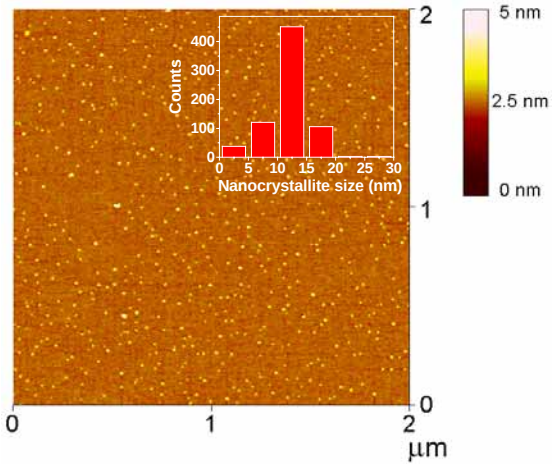


Fig. 2. AFM image of ZnO nanocrystallites obtained by oxidation at 700ºC of a 7-monolayer ZnA LB multilayer transferred on mica substrate at subphase pH value of 5.0.

SYNTHESIS OF CARBON NANOTUBES (CNT) BY PLASMA – CHEMICAL METHODS AND THE INFLUENCE OF PLASMA PARAMETERS ON NANOTUBES GROWTH

Smovzh Dmitry Vladimirovich
Institute of termophysics SB RAS
630090, Russia, Novosibirsk, prosp. Lavrentyev 1.
smovzh@itp.nsc.ru

Carbon nanotubes (CNTs) are one of the most exciting nanoscale structures to have been produced in recent years. Chemical vapour deposition (CVD) is the most flexible method of producing carbon nanotubes. Depending on the conditions of growth one can obtain individual single walled nanotubes (SWNT), bundles of SWNT, multi-walled nanotubes (MWNT) and films of aligned MWNT. However, the quality of the grown material is often less than optimal. Moreover, the variety of different types of CNTs might be disadvantageous for specific applications. Plasma CVD on the other hand does make it possible to increase growth rates and, in addition, the charged nanotubes become sensitive to external electric fields and might be manipulated in the required manner. In the present work, demonstrate the efficient bulk production of SWNT in a novel low-pressure CVD reactor combined with an electrophoretic cell. We illustrate for the first time that *in situ* dc electrophoresis can be used to efficiently extract SWNT from other carbon-containing materials produced in the gas phase CVD process. The results indicate that the nanotubes are negatively charged during gas phase growth, providing a powerful tool for manipulation and further purification.

Experimental setup.

Our novel growth reactor exploits a combination of low–pressure gas phase CVD growth with an electrophoretic cell. It consists of a gas feedthrough system, an evacuated bell jar with heated stainless steel tube and a cylindrical electrode (Fig.1). A gas mixture containing the carbon feedstock gas (C_2H_2) and buffer gases (Ar, H_2) is blown through the hot vertical stainless steel tube with a flow rate in the range of 50-100 sccm. Iron catalyst particles are synthesized by thermal decomposition of iron pentacarbonyl directly in the reactor. The pentacarbonyl is delivered to the reaction zone by bubbling C_2H_2 through a vessel containing liquid iron pentacarbonyl at 0^o C. The thermally isolated hot tube is placed inside the vacuum chamber and connected to a vacuum pump through a filter, where carbon soot is collected. The inner diameter of the tube is 20 mm and the length of the hot zone is 180 mm. The gas temperature is measured by a thermocouple suspended on the reactor axis in the gas flow. Pressure is varied by control of the gas flow rate and the pumping speed by inlet and outlet valves. An electric field can be generated by applying a voltage between the hot tube wall and a retractable coaxial central electrode of 1,5 mm diameter and some experiments were carried out with hollow cathode (when central electrode was before the hot zone of tube). Three regimes were explored - "thermal CVD" without field, "PECVD" with field higher than breakdown value, and "electro trapped CVD" with intermediate field.

The carbon-containing material was collected from the electrodes and the output filter and imaged by scanning and transmission electron microscopy (SEM (JSM 6301F)/TEM (JEM2010)) and investigated by micro-Raman spectroscopy (inVia Renishaw microscope with 488, 514, 568, 785 nm excitation wavelengths) after dispersion in organic solvents without surfactants.

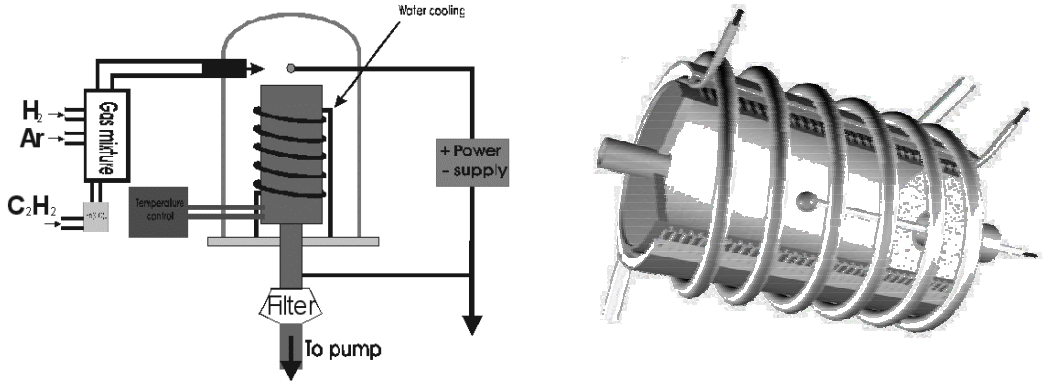


Fig.1 Experimental setup. With hollow cathode – left. And modification of heated tube for experiments with central electrode - right.

Results.

A preliminary set of experiments was performed without the presence of an electric field to determine the range of parameters optimal for CNT production. TEM was used for a qualitative estimation of the dimensions and partial yield of CNTs. In carbon material collected from the filter after an experiment using a $C_2H_2/Ar/H_2$ mixture at 5/80/10 sccm flow rates, at a pressure of 15 Torr and a temperature of 800^o C, two main fractions of carbon material were found – SWNTs and encapsulated metallic particles. No CNTs were found on the filter after experiments with the hollow cathode gas discharge. TEM investigation of the carbon deposit did not show any changes in the distribution of encapsulated particles compared to the results discussed above, which means that the absence of CNTs is not related to the catalyst transformation. Surprisingly, carbon nanotubes were found on the anode surface placed upstream in the cold zone. These CNTs were not formed at the anode surface but were transported from the hot zone by the electric field. We conclude that the electrophoretic force is large enough to transport the nanotubes even inside the hollow cathode where the electric field is relatively small.

Further investigation was aimed at carbon species separation by using a radial electric field inside the hot tube. The electrode was placed coaxially inside the grounded hot tube. Soot was collected from both electrodes and filter and investigated with SEM/TEM and micro-Raman for different gas compositions and electric field distributions. In all experiments with different polarity the structure of the material deposited on the “filter” looks closer to amorphous with encapsulated metallic particles, only very slight percent of short SWNT were found. More importantly, there is a clear difference in the structure of the material collected from the anode and the cathode. The cathode material contains more encapsulated particles and the relative yield of CNTs is much lower than for the anode material.

The obtained results showed that electrophoresis of CNTs at relatively low electric fields caused the motion of CNTs to the electrodes, predominantly to the anode. On other hand, dielectrophoresis of CNTs is known to be the most promising method for CNT separation into semiconducting and metallic materials after growth. Analysis of the times required for such a CNT separation, taking into consideration the viscous forces and growth time in a thermal CVD reactor, does not allow to combine them in one set up. CNT charging in a plasma creates a much more powerful way of controlling CNT transport and separation. The most promising application of this study might be in situ control over different nanometre – scaled carbon particles and their separation according to electronic properties, directly in the preparation stage.

STRUCTURAL AND OPTICAL PROPERTIES OF BI_2S_3 NANOPARTICLE FILMS PREPARED BY CHEMICAL BATH DEPOSITION

L.I. Soliman

National Research Centre, Cairo, Egypt

The structural and optical properties of thin films of Bi_2S_3 prepared by the chemical bath deposition technique are described. X-ray diffraction, electron microscope measurements and energy – dispersive X-ray analysis showed that the films have nearly stoichiometric nanoparticles structure. All prepared films were uniform and adhesive with mean diameter varying from 7 to 34 nm. The investigated samples were characterized by measuring the transmission and reflection spectra with wavelength range from 500 to 2500 nm. The optical studied revealed that the Bi_2S_3 films have an absorption coefficient $\alpha \approx 10^4$ cm^{-1} and their optical band gap varies between 2.06 to 1.65 eV. This is attributed to the quantum size. The effect of bath temperature on the structural and optical properties is studied.

Poster

THE MECHANISM OF METALLIC NANOPARTICLES FORMATION DURING THERMOLYSIS OF LAYERED DOUBLE HYDROXIDES CONTAINING $[M(edta)]^{2-}$ COMPLEXES (M = Ni, Co, Cu)

Starikova E.V.[1,2], Isupov V.P.[1], Chupakhina L.E.[1], Mitrofanova R.P[1]., Tarasov K.A.[1], Yulikov M.M.[3]

[1]Institute of Solid State Chemistry and Mechanochemistry SB RAS, 630128, ul. Kutateladze, 18, Novosibirsk, Russia

[2]Novosibirsk State Univesity, 630090, ul. Pirogova, 2, Novosibirsk, Russia

[3]Boreskov Institute of Catalysis SB RAS, 630090, Pr. Lavrent'eva, 5, Novosibirsk, Russia

Katya@solid.nsc.ruT

Due to the unique properties of the metallic nanoparticles, the preparation of nanocomposites is of special significance. Such materials offer some attractive possibilities in biomedicine, catalysis, magneto- and radiotechnology and so on. Recently it has been shown that the layered intercalation compounds such as layered double hydroxides pillared with the organic complexes of transition metals can be used as precursors that give composites containing stable metallic nanoparticles inserted into oxide matrix [1, 2].

Layered double hydroxides (LDHs) have the general formula $[M^{2+}_{1-x}M^{3+}_{x}(OH)_2]^{x+}(A^{n-})_{x/n}\cdot mH_2O$, where $M^{2+} = Mg^{2+}$, Ni^{2+}, Co^{2+}, etc. and $M^{3+} = Al^{3+}$, Cr^{3+}, Fe^{3+}, etc. Their structure consists of positively charged layers separated by interlayer anions A^{n-} and solvent molecules. If LDH contain an organic complexes of transition metals as anion A^{n-}, its thermolysis in vacuum results in the reduction of transition metal cation. Hydroxide layers decomposition and the destruction of metallic complex can can be either simultaneous or not, which in turn has an effect on the properties of the particles obtained this way. Consequently, LDH can be considered as nanoreactors. The properties of composites obtained in them, depends on nanoreactor properties. Understanding the nanoparticles formation mechanism occuring in LDH and the principles of nanoparticle stabilization allows to control the desired properties of the composites prepared.

We have synthesized LDHs formed by couples of metals M^1-Al (M^1 = Li, Ni, Co) and pillared with complexes $[M^2(edta)]^{2-}$ (M^2 = Ni, Co, Cu; *edta* = ***e**thylene**d**iamine**t**etera**a**cetate*) (further referred to as M^1,Al-M^2(*edta*)). M^1,Al-M^2*(edta)* ($M^1 = M^2$ = Ni, Co) are of particular interest since they contain transition metal cations capable of reducing to metallic state and located both in the hydroxide layers $[M^{2+}_{1-x}Al_x(OH)_2]^{x+}$ ("in-layer" metal) and between them as interlayer species $[M^2(edta)]^{2-}$ ("interlayer" metal). In contrast, Li,Al-M^2(edta) (M^2 = Ni, Co, Cu) lacks "in-layer" metal.

The aim of the work was to investigate the thermal behaviour of these precursors, to reveal the mechanism of their thermolysis and to find the peculiarities of the resulted composites.

The precursors M^1,Al-M^2*(edta)* (M^1 = Li, Ni, Co; M^2 = Ni, Co, Cu) were obtained by the anion exchange of choride anions by $[M^2(edta)]^{2-}$. The chloride forms of M^1,Al-LDHs (M^1 = Ni, Co) were synthesized by the interaction of solid dawsonite $NaAl(OH)_2CO_3\cdot nH_2O$ with the aqueous solutions of transition metal salts [3]. The chloride form of Li,Al-LDH was prepared by the intercalation of lithium chloride into gibbcite $Al(OH)_3$ [4]. Thereafter, precursors containing organic metal complexes were thermally decomposed in vacuum at different temperatures. To gain a better understanding of complex thermolysis of LDHs with organic anions thermal decomposition of individual parts (i.e. LDH matrixes and salts of EDTA) are also analyzed. The thermolysis processes and the products of pyrolysis were investigated by thermal analysis, mass-spectrometry of gaseous thermolysis products, XRD, IR-spectroscopy, ferromagnetic resonance, SEM, TEM, chemical analysis.

Powder XRD data indicate that the interlayer distance in all M^1,Al-M^2*(edta)* decreases on ~2-3 Å during heating in vacuum up to 200°C. This can be attributed to the removal of the molecular water from the interlayer space as it was confirmed by DSC and TG analysis. Obviously this process is accompanied by the re-orientation of *edta* complexes. The

dehydration of the hydroxide layers starts above 200°C. Amorphious product is formed at 300-325°C. The "grafting" effect is observed for Li,Al-M(edta) (M = Ni, Co), i.e. the oxygen atoms of *edta* enter partially into the hydroxide layers.

IR-spectra of thermally treated M^1,Al-M^2*(edta)* (M^1 = M^2 = Ni, Co) show the organic ligand EDTA begins to decompose above 315-325°C. This is in good agreement with the results of mass-spectometry of gaseous products evolving during the thermal decomposition.

The formation of metallic nickel and cobalt from M^1,Al-M^2*(edta)* and Li,Al-M^2*(edta)* (M^1 = M^2 = Ni, Co) was detected by XRD. The temperature of thermolysis necessary for their formation is 340-350°C for Ni and 400°C for Co. The estimated grain size of metal particles obtained from M^1,Al-M^2*(edta)* (M^1 = M^2 = Ni, Co) and Li,Al-Ni*(edta)* is about 2-5 nm. The size of cobalt particles as well as those of copper obtained via the thermolysis of Li,Al-Cu*(edta)* at 250°C varies in the range of 5-100 nm.

Also the fact of the growth of Ni and Co phase was detected by ferromagnetic resonance method (FMR). The FMR signal of Ni,Al-Ni*(edta)* is observed during the thermolysis above 325°C, which evidences the formation of the superparamagnetic nickel particles. It was shown that the thermolysis at 340-400°C leads to the formation of isotropic nickel particles. Above 400°C the metal particles can have both isotropic and anisotropic geometry. This is likely due to the formation of particles from the different fragments of the initial structure. At first, the "interlayer" nickel forms isotropic particles. This process is than followed by the reduction of the "in-layer" nickel yielding anisotropic particles of larger sizes. Analysis of FMR spectra of Li,Al-Ni*(edta)* calcinated at 400°C shows only the presence of the isotropic particles. The formation of small superparamagnetic (Co,Al-Co(edta) as precursor) and large ferromagnetic (Li,Al-Co(edta) as precursor) particles is evident from the FMR spectra.

TEM data of M^1,Al-M^2*(edta)* (M^1 = M^2 = Ni, Co) calcinated at 400°C are presented on Fig. 1.

The thermolysis of Na_2M(edta) (M = Ni, Co, Cu) was also studied and the results obtained allows to explain the metal particle formation mechanism in detail.

This work was supported by CRDF (Grant NO-008-X1), RFBR (№ 06-03-32107), the programme of Presidium of RAS (№ 8.16), the programme “Chemistry and physical chemistry of supramolecular systems and atomic clusters” (grant № 5.7.3).

References:

[1] V.P.Isupov, L.E.Chupakhina, et al. Solid State Ionics. **101-103** (1997) p. 265-270.
[2] K.A. Tarasov, V.P. Isupov et al. J. of Mater. Synth. Proc. **1** (2000) p. 21-27.
[3] Starikova E.V., Isupov V.P., et al. J. of Struct. Chem. Application. **45** (2004) p. 116-121.
[4] Nemudry A.P., Isupov V.P., et al. Reactivity of Solids. **1** (1986) p. 221-226.

Figures:

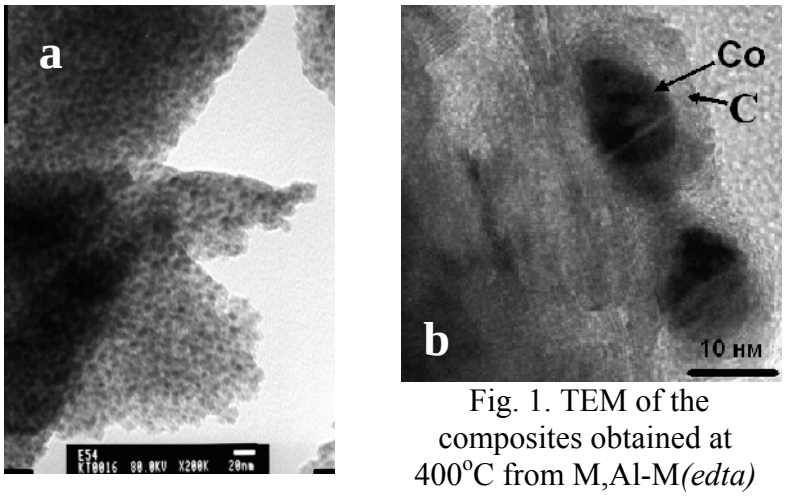


Fig. 1. TEM of the composites obtained at 400°C from M,Al-M*(edta)* (M = Ni (a), Co (b))

ION BEAM DEPOSITION OF NANOSCALED Ti AND TiN FILMS ON SILICON

A. Styervoyedov [a, b], *V. Farenik* [a, b]
[a] *Scientific Centre of Physical Technologies of MES and NAS of Ukraine, Svobody sq.6, 61022 Kharkiv, Ukraine*
[b] *V.N. Karazin Kharkiv National University, Svobody sq. 4, 61077 Kharkiv, Ukraine*
E-mail: standrey@yahoo.com

Titanium and titanium nitride films are more and more used as wear- and corrosion resistant coatings, including ultra-thin coatings for nanotechnologies. From the other side, titanium compounds play one of the important roles in modern micro- and nanoelectronics, where they are intensively used as, for example, optical coatings [1], buffer layers in multilayer structures [2, 3] and high-temperature contacts [4]. X-ray photoelectron spectroscopy (XPS) is one of the few instruments for chemical state analysis of surface due to its perfect elemental sensitivity. High surface sensitivity makes XPS more and more popular because of great interest to investigations of ultra-thin films for nanotechnology and nanoelectronics applications. When the film thickness doesn't exceed several monolayers, XPS also allows to investigate film / substrate interface and reactions, which occur there as the result of thermal annealing or ion bombardment. Such investigations are very interesting, for example, in nanoelectronics where the formation of different oxides or silicates (in the case of Si or SiC) on the interface strongly influences on electric characteristics of obtained structures. The aim of present work was formation of ultra-thin titanium and titanium nitride films, including Ti / TiN nanoscaled layers, by low current argon ions beam sputtering of pure titanium target in vacuum and nitrogen atmosphere and investigations of obtained films with X-ray photoelectron spectroscopy.

Ultra-thin (~ 5 nm) titanium and titanium nitride films were obtained by ion beam sputtering of titanium target of 99.99% purity in vacuum (Ti) and nitrogen atmosphere (TiN) using cold cathode ion gun. Ion gun was installed with the possibility of ion beam direction changing during the experiment, as shown on Fig.1. Such installation allows us to clean both the target and substrate with ions from natural oxides and contaminations before deposition. Titanium was sputtered by argon ions with the 5 keV energy and 15 $\mu A/cm^2$ ion current density. Vacuum before switching on the ion source was $4 \cdot 10^{-8}$ mbar. During switching on the ion source, Ar gas was introduced into discharge chamber of ion source up to the vacuum chamber pressure of $5 \cdot 10^{-6}$ mbar. To get Ti / TiN nanoscaled layers titanium target was sputtered on Si substrate, previously cleaned by ion beam, for 10 minutes without nitrogen leaking. After that nitrogen was introduced into the vacuum chamber and sputtering was continued for another 10 minutes. The substrate temperature during deposition was 350°C.

After deposition samples were transported from the preparation chamber to the analytical chamber without breaking vacuum for investigation by XPS. X-ray characterization was performed at the pressure of $5 \cdot 10^{-10}$ mbar using X-ray radiation of Mg-Kα. After the primary analysis samples were annealed for 5 minutes at the temperatures of 650°C and 750°C by electric current going directly through the sample. After each stage of annealing samples were investigated by XPS (Fig.2).

It was shown that it is possible to form both ultra-thin titanium films (sputtering in residual vacuum) and ultra-thin titanium nitride films (sputtering in the nitrogen atmosphere) in the same temperature conditions. In both cases oxygen is captured by titanium molecules from residual gas medium during deposition forming oxide component that decreases during annealing at 650^o C and almost completely disappears at 750^o C. It was also shown that by

low current Ar ion beam sputtering it is possible to form Ti/TiN nanoscaled layers by manipulation of nitrogen leaking to the vacuum chamber.

References:

[1] J.E. Klemberg-Sapieha et al., Applied Optics, Vol. **43**, No.13 (2004) 2670.
[2] P. Tiwari et al. Appl. Phys. Lett., **65** (21) (1994) 2693.
[3] H. Wang, Ashutosh Tiwari, A. Kvit, X. Zhang, and J. Narayanet, Appl. Phys. Lett., **80** (2002) 2323.
[4] J.R. Waldrop, Appl. Phys. Lett., **43** (1983) 87.

Figures:

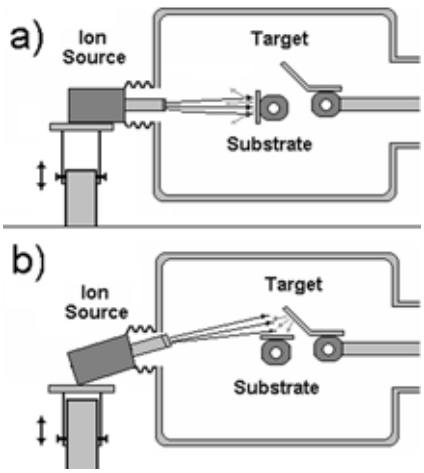


Fig.1. Schematic sketch of ion gun installation: a) substrate cleaning; b) ion beam sputter deposition.

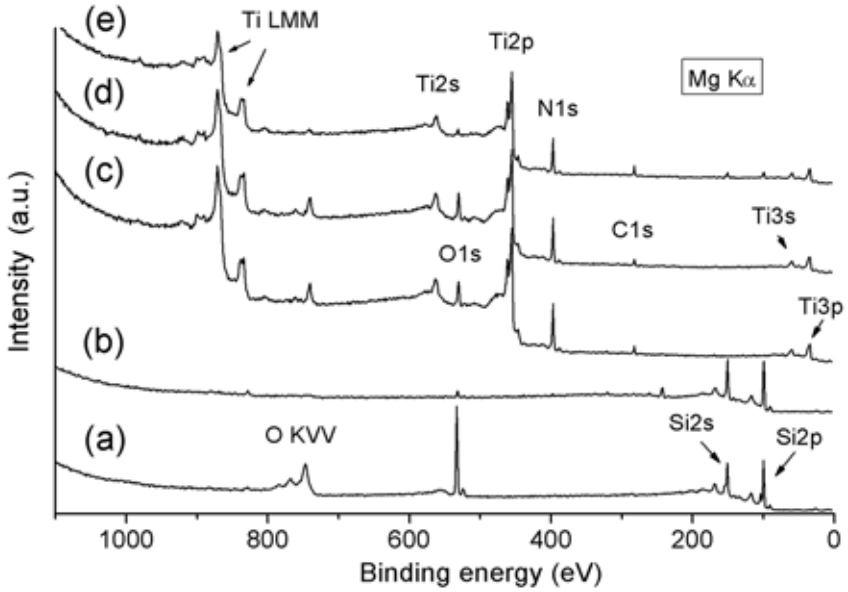


Fig.2. Wide scan XPS spectra of sample surface: (a) substrate before cleaning by ion beam; (b) after cleaning; (c) after titanium sputtering in nitrogen atmosphere; (d) after temperature annealing at 650°C 5 min; (e) after annealing at 750°C 5 min.

PREPARATION AND MICROSTRUCTURE OF TiO_2-NANOWIRE DISPERSED COMPOSITE ELECTRODE FOR DYE-SENSITIZED SOLAR CELLS

Yoshikazu Suzuki, Asagoe, Keisuke, Supachai Ngamsinlapasathian, and Susumu Yoshikawa
Institute of Advanced Energy, Kyoto University, Uji, Kyoto 611-0011, Japan
suzuki@iae.kyoto-u.ac.jp

TiO_2 powders are widely used for industrial applications, such as pigments, cosmetics, electronic devises, photocatalysts, catalyst supports, dye-sensitized solar cells, and so on. In order to improve various functions of TiO_2 powders, phase, size and morphology controlling have been extensively studied. Since the innovative work by Kasuga et al. in 1998-99 [1,2], TiO_2-derived one-dimensional (1-D) nanomaterials synthesized by the hydrothermal alkali treatment method, such as nanotubes, nanowires, and nanofibers, have attracted much attention because of their unique microstructure and promising energy-related applications. *e.g.*, lithium ion batteries, hydrogen storage, and dye-sensitized solar cells (DSCs) [3-5].

Since O'Regan and Grätzel firstly reported DSCs using nanocrystalline porous TiO_2 electrode in 1991 [6], a variety of semiconductor electrode have been investigated. Targeting on preparing efficient electron transfer paths through the electrode of DSCs, porous film electrodes composed of various 1-D nanomaterials have been fabricated. Using 1-D TiO_2 nanomaterials (as well as hydrogen titanates, which transform into TiO_2 at high temperatures) is a straightforward way to realize the "electron expressway concept [3]" (Fig. 1). An example of TiO_2-nanowire dispersed composite electrode is shown in Fig. 2.

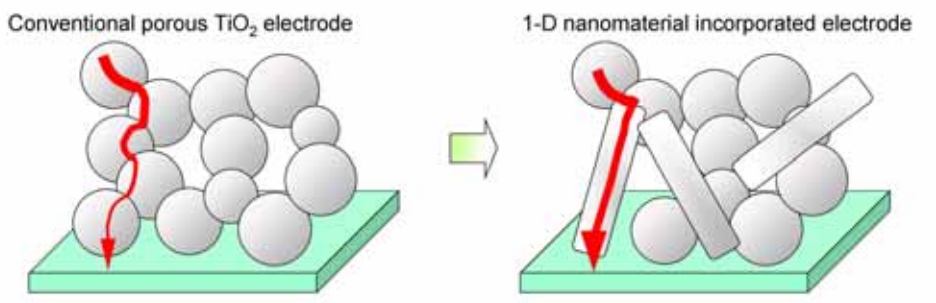


Fig. 1 "Electron expressway concept" by the incorporation of 1-D nanomaterials for DSC electrode. Arrow through particles means the electron transfer [3].

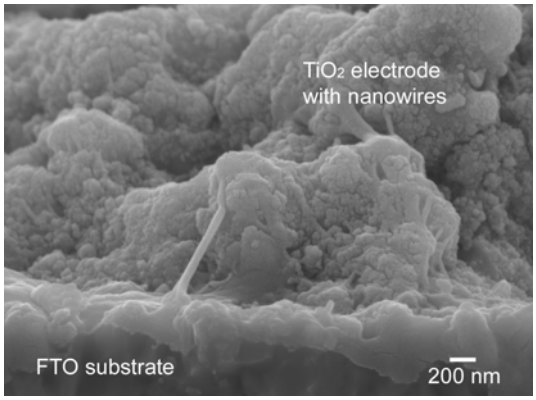


Fig. 2 An example of TiO_2-nanowire dispersed composite electrode prepared by a middle-stage (i.e., incomplete) hydrothermal treatment [3].

To harmonize the 1-D nanostructure and the high surface area of the electrode, we have attempted to fabricate partially nanowire-structured TiO_2, via a modified hydrothermal process, and to apply it for DSCs [3-5]. The idea is an analogy with "a road network system" where truck lines and narrow paths are combined for efficient mass transportation. To prepare the TiO_2 1-D nanomaterial/TiO_2 nanoparticle composite structure, several routes can be available:

(a) Simple mixing of pure 1-D nanomaterial and pure nanoparticles (similarly to the carbon nanotubes addition to TiO_2 powder in the literatures)
(b) Preparing 1-D nanomaterial/nanoparticle mixed (or composite) powder by using chemical fragmentation of 1-D nanomaterials in acid solution at low pH (pH ~ 0)
(c) Preparing 1-D nanomaterial/nanoparticle mixed (or composite) powder by using middle-stage (i.e., incomplete) hydrothermal treatment in rather short period
(d) Preparing nanowire/nanoparticle mixed (or composite) powder by using thermal fragmentation of thermally unstable 1-D nanomaterials (e.g., titania nanotubes), or *in situ* thermal fragmentation during the sintering process for DSC devices.

In this work, we report the preparation and microstructure of TiO_2-nanowire dispersed composite electrode for high-performance dye-sensitized solar cells in various preparation methods. Crystal structure, device structure and cell performances will be discussed in detail.

References:

[1] T. Kasuga, M. Hiramatsu, A. Hoson, T. Sekino and K. Niihara, Langmuir, **14**, (1998), 3160.
[2] T. Kasuga, M. Hiramatsu, A. Hoson, T. Sekino and K. Niihara, Adv. Mater., **11** (1999) 1307.
[3] Y. Suzuki, S. Ngamsinlapasathian, R. Yoshida and S. Yoshikawa, Central Euro. J. Chem., in press (DOI: 10.2478/s11532-006-0015-3).
[4] S. Pavasupree, S. Ngamsinlapasathian, M. Nakajima, Y. Suzuki and S. Yoshikawa, J. Photochem. Photobio. A: Chem, in press (DOI:10.1016/j.jphotochem.2006.04.010)
[5] K. Asagoe, S. Ngamsinlapasathian, Y. Suzuki and S. Yoshikawa, Central Euro. J. Chem., in contribution.
[6] B. O'Regan and M. Grätzel, Nature, **353** (1991) 737.

OUT-OF-EQUILIBRIUM SELF-ASSEMBLY OF BINARY MIXTURES OF NANOPARTICLES

Claudia G. Sztrum and Eran Rabani
School of Chemistry, The Sackler Faculty of Exact Sciences Tel Aviv University, Tel Aviv 69978 Israel
sztrumcl@post.tau.ac.ill

A coarse-grained lattice-gas model is developed to study drying-mediated self-assembly of binary mixtures of nanoparticles. Out-of-equilibrium simulations of the model provide insight into the dynamics of solvent evaporation and the formation of self-assembled superstructure domains. Three model systems are considered, corresponding to equilibrium phase separation between nanoparticles of type A and B, to an amorphous state, and to an ordered, checkerboard-like, superstructure. Interestingly, the mechanism for self-ordering depends on the nature of equilibrium superstructure and on the dynamical coupling to the evaporating solvent. In a certain limit of evaporation, the system shows complex behavior common to arrested micro-phase separation of glassy materials. Several qualitative features are discussed and scaling laws for the growth of domains are determined numerically.

Poster

FM-NCAFM INVESTIGATION OF INDIVIDUAL ORGANIC MOLECULES ON INSULATING SUBSTRATES

Shukichi Tanaka, Hitoshi Suzuki, Mitsuru Inada, Toshiya Kamikado, Shiyoshi Yokoyama
Nanotechnology Section, Kobe Advanced ICT Research Centre, National Institute of Information and Communications Technology (KARC-NiCT)
588-2 Iwaoka, Kobe 651-2492, Japan
e-mail:tanakas@nict.go.jp

The developments of smallest scale devices has focused research attention onto the possibilities offered by nanometre scale single molecules, such as porphyrins, whose chemical, physical and electrical properties can be tuned by chemical synthetic techniques.

For device designing, the precise positional control of individual molecule units on the substrate is one of the important subjects. In the case of organic molecules on the metal substrates, there can be found some number of successful reports to control the mobility of molecules on the surface by means of attractive interaction between molecules and substrates appropriately[1, 2]. However, as long as the substrate is conductive, possibilities to design electronic devices using supra-molecular system on the substrate should be strongly limited.

By considering the successful example of mobility control of molecules on the conductive substrates, we adopted the oxide surfaces as candidates for insulating substrates [3, 4]. However, the sub-nanometre scale features of non-defect surfaces of oxides and its applicability to the molecule systems in UHV condition have not been well investigated because of the lack of suitable experimental methods to investigate the sub-nanometre scale conformational features of insulating oxide surfaces with organic molecules.

Non-contact atomic force microscopy operated in the force feed-back mode (FM-NCAFM) is one of the versatile tools for this purpose because of its ability to access insulating substrates with excellent spatial resolution. FM-NCAFM uses atomic interaction force to regulate the distance between the tip apex and the surface, and that the conductivity of the sample is not necessary for measurements.

In this paper, we report the experimental results of FM-NCAFM observations of sub-nanometre scale conformational features of non-defected insulating oxide surfaces produced by heat treatments, and discuss their stability during the fabrication process in UHV. Following the results of FM-NCAFM observations of oxide substrate with organic molecules are presented, and then their conformational features in sub-molecular scale on the substrates are discussed.

[1] S. Tanaka, H. Suzuki, T. Kamikado and S. Mashiko Thin Solid Films 438-439 (2002) 56.

[2] S. Tanaka, H. Suzuki, T. Kamikado, S. Mashiko, Nanotechnology 15 (2004) 87.

[3] S. Tanaka, H. Suzuki, M. Inada, T. Kamikado, S. Mashiko, Nanotechnology 16 (2005) 107.

[4] S. Tanaka, H. Suzuki, M.Inada, T. Kamikado, S. Mashiko, JJAP, 45 (2006) pp2045.

Poster

Sol-gel Preparation and Studies of Co(II) and Co(III)-Substituted Barium Ferrite Nanoparticles

Geok-Bee Teh*, *N. Saravanan* and D. A. Jefferson*[+]*,
**Department of Bioscience and Chemistry, Faculty of Engineering and Science, Universiti Tunku Abdul Rahman, 53300 Kuala Lumpur, Malaysia*
[+2]Department of Chemistry, University of Cambridge, Lensfield Road,
Cambridge CB2 1EW, United Kingdom.
tehgb@mail.utar.edu.my

The sol-gel preparative method was employed to synthesise Co(II) and Co(III)-substituted barium ferrite. This method was attempted to achieve higher homogeneity of the final product. Co(II) substituted barium ferrite was found to have oxygen vacancies which was confirmed by TGA analysis. Samples of substituted ferrites were characterised by various experimental techniques including High Resolution Transmission Electron Microscopy, X-ray diffraction analysis, magnetometry and thermal gravimetric analysis. These cobalt ions substituted barium ferrite were found to have a long-axis range ordering and the microstructures were not affected by the cobalt substitutions. Disordered intergrowth of cobalt-substituted barium ferrites particles were found and proved that barium ferrite phase crystallized on the {111} of spinel-structured iron oxide.

Keywords: sol-gel growth, nanostructures, barium ferrite, magnetic material

References:

[1] A. Grusková, J. Lipka, M. Papánová, D. Kevická, A. González, G. Mendoza, I. Tóth, J. Sláma, *Hyp. Inter.,* 156 (2004) 187.
[2] J.C. Corral-Huacuz, G. Mendoza-Suárez, *J. Magn. Magn. Mater.,* 242 (2002) 430.
[3] J. Smit, H.P.J. Wijn, Ferrites: Physical Properties of ferrimagnetic oxides in relation to their technical applications, Philips Technical Library, 1959.

Figures:

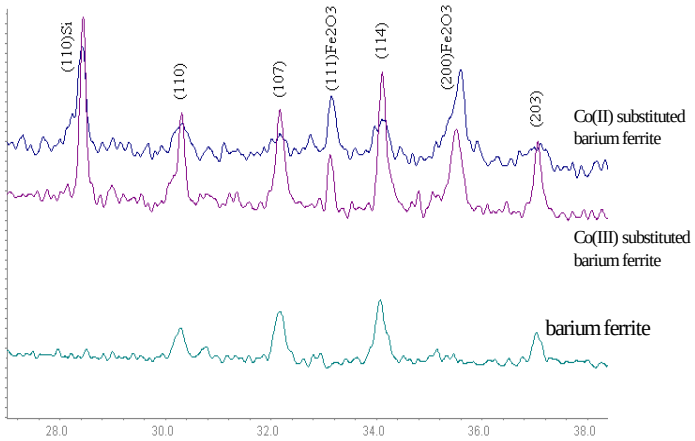


Figure 1: XRD patterns of $BaFe_{12}O_{19}$, Co(II) and Co(III) substituted barium ferrites. Peak marked as '(110)Si' is the peak for the silicon powder which was added as the internal standard.

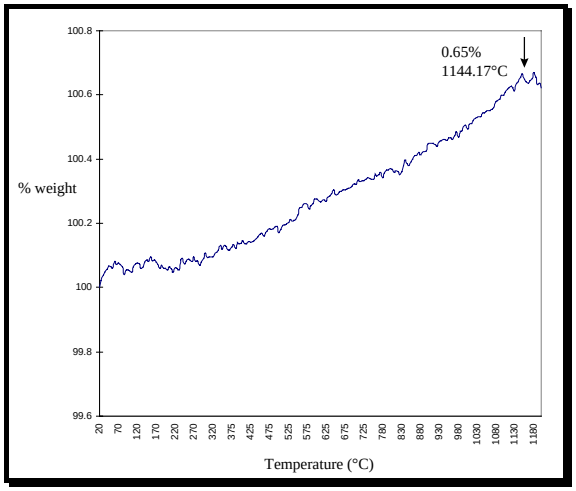


Figure 2 : TG scan for a sample of 13.903 mg of Co(II) substituted $BaFe_{12}O_{19}$

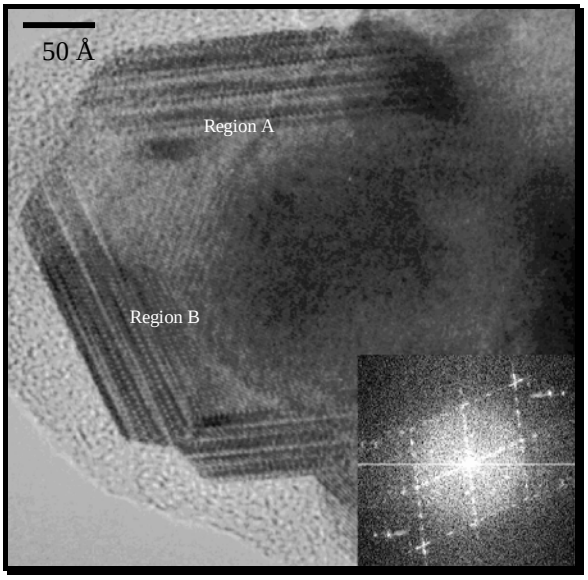


Figure 3 : HRTEM micrograph of a spinel crystal encapsulated by M-type barium ferrite in the specimen of Co(II) substituted barium ferrite. The inset shows the power spectrum of the lattice fringe image (*G. B. Teh et. al., J. of Solid State Chem., **2002**, 167, 254-257.)*

Poster

NEW TYPES OF NANOELECTRONICS CONTACTS

Israel Temprano, Nathalie Dubuc, Mohamed Siaj and Peter H. McBreen
Université Laval, G1K 7P4, Quebec, Canada
chmite@hermes.ulaval.ca

The ability to develop new methods to enhance electrical contact between organic molecules and electrodes is fundamental to the design of devices that require electron flow between an organic component and a metallic component. Examples of such devices are organic thin film field effect transistors, where electrons flow from the source to drain electrodes through the organic film. The metal-organic contacts are the 'electrical plugs' in such a system. Metal-organic contacts using double and triple bonds is a promising approach in that it combines three advantages. These advantages are as follows: better electrical contact than for thiols, enhanced thermal stability, and activity for olefin-metathesis add-on chemistry[1].

The data presented in this poster show a new surface reaction leading to the formation of C=Mo double bonds to the surface of a conducting material, molybdenum carbide[2-5]. The metal-molecule contacts are found to be active for transalkylidenation and ring-openining polymerization (ROMP)[6] reactions. For example, olefin-metathesis may be used to grow conjugated polymers directly from the carbide surface. Hence, the data suggest that olefin-metathesis procedures may be used to interconnect electrodes in nanodevices. Self-assembly of conjugated polymers may allow their targeted insertion into electronic and electrooptical devices.

References:

[1] Tulevski, G.S., Myers, M.B., Hybertsen, M.S., Steigerwald, M.L., Nuckolls C., Science, **309** (2005) 591.

[2] Zahidi, E-M., Oudghiri-Hassani, H., McBreen, P.H., Nature, **409** (2001), 1023

[3] Siaj, M., Reed, C., Oyama, T., Scott, S.L., McBreen, P.H., J. Am. Chem. Soc, **126** (2004) 9514

[4] Siaj, M., Oudghiri-Hassani, H., Zahidi, E-M., McBreen, P.H., Surf. Sci., **579** (2005) 1

[5] Oudghiri-Hassani, H., Zahidi, E-M., Siaj, M., McBreen, P.H., App. Surf. Sci., **212-213** (2003) 4

[6] Siaj, M., McBreen, P.H., Science, **309** (2005) 588

[7] http://nobelprize.org/nobel_prizes/chemistry/laureates/2005/chemadv05.pdf

Figures:

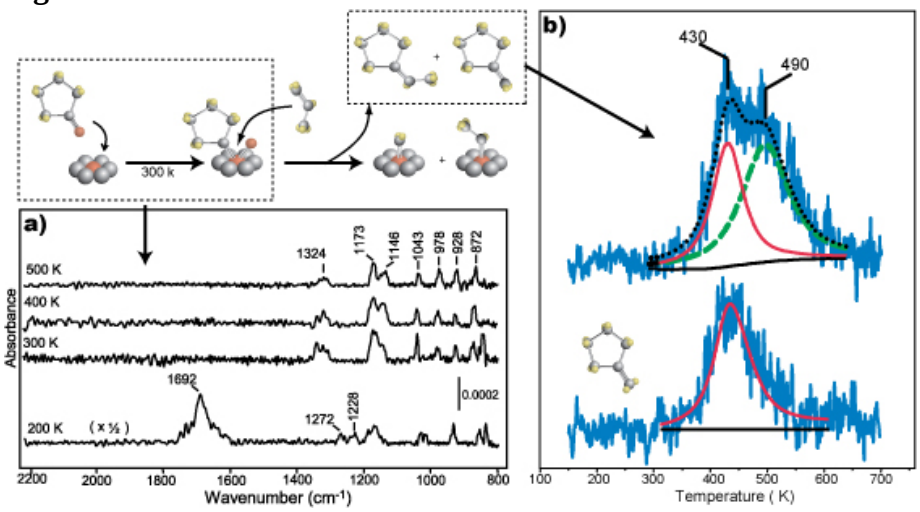


Figure 1

a) RAIRS and b) TPR spectra of active site formation for metathesis reaction on molybdenum carbide

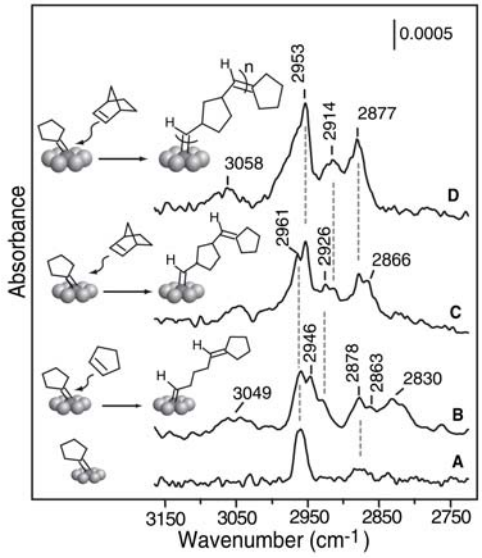


Figure 2

a) RAIRS spectra of Ring Opening Metathesis Polymerization from cyclopentylidene initiation sites on molybdenum carbide

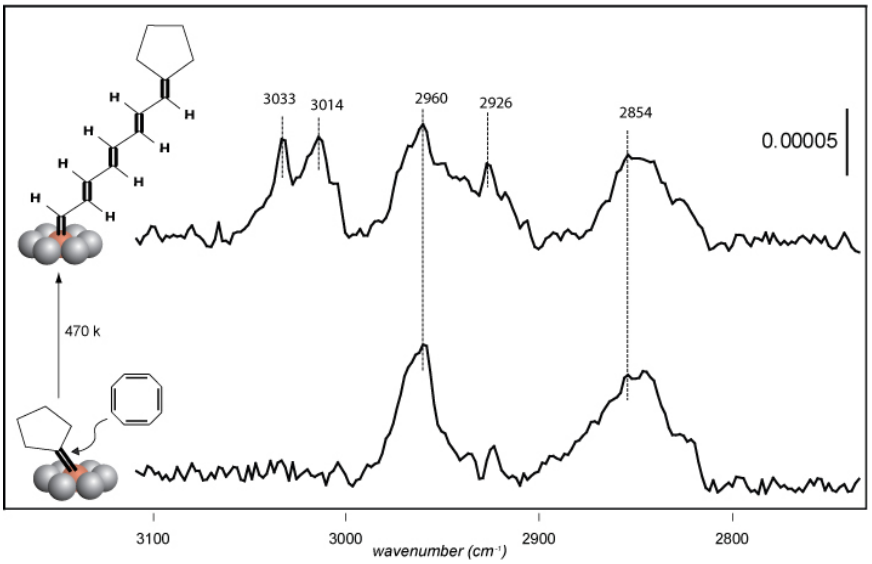


Figure 3

a) RAIRS spectra of a conjugated organic chain made by Ring Opening Metathesis Polymerization (ROMP) from cyclopentylidene initiation sites on molybdenum carbide

Poster

SIMILARITY LAWS DETERMINING THERMODYNAMIC CHARACTERISTICS OF FULLERITE CRYSTALS

Francisco Torrens, Gloria Castellano
Institut Universitari de Ciència Molecular, Universitat de València, Edifici d'Instituts de Paterna, P. O. Box 22085, 46071, Departamento de Química, Universidad Politécnica de Valencia, and Facultad de Ciencias Experimentales, Universidad Católica de Valencia San Vicente Mártir, *46003, València, Spain*
francisco.torrens@uv.es

It is discussed the existence of single-wall carbon nanotubes (SWNTs) in organic solvents in the form of clusters. A theory is developed based on a *bundlet* model, which enables describing the cluster-size distribution function [1–3]. Comparison of calculated solubilities with experiments would permit obtaining energetic parameters characterizing the interaction of an SWNT with its surrounding. Fullerenes and SWNTs are objects whose behaviour in many physical situations is characterized by peculiarities, which show up in that these systems represent the only soluble forms of carbon, what is related to their molecular structures. The fullerene molecule is a virtually uniform closed spherical–spheroidal surface, and an SWNT is a smooth cylindrical unit. Both structures give rise to weak interactions between the neighbouring units in a crystal and promote their interaction with solvent molecules. Another peculiarity is related to their trend to form clusters consisting of a number of fullerene molecules or SWNTs. The interaction energy of a fullerene molecule or SWNT with solvent molecules is proportional to the surface of the former and roughly independent of the orientation of the latter. The phenomena have a unified explanation in the bundlet model, in which the free energy of an SWNT in a cluster is combined from two components, *viz*. a volume one proportional to the number of molecules n in a cluster, and a surface one, proportional to $n^{1/2}$. Growth mechanisms of fractal clusters in fullerene solutions are analyzed along with similarity laws determining the thermodynamic characteristics of fullerite crystals (Fig. 1). Hierarchical principal component analysis (HPCA) for the thermodynamic properties of inert-gas and fullerite crystals classifies these crystals (Fig. 2). Provisional conclusions follow. (1) For a cluster nature of SWNT solubility to be completely established direct experimental exploration is necessary, *e.g*., the measurements of infrared absorption spectra or the application of Raoult's law. (2) The establishment of the *membranous character* of growth process in clusters allows explaining the high dispersion and contradiction of existing experimental data in the literature. In earlier reports on growth process nobody never posed the question of the existence of pores. (3) In accordance with the similarity laws for inert gases, the values of this dimensionless parameter for all crystals belonging to considered class should be close. The Debye temperatures θ_0 are determined *via* similarity relation from experimental and estimated data. The similarity relation is fulfilled quite well for the inert-gas crystals. Some violation of this relation for Ne is attributed to well-known quantum effects at low temperatures. The value of θ_0 for fullerite is about twice as high as that for inert-gas crystals. Such a deviation of fullerite Debye temperature from the value followed from similarity relation does not appear to be surprising since, over a temperature range near the Debye point, the fullerite crystal is orientationally ordered so that its structure is dissimilar to FCC. A fullerene molecule whose thermal rotation is frozen cannot be considered as a spherically symmetric particle. The fulfilment of the similarity laws that are valuable for particles with spherically symmetric interaction potential would hardly be expected. Some contribution to the Debye spectrum of fullerite is made by intramolecular vibrations, which of course are not considered in formulating the similarity laws. (4) In the case of many or conflicting data, modelling allows a simplified analysis, substituting each group of similar properties by its most important one. Hierarchical modelling improves the interpretability of conflicting data and is preferred to variable selection because all variables are retained, leading to more stable and more robust models. We thank Universitat de València–Mediscovery.

References:

[1] F. Torrens and G. Castellano, Comput. Lett., **1** (2005) 331.
[2] F. Torrens and G. Castellano, Phys. Status Solidi C, submitted for publication.
[3] F. Torrens and G. Castellano, Microelectron. J., in press.

Figures:

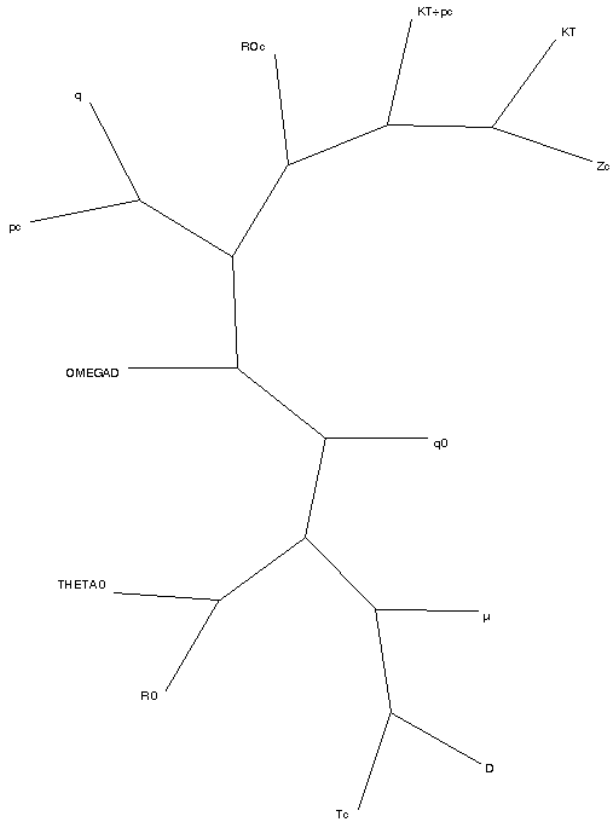


Fig. 1. Radial tree for the thermodynamic properties of the inert-gas and fullerite C_{60} crystals.

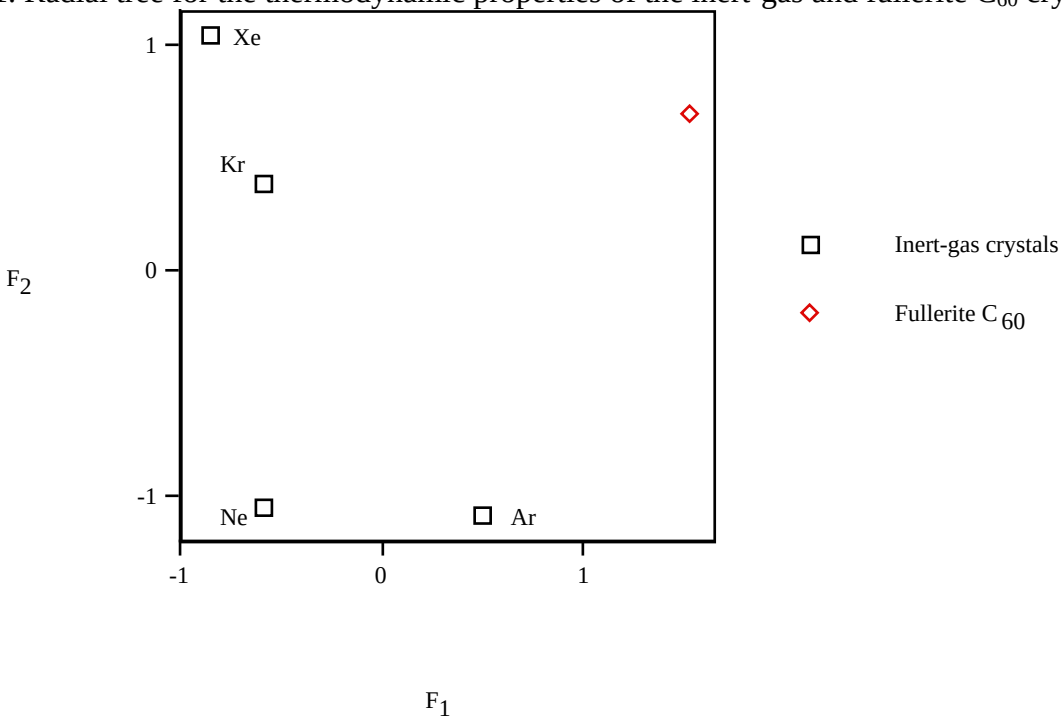


Fig. 2. Hierarchical PCA plot for thermodynamic properties of inert-gas/fullerite C_{60} crystals.

DC electrostatic manipulation of gold nanoparticles with Atomic Force Microscopy

Jordi Toset, Gabriel Gomila, Josep Samitier.
Departament d'Electrònica, Universitat de Barcelona,
Laboratori de Nanobioenginyeria-CREBEC, Parc Científic de Barcelona
C/Josep Samitier 1-5, 08028, Barcelona, Spain
jtoset@pcb.ub.es

There exist tools such as Atomic Force Microscopy (AFM), Scanning Tunneling Microscopy (STM), and Scanning Electron Microspy (SEM) [1]-[2] that enable to manipulate particles of nanometric sizes. In the present contribution we extend existing techniques by report on the electrostatic manipulation of gold nanoparticles with AFM

Initial attempts at manipulation of nanoparticles with the AFM were based on pushing the nanoparticle with the AFM tip [2-5]. However, the pushing process does not enable building 3D structures nor provides feedback on how the nanomaniplation process is proceeding. We have shown that the electrostatic manipulation overcomes these limitations.

Electrostatic nanomanipulation uses electrostatic forces to detach the particle form the substrate and Van der Waals forces [6] to attach back the particle to the substrate (or viceversa). The election of one procedure or another depends on the relative value of the Van der Waals forces of the particle-susbtrate and particle-tip systems. In both cases, during the translation process, the nanoparticle remains adhered to the tip.

To perform the electrostatic manipulation [7] the tip must be situated at a fixed distance on top of the nanoparticle and then a potential difference has to be applied between the AFM tip and the substrate high enough to overcome the Van der Waals force and hence to detach the nanoparticle from the substrate.

In order to perform such an experiment one has to estimate the value of the force necessary to detach the nanoparticle. This value determines the applied bias necessary. Once the applied bias is known one has to determine the initial distance between tip and nanoparticle. This distance has to be chosen such as not to be too far from the nanoparticle (the transfer does not occur) nor too close to the particle such as the application of the DC bias makes the tip to collapse onto the nanoparticle [8] [9]. In order to assist in this tip positioning we have developed a theoretical model able to predict for a given probe geometry and for every initial distance to the nanoparticle, the maximum applied potential at which the tip will collapse onto the nanoparticle (Vc) (or conversely the distance at which collapse will start (Dc)) (Fig. 1). This modeling has enabled us to choose the correct probe (e.g. elastic constant) and the parameters (initial distance) to perform the experiments.

In Fig. 2a and 2b successful transport of a 50 nm gold nanoparticle from position A to position B performed electrostatically with the AFM is shown.

A graph of the deflection signal as a function of time during the nanomanipulation experiment is shown in Fig. 3. From this type of signal one can monitor the nanomanipulation experiment by detecting, in particular, the instant at which the detachment of the nanoparticle from the substrate takes place (big spike in the deflection signal in Fig. 3) or any eventual loss of the nanoparticle during the transport (not shown in Fig. 3).

To create 3D structures we need to transport one particle over other particles and deposit it with precision, otherwise, we can destroy the structure. The images in figure 4 show the possibility of positioning a nanoparticle on top of other nanoparticles by means of electrostatic manipulation with AFM.

References:

[1] Kasaya, T.; Miyazaki, H.T.; Saito, S.; Koyano, K.; Yamaura, T.; Sato, T.; Rewiew of scientific instruments, 75,6, 2004,203-2042.
[2]Sitti, M.; Hashimoto, H.; IEEE/ASME Transactions on mechatronics, 5,2; 2000, 199-211.

[3] Baur, C.; Bugacov, A.; Koel, B.E.; Madhukar, A.; Montoya, N.; Ramachandran, T.R.; Requicha, A.A.G.; Resch, R.; Will, P.; Nanotechnology, 9, 1998, 360-364.
[4] Fahlbusch, S.; Shirinov, A.; Fatikow, S.; Proceedings of the 2002 IEEE/RSJ, Conference on Intelligent Robots and Systems, 2002.
[5] Resch, R.; Lewis, D.; Meltzer, S.; Montoya, N.; Koel, B.E.; Madhukar, A.; Requicha, A.A.G.; Will, P.; Ultramicroscopy, 82, 2000, 135-139.
[6] Argento, C.; French, R.H.; Journal of Applied Physics, 80, 1996, 6081-6090.
[7] Decossas, S.; Mazen, F.; Baron, T.; Brémond, G.; Souifi, A.; Nanotechnology, 14, 2003, 1272-1278.
[8] Tas, N.; Sonnenberg, T.; Jansen, H.; Legtenberg, R.; Elwenspoek, M.; J. Micromech. Microeng., 6, 1996, 385-397.
[9] Abadal, G.; Davis, Z.J.; Helbo, B.; Borrisé, X.; Ruiz, R.; Boisen, A.; Campabadal, F.; Esteve, J.; Figueras, E.; Perez-Murano, F.; Barniol, N.; Nanotechnology, 12, 2001, 100-104.

Figures:

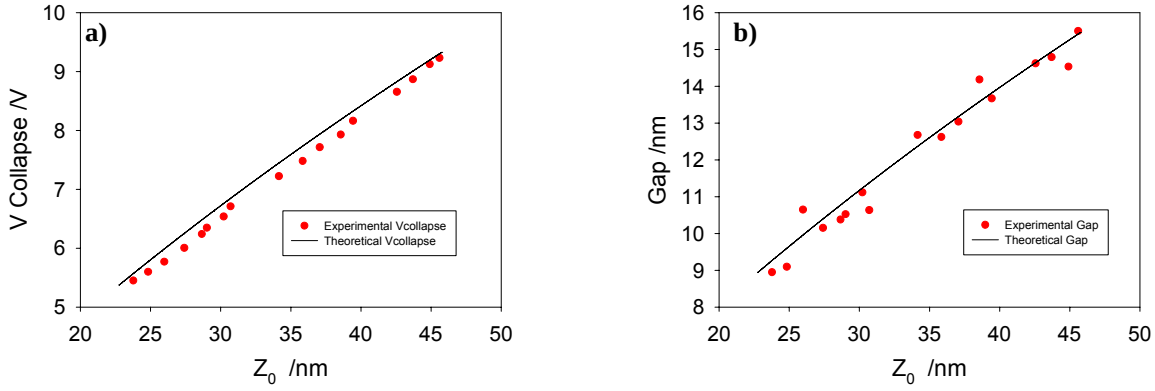
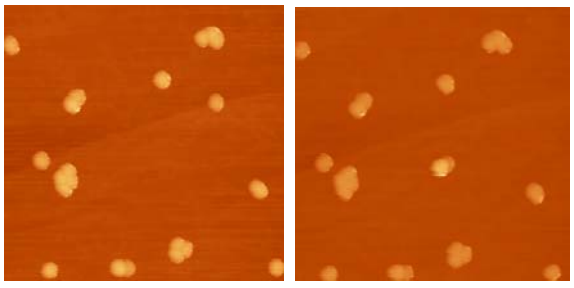


Figure 1: a) Collapse potential vs initial distance for a probe with elastic constant k=1.5 N/m AFM tip. b) Collapse distance vs initial distance for the same probe (solid line theoreticla model, red circles experimental results).



2a) 2b)

Figure 2: 2a and 2b we show the transport of a gold nanoparticle from position A to position B performed electrostatically.

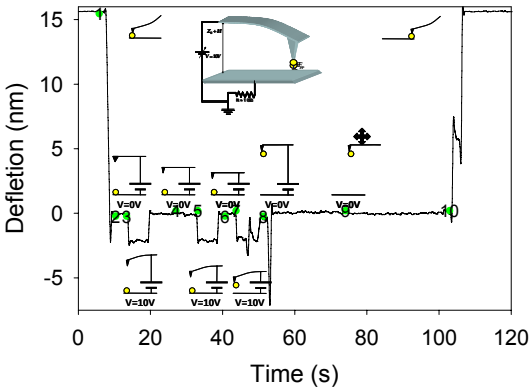
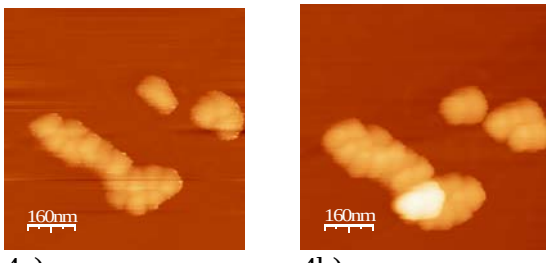


Figure3: Deflection signal as a function of time during the nanomanipulation experiment.



4a) 4b)

Figure 4: (a) and (b) 2D AFM images before and after the deposition of a nanoparticle on top of an aggregation of nanopartícles.

SIMULATIONS OF CONTROLLED SINGLE ATOM MANIPULATION IN NON-CONTACT ATOMIC FORCE MICROSCOPY

T. Trevethan[1], M. Watkins[1], L.N. Kantorovich[2] and A.L. Shluger[1]
[1]Department of Physics and Astronomy, University College London, London, UK
[2]Department of Physics, Kings College London, London, UK
t.trevethan@ucl.ac.uk

One of the great achievements of scanning probe microscopy is the controlled manipulation of individual atoms on surfaces. Non-contact atomic force microscopy (NC-AFM) is the only tool capable of imaging and now manipulating individual atoms of the surfaces of insulating materials [1]. We present the results of calculations performed to model the process of manipulation using two model but technologically important systems: an oxygen vacancy and a metal adatom on the regular MgO (001) surface. The accessible states of the systems and the barriers that separate them are determined as a function of tip height and position above the surface from atomistic calculations. The dynamical evolution of the system in real time as the tip is oscillated and at a finite temperature is then determined using a Kinetic Monte Carlo method. It is found that the point at which the manipulation occurs is sensitive to both the temperature and the trajectory of the cantilever. Based on the results of these calculations we are able to identify the most favourable experimental conditions and the procedure to achieve the desired manipulation.

We show how the manipulation occurs as a single atomic scale event, which results in a large and sudden change in the force-field experienced by the tip during a single oscillation cycle. Using a Virtual dynamic atomic force microscope [2], which explicitly simulates the operation and response of the real apparatus, we show how this single atomic scale event can be registered by the instrument and used as an experimental signal that the manipulation has been achieved.

References:

[1] Y. Sugimoto, M. Abe, S. Hirayama, N. Oyabu, O. Custance, and S. Morita, Nature Materials, **4**, (2005) 156.
[2] J. Polesel-Maris and S. Gauthier, J. Appl. Phys., **97**, (2005) 1.

Computational Design of Metallofullerene Production: X@C_{74}

Filip Uhlík,[1] *Zdeněk Slanina*[2,3] *and Shigeru Nagase*[2]

[1] *School of Science, Charles University*
CZ-128 43 Prague 2, Czech Republic
[2] *Department of Theoretical Molecular Science*
Institute for Molecular Science
Myodaiji, Okazaki 444-8585, Japan
[3] *Institute of Chemistry, Academia Sinica*
Nankang, Taipei 11529, Taiwan-ROC

Various endohedral cage compounds have been suggested as possible candidate species for molecular memories and other future nanotechnological applications. One approach is built on endohedral species with two possible location sites of the encapsulated atom [1] while another concept of quantum computing aims at a usage of spin states of N@C_{60} [2] or fullerene-based molecular transistors [3]. The properties of metallofullerenes can further be tuned by external cage derivatizations. At present, however, a deeper knowledge of various molecular and production aspects of the endohedral compounds is needed before their tailoring to nanotechnology applications is possible.

The C_{74} fullerene endohedral family is rather extended as encapsulations like Ca@C_{74}, Sr@C_{74}, Ba@C_{74}, La@C_{74}, Eu@C_{74}, Yb@C_{74}, Sc_2@C_{74}, or Er_3@C_{74} are known from previous experimental studies. The family is also interesting as there is just one C_{74} cage that obeys the isolated pentagon rule, namely of D_{3h} symmetry. The cage was experimentally confirmed in Ca@C_{74}, Ba@C_{74}, and La@C_{74}. However, the empty C_{74} (and also C_{72}) species could not be isolated yet, perhaps owing to solubility problems.

The experimental findings are thus of computational interest and calculations on several of the species will be reported based on the density functional methods in order to clarify structure, energy, stability as well as spectral aspects. As far as metallofullerene production is concerned, there is a general stability problem which members of a series, like X@C_{74}, are produced in high/low yields. Under equilibrium conditions we shall deal with the encapsulation equilibrium constants $K_{@,X,p}$. Temperature dependency of the encapsulation equilibrium constant $K_{@,X,p}$ is described by the van't Hoff equation controlled by the (negative) standard change of enthalpy upon encapsulation. In other words, $K_{@,X,p}$ must be decreasing with temperature. Let the metal pressure is close to its saturated pressure p_{sat}(X). We suggest a product, $p_{sat}(\mathrm{X})K_{@,X,p}$, as a pratical stability measure in a metallofullerene series. Interestingly enough, the product increases with temperature which is the basic scenario of the metallofullerene formation in, e.g., the electric-arc technique. The encapsulation equilibrium constants $K_{@,X,p}$ are computed using the potential-energy change evaluated at the B3LYP/6-31G* level and the partition functions at the B3LYP/3-21G level.

[1] J. K. Gimzewski, in The Chemical Physics of Fullerenes 10 (and 5) Years Later, W. Andreoni (ed.), Kluwer Academic Publishers, Dordrecht, 1996, p. 117; [2] W. Harneit, M. Waiblinger, C. Meyer, K. Lips and A. Weidinger, in Recent Advances in the Chemistry and Physics of Fullerenes and Related Materials, Vol. 11, Fullerenes for the New Millennium, K. M. Kadish, P. V. Kamat and D. Guldi (eds.), Electrochemical Society, Pennington, 2001, p. 358; [3] N. Hiroshiba, K. Tanigaki, R. Kumashiro, H. Ohashi, T. Wakahara and T. Akasaka Chem. Phys. Lett. 400 (2004) 235.

ELECTRONIC TRANSPORT AND MAGNETISM IN ATOMIC-SIZED STRUCTURES

Carlos Untiedt
LT-Nanolab. Dep. de Física Aplicada. Facultad de Ciencias. Universidad de Alicante. Spain
untiedt@ua.es

Different techniques such as the Scanning tunnelling microscope, the mechanically controlled break junctions, electrochemical methods, or several others, make it possible to control the formation of atomic-sized structures connected to macroscopic electrodes. In this way the ultimate structures: atomic-contact, atomic wire or molecular bridge, have been achieved.

In the last decade there has been a great success in measuring the properties of the electronic transport over these structures [1]. There, the conductance (G) is described by the Landauer's formulae: $G = G0 \Sigma Ti$ where $G0=2e2/h$ the conductance quanta, Ti is the transmission of the ith channel and the summation goes over all the conduction channels available for the structure. For the case of magnetic materials, the spin degeneracy is removed and then we should distinguish channels for the different spins, each of these with conduction up to G0/2.

Several attempts have been made in order to measure signatures of these fractional quanta of conductance, although we can show that for most of the cases this is not straight forward and contamination can give misleading results [2]. Finally we will show new approaches to obtain information of magnetism using transport properties in atomic contacts of magnetic materials that can help in the areas of spintronics and molecular electronics[3]..

References:

[1] N. Agraït, A. Levy-Yeyati, J.M. van Ruitenbeek. Phys. Rep. 377, 81, (2003)

[2] C. Untiedt, D.M.T. Dekker, D. Djukic, and J.M van Ruitenbeek. Phys. Rev. B. 69, 081401(R) (2004)

[3] J. Fernandez-Rossier, D. Jacob, C. Untiedt, and J.J. Palacios. Phys. Rev. B.72, 224418 (2005)

SCIENCE AND TECHNOLOGY CENTER IN UKRAINE – MORE THAN 10 YEARS OF SUCCESSFUL COOPERATION

Svitlana Us
Science and Technology Center in Ukraine, 21 Kamenyariv street, Kyiv, Ukraine
svitlana.us@stcu.int
www.stcu.int

The Science and Technology Center in Ukraine (STCU) is an intergovernmental, non-profit organization established on October 25, 1993 by Canada, U.S.A., Ukraine and Sweden (subsequently replaced by the EU) with the goal of aiding unemployed or underemployed scientists previously working on the development of weapons of mass destruction.

Mission

Nonproliferation: Prevent the spread of weapons mass distraction (WMD) expertise by supporting civilian R&D activities of Azeri, Georgian, Moldovan, Ukrainian and Uzbek scientists and engineers formerly involved WMD and their means of delivery.

Sustainable Redirection: Create opportunities for former WMD scientists and engineers to develop sustainable civilian research work that contributes to the economic development of their countries, finds solutions to national/international S&T problems, and builds successful research groups.

The STCU finances projects in the following R&D areas : 1- Biotechnologies; 2- Materials Science; 3- Chemistry; 4- Environmental and Non-Nuclear Research; 5- Industrial Technologies; 6- Sensors; 7- Nuclear Energy & Safety; 8- Physics; 9- Other (Basic science). Other than government funded projects, the STCU also works in a number of other spheres of activity: Matchmaking; Promotional Missions; Seminars and Workshops; Partnership Projects; Travel Grants; and Patent Support.

The total funding to date including all twenty-two (22) Governing Boards stands at approximately **$142.6 million**, with the donor countries contributing the following amounts: **Canada - $3.3m, U.S.A.- $73.0m, European Union - $25.4m (€21.5m), Non-Government Partners Sector - $14.0m, Government Partners Sector - $25.9m and Other (Japan, CERN) - $1.0m.**

The area of Materials Science is one of the most represented among the STCU categorization. At the moment the STCU has funded **152 projects**, employing a total of **3759 scientists**. The total funding for the materials science related projects is **$16,134,299 and 3,687,064€.** The area of materials science includes the following directions: new materials, nanotechnology, equipment & devices, coatings.

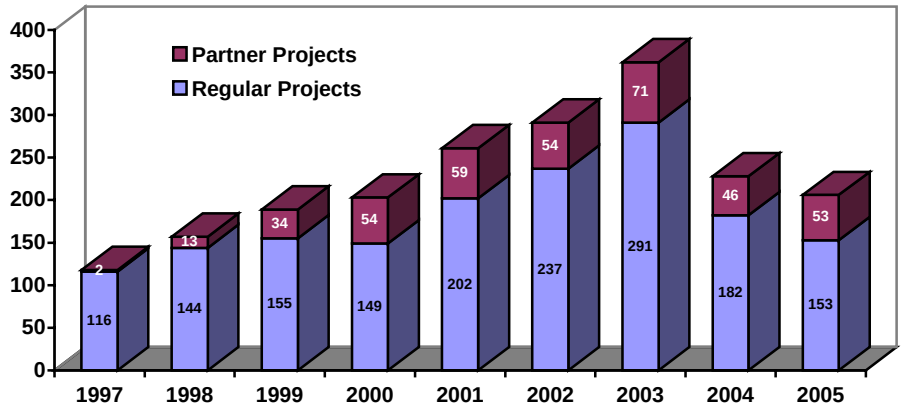
"From Science to Business" – STCU-NATO Workshop in Kyiv (October 11-12, 2006)

[Direct link to workshop information page: http://www.stcu.int/workshop/index.php]

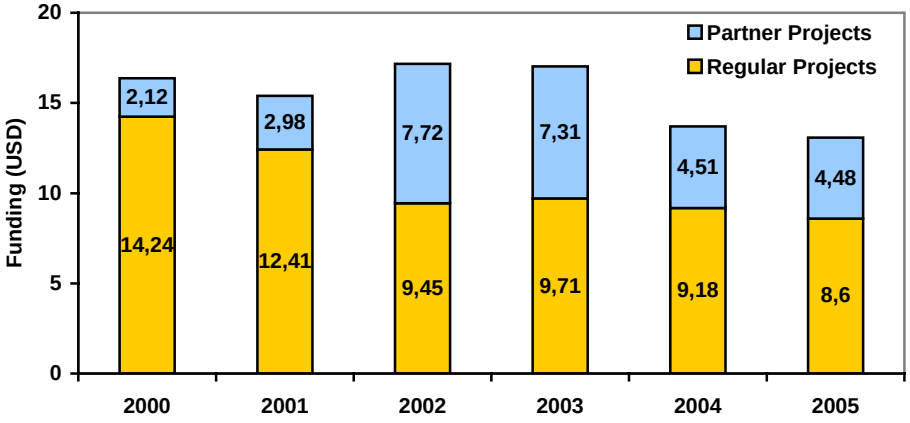
In line with the Center main objectives, the Workshop serves the purpose of bringing former Soviet Weapon Scientists to Civilian Business. The focus will be specifically on delivering know-how to Ukrainian Scientists. Simultaneously the event shall offer Foreign Companies a platform to initiate relations leading possibly to industrial research and technology transfer opportunities. **Day One (Wednesday Oct. 11)** will gather some 200 pre-selected Local Scientists and deliver them most up-to-date presentations and speeches by Key Speakers from STCU Funding Parties Countries and NATO "Security Through Science" Program. The themes selected are: Technology Transfer Issues, Intellectual Property Rights Protection, Mechanisms of Commercializing Research Results and Methods for Attracting Financing. Participants will be walked through a Technology Exhibition where Ukrainian Scientists will defend their posters.

Day Two (Thursday Oct. 12) will give the occasion for a reduced number of Local Scientists (100 also pre-identified), to split between five Panel Groups, including **New Materials and Nanotechnology**, and to engage in a real dialogue with Company representatives. Each Group shall focus on debating innovative technologies and potential commercialization (some Technology Profile Forms are now available).

Number of Active STCU Projects Per Year



Approved STCU Projects Financing (Past Five Years)



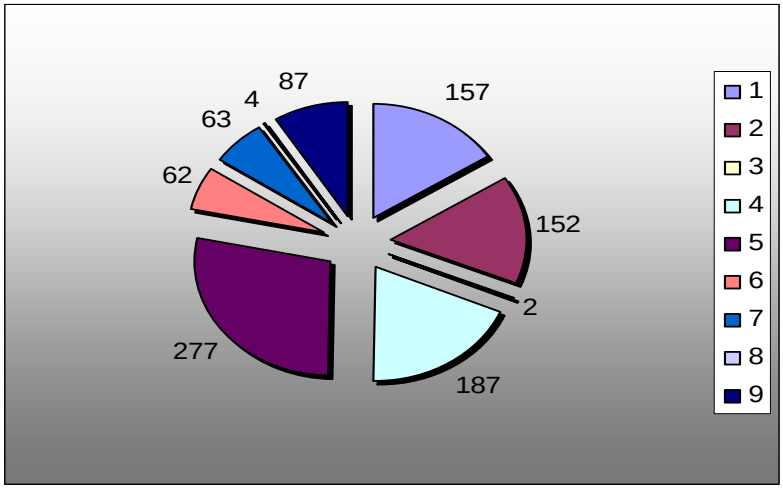
STCU Programs Focused On "Permanent Redirection" And Self-Sustainability

- **Less on project Volume**
- **More on Opportunities in:**

· **Private Sector Partners**
· **Commercialization**
· **National / International Research Programs**
· **Specific Party Programs/ Goals**

Encouraging Partnership/ Co-Financing with Recipient Parties

Distribution of the STCU Funded Projects by Technical Areas



1- Biotechnologies; 2- Materials Science; 3- Chemistry; 4- Environmental and Non-Nuclear Research; 5- Industrial Technologies; 6- Sensors; 7- Nuclear Energy & Safety; 8 - Physics; 9- Other (Basic Science, etc.)

PREPARATION OF VERMICULITE PARTICLES FOR UTILIZATION IN CLAY/POLYMER NANOCOMPOSITES

M. Valášková[1], V. Matějka[1], M. Pospíšil[2], K. Barabaszová[1], M. Šupová-Křístková[1], G. Kratošová[1]*

[1]Institute of Materials Chemistry, VŠB-Technical University Ostrava, Ostrava-Poruba 708 33, Czech Republic

[2]Faculty of Mathematics and Physics, Charles University Prague, Ke Karlovu 3, 121 16 Prague, Czech Republic

marta.valaskova@vsb.cz

Layered silicates (phyllosilicates) represent important native clay materials, which improve stiffness, strength, toughness, and thermal stability of the polymer/layered silicate nanocomposites. Chemical modification is important for preparation of nanoclays particles to make them compatible (organophilic) with organic monomers and polymers. Nanoclays combined with monomers or polymers form nanocomposites. The best properties of polymer/clay nanocomposites are achieved when exfoliated phyllosilicate particles are homogenously dispersed in polymer matrices. Especially suitable are 2:1 phyllosilicates with molecular water in the interlayer, because their exfoliation results from a spontaneous escape of the interlayer water. Vermiculite (VER) is abundant 2:1 phyllosilicate that is much cheaper compared to widely used montmorilonite, hectorite and saponite.

We decided to choose octadecylamine (ODA) with a long alkyl chain for intercalation of VER. The main goal of this intercalation is to achieve organophilization of VER and its exfoliation. Low-temperature intercalation of VER with ODA forms VER/ODA complex which consist of exfoliated vermiculite particles with the grafted nano-layers of ODA chains on the surface of micro-flakes [1].

We have studied two combining procedures for the exfoliation/delamination of VER particles:

- Exfoliation/delamination with ODA after previous treatment of VER particles with oxidizing agents [2, 3];
- Exfoliation/delamination of VER particles using intercalation with ODA and its subsequent micronization using jet mill.

Exfoliated/delaminated vermiculite was evaluated using X-ray powder diffraction (XRPD), scanning electron microscope (SEM), atomic force microscope (AFM) and structure was simulated using molecular modeling.

References:

[1] Weiss Z., Valášková M., Křístková M., Čapková P.& Pospíšil M., Clays and Clay Miner., **51** (2003) 555.

[2] Weiss Z., Valášková M., Seidlerová J., Křístková-Šupová M., Šustai O. Matějka V. & Čapková P., J. Nanosci. Nanotechnol., **3** (2006) 726.

[3] Matějka V., Šupová-Křístková M., Kratošová G. & Valášková M., J. Nanosci. Nanotechnol., **6**, (2006) 2484.

Figures:

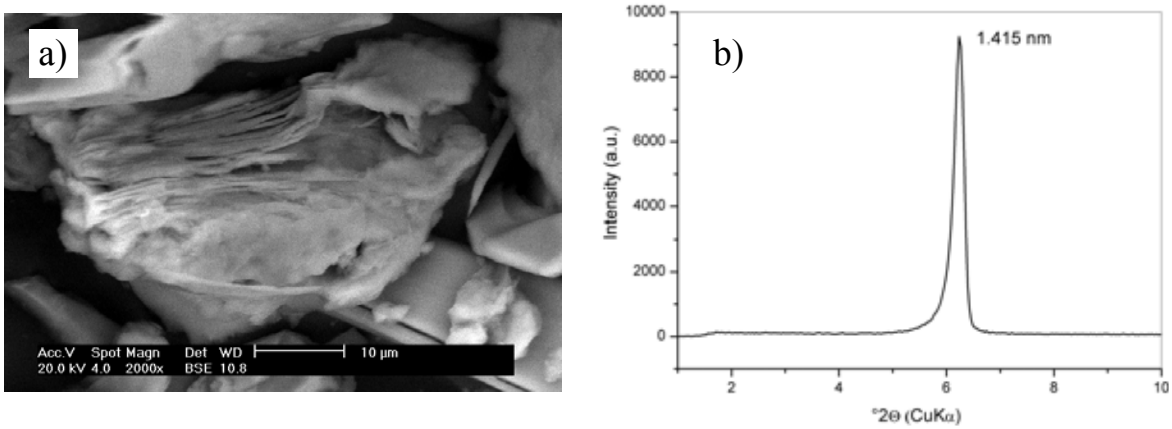


Figure 1. Untreated VER sample: a) SEM micrograph, b) XRPD pattern (part from 1 to 10 °2 θ)

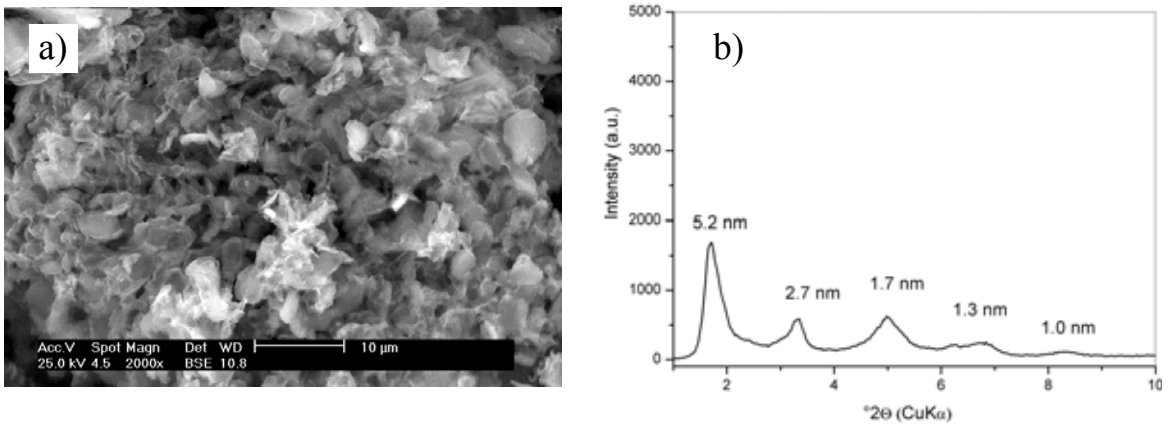


Figure 2. VER/ODA intercalates after jet milling: a) SEM micrograph, b) XRPD pattern (part from 1 to 10 °2 θ)

CHARACTERIZATION OF SINGLE-WALLED CARBON NANOTUBES CONTAINING DEFECTS FROM THEIR LOCAL VIBRATIONAL DENSITIES OF STATES

M. Vandescuren[1], *H. Amara*[1,2] *and Ph. Lambin*[1]
[1]*Laboratoire de Physique du Solide, Facultés Universitaires Notre-Dame de la Paix, Rue de Bruxelles 61,*
5000 Namur, Belgium
[2]*PCPM, Université Catholique de Louvain, Place Croix du Sud 1, 1348 Louvain-la-Neuve, Belgium*
matthieu.vandescuren@fundp.ac.be

The study of local vibrational properties of nanostructures is becoming of great interest since the development of resonant Raman enhanced spectroscopy, inelastic tunneling spectroscopy,... The latter technique has the advantage to authorize atomic resolution and could be used to detect the presence of a defect from the perturbation of the vibrational spectrum it induces. In this context, this work aims at exploring local vibrational structures of typical defects in carbon nanotubes.
We present a vibrational study of an isotopic substitution impurity in a (10,9) chiral nanotube, a Stone-Wales defect in a series of armchair tubes and, in addition, we have considered a intramolecular jonction between (12,0) and (9,0) nanotubes. Our study emphasizes the differences of local vibrational densities of state (lVDOS) between perfect and imperfect nanotubes. We use a dynamical model where carbons interact up to their third nearest neighbours with force constants fitted to graphene [1]. lVDOS are computed with the recursion method. Our study is a first step towards a more complete approach for characterizing defects in carbon nanotube structures based on the recognition of local vibrational fingerprints of these defects.

This work has been performed within the IUAP program P5/01 "Quantum size effects in nanostructured materials of the Belgian science policy programming services".

Reference

[1] R.A. Jishi and G. Dresselhaus, Phys. Rev. B **26** (1982), 4514-22

BIOMIMETIC HYBRIDS FOR MULTIFUNCTIONAL NANOREACTOR CREATION

M.Vantsian[1], D.Alekperov[1], G.Popova[1], H.Ihara[2]
[1]Mendeleyev University of Chemical Technology of Russia, Address 125190, Miusskaya sq. 9, Moscow, Russia
[2]Kumamoto University, 2-39-1, Kurokami, 860-8555, Kumamoto, Japan
galina@muctr.edu.ru

The research is aimed at creation of nanoscale biocatalyst which is effective under industrial hydrolysis conditions. Pathways for preparation of multi-purpose organic/inorganic matrix based on non-toxic biocompatible and biodegradable compounds –cyclotriphosphazene and polyglutamic acid are elaborated. Molecular architecture of biomimetic nanoparticle is studied (trans-oriented 3 α-helix bundles). Conventional methods of physical chemistry (optical spectroscopy, SWAXS, DCS etc.) as well as computer simulation which included geometry optimization, electron density calculations etc. have been applied for structural study. It was shown that biologically active ingredients (enzymes) can be introduced to the matrix; fully substituted and non-fully substituted products can be obtained. In case of non-fully substituted products free amino-groups can bind to biological substrates while biologically active fragments may participate in other reactions, in our case enzymatic cleavage.

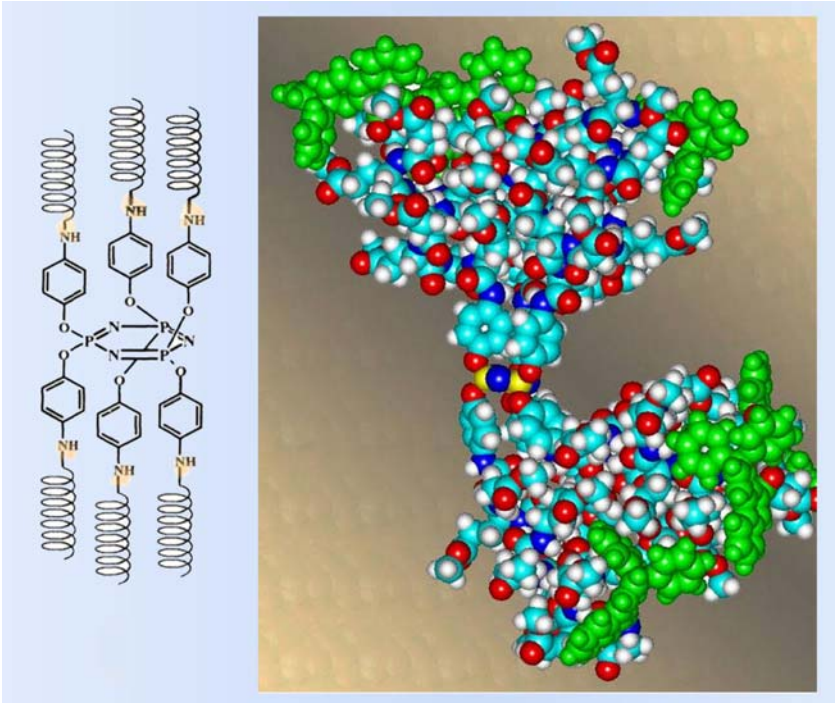
Purified and extracted substances – ribonuclease and lipase were immobilized at hybrid matrix at all reaction centers. The complex was well soluble in alcohol, partially soluble in water. Its enzymatic activity was very high in reactions with yeast ribonuclease. An increased active centers density allows to decrease the concentration of the reagent which is more active than non-immobilized enzyme at $t<60\ ^0C$ and at $pH<4$. It was shown that under industrial conditions the substrate splitting passes faster when applying the hybrid matrix. The catalyst continues to act under addition of new amounts of the substrate. The process of the enzymatic hydrolysis catalysed by multi-centered nanobiocatalyst will be extensively studied in future.

The data obtained show that nanoreactor is stable in acidic medium and that hydrolysis rate is 30 % faster than for pure (“free”) enzymes.

References:

[1] G. Popova, V. Kireev, A. Spitsyn, H. Ihara, M. Scherbina, S. Chvalun, Mol. Cryst. Liq. Cryst. **390** (2003) 91.
[2] G. Popova, A. Spitsyn, (Rev.) At the memory of Prof. N.N.Suvorov. Nanotechnics (Rus.) **2** (2005) 84.
[3] M.Takafuji, T.Shirosaki, S.Chowdhury, D.Alekperov, G.Popova, H.Hachisako, H.Ihara, J. Materials Research **3** (2006) in press.

Figures:



TREATMENT FOR STROKE USING NANOTECHNOLOGY

Arunkumaran Varadharajan, Sesh Narayanan
R.M.K Engineering College, 10 Munusamy Salai,K.K.Nagar, Chennai, India
arunkumaran@rediffmail.com

From the day of the evolution of mankind on this blue planet, man has maintained a symbiotic relationship with technology and comfort. Nanotechnology is the precise and purposeful manipulation of matter at atomic level. The size of each and every part in Nanotechnology is of the order of nanometers (10-9m).As,

"NECESSITY IS THE MOTHER OF INVENTIONS"
The need for the survival and betterment of mankind, we exploit our own innovative idea in this paper to treat stroke in a better way using Nanotechnology.

Blood supply to all the parts of the body is an essential criterion for perfect health. A clot formed in the blood vessel blocks the lumen and therefore hinders the blood supply. Stroke is a condition wherein, the blood supply to the brain is reduced or completely inhibited, as a result of thrombosis, which apparently leads to paralysis. Warfarin a biochemical compound which has the ability to dissolve clots that is formed in the blood vessels.

Nanorobots can be employed to deliver Warfarin targeted to the specific sites in order to dissolve the clots in the lumen of the blood vessel. The biochemical Warfarin is stored in a tank in a torpedo shaped Nanorobot. This paper deals with the shape, design, construction and treatment for stroke. This paper also deals with the nanodrive mechanism fixed to the torpedo shaped Nanorobot for the propulsion of the robot.

OPTICAL PROPERTIES OF Ho^{3+}-Yb^{3+} AND Nd^{3+} DOPED SiO_2-LaF_3 GLASS-CERAMICS BY SOL-GEL METHOD

J.J. VELÁZQUEZ[1], A.C. YANES[2], J. MÉNDEZ-RAMOS[1], J. DEL-CASTILLO[2] AND V.D. RODRÍGUEZ[1]

[1]*Dpto. Física Fundamental y Experimental, Electrónica y Sistemas, Universidad de La Laguna, 38206 La Laguna, Tenerife, SPAIN*
e-mail: josvel@ull.es

[2]*Dpto. Física Básica, Universidad de La Laguna, 38206 La Laguna, Tenerife, SPAIN*
e-mail: ayanesh@ull.es

At present time, rare earth ions doped oxyfluoride glass-ceramics have a great interest in the development of optical devices as lasers, optical amplifiers and upconverters. These materials have the spectroscopic advantages of the fluoride hosts, due to their low phonon energies, and the good mechanical and chemical properties of the oxide glasses. Moreover, they remain transparent due to the nanoscale of the fluoride crystals [1].

The upconversion and near-infrared emissions of Ho^{3+} ions have been investigated in oxyfluoride glass-ceramics obtained by conventional melting method [2]. Upconversion emissions have been also obtained in Ho^{3+}-Yb^{3+} co-doped oxyfluoride glass-ceramics prepared by sol-gel method [3]. On the other hand, infrared emission at 1.06 μm of Nd^{3+} ions is one of the most widely studied infrared emissions for lasers devices. However, there are only few works related the lasers properties of Nd^{3+} in glass-ceramics [4].

In this work, the optical properties of rare earth doped SiO_2-LaF_3 oxyfluoride glass-ceramics prepared by sol-gel method are studied, focusing attention on UV and VIS up-conversion emissions for Ho^{3+}-Yb^{3+} co-doped samples and near infrared emission for Nd^{3+}-doped samples.

Oxyfluoride glass-ceramics with composition $5LaF_3$-$95SiO_2$ codoped with 0.1 Ho^{3+}-0.3 Yb^{3+} (mol%) or doped with 0.1 Nd^{3+} (mol%) were prepared by sol-gel method in a similar way as Fujihara et al.[5]. Nanocrystals of LaF_3 were precipitated by heat-treatment and identified by X-ray Diffraction. In previous work we used sol-gel technique for the preparation of silica based transparent glass-ceramics doped with Eu^{3+} ions [6].

The optical spectra indicate that a fraction of the Ho^{3+} ions are incorporated to the LaF_3 nanocrystals. As a consequence, efficient UV and VIS upconversion emissions are observed under direct infrared excitation of the Yb^{3+} ions at 980 nm (see Fig.1). The upconversion mechanisms were investigated: UV emission is obtained by a three-photon process whereas only two photons are necessary to obtain the VIS emission. On the other hand, for the Nd^{3+}, the stimulated emission cross-section has been calculated using the F-L equation based on the spontaneous emission spectrum (see Fig. 2). The absorption cross-section has been derived from emission spectrum on the basis of reciprocity method of McCumber. As a result, gain cross-section wavelength dependence has been computed, as a function of population inversion of involved states.

[1] Y. Wang and J. Ohwaki, Appl. Phys. Letters 63 (24), 3628 (1993).
[2] A.S. Gouveia-Neto, E.B. da Costa, L.A. Bueno, S.J.L. Ribeiro, J. of Luminescense (2004).
[3] A. Biswas, G.S. Maciel, C.S. Friend and P.N. Prasad, J. Non-Cryst Solids **316**, 393 (2003).
[4] U.K. Kang, T.I. Chuvaeca, A.A. Onushchenko, A.V. Shashkin, A.A. Zhilin, H. Kim and Y. Chang, J. Non-Cryst. Solids 278, 75 (2000).
[5] S. Fujihara, C. Mochizuki and T. Kimura, J. Non Crist. Solids **244**, 267 (1999).
[6] A.C. Yanes, J. Del Castillo, M.E. Torres, J. Peraza, V.D. Rodríguez and J. Méndez-Ramos, Appl. Phys. Letters 85, 2343 (2004); A.C. Yanes, J. Del Castillo, J. Méndez-Ramos, V.D. Rodríguez, M. Torres, J. Arbiol, Optical Materials 2006 (in press).

TOPICS: Nanophysics, nanomaterials and nanotechnology.

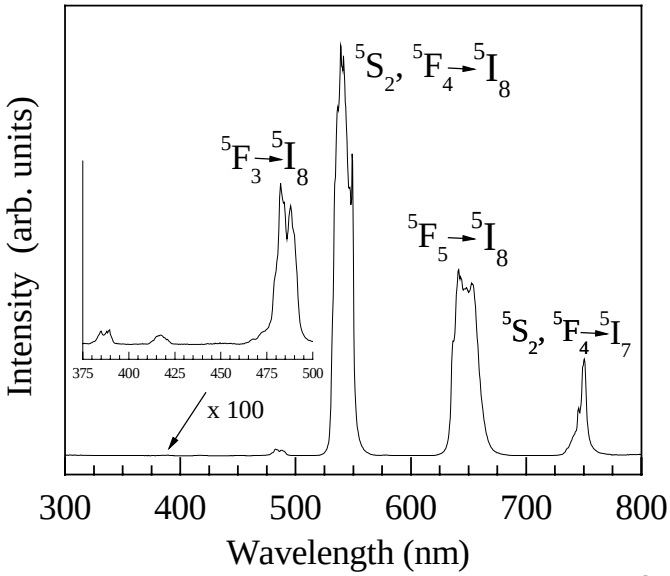


Fig 1. Up-conversion emission spectrum of $95SiO_2$-$5LaF_3$: $0.1Ho^{3+}$- $0.3Yb^{3+}$ (mol%) glass-ceramics obtained under 980 nm excitation at room temperature (inset: magnified spectrum in the wavelength range of 375 - 500 nm).

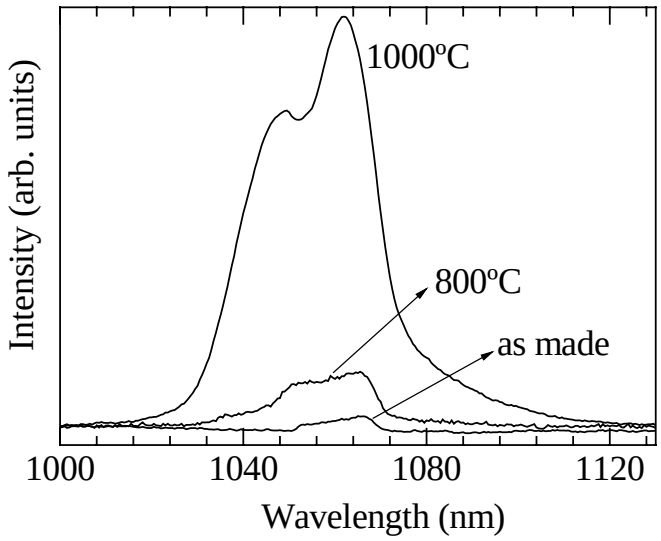


Fig 2. Emission spectra of $95SiO_2$-$5LaF_3$ doped with 0.1mol% of Nd^{3+} samples, as made and heat treated at 800 and 1000ºC respectively, exciting at 800 nm.

NANOSTRUCTURED MATERIALS WITH APPLICATIONS IN BIOSENSING AND BIOCOMPATIBILITY

Fiorenzo Vetrone[1], *Fabio Variola*[1], *Antonio Nanci*[2], *Federico Rosei*[1]

[1] *Institut National de la Recherche Scientifique-Énergie, Matériaux et Télécommunications, Université du Québec, Varennes, Québec J3X 1S2, Canada*
[2] *Laboratory for the Study of Calcified Tissues & Biomaterials, Faculté de Médecine Dentaire, de Montréal, Montréal, Québec H3C 3J7, Canada*
vetrone@emt.inrs.ca

Advanced materials in the sub-100 nm regime have been shown to have novel and improved physical, chemical, and biological properties compared to traditional materials [1]. In this presentation, we will explore two diverse examples of nanostructured materials with applications in biology. First, we will focus on luminescent nanoparticles doped with lanthanide ions that have the capability to (up)convert infrared light to visible and/or ultraviolet. The small size of these materials (sub-20 nm) allow for the development of a "sandwich-type" bioassay where the analyte of interest is wedged between donor and acceptor labels and operates on the principle of fluorescence resonance energy transfer (FRET). Secondly, we will discuss biocompatible materials whose surfaces have been modified to create a nanotopography, which has yielded promising results.

(i) Conventional fluorescent sandwich assays use blue light to excite the donor label and have already been commercialized (Fig. 1a). However, the blue (high-energy) light absorbs readily by proteins (often damaging them) and also excites all fluorescent contaminants in the sample, resulting in poor sensitivity. By replacing the donor label with an Ln-doped upconverting nanoparticle, it becomes feasible to use an NIR light source, which selectively excites that label (Fig. 1b). However, before the biomedical studies of such assays are performed, it is essential to fully understand the mechanism(s) that lead to upconversion in nanosystems.

We developed for the first time erbium (Er^{3+}) doped nanomaterials that are capable of upconverting NIR light to green and red (Fig. 2). This ion is ideal for use in FRET assays since it has no emission in the region where the acceptor label would emit. Initially, we prepared Er^{3+}-doped binary nanocrystalline oxides (e.g. Y_2O_3:Er^{3+}) and studied various parameters that may influence the upconversion of the Er^{3+} ion [2, 3]. We found that after excitation with NIR radiation (980 nm) the nanocrystals emitted green and red light. However, when compared to an identically doped bulk sample, the intensity of the upconversion was several orders of magnitude lower. This was due to the presence of surface species bound to the outside of the nanoparticle that quenched the luminescence. We also proved that as a result of these species, the fundamental mechanism of upconversion was significantly altered and led to drastically different upconversion spectra. Subsequently, we investigated more complex ternary nanocrystalline oxides ($Gd_3Ga_5O_{12}$:Er^{3+}) and showed that these materials are much more promising. They do not suffer from surface contamination and as a result, their upconversion intensity was much stronger and ideal for use in assays. Upconversion emission was observed when pumping with low energy (5 mW) from inexpensive solid state NIR sources.

(ii) Titanium and its alloys are widely used in implants due to their excellent biocompatibility. To improve implants, it is essential to engineer biomaterials in ways that promote tissue integration and improve biological function. The key to the design of novel biomaterials is to properly manage the interaction of the surface and the interface between the material and the

host tissue since in the human body, most reactions occur at surface and interfaces. Using a simple chemical treatment, we produced a unique nanostructured topography (Fig. 3) [4]. These surfaces selectively inhibit fibroblastic cell growth while promoting osteogenic cell activity. Such intelligent surfaces may be used for various applications, including implantable biomaterials as well as drug delivery and biosensors, with broad implications and a significant impact in nanomedicine.

References:

[1] F. Rosei, J. Phys.: Condens. Matter., **16** (2004) S1373-S1436.
[2] F. Vetrone, J. C. Boyer, J. A. Capobianco, *"Yttrium oxide nanocrystals: Luminescent properties and applications"*. In The Encyclopedia of Nanoscience and Nanotechnology. Edited by Nalwa, H. S. American Scientific Publishers. Stevenson Ranch, CA, **10** (2004) 725-765.
[3] F. Vetrone, J. C. Boyer, J. A. Capobianco, A. Speghini, M. Bettinelli, Chem. Mater., **15** (2003) 2737-2743.
[4] P. Tambasco de Oliveira, A. Nanci, *Biomaterials*, **25** (2004) 403-413.

Figures:

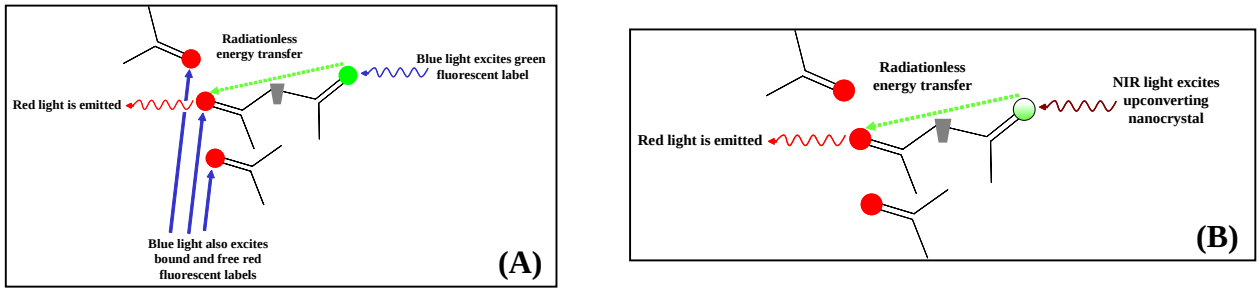


Figure 1: (A) Schematic representation of a conventional FRET assay. (B) Schematic representation of an upconversion FRET assay.

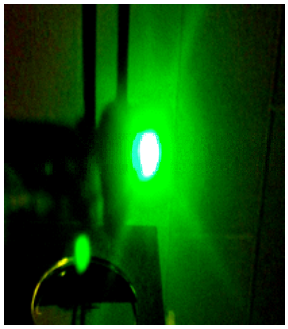


Figure 2: Upconversion luminescence of Y_2O_3:Er^{3+}, Yb^{3+} nanocrystals

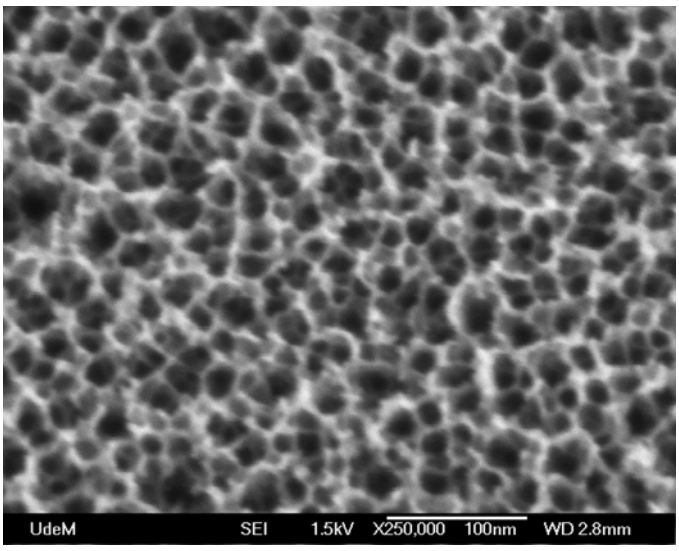


Figure 3: SEM image of nanostructured titanium alloy surface

Poster

Fabrication of Opals and Inverse Opals with a Planar Defect

Likui Wang, (George) X. S. Zhao*

Department of Chemical and Biomolecular Engineering, National University of Singapore, 10 Kent Ridge Crescent, Singapore 117576

Nanoscience and Nanotechnology Initiative, National University of Singapore, 10 Kent Ridge Crescent, Singapore 117576

Email: chezxs@nus.edu.sg

A facile method of fabricating opal and inverse opal structures with a planar defect was demonstrated. A single layer of silica beads was embedded into polystyrene opals by combining an inward-growing self-assembly method with spin-coating technique. After infiltration of silica, followed by removal of the polystyrene beads by calcination, an inverted structure was obtained. The silica beads were connected together by the infiltrated silica, thus a solid silica phase with the silica beads as a planar defect embedded in the inverse silica opal was obtained. The thickness of the defect layer can be adjusted by changing the size of silica beads. Scanning electron microscope images showed good quality of the crystal and uniformity of the defect layer. Optical transmission spectra indicated the existence of defect state induced by the defect layer in both the opal and inverse opal structures. High-cost techniques such as lithography and chemical vapor deposition are not involved in the fabrication of inverse opals with planar defects.

Figures:

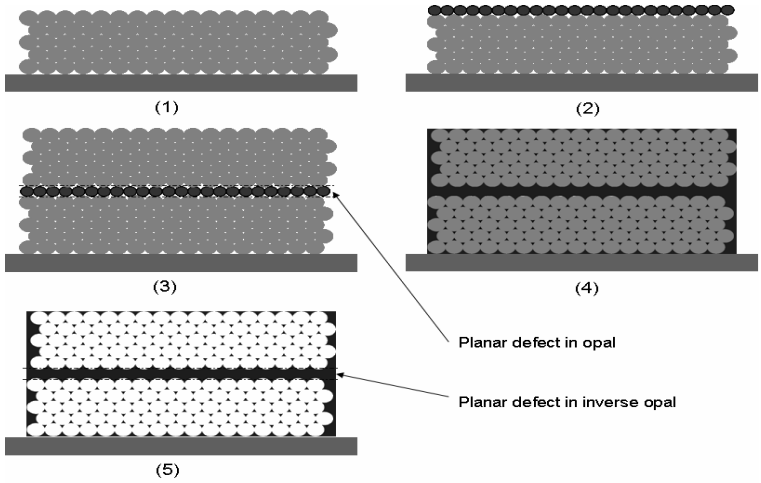


Figure 1. A scheme showing the steps of fabricating a planar defect embedded in an opal and inverse opal: (1) Growth of the first PS multilayer on a glass substrate by using an inward-growing self-assembly method; (2) Spin coating of a monolayer of silica beads on the surface of the PS colloidal crystal; (3) Growth of the second PS multilayer on the surface of the silica beads; (4) Infiltration with silica; (5) Removal of the PS particles by calcination.

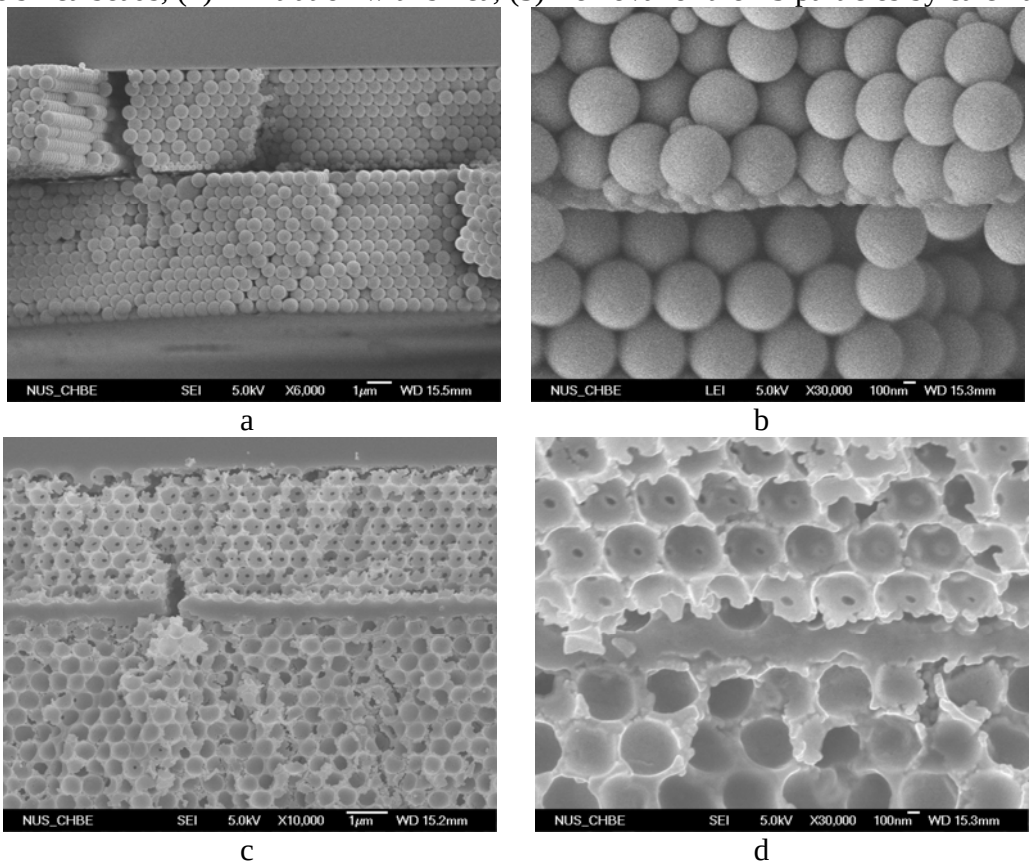


Figure 2. SEM images of an opal with planar defect and its inverted structure: (a, b) 20 layers of 560nm PS spheres embedded with a 225nm silica bead monolayer, low and high magnification; (c, d) the inverted opal sample, low and high magnification.

TEMPERATURE INDUCED CONFORMATIONAL CHANGE OF TETRAPYRIDYLPORPHYRIN ON Cu(111)

Alexander Weber-Bargioni[1], Willi Auwärter, Andreas Riemann, Agustin Schiffrin, and Johannes V. Barth

[1] *Departments of Physics & Astronomy and Chemistry, University of British Columbia, Vancouver, B.C. V6T 1Z4, Canada*

aweber@physics.ubc.ca

Recently there has been much interest in the self-assembly of functional organic molecules on various metal substrates, preparing the ground for the control and synthesis of low-dimensional supramolecular nanosystems, which are potentially useful for a variety of applications (e.g., molecular electronics, sensing, nano-optics or molecular magnetic devices).

Here we present Low-Temperature Scanning Tunneling Microscopy (LT-STM) and Scanning Tunneling Spectroscopy (STS) results of tetrapyridylporphyrin molecules ($C_{40}H_{26}N_8$, TPyP) adsorbed on a Cu(111) surface. In particular, we discuss the molecular ordering at various substrate temperatures and address a temperature induced conformational change. Figure 1 shows STM images of TPyP molecules deposited on Cu(111) at 270K, 390K and 510K. All STM data were recorded after cooling the sample below 15K.
Evaporated at room temperature, the TPyP molecules adsorb individually along the 6-fold symmetry of the substrate surface. In STM images the molecules exhibit a two-fold symmetry showing no change in appearance over a wide bias voltage range from -2 eV to +2 eV. Above room temperature the TPyPs form one-dimensional chain segments and hexagonal structures. In contrast, on Ag(111) densely packed molecular islands readily evolve already at low coverage, indicating appreciable molecular surface mobility and moderate substrate coupling [1,2].
To determine the adsorption sites of TPyP on the Cu(111) surface, CO molecules were deposited in-situ. In the low coverage regime they exclusively decorate the on-top adsorbtion sites on Cu(111) and can consequently be used as markers for the substrate lattice, (compare figure 2).
Once the sample is annealed over 470K, the molecular contrast changes considerably: the TPyP molecules appear as four lobes, supposing a conformational change of the TPyP on the substrate. In this new state, we can further distinguish two types of molecules by considering subtle contrast variations: One appearing hollow in the center and the other one showing contrast in the center (compare figure 3).
This conformational change is also underlined by differences in the tunneling spectroscopy over the admolecules. Tunneling spectra on single TPyPs adsorbed at room temperature do not show any contribution from additional molecular electronic states and strongly resemble the data taken on the pure Cu(111) substrate. In the new state after annealing, the spectra taken on the hollow appearing TPyPs, show an electronic state at 2 eV, which is 300 meV wide.
Furthermore, the conformational change of the molecules is accompanied by a change in the nearest neighbor distance between the molecules in the one-dimensional chain segments.

The formation of one dimensional chains on Cu(111) above room temperature along the substrate surface symmetry we account to interactions of Cu adatoms with TPyP. This assumption is supported by experiments, exploiting coordination interactions between the pyridil functional moiety and co-deposited metal atoms. This work is part of a strategy to fabricate metallosupramolecular networks with specific topologies and a high structural stability.

References:

[1] Self-assembly and conformation of Tetrapyridil-porphyrin molecules on Ag(111**)** W.Auwärter, A. Weber-Bargioni, A. Riemann, A. Schiffrin, O. Gröning, R.Fasel and J.V. Barth, **J. Chem. Phys.** 124(2006), 194708

[2] The make of metallo-porphyrins in two dimensions W. Auwärter, A. Weber-Bargioni, S. Brink, A. Riemann, A. Schiffrin, M. Ruben and J.V. Barth, to be publishedP

Figures:

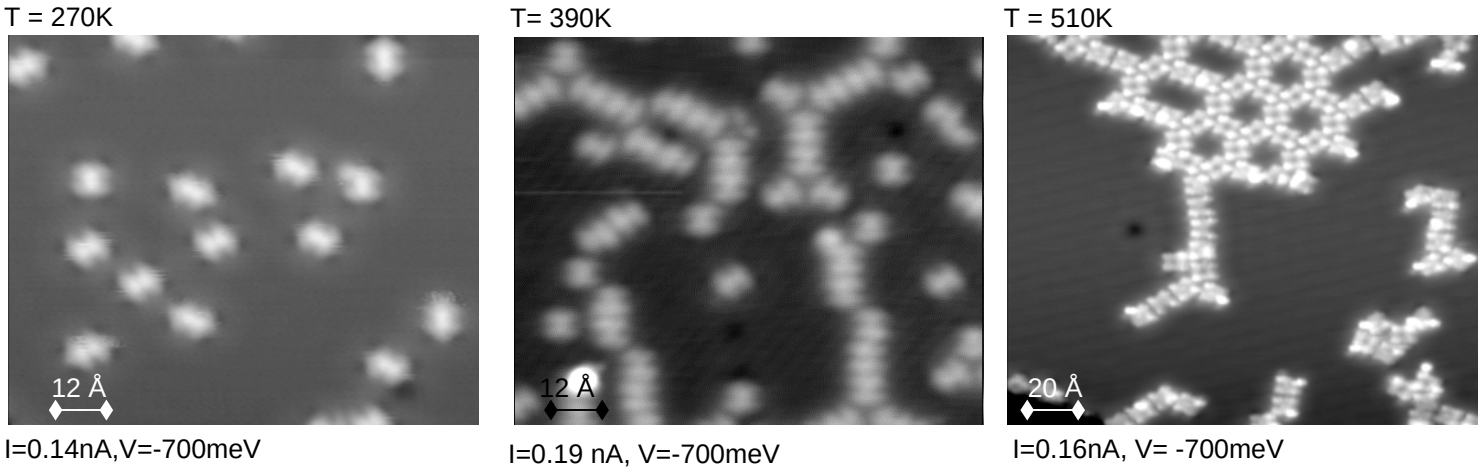


Figure 1: TPyP deposited at 270K, 390K and 510K on Cu111. The admolecules assemble to complex structures at higher temperatures and show a conformational change above 450K

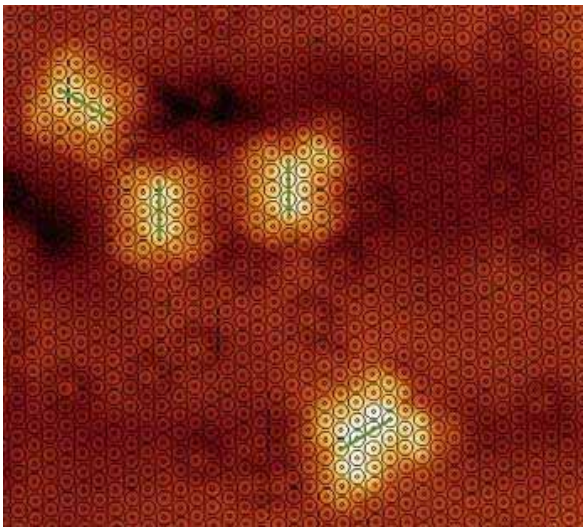


Figure 3: after annealing at 470K two different contrasts are observable in the center. The hollow appearing admolecules show information in STS

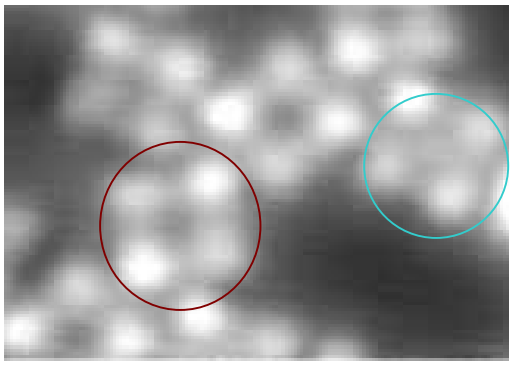


Figure 2: determination of adsorption site on the Cu111 via C-O admolecules as markers.

Comparative study of the conductance in multiwall carbon nanotubes and semiconductor nanowires

J-E Wegrowe, J.-F Dayen,T. Wade,X. Jehl, M. Sanquer
Laboratoire des solides irradiés, Ecole Polytechnique,Paleseau
et CEA-DRFMC, Grenoble, France

wegrowe@poly.polytechnique.fr

We compare the electronic transport of an ensemble of multiwall carbon nanotubes and semiconductor nanowires of typically W=20nm diameter and l=1000 nanometer long. The nanotubes and nanowires were obtained by template synthesis in porous membranes [1]. The templates used are anodized alumina and commercial track etched polycarbonate membranes. The pores of the membranes are partially filled with electrodeposited catalysts or entirely with semiconductors (Te, Se or ZnO nanowires). Thermal CVD allows carbon nanotubes and Si nanowires to be obtained from the electrodeposited catalysts (Co, Ni, Au and Cu). In the case of electrodeposited nanowires, a single wire is contacted inside the membrane with an in-situ method.

For all samples (about 50, with the exception of a couples of samples), the non-ohmic behavior of the conductance, the so-called zero bias anomaly, shows a temperature dependence that scales with the voltage dependence. The conductance G(V,T) is described by a single scaling coefficient α. A statistic of the coefficient α is performed, and a universal law as a function of α was found for all samples [2]. This law seems to be a characteristic of Coulomb Blockade effects in our structures, and fit with the following prediction of non-conventional CB theories [3, 4] for all sample.

In parallel, the magnetoresistance measurements show systematically a weak localization effect that seems to follow the expression of the quasi-1D weak localization formula as a function of the amplitude of the perpendicular magnetic field. This allows one to fit the $\Delta G(H)$ curve for different temperatures, and for all samples (i.e. for various coefficient α), and to deduce the phase coherence length $L\phi$. The expected temperature dependence for $L\phi$. - proportional to $T^{-1/3}$ - is observed. The relation between $L\phi$. and the scaling coefficient α is then deduced (Fig. 1).

Independently, the measurements at very low temperatures, down to 50 mK show a weak to strong localization transition [5] beyond the Coulomb regime (Fig. 2). In the case of strong localization, zero bias anomaly and scaling laws are no longer observed, and a metal-insulator transition from 10^5 to 10^9 ohm occurs at the critical bias (Inset in Fig. 2, left). The CB regime is restored at high voltage, beyond the strong to weak localization transition. Activation energies E_a are deduced in the hopping regime, and correlated to the scaling coefficient α.(here, only six samples have been measured below 1K: three CNT and three Te nanowires). The relation between the activation energy and the coherence length is deduced. The behaviour observed, $Ea \sim Cst./L\phi$, is in agreement with hopping processes in quasi-1D wires, where the phase coherence length is defined, like here, at the critical point where the two regime coexist.

The comparative study between different kind of nanowires and nanotubes shows that the main properties of the electric conduction are due to Coulomb blockade in a disordered structure. The disorder is indirectly measured through the phase coherence length (range from 50 to 200 nm). In the coulomb blockade regime, each sample is characterized by its scaling coefficient α, and by the phase coherence length, i.e. by each specific configuration of the

disorder at the nanoscopic scales. Beyond the above conclusions, the role of the intrinsic properties is expected in pure single crystalline Si nanowires.

References:

[1] Wade, T. L. and Wegrowe, J.-E., J. Phys. Appl. Phys. 29 (2005) 3.
[2] Dayen, J. –F., Wade, T.L., Konczykowski M., Hoffer X. and Wegrowe, J.-E., Phys. Rev. B 72 (2005) 073402.
[3] Rollbuehler, J. and Graber, H Phys. Rev. Lett. 87 .(2001) 126804.
[4] Egger, R. Gogolin, A. O. Phys. Rev. Lett. 87 (2001) 066401.
[5] Khavin, Yu., Gershenson B, M. E., and Bogdanov, A. L. Phys. Rev. B 58 (1998). 8009.

Figures:

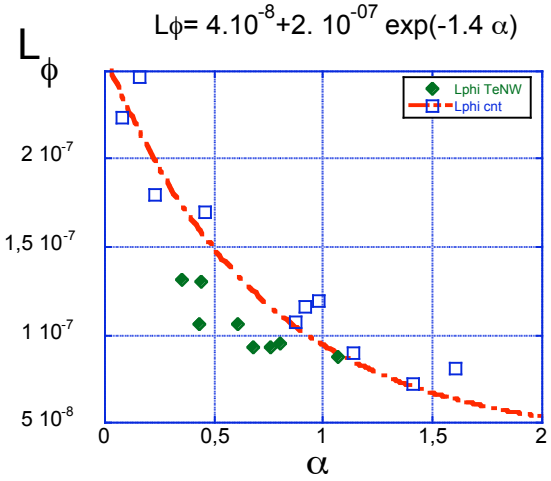


Fig1: Phase coherence length as a function of the scaling coefficient α for MWCNT and Te nanowires.

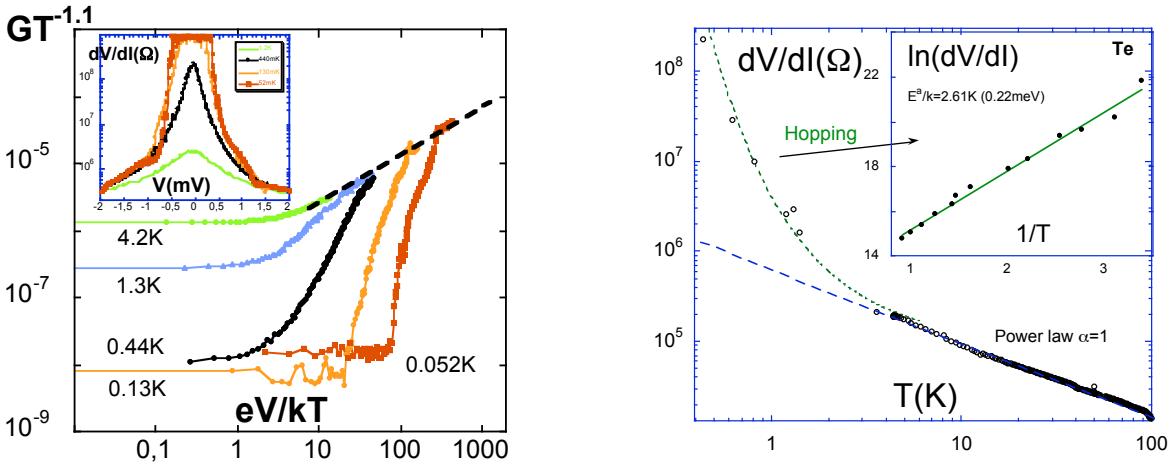


Fig2: Scaling plot at very low temperature: the hopping conduction destroys the coulomb blockade regime. Inset: conductance as a function of bias voltage. Right: transition from coulomb blockade to hopping regime as a function of the temperature. Inset: the Arrhenius Plot shows the hopping regime.

Formation of single-crystallized nanowires of manganese and vanadium oxides by a soft chemical process

Mingdeng Wei,[ab] Hideki Sugihara,[b] Itaru Honma,[b] Haoshen Zhou [ab]

[a] Japan Science and Technology Agency (JST), Light and Control Research Group, PRESTO, Kawagoe, Saitama 3320012, Japan
[b] National Institute of Advanced Industrial Science and Technology (AIST), AIST Tsukuba Center, Ibaraki 305-8568, Japan.
wei-mingdeng@aist.go.jp; hs.zhou@aist.go.jp

One-dimensional (1D) nanostructures include nanotubes, nanowires, nanorods, nanofibers, nanobelts and nanoribbons. In the past decade, a larger number of 1D structural nanoscale materials have been synthesized using variously synthetic routes, such as chemical reaction[1], template technique[2], and so on. For all of these routes, additional reagents or templates were introduced into the reaction system, As such, the synthetic process is complicated, and might bring about an increase of impurity concentration in the final product. In this study, a simple method was used to synthesize nanowires of manganese and vanadium oxides using only the raw material and water.

Synthesis of nanowires of manganese and vanadium oxides was performed by a soft chemical process [3-4]. In a typical synthesis, 0.15 g commercial γ-MnO_2 or V_2O_4 powder was dispersed into a 15 ml H_2O, then was transferred into a 20 ml autoclave, and kept it in oven at 100 - 200 °C for 1-14 days. The as product was filtered, and died at in air. Finally, the product was characterized by XRD, TGA, SEM and TEM measurements.

Synthesis of single-crystal α- and β-MnO_2

Figure 1A shows the XRD patterns of the raw material and products synthesized at 140, 170 and 200 °C for 3 days. It clearly indicates that diffractions of the products are significantly different from the raw material. As shown in Fig. 1A curves b-d, the crystal phase of the products varied with increasing with increasing temperature, and could be indexed onto α-MnO_2, β-MnO_2 and MnOOH, respectively (JCPDS 44-0141, 24-0735, 74-1632). This result indicates that MnO_2 polymorphic forms can be synthesized by selected-control reaction temperature.

SEM images of α- and β-MnO_2 are shown in Fig. 1B-C and reveal the presence of a larger number of nanowires with a long length. TEM measurement further confirmed the formation of nanowires with a diameter ca. 10-30 nm, as depicted in Fig. 1D-E. High magnification images clearly reveal very crystallized nanowires and the lattice fringes correspond to d-spacing of 0.69 and 0.31 nm for α- and β-MnO_2, respectively.

Synthesis of single-crystal $V_2O_4 \cdot 0.25H_2O$ nanowires

Figure 2A depicts the XRD patterns of the raw material (curve a) and product synthesized at 170 °C for 1, 3, 7, 14 days (curves b-e), respectively. It is notable that a peak at 2θ = 10 ° was observed after the reaction time is more than 3 days, and became more intense with increasing reaction time. This is a characteristic of layered compound, and also was observed in layered hydrate $VO_2 \cdot 1/2H_2O$ and $V_2O_4 \cdot 2H_2O$. This result indicates that the product is a vanadium oxide hydrate $V_2O_4 \cdot nH_2O$ with layered structure. However, all the diffraction peaks can not be indexed onto a vanadium oxide hydrate reported in publications, indicating that the product is a new metastable phase of vanadium oxide hydrate. Using the least-squares method, all the diffraction peaks could be indexed onto the basis of monoclinic symmetry with the lattice parameters a = 16.690 Å, b = 6.200 Å, c = 9.580 Å, and β = 92.20 °. After the product

(synthesized at 200 °C for 3 days) was calcined at 300 °C, the peak at 2θ = 10 ° disappeared (see Fig. 2A curve f), indicating that water of crystallization in product was removed. TG analysis indicates the weight of crystal water is ca. 2.58%, and closes to the theoretical weight of crystal water. Therefore, we suggest that the phase of products is $V_2O_4 \cdot 0.25H_2O$. SEM and TEM images reveal the presence of highly crystallized nanowires.

In order to investigate the formation process of nanowires, a series of the samples were prepared under different reaction conditions and further characterized by XRD, SEM and TEM. Based on the experimental results, the possible formation model of manganese and vanadium oxides was proposed.

References:

[1] Z. Gui, R. Fan, W. Q. Mo, X. H. Chen, L. Yang, S. Y. Zhang, Y. Hu, Z. Z. Wang, W. C. Fang, Chem. Mater., 14 (2002) 5053.
[2] M. Adachi, Y. Murata, M. Harada, Chem. Lett., 29 (2000) 942.
[3] M. D. Wei, Y. Konishi, H. S. Zhou, H. Sugihara, H. Arakawa, Nanotech., 16 (2005) 245.
[4] M. D. Wei, H. Sugihara, I. Honma, M. Ichihara, H. S. Zhou, Adv. Mater., 17 (2005) 2964.

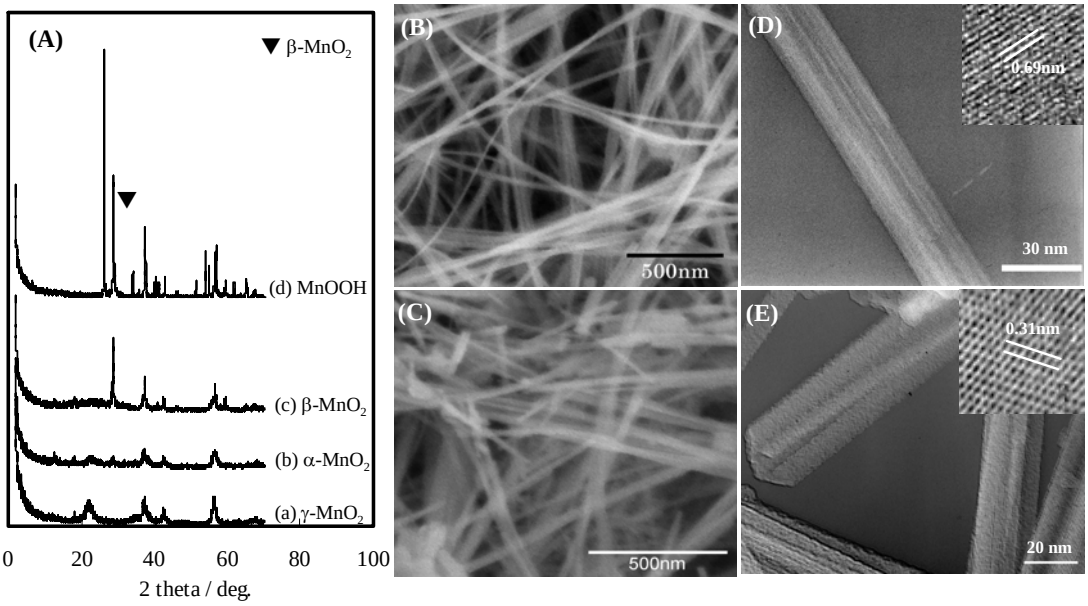


Figure 1 The XRD patterns, SEM and TEM images of manganese oxides obtained at different temperatures.

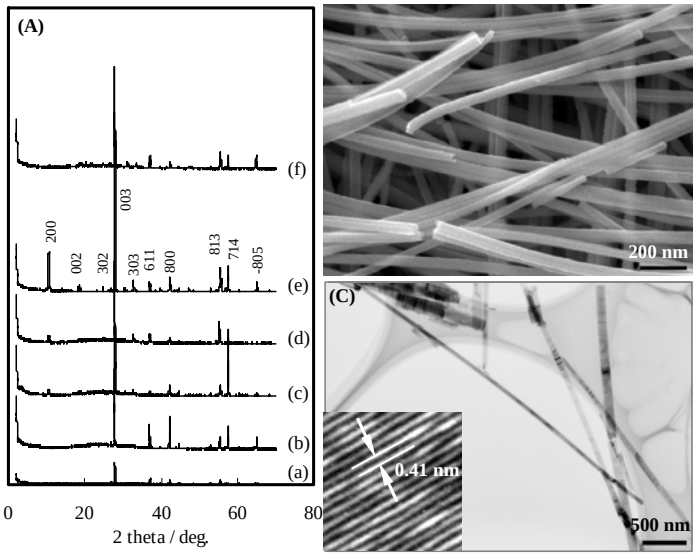


Figure 2 The XRD patterns, SEM and TEM images of vanadium oxide obtained at 170 °C for 14 days.

Poster

SHAPE CONTROLLED SYNTHESIS OF AU NANOPARTICLES

Sung Ik Yang, Seon Ho Kim, S un Young Park
College of Environment and Applied Chemistry, Materials Research Center for Information Display, Kyung Hee University, Yongin, 449-701, Republic of Korea
siyang@khu.ac.kr

Inorganic nanoparticles have attracted great attention to the scientific community due to their potential applications in nanoelectrons, nanophotonics, chemical sensing, and biological imaging [1-3]. In particular, noble metal nanoparticles have been of considerable interest since chemical and physical properties of metal nanoparticles are strongly influenced by the size and shape due to surface and quantum size effect [4,5]. For example, the absorption wavelength of the surface plasmon band of spherical Au nanoparticles is 530 nm, whereas that of the rod shape of Au nanoparticles with aspect ratio 4 is 780 nm.
Xia *et al*. have prepared single crystal cubes and tetrahedrons through selective etching and dissolution processes [6,7]. Murphy and El-Sayed group have synthesized various aspect ratio of Au nanorods via seed-mediated growth method [8-10].
We have synthesized Au nanoparticles with controllable shape via seed-mediated growth method with modification and characterized their optical properties as a function of shape. We examine the nucleation and growth conditions to understand the growth mechanism and reaction parameters that determine the shape of nanoparticles. To synthesize various shapes of Au nanoparticles, we prepared Au seed particles by reducing gold chloride with $NaBH_4$ in the presence of cetyltrimethylammonium bromide (CTAB). We prepared aqueous growth solution with $HAuCl_4$, ascorbic acid (AA), $AgNO_3$ and CTAB. Tehn we added an appropriate quantity of Au seed to the aqueous growth solution. The shapes of Au nanoparticles strongly depend on the ratio of the concentration of seed solution, AA and CTAB and could be controlled from sphere to square to star by varying the ratio of seed over AA and CTAB.
The synthesized Au nanostructures were observed by TEM. The bright-field plan-view images for Au nanoparticels with sphere, cube, and multipod are shown in Fig. 2. In Fig. 2 (B), the particles synthesized at room temperature are round and have an average diameter of around 13 nm. By controlling the additional AA quantity, Au particles with various shapes were observed; adding 0.6 ml AA resulted in mono-dispersed cube nanoparticles with 17 nm in diameter. As we increased the concentration of $AgNO_3$, we could obtain multipod with 21 nm in diameter.
Fig. 1 shows the electronic absorption spectra of Au nanoparticles in hexane solutions as a function of shape, which is consistent with previously reported results. According to the Mie theory [11], the decrease in the size gives rise to intense surface plasmon absorption around 530 nm due to the coherent oscillation of the free electrons from the surface of the silver nanoparticles. Plasmon absorption maximum slightly shifted to red at 550 and 560 nm upon forming cube and multi-pod, respectively. In particular, the absorption spectrum of star shaped has two strong plasmon absorption bands at 560 and 850 nm which is related with the transverse and longitudinal plasmon absorption, respectively of Au nanoparticles.
In conclusion, we have synthesized various shape of Au nanoparticles via seed-mediated growth and characterized their optical properties.

References:

[1] Y. Huang, X. Duan and C. M. Lieber, Science **291** (2001) 630.
[2] S. A. Maier, M. L. Brongersma, P. G. Kik, S. Meltzer, A. A. G. Requichia and H. A. Atwater, Adv. Mater. **13** (2001) 1501.
[3] R. Jin, Y. W. Cao, C. A. Mirkin, K. L. Kelly, G. C. Schatz and J. G. Zheng, Science **294** (2001) 1901.
[4] M. A. El-Sayed, Acc. Chem. Res. **34** (2001) 257.
[5] N. Toshima, M. Kuriyama, Y. Yamada and H. Hirai, Chem. Lett . **10** (1981) 793.

[6] B. Wiley, T. Herricks, Y. Sun and Y. Xia, Nano Lett. **4** (2004) 1733.
[7] S. H. Im, Y. T. Lee, B. Wiley and Y. Xia, Angew. Chem. Int. Ed. **44** (2005) 2154.
[8] G. Linfeng, C. J. Murphy, Chem. Mater. **17** (2005) 3668.
[9] Nikoobakht, B.; El-Sayed, M. A. Chem. Mater. **15** (2003) 1957.
[10] T. K. Sau, C. J. Murphy, C. J. Langmuir 20 (2004) 6414.
[11] G. Mie, Ann. Phys. **25** (1908) 329.

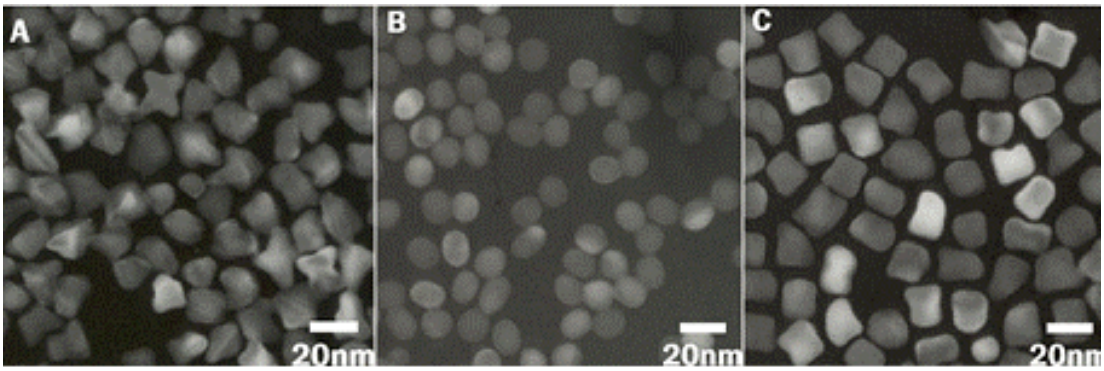


Figure 1. TEM images of (A) mulipod, (B) sphere, and (C) cube Au nanoparticles

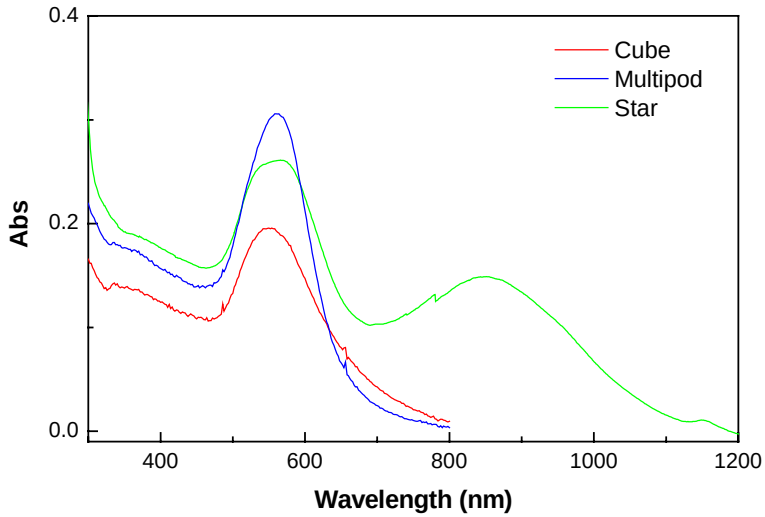


Figure 2. Absorption spectra of cube, multipod, and star shaped Au nanoparticles.

ATOMISTIC SIMULATION OF INTERACTIONS OF CARBON NANOPARTICLES WITH ORGANIC COATINGS

Irene Yarovsky, David Henry, George Yiapanis, Evan Evans
RMIT University, GPO Box 2476V, Melbourne, Australia
Irene.yarovsky@rmit.edu.au

Polyester paint coatings may discolor when exposed to long term harsh weathering conditions. The principal source of contamination has been suggested as rain or air carried carbonaceous particles that adhere to the paint surface. Computational studies of interfacial adhesion between modified polyester and carbon surfaces can provide valuable insight into the design of contamination resistant paint coatings. To enable a realistic nanoscale representation of a cured paint surface, we have developed a methodology for construction of atomistic models of crosslinked polymer networks[1]. In this study, the fully atomistic model of crosslinked polyester has been modified on the atomic scale, using hydrophobic and hydrophilic functional groups, with varying degree of surface coverage. Graphite, amorphous carbon[3] and fullerene models have been used to simulate the carbonaceous contaminants.

Theoretical adhesion calculations[2,4] have been used to characterize the interfacial interactions between polyester and carbon surfaces under a variety of computational protocols which include accentuation of polyester atomic surface roughness (Figure 1) and relaxation of the interface. Adhesion energetics have been calculated using the COMPASS forcefield[5] to describe interatomic interactions. COMPASS (Condensed – phase Optimized Molecular Potential for Atomistic Simulation Studies) is an ab-initio force field with parameters derived from approximate solutions of the full Hartree Fock equations, and optimized for a wide range of condensed matter properties using experimental data. The parameterization to condensed phase properties used in this forcefield is ideal for application to adhesive energy calculations between dense surfaces and has been demonstrated to produce reliable results for our systems of interest [1,2,4,5].

Results show that chemical modification and atomic scale roughness of a polyester surface can significantly affect adhesion with the carbonaceous solids (Figure 2). Relaxation of the interface leads to reorganisation of the polyester substituents, increasing the interfacial contact area and thereby reducing the effects of atomic surface roughness. This is more pronounced at elevated temperatures where the mobility of the polyester components is far greater.

We have also examined the interaction of neutral and charged fullerenes with model silica and polyester surfaces. Classical Molecular Dynamics simulations at 298 K indicate that Van der Waals forces are sufficiently strong in most cases to cause physisorption of the neutral fullerene particle on to the surfaces (Figure 3). The adhesion of C_{60} to both the silica and polyester surfaces depends greatly on the charge on the particle. Crosslinking and functionalization of the polyester can improve resistance to the neutral fullerene. However, for charged fullerenes, the same functionalization can actually reduce resistance to adhesion.

References:

[1] Yarovsky, I., Evans, E., Polymer **43** (2002) 963.
[2] Henry, D. J.; Yiapanis, G.; Evans, E.; Yarovsky, I., J. Phys. Chem. B **109** (2005) 17224.
[3] Petersen, T., Yarovsky, I., Snook, I., McCulloch, D., Opletal, G., Carbon **42** (2004) 2457.
[4] Henry, D. J., Lukey, C. A., Evans, E., Yarovsky, I., Mol. Simul. **31** (2005) 449.
[5] Sun, H., J. Phys. Chem. B **102** (1998) 7338.

Figure 1. Schematic representation of polyester / amorphous carbon interface.

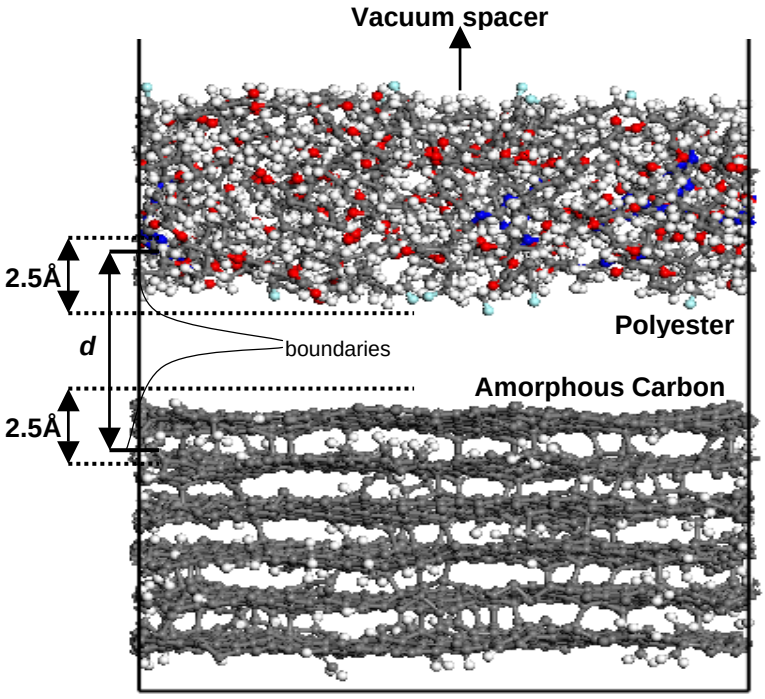


Figure 2. Sample adhesion curves for Graphite – Polyester interfaces showing the effects of nanoscale polyester surface treatments.

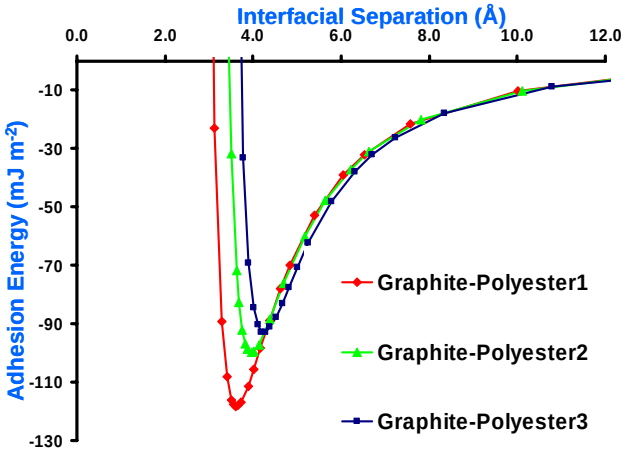
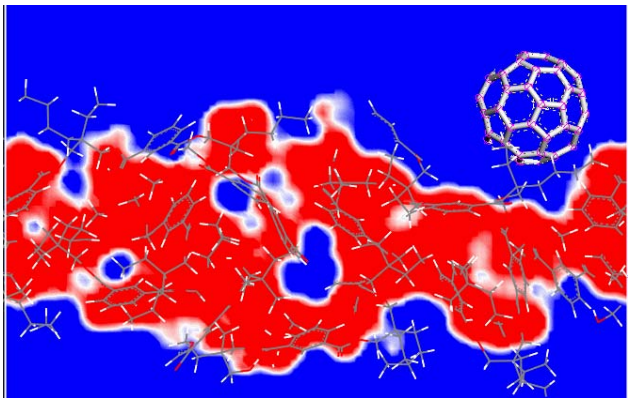


Figure 3. Slice of Van der Waals surface highlighting interaction of fullerene with polyester surface.



SWITCHABLE MAGNETISM FOR ARSENIC REMOVAL AND BIOMAGNETIC SEPARATION

Cafer T. Yavuz[1], J. T. Mayo[2], William W Yu[1], Joshua C. Falkner[1], Sujin Yean[3], Li Li Cong[4], Amy T. Kan[5], Mason Tomson[3], and Vicki L. Colvin[1].

(1) Department of Chemistry, Rice University, 6100 Main St. MS-60, Houston, TX 77005, Fax: 713-348-2578, cafer@rice.edu,
(2) Department of Chemistry, University of St. Thomas,
(3) Department of Civil and Environmental Engineering, Rice University,
(4) Department of Environmental Science and Engineering, Rice University,
(5) Civil and Environmental Engineering, Rice University

Uniform size and highly monodisperse (ó = 5-10%) magnetite (Fe_3O_4) nanocrystals were synthesized utilizing two different solvothermal reactions of iron (III) species (FeOOH and $Fe(acac)_3$). Wide range of sizes (4, 6, 8, 11, 12, 14, 20, 26, 33 nm) achieved, characterized and used for further applications. Size dependent magnetic separation was studied and applied to polydisperse samples successfully. Magnetic field strength vs. percent retention of individual sizes reported. Magnetic multiplex separation method is created and proposed for bio-magnetic separations. Superparamagnetic limit for magnetite (Rc = 16 nm) is experimentally reported for the first time. Superparamagnetic property is used to turn on and off the magnetic activity of particles. Arsenic adsorption, 100% removal from wastewaters by nanosize magnetite is shown and compared to bulk material (100x better).

ELECTROSPUN STARCH-POLYCAPROLACTONE NANO FIBER BASED CONSTRUCTS FOR TISSUE ENGINEERING.

H Ylikauppila[1], L Nikkola[1], M Gomes[2], R Reis[2], N Ashammakhi[1]
[1]Tampere University of Technology, Institute of Biomaterials, Tampere, Finland
[2]3B's Research Group, University of Minho, 4710 Braga, Portugal and Dept of Polymer Eng, Campus de Azurém, U. Minho, 4800 Guimarães, Portugal.
mailto:nureddin.ashammakhi@tut.fi

Starch based polymers have been widely studied for several different applications within the biomaterials field, including as scaffolds for tissue engineering. Recently electrospinning has been gaining interest as a promising method to manufacture highly porous 3D structures which provide high surface area for cell attachment and proliferation, being adequate for several uses in tissue engineering. The aim of this work was to develop nanofiber-based constructs from starch-polycaprolactone (SPCL 30/70 wt%) blends using electrospinning.

SPCL was dissolved in acetic acid or chloroform to form solutions with 3 different concentrations and stirred to produce a homogenous solution. About 2 ml of polymer-solvent solution was electrospun onto substrate. The distance between needle tip and the substrate was 25 cm and the voltage used was 30 kV. The microstructure of the obtained constructs was characterized by using scanning electron microscopy (SEM).

It was possible to obtain highly porous 3D scaffold with a typical nanofiber-mesh structure by using electrospinning as a method from SPCL-solvent solutions. The process was most successful with higher concentrations. With lower concentrations it was not possible to obtain nanofibers and the process was rather electrospraying than electrospinning. SEM analysis revealed the presence of particles (with an average size 6 μm) which were interconnected by the polycaprolactone nanofibres of about 150 nm. The particles can be assumed to be starch and the fibers are probably composed of polycaprolactone.

It is possible to produce highly porous nano-fiber based constructs from SPCL using electrospinning. Such constructs may have applications in tissue engineering of different tissues, such as bone, skin and cartilage.

This study is in the scope of the European Commission project EXPERTISSUES (NMP3-CT-2004-500283).

AN X-RAY SPECTROSCOPY SDUDY AND EVALUATION OF CHANGES OF INTERNAL ENERGY OF NANOPOWDERS DUE TO THEIR ULTRADISPERSION

Ya. V. Zaulychny
Frantsevych Institute for Problems of Materials Science, National Academy of Sciences of Ukraine, 3 Krzhyzhanivsky Str., Kiev UA-03142, Ukraine
zaulychnyj@ipms.kiev.ua

Changes of the electronic structure and chemical bonding due dispersion of crystals possessing different types of the chemical bonding and atomic-crystal structures have been studied using the utra-soft X-ray emission spectroscopy method. The spectra of nanoparticles were obtained with electron excitation, that allows to clean the nanoparticles from chemisorbed atoms.

The effect of narrowing of the X-ray emission bands and changing their shapes due to energy redistribution of valent electrons all the crystal components as a resuls of dispersion of the crystals up to nanoscale sizes has been observed. It has beeen shown that, this effect is due to localization of the energy levels during wanishing their sptitting after breaking chemical bonding because in nanoparticles the number of surface atoms is comparable with that in the bulk. Investigations of this effect in covalent diamond, covalent-ionic boron nitride, metal-covalent titanium carbide and nitride, titanium dioxide and barium titanate show that the value of specific narrowing and the character of energy redistribution of valent electrons depends on filling the atomic valent states by electrons, i.e. the higher filling of valent states of the atom emitting the emission band the higher specific narrowing.

It has been shown that energy distribution of the states involving into pi-bonds of carbon nanomaterials, fullerenes, nanotubes and nanofibres depends on their diameters and narrowes during decreasing the diameters. Breaking sigma-bonds after washing the nanotubes from metal-catalysts incerted into their walls leads also to narrowing energy distribution of the sigma-states.

The method of evaluation of changes the internal energy of materials when going from grain paricles to nanoscale particle sdue to increasing band energy taking into account the energy redistribution intensities of the emission bands reflecting densities of the valent electronic states has been elaborated. Our calculations of ratios of the band energies of grain particles (200 mkm) and nanopowder (30 nm) of titanium dioxide (rutile) reveal that the band energy of the nanopowder increases by 17 per cent as compared with that of the grain particles.

CHARGING EFFECTS IN CARBON NANOTUBES

M. Zdrojek[1,2], T. Mélin[1], W. Gebicki[2], D. Stiévenard[1], L. Adamowicz[2]
1. Institut d'Electronique, de Microélectronique et de Nanotechnologie, CNRS UMR 8520, Avenue Poincaré, F-59652 Villeneuve d'Ascq, France
2. Faculty of Physics, Warsaw University of Technology, Koszykowa 75, 00-661 Warsaw
zdrojekt@if.pw.edu.pl

In this contribution , we will describe the issue of electrostatic and emission properties of separated carbon nanotubes (CNTs) deposited on a insulating layer have been investigated by charge injection and Electric Force Microscopy (EFM) experiments [1]. We found that upon local injection charges were delocalized over the whole nanotube length (up to more then 40µm). We will describe the phenomenological behaviours of SWCNTs and MWCNTs upon charging.

We will present experiments aiming to dissociate between *capacitive* charging mechanisms [2] (in which the nanotubes are capacitively put at the EFM tip bias during the charging, and the charge is stored in the nanotube outer shells) and *inner-shell* charging mechanisms, associated with tunnelling processes through the nanotube shells.

Depending on the CNT diameter (number of walls) we observed different discharge behaviours:

- fast (see Fig. 1) and abrubt discharge
- charge storage with long time retention of charge

In addition, the insulating layer supporting the nanotubes is shown to act as a charge-sensitive plate for electrons emitted from the CNTs at low electric fields, thus allowing the spatial mapping of nanotubes field emission patterns. We will present that one of the important factor during field emission from nanotubes is the cap diameter (see Fig.2) and cap structure[3].

References:

[1] M. Zdrojek, T. Melin, C. Boyaval, B. Jouault, M. Wozniak, W. Gebicki, A. Huczko, D. Stievenard and L. Adamowicz, Appl. Phys. Lett. **86** 213114 (2005).

[2] M. Paillet *et al.*, Phys. Rev. Lett. **94** 186801 (2005) ; M. Zdrojek *et al.*, Phys. Rev. Lett. **96** 039703 (2006); M. Paillet *et al.*, Phys. Rev. Lett. **96** 039704 (2006).

[3] A. Buldum, *et. al.*, Phys. Rev. Lett. **91** 236801 (2003).

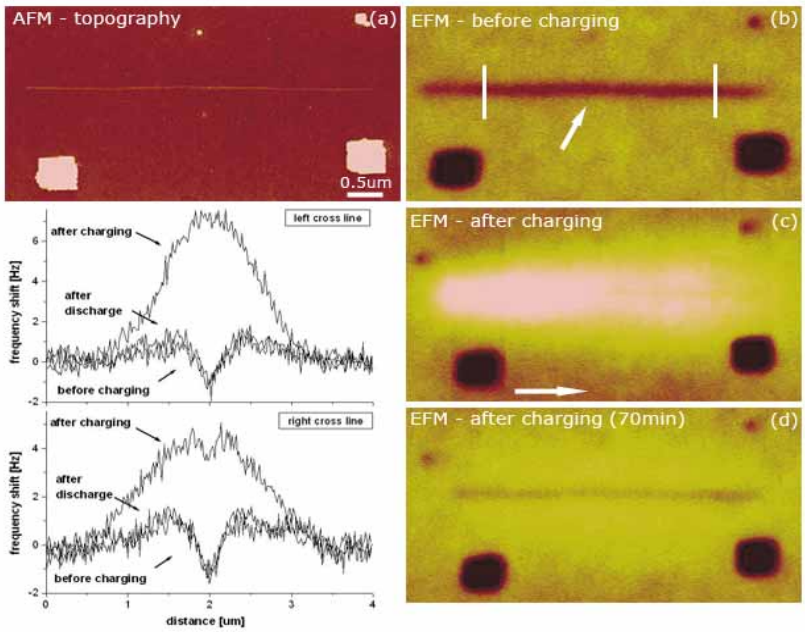


Fig.1 (a) AFM topography scan of 5 µm long SWNT (1.5 nm of diameter). Metal square markers are visible below the nanotube. (b) EFM image before charging. The white arrow indicates the injection point. Both, nanotube and markers remain uncharged (dark features) during this scan. Vertical bars indicate the place where the cross section are taken (see the chart inset). The cross sections before charging are shown on the graph inset. The lift scan height was 90 nm. (c) EFM picture after charge injection (V_{inj} = -5 V for 3 min). The white arrow shows the scan direction. The left part of the nanotube is brighter than the right one, which means that here the nanotube undergoes the discharge process. Two cross-sections are taken from this scan and shown on the graph inset. The left cross-section shows a regular peak shape of the frequency shift of the charged nanotube, while the right cross line already exhibits capacitive effect. Metal markers are still uncharged. (d) EFM scan after 70 min after charging. The nanotube is already uncharged. Cross sections after discharge are shown on the graph inset.

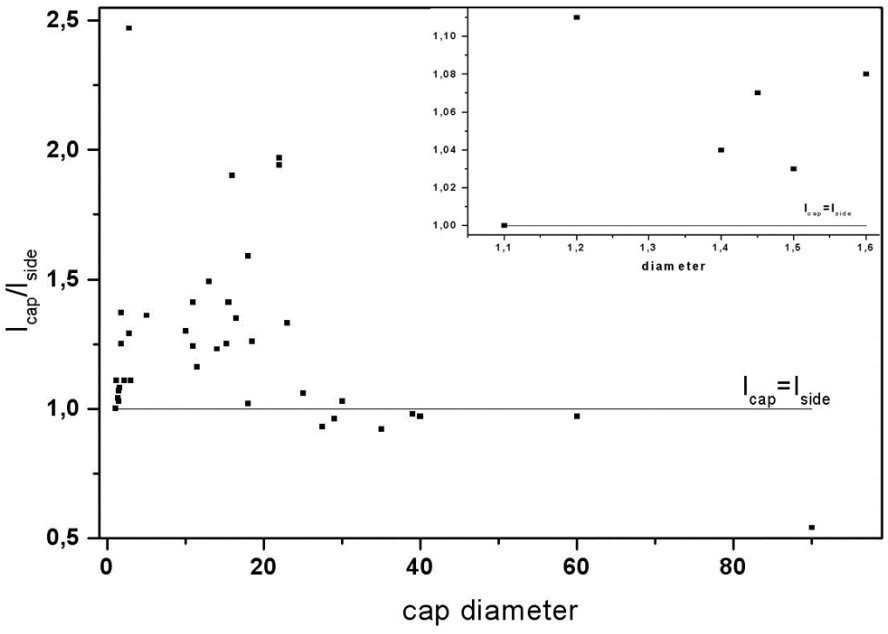


Fig. 2 (a) Comparison of charge emission from the nanotube cap and through the side walls. On the plot we show ratio of frequency shift in front of the nanotube apex and on side of the nantube (I_{cap}/I_{side}) as a function of the nanotube diameter. (inset) Data zoom for single-walled nanotubes.